Pacific Northwest
NATIONAL LABORATORY

PNNL-36304, Rev. 1
EWG-RPT-048, Rev. 1

Expansion of the Direct Feed High-Level Waste Glass Composition in the High Al Range

September 2025

RL Russell
V Gervasio
X Lu
NA Lumetta
NL Canfield
LM Seymour
JT Reiser
JJ Neeway
S Chong
JL George
JD Vienna

U.S. DEPARTMENT of ENERGY

Prepared for the U.S. Department of Energy
under Contract DE-AC05-76RL01830

DISCLAIMER

PACIFIC NORTHWEST NATIONAL LABORATORY
operated by
BATTELLE
for the
UNITED STATES DEPARTMENT OF ENERGY
under Contract DE-AC05-76RL01830

Printed in the United States of America

Available to DOE and DOE contractors from
the Office of Scientific and Technical Information,
P.O. Box 62, Oak Ridge, TN 37831-0062
www.osti.gov
ph: (865) 576-8401
fox: (865) 576-5728
email: reports@osti.gov

Available to the public from the National Technical Information Service
5301 Shawnee Rd., Alexandria, VA 22312
ph: (800) 553-NTIS (6847)
or (703) 605-6000
email: info@ntis.gov
Online ordering: http://www.ntis.gov

PNNL-36304, Rev. 1
EWG-RPT-048, Rev. 1

Expansion of the Direct Feed High-Level Waste Glass Composition in the High Al Range

September 2025

RL Russell, V Gervasio, X Lu, NA Lumetta, NL Canfield, LM Seymour, JT Reiser, JJ Neeway, S Chong, JL George, JD Vienna

Prepared for
the U.S. Department of Energy
under Contract DE-AC05-76RL01830

Pacific Northwest National Laboratory
Richland, Washington 99354

Abstract

Baseline glass compositions have been developed and demonstrated for successful immobilization of Hanford high-level waste (HLW) prepared through a pretreatment process. Recent enhanced waste glass formulations have shown promise to increase the waste loading of pretreated sludge compositions from a broader range of HLW feeds. This project proposes to increase the loading of minimally pretreated (e.g., direct feed scenario) Hanford HLW in glass by expanding the existing glass property-composition database and models. To expand the anticipated HLW glass region, projections must first be developed and compared with existing data to identify coverage gaps. These gaps can then be addressed to ensure sufficient representation across the anticipated HLW glass region, enabling model updates. Estimated direct-feed high-level waste (DFHLW) compositions, generated by the Hanford Tank Operations Contractor, were used by Pacific Northwest National Laboratory to define target glass compositions. Through this process, several data gaps were identified, including a high-priority gap in the high-Al compositional region. This report summarizes the data collected during the characterization of the DFHLW High Al Glass Matrix.

These glasses were intentionally designed with high aluminum concentrations (15 to 30 wt%) and a high likelihood of nepheline formation, which could negatively affect glass durability. Some glasses were predicted to either fail or approach property constraints to fill data gaps in poorly understood regions of the compositional space due to lack of existing data.

Out of the 50 glasses tested, 14 glasses formed nepheline, while the model predicted nepheline formation in 20 glasses, providing valuable information to update the conservative nepheline models. All quenched glasses met the product consistency test durability constraint; however, 8 glasses failed this constraint after undergoing the canister centerline cooling treatment due to crystal formations (including nepheline and other crystals). Additionally, 17 glasses did not meet the viscosity constraints, 4 failed the EC constraints, and 2 exceeded the allowable T2% for spinel crystal formation. All glasses satisfied the SO_3 solubility limit. It should be emphasized that failures in specific properties were anticipated and are necessary to establish acceptable processing envelopes for DFHLW operations.

The resulting dataset provides valuable information to improve model accuracy and reduce prediction uncertainty. These insights will ultimately support the development of more robust glass formulation strategies, enabling higher waste loadings, reducing operational risks, and expanding the processing envelope.

Acknowledgments

The authors gratefully acknowledge the financial support provided by the U.S. Department of Energy Office (DOE) of Environmental Management. We are thankful to Ming Zhu, John Kelley, and Albert Kruger (DOE) for their oversight and collaboration.

The following Pacific Northwest National Laboratory staff members are acknowledged for their contributions: Pavel Ferkl for technical review of the report, David MacPherson and Aaron Sachs for quality assurance, Chrissy Charron and Cassie Martin for programmatic support during this work, Vivianaluxa Gervasio and Renee Russell for project management.

All of the other PNNL staff helping in the laboratory to complete this work are greatly appreciated and acknowledged: P Metheny, M Torres, DA Cutforth, JM Westman, JM Oshiro, JV Crum, J Kroll, S Choi, J Marcial, A Zwoster, ML Blazon, J Bai, and D Wang.

Acronyms and Abbreviations

3TS	three times saturation (method)
CCC	canister centerline cooling(ed)
CF	crystal fraction
DFHLW	Direct Feed High-Level Waste
DOE	U.S. Department of Energy
DWPF	Defense Waste Processing Facility
EC	electrical conductivity
EPMA	electron probe micro-analyzer(sis)
EWG	enhanced waste glass
EWG1	first iteration of enhanced waste glass models
EWG2	second iteration of enhanced waste glass models
HAL	High Al_2O_3 glass matrix
HLW	high-level waste
HTWOS	Hanford Tank Waste Operations Simulator
NL	normalized loss by 7-day PCT
NQAP	Nuclear Quality Assurance Program
PCT	product consistency test
PNNL	Pacific Northwest National Laboratory
Q	quenched (glasses)
QA	quality assurance
SSM	sulfur-saturated melt
T_L	liquidus temperature
TCLP	toxicity characteristic leaching procedure
TPMF	Tilt-Pour melting furnace
VFT	Vogel–Fulcher–Tammann
WC	tungsten carbide
wSO_3	SO_3 solubility
wt%	weight percent
WTP	Waste Treatment and Immobilization Plant
XRD	X-ray diffraction

Contents

Figures

Tables

1.0 Introduction

Baseline glass compositions have been developed and demonstrated for successful immobilization of Hanford high-level waste (HLW) (Vienna and Kim 2014). These formulations were developed to start up the Hanford Waste Treatment and Immobilization Plant (WTP) and therefore were developed over a narrow range of waste compositions based on fully leached and washed tank sludges with modest waste loading (Peeler et al. 2015). Recent enhanced waste glass (EWG) formulations have shown promise in increasing the waste loading of pretreated sludge compositions from a broader range of HLW feeds (Vienna et al. 2016). Advancements in formulations through the EWG program have recently led to the possibility that the WTP HLW Facility can be efficiently started under a Direct Feed High-Level Waste (DFHLW) mode (Vienna et al. 2023) which could be based on minimal pretreatment or conditioning of waste prior to vitrification. Minimal pretreatment and significant concentrations of tank supernate can decrease mission life by 5-10 years and reduce the cost of cleanup by $12.5B-$25.0B (Herman et al. 2022).

DFHLW feeds are projected to have several key compositional differences from those of leached and washed (e.g., pretreated) sludges that ultimately could limit waste loading:

1. DFHLW feeds will likely be retrieved with tank supernate to improve the ability to mobilize solids and deliver them from tank farms to the HLW Facility. The supernate is rich in sodium (typically up to 4 $mol \cdot L^{-1}$ [Na]), sulfate, and other components that are generally washed out of pretreated sludge and managed in the low-activity waste treatment flowsheet (Britton 2023). This results in higher ranges of Na_2O and SO_3 in DFHLW feed, requiring expanded composition bounds to allow for increased waste loading in glass.
2. Aluminum leaching was projected to be a primary function of the pretreatment process. Caustic leaching removed a weighted average of 77% of the Al in tank waste sludge (Certa et al. 2005). The lack of leaching requires broader composition ranges for Al_2O_3 in DFHLW glasses.
3. The concentrations of other components (e.g., Cr_2O_3, F, P_2O_5, Cl, K_2O) are projected to be increased by the reduced washing and lack of leaching anticipated in the DFHLW flowsheet.

This project proposes to increase the loading of potential DFHLW feeds in glass by expanding the existing database (Lu et al. 2023) and glass property-composition models (Vienna et al. 2016) in the high Al, high S, and high Na compositional region.

- **Al_2O_3:** As concentrations of Al_2O_3 and Na_2O increase in glass, so does the probability of nepheline [$NaAlSiO_4$] formation (Lu et al. 2021). Nepheline formation during slow cooling in the HLW glass canister is likely to cause the glass to fail to satisfy chemical durability requirements (Vienna et al. 2017). Although some data in the higher Al_2O_3 and Na_2O composition region has been developed, much more is required to expand the composition region and reduce the prediction uncertainty for nepheline models. Early estimates suggest that Al_2O_3 concentrations in HLW glass limited by nepheline can be increased from the Vienna et al. (2013) limit of 23 wt% or the WTP baseline (Vienna and Kim 2014) of 13 wt% to over 30 wt% (Kroll et al. 2019).
- **Na_2O:** Increasing data and model validity for glasses with increased Na_2O content is paramount for minimizing impacts to the HLW flowsheet. At some point, increasing the concentration of Na_2O will decrease the chemical durability of glass, increase the corrosion rate of melter components and the electrical conductivity (EC) of the melt, and decrease the melt viscosity. Several data sets exist for low-activity waste formulations that can augment the current HLW models (Vienna et al. 2022). However, the composition regions are not the same, so data on additional glasses is required to bridge the gap. Early estimates suggest that Na_2O concentration in HLW glass can be increased from

the Vienna et al. (2013) limit of 23 wt% or the WTP baseline (Vienna and Kim 2014) of 20 wt% to near 30 wt% (Vienna et al. 2018).

- **SO_3:** As concentrations of SO_3, Cl, Cr_2O_3, F, and P_2O_5 increase, so does the propensity for molten salt accumulation in the melter (Vienna and Kim 2014; Skidmore et al. 2019). As the concentrations of these components are higher in DFHLW feeds compared to pretreated feeds, the concentration ranges of these components need to be expanded and the solubility measured to improve loading of DFHLW in glass. Early estimates suggest that SO_3 concentration in HLW melter feed can be increased from the WTP baseline (Vienna and Kim 2014) of 0.44 wt% to roughly 2 wt% (Skidmore et al. 2019 and Jin et al. 2018).

This report documents the design of a high Al_2O_3 matrix to extend DFHLW glass compositional ranges, glass preparation, characterization, and measured vs. predicted values comparison using current models (Section 2.1.3).

1.1 Quality Assurance

This work was performed in accordance with the Pacific Northwest National Laboratory (PNNL) Nuclear Quality Assurance Program (NQAP). The NQAP complies with the DOE Order 414.1D, *Quality Assurance*, and 10 CFR 830, Subpart A, *Quality Assurance Requirements*. The NQAP uses NQA-1-2012*, Quality Assurance Requirements for Nuclear Facility Applications*, and DOE/RW-0333P Revision 20, *Quality Assurance Requirements Document* (QARD), as consensus standards and NQA-1-2012, Subpart 4.2.1, as the basis for its graded approach to quality.

The NQAP works in conjunction with PNNL's laboratory-level Quality Management Program, which is based on the requirements as defined in DOE Order 414.1D and 10 CFR 830 Subpart A.

The work of this report was performed at a technology readiness level of 5. Experimental activities supporting this report were performed in compliance with DOE/RW-0333P requirements.

2.0 Test Methods

This section describes how the test matrix of 50 glasses was designed and data were obtained. The descriptions include the methods for (1) glass matrix design, (2) glass fabrication and chemical composition analysis, (3) secondary phase identification from canister centerline cooled (CCC) samples, (4) isothermal crystal fraction (CF) and liquidus temperature (T_L) measurement, (5) sulfur solubility measurement, (6) density (ρ) determination, (7) viscosity (η) measurement, (8) electrical conductivity (EC) measurement, (9) product consistency test (PCT) measurement, and (10) toxicity characteristic leaching procedure (TCLP) measurement.

2.1 Matrix Design

This section describes how the glasses were formulated for representative DFHLW feed composition estimates using the current state-of-the-art glass property-composition models and constraint sets applicable to DFHLW.

2.1.1 Design Method

The region with relatively high Al_2O_3 is a specific focus of this design. The space-filling experimental design capabilities of JMP® (statistical software, SAS Institute) were used to develop a glass composition matrix for HLW glass composition region. JMP® has a unique proprietary approach to space-filling designs that are not available in other software packages and are widely considered the most appropriate method for developing such a matrix (Joseph et al. 2015). Standard software default assumptions were used to design the matrix of glasses with a fixed set of single-component constraints for individual oxide concentration ranges. HLW glasses from an existing database of glasses in the same composition region will be augmented by this design. The matrix design was required to meet predefined acceptance ranges defined by the single-component restraints and also broad dispersion of points across the range compared to those ranges.

A successful matrix must meet two criteria: (1) the dispersion value of each component must be below 0.90 and (2) the relative range of individual components across the glasses in the matrix should be greater than or equal to 0.80 for components that can achieve their full design range. The methods for calculating these two values are given below.

1. The dispersion ratio of a matrix is defined as follows:

Given a vector x of n values for a particular component (so x is a vector of length n) that are <u>sorted</u> in increasing order, define the d to be the differences of the entries in x. So, d is a vector of length $n – 1$, such that

$$d_i = x_{i+1} - x_i \quad \text{for } i = 1, 2, 3, \ldots, n-1 \qquad (2.1)$$

So, these d_i values are the lengths of the segments of the partition formed by the component values contained in the vector x.

The formula for the dispersion metric (D) is:

$$D = \frac{\sum_{i=1}^{n-1}\left|d_i - \frac{R}{n-1}\right|}{R} \tag{2.2}$$

where R = the intended range of the particular component or predicted property
n = number of glasses in the matrix
d_i is as defined above

Note that if the points formed an "ideal" uniform or regular partition of the range of the particular component, each d_i would have a length of $\frac{R}{n-1}$, and D would be 0. So, the dispersion metric describes the sum of absolute differences from a uniform or regular partition of the range of the particular component, relative to the range of the component. Thus, a value of $D = 1.45$ would mean that the absolute differences in the actual segment lengths of the partition formed by the vector x and the length of an "ideal" segment would sum to 1.45 times the intended range of the component. Additionally, the dispersion metric, D, rewards sets of component values that are close to a uniform or regular partition. Smaller values of D are better in the sense that the corresponding x vector would be closer to a regular partition.

2. The relative range of each individual component across the glasses in the matrix is calculated according to:

$$[\min(g_{matrix})-\max(g_{matrix})]/[\min(g_{target})-\max(g_{target})] \tag{2.3}$$

where g_{target} is the target mass fraction of a component and g_{matrix} is the mass fraction of a component in the matrix.

The matrix was designed following these general steps:

1. Identify compositional gaps (Lu et al. 2023).
2. Set component concentration boundaries and property boundaries (both within and outside the typical processing and product quality constraints so that constraints can be successfully predicted).
3. Generate a significant amount (e.g., 40,000) of simulated glasses using JMP to fill in the space within boundaries.
4. Calculate the predicted properties using various models.
5. Select the glasses that satisfy the property targets among the 40,000 simulated glasses.
6. Combine the selected glasses with existing data that are within the component concentration boundaries, as well as adding duplicates from previous tested glass matrices.
7. Design candidate glass matrices using JMP to back fill with a few different random seeds (e.g., 5).
8. Calculate matrix dispersion and range coverage to select one matrix for testing.
9. Plot figures to check compositional coverage and property distribution.

2.1.2 Compositional Boundaries

Component concentration boundaries were obtained by examining the minimum and maximum values of each component from different datasets (e.g., existing nepheline data that satisfy quality assurance (QA) requirements, glasses formulated using EWG methods). Table 2.1 shows these boundaries and rationales of the matrix design ranges. Table 2.2 shows the components contained in the "Others" component listed in Table 2.1. These minor components were grouped together with a fixed concentration in "Others."

Table 2.1. Minimum and maximum values (wt%) of major components from existing nepheline (NP) data conducted under required QA program, glasses formulated using EWG1 and EWG2 method, matrix design ranges and rationales.

	Existing QA NP Data		EWG1		EWG2		Matrix Design		Rationale
Ref.:	Lu et al. 2023		Vienna et al. 2016 and Lu et al. 2023		Vienna et al. 2023 and Gervasio et al. 2024		This study		This study
	Min	Max	Min	Max	Min	Max	Min	Max	
Al_2O_3	15.0	20.0	15.2	26.3	15.1	26.2	15.0	30.0	Range of existing data + expansion
B_2O_3	5.0	20.0	13.8	22.0	16.8	22.0	13.5	24.0	Range for EWG + expansion
CaO	0.0	10.0	0.1	10.0	0.0	1.6	0.0	10.0	Range of existing data and EWG1
Cr_2O_3	0.0	3.0	0.1	0.9	0.1	0.9	0.0	1.0	Range of EWG rounded
F	0.0	0.5	0.1	1.9	0.2	0.5	0.0	2.0	Range of EWG1 rounded
Fe_2O_3	0.0	11.4	0.2	6.5	2.4	6.8	0.0	7.0	Range of EWG rounded
Li_2O	0.5	7.3	0.0	2.2	0.0	2.1	0.0	2.5	Range of EWG + expansion
Na_2O	5.0	19.0	11.1	22.9	15.0	23.0	11.0	23.0	Range of EWG
P_2O_5	0.0	0.5	0.2	3.9	0.4	3.9	0.0	4.0	Range of EWG rounded
SiO_2	32.3	55.0	24.7	33.7	24.6	37.5	24.0	38.0	Range of EWG2 rounded
SO_3	0.0	0.5	0.2	1.5	0.3	0.9	0.0	1.5	Range of EWG1
V_2O_5	0.0	0.0	0.0	4.1	0.0	2.0	0.0	4.1	Range of EWG1
ZnO	0.0	2.0	0.0	4.0	0.0	0.0	0.0	4.0	Range of EWG1
ZrO_2	0.0	4.0	0.1	0.4	0.0	0.2	0.0	4.0	Range of existing data
Others[(a)]	-	-	-	-	-	-	0.873	2.619	Arbitrary

(a) Components contained in "Others" are shown in Table 2.2.
EWG1 = first iteration of enhanced waste glass models; EWG2 = second iteration of enhanced waste glass models.

Table 2.2. Minor components in "Others".

"Others"	Mean wt%	wt% in "Others" [b]
Bi_2O_3	0.11	6
Cl	0.13	8
K_2O	0.29	16
LN_2O_3[a]	0.04	2
MgO	0.48	27
MnO	0.22	12
NiO	0.30	17
PbO	0.14	8
SrO	0.01	1
TiO_2	0.02	1
Total	1.75	100

(a) LN_2O_3 represents lanthanide oxides.
(b) These minor components were grouped together with a fixed concentrations in "Others."

2.1.3 Property Constraints

Table 2.3 shows the property constraints used to select glasses generated from the space-filling step. These constraints were relaxed compared to the previous or original EWG limits, so that the glasses that have predicted values at or near the limits could be included in testing.

Table 2.3. Property constraints used in matrix design.

Property	EWG2 Limit	Design Limit	Unit	Models
Spinel $T_{2\%}$	< 950	< 1000	°C	Vienna et al. (2016)
PCT NL_{Ave}[a]	< 4	< 10	g/m^2	Vienna and Crum (2018)
PCT NC_B [a]	< 8	< 20	g/L	Kot et al. (2019)
Viscosity at 1150 °C (η_{1150})	40 to 60	10 to 100	Poise	Vienna et al. (2022), and Kot et al. (2019)
EC at 1150 °C (ε_{1150})	12 to 59	8 to 100	S/m	Vienna et al. (2022), and Vienna et al. (2009)
Three times saturation (3TS) SO_3 solubility (w_{SO3})	< w_{SO3}	< 0.75 × w_{SO3}	Mass ratio	Vienna et al. (2024)
Nepheline formation	> 0	> -0.05	Distance to the line	Lu et al. (2021)

(a) PCT responses are modeled in normalized concentration (NC) and normalized loss (NL).

2.1.4 Designed Matrix Compositions

Figure 2.1 shows the scatterplot matrix for the designed 50 high Al_2O_3 glasses. Table 2.4 to Table 2.8 list the compositions of these glasses. The compositions were separated into two testing phases for program logistical purposes: HAL24M1 and HAL24M2. Two replicate glasses (HAL24M1-29 and HAL24M1-30) were included in the design: APPS-01 and APPS-02 from Gervasio et al. (2024), respectively. Heatmaps showing the pair correlations of a few major glass components can be found in Appendix A. Those figures show the comparison between the design space, existing glasses, and the designed 50 high Al_2O_3 glasses.

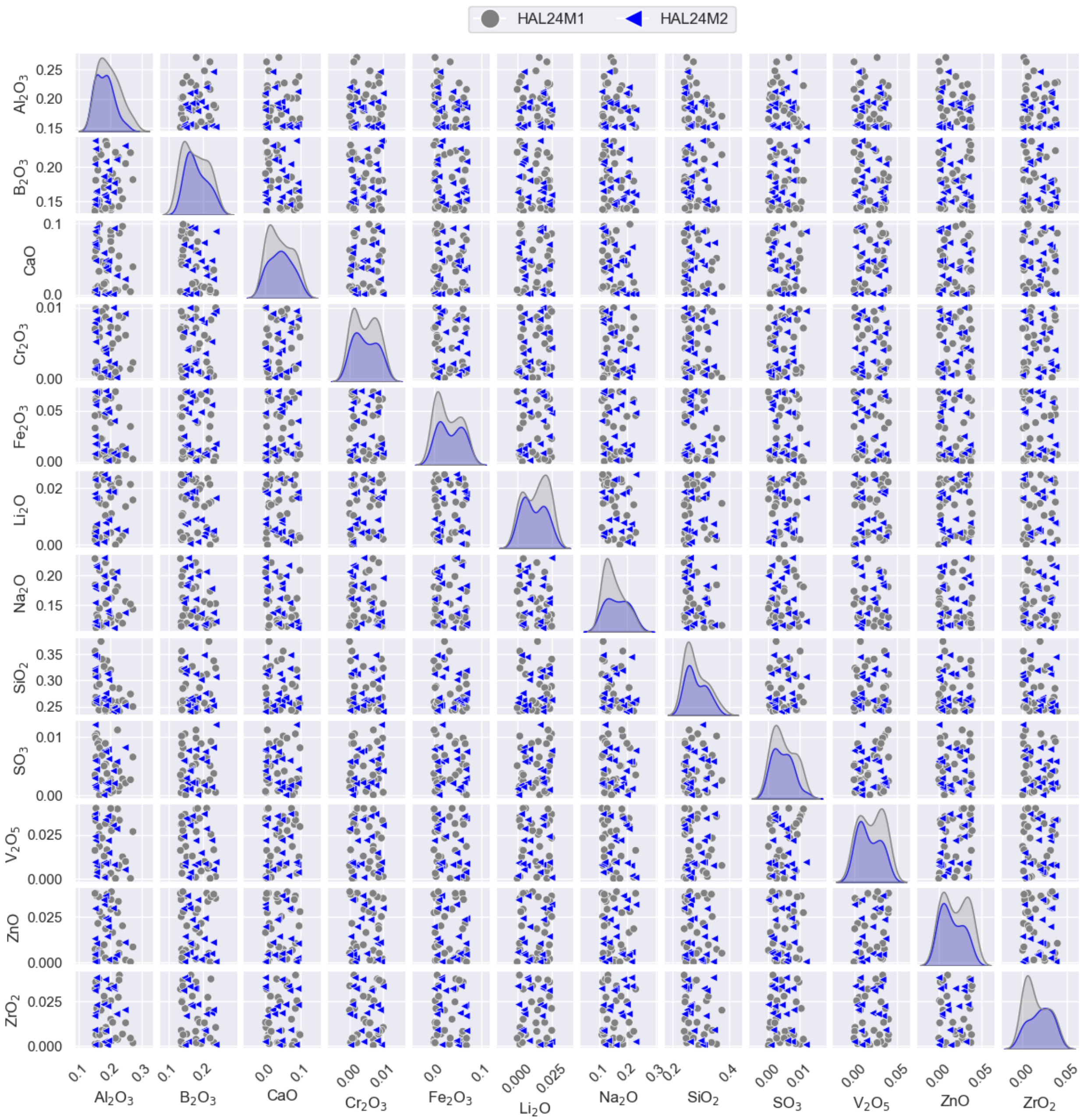

Figure 2.1. Scatterplot matrix for the designed 50 high Al_2O_3 glasses.

Table 2.4. Glass compositions (mass fraction) for HAL24M1-01 to HAL24M1-10.

Glass ID	HAL24M1-01	HAL24M1-02	HAL24M1-03	HAL24M1-04	HAL24M1-05	HAL24M1-06	HAL24M1-07	HAL24M1-08	HAL24M1-09	HAL24M1-10
Al_2O_3	0.15604	0.15109	0.15287	0.18473	0.22217	0.22475	0.15387	0.16337	0.20133	0.15994
B_2O_3	0.14885	0.13901	0.18062	0.23779	0.1804	0.21486	0.21174	0.22395	0.13714	0.19543
CaO	0.08596	0.05127	0.06206	0.00251	0.00591	0.03686	0.00903	0.03271	0.08291	0.01149
Cr_2O_3	0.00153	0.0008	0.0098	0.00997	0.00709	0.0056	0.00232	0.00826	0.00166	0.00072
F	0.0199	0.01831	0.00449	0.01224	0.01904	0.01773	0.00826	0.00104	0.01323	0.01797
Fe_2O_3	0.00444	0.03279	0.06138	0.00461	0.00056	0.01064	0.05977	0.04601	0.06237	0.06584
Li_2O	0.02464	0.00183	0.02327	0.00198	0.02216	0.02336	0.00606	0.01508	0.02111	0.02099
Na_2O	0.13294	0.18382	0.11305	0.15195	0.18037	0.12454	0.11073	0.1229	0.11995	0.12843
P_2O_5	0.00757	0.00272	0.03346	0.01209	0.00979	0.00613	0.02719	0.02014	0.02967	0.03714
SiO_2	0.28838	0.3553	0.26769	0.32306	0.25845	0.24606	0.31127	0.24354	0.25265	0.30795
SO_3	0.01056	0.01019	0.00983	0.00053	0.01122	0.00079	0.00657	0.00925	0.00048	0.00887
V_2O_5	0.03665	0.03532	0.03309	0.00113	0.03962	0.00579	0.04004	0.02519	0.0309	0.00425
ZnO	0.03661	0.00708	0.00175	0.03536	0.02736	0.03362	0.03819	0.03613	0.03465	0.02144
ZrO_2	0.02085	0.00092	0.03564	0.01028	0.00364	0.0271	0.00621	0.03733	0.0024	0.0012
Bi_2O_3	0.0016	0.00061	0.0007	0.00075	0.00078	0.00141	0.00056	0.00096	0.00061	0.00117
Cl	0.00191	0.00073	0.00084	0.0009	0.00093	0.00169	0.00067	0.00115	0.00073	0.0014
K_2O	0.0041	0.00156	0.0018	0.00192	0.00199	0.00362	0.00143	0.00246	0.00156	0.00299
Nd_2O_3	0.00058	0.00022	0.00025	0.00027	0.00028	0.00051	0.0002	0.00035	0.00022	0.00042
MgO	0.00689	0.00262	0.00302	0.00323	0.00336	0.00609	0.0024	0.00415	0.00262	0.00504
MnO	0.00313	0.00119	0.00137	0.00147	0.00152	0.00276	0.00109	0.00188	0.00119	0.00229
NiO	0.0043	0.00164	0.00189	0.00202	0.0021	0.00381	0.0015	0.00259	0.00164	0.00315
PbO	0.00205	0.00078	0.0009	0.00096	0.001	0.00182	0.00072	0.00124	0.00078	0.0015
SrO	0.00018	0.00007	0.00008	0.00009	0.00009	0.00016	0.00006	0.00011	0.00007	0.00013
TiO_2	0.00034	0.00013	0.00015	0.00016	0.00017	0.0003	0.00012	0.00021	0.00013	0.00025
SUM	1	1	1	1	1	1	1	1	1	1

Table 2.5. Glass compositions (mass fraction) for HAL24M1-11 to HAL24M1-20.

Glass ID	HAL24M1-11	HAL24M1-12	HAL24M1-13	HAL24M1-14	HAL24M1-15	HAL24M1-16	HAL24M1-17	HAL24M1-18	HAL24M1-19	HAL24M1-20
Al_2O_3	0.23789	0.2008	0.22806	0.16461	0.20068	0.22679	0.18871	0.17319	0.16968	0.27083
B_2O_3	0.15372	0.13969	0.16574	0.15048	0.18528	0.14224	0.23224	0.13781	0.21813	0.18152
CaO	0.09635	0.09031	0.08666	0.07719	0.07491	0.05452	0.03464	0.04631	0.01113	0.0391
Cr_2O_3	0.0086	0.00723	0.00137	0.00706	0.00427	0.00881	0.00036	0.00943	0.00006	0.00222
F	0.00188	0.01621	0.00485	0.00381	0.00135	0.00078	0.00022	0.01609	0.00405	0.01558
Fe_2O_3	0.01485	0.00294	0.00686	0.06838	0.0381	0.05302	0.00024	0.02247	0.02241	0.0025
Li_2O	0.00315	0.01682	0.0016	0.01614	0.00426	0.02189	0.00366	0.02477	0.01459	0.0158
Na_2O	0.11843	0.16087	0.13179	0.14385	0.12887	0.13119	0.11894	0.11329	0.11491	0.14236
P_2O_5	0.03607	0.00459	0.03878	0.03944	0.00885	0.00147	0.00508	0.02878	0.02413	0.02234
SiO_2	0.26164	0.31962	0.24088	0.29252	0.24315	0.2844	0.33697	0.33999	0.37372	0.24987
SO_3	0.00284	0.00281	0.00152	0.00007	0.00245	0.00417	0.00375	0.00688	0.00256	0.00658
V_2O_5	0.01236	0.00299	0.03324	0.01831	0.03997	0.00748	0.01634	0.0231	0.0074	0.02677
ZnO	0.02005	0.0009	0.01037	0.00654	0.02926	0.00487	0.03757	0.0252	0.00492	0.00836
ZrO_2	0.00655	0.02521	0.0395	0.00023	0.01485	0.03673	0.00185	0.00861	0.01988	0.00168
Bi_2O_3	0.00163	0.00057	0.00056	0.00072	0.00151	0.00138	0.00124	0.00153	0.00079	0.00092
Cl	0.00195	0.00069	0.00067	0.00087	0.00181	0.00165	0.00148	0.00184	0.00095	0.0011
K_2O	0.00418	0.00147	0.00143	0.00186	0.00388	0.00353	0.00317	0.00393	0.00203	0.00236
Nd_2O_3	0.00059	0.00021	0.0002	0.00026	0.00055	0.0005	0.00045	0.00055	0.00029	0.00033
MgO	0.00704	0.00247	0.00241	0.00312	0.00652	0.00594	0.00534	0.00662	0.00341	0.00398
MnO	0.00319	0.00112	0.0011	0.00142	0.00296	0.0027	0.00242	0.003	0.00155	0.00181
NiO	0.0044	0.00155	0.00151	0.00195	0.00408	0.00371	0.00333	0.00413	0.00213	0.00249
PbO	0.0021	0.00074	0.00072	0.00093	0.00194	0.00177	0.00159	0.00197	0.00102	0.00119
SrO	0.00019	0.00007	0.00006	0.00008	0.00017	0.00016	0.00014	0.00018	0.00009	0.00011
TiO_2	0.00035	0.00012	0.00012	0.00016	0.00033	0.0003	0.00027	0.00033	0.00017	0.0002
SUM	1	1	1	1	1	1	1	1	1	1

Table 2.6. Glass compositions (mass fraction) for HAL24M1-21 to HAL24M1-30.

Glass ID	HAL24M1-21	HAL24M1-22	HAL24M1-23	HAL24M1-24	HAL24M1-25	HAL24M1-26	HAL24M1-27	HAL24M1-28	HAL24M1-29	HAL24M1-30
Al_2O_3	0.20678	0.24772	0.15053	0.16535	0.18429	0.20265	0.18366	0.1794	0.26321	0.21577
B_2O_3	0.19064	0.20515	0.13546	0.14325	0.17947	0.14228	0.13944	0.16996	0.22104	0.22169
CaO	0.00081	0.0104	0.00435	0.09923	0.01713	0.06274	0.04247	0.01515	0.00409	0.00669
Cr_2O_3	0.00491	0.00608	0.00696	0.00583	0.00865	0.00011	0.00123	0.00413	0.00131	0.00089
F	0.00273	0.00672	0.01699	0.00966	0.01681	0.00619	0.01215	0.00587	0.00211	0.00455
Fe_2O_3	0.00259	0.00652	0.04504	0.007	0.06055	0.00954	0.04424	0.00995	0.03434	0.0685
Li_2O	0.01969	0.01348	0.00435	0.00255	0.01411	0.01099	0.01031	0.02302	0.02131	0
Na_2O	0.20553	0.15564	0.22866	0.20866	0.2219	0.16186	0.19825	0.17782	0.15113	0.17324
P_2O_5	0.0056	0.03986	0.03842	0.02044	0.00306	0.01668	0.03753	0.0178	0.0037	0.02298
SiO_2	0.286	0.25644	0.25661	0.25608	0.24131	0.2611	0.2439	0.32628	0.27371	0.24775
SO_3	0.00069	0.00213	0.00351	0.00817	0.00537	0.00135	0.00893	0.00505	0.00269	0.0051
V_2O_5	0.03429	0.0097	0.01602	0.02958	0.00072	0.02731	0.03131	0.01273	0.00003	0
ZnO	0.01636	0.00117	0.03805	0.02792	0.01844	0.039	0.00231	0.00956	0.00007	0.00007
ZrO_2	0.01306	0.01284	0.03167	0.00616	0.00808	0.03352	0.02452	0.02767	0.00426	0.00422
Bi_2O_3	0.00066	0.00166	0.00149	0.00064	0.00128	0.00157	0.00126	0.00099	0.00093	0.00456
Cl	0.00079	0.00199	0.00178	0.00077	0.00153	0.00188	0.0015	0.00119	0.00194	0.00202
K_2O	0.00168	0.00427	0.00382	0.00166	0.00328	0.00403	0.00323	0.00255	0.00202	0.00066
Nd_2O_3	0.00024	0.0006	0.00054	0.00023	0.00046	0.00057	0.00045	0.00036	0.00325	0.00766
MgO	0.00283	0.00719	0.00642	0.00278	0.00552	0.00678	0.00543	0.00429	0.00014	0.00013
MnO	0.00129	0.00326	0.00292	0.00126	0.00251	0.00308	0.00246	0.00195	0.00347	0.00284
NiO	0.00177	0.00449	0.00401	0.00174	0.00345	0.00423	0.00339	0.00268	0.00341	0.00582
PbO	0.00084	0.00214	0.00191	0.00083	0.00165	0.00202	0.00162	0.00128	0.00184	0.00486
SrO	0.00008	0.00019	0.00017	0.00007	0.00015	0.00018	0.00014	0.00011	0	0
TiO_2	0.00014	0.00036	0.00032	0.00014	0.00028	0.00034	0.00027	0.00021	0	0
SUM	1	1	1	1	1	1	1	1	1	1

Table 2.7. Glass compositions (mass fraction) for HAL24M2-01 to HAL24M2-10.

Glass ID	HAL24M2-01	HAL24M2-02	HAL24M2-03	HAL24M2-04	HAL24M2-05	HAL24M2-06	HAL24M2-07	HAL24M2-08	HAL24M2-09	HAL24M2-10
Al_2O_3	0.15453	0.18027	0.19261	0.15577	0.18987	0.15027	0.18428	0.15588	0.15279	0.21186
B_2O_3	0.16304	0.15892	0.18026	0.14803	0.14923	0.20417	0.15607	0.16479	0.22661	0.17641
CaO	0.06703	0.00032	0.00154	0.00065	0.04108	0.07297	0.04776	0.09454	0.04778	0.09339
Cr_2O_3	0.00112	0.00428	0.00239	0.00168	0.00045	0.00782	0.00396	0.0083	0.00515	0.00206
F	0.01425	0.00028	0.00093	0.0071	0.01951	0.01313	0.01948	0.01942	0.00075	0.01673
Fe_2O_3	0.05787	0.04748	0.00106	0.01599	0.05126	0.00747	0.0163	0.06713	0.05535	0.03975
Li_2O	0.00034	0.02475	0.00903	0.00729	0.02314	0.00305	0.00773	0.01649	0.00467	0.01855
Na_2O	0.21668	0.22977	0.15937	0.21417	0.16024	0.11517	0.18639	0.1147	0.17732	0.11
P_2O_5	0.00769	0.03912	0.03764	0.03964	0.00227	0.00097	0.00543	0.03136	0.01303	0.01493
SiO_2	0.25698	0.26233	0.31156	0.34377	0.31231	0.34748	0.25216	0.26575	0.2615	0.24752
SO_3	0.00112	0.00767	0.00789	0.0058	0.00095	0.00172	0.00215	0.00445	0.00142	0.00206
V_2O_5	0.00144	0.00047	0.02158	0.00728	0.00916	0.03675	0.03344	0.00351	0.02174	0.00777
ZnO	0.00542	0.03183	0.01952	0.00012	0.01413	0.0129	0.03666	0.01024	0.00464	0.00213
ZrO_2	0.03328	0.00223	0.03201	0.03804	0.00029	0.0088	0.03695	0.02276	0.01824	0.03193
Bi_2O_3	0.00122	0.00065	0.00144	0.00093	0.00166	0.0011	0.00071	0.00131	0.00057	0.00158
Cl	0.00146	0.00078	0.00172	0.00112	0.00199	0.00132	0.00086	0.00158	0.00069	0.0019
K_2O	0.00314	0.00168	0.00369	0.00239	0.00426	0.00283	0.00184	0.00338	0.00147	0.00407
Nd_2O_3	0.00044	0.00024	0.00052	0.00034	0.0006	0.0004	0.00026	0.00048	0.00021	0.00057
MgO	0.00528	0.00283	0.00621	0.00403	0.00717	0.00476	0.00309	0.00568	0.00247	0.00684
MnO	0.0024	0.00128	0.00282	0.00183	0.00326	0.00216	0.0014	0.00258	0.00112	0.00311
NiO	0.0033	0.00176	0.00388	0.00252	0.00448	0.00297	0.00193	0.00355	0.00155	0.00428
PbO	0.00157	0.00084	0.00185	0.0012	0.00214	0.00142	0.00092	0.00169	0.00074	0.00204
SrO	0.00014	0.00008	0.00017	0.00011	0.00019	0.00013	0.00008	0.00015	0.00007	0.00018
TiO_2	0.00026	0.00014	0.00031	0.0002	0.00036	0.00024	0.00015	0.00028	0.00012	0.00034
SUM	1	1	1	1	1	1	1	1	1	1

Table 2.8. Glass compositions (mass fraction) for HAL24M2-11 to HAL24M2-20.

Glass ID	HAL24M2-11	HAL24M2-12	HAL24M2-13	HAL24M2-14	HAL24M2-15	HAL24M2-16	HAL24M2-17	HAL24M2-18	HAL24M2-19	HAL24M2-20
Al_2O_3	0.15122	0.20904	0.2459	0.15001	0.17843	0.18502	0.15112	0.19466	0.21933	0.19187
B_2O_3	0.1449	0.16294	0.23104	0.15231	0.18607	0.20795	0.23846	0.19549	0.21083	0.16985
CaO	0.07047	0.00006	0.02156	0.00635	0.05854	0.0378	0.08901	0.04724	0.02651	0.0344
Cr_2O_3	0.00651	0.00995	0.00912	0.00133	0.00092	0.00349	0.00948	0.00827	0.00009	0.00634
F	0.00025	0.01535	0.00017	0.01074	0.00126	0.00464	0.00309	0.01324	0.01444	0.00987
Fe_2O_3	0.02473	0.00816	0.01267	0.06818	0.01088	0.06901	0.01728	0.04833	0.00629	0.06423
Li_2O	0.0229	0.0186	0.0049	0.01793	0.00099	0.00418	0.01645	0.00872	0.00547	0.01885
Na_2O	0.15315	0.19536	0.1362	0.18213	0.19921	0.11772	0.12127	0.13488	0.2061	0.13945
P_2O_5	0.00237	0.02567	0.0292	0.0124	0.01988	0.03268	0.00206	0.01092	0.00144	0.0035
SiO_2	0.32195	0.24037	0.25153	0.31824	0.26648	0.27514	0.30601	0.3005	0.2425	0.26233
SO_3	0.00597	0.0042	0.0082	0.00293	0.00006	0.00748	0.01211	0.00625	0.00578	0.0022
V_2O_5	0.02393	0.03024	0.005	0.03424	0.0088	0.00834	0.00924	0.01453	0.02829	0.03556
ZnO	0.02961	0.02981	0.01082	0.00418	0.03439	0.02419	0.00014	0.00134	0.00389	0.02344
ZrO_2	0.03084	0.03313	0.01999	0.01666	0.02303	0.00835	0.00055	0.00282	0.01773	0.02207
Bi_2O_3	0.00071	0.00109	0.00087	0.00142	0.0007	0.00089	0.00151	0.00081	0.00072	0.00102
Cl	0.00085	0.0013	0.00104	0.0017	0.00084	0.00107	0.00181	0.00098	0.00086	0.00122
K_2O	0.00183	0.0028	0.00224	0.00365	0.00181	0.00229	0.00387	0.00209	0.00185	0.00262
Nd_2O_3	0.00026	0.00039	0.00032	0.00052	0.00025	0.00032	0.00055	0.00029	0.00026	0.00037
MgO	0.00308	0.0047	0.00376	0.00615	0.00304	0.00385	0.00652	0.00352	0.00311	0.00441
MnO	0.0014	0.00214	0.00171	0.00279	0.00138	0.00175	0.00296	0.0016	0.00141	0.002
NiO	0.00192	0.00294	0.00235	0.00384	0.0019	0.0024	0.00407	0.0022	0.00194	0.00275
PbO	0.00092	0.0014	0.00112	0.00183	0.00091	0.00115	0.00194	0.00105	0.00093	0.00131
SrO	0.00008	0.00013	0.0001	0.00016	0.00008	0.0001	0.00017	0.00009	0.00008	0.00012
TiO_2	0.00015	0.00023	0.00019	0.00031	0.00015	0.00019	0.00033	0.00018	0.00015	0.00022
SUM	1	1	1	1	1	1	1	1	1	1

2.1.5 Predicted Properties

Figure 2.2 shows the predicted properties (model listed in Table 2.3) including viscosity at 1150 °C (η_{1150}), EC at 1150 °C (ε_{1150}), PCT response, 2% spinel temperature ($T_{2\%}$), three times saturation method (3TS) sulfur solubility (w_{SO3}), and nepheline formation probability for the 50 designed glasses.

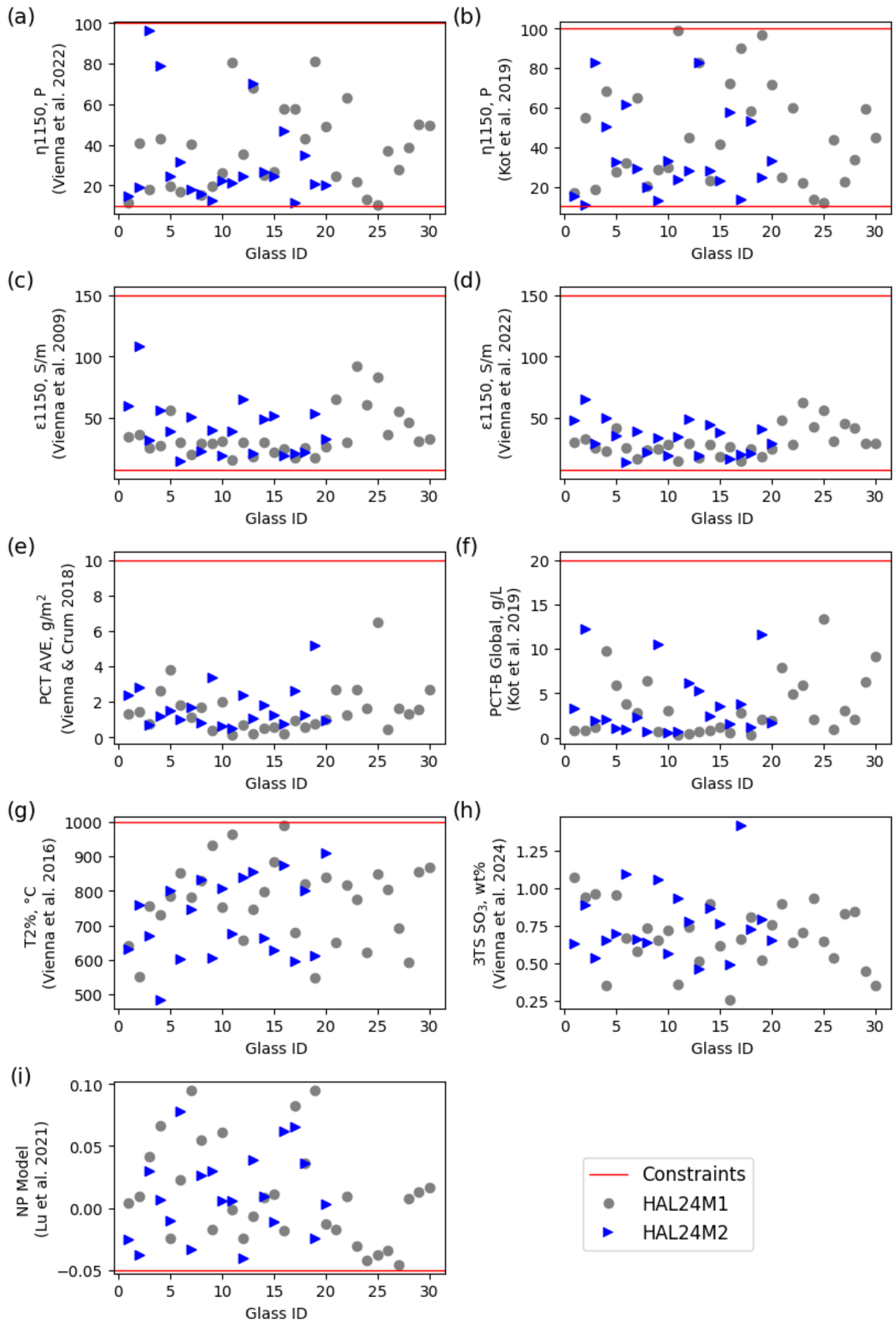

Figure 2.2. Predicted properties, including η_{1150} (a, b), ε_{1150} (c, d), PCT response (e, f), spinel $T_{2\%}$ temperature (g), 3TS w_{SO3} (h), and nepheline formation probability (i) for the 50 designed glasses.

2.2 Glass Fabrication and Characterization

The designed glass compositions were made and characterized. This section describes the fabrication method of the 50 high-Al glasses (HAL24) and their characterization.

The following properties of the glasses were characterized:

- Glass-forming ability and melting temperature for each glass by visual observation
- Elemental and oxide composition of quenched (Q) glasses analyzed by electron probe micro-analyzer (EPMA) and laser-induced breakdown spectroscopy to verify accurate batching for the glasses
- Secondary crystalline phase formation after slow cooling using the CCC profile
- Isothermal CF formation as a function of temperature of Q glasses and liquidus temperature (T_L)
- Density of Q glasses
- Viscosity and EC of melt as a function of temperature
- Q and CCC glass PCT normalized boron, sodium, lithium, and silicon releases
- Q and CCC glass toxicity leaching characteristic procedure (TCLP) response
- Sulfate solubility by 3TS method

K3 refractory corrosion testing was performed and reported separately.

2.2.1 Glass Fabrication

The glasses were batched using appropriate masses of single-metal oxides, single-metal carbonates, sodium salts, and boric acid to form the target compositions. The batched powders (Appendix B) were melted in platinum (Pt)-10% rhodium (Rh) crucibles. Laboratory crucible-scale fabrication of glasses is intended to fabricate a glass sample with a controlled composition for property testing, and it is not intended to mimic the actual melter process or feed processability. The batched powders were thoroughly mixed in a plastic bag for at least 30 s until the mixture was a uniform color. The powders were transferred to an agate milling chamber and milled for 4 min in a vibratory mill (Angstrom TE110) and placed into a clean Pt-10% Rh crucible for melting.

Glasses melted in the Deltech furnace (Deltech Model DT-31-RS, Denver, Colorado) were melted at least two times. First and second melts were performed at 1150 ± 10 °C for 1 h ± 10 min. After the first melt, the glass was air quenched on a stainless-steel pouring plate, ground to a fine powder for 5 min (+ 1 min if glass chunks were still present) in a tungsten carbide (WC) vibratory mill (AngstromTE110), and melted a second time. After each melt, the glass was observed under an optical microscope and the presence of undissolved particles and/or salts was reported. When the glass presented a large amount of undissolved particles, a third melt was performed at 1200 °C for 1 h ± 10 min after the glass was reduced to powder as described above.

For the tilt-pour furnace (UltraMELT, TLT-2P, Ronkonkoma, New York), melting was performed by following the *Operating Procedure for the Tilt-Pour Furnace*, EWG-OP-086, Rev. 1.0.[1] Melting with a tilt-pour furnace took about 1 h for charging glass powders at 1150 ± 50 °C, and the powder was melted for 1 to 1.5 h after charging. The melt was stirred every 10 to 15 min for < 1 min to obtain homogeneous distribution of the glass melt. After the first melt was air quenched on a pouring plate, the glass was

[1] Neeway JJ. 2024. *Operating Procedure for Tilt-Pour Furnace*. EWG-OP-086, Rev. 1.0.

observed under an optical microscope and the presence of undissolved particles and/or salts was reported. A second melt was performed for the glasses with large amounts of undissolved particles and/or salts present.

Table 2.9 presents details on the furnace type used, number of melts, and final melting temperature. Photos of the melted glasses are provided in Appendix B. The averages of the 10 different measured components in weight percent in the Q glasses are compared to the target concentrations in Appendix C along with the relative percentage difference.

Table 2.9. Number of melts and type of furnace used. The final melt was performed at 1150 °C unless otherwise noted.

Glass ID	Number of Melts	Melting Furnace[(a)] (1st/2nd and 3rd melt[(b)])	Glass ID	Number of Melts	Melting Furnace[(a)] (1st/2nd and 3rd melt[(b)])
HAL24M1-01	1	TPMF	HAL24M2-01	2	Deltech
HAL24M1-02	1	TPMF	HAL24M2-02	2	Deltech
HAL24M1-03	1	TPMF	HAL24M2-03	2	Deltech
HAL24M1-04	2	TPMF	HAL24M2-04-1[(c)]	3	Deltech
HAL24M1-05	2	TPMF	HAL24M2-05	2	Deltech
HAL24M1-06	2	TPMF/Deltech	HAL24M2-06	2	Deltech
HAL24M1-07	1	TPMF	HAL24M2-07[(c)]	3	Deltech
HAL24M1-08	2	TPMF/Deltech	HAL24M2-08[(d)]	2	Deltech
HAL24M1-09	2	TPMF/Deltech	HAL24M2-09	2	Deltech
HAL24M1-10	2	TPMF/Deltech	HAL24M2-10[(c)]	3	Deltech
HAL24M1-11	3	TPMF/Deltech	HAL24M2-11[(d)]	3	Deltech
HAL24M1-12	3	TPMF/Deltech	HAL24M2-12	2	Deltech
HAL24M1-13-1	1	TPMF	HAL24M2-13[(c)]	3	Deltech
HAL24M1-14	3	TPMF/Deltech	HAL24M2-14[(c)]	2	Deltech
HAL24M1-15	1	TPMF	HAL24M2-15	2	Deltech
HAL24M1-16	1	TPMF	HAL24M2-16[(c)]	3	Deltech
HAL24M1-17	1	TPMF	HAL24M2-17[(c)]	3	Deltech
HAL24M1-18	2	TPMF/Deltech	HAL24M2-18	2	Deltech
HAL24M1-19	1	TPMF	HAL24M2-19	2	Deltech
HAL24M1-20	1	TPMF	HAL24M2-20	2	Deltech
HAL24M1-21	1	TPMF			
HAL24M1-22	1	TPMF			
HAL24M1-23	1	TPMF			
HAL24M1-24	1	TPMF			
HAL24M1-25	1	TPMF			
HAL24M1-26	1	TPMF			
HAL24M1-27	2	TPMF/Deltech			
HAL24M1-28	1	TPMF			
HAL24M1-29-1	2	TPMF/Deltech			
HAL24M1-30-1	2	Deltech			

(a) TPMF = Tilt-Pour melting furnace
(b) The first furnace type listed was used for the first melt. If the subsequent melt(s) used a different furnace, the type is listed.
(c) Final melt performed at 1200 °C for 1 h ± 10 min.
(d) Final melt performed at 1250 °C for 1 h ± 10 min.

Four glasses (HAL24M1-13, HAL24M1-29, HAL24M1-30, and HAL24M2-04) were re-batched and given a replicate number starting with -1. Table 2.10 gives the full list of the samples that were re-batched.

Table 2.10. Sample identification for the glasses that were re-batched.

Composition Name	Sample Name Used
HAL24M1-13	HAL24M1-13-1
HAL24M1-29	HAL24M1-29-1
HAL24M1-30	HAL24M1-30-1
HAL24M2-04	HAL24M2-04-1

The glass compositions were checked using EPMA, and the crystalline phases in the glass were identified and quantified using X-ray diffraction (XRD). The results are discussed in Section 3.1 and presented in Appendix D.

2.3 Secondary Phase Investigation

XRD analysis was performed to identify and quantify the crystalline phases within the glasses. Powdered glass samples were prepared for XRD using ~5 mass% CeO_2 as an internal standard phase with between 1 and 2 g of powdered glass. A glass piece representative of the whole sample was milled alone for 1 min and then homogenized with the CeO_2 for 30 s in a 10-cm^3 WC disc mill. The homogenized samples were loaded into plastic holders and analyzed using a Bruker D8 Advance XRD (Bruker AXS Inc., Madison, Wisconsin) with Cu Kα emission. Samples were scanned at a 0.015° 2θ step size with 1.5-s dwell time from 5° to 75° 2θ scan range. XRD spectra were analyzed with DIFFRAC.EVA (Bruker Corporation, Billerica, Massachusetts) for phase identification. Full-pattern Rietveld refinement using TOPAS 5 Software (Bruker AXS Inc., Madison) was performed to quantify the fraction of each crystal phase present. Comparing the quantified fraction by Rietveld refinement to the quantity of the crystalline internal standard used allowed quantification of the crystalline phases and amorphous phase in the sample.

2.4 Chemical Composition Analysis

A representative sample of each glass was analyzed using EPMA/wavelength dispersive spectroscopy with a JEOL JXA-8530F Hyperprobe (JEOL USA Inc., Peabody, Massachusetts) to confirm that the composition of the glasses corresponded to the specified target compositions of the elements in the glass with atomic numbers > 4 (which excludes Li, assumed to be on target). The glass pieces were mounted in 1-in. epoxy pucks and then polished. The samples were ground with 1500 grit paper and polished to a finish of 1 µm using 9-, 3-, and 1-µm diamond pads and polishing compound. Samples were then coated with iridium to dissipate charging.

The EPMA instrument used a field-emission gun equipped with five wavelength dispersive spectrometers, each with a take-off angle of 40°. The microprobe data was collected at an accelerating voltage of 15 kV, beam current of 40 nA, and beam size of 100 µm.

Appropriate standards were used for each element analyzed. Interferences were identified and corrected by applying interference standards for each element. Wave scans were collected using arbitrarily chosen coupons to fit background functions for each glass composition. Oxygen and lithium were not directly analyzed. Instead, oxygen was calculated based on stoichiometry of the oxides analyzed. The presence of lithium was qualitatively confirmed using laser-induced breakdown spectroscopy.

2.5 Canister Centerline Cooling

A portion (~150 g) of each test glass was subjected to the simulated CCC temperature profile shown in Table 2.11 and Figure 2.3.

Table 2.11. Canister centerline cooling profile for the DFHLW samples.

Segment	Start Temp (°C)	Stop Temp (°C)	Rate (°C/min)
1[a]	1150	1150	0.000[a]
2[b]	1150	1050	free fall[b]
3	1050	980	-1.556
4	980	930	-0.806
5	930	875	-0.591
6	875	825	-0.388
7	825	775	-0.253
8	775	725	-0.278
9	725	400	-0.304

(a) Segment 1 is a 30-min dwell at 1150 °C.
(b) Segment 2 free fall is at an estimated rate of -12.5 °C/min.

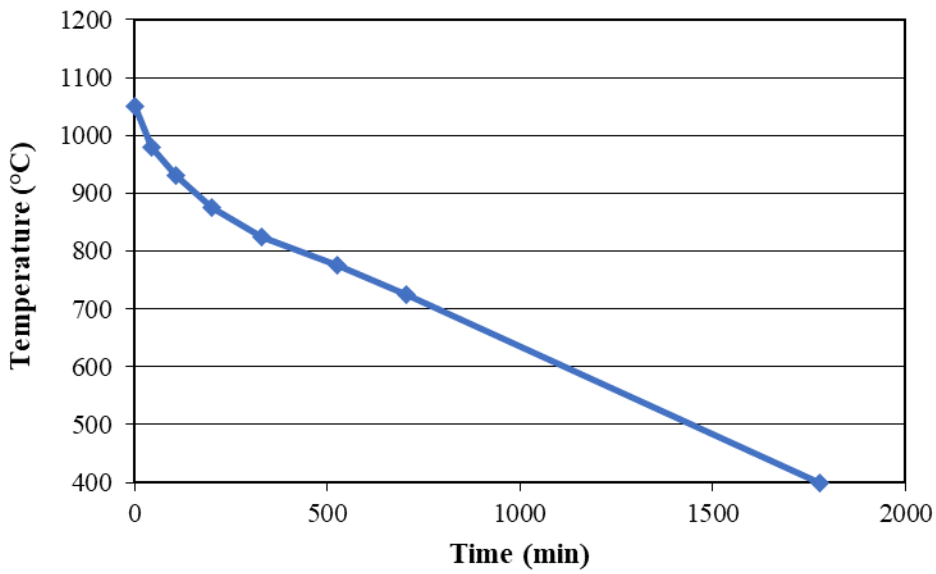

Figure 2.3. Plot of target temperature schedule during CCC treatment.

This profile is the temperature schedule of CCC treatment for Hanford HLW glasses planned for use at the WTP (Petkus 2003) and modified by PNNL to include a 30-min soak at 1150 °C before the cooling began. Pieces of Q glass, < 3 cm in diameter, were placed in a Pt-alloy crucible and covered with a Pt-alloy lid. The glass samples were placed in a furnace preheated to 1150 °C. After 30 min at 1150 °C, the furnace temperature was quickly reduced to 1050 °C and the cooling profile started. The furnace temperature was decreased to at least 400 °C based on seven cooling segments shown in Table 2.11 and Figure 2.3. The starting temperatures for the seven segments of cooling were 1050, 980, 930, 875, 825, 775, and 725 °C.

Appendix E presents photos of the heat-treated glasses. The amounts and types of crystalline phases that formed during CCC treatment were analyzed using XRD according to Section 2.3. These results are discussed in Section 3.2 and presented in Appendix F.

2.6 Isothermal Crystal Fraction and Liquidus Temperature (T_L)

Isothermal CF as a function of temperature was measured in Pt-alloy crucibles with tight-fitting lids to minimize volatility according to the ASTM C1720 procedure. Prior to measuring the CF, the furnace temperature accuracy was verified using ARG-1 glass (Smith 1993).

Isothermal CF heat treatments were completed on each composition by selecting pieces of glass between 4 mm and 425 µm, washing with deionized water (three times) in a sonic bath, then performing a final wash with clean ethanol and drying in air for at least 12 h or by using an appropriate explosion-proof drying oven at 90 °C for at least 2 h. These pieces were loaded into a Pt-alloy crucible of roughly 1 cm^3 prepared following the ASTM C1720 procedure. The crucible was first held for 30 min at 1150 °C prior to moving into a second furnace pre-heated to the desired temperature for the isothermal CF heat treatment. The heat treatment times and temperatures are reported in Table 2.12 and Table 2.13. The Pt-alloy crucibles were removed from the furnace and placed on a ceramic brick to cool. Due to the small size, water quenching was unnecessary to prevent crystal formation from cooling. Photos of these glasses are shown in Appendix G. The crystals that formed during heat treatment were analyzed using XRD according to Section 2.3 and are discussed in Section 3.3 and shown in Appendix H.

Table 2.12. Heat treatment temperatures and duration used for CF measurements of HAL24M1 samples.

Heat Treatment Temperatures and Duration	Glasses Tested
750 °C–72 h	-01, -02, 03, -04, -12, -16, -17, -19, -28
800 °C–48 h	-01, -02
850 °C–48 h	All 30 glasses
875 °C–48 h	-01, -02
900 °C–24 h	All 30 glasses except for -02
950 °C–24 h	All glasses except for -01, -02
1000 °C–24 h	-07, -09, -13-1, -15, -20, -24, -26
1050 °C–24 h	-06, -15, -27, 29-1, -30-1
1100 °C–24 h	-06, -08, -09, -18, -26
1150 °C–24 h	-03, -04, -05, -11, -13-1, -21, -27
1300°C–24 h	-04, -05, -11, -14, -22

Table 2.13. Heat treatment temperatures and duration used for CF measurements of HAL24M2 samples.

Heat Treatment Temperatures and Duration	Glasses Tested
750 °C–72 h	-01, -02, -04-1, -05, -07, -09, -11, -14, -15, -17, -18, -19
800 °C–48 h	-05, -11, -13, -14, -15, -19
850 °C–48 h	All glasses except for -03, -08, -13
900 °C–24 h	-01, -02, -08, -14, -15
950 °C–24 h	All 20 glasses
1025 °C–24 h	-03, -06, -08, -09, -10, -11, -12, -15, -18, -20
1050 °C–24 h	-16
1100°C–24 h	-01, -02, -03, -04-1, -05, -06, -08, -09, -10, -12, -13, -14, -18

The liquidus temperature (T_L) of the test-matrix glasses was determined using the CF extrapolation method outlined in the ASTM C1720 procedure. This involved extrapolating the CF as a function of temperature to zero crystals. The coefficient of determination (R-squared) was used to indicate how well temperature variations could predict crystallinity formation. Generally, an R-squared value near 1 suggests a strong predictive relationship. If the value significantly deviated from 1, a non-linear fit was also evaluated. The non-linear fit of the CF was calculated using a modified ideal-solution equation (Alton et al. 2002):

$$C_0 = C_{\max}\left\{1 - \exp\left[-B_L\left(\frac{1}{T} - \frac{1}{T_L}\right)\right]\right\} \tag{2.4}$$

where C_0 is the crystalline mass fraction at equilibrium, C_{max} is the total solute mass fraction in glass, B_L is crystal phase solubility temperature coefficient in K, T is temperature in K from isothermal heat treatment, and T_L is glass liquidus temperature in K. The GRG Nonlinear Solver method in Excel was selected to adjust C_{max}, B_L, and T_L to minimize the sum of squares difference between the measured and calculated CFs as a function of temperature.

The CF and T_L results are discussed in Section 3.3.

2.7 SO_3 Solubility

The method to measure sulfur solubility in glass melts has been reassessed in recent years. In Gervasio et al. (2024), SO_3 concentrations of crushed (to maximize surface area), sieved, and washed (to remove excess sulfate) from sulfur-saturated melt (SSM) samples measured using EPMA provided more conservative SO_3 concentrations than concentrations measured from similarly prepared SSM glasses using inductively coupled plasma-optical emission spectroscopy (ICP-OES). EPMA provided a major practical benefit in that results are obtained simpler, quicker, and less expensively. However, EPMA requires particles to be larger than the beam size of the probe, which can vary depending on glass composition (e.g., larger beam size is required for high Na glasses). This complicates sample preparation as the glass particles must be sieved to the appropriate range for the beam, which may be difficult to predict before performing EPMA measurements. Therefore, alternative preparation methods were pursued, including analyzing as-melted SSM glass monoliths – both washed monoliths using the same procedure as with the sieved particles and unwashed monoliths. The washing procedure was proposed to be superfluous with monoliths as only the surface of the monolith is washed, and the interior of the monolith is characterized after the monolith is epoxied and polished before EPMA characterization. Figure 2.4 summarizes the preparation steps used for the particle and monolith approaches.

A subset of the SSM glasses was prepared with all three methods and measured via EPMA to determine whether the preparation method affects the SO_3 composition of the SSM. The results from the sample subset determined the preparation method for the remaining glasses.

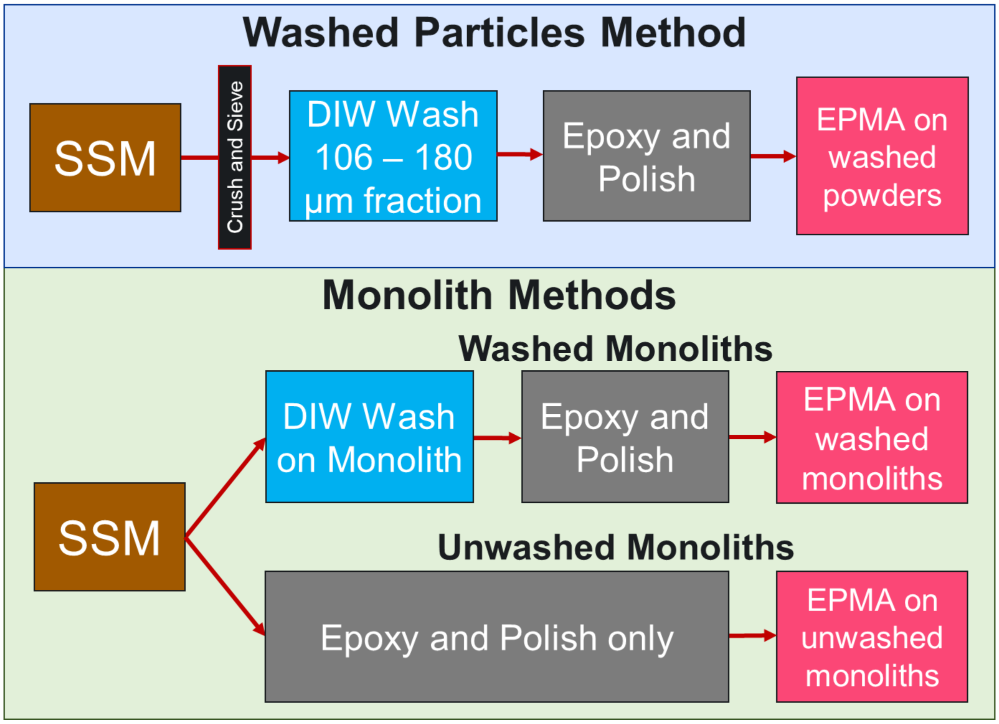

Figure 2.4. Summary of SSM preparation procedure options.

For all glasses, w_{SO3} was determined using the 3TS method. Approximately 52 to 60 g of the Q HAL24 glasses were milled in a WC chamber in the Angstrom milling instrument for 2 to 3 min to generate fines. For each glass, 3.84 g of Na_2SO_4 (Fisher Chemical) was added to 50.00 g of the crushed Q glass fraction and homogenized with the WC mill for 30 s. The Na_2SO_4 + glass mixtures were melted in Pt/Rh crucibles at 1150 °C for 1 h. After 1 h, each melt was quenched on a stainless-steel pouring plate, resulting in a glass and a sulfate salt separated phase. Once cooled, each glass was crushed to fines in the WC mill and remelted for 1 h at 1150 °C. This process continued until three melts were completed to generate the SSM glasses.

For the SSM glasses that were prepared using the washed particle method, the glasses were crushed incrementally in the WC mill for ~1.2 s and sieved to obtain a 106 – 180 µm fraction using a Ro-Tap shaker (RX-29 model, W.C. Tyler) for 6 min for each session. Approximately 5 to 10 sessions were required to crush and sieve the SSM glass fraction, resulting in > 15 g of the 106- to 180-µm fraction available for the washing steps. From the > 15 g of the 106- to 180-µm glass fraction, 2.0 g of SSM glass and 20 g of deionized water were transferred into a centrifuge tube equipped with a 0.45-µm nylon filter. The centrifuge tube was closed and shaken by hand for ~2 min to ensure that the glass was completely exposed to the solution. After shaking, the centrifuge tubes were centrifuged at 3175 rpm for 5 min in a centrifuge instrument (Sorvall Legend Mach 1.6 model, Thermo Electron Corporation). The centrifuge filter with the washed glass powder was removed, and the rinse solution was decanted and stored for potential future use. The filter with glass powder was returned to the centrifuge tube and the washing procedure was repeated. After the second washing, the filter with glass powder was dried overnight in an 80 °C oven. The dried powder was separated from the centrifuge filter and prepared for EPMA analysis. A few milligrams of the dried washed SSM glass powders were mounted into an aluminum puck with epoxy (EpoxySet, Allied High-Tech Products, Inc.). The mounted samples were analyzed by EPMA following the same procedure described in Section 2.4.

For SSM glasses prepared using the monolith methods, monoliths (with diameters > 5 mm) were selected after the SSM glasses had cooled. The washed monoliths were washed using the same method as the washed particles and then mounted in epoxy and polished, while the unwashed monoliths were mounted directly in epoxy and polished without further treatment. The mounted samples were analyzed by EPMA following the same procedure described in Section 2.4.

2.8 Density

Density of each glass was measured at room temperature using a MicroMeritics AccuPyc II 1340 gas pycnometer (MicroMeritics, Norcross, Georgia). Approximately 1 g of glass was loaded into a sample holder and placed within the instrument. The pycnometer was purged 10 times with He gas prior to volume measurement, and the volume of each glass was measured 10 times. The average of 10 volume measurements and the measured mass of the sample were used to calculate the glass density. The pycnometer calibration was verified before and after measurements for that day using a National Institute of Standards and Technology traceable standard WC ball.

These results are discussed in Section 3.5.

2.9 Viscosity

The viscosity of each glass was measured as a function of temperature using the shear stress dependance to the shear rate:

$$\eta = \frac{\tau}{\gamma} \tag{2.5}$$

where η is the viscosity, γ is the shear rate, and τ is the shear stress.

A rotating spindle digital viscometer capable of measuring viscosities from 1 to 100 Pa·s (Brookfield Digital Model LVTD) was staged above a high-temperature Deltech furnace (Deltech Model DT-31-RS, Denver, Colorado) equipped with a Pt/Rh spindle to fit through a hole in the top of the furnace. A 50-mL glass sample was added to a 100-mL Pt/Rh alloy crucible with approximate dimensions of 5 cm diameter × 6 cm height. The crucible was placed into the furnace, which was set at 1150 °C, and the glass was left to melt for about 20 min. The spindle was then lowered into the molten glass in the center of the crucible with the lower end of the rod suspended 1 cm above the bottom of the crucible. The furnace was programmed to follow a set ramp schedule at the following temperatures: 1150, 1050, 950, 1150, 1200 °C, and back to 1150 °C. The soak time was 45 min at each temperature. This temperature profile allowed for the potential impacts of crystallization (at lower temperatures) and volatility (at higher temperatures) to be assessed (via reproducibility) at the repeated 1150 °C temperature. The viscometer was calibrated using the Defense Waste Processing Facility (DWPF) startup frit. At each target temperature, the maximum and minimum spindle torque values were recorded three times each at 3-min intervals. The average of the three measurements was used for data analysis. A secondary thermocouple was placed below the crucible and temperature was recorded continuously during measurement to ensure thermal equilibrium was reached before measurement. Results are discussed in Section 3.6.

2.10 Electrical Conductivity

The EC (ε in S/m) as a function of temperature was calculated from the resistance (R' in Ω) and cell constant (K in m^{-1}) using:

$$\varepsilon = K/R_s \tag{2.6}$$

where R_s is the solution resistance obtained for the KCl calibration solutions and K is the cell constant and is linked to the geometry of the system.

A Biologic VSP-3E potentiostat connected to a two-blade Pt/Rh probe staged above a high-temperature Sentrotech furnace (Sentrotech Model ST-1200-7812, Strongsville, Ohio) was used to measure the molten glass impedance. Data was recorded at 1200, 1150, 1050, and 950 °C after roughly 30-min soaks at each temperature, allowing the program to collect impedance data at an applied voltage of 100 mV and frequencies of 0.5 – $5\text{x}10^5$ Hz, measuring 25 data points per decade, and repeating the scan three times for a total of four measurements per glass per temperature.

Approximately 18 g of Q glass was added to an alumina crucible with the two-blade Pt/Rh probes attached perpendicular to one another 20 mm apart, and the assembly was loaded into the furnace at room temperature. The furnace was then slowly (~10 °C/min) ramped to 900 °C to prevent thermal shock to the crucibles and was successively fast ramped to 1200 °C to complete glass melting. The furnace was then held (~30 min) at 1200 °C to homogenize the glass before taking the first measurement. Each change in temperature was performed at a slow rate (~10 °C/min) and the glass was allowed to equilibrate at each temperature for ~ 30 min before the corresponding measurement was taken.

Solution resistance (R_s) was calculated by fitting the impedance spectra (i.e., Nyquist plots). A cell constant was determined using 0.1 M and 1.0 M KCl solutions measured at the same volume in the same alumina crucible and Pt/Rh probe apparatus. The conductivity was then calculated from Eq. (2.6).

These results are discussed in Section 3.7.

2.11 Product Consistency Test

The PCT responses were measured for Q and CCC samples of each glass using Method A of ASTM C1285, *Standard Test Methods for Determining Chemical Durability of Nuclear, Hazardous, and Mixed Waste Glasses and Multiphase Glass Ceramics: The Product Consistency Test (PCT)*. Tests were performed in triplicate for each Q and CCC glass. Alongside each triplicate set of test glass, the Approved Reference Material-1 (ARM-1, Mellinger and Daniel 1984) glass was also tested in triplicate. Two blanks, which consisted of deionized water in a cleaned vessel without glass, were added with each set of tests. Glasses were ground, sieved to -100 +200 mesh, washed, and prepared according to Section 19.6 of the ASTM C1285 procedure. Then, 1.5 g of the prepared glass was added to 15 mL of deionized water in a Type 304L Parr stainless steel vessels with a polytetrafluoroethylene (PTFE) gasket. The vessels were closed, sealed, and placed into an oven at 90 ± 2 °C for 7 days ± 3 h.

After 7 days, the vessels were removed from the oven and cooled until they were cool to the touch. The final mass of the vessel and the solution pH were recorded. The leachate from each test vessel was then filtered through a 0.45-µm-size filter and acidified with concentrated, high-purity HNO_3 to 1 vol% before analysis. The leachates were analyzed using ICP-OES for Si, Na, Li. and B at the Southwest Research Institute.

Normalized concentrations (NC, g L^{-1}) were calculated with the following formula:

$$\mathrm{NC}_i = \frac{C_i}{f_i} \tag{2.7}$$

where: C_i = the concentration of element i in solution ($g_i \cdot L^{-1}$)
f_i = mass fraction of element i in the glass ($g_i \cdot g_{glass}^{-1}$)

These results are discussed in Section 3.5.

2.12 Toxicity Characteristic Leaching Procedure

The TCLP based on EPA Method 1311 with notable exceptions was performed on the Q and CCC glasses to measure the release of toxic elements present in the glasses (Cr, Ni, Pb, V, Zn) compared to their delisting limit concentrations provided in Table 2.14 and to predicted TCLP releases from various models discussed in Section 3.9.

Table 2.14. WTP delisting limits and Resource Conservation and Recovery Act (RCRA) toxicity and universal treatment standards (UTS) limits for TCLP (40 CFR 268. 2015).

Element	Ag	As	Ba	Cd	Cr	Hg	Ni	Pb	Se	V	Zn
WTP Delisting Limit (mg/L)	3.07	0.616	100	0.48	4.95	0.2	22.6	5	1	16.9	225
RCRA Toxicity Limit (mg/L)	5	5	100	1	5	0.2	--	5	1	--	--
RCRA UTS Limit (mg/L)	0.14	5	21	0.11	0.6	0.025	--	0.75	5.7	--	--

The notable exceptions to EPA Method 1311 included glasses being size-reduced to pass through a sieve < 5.0 mm according to ASTM D6323-D19 rather than < 9.5 mm as described in EPA Method 1311. Additionally, the amount of glass tested was reduced from 100 to 15 g and the corresponding extraction fluid volume was reduced from 2000 to 300 mL. These changes to the test method were agreed upon for application to Hanford HLW glasses by the Washington State Department of Ecology, the U.S. Department of Energy, Vanderbilt University, and PNNL (Kruger 2023). A pretest was performed on each Q and CCC glass to identify the extraction fluid used for testing according to EPA Method 1311.

Glasses were tested in duplicate tests. Each campaign of tests was conducted for 18 ± 2 h in ambient temperatures of 23 ± 2 °C. One blank vessel for each extraction fluid used in a campaign was tested in parallel with tests in the campaign. After 18 ± 2 h, the TCLP leachate was filtered with 0.45-µm PTFE filters, preserved with 100-µL Optima concentrated HNO_3, and refrigerated until the samples were ready for solution analysis. The solutions were sent to Southwest Research Institute for ICP-OES analysis. The normalized concentration of B (NC_B) was calculated to compare with predicted normalized concentrations from models. NC_B was determined using:

$$NC_B = \frac{c_B}{f_B} \tag{2.8}$$

where c_B is the TCLP leachate concentration of B and f_B is the mass fraction of boron in the unaltered glass. Other components were calculated in the same way. The TCLP results are discussed in Section 3.9.

3.0 Results and Discussion

This section describes the results for the chemical composition, CCC and CF crystallinity (including T_L), sulfur solubility, density, viscosity, EC, PCT, and TCLP.

3.1 Glass Composition

Optical images of the Q HAL24 glasses after the second or third melt are presented in Appendix C. The target and EPMA measured compositions of HAL24 glasses in wt% along with and without the target Li_2O are presented in Appendix D. The EPMA results of all glasses showed that the sums of measured oxides with added target masses of Li_2O were between 94.2 and 101.5 wt%, indicating acceptable recovery of the glass components. The target mass (< 2.5 wt%) of Li_2O was used to better approximate the total weight percent of each glass.

EPMA results were as follows:

- The relative percentage difference (RPD) of Al_2O_3, B_2O_3, Na_2O, and SiO_2 were less than 10%, 16%, 5%, and 13%, respectively.
- RPD values of Cl were in the range of 10% to 46%.
- RPD values of F were in the range of 1% to 141%.
- 27 HAL24 glasses had SO_3 retention values of > 80 %, 17 glasses showed SO_3 retention values between 50% and 80%, and 6 glasses showed the SO_3 retention values of < 50%.
- 38 HAL24 glasses had RPD values of < 10% for MgO.
- 17 HAL24 glasses had RPD values of < 5% for NiO.

The relatively high fluctuation of RPD values for Cl, F, and SO_3 was due to their volatility during the melting process. The target mass values for Bi_2O_3, Cr_2O_3, K_2O, Li_2O, MgO, MnO, NiO, Nd_2O_3, P_2O_5, PbO, SrO, TiO_2, V_2O_5, ZnO, and ZrO_2 were generally < 1 wt%, and the RPD values were inconsistent or high for the components with low target wt% (< 0.5 wt%). These inconsistencies in RPD are likely due to the experimental and instrument uncertainties.

3.1.1 Secondary Phase Investigation in Quenched Glasses

The crystalline phases and their wt% values are presented in Table 3.1. The refined XRD plots with quantified crystalline fractions are presented in Appendix E. The normalized wt% was calculated using Eq. (3.1), where *P* is the phase wt%, *C* is the standard crystallinity of 51.28%, and *S* is the added standard wt%:

$$\text{Normalized wt\% of a Phase} = \frac{PC}{100 - S} \quad (3.1)$$

Among the 50 HAL24 glasses, 18 glasses were fully amorphous and 32 glasses showed between 0.18 and 8.74 wt% of crystalline phases within the quenched sample. For the crystalline phase, apatite phases [$Ca_{10}(PO_4)_6F_2$ and $Ca_{10}(SiO_4)_3(SO_4)_3F_2$], silicate ($Na_2Si_3O_7$), eskolaite ($Cr_2O_3$), and variations of spinel phases were observed using XRD. The eskolaite phase was only observed in HAL24M2-17 and HAL24M2-18, which had relatively high target masses of Cr_2O_3 compared to the other glasses. The spinel phases identified by closest structure parameter fits included $ZnCr_{1.8}Al_{0.2}O_4$, $ZnCr_2O_4$, $ZnFeAlO_4$, $NiFe_2O_4$, $Zn(Fe_{1.9}Cr_{0.1})O_4$, $NiCr_2O_4$, and Fe_3O_4.

Table 3.1. Crystalline phases and wt% in HAL24 Q glasses.

Glass ID	Crystalline Phase	wt%
HAL24M1-01	None	-
HAL24M1-02	$Ca_{10}(PO_4)_6F_2$	5.72
HAL24M1-03	$Ca_{10}(PO_4)_6F_2$	6.07
HAL24M1-04	$ZnCr_{1.8}Al_{0.2}O_4$	0.94
HAL24M1-05	$ZnCr_2O_4$	0.57
HAL24M1-06	$ZnFeAlO_4$	0.59
HAL24M1-07	Fe_3O_4	0.6
HAL24M1-08	$ZnCr_{1.8}Al_{0.2}O_4$	1.96
HAL24M1-09	$Ca_{10}(PO_4)_6F_2$, $ZnCr_{1.8}Al_{0.2}O_4$	1.22, 0.61
HAL24M1-10	None	-
HAL24M1-11	$Ca_{10}(PO_4)_6F_2$, $ZnCr_{1.8}Al_{0.2}O_4$	7.32, 1.28
HAL24M1-12	None	-
HAL24M1-13-1	$Ca_{10}(SiO_4)_3(SO_4)_3F_2$	8.74
HAL24M1-14	$Ca_{10}(PO_4)_6F_2$, $NiFe_2O_4$	3.44, 0.51
HAL24M1-15	$ZnFeAlO_4$	0.48
HAL24M1-16	$Zn(Fe_{1.9}Cr_{0.1})O_4$	0.52
HAL24M1-17	None	-
HAL24M1-18	$Ca_{10}(PO_4)_6F_2$, $ZnCr_{1.8}Al_{0.2}O_4$	3.66, 0.85
HAL24M1-19	None	-
HAL24M1-20	$Ca_{10}(SiO_4)_3(SO_4)_3F_2$	2.37
HAL24M1-21	$NiCr_2O_4$	0.28
HAL24M1-22	None	-
HAL24M1-23	$ZnCr_{1.8}Al_{0.2}O_4$	0.45
HAL24M1-24	$ZnCr_{1.8}Al_{0.2}O_4$	0.25
HAL24M1-25	$ZnCr_{1.8}Al_{0.2}O_4$	0.65
HAL24M1-26	None	-
HAL24M1-27	$Ca_{10}(PO_4)_6F_2$, $Na_2Si_3O_7$	2.67, 3.87
HAL24M1-28	None	-
HAL24M1-29-1	$NiCr_2O_4$	0.21
HAL24M1-30-1	None	-
HAL24M2-01	None	-
HAL24M2-02	$Ca_{10}(PO_4)_6F_2$	0.18
HAL24M2-03	$ZnCr_2O_4$	0.17
HAL24M2-04-1	None	-
HAL24M2-05	None	-
HAL24M2-06	$ZnCr_{1.8}Al_{0.2}O_4$	0.77
HAL24M2-07	$ZnFeAlO_4$	0.27
HAL24M2-08	$Ca_{10}(PO_4)_6F_2$, $Zn(Fe_{1.9}Cr_{0.1})O_4$	5.93, 0.45
HAL24M2-09	None	-
HAL24M2-10	None	-
HAL24M2-11	None	-
HAL24M2-12	$ZnCr_2O_4$	0.97
HAL24M2-13	$ZnFeAlO_4$	1.2
HAL24M2-14	None	-
HAL24M2-15	None	-
HAL24M2-16	$ZnCr_{1.8}Al_{0.2}O_4$	0.85
HAL24M2-17	Cr_2O_3	0.37
HAL24M2-18	$Ca_{10}(PO_4)_6F_2$, Cr_2O_3	2.26, 0.64
HAL24M2-19	None	-
HAL24M2-20	$ZnCr_{1.8}Al_{0.2}O_4$	1.44

The XRD results showed that Zn, Cr, Fe, Ni, and Al interact with one another and form spinel phases at the melting temperature of 1150 °C. Crystallization of spinel seems to occur rapidly during quenching, which is interesting as the typical crystallization and growth occur through the slow cooling process.

With small amounts of spinel phases in the glasses, only two small peaks from diffraction from (h k l) planes of (2 2 0) and (3 1 1) were present in the XRD patterns. Different elements in the spinel phases affect the unit cell parameters and shifts in peak positions, but it is still difficult to identify the exact chemistries of spinel phases solely based on XRD analysis, especially with small intensity peaks. All the spinel phases contained Zn or Ni at +2 cation site and different +3 cations, including Al, Cr, and/or Fe. Figure 3.1 shows the structures of crystalline phases found in HAL24 glasses.

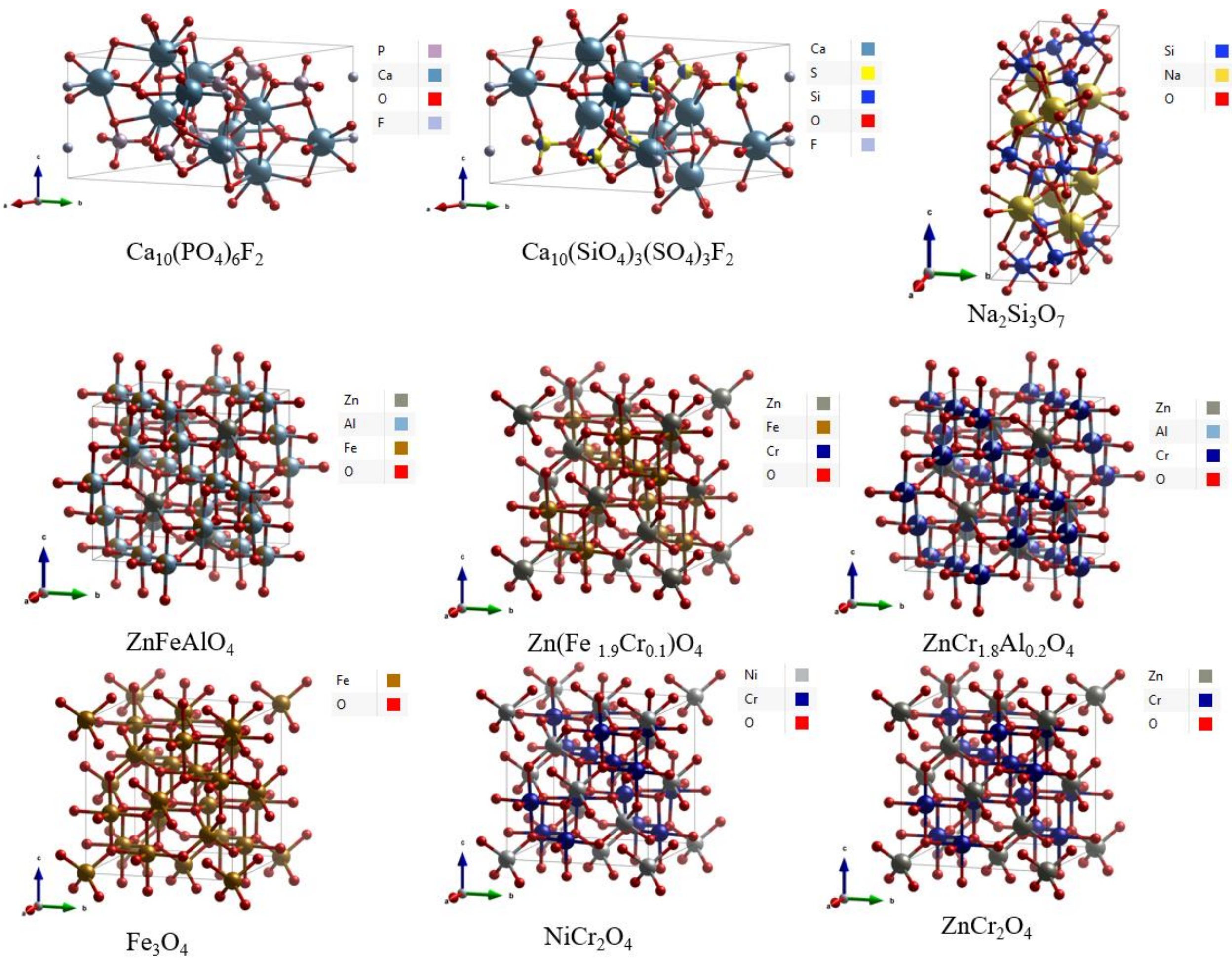

Figure 3.1. Structures of crystalline phases in HAL24 glasses. $NiFe_2O_4$ has the same structure as $NiCr_2O_4$, and Cr_2O_3 structure is not included.

3.2 Crystal Identification in Canister Centerline Cooling Glasses

The slow cooling of the molten glass in the canister core might impact glass durability by changing the residual glass composition (Kim et al. 1995; Kroll et al. 2019). Not all crystals affect durability in the same way, so identifying the crystal content after CCC is an important step toward understanding crystallization impacts on glass durability. Moreover, property-prediction models were formulated using quenched data; therefore, differences of glass durability responses after CCC via PCT and TCLP were evaluated.

This section presents and discusses the CF results from the CCC glasses obtained using the methods discussed in Section 2.3. The effects of CCC on PCT and TCLP are reported in Sections 3.8 and 3.9, respectively.

Among the 50 total glasses, 5 were found to be amorphous by XRD after CCC. Of the remaining glasses, 9 had CF ≤ 1 wt%, 15 had CF ≤ 4 wt%, and 21 had CF > 4 wt%. XRD analysis revealed a range of different crystal phases. The XRD phases and wt% crystallinity results are summarized in Table 3.2.

There are five glasses without any crystal phases observed in CCC (HAL24M1-02, -17, and HAL24M2-05, -14, -19.) The highest CF weight percentage was observed in glass HAL24M1-12, which contained 25.2% nepheline. The most prevalent crystal phases after CCC are nepheline and apatite [$Ca_{10}(PO_4)_6F_2$], appearing in 10 and 21 glasses, respectively. Note that fluorapatite phase was used for XRD refinement, but different anions (e.g., Cl, F, OH) can occupy the -1 anion site, and the actual chemistry of apatite is difficult to identify accurately with XRD analysis alone, especially with small peak intensities of apatite phase.

As the spinel phases have similar peak positions, different spinel phases were used for refinement based on the glass compositions. Spinel phases are frequently present, with $ZnCr_{1.8}Al_{0.2}O_4$ found in 16 glasses, followed by $ZnFeAlO_4$ in 6 glasses, $NiFe_2O_4$ in 6 glasses, and $ZnCr_2O_4$ in 2 glasses.

Baddeleyite (ZrO_2) was seen in seven glasses, of which five had ZrO_2 higher than 3.3 wt%, indicating they could be above the solubility of the Zr.

Sodalite type phases including $Na_8(Al_6Si_6O_{24})(SO_4)$ and $Na_6Ca_2Al_6Si_6O_{24}(SO_4)_2$ were also observed. Less common phases such as AlF_3, $NaFe_3(PO_4)_3$, Fe_2O_3, $Na_4Zn(PO_4)_2$, and $Na_{1.14}AlSiO_4$, were also found. Eskolaite (Cr_2O_3) was observed in HAL24M2-17 glass with a relatively high target Cr_2O_3 wt% (> 0.9 wt%). Note that eskolaite and hematite (Fe_2O_3) have the same space group, and their XRD peak positions are similar such that glasses with a small amount of either Cr_2O_3 or Fe_2O_3 will have small diffraction peaks that might be difficult to differentiate.

Eight of the 50 glasses have sufficient nepheline to significantly reduced chemical durability (> 5 wt%): HAL24M1-12, -16, -24, -25, -26, HAL24M2-02, and -12, although other phases may also impact durability.

This diverse distribution underscores the variety of crystalline and amorphous phases present in these glasses, with certain phases like nepheline and apatite being significantly more ubiquitous compared to others. Appendix F and Appendix G present images of glasses after CCC and XRD scans when applicable.

Table 3.2. Crystalline phases and wt% in CCC glasses.

Glass ID	Crystalline Phase	wt%
HAL24M1-01	$ZnCr_{1.8}Al_{0.2}O_4$ (Spinel)	0.1
HAL24M1-02	None	-
HAL24M1-03	$Ca_{10}(PO_4)_6F_2$, Fe_2O_3 , ZrO_2	4.5, 1.6, 0.5
HAL24M1-04	$ZnCr_{1.8}Al_{0.2}O_4$ (Spinel)	1.3
HAL24M1-05	$ZnCr_2O_4$ (Spinel), $NaAlSiO_4$, $Na_6Ca_2Al_6Si_6O_{24}(SO_4)_2$	0.7, 0.6, 0.2
HAL24M1-06	$ZnFeAlO_4$ (Spinel), ZrO_2	1.2, 0.4
HAL24M1-07	$ZnAl_{0.2}Fe_{1.8}O_4$ (Spinel), $Ca_{10}(PO_4)_6F_2$	4.1, 1.1
HAL24M1-08	$NiFe_2O_4$ (Spinel), $Ca_{10}(PO_4)_6F_2$, $ZnCr_{1.8}Al_{0.2}O_4$ (Spinel), ZrO_2	2.8, 2.4, 1.0, 0.4
HAL24M1-09	$ZnCr_{1.8}Al_{0.2}O_4$ (Spinel), $Ca_{10}(PO_4)_6F_2$	5.8, 4.8
HAL24M1-10	$ZnAl_{0.2}Fe_{1.8}O_4$ (Spinel), $Ca_{10}(PO_4)_6F_2$	4.1, 1.4
HAL24M1-11	$Ca_{10}(PO_4)_6F_2$, $ZnCr_2O_4$ (Spinel)	5.7, 2.0
HAL24M1-12	$NaAlSiO_4$	25.2
HAL24M1-13-1	$Ca_{10}(PO_4)_6F_2$, ZrO_2	6.7, 2.8
HAL24M1-14	$Ca_{10}(PO_4)_6F_2$, $ZnFeAlO_4$ (Spinel)	5.2, 1.9
HAL24M1-15	$ZnFeAlO_4$ (Spinel), $ZnCr_{1.8}Al_{0.2}O_4$ (Spinel)	1.3, 0.9
HAL24M1-16	$NaAlSiO_4$, $ZnAl_{0.2}Fe_{1.8}O_4$, ZrO_2	24.4, 3.0, 1.7
HAL24M1-17	None	-
HAL24M1-18	$Ca_{10}(PO_4)_6F_2$, $ZnCr_{1.8}Al_{0.2}O_4$ (Spinel)	3.6, 1.2
HAL24M1-19	$Ca_{10}(PO_4)_6F_2$	1.5
HAL24M1-20	$Ca_{10}(PO_4)_6F_2$, $ZnCr_{1.8}Al_{0.2}O_4$ (Spinel)	2.5, 0.4
HAL24M1-21	$ZnCr_{1.8}Al_{0.2}O_4$ (Spinel)	0.5
HAL24M1-22	$Ca_{10}(PO_4)_6F_2$, $ZnCr_{1.8}Al_{0.2}O_4$ (Spinel)	1.1, 1.0
HAL24M1-23	$ZnCr_{1.8}Al_{0.2}O_4$ (Spinel), $Na_4Zn(PO_4)_2$	1.9, 1.6
HAL24M1-24	$NaAlSiO_4$, $Na_8(Al_6Si_6O_{24})(SO_4)$, $Ca_{10}(PO_4)_6F_2$	10.3, 6.0, 2.5
HAL24M1-25	$NaAlSiO_4$, $Na_8(Al_6Si_6O_{24})(SO_4)$, $NaFe_3(PO_4)_3$, $ZnCr_{1.8}Al_{0.2}O_4$ (Spinel), AlF_3	12.6, 5.3, 3.4, 3.0, 2.7
HAL24M1-26	$NaAlSiO_4$, $Ca_{10}(PO_4)_6F_2$, ZrO_2	8.9, 2.9, 0.5
HAL24M1-27	$Ca_{10}(PO_4)_6F_2$, $Na_8(Al_6Si_6O_{24})(SO_4)$	3.9, 2.0
HAL24M1-28	$ZnCr_{1.8}Al_{0.2}O_4$ (Spinel)	0.3
HAL24M1-29-1	$NiFe_2O_4$ (Spinel)	1.4
HAL24M1-30-1	$NiFe_2O_4$ (Spinel), $Ca_{10}(PO_4)_6F_2$	2.7, 0.5
HAL24M2-01	$NaAlSiO_4$	1.9
HAL24M2-02	$NaAlSiO_4$, $Na_8(Al_6Si_6O_{24})(SO_4)$, $ZnFeAlO_4$ (Spinel)	14.6, 8.1, 1.8
HAL24M2-03	$ZnCr_{1.8}Al_{0.2}O_4$ (Spinel)	0.3
HAL24M2-04-1	$Na_{1.14}AlSiO_4$	1.7
HAL24M2-05	None	-
HAL24M2-06	$NiFe_2O_4$ (Spinel)	0.7
HAL24M2-07	$ZnCr_{1.8}Al_{0.2}O_4$ (Spinel)	0.7
HAL24M2-08	$Ca_{10}(PO_4)_6F_2$, $ZnCr_{1.8}Al_{0.2}O_4$ (Spinel)	4.8, 3.5
HAL24M2-09	$NaAlSiO_4$	2.2
HAL24M2-10	$Ca_{10}(PO_4)_6F_2$, $ZnCr_{1.8}Al_{0.2}O_4$ (Spinel)	2.3, 2.0
HAL24M2-11	$Na_8(Al_6Si_6O_{24})(SO_4)$, $Zn(Fe_{1.9}Cr_{0.1})O_4$ (Spinel)	0.5, 0.4
HAL24M2-12	Nepheline, $ZnFeAlO_4$ (Spinel)	9.3, 1.6
HAL24M2-13	$ZnFeAlO_4$ (Spinel), ZrO_2	1.9, 1.1
HAL24M2-14	None	-
HAL24M2-15	$Ca_{10}(PO_4)_6F_2$	0.6
HAL24M2-16	$NiFe_2O_4$ (Spinel), $Ca_{10}(PO_4)_6F_2$	5.4, 3.7
HAL24M2-17	Cr_2O_3	0.6
HAL24M2-18	Fe_2O_3, $Ca_{10}(PO_4)_6F_2$, $NiFe_2O_4$ (Spinel)	1.9, 1.5, 0.5
HAL24M2-19	None	-
HAL24M2-20	$Zn(Fe_{1.9}Cr_{0.1})O_4)$ (Spinel)	3.8

3.3 Crystal Fraction and Liquidus Temperature

The long idling of the melter at low temperatures might promote crystal formation, impacting glass processability by settling in the melter and clogging the pour spout (Vienna et al. 2001; Matyáš et al. 2010). Therefore, the study of crystalline phases, quantities, and T_L in isothermal heat-treatments is part of the regular investigation of HLW glasses.

This section presents and discusses the isothermal CF and T_L results obtained using the methodologies detailed in Section 2.4. When the T_L was estimated to be greater than 850 °C, the glass analysis included the measured temperatures (°C), crystal content (mass percentage), and a plot of the primary crystalline phase, as well as XRD analysis (see Appendix H). XRD scans are omitted when the glass retains an amorphous structure. Table 3.3 summarizes the temperatures run, CF (wt%), identified phases, and T_L values. It is important to note that T_L is calculated based on the primary crystal phase only.

Table 3.3. Crystalline phases, wt%, vol% at 950 °C, and T_L for isothermally heat-treated glasses.

Glass ID	T (°C)	Phases	wt%	vol%$_{950}$	T_L (°C)
HAL24M1-01	750	$Ca_{10}(SiO_4)_3(SO_4)_3F_2$, $Na_6Ca_2Al_6Si_6O_{24}(SO_4)_2$	1.52, 2.01	NA	979
	800	$Ca_{10}(SiO_4)_3(SO_4)_3F_2$, $Na_6Ca_2Al_6Si_6O_{24}(SO_4)_2$	1.17, 0.10		
	850	$Ca_{10}(SiO_4)_3(SO_4)_3F_2$, $Na_6Ca_2Al_6Si_6O_{24}(SO_4)_2$	0.81, 0.17		
	875	$Ca_{10}(SiO_4)_3(SO_4)_3F_2$	0.69		
	900	None	NA		
HAL24M1-02	750	$Na_8(Al_6Si_6O_{24})(SO_4)$	3.43	NA	844
	800	$Na_8(Al_6Si_6O_{24})(SO_4)$	0.24		
	850	$Na_8(Al_6Si_6O_{24})(SO_4)$	0.33		
	900	None	NA		
HAL24M1-03	750	$Ca_{10}(PO_4)_6F_2$, ZrO_2, Fe_2O_3	4.94, 1.77, 1.73	2.63, 0.39, 0.50	1150 < T_L
	850	$Ca_{10}(PO_4)_6F_2$, ZrO_2, Fe_2O_3	4.57, 1.37, 1.24		
	900	$Ca_{10}(PO_4)_6F_2$, ZrO_2, Fe_2O_3	4.02, 1.06, 0.89		
	950	$Ca_{10}(PO_4)_6F_2$, ZrO_2, Fe_2O_3	3.14, 0.84, 0.99		
	1150	$Ca_{10}(PO_4)_6F_2$, ZrO_2, Fe_2O_3	2.73, 0.54, 0.34		
HAL24M1-04	750	$ZnCr_{1.8}Al_{0.2}O_4$	1.27	0.55	1150 < T_L
	850	$ZnCr_{1.8}Al_{0.2}O_4$	1.16		
	900	$ZnCr_{1.8}Al_{0.2}O_4$	1.22		
	950	$ZnCr_{1.8}Al_{0.2}O_4$	1.09		
	1150	$ZnCr_{1.8}Al_{0.2}O_4$	1.08		
	1300	$ZnCr_{1.8}Al_{0.2}O_4$	1.00		
HAL24M1-05	750	$NaAlSiO_4$, $Na_6Ca_2Al_6Si_6O_{24}(SO_4)_2$, $Na_8(Al_6Si_6O_{24})(SO_4)$, $ZnCr_2O_4$	0.71, 0.29, 6.73, 0.80	0.29	1150 < T_L
	850	$Na_6Ca_2Al_6Si_6O_{24}(SO_4)_2$, $ZnCr_2O_4$	0.64, 0.65		
	900	$ZnCr_2O_4$	0.60		
	950	$ZnCr_2O_4$	0.58		
	1150	$ZnCr_2O_4$, $ZnCr_{0.4}Al_{1.6}O_4$	0.26, 1.05		
	1300	$ZnCr_{0.4}Al_{1.6}O_4$	1.94		
HAL24M1-06	850	$ZnFeAlO_4$, ZrO_2	1.04, 0.96	0.42, 0.34	1150 < T_L
	900	$ZnFeAlO_4$, ZrO_2	0.87, 0.83		
	950	$ZnFeAlO_4$, ZrO_2	0.78, 0.73		
	1050	$ZnFeAlO_4$, ZrO_2	0.57, 0.50		
	1100	$ZnFeAlO_4$, ZrO_2	0.52, 0.36		
HAL24M1-07	850	$Ca_{10}(PO_4)_6F_2$, $ZnAl_{0.2}Fe_{1.8}O_4$	0.39, 2.96	0.05, 0.77	1059
	900	$Ca_{10}(PO_4)_6F_2$, $ZnAl_{0.2}Fe_{1.8}O_4$	0.06, 2.05		
	950	$Ca_{10}(PO_4)_6F_2$, $ZnAl_{0.2}Fe_{1.8}O_4$	0.06, 1.52		
	1000	$ZnAl_{0.2}Fe_{1.8}O_4$	0.87		

Glass ID	T (°C)	Phases	wt%	vol%$_{950}$	T_L (°C)
HAL24M1-08	850	$Ca_{10}(PO_4)_6F_2$, $NiFe_2O_4$, $ZnCr_{1.8}Al_{0.2}O_4$, ZrO2	0.98, 1.34, 0.77, 1.44	0.37, 0.42, 0.27, 0.50	1150 < T_L
	900	$Ca_{10}(PO_4)_6F_2$, $NiFe_2O_4$, $ZnCr_{1.8}Al_{0.2}O_4$, ZrO2	0.76, 0.98, 0.64, 1.18		
	950	$Ca_{10}(PO_4)_6F_2$, $NiFe_2O_4$, $ZnCr_{1.8}Al_{0.2}O_4$, ZrO2	0.44, 0.83, 0.54, 1.08		
	1100	$NiFe_2O_4$, $ZnCr_{1.8}Al_{0.2}O_4$, ZrO_2	0.54, 0.42, 0.47		
HAL24M1-09	850	$Ca_{10}(PO_4)_6F_2$, $ZnCr_{1.8}Al_{0.2}O_4$	4.48, 4.10	2.56, 1.24	1150 < T_L
	900	$Ca_{10}(PO_4)_6F_2$, $ZnCr_{1.8}Al_{0.2}O_4$	4.34, 3.29		
	950	$Ca_{10}(PO_4)_6F_2$, $ZnCr_{1.8}Al_{0.2}O_4$	3.04, 2.43		
	1000	$Ca_{10}(PO_4)_6F_2$, $ZnCr_{1.8}Al_{0.2}O_4$	2.43, 1.78		
	1100	$Ca_{10}(PO_4)_6F_2$, $ZnCr_{1.8}Al_{0.2}O_4$	2.31, 1.01		
HAL24M1-10	850	$NiFe_2O_4$	0.87	0.09	964
	900	$NiFe_2O_4$	0.34		
	950	$NiFe_2O_4$	0.17		
HAL24M1-11	850	$Ca_{10}(PO_4)_6F_2$, $ZnCr_2O_4$	5.92, 2.73	4.03, 0.85	1150 < T_L
	900	$Ca_{10}(PO_4)_6F_2$, $ZnCr_2O_4$	5.46, 2.19		
	950	$Ca_{10}(PO_4)_6F_2$, $ZnCr_2O_4$	4.79, 1.71		
	1150	$Ca_{10}(PO_4)_6F_2$, $ZnCr_2O_4$	5.72, 1.11		
	1300	$ZnCr_2O_4$	0.86		
HAL24M1-12	750	$NaAlSiO_4$, Na_2CaSiO_4	19.48, 0.45	0.10	982
	850	$NaAlSiO_4$, Na_2CaSiO_4	9.32, 0.33		
	900	$NaAlSiO_4$, Na_2CaSiO_4	0.62, 0.13		
	950	Na_2CaSiO_4	0.11		
HAL24M1-13	850	$Ca_{10}(PO_4)_6F_2$, ZrO_2	6.15, 2.68	5.16, 1.15, 0.05	1150 < T_L
	900	$Ca_{10}(PO_4)_6F_2$, ZrO_2	6.13, 1.60		
	950	$Ca_{10}(PO_4)_6F_2$, ZrO_2	6.07, 2.58		
	1000	$Ca_{10}(PO_4)_6F_2$, ZrO_2	4.92, 2.08		
	1150	$Ca_{10}(PO_4)_6F_2$, ZrO_2	4.87, 1.21		
HAL24M1-14	850	$Ca_{10}(PO_4)_6F_2$, $ZnFeAlO_4$	5.29, 0.95	3.60, 0.33	1077
	900	$Ca_{10}(PO_4)_6F_2$, $ZnFeAlO_4$	4.94, 0.77		
	950	$Ca_{10}(PO_4)_6F_2$, $ZnFeAlO_4$	4.31, 0.61		
	1300	None	NA		
HAL24M1-15	850	$Ca_{10}(PO_4)_6F_2$, $ZnFeAlO_4$	0.59, 1.10	0.38	1178
	900	$Ca_{10}(PO_4)_6F_2$, $ZnFeAlO_4$	0.67, 1.00		
	950	$ZnFeAlO_4$	0.71		
	1000	$ZnFeAlO_4$	0.64		
	1050	$ZnFeAlO_4$	0.44		
HAL24M1-16	750	None	NA	NA	T_L <750
HAL24M1-17	750	None	NA	NA	T_L <750
HAL24M1-18	850	$Ca_{10}(PO_4)_6F_2$, $ZnCr_{1.8}Al_{0.2}O_4$	3.69, 1.11	2.08, 0.47	1159
	900	$Ca_{10}(PO_4)_6F_2$, $ZnCr_{1.8}Al_{0.2}O_4$	3.19, 1.03		
	950	$Ca_{10}(PO_4)_6F_2$, $ZnCr_{1.8}Al_{0.2}O_4$	2.49, 0.93		
	1100	$Ca_{10}(PO_4)_6F_2$, $ZnCr_{1.8}Al_{0.2}O_4$	3.34, 0.76		
HAL24M1-19	750	$Ca_{10}(PO_4)_6F_2$	1.12	0.24	1001
	850	$Ca_{10}(PO_4)_6F_2$	0.65		
	900	$Ca_{10}(PO_4)_6F_2$	0.36		
	950	$Ca_{10}(PO_4)_6F_2$	0.29		
HAL24M1-20	850	$Ca_{10}(PO_4)_6F_2$	2.45	1.15	1071
	900	$Ca_{10}(PO_4)_6F_2$	2.16		
	950	$Ca_{10}(PO_4)_6F_2$	1.38		
	1000	$Ca_{10}(PO_4)_6F_2$	0.79		

Glass ID	T (°C)	Phases	wt%	vol%$_{950}$	T_L (°C)
HAL24M1-21	750	$NaAlSiO_4$, $ZnCr_{1.8}Al_{0.2}O_4$	7.33, 0.57	0.22	1134
	850	$ZnCr_{1.8}Al_{0.2}O_4$	0.53		
	900	$ZnCr_{1.8}Al_{0.2}O_4$	0.47		
	950	$ZnCr_{1.8}Al_{0.2}O_4$	0.44		
	1150	None	NA		
HAL24M1-22	750	$Ca_{10}(PO_4)_6F_2$, $ZnCr_{1.8}Al_{0.2}O_4$, ZrO2	1.02, 0.68, 0.77	0.36	1150 < T_L
	850	$ZnCr_{1.8}Al_{0.2}O_4$	0.83		
	900	$ZnCr_{1.8}Al_{0.2}O_4$	0.76		
	950	$ZnCr_{1.8}Al_{0.2}O_4$	0.71		
	1300	None	NA		
HAL24M1-23	850	$Na_6Ca_2Al_6Si_6O_{24}(SO_4)_2$, $ZnCr_{1.8}Al_{0.2}O_4$	0.38, 1.19	0.23	1017
	900	$Na_6Ca_2Al_6Si_6O_{24}(SO_4)_2$, $ZnCr_{1.8}Al_{0.2}O_4$	0.11, 0.85		
	950	$ZnCr_{1.8}Al_{0.2}O_4$	0.46		
HAL24M1-24	850	$Ca_{10}(PO_4)_6F_2$, $Na_8(Al_6Si_6O_{24})(SO_4)$, $NaAlSiO_4$	1.74, 7.46, 2.55	3.68, 1.92	1029
	900	$Ca_{10}(PO_4)_6F_2$, $Na_8(Al_6Si_6O_{24})(SO_4)$, $NaAlSiO_4$, $ZnCr_{1.8}Al_{0.2}O_4$	1.56, 1.33, 1.33, 0.51		
	950	$Na_8(Al_6Si_6O_{24})(SO_4)$, $NaAlSiO_4$	3.10, 1.95		
	1000	$Na_8(Al_6Si_6O_{24})(SO_4)$	1.23		
HAL24M1-25	850	$Na_6Ca_2Al_6Si_6O_{24}(SO_4)_2$, $Na_8(Al_6Si_6O_{24})(SO_4)$, $ZnCr_{1.8}Al_{0.2}O_4$	0.34, 4.69, 1.69	0.28	1003
	900	$Na_8(Al_6Si_6O_{24})(SO_4)$, $ZnCr_{1.8}Al_{0.2}O_4$	0.73, 1.14		
	950	$ZnCr_{1.8}Al_{0.2}O_4$	0.57		
HAL24M1-26	850	$Ca_{10}(PO_4)_6F_2$, $NaAlSiO_4$, ZrO_2	2.09, 9.20, 1.21	0.47	1150 < T_L
	900	$Ca_{10}(PO_4)_6F_2$, $NaAlSiO_4$, ZrO_2	1.28, 1.49, 1.26		
	950	ZrO_2	1.03		
	1000	ZrO_2	0.81		
	1100	ZrO_2	0.60		
HAL24M1-27	850	$Ca_{10}(PO_4)_6F_2$, $Na_6Ca_2Al_6Si_6O_{24}(SO_4)_2$, $Na_8(Al_6Si_6O_{24})(SO_4)$,	2.80, 0.43, 6.21	1.76, 0.86	1150 < T_L
	900	$Ca_{10}(PO_4)_6F_2$, $Na_8(Al_6Si_6O_{24})(SO_4)$,	2.50, 0.86		
	950	$Ca_{10}(PO_4)_6F_2$, $CaFe_2O_5$	2.11, 1.30		
	1050	$Ca_{10}(PO_4)_6F_2$, $CaFe_2O_5$	2.12, 2.20		
	1150	$Ca_{10}(PO_4)_6F_2$, $CaFe_2O_5$	2.09, 1.71		
HAL24M1-28	750	$Ca_{10}(PO_4)_6F_2$, $ZnCr_{1.8}Al_{0.2}O_4$	0.65, 0.43	0.08	1005
	850	$ZnCr_{1.8}Al_{0.2}O_4$	0.34		
	900	$ZnCr_{1.8}Al_{0.2}O_4$	0.28		
	950	$ZnCr_{1.8}Al_{0.2}O_4$	0.16		
HAL24M1-29	850	$NiFe_2O_4$	0.89	0.27	1108
	900	$NiFe_2O_4$	0.70		
	950	$NiFe_2O_4$	0.53		
	1050	$NiFe_2O_4$	0.20		
HAL24M1-30	850	$NiFe_2O_4$	1.85	0.61	1193
	900	$NiFe_2O_4$	1.65		
	950	$NiFe_2O_4$	1.21		
	1050	$NiFe_2O_4$	0.80		
HAL24M2-01	750	$NaAlSiO_4$	13.85	NA	887
	850	$NaAlSiO_4$	1.46		
	900	None	NA		
	950	None	NA		
	1100	None	NA		

Glass ID	T (°C)	Phases	wt%	$vol\%_{950}$	T_L (°C)
HAL24M2-02	750	$NaAlSiO_4$, $Na_8(Al_6Si_6O_{24})(SO_4)$	12.89, 6.19	0.22	953
	850	$NaAlSiO_4$, $Na_8(Al_6Si_6O_{24})(SO_4)$	0.47, 7.43		
	900	$Na_8(Al_6Si_6O_{24})(SO_4)$	4.38		
	950	$Na_8(Al_6Si_6O_{24})(SO_4)$	0.18		
	1100	None	NA		
HAL24M2-03	950	$ZnCr_{1.8}Al_{0.2}O_4$, ZrO2	0.36, 0.57	0.18, 0.26	1150 < T_L
	1025	$ZnCr_{1.8}Al_{0.2}O_4$	0.24		
	1100	$ZnCr_{1.8}Al_{0.2}O_4$	0.15		
HAL24M2-04-1	750	$Na_{1.14}AlSiO_4$	0.72	NA	T_L < 850
	850	None	NA		
	950	None	NA		
	1100	None	NA		
HAL24M2-05	750	$NaAlSiO_4$, $ZnAl_{0.2}Fe_{1.8}O_4$	4.09, 0.68	NA	890
	800	$NaAlSiO_4$, $ZnAl_{0.2}Fe_{1.8}O_4$	2.36, 0.36		
	850	$ZnAl_{0.2}Fe_{1.8}O_4$	0.21		
	950	None	NA		
	1100	None	NA		
HAL24M2-06	850	$NiFe_2O_4$	0.80	0.38	1150 < T_L
	950	$NiFe_2O_4$	0.76		
	1025	$NiFe_2O_4$	0.63		
	1100	$NiFe_2O_4$	0.54		
HAL24M2-07	750	$NaAlSiO_4$, $ZnCr_{1.8}Al_{0.2}O_4$	13.58, 0.98	0.16	1034
	850	$NaAlSiO_4$, $ZnCr_{1.8}Al_{0.2}O_4$	1.78, 0.49		
	950	$ZnCr_{1.8}Al_{0.2}O_4$	0.33		
HAL24M2-08	900	$Ca_{10}(PO_4)_6F_2$, $ZnCr_{1.8}Al_{0.2}O_4$	4.37, 2.03	3.28, 0.82	1150 < T_L
	950	$Ca_{10}(PO_4)_6F_2$, $ZnCr_{1.8}Al_{0.2}O_4$	3.90, 1.62		
	1025	$Ca_{10}(PO_4)_6F_2$, $ZnCr_{1.8}Al_{0.2}O_4$	3.02, 1.35		
	1100	$Ca_{10}(PO_4)_6F_2$, $ZnCr_{1.8}Al_{0.2}O_4$	3.00, 0.90		
HAL24M2-09	750	$Ca_{10}(PO_4)_6F_2$, $ZnCr_{1.8}Al_{0.2}O_4$	1.98, 0.73	0.14	1060
	850	$Ca_{10}(PO_4)_6F_2$, $ZnCr_{1.8}Al_{0.2}O_4$	0.97, 0.43		
	950	$ZnCr_{1.8}Al_{0.2}O_4$	0.28		
	1025	None	NA		
	1100	None	NA		
HAL24M2-10	850	$Ca_{10}(PO_4)_6F_2$, $ZnCr_{1.8}Al_{0.2}O_4$, ZrO2	2.19, 1.16, 1.42	0.98, 0.34, 0.41	1194
	950	$Ca_{10}(PO_4)_6F_2$, $ZnCr_{1.8}Al_{0.2}O_4$, ZrO2	1.18, 0.68, 0.89		
	1025	$ZnCr_{1.8}Al_{0.2}O_4$, ZrO2	0.31, 0.74		
	1100	None	NA		
HAL24M2-11	750	$NaAlSiO_4$, $Na_8(Al_6Si_6O_{24})(SO_4)$, $ZnCr_{1.8}Al_{0.2}O_4$	0.98, 3.78, 1.24	0.32	962
	800	$Na_8(Al_6Si_6O_{24})(SO_4)$, $ZnCr_{1.8}Al_{0.2}O_4$	3.42, 0.85		
	850	$Na_8(Al_6Si_6O_{24})(SO_4)$, $ZnCr_{1.8}Al_{0.2}O_4$	0.24, 0.66		
	950	$ZnCr_{1.8}Al_{0.2}O_4$	0.64		
	1100	None	NA		
HAL24M2-12	850	$ZnFeAlO_4$, ZrO_2	1.30, 0.55	0.60, 0.24	1150 < T_L
	950	$ZnFeAlO_4$, ZrO_2	1.12, 0.53		
	1025	$ZnFeAlO_4$, ZrO_2	0.92, 0.59		
	1100	$ZnFeAlO_4$	0.65		
HAL24M2-13	800	$ZnFeAlO_4$, ZrO_2	2.14, 1.24	0.74, 0.41	1150 < T_L
	950	$ZnFeAlO_4$, ZrO_2	1.38, 0.88		
	1100	$ZnFeAlO_4$, ZrO_2	1.23, 0.50		

Glass ID	T (°C)	Phases	wt%	vol%$_{950}$	T_L (°C)
HAL24M2-14	750	$Ca_{10}(PO_4)_6F_2$, $NaAlSiO_4$, $ZnAl_{0.2}Fe_{1.8}O_4$	0.23, 0.59, 0.34	NA	850 < T_L < 900
	800	$ZnAl_{0.2}Fe_{1.8}O_4$	0.16		
	850	$ZnAl_{0.2}Fe_{1.8}O_4$	0.35		
	900	None	NA		
	950	None	NA		
	1100	None	NA		
HAL24M2-15	750	$Ca_{10}(PO_4)_6F_2$, $NaAlSiO_4$	1.76, 12.27	NA	850 < T_L < 900
	800	$Ca_{10}(PO_4)_6F_2$, $NaAlSiO_4$	1.60, 0.66		
	850	$Ca_{10}(PO_4)_6F_2$	1.64		
	900	None	NA		
	950	None	NA		
	1025	None	NA		
HAL24M2-16	850	$Ca_{10}(PO_4)_6F_2$, $ZnFe_{1.9}Cr_{0.1}O_4$	3.45, 3.95	1.83, 1.23	1124
	950	$Ca_{10}(PO_4)_6F_2$, $ZnFe_{1.9}Cr_{0.1}O_4$	2.18, 2.53		
	1050	$ZnFe_{1.9}Cr_{0.1}O_4$	1.08		
HAL24M2-17	750	Cr_2O_3	0.76	0.19	1122
	850	Cr_2O_3	0.47		
	950	Cr_2O_3	0.37		
HAL24M2-18	750	$Ca_{10}(PO_4)_6F_2$, $NiFe_2O_4$	2.03, 1.07	0.89, 0.39	1150 < T_L
	850	$Ca_{10}(PO_4)_6F_2$, $NiFe_2O_4$	1.48, 1.01		
	950	$Ca_{10}(PO_4)_6F_2$, $NiFe_2O_4$	1.07, 0.77		
	1025	$NiFe_2O_4$	0.51		
	1100	$NiFe_2O_4$	0.30		
HAL24M2-19	750	$NaAlSiO_4$, $Na_8(Al_6Si_6O_{24})(SO_4)$	4.45, 3.81	NA	861
	800	$NaAlSiO_4$, $Na_8(Al_6Si_6O_{24})(SO_4)$	0.92, 1.99		
	850	$Na_8(Al_6Si_6O_{24})(SO_4)$	0.38		
	950	None	NA		
HAL24M2-20	850	$ZnFe_{1.9}Cr_{0.1}O_4$, ZrO_2	2.70, 0.50	0.92	1176
	950	$ZnFe_{1.9}Cr_{0.1}O_4$	1.90		
	1025	$ZnFe_{1.9}Cr_{0.1}O_4$	1.25		

Out of 50 HAL glasses, 10 glasses were fully amorphous without any crystalline phases at or below 950 °C: HAL24M1-01, -02, -16, -17, and HAL24M2-01, -04, -05, -14, -15, -19. This indicates that these glasses remained amorphous below the melter pour-spout temperature of 950 °C. The most common crystal phase among the glasses was spinel with different chemistries, containing Al, Cr, Fe, Ni, and/or Zn (Figure 3.1). Spinel phases are problematic in the melter operation as they can settle to the melter bottom and accumulate, impacting melter operation and lifespan. Spinel phases were present in various glass compositions, which contributed to the overall diversity of crystal phases identified. The next most common phase was apatite and fluorapatite [$Ca_{10}(PO_4)_6F_2$]. In the apatite structure, different cations including Na, Mg, and Sr can occupy Ca site, and Cl can occupy F site. The sodium aluminosilicate phases including nepheline and nosean were observed in some glasses. These phases have a negative effect on the chemical durability of glasses as they remove Al and Si from the glass matrix. The highest wt% of nepheline was observed in HAL24M1-12 at 750 °C with 19.48 wt%, followed by HAL24M2-01 and -02 (13.8 wt% and 12.9 wt%) and by HAL24M2-07 and -15 with 13.6 and 12.27 wt%, respectively. Baddeleyite (ZrO_2) was generally observed in nine compositions with relatively high ZrO_2 target wt% (2-4 wt%).

T_L was obtained by linear or nonlinear fitting of wt% crystals at three or more different temperatures. The nonlinear fitting was used on four glasses as it improved the correlation coefficient. Among the observed phases, spinel phases generally crystallized across the tested temperature ranges with small decrease in wt% at temperature increment, resulting in high T_L. The sodium aluminosilicate phases such as nepheline and nosean decomposed above 1150 °C.

3.4 SO_3 Solubility

The SO_3 saturation concentration is controlled to avoid excessive corrosion of melter materials at the melt-line. This section summarizes the SSM study on the HAL24 glasses. The SO_3 concentrations of SSM and Q glasses were compared. In addition, the predicted SO_3 solubilities from different models were compared.

3.4.1 SSM Preparation Method Investigations

HAL24 glasses HAL24M1-05, HAL24M1-06, and HAL24M1-07 were selected to be prepared using the washed particles, washed monolith, and unwashed monolith methods and analyzed via EPMA. These glasses were chosen as they represented glass compositions with ranges that span low to high Na, S, and Si in various combinations. Additionally, the washed coupons were analyzed by EPMA using a scattered and linear approach where points were selected randomly along the monolith using the scattered approach and where points were selected in a straight line equidistantly apart in the linear approach to observe whether a compositional gradient exists on the monoliths.

Table 3.4 presents the results from each sample and their average concentration and standard deviation. Some variation exists between the methods, which has been attributed to suspected outliers and differences in the EPMA calibration. Even with the variations, the standard deviation of each glass is less than the pooled standard deviation of SO_3 concentration in SSM samples determined from glasses analyzed with ICP-OES (0.1548 wt%). Also, no obvious trends in method were observed for the three samples (e.g., each method produced results both above and below the mean for different samples). This implies that any effect of preparation and analysis methods on the final SO_3 concentration is within test experimental error. The simplest preparation method, unwashed monolith, was selected for the remaining glasses using the scattered analysis approach with the exception of HAL24M1-01, HAL24M1-02, and HAL24M1-04, which were prepared with the washed particle method.

Table 3.4. Measured SO_3 concentrations of subset of samples prepared via the various methods and the average concentration and standard deviation of all the methods.

Glass ID	Washed Powder (wt%)	Washed Monolith (linear analysis, wt%)	Washed Monolith (scattered analysis, wt%)	Unwashed Monolith (wt%)	Average (wt%)	Standard Deviation (wt%)
HAL24M1-05	1.31	1.35	1.34	1.19	1.30	0.07
HAL24M1-06	1.28	1.46	1.13	1.30	1.29	0.13
HAL24M1-07	1.06	1.07	0.84	1.01	0.99	0.11

3.4.2 SSM SO_3 Concentrations

For each HAL24 glass, an excess sulfate phase was observed in all three melts as seen for HAL24M1-12 in Figure 3.2 as an example. The excess sulfate phase is expected as the amount of Na_2SO_4 added exceeds the conservative sulfur limit for WTP used in the 2014 algorithm by more than 9× (4 vs. 0.44 wt% SO_4) (Vienna and Kim 2014). However, while the excess phase may form for the first two melts, Jin et al. (2019) provided evidence that the glass is not completely saturated with SO_3 until the third melt.

Figure 3.2. Photos of the three melts (*left to right*): melts 1, 2, and 3 (i.e., the SSM) for HAL24M1-12.

Table 3.5 presents the SO_3 concentrations of the HAL24 glass SSM samples measured by EPMA. The SO_3 concentrations range from 0.76 to 1.79 wt% with a median value of 1.17 wt%.

Table 3.5. Measured SO_3 concentrations (wt%) of SSM glasses from the HAL24 matrix.

Glass ID	SO_3 (wt %)	Glass ID	SO_3 (wt %)
HAL24M1-01-SSM	1.79	HAL24M1-26-SSM	1.17
HAL24M1-02-SSM	1.18	HAL24M1-27-SSM	1.25
HAL24M1-03-SSM	1.13	HAL24M1-28-SSM	1.05
HAL24M1-04-SSM	0.76	HAL24M1-29-1-SSM	0.87
HAL24M1-05-SSM	1.19	HAL24M1-30-1-SSM	0.93
HAL24M1-06-SSM	1.30	HAL24M2-01-SSM	1.22
HAL24M1-07-SSM	1.01	HAL24M2-02-SSM	1.32
HAL24M1-08-SSM	1.42	HAL24M2-03-SSM	0.91
HAL24M1-09-SSM	1.58	HAL24M2-04-1-SSM	0.85
HAL24M1-10-SSM	1.07	HAL24M2-05-SSM	1.14
HAL24M1-11-SSM	1.60	HAL24M2-06-SSM	1.21
HAL24M1-12-SSM	1.24	HAL24M2-07-SSM	1.14
HAL24M1-13-1-SSM	1.44	HAL24M2-08-SSM	1.65
HAL24M1-14-SSM	1.60	HAL24M2-09-SSM	1.42
HAL24M1-15-SSM	1.38	HAL24M2-10-SSM	1.40
HAL24M1-16-SSM	0.92	HAL24M2-11-SSM	1.30
HAL24M1-17-SSM	0.85	HAL24M2-12-SSM	1.08
HAL24M1-18-SSM	0.99	HAL24M2-13-SSM	1.08
HAL24M1-19-SSM	0.84	HAL24M2-14-SSM	1.08
HAL24M1-20-SSM	1.19	HAL24M2-15-SSM	1.27
HAL24M1-21-SSM	1.17	HAL24M2-16-SSM	1.20
HAL24M1-22-SSM	1.07	HAL24M2-17-SSM	1.65
HAL24M1-23-SSM	1.06	HAL24M2-18-SSM	1.17
HAL24M1-24-SSM	1.64	HAL24M2-19-SSM	1.20
HAL24M1-25-SSM	1.09	HAL24M2-20-SSM	1.13

3.4.3 Comparisons to Predicted SO_3 Saturation Concentrations

The SO_3 saturation concentrations determined experimentally for the HAL24 matrix were compared to SO_3 saturation predicted concentrations generated from the 3TS-SO_3-PQMM model (EWG 2.5, Vienna et al. 2024). None of these glasses were designed to fail SO_3 solubility.

Figure 3.3 provides a one-to-one comparison of the measured and predicted SO_3 solubilities using the 3TS-SO_3-PQMM (EWG 2.5, Vienna et al. 2024) model. The data is provided without the 0.33 wt% melter data offset, but the offset effects are indicated by the dark blue dashed line in Figure 3.3. Overall, the predicted SSM SO_3 concentrations are consistent with the measured concentrations but have larger uncertainties.

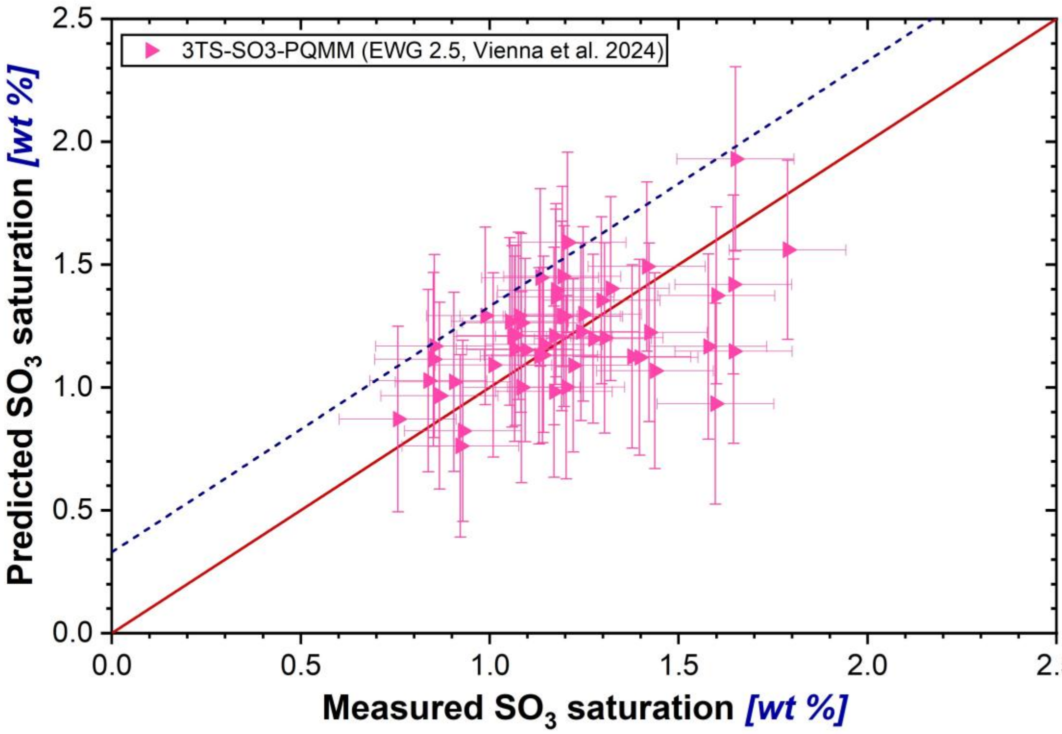

Figure 3.3. Measured SO_3 saturation and predicted SO_3 saturation concentrations for HAL24 glasses from the 3TS-SO_3-PQMM (EWG 2.5, Vienna et al. 2024) model. The red line is the 1-1 line whereas the dashed dark blue line shows the 0.33 wt% melter offset (Skidmore et al. 2019).

3.5 Density

Densities of the HAL24M1 and HAL24M2 glasses were obtained using the methods discussed in Section 2.8 and are presented in Table 3.6. The average density of the HAL24 glasses was 2.55 g/cm³.

Table 3.6. Measured densities of HAL24 glasses in g/cm³.

Glass ID	Density (g/cm³)	Glass ID	Density (g/cm³)
HAL24M1-01	2.64	HAL24M1-26	2.63
HAL24M1-02	2.55	HAL24M1-27	2.59
HAL24M1-03	2.60	HAL24M1-28	2.53
HAL24M1-04	2.44	HAL24M1-29-1	2.44
HAL24M1-05	2.50	HAL24M1-30-1	2.49
HAL24M1-06	2.54	HAL24M2-01	2.65
HAL24M1-07	2.50	HAL24M2-02	2.57
HAL24M1-08	2.58	HAL24M2-03	2.48
HAL24M1-09	2.64	HAL24M2-04-1	2.53
HAL24M1-10	2.51	HAL24M2-05	2.59
HAL24M1-11	2.55	HAL24M2-06	2.53
HAL24M1-12	2.58	HAL24M2-07	2.62
HAL24M1-13-1	2.57	HAL24M2-08	2.66
HAL24M1-14	2.61	HAL24M2-09	2.57
HAL24M1-15	2.62	HAL24M2-10	2.62
HAL24M1-16	2.62	HAL24M2-11	2.61
HAL24M1-17	2.46	HAL24M2-12	2.54
HAL24M1-18	2.57	HAL24M2-13	2.43
HAL24M1-19	2.42	HAL24M2-14	2.57
HAL24M1-20	2.46	HAL24M2-15	2.58
HAL24M1-21	2.50	HAL24M2-16	2.53
HAL24M1-22	2.44	HAL24M2-17	2.56
HAL24M1-23	2.63	HAL24M2-18	2.51
HAL24M1-24	2.62	HAL24M2-19	2.50
HAL24M1-25	2.59	HAL24M2-20	2.62

Measured densities of the HAL24 glasses were compared to predicted densities from models by Vienna et al. (2002) and the Hanford Tank Waste Operations Simulator (HTWOS) model (Vienna et al. 2009). For HAL24M1, predicted values from Vienna et al. (2002) are closer to measured values compared to values from the HTWOS model (Vienna et al. 2009), and predicted densities from both models were generally higher than measured values (Figure 3.4). Overall, the linearity of predicted values from both models was in good agreement but just shifted to higher density values as seen in Figure 3.4. For HAL24M2, the difference between predicted and measured densities was greater compared to HAL24M1, and the scatterplot did not show a specific relationship between predicted and measured values (Figure 3.5).

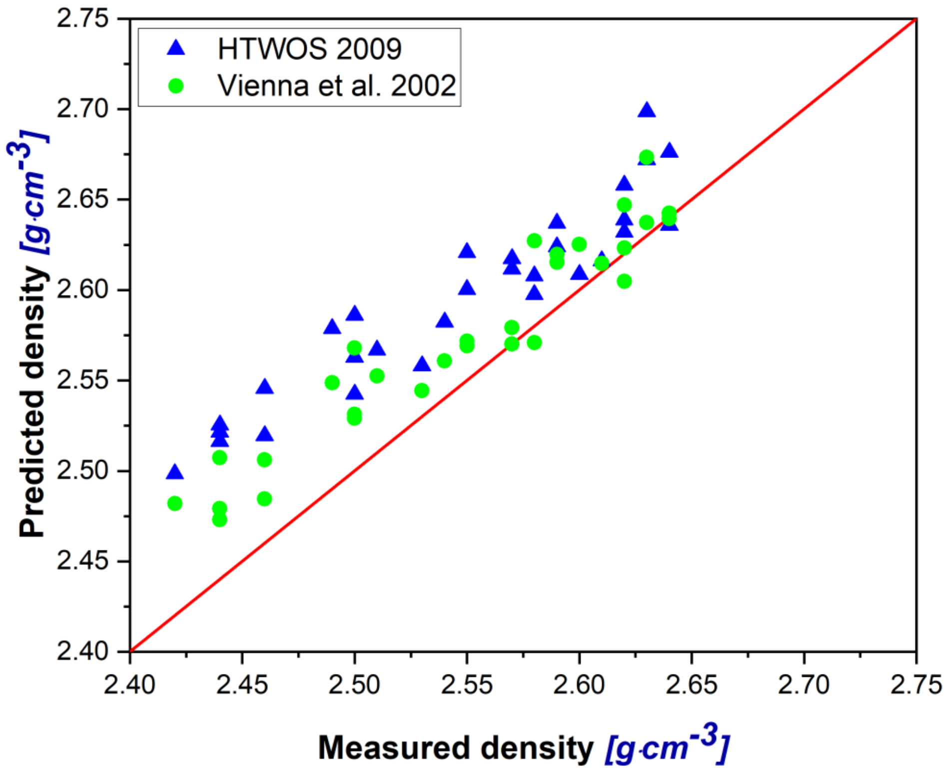

Figure 3.4. Measured and predicted densities for HAL24M1 glasses (For Information Only).

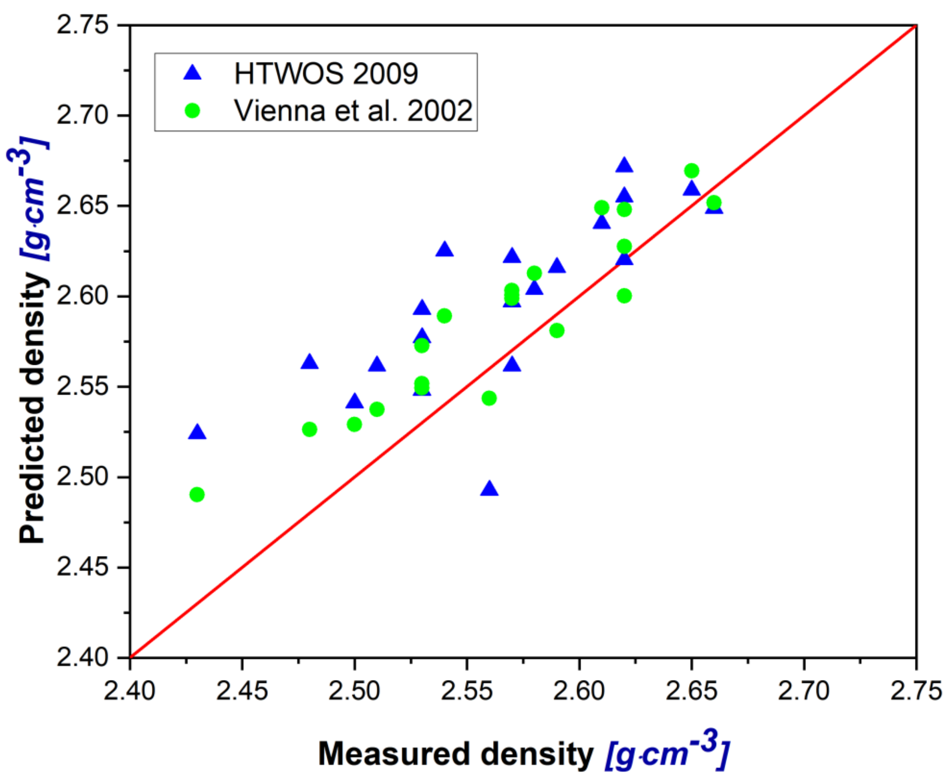

Figure 3.5. Measured and predicted densities for HAL24M2 glasses (For Information Only).

3.6 Viscosity

This section presents the viscosity results obtained using the methods discussed in Section 2.9. The results are summarized in Table 3.7 and individually reported in Appendix J. Note that the reported temperatures may be different than target temperatures listed in Section 2.9 because of a difference between the furnace control thermocouple and the viscosity measurement thermocouple. For some glasses, readings at 950 and 1050 °C were outside of the limitations of the viscometer because the viscosity of the glass was too high, likely due to these glasses crystallizing at lower temperatures. For all such glasses, raising the temperature back to 1150 °C allowed for a measurement again. Glass HAL24M1-17 showed a higher viscosity value at the last 1150 °C reading, indicating that alkali may have volatilized from the glass at the previous 1250 °C reading. Glass HAL24M2-12 shows a lot of scatter, particularly for the repeat 1150 °C, and that datapoint should be used with caution. Most glasses showed good agreement between the three 1150 °C readings and good Arrhenius fits, which are reported in Appendix J.

Table 3.7. Measured ln η (Pa-s) values vs. target temperature (in the sequence of measurement).

Target T, °C	1150	1050	950	1150	1250	1150
Glass ID	ln η (Pa-s)[(a)]	ln η (Pa-s)[(a)]	ln η (Pa-s)[(a)]	ln η (Pa-s)[(a)]	ln η (Pa-s)[(a)]	ln η (Pa-s)[(a)]
HAL24M1-01	0.200	0.875	1.736	0.143	-0.397	0.162
HAL24M1-02	1.299	2.024	2.944	1.325	0.722	1.341
HAL24M1-03	0.771	1.480	2.947	0.752	-0.272	0.741
HAL24M1-04	2.079	2.911	3.932	2.208	1.583	2.226
HAL24M1-05	0.753	1.443	2.191	0.732	0.178	0.761
HAL24M1-06	0.665	1.485	2.392	0.718	0.048	0.688
HAL24M1-07	1.862	2.697	3.735	1.863	1.071	1.855
HAL24M1-08	1.475	2.143	2.985	1.498	0.404	1.473
HAL24M1-09	0.492	1.595	2.753	0.514	-0.183	0.459
HAL24M1-10	1.278	2.036	2.923	1.300	0.685	1.289
HAL24M1-11	1.868	2.544	2.765	1.908	1.081	1.835
HAL24M1-12	1.107	1.793	2.841	1.110	0.375	1.023
HAL24M1-13-1	2.244	2.547	4.826	2.247	0.697	2.217
HAL24M1-14	0.952	--[(b)]	--[(b)]	0.931	0.272	0.924
HAL24M1-15	0.853	1.673	2.695	0.841	0.146	0.835
HAL24M1-16	1.697	2.845	3.792	1.708	0.876	1.700
HAL24M1-17	2.002	2.886	3.944	2.020	1.299	2.347
HAL24M1-18	1.576	2.382	2.765	1.602	0.899	1.580
HAL24M1-19	2.222	3.066	4.286	2.249	1.607	2.198
HAL24M1-20	1.653	2.523	3.520	1.683	0.977	1.642
HAL24M1-21	0.811	1.376	2.153	0.797	0.282	0.785
HAL24M1-22	2.045	2.880	3.936	2.098	1.353	2.080
HAL24M1-23	0.435	1.100	1.913	0.425	-0.038	0.443
HAL24M1-24	0.271	0.969	1.898	0.261	-0.321	0.261
HAL24M1-25	0.065	0.702	1.466	0.077	-0.433	0.053
HAL24M1-26	1.004	1.829	2.859	1.016	0.322	0.993
HAL24M1-27	0.729	1.487	2.331	0.750	0.126	0.727
HAL24M1-28	1.280	2.005	2.940	1.268	0.672	1.305

Target *T*, °C	1150	1050	950	1150	1250	1150
HAL24M1-29-1	1.803	2.452	3.562	1.791	0.987	1.769
HAL24M1-30-1	1.870	2.762	3.702	1.908	1.224	1.854
HAL24M2-01	0.372	1.108	1.973	0.341	-0.249	0.332
HAL24M2-02	0.428	1.092	1.872	0.427	-0.123	0.447
HAL24M2-03	2.180	3.124	4.204	2.220	1.430	2.177
HAL24M2-04-1	1.721	2.503	3.514	1.758	0.144	1.746
HAL24M2-05	0.851	1.601	2.480	0.874	0.274	0.875
HAL24M2-06	1.652	3.059	3.752	1.755	1.024	1.764
HAL24M2-07	0.629	1.396	2.348	0.566	-0.082	0.554
HAL24M2-08	0.654	--(b)	--(b)	0.612	-0.147	0.589
HAL24M2-09	0.456	1.215	2.173	0.409	-0.188	0.407
HAL24M2-10	0.805	1.710	--(b)	0.822	0.112	0.795
HAL24M2-11	0.796	1.580	2.581	0.768	0.089	0.737
HAL24M2-12	1.260	1.978	2.847	1.156	0.362	0.918
HAL24M2-13	2.646	3.722	5.097	2.721	1.858	2.616
HAL24M2-14	0.817	1.497	2.344	0.790	0.247	0.824
HAL24M2-15	0.661	1.407	2.359	0.645	0.037	0.663
HAL24M2-16	1.818	2.946	--(b)	1.931	1.023	1.751
HAL24M2-17	0.532	1.289	2.235	0.487	-0.155	0.441
HAL24M2-18	1.605	2.620	--(b)	1.690	0.910	1.619
HAL24M2-19	0.748	1.420	2.273	0.712	0.183	0.748
HAL24M2-20	0.978	1.937	3.109	0.956	0.241	0.911

(a) Average of three measurements.
(b) Too thick to get a reading.

The Arrhenius model was used to fit the viscosity-temperature data for each waste glass. The model form is the Arrhenius equation:

$$\ln(\eta) = A + \frac{B}{T_K} \tag{3.2}$$

where A and B are independent of temperature (T_K), which is in Kelvin (T(°C) + 273.15). For each glass, Table 3.8 provides the values for the A and B coefficients and summarizes the viscosity results at six target temperatures calculated using the Arrhenius Eq. (3.2).

The η_{1150} values interpolated from measured data were compared to predicted values from Vienna et al. (2022) (Figure 3.6). Both the HAL24M1 and HAL24M2 glasses present some scatter around the 45° line. Both matrices show similar results, with most glasses touching the line and a few glasses being underpredicted, indicating good agreement with the model for most glasses.

Table 3.8. Fit of Arrhenius coefficients and calculated η for various temperatures.

	Arrhenius Coefficients		Temperature (°C)					
	A	B	950	1050	1100	1150	1200	1250
Glass ID	(ln Pa-s)	(ln Pa-s*K)	ln η [Pa-s]					
HAL24M1-01	-9.1852	13330.0	1.714	0.890	0.523	0.182	-0.136	-0.4328
HAL24M1-02	-8.3674	13797.5	2.914	2.062	1.682	1.329	1.000	0.692
HAL24M1-03	-12.7361	19094.0	2.876	1.696	1.171	0.682	0.227	-0.199
HAL24M1-04	-8.1149	14666.5	3.877	2.971	2.567	2.192	1.842	1.515
HAL24M1-05	-8.0828	12574.8	2.199	1.422	1.076	0.754	0.454	0.174
HAL24M1-06	-9.5918	14647.5	2.385	1.480	1.076	0.702	0.352	0.026
HAL24M1-07	-9.6839	16408.8	3.733	2.719	2.267	1.847	1.456	1.090
HAL24M1-08	-9.1967	15019.2	3.084	2.156	1.742	1.358	1.000	0.665
HAL24M1-09	-12.6877	18845.5	2.722	1.557	1.038	0.556	0.106	-0.314
HAL24M1-10	-8.5237	13980.8	2.908	2.044	1.659	1.301	0.968	0.656
HAL24M1-11	-5.3424	10154.9	2.961	2.333	2.054	1.794	1.552	1.325
HAL24M1-12	-9.5457	15103.3	2.804	1.870	1.454	1.068	0.708	0.371
HAL24M1-13-1	-14.0232	22800.8	4.620	3.211	2.583	2.000	1.456	0.948
HAL24M1-14	-9.1734	14385.1	2.589	1.700	1.304	0.936	0.592	0.272
HAL24M1-15	-10.2957	15862.5	2.674	1.694	1.257	0.852	0.473	0.120
HAL24M1-16	-11.2761	18503.5	3.853	2.710	2.201	1.727	1.286	0.873
HAL24M1-17	-9.2050	16072.5	3.937	2.944	2.501	2.090	1.706	1.348
HAL24M1-18	-6.6487	11685.7	2.906	2.184	1.862	1.563	1.285	1.024
HAL24M1-19	-9.5586	16822.1	4.196	3.156	2.693	2.263	1.862	1.487
HAL24M1-20	-9.5149	15925.1	3.506	2.522	2.084	1.676	1.296	0.941
HAL24M1-21	-7.3358	11575.4	2.129	1.414	1.095	0.799	0.523	0.265
HAL24M1-22	-9.1493	15971.3	3.910	2.923	2.483	2.074	1.693	1.337
HAL24M1-23	-8.1905	12313.8	1.878	1.117	0.778	0.463	0.169	-0.105
HAL24M1-24	-9.3755	13668.7	1.801	0.956	0.580	0.230	-0.096	-0.401
HAL24M1-25	-8.2783	11893.7	1.447	0.712	0.384	0.080	-0.204	-0.469
HAL24M1-26	-10.0951	15810.7	2.833	1.856	1.420	1.016	0.639	0.286
HAL24M1-27	-8.9408	13782.9	2.329	1.477	1.098	0.745	0.416	0.109
HAL24M1-28	-8.6083	14088.5	2.911	2.041	1.653	1.292	0.956	0.642
HAL24M1-29-1	-9.1381	15488.3	3.526	2.569	2.142	1.746	1.377	1.031
HAL24M1-30-1	-9.0791	15626.8	3.698	2.733	2.302	1.902	1.530	1.181
HAL24M2-01	-10.5296	15586.5	2.215	1.252	0.823	0.424	0.052	-0.295
HAL24M2-02	-9.3250	13964.2	2.093	1.230	0.846	0.488	0.155	-0.156
HAL24M2-03	-11.3624	19415.0	4.513	3.313	2.778	2.281	1.818	1.386
HAL24M2-04-1	-13.4847	21446.9	4.052	2.726	2.136	1.587	1.075	0.597
HAL24M2-05	-9.9494	15490.6	2.717	1.759	1.333	0.936	0.567	0.222
HAL24M2-06	-12.3262	20227.2	4.213	2.963	2.406	1.888	1.406	0.955
HAL24M2-07	-8.9952	13693.8	2.202	1.355	0.978	0.628	0.301	-0.004
HAL24M2-08	-12.3756	18592.3	2.827	1.678	1.166	0.690	0.247	-0.168
HAL24M2-09	-11.2002	16649.1	2.413	1.384	0.926	0.500	0.103	-0.268
HAL24M2-10	-11.8788	18178.2	2.985	1.861	1.361	0.896	0.462	0.057
HAL24M2-11	-11.4087	17418.6	2.834	1.757	1.278	0.832	0.417	0.028
HAL24M2-12	-9.7167	15466.3	2.930	1.974	1.548	1.152	0.783	0.438
HAL24M2-13	-13.2897	22868.4	5.409	3.996	3.366	2.781	2.235	1.726
HAL24M2-14	-9.4234	14658.6	2.562	1.253	1.253	0.878	0.528	0.201
HAL24M2-15	-10.7101	16281.9	2.603	1.149	1.149	0.732	0.343	-0.019
HAL24M2-16	-13.2540	21613.7	4.419	2.488	2.488	1.935	1.419	0.938
HAL24M2-17	-11.3337	16937.2	2.515	1.002	1.002	0.569	0.165	-0.213
HAL24M2-18	-11.1747	18341.7	3.823	2.184	2.184	1.715	1.277	0.868
HAL24M2-19	-9.4853	14651.4	2.495	1.186	1.186	0.811	0.461	0.135
HAL24M2-20	-13.1803	20283.6	3.405	1.593	1.593	1.074	0.590	0.138

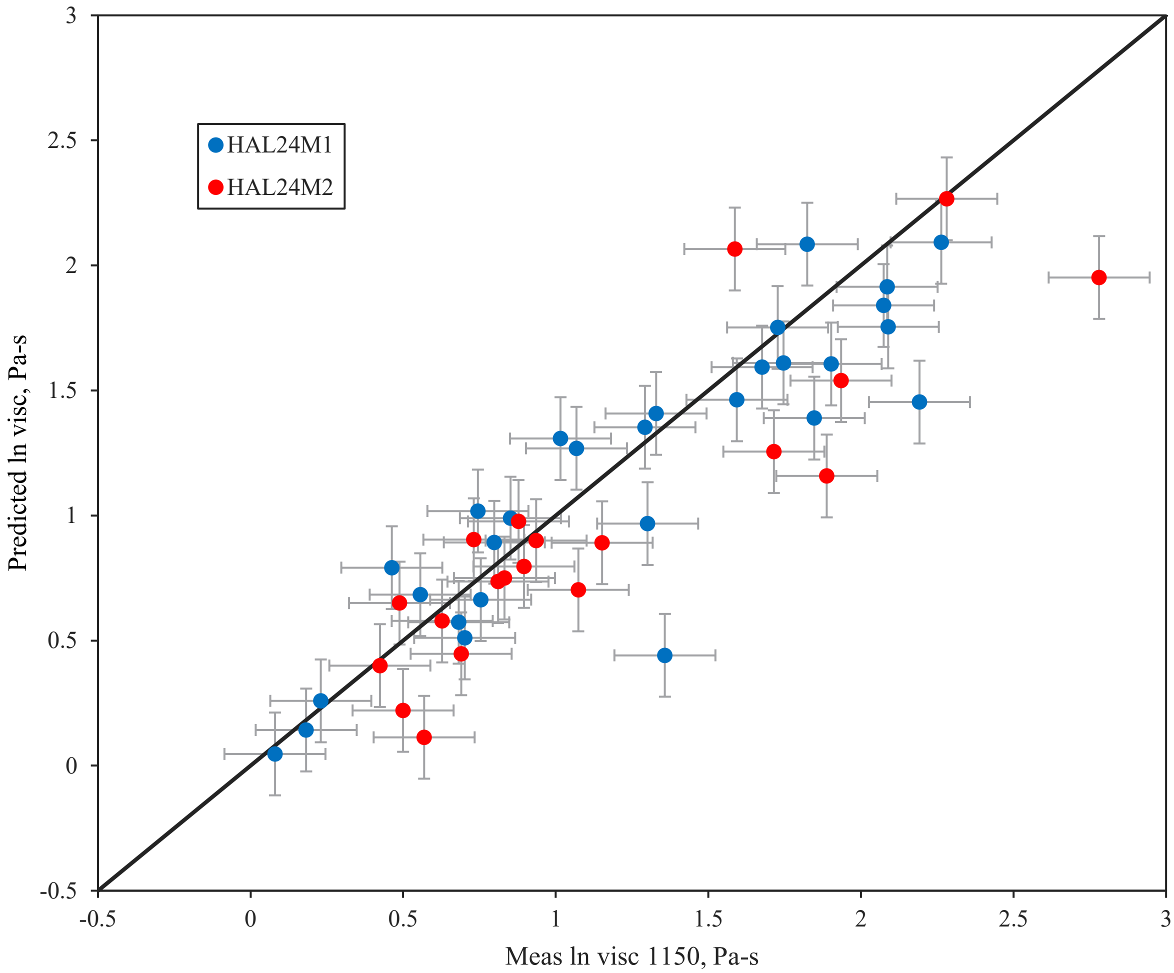

Figure 3.6. Measured vs. predicted ln(η_{1150}), where the model predicted for Pa·s shown. Uncertainties for measured values are represented by SD_{pooled} reported in Vienna et al. (2022).

3.7 Electrical Conductivity

This section presents the EC results obtained using the methods discussed in Section 2.10. The results are summarized in Table 3.9. Measured EC (S/m) values vs. temperatures are individually reported in Appendix K. The Arrhenius equation [Eq. (3.2)] was used to fit EC-temperature data for each waste glass. Arrhenius coefficients and calculated ε_{1150} are reported in Table 3.10. Figure 3.7 shows a comparison between measured and predicted values using Vienna et al. (2022) and Kot et al. (2019) model. Overall, there is good agreement between the predictions and measured values, with data points slightly shifted to a higher measured conductivity than predicted.

Table 3.9. Measured electrical conductivity (S/m) values vs. temperatures.

Target *T*, °C	950	1050	1150	1200
Glass ID		S/m		
HAL24M1-01	12.95	22.06	33.37	40.42
HAL24M1-02	17.76	26.69	36.27	41.88
HAL24M1-03	15.96	26.79	40.21	47.97
HAL24M1-04	18.25	27.36	37.06	42.03
HAL24M1-05	31.32	45.55	60.33	69.11
HAL24M1-06	10.55	17.56	26.43	31.67
HAL24M1-07	16.52	25.45	33.24	41.48
HAL24M1-08	14.45	23.72	35.27	42.19
HAL24M1-09	16.87	27.62	40.01	46.69
HAL24M1-10	17.57	27.24	37.95	43.61
HAL24M1-11	6.20	10.51	17.20	21.32
HAL24M1-12	15.58	25.93	38.09	44.85
HAL24M1-13-1	11.91	18.54	26.95	31.89
HAL24M1-14	27.16	41.68	58.76	67.74
HAL24M1-15	8.96	15.11	22.59	26.66
HAL24M1-16	15.32	24.16	32.17	38.00
HAL24M1-17	7.82	13.04	19.22	22.80
HAL24M1-18	12.40	19.59	28.55	33.89
HAL24M1-19	13.22	20.96	29.90	35.08
HAL24M1-20	16.06	24.11	32.48	36.56
HAL24M1-21	34.62	48.74	63.39	72.41
HAL24M1-22	19.42	28.78	39.02	44.13
HAL24M1-23	41.72	57.06	72.48	81.12
HAL24M1-24	20.94	32.04	44.65	51.98
HAL24M1-25	47.05	65.82	84.50	95.87
HAL24M1-26	16.75	26.62	38.00	44.50
HAL24M1-27	31.76	47.02	64.01	74.39
HAL24M1-28	25.02	37.20	50.07	59.16
HAL24M1-29-1	19.59	30.07	42.17	49.72
HAL24M1-30-1	18.00	26.74	36.26	41.61
HAL24M2-01	24.88	37.37	51.78	60.70
HAL24M2-02	50.10	67.80	84.72	95.81
HAL24M2-03	22.36	33.53	45.29	51.44
HAL24M2-04-1	39.77	55.14	71.62	80.96
HAL24M2-05	19.34	30.02	42.12	49.38
HAL24M2-06	8.85	15.20	23.27	28.56
HAL24M2-07	26.13	39.43	53.64	62.93
HAL24M2-08	10.91	18.44	29.28	36.06
HAL24M2-09	19.51	30.24	43.33	51.44
HAL24M2-10	9.88	18.20	30.72	38.08
HAL24M2-11	17.05	28.43	40.84	47.91
HAL24M2-12	30.80	43.69	56.24	62.68
HAL24M2-13	14.72	23.84	35.14	40.03
HAL24M2-14	25.84	37.80	50.55	57.90
HAL24M2-15	23.41	35.46	48.59	56.16
HAL24M2-16	8.23	13.32	19.56	23.41
HAL24M2-17	9.74	17.02	26.35	32.40
HAL24M2-18	11.29	18.48	27.08	32.71
HAL24M2-19	29.64	43.09	57.14	65.28
HAL24M2-20	14.73	23.17	33.29	39.00

Table 3.10. Fitted coefficients of Arrhenius model for ε_{1150}.

	Arrhenius Coefficients		
Glass ID	A, ln[S/m]	B, ln[S/m]·K	ε_{1150} (S/m)
HAL24M1-01	9.2556	-8175.7	33.45
HAL24M1-02	7.9181	-6153.8	36.36
HAL24M1-03	9.2639	-7929.6	40.10
HAL24M1-04	7.8364	-6017.1	36.89
HAL24M1-05	8.0896	-5671.3	60.59
HAL24M1-06	8.8372	-7917.4	26.40
HAL24M1-07	8.0468	-6401.4	34.75
HAL24M1-08	8.9819	-7710.5	35.28
HAL24M1-09	8.8422	-7340.4	39.80
HAL24M1-10	8.2386	-6555.4	37.78
HAL24M1-11	9.1148	-8926.0	17.15
HAL24M1-12	8.9917	-7621.3	37.94
HAL24M1-13-1	8.2787	-7093.2	26.95
HAL24M1-14	8.7066	-6600.5	58.45
HAL24M1-15	8.6395	-7867.1	22.44
HAL24M1-16	8.0104	-6435.9	32.71
HAL24M1-17	8.3653	-7699.6	19.19
HAL24M1-18	8.4379	-7236.3	28.58
HAL24M1-19	8.3286	-7016.4	29.90
HAL24M1-20	7.6480	-5940.0	32.26
HAL24M1-21	7.8653	-5278.5	63.81
HAL24M1-22	7.8245	-5928.9	38.78
HAL24M1-23	7.6382	-4770.9	72.64
HAL24M1-24	8.3914	-6533.3	44.71
HAL24M1-25	8.0190	-5088.8	85.02
HAL24M1-26	8.5787	-7032.5	37.97
HAL24M1-27	8.4515	-6100.8	64.34
HAL24M1-28	8.2300	-6121.7	50.80
HAL24M1-29-1	8.4397	-6677.3	42.41
HAL24M1-30-1	7.8250	-6024.9	36.27
HAL24M2-01	8.4472	-6396.0	52.06
HAL24M2-02	7.6925	-4614.9	85.58
HAL24M2-03	8.0286	-6003.6	45.14
HAL24M2-04-1	7.8622	-5106.5	71.78
HAL24M2-05	8.4724	-6729.2	42.25
HAL24M2-06	9.0570	-8401.1	23.41
HAL24M2-07	8.4030	-6277.2	54.15
HAL24M2-08	9.4333	-8617.9	29.29
HAL24M2-09	8.6637	-6959.3	43.52
HAL24M2-10	10.2737	-9758.6	30.44
HAL24M2-11	8.9269	-7426.2	40.78
HAL24M2-12	7.6210	-5113.7	56.12
HAL24M2-13	8.6591	-7284.5	34.47
HAL24M2-14	7.9952	-5791.6	50.66
HAL24M2-15	8.3026	-6286.5	48.66
HAL24M2-16	8.2537	-7509.4	19.62
HAL24M2-17	9.3376	-8625.8	26.47
HAL24M2-18	8.6590	-7617.0	27.28
HAL24M2-19	8.0276	-5662.5	57.30
HAL24M2-20	8.4339	-7016.5	33.22

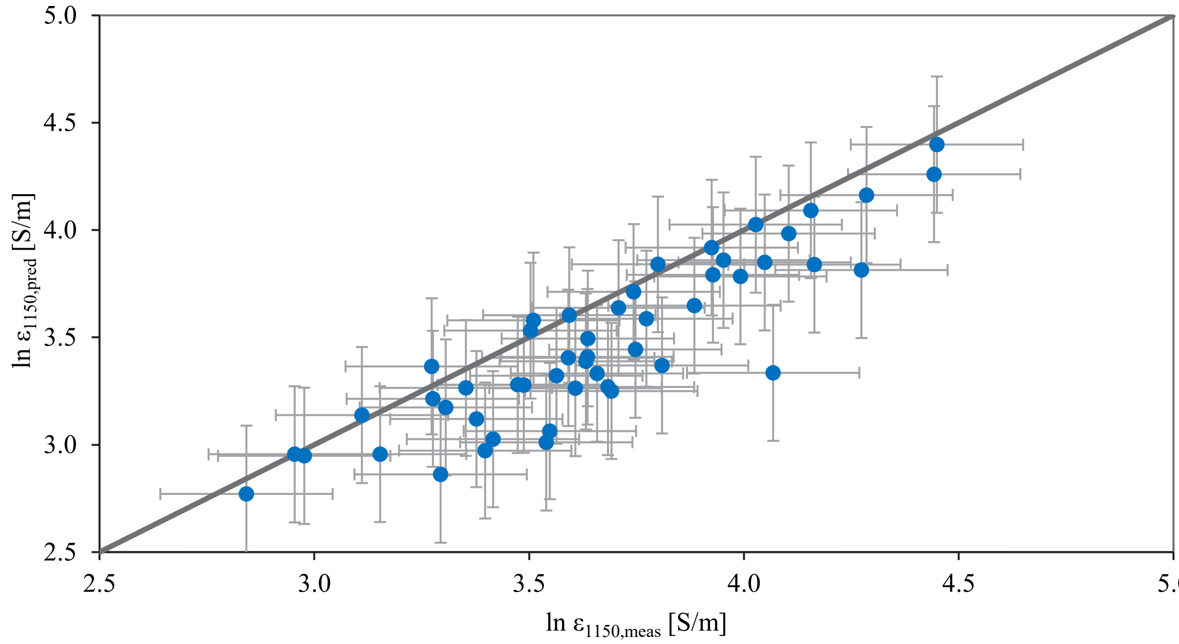

Figure 3.7. Measured vs. predicted ln(ε_{1150}). Uncertainties for measured values are represented by SD_{pooled} reported in Vienna et al. (2022).

3.8 Product Consistency Test

This section presents the PCT results obtained using the methods discussed in Section 2.11.

Per the WTP contract (DOE 2000), the Waste Acceptance Product Specification (DOE 1996) must be adhered to. That requires the NC_B, NC_{Na}, and NC_{Li} values to be below the associated values of the DWPF Environmental Assessment glass (Jantzen et al. 1993), which is presented in Table 3.13. The average normalized concentrations [NC_i; see Eq. (3.3)] for B, Na, Si, and Li for Q and CCC glass are reported in Table 3.12 and Table 3.13. As per ASTM C1285, the NC_i values presented in Table 3.12 and Table 3.13 are determined from triplicate tests with the following expression:

$$\mathrm{NC}_i = exp\,[avg\,\ln(\mathrm{NC}_i)] \qquad (3.3)$$

The NC_i for the individual tests are presented in Appendix L. The relative standard deviation between triplicate samples is less than 5%. The standard glass (ARM-1) was within the acceptance limits.

No glasses exceed the contract limits for the Q glasses, while several of the CCC glasses failed the contract limit, and these are bolded in Table 3.13. The nine glasses that failed the contract limit after CCC are HAL24M1-07, HAL24M1-16, HAL24M1-24, HAL24M1-25, HAL24M1-26, HAL24M1-27, HAL24M2-02, HAL24M2-09, and HAL24M2-12. In the CCC samples, HAL24M1-16, HAL24M1-24, HAL24M1-25, HAL24M1-26, HAL24M2-02, and HAL24M2-12 also have some of the highest nepheline contents (>8.9 wt%). HAL24M1-27 does not contain nepheline but does contain the sodalite phase nosean [$Na_8(Al_6Si_6O_{24})(SO_4)$], which removes the network formers Si and Al from the glass, which may result in the poor durability of this CCC glass. Lastly, a characteristic of this set of high-Al glasses is that the NC_{Na} values tend to bias lower than NC_B and NC_{Li}, especially for the glasses with higher NC_i values. This characteristic can be attributed to the need for charge compensation of $[AlO_4]^-$ units in the alteration layer. The charge compensation is initially performed by Ca^{2+}, but when that source has been exhausted, Na^{+} is retained.

Table 3.11. WTP PCT normalized release limits to HLW glass (g/L).

Constraint Description	Value	Source
PCT normalized B release	NC_B < 16.70 (g/L) ln(NC_B), g/L < 2.82	DOE 2000
PCT normalized Li release	NC_{Li} < 9.57 (g/L) ln($NC_{Li,}$), g/L < 2.26	DOE 2000
PCT normalized Na release	NC_{Na} < 13.35 (g/L) ln(NC_{Na}), g/L < 2.59	DOE 2000

Table 3.12. Average normalized concentrations (NC_i) in g/L for the HAL24 Q glasses. No values exceed the DWPF Environmental Assessment glass threshold listed in Table 3.11.

Glass ID	Boron	Silicon	Sodium	Lithium
HAL24M1-01	0.94	0.17	1.02	0.90
HAL24M1-02	2.38	0.26	1.84	1.82
HAL24M1-03	2.79	0.25	1.72	2.44
HAL24M1-04	11.56	0.17	6.11	9.46
HAL24M1-05	9.31	0.22	5.73	7.48
HAL24M1-06	2.32	0.23	2.03	2.26
HAL24M1-07	9.33	0.20	3.95	6.64
HAL24M1-08	4.94	0.19	3.46	4.30
HAL24M1-09	0.74	0.31	0.77	0.76
HAL24M1-10	7.52	0.22	3.73	5.50
HAL24M1-11	0.29	0.13	0.40	0.52
HAL24M1-12	0.43	0.11	0.53	0.37
HAL24M1-13	0.68	0.25	0.74	1.03
HAL24M1-14	0.52	0.23	0.61	0.52
HAL24M1-15	0.67	0.14	0.76	0.64
HAL24M1-16	0.60	0.17	0.68	0.64
HAL24M1-17	3.45	0.21	2.36	3.18
HAL24M1-18	0.46	0.25	0.42	0.65
HAL24M1-19	8.16	0.20	3.12	5.87
HAL24M1-20	2.85	0.32	2.13	2.61
HAL24M1-21	10.26	0.25	6.02	7.96
HAL24M1-22	5.33	0.23	3.36	4.22
HAL24M1-23	6.97	0.29	4.63	4.16
HAL24M1-24	1.42	0.32	1.62	0.81
HAL24M1-25	6.43	0.37	5.30	5.26
HAL24M1-26	1.13	0.20	1.19	0.99
HAL24M1-27	2.33	0.28	1.90	1.41
HAL24M1-28	3.78	0.25	2.31	2.93
HAL24M1-29	5.62	0.24	3.72	4.57
HAL24M1-30	9.23	0.20	5.84	---
HAL24M2-01	2.18	0.26	2.12	4.79
HAL24M2-02	7.70	0.62	5.34	4.39
HAL24M2-03	5.00	0.20	2.38	3.62
HAL24M2-04	6.56	0.22	3.63	3.58
HAL24M2-05	1.21	0.30	1.10	0.97
HAL24M2-06	2.74	0.14	2.29	2.66
HAL24M2-07	2.38	0.23	2.09	1.84
HAL24M2-08	0.65	0.16	0.72	0.68
HAL24M2-09	5.16	0.20	4.00	4.61
HAL24M2-10	0.55	0.09	0.63	0.61
HAL24M2-11	0.77	0.20	0.92	0.71
HAL24M2-12	8.08	0.20	5.31	6.22
HAL24M2-13	5.33	0.22	3.55	4.48
HAL24M2-14	6.32	0.25	3.69	4.69
HAL24M2-15	2.53	0.27	2.31	1.75
HAL24M2-16	2.05	0.24	1.60	1.97
HAL24M2-17	2.01	0.17	2.02	2.10
HAL24M2-18	2.26	0.24	1.70	2.13
HAL24M2-19	7.40	0.22	5.69	6.39
HAL24M2-20	1.56	0.27	1.32	1.47

Table 3.13. Average normalized concentrations (NC_i) in g/L for the HAL24 CCC glasses. Values exceed the DWPF Environmental Assessment glass threshold listed in Table 3.11 are in bold.

Glass ID	Boron	Silicon	Sodium	Lithium
HAL24M1-01	1.03	0.18	1.17	1.13
HAL24M1-02	1.45	0.27	1.23	1.17
HAL24M1-03	4.43	0.27	2.51	3.69
HAL24M1-04	10.04	0.18	5.36	8.28
HAL24M1-05	12.07	0.21	6.69	9.23
HAL24M1-06	2.02	0.27	1.78	1.98
HAL24M1-07	**20.35**	0.22	6.80	**13.83**
HAL24M1-08	8.11	0.23	4.92	6.89
HAL24M1-09	0.54	0.18	0.51	0.57
HAL24M1-10	11.90	0.22	4.99	7.39
HAL24M1-11	0.29	0.13	0.36	0.52
HAL24M1-12	6.42	0.06	2.95	7.56
HAL24M1-13	0.74	0.29	0.78	1.03
HAL24M1-14	1.36	0.25	0.99	1.15
HAL24M1-15	0.51	0.14	0.60	0.54
HAL24M1-16	**41.87**	0.05	**13.83**	**51.53**
HAL24M1-17	2.87	0.21	2.01	2.65
HAL24M1-18	0.50	0.32	0.43	0.66
HAL24M1-19	7.52	0.20	2.71	5.22
HAL24M1-20	2.59	0.32	1.96	2.43
HAL24M1-21	10.34	0.24	5.83	8.01
HAL24M1-22	6.20	0.24	3.70	4.76
HAL24M1-23	5.04	0.25	4.42	3.97
HAL24M1-24	**24.52**	0.31	**18.71**	**28.26**
HAL24M1-25	**89.25**	0.12	**43.26**	**78.76**
HAL24M1-26	**21.54**	0.07	10.89	**20.38**
HAL24M1-27	**44.44**	0.13	**18.67**	**34.46**
HAL24M1-28	3.71	0.21	2.18	2.78
HAL24M1-29	5.12	0.25	3.32	4.04
HAL24M1-30	10.93	0.21	6.49	--
HAL24M2-01	8.98	0.15	6.83	6.15
HAL24M2-02	**83.45**	0.17	**34.21**	**22.30**
HAL24M2-03	3.89	0.24	1.92	2.76
HAL24M2-04	4.38	0.23	2.43	1.40
HAL24M2-05	0.78	0.21	0.70	0.68
HAL24M2-06	0.39	0.11	0.43	0.53
HAL24M2-07	2.43	0.17	1.88	1.94
HAL24M2-08	0.80	0.19	0.81	0.80
HAL24M2-09	**20.58**	0.11	**13.76**	**20.45**
HAL24M2-10	0.38	0.10	0.40	0.42
HAL24M2-11	0.72	0.19	0.82	0.74
HAL24M2-12	**46.46**	0.32	**66.08**	**23.14**
HAL24M2-13	5.76	0.24	3.68	4.64
HAL24M2-14	3.68	0.27	2.25	2.86
HAL24M2-15	3.15	0.22	2.62	2.41
HAL24M2-16	11.73	0.24	5.46	8.48
HAL24M2-17	1.81	0.17	1.82	1.86
HAL24M2-18	3.25	0.24	2.19	2.88
HAL24M2-19	6.66	0.19	4.96	5.69
HAL24M2-20	2.01	0.28	1.55	1.80

A method that relies on a pooled standard deviation of PCT responses can be employed to determine if the difference between Q and CCC heat-treated glasses are within experimental error (Russell et al. 2025). Briefly, the method creates a range for $\ln(NC_{Na})$ and $\ln(NC_{Li})$ where if the measured $\ln(NC_{Na})$ and $\ln(NC_{Li})$ for Q and CCC glasses fall within that range, then the Q and CCC responses can be considered to be within experimental uncertainty. Fourteen of the 50 HAL24 glasses did not have Q and CCC PCT responses that were within experimental uncertainty: HAL24M1-07 [this glass passed for $\ln(NC_{Na})$ but failed for $\ln(NC_{Li})$ and $\ln(NC_{B})$], HAL24M1-12, HAL24M1-14, HAL24M1-16, HAL24M1-24, HAL24M1-25, HAL24M1-26, HAL24M1-27, HAL24M2-01, HAL24M2-02, HAL24M2-06, HAL24M2-09, HAL24M2-12, and HAL24M2-16.

Figure 3.8 presents the differences between $\ln(NC_{i})$ values for Q and CCC glasses. For most of the Q and CCC responses, the high degree of crystallinity in the CCC resulted in a disruption to the network connectivity and less durable glass. All of the HAL24 glasses with statistically significant differences between Q and CCC responses contained more than 5 wt% of crystals in the CCC glass except for HAL24M2-09, which contained 2.2 wt% nepheline. Glasses HAL24M1-12, HAL24M1-16, HAL24M1-24, HAL24M1-25, and HAL24M2-02 contained more than 20 wt% crystalline phases. HAL24M1-12 has 25.2 wt% nepheline, and although it met the contract requirements for NC_{i} there was a statical difference between Q and CCC values due to crystallization. However, the presence of nepheline is only an indicator that the glass will be less durable. But there's so many coupled effects in these complex glasses, it's hard to isolate these impacts. The general contributors that lead to less durable glasses are understood, but occasionally there are outliers that require much more research to determine the cause of this behavior.

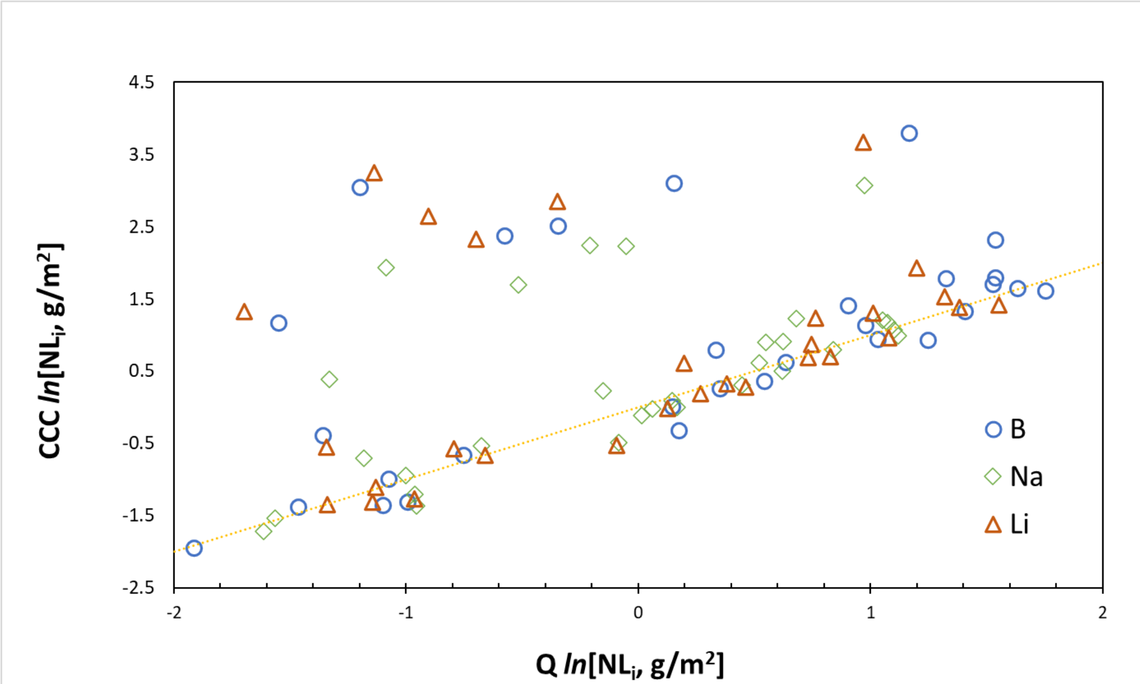

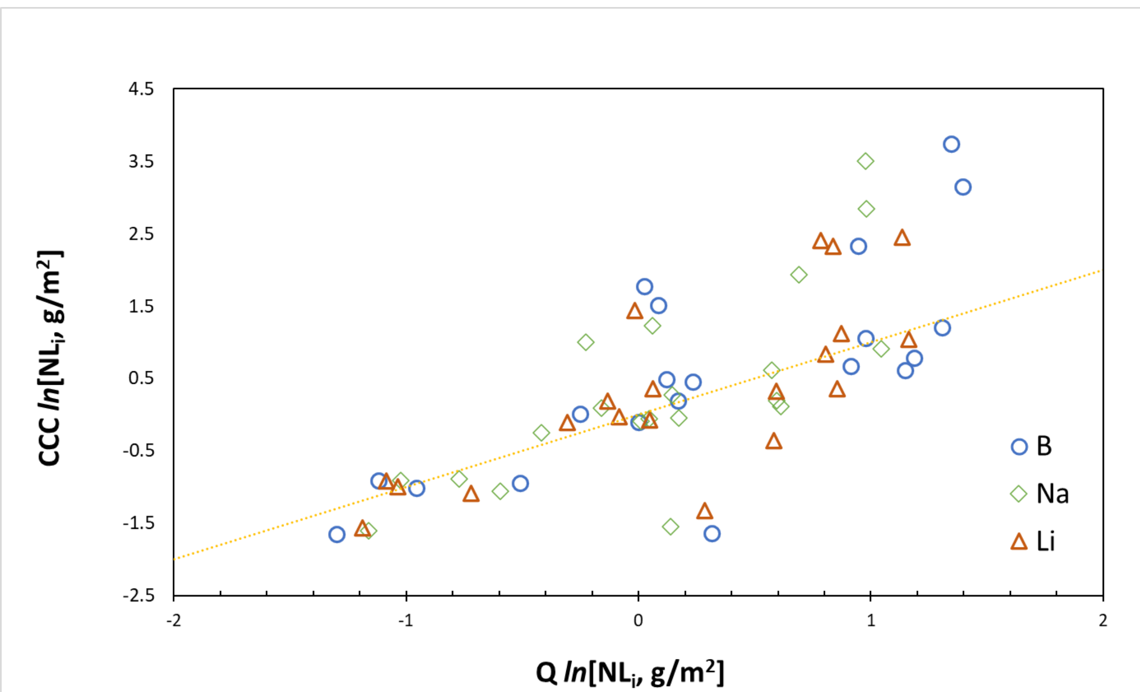

Figure 3.8. Normalized NL_B, NL_{Li}, and NL_{Na} release in natural logarithm scale of Q vs. CCC for HAL24M1 glasses (top) and HAL24M2 glasses (bottom).

Figure 3.9 shows measured average $\ln(NL_B)$ and $\ln(NL_{Na})$ values plotted against model predictions from Vienna et al. (2024) and Vienna and Crum (2018). All HAL24 glasses were designed to have a release less than < 10 g/L, and all of the quenched samples were within this limit. Visually, the Vienna and Crum (2018) model seems to predict better than the Vienna et al. (2024) model.

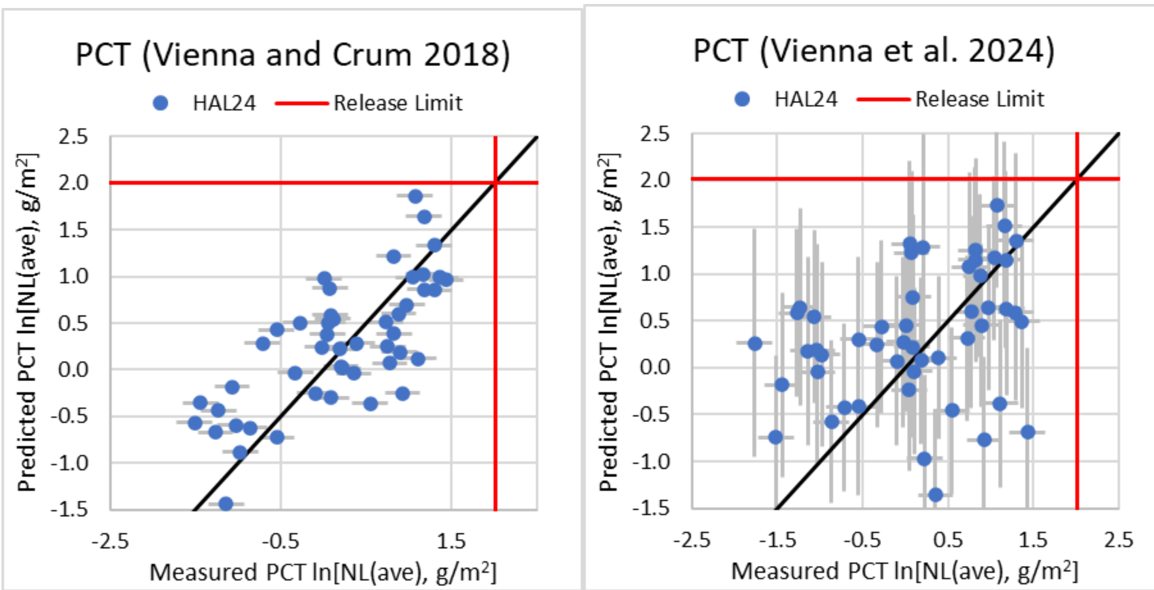

Figure 3.9. Uncertainties for measured values are represented by SD_{pooled} reported in Vienna et al. (2022). The release limit is the average of the B and Na release limit presented in Table 3.12.

3.9 Toxicity Characteristic Leaching Procedure

This section presents the TCLP results obtained using the methods discussed in Section 2.7.

3.9.1 Results and Comparisons to the Delisting Results

Figure 3.10 summarizes the measured TCLP leachate concentrations of B, Cr, Ni, Pb, V, and Zn for Q and CCC HAL24 glasses compared to the analytical detection limits and the delisting limits for the constituent of concerns (Blumenkranz 2006). The detection limit value is provided for tests that returned concentrations below detection limits. Full results are presented in Appendix L. For Cr, Ni, and Pb, most glasses had TCLP leachate concentrations below detection limits. When TCLP leachate concentrations registered above detection limits, they mostly originated from CCC glasses. No glass surpassed the delisting limits for Pb and Ni, while only HAL24M2-02-CCC surpassed the delisting limit for Cr. Several glasses – both Q and CCC glasses – had measured TCLP leachate concentrations above detection limits for V and Zn. No glasses surpassed the Zn delisting limit, but HAL24M1-09-CCC and HAL24M1-24-CCC each surpassed the V delisting limit.

Figure 3.11 plots the CCC and Q measured TCLP leachate concentrations together. In general, the CCC glasses release higher concentrations of B, Cr, Ni, Pb, V, and Zn than the Q glasses, with some exceptions (see Figure 3.10 and Appendix M).

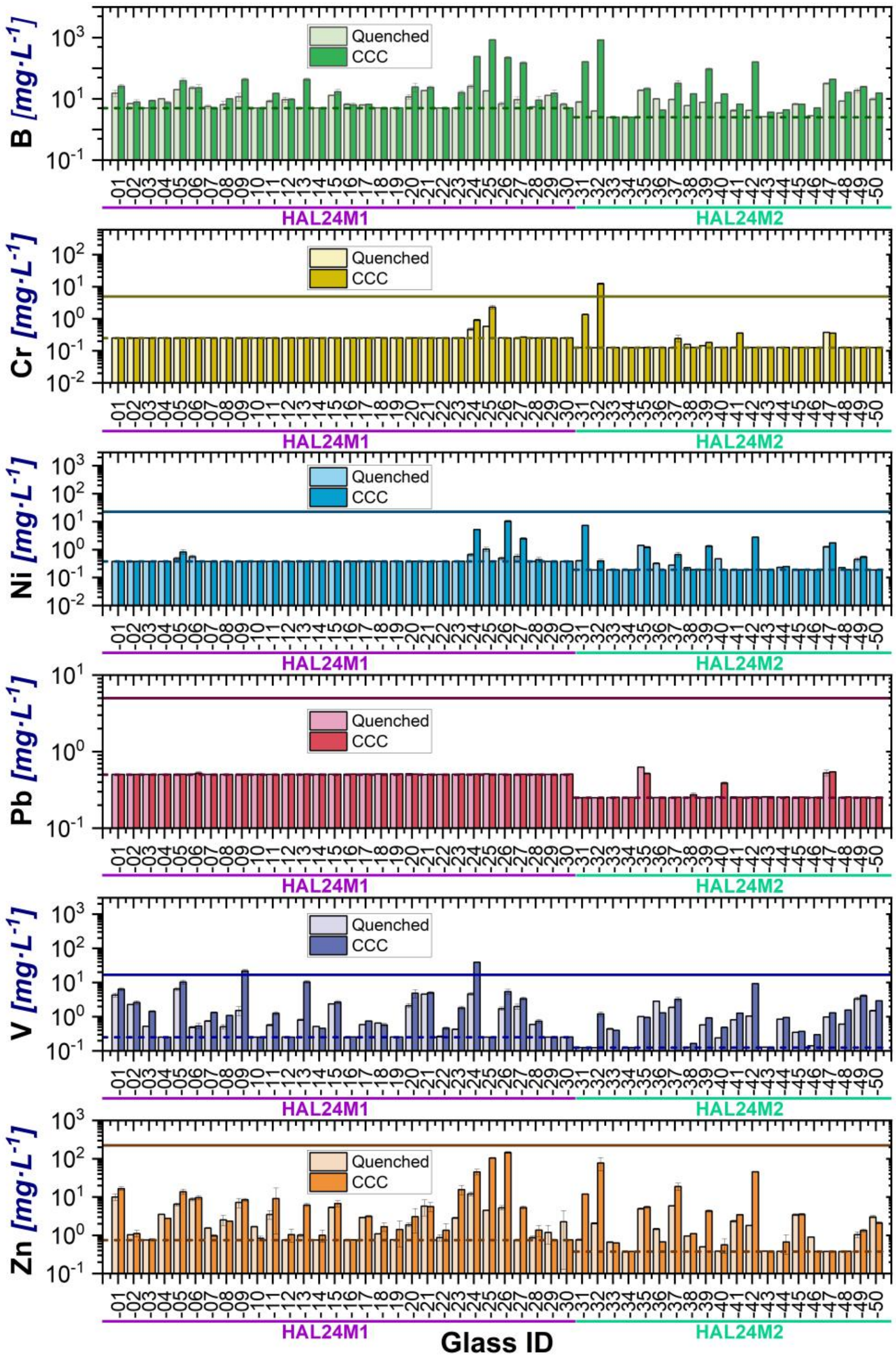

Figure 3.10. TCLP leachate concentrations for B, Cr, Ni, Pb, V, and Zn for Q and CCC HAL24 glasses. The HAL24M1 and HAL24M2 series are indicated for each plot. The solid color line represents the delisting limits while the dashed lines specify the analytical detection limit. Note that HAL24M1 and HAL24M2 have different detection limits.

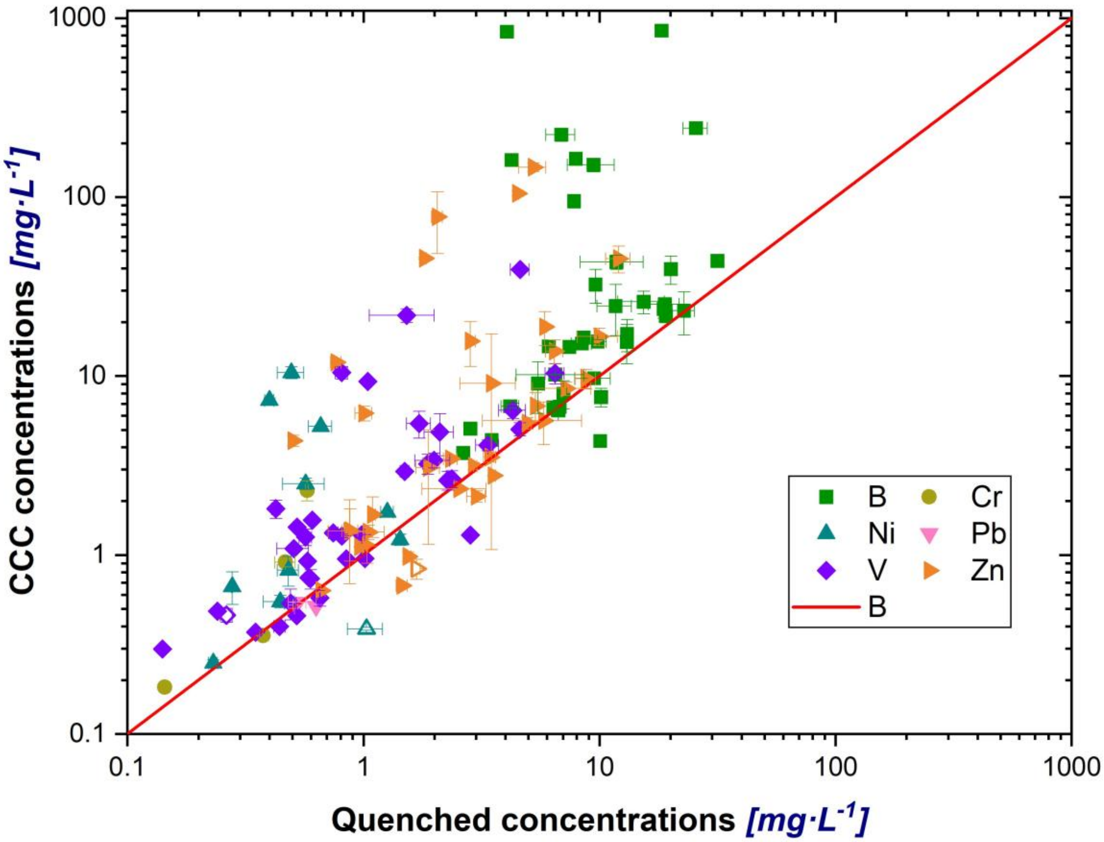

Figure 3.11. Measured TCLP leachate concentrations for B, Cr, Ni, Pb, V, and Zn for Q and CCC HAL24 glasses. All results that were below detections for both replicates were excluded. Open symbols represent results determined from one replicate with its measured value and one replicate with the detection limit. The red line represents the 1-1 correlation between the Q and CCC values.

3.9.2 Comparisons of Measured to Predicted TCLP Leachate Concentrations

The NC_B values from the Q glasses determined experimentally for the HAL24 matrix were compared to predicted NC_B values generated from the TCLP models in Vienna et al. (2009) and Kim and Vienna (2002) and are presented in Figure 3.12. Both models provide NC_B values that are quite scattered across the 1-1 correlation line; however, in general, the predicted NC_B values were higher.

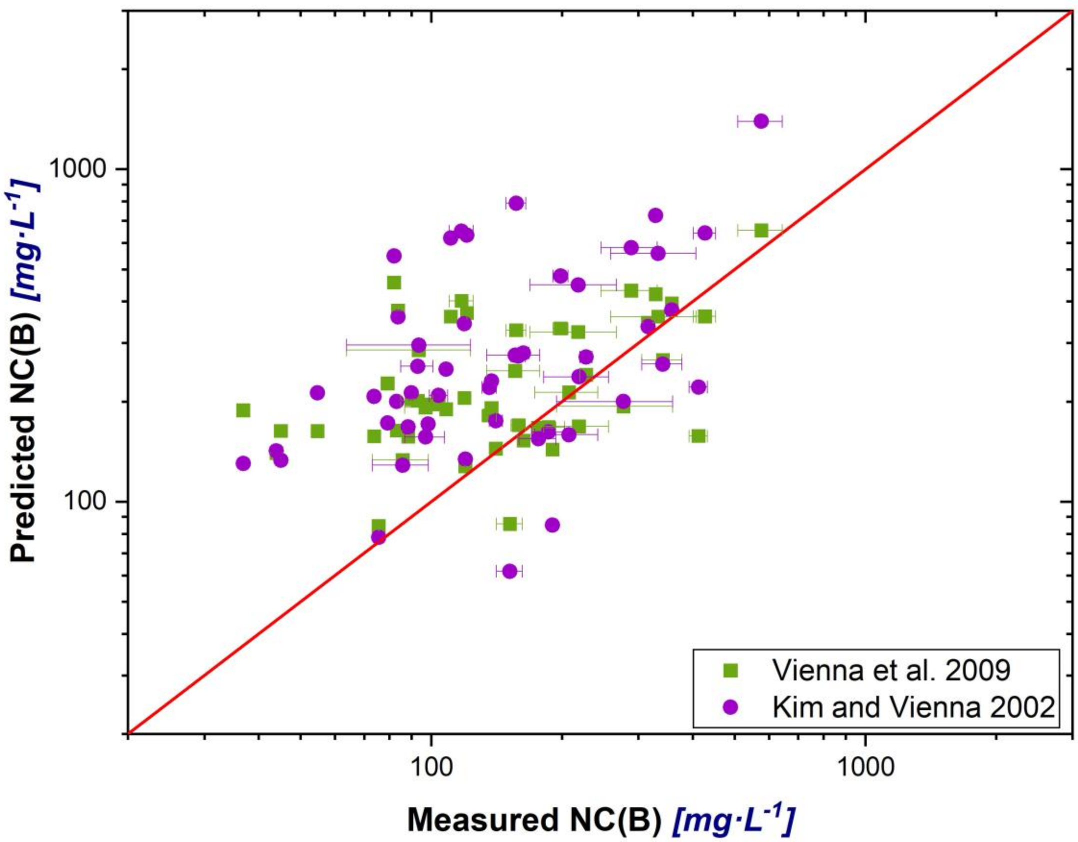

Figure 3.12. Measured and predicted NC_B from the Vienna et al. (2009) and Kim and Vienna (2002) models. Results are only provided for measured NC_B with results above the detection limits. The red line represents the 1-1 correlation between the measured and predicted values.

Predicted TCLP leachate concentrations of element *i* ($c_{i,pred}$) were calculated using the following equation from Kim and Vienna (2004).

$$c_{i,pred} = NC(B)_{pred} \cdot f_i \tag{3.4}$$

where $NC_{B,pred}$ is the predicted NC_B using the Kim and Vienna (2002) and Vienna et al. (2009) models and f_i is the mass fraction of element *i* in the unaltered glass.

Figure 3.13 and Figure 3.14 show measured and predicted TCLP releases from Kim and Vienna (2002) and Vienna et al. (2009) for Cr, Ni, Pb, V, and Zn. All measured values below the detection limit were excluded. As a result, fewer results are available for some species such as Cr and Pb compared to other species such as V and Zn. The predicted values follow the same trend as the 1-1 correlation line, but the predicted values in general are higher than the experimental values.

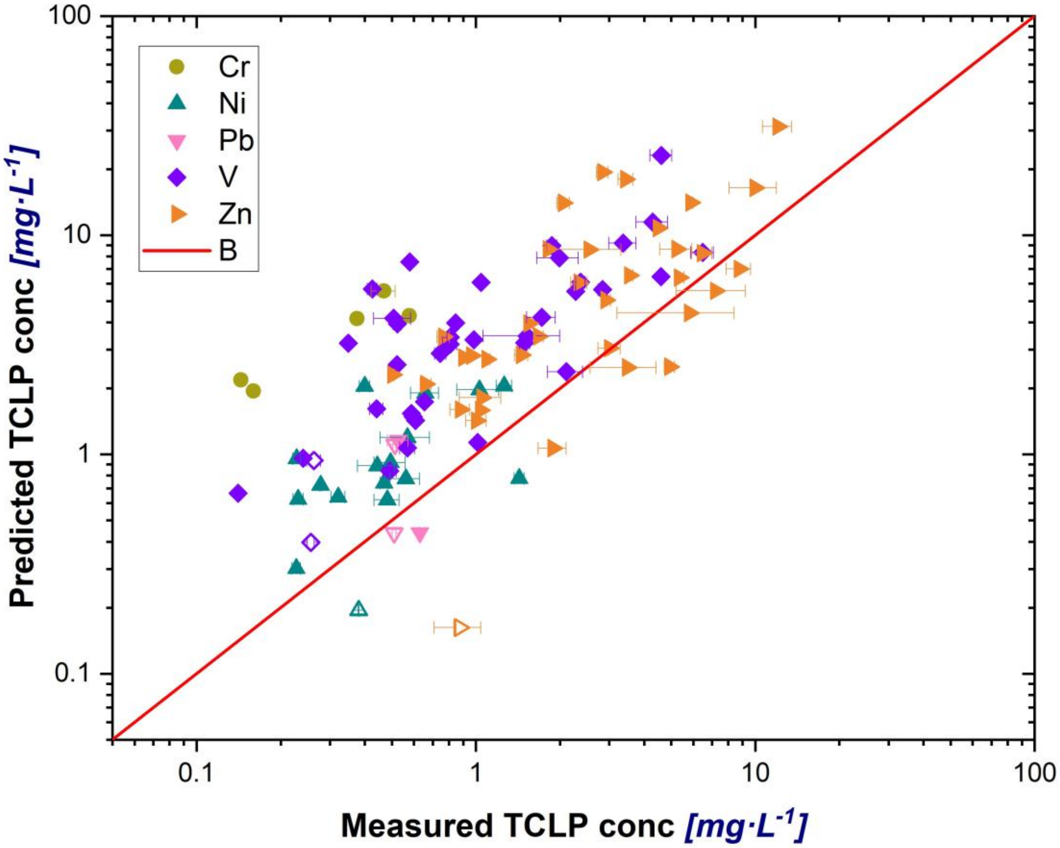

Figure 3.13. Measured and predicted TCLP releases from Kim and Vienna (2002) for Cr, Ni, Pb, V, and Zn. All measured values below detection limits for both replicates were excluded. Open symbols represent results determined from one replicate with its measured value and one replicate with the detection limit. The red line represents the 1-1 correlation between the measured and predicted values.

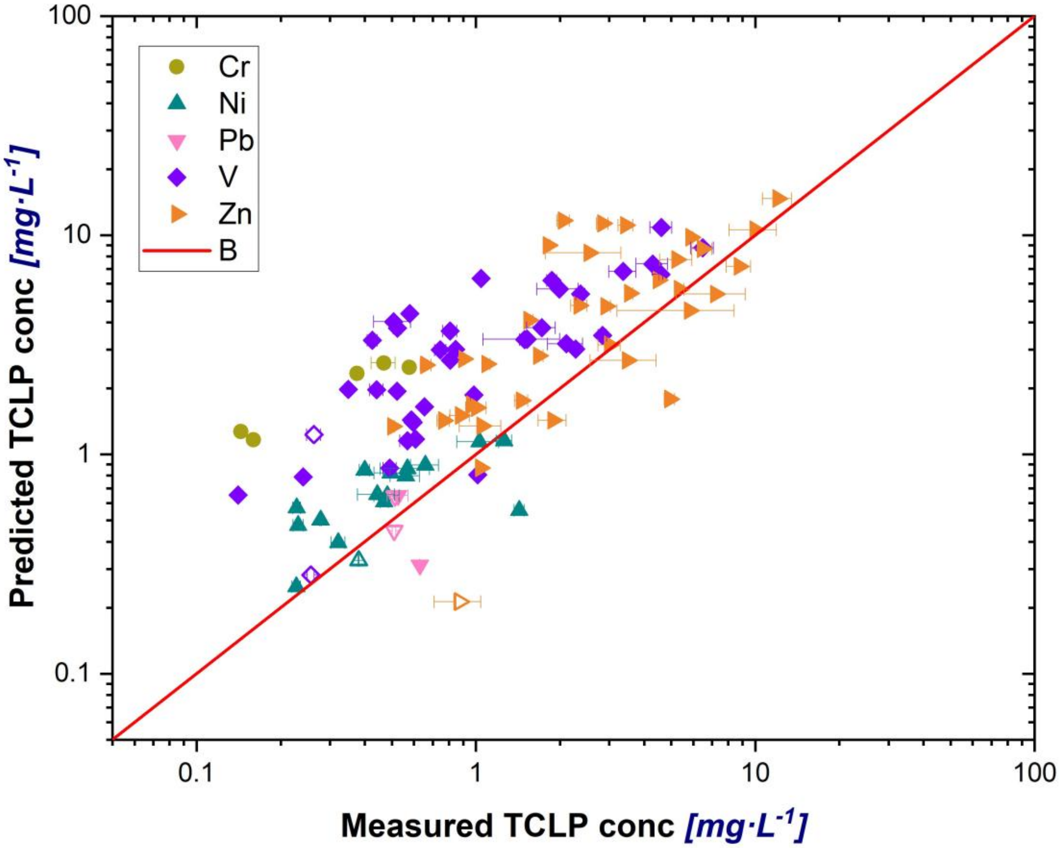

Figure 3.14. Measured and predicted TCLP releases from Vienna et al. (2009) for Cr, Ni, Pb, V, and Zn. All measured values below detection limits for both replicates were excluded. Open symbols represent results determined from one replicate with its measured value and one replicate with the detection limit. The red line represents the 1-1 correlation between the measured and predicted values.

4.0 Conclusions

A glass matrix containing high Al_2O_3 with a total of 50 glasses was designed in this study, expanding DFHLW glass compositional ranges. This matrix was designed using a space-filling method with component concentration boundaries obtained by expanding the existing database and results from the EWG-based formulations. This 50-glass matrix satisfied the success criteria for the dispersion ratio and range of coverage. The designed glass compositions were fabricated and tested, including compositions, CCC and isothermal heat treatments, density, viscosity, EC, PCT, TCLP, and sulfate solubility.

Table 4.1 summarizes the HAL24 glasses passing or failing the property constraints. Out of the 50 glasses tested, 14 glasses formed nepheline, while the model predicted nepheline formation in 20 glasses. All Q glasses satisfy the PCT durability constraint; however, 8 glasses failed this constraint after undergoing the CCC treatment. Additionally, 17 glasses did not satisfy the viscosity constraints, 4 failed the EC constraints, and 2 exceeded the allowable $T_{2\%}$ for spinel crystal formation. All glasses satisfied the SO_3 solubility limit. The failures in specific properties were intentionally incorporated during matrix design and are essential for defining acceptable processing envelopes for DFHLW operations. Data generated near property constraint boundaries are particularly critical, as they improve model accuracy and robustness, increase predictive accuracy in boundary regions, and reduce uncertainties in defining processing limits.

These glasses were intentionally designed with high aluminum concentrations (15 to 30 wt%) and a high likelihood of nepheline formation, which is known to negatively affect glass durability. Some glasses were expected to either fail or approach property constraints to fill data gaps in poorly understood regions of the compositional space due to lack of data.

The resulting dataset provides valuable information to improve model accuracy and reduce prediction uncertainty. These insights will ultimately support the development of more robust glass formulation strategies, enabling higher waste loadings, reducing operational risks, and expanding the processing envelope.

Table 4.1. Summary of the 50 HAL24 glasses passing or failing property constraints. Property constraints were taken from Vienna et al. (2025).

z	w_{SO3}	η_{1150}	ε_{1150}	PCT Q	PCT CCC	Pred NP F/P	Meas NP F/P	Spinel $T_{2\%}$
Constraints	SO_3 in glass < w_{SO3}	20 to 80 Poise	10 to 70 S/m	<6.44 g/m^2	<6.44 g/m^2	Model Predicted Nepheline Formation	Measured Nepheline Formation	F if Spinel vol% >2% at 950 °C
HAL24M1-01	P	F	P	P	P	P	P	P
HAL24M1-02	P	P	P	P	P	P	P	P
HAL24M1-03	P	F	P	P	P	P	P	P
HAL24M1-04	P	F	P	P	P	P	P	P
HAL24M1-05	P	P	P	P	P	F	F	P
HAL24M1-06	P	P	P	P	P	P	P	P
HAL24M1-07	P	P	P	P	P	P	P	P
HAL24M1-08	P	P	P	P	P	P	P	P
HAL24M1-09	P	F	P	P	P	F	P	F
HAL24M1-10	P	P	P	P	P	P	P	P
HAL24M1-11	P	P	P	P	P	F	P	F
HAL24M1-12	P	P	P	P	P	F	P	P
HAL24M1-13	P	P	P	P	P	F	P	P

z	w_{SO3}	η_{1150}	ε_{1150}	PCT Q	PCT CCC	Pred NP F/P	Meas NP F/P	Spinel $T_{2\%}$
Constraints	SO_3 in glass < w_{SO3}	20 to 80 Poise	10 to 70 S/m	<6.44 g/m^2	<6.44 g/m^2	Model Predicted Nepheline Formation	Measured Nepheline Formation	F if Spinel vol% >2% at 950 °C
HAL24M1-14	P	P	P	P	P	P	P	P
HAL24M1-15	P	P	P	P	P	P	P	P
HAL24M1-16	P	P	P	P	F	F	F	P
HAL24M1-17	P	F	P	P	P	P	P	P
HAL24M1-18	P	P	P	P	P	P	P	P
HAL24M1-19	P	F	P	P	P	P	P	P
HAL24M1-20	P	P	P	P	P	F	P	P
HAL24M1-21	P	P	P	P	P	F	P	P
HAL24M1-22	P	P	P	P	P	P	P	P
HAL24M1-23	P	F	F	P	P	F	F	P
HAL24M1-24	P	F	P	P	F	F	F	P
HAL24M1-25	P	F	F	P	F	F	F	P
HAL24M1-26	P	P	P	P	F	F	F	P
HAL24M1-27	P	P	P	P	F	F	F	P
HAL24M1-28	P	P	P	P	P	P	P	P
HAL24M1-29	P	P	P	P	P	P	P	P
HAL24M1-30	P	P	P	P	P	P	P	P
HAL24M2-01	P	F	P	P	P	F	F	P
HAL24M2-02	P	F	F	P	F	F	F	P
HAL24M2-03	P	F	P	P	P	P	F	P
HAL24M2-04	P	P	F	P	P	P	F	P
HAL24M2-05	P	P	P	P	P	F	P	P
HAL24M2-06	P	P	P	P	P	P	P	P
HAL24M2-07	P	F	P	P	P	F	P	P
HAL24M2-08	P	F	P	P	P	P	P	P
HAL24M2-09	P	F	P	P	F	P	F	P
HAL24M2-10	P	P	P	P	P	P	P	P
HAL24M2-11	P	P	P	P	P	P	F	P
HAL24M2-12	P	P	P	P	F	F	F	P
HAL24M2-13	P	F	P	P	P	P	P	P
HAL24M2-14	P	P	P	P	P	P	P	P
HAL24M2-15	P	P	P	P	P	F	P	P
HAL24M2-16	P	P	P	P	P	P	P	P
HAL24M2-17	P	F	P	P	P	P	P	P
HAL24M2-18	P	P	P	P	P	P	P	P
HAL24M2-19	P	P	P	P	P	F	P	P
HAL24M2-20	P	P	P	P	P	P	P	P
Total F	0	17	4	0	8	20	14	2

5.0 Bibliography

10 CFR 830, *Nuclear Safety Management*. Code of Federal Regulations, as amended.

Alton J, J Plaisted, and P Hrma. 2002. "Kinetics of Growth of Spinel Crystals in a Borosilicate Glass." *Chemical Engineering Science* 57:2503-2509.

ASTM C1720, *Standard Test Method for Determining Liquidus Temperature of Immobilized Waste Glasses and Simulated Waste Glasses*. ASTM International, West Conshohocken, PA.

ASTM C1285, *Standard Test Methods for Determining Chemical Durability of Nuclear, Hazardous, and Mixed Waste Glasses and Multiphase Glass Ceramics: The Product Consistency Test (PCT).* ASTM International, West Conshohocken, PA.

ASTM D6323-19, *Standard Guide for Laboratory Subsampling of Media Related to Waste Management Activities*. West Conshohocken, PA, ASTM International, West Conshohocken, PA.

Blumenkranz DB. 2006. *Petition to Delist Immobilized High-Level Waste Generated at the Hanford Tank Waste Treatment and Immobilization Plant.* 24590-WTP-RPT- DB ENV-06-001, Rev. 0, River Protection Project, Hanford Waste Treatment and Immobilization Plant, Richland, WA.

Britton MD. 2023. "Preliminary Direct-Feed High-Level Waste Washing and Blending Study Results." Memo to T Wagnon, Jan 27, 2023, WRPS-2300408, Washington River Protection Solutions, Richland, WA.

Certa PJ, TM Hohl, AM Johnson, SL Orcutt, RS Wittman, and DS Kim. 2005. *Sensitivity of Hanford Immobilized High Level Waste Glass Mass to Chromium and Aluminum Partitioning Assumptions*. RPP-20003, Rev. 1, CH2M Hill Hanford Group, Richland, WA.

DOE. 1996. *Waste Acceptance Product Specifications for Vitrified High-Level Waste Forms (WAPS)*. DOE/EM-0093, U.S. Department of Energy, Office of Environmental Management, Washington, D.C.

DOE. 2000. *Design, Construction, and Commissioning of the Hanford Tank Waste Treatment and Immobilization Plant*. Contract DE-AC27-01RV14136, as amended, U.S. Department of Energy, Office of River Protection, Richland, WA.

DOE Order 414.1D, *Quality Assurance*. U.S. Department of Energy, Washington, D.C.

EPA Method 1311, "Toxicity Characteristic Leaching Procedure (TCLP)." In *Test Methods for Evaluating Solid Waste, Physical/Chemical Methods*. EPA Publication SW-846, U.S. Environmental Protection Agency, Washington, D.C.

Gervasio V, X Lu, JT Reiser, M Peterson, NL Canfield, JB Lang, JC Rigby, J George, DA Cutforth, JM Westman, et al. 2024. *Direct Feed High-Level Waste APPS Model Glass Testing (DFHLW APPS) Matrix*. PNNL-35503, Pacific Northwest Laboratory, Richland, WA.

Herman CC, PR Dixon, TM Brouns, ME Stone, RT Jubin, KG Picha, MS Vassiliou, RP Miklos, SM Robinson, MJ Rigali, et al. 2022. *R&D Roadmap for Hanford Tank Waste Mission Acceleration*. NNLEMS-2022-00005, Rev. 0, Network of National Laboratories for Environmental Management and Stewardship, Washington, D.C.

Jantzen CM, NE Bibler, DC Beam, CL Crawford, and MA Pickett. 1993. *Characterization of the Defense Waste Processing Facility (DWPF) Environmental Assessment (EA) Glass Standard Reference Material*. WSRC-TR-92-346, Rev. 1, Westinghouse Savannah River Company, Aiken, SC.

Jin T, DS Kim, LP Darnell, BL Weese, NL Canfield, M Bliss, MJ Schweiger, JD Vienna, and AA Kruger. 2018. "A Crucible Salt Saturation Method for Determining Sulfur Solubility in Glass Melt." *International Journal of Applied Glass Science* 10:92-102.

Joseph R, E Gui, and S Ba. 2015. "Maximum Projection Designs for Computer Experiments." *Biometrika* 102(2):371-380.

Kim DS, D Peeler, and P Hrma. 1995. "Effect of Crystallization on the Chemical Durability of Simulated Nuclear Waste Glasses." In *Environmental Issues and Waste Management Technologies in the Ceramic and Nuclear Industries* 177-186.

Kim DS and JD Vienna. 2002. *Model for TCLP Releases from Waste Glasses*. PNNL-14061, Pacific Northwest National Laboratory, Richland, WA.

Kim D and JD Vienna. 2004. "Glass Composition-TCLP Response Model for Waste Glasses." In *Environmental Issues and Waste Management Technologies in the Ceramic and Nuclear Industries IX*. John Wiley & Sons, Hoboken, NJ.

Kot WK, K Gilbo, H Gan, and IL Pegg. 2019. *Enhancement of HLW Glass Property-Composition Models*. VSL-19R4480-1, Vitreous State Laboratory, The Catholic University of America, Washington, D.C.

Kroll JO, ZJ Nelson, CH Skidmore, DA Dixon, and JD Vienna. 2019. "Formulation of High-Al_2O_3 Waste Glasses from Projected Hanford Waste Compositions and Assessment of Current Glass Property Models." *Journal of Non-Crystalline Solids* 517:17-25.

Kruger A. 2023. *Toxicity Characteristic Leaching Procedure (TCLP) Testing of Selected High-Level Waste (HLW) Simulant Glasses*. QAPP ID# CRESP-VU-ORP-2023-0001, U.S. Department of Energy, Office of River Protection, Richland, WA.

Lu X, T Jin, JD Vienna, and CL Trivelpiece. 2023. *Waste Glass Property Database and Data Qualification Plan*. PNNL-34447, Pacific Northwest National Laboratory, Richland, WA.

Lu X, I Sargin, and JD Vienna. 2021. "Predicting nepheline precipitation in waste glasses using ternary submixture model and machine learning." *Journal of American Ceramic Society* 104:5636-5647.

Matyáš J, JD Vienna, A Kimura, M Schaible, and RM Tate. 2010. "Development of Crystal-Tolerant Waste Glasses." *Ceramic Transactions* 222:41-51.

Mellinger GB and JL Daniel. 1984. *Approved Reference and Testing Materials for Use in Nuclear Waste Management Research and Development Programs*. PNL-4955-2, Pacific Northwest Laboratory, Richland, WA. https://doi.org/10.2172/6224421

NQA-1-2012, *Quality Assurance Requirements for Nuclear Facility Applications*. American Society of Mechanical Engineers, New York, NY.

Peeler DK, JD Vienna, MJ Schweiger, and KM Fox. 2015. *Advanced High-Level Waste Glass Research and Development Plan*. PNNL-24450, Pacific Northwest National Laboratory, Richland, WA.

Petkus LL. 2003. "Canister Centerline Cooling Data, Revision 1." To CA Musick, Oct 29, 2003. CCN 074851, River Protection Project, Waste Treatment and Immobilization Plant, Richland, WA.

Russell RL, V Gervasio, X Lu, S Chong, JT Reiser, NL Canfield, JL George, NA Lumetta, J Neeway, LM Seymour. 2025. *Direct Feed High Level Waste APPS Model Glass Testing (DFHLW APPS) Matrix, Phase 2*. PNNL-37506, Pacific Northwest National Laboratory, Richland, WA.

Skidmore CH, JD Vienna, T Jin, D Kim, BA Stanfill, KM Fox, and AA Kruger. 2019. "Sulfur solubility in low activity waste glass and its correlation to melter tolerance." *International Journal of Applied Glass Science* 10(4):558-568.

Smith GL. 1993. *Characterization of Analytical Reference Glass-1 (ARG-1)*. PNL-8992, Pacific Northwest Laboratory, Richland, WA.

Vienna, JD, P Hrma, JV Crum, and M Mika. 2001. "Liquidus temperature-composition model for multi-component glasses in the Fe, Cr, Ni, and Mn spinel primary phase field." *Journal of Non-Crystalline Solids* 292(1-3):1-24.

Vienna, JD, D Kim, and P Hrma. 2002. *Database and Interim Glass Property Models for Hanford HLW and LAW Glasses*. PNNL-14060, Pacific Northwest National Laboratory, Richland, WA.

Vienna JD, A Fluegel, DS Kim, and P Hrma. 2009. *Glass Property Data and Models for Estimating High-Level Waste Glass Volume*. PNNL-18501, Pacific Northwest National Laboratory, Richland, WA.

Vienna JD, DC Skorski, DS Kim, and J Matyáš. 2013. *Glass Property Models and Constraints for Estimating the Glass to be Produced at Hanford by Implementing Current Advanced Glass Formulation Efforts*. PNNL-22631, Rev. 1, Pacific Northwest National Laboratory, Richland, WA.

Vienna JD and DS Kim. 2014. *Preliminary IHLW Formulation Algorithm Description*. 24590-HLW-RPT-RT-05-001, Rev. 1, River Protection Project, Waste Treatment and Immobilization Plant, Richland, WA.

Vienna JD, GF Piepel, DS Kim, JV Crum, CE Lonergan, BA Stanfill, BJ Riley, SK Cooley, and T Jin. 2016. *2016 Update of Hanford Glass Property Models and Constraints for Use in Estimating the Glass Mass to be Produced at Hanford by Implementing Current Enhanced Glass Formulation Efforts*. PNNL-25835, Pacific Northwest National Laboratory, Richland, WA.

Vienna JD, JO Kroll, PR Hrma, JB Lang, and JV Crum. 2017. "Submixture model to predict nepheline precipitation in waste glasses." *International Journal of Applied Glass Science* 8(2):143-157.

Vienna JD and JV Crum. 2018. "Non-linear effects of alumina concentration on Product Consistency Test response of waste glasses." *Journal of Nuclear Materials* 511:396-405.

Vienna JD, A Heredia-Langner, SK Cooley, AE Holmes, DS Kim, and NA Lumetta. 2022. *Glass Property-Composition Models for Support of Hanford WTP LAW Facility Operation*. PNNL-30932, Rev. 2, Pacific Northwest National Laboratory, Richland, WA.

Vienna JD, X Lu, P Ferkl, J Marcial, MS Fountain, M Trenidad, R Hanson, MD Britton, L Cree, and W Abdul. 2023. "High-Level Waste Glass Processing over Broad Range of Alternative Feed Compositions." Waste Management Symposia 2023, February 26-March 2, 2023, Phoenix, AZ.

Vienna JD, X Lu, P Ferkl, LL Gunnell, A Heredia-Langner, NA Lumetta, T Jin, et al. 2024. *Glass Property-Composition Models Update for Use in Direct Feed High-Level Waste Flowsheet Development*. PNNL-35884, Pacific Northwest National Laboratory, Richland, WA.

Vienna JD, X Lu, P Ferkl, D Kim, J Marcial, J Bai, JV Crum, et al. 2025. *Glass Property-Composition Models Update for Use in Direct Feed High-Level Waste Flowsheet Development: EWG2.6*. PNNL-37762, Pacific Northwest National Laboratory, Richland, WA.

.

Appendix A – Heatmap and Scatter Plots

The information in this appendix is to be used for information only. These figures show the pair correlations of a few major glass components (e.g., Al_2O_3, B_2O_3, SiO_2, Na_2O). Figures on the left show the design space (whole ranges) as blue heatmaps, 50 glasses for tests as black x's, nepheline data that were conducted/collected under insufficient quality assurance (QA) requirements as pink triangles. Figures on the right show the design space (where glasses pass the property constraints) as blue heatmaps, 50 glasses for tests as black x's, nepheline data that were conducted/collected under sufficient QA requirements as pink dots.

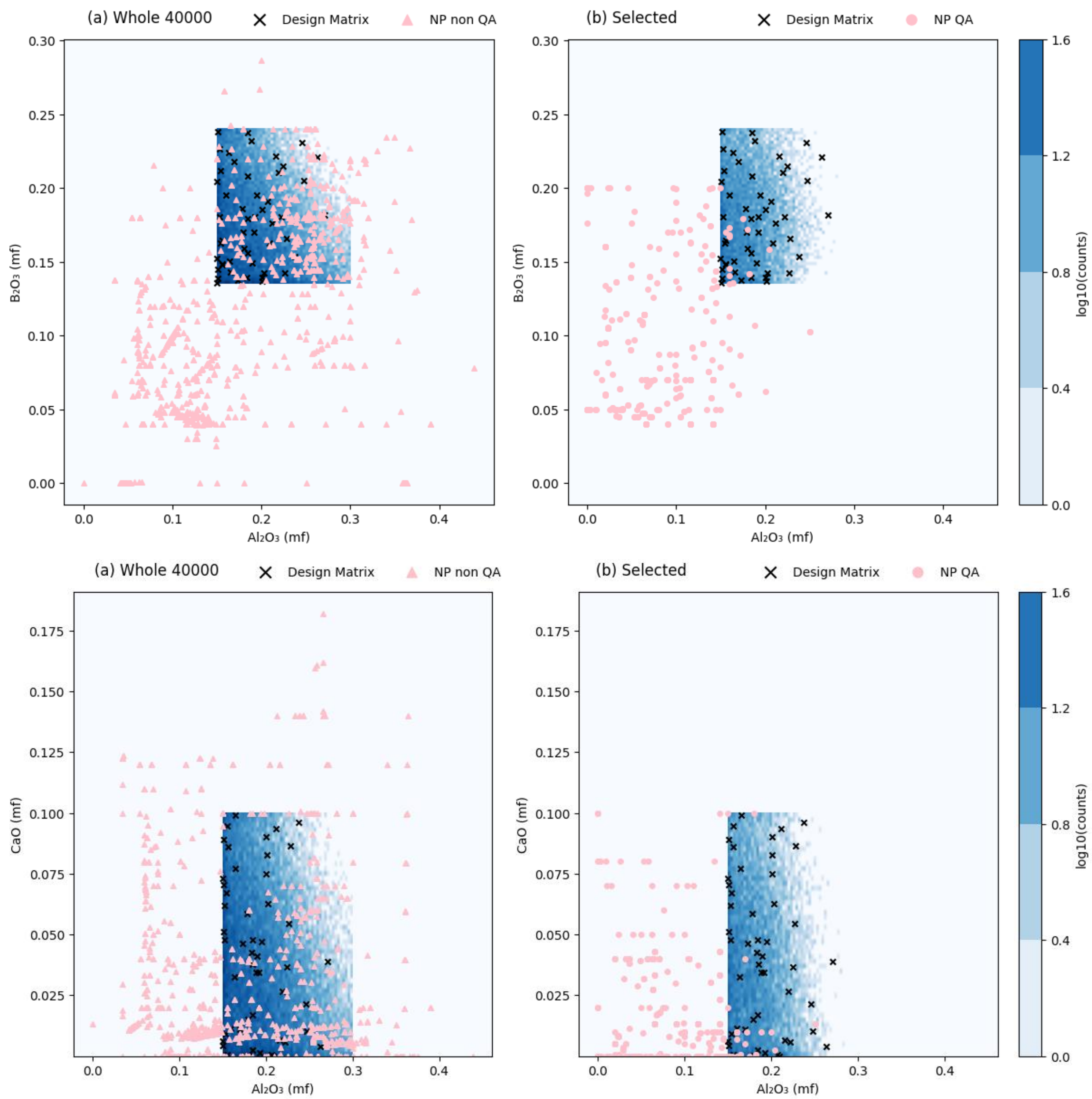

Figure A.1. Heatmaps of Al_2O_3 vs. B_2O_3 and CaO.

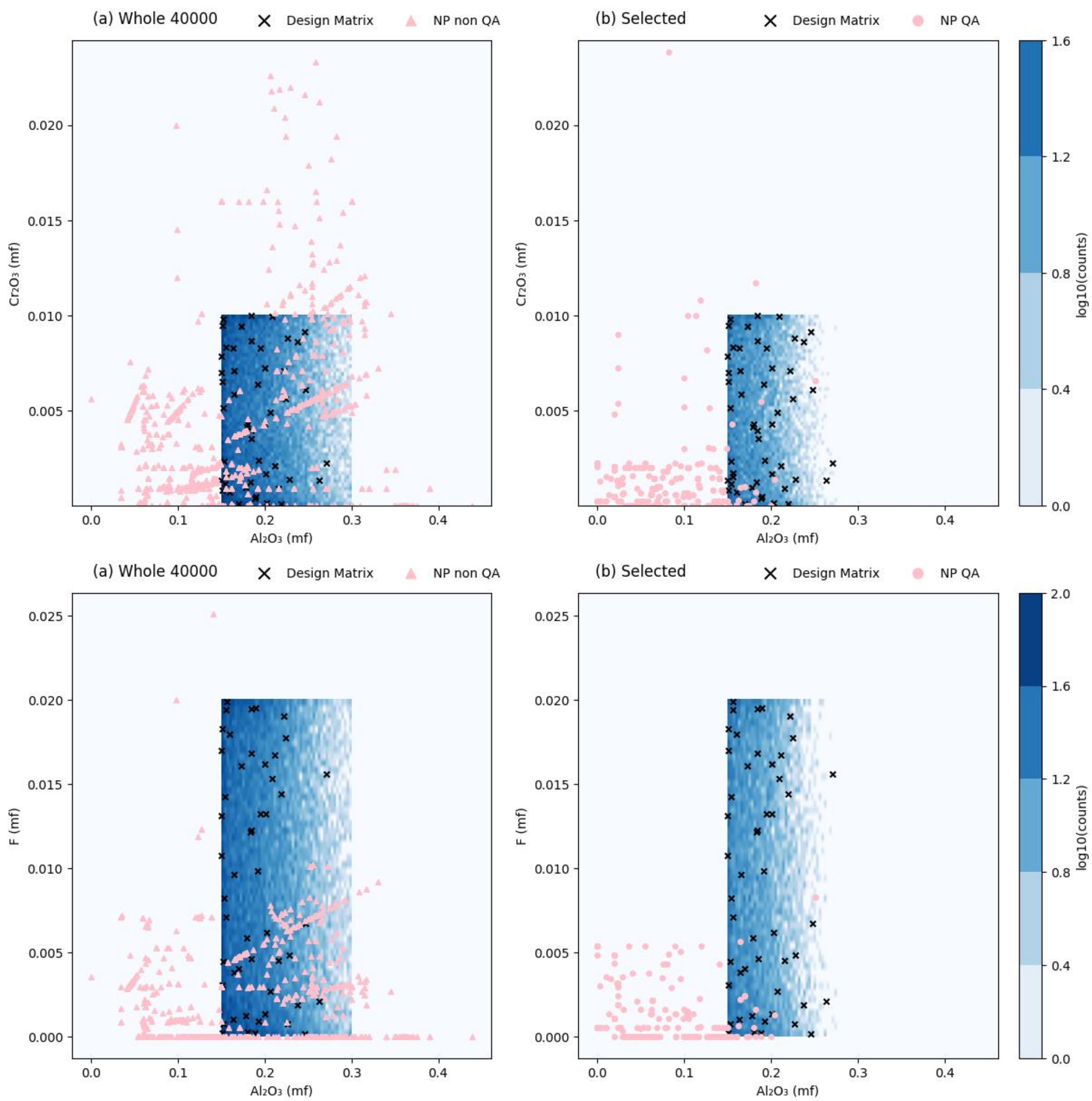

Figure A.2. Heatmaps of Al_2O_3 vs. Cr_2O_3 and F.

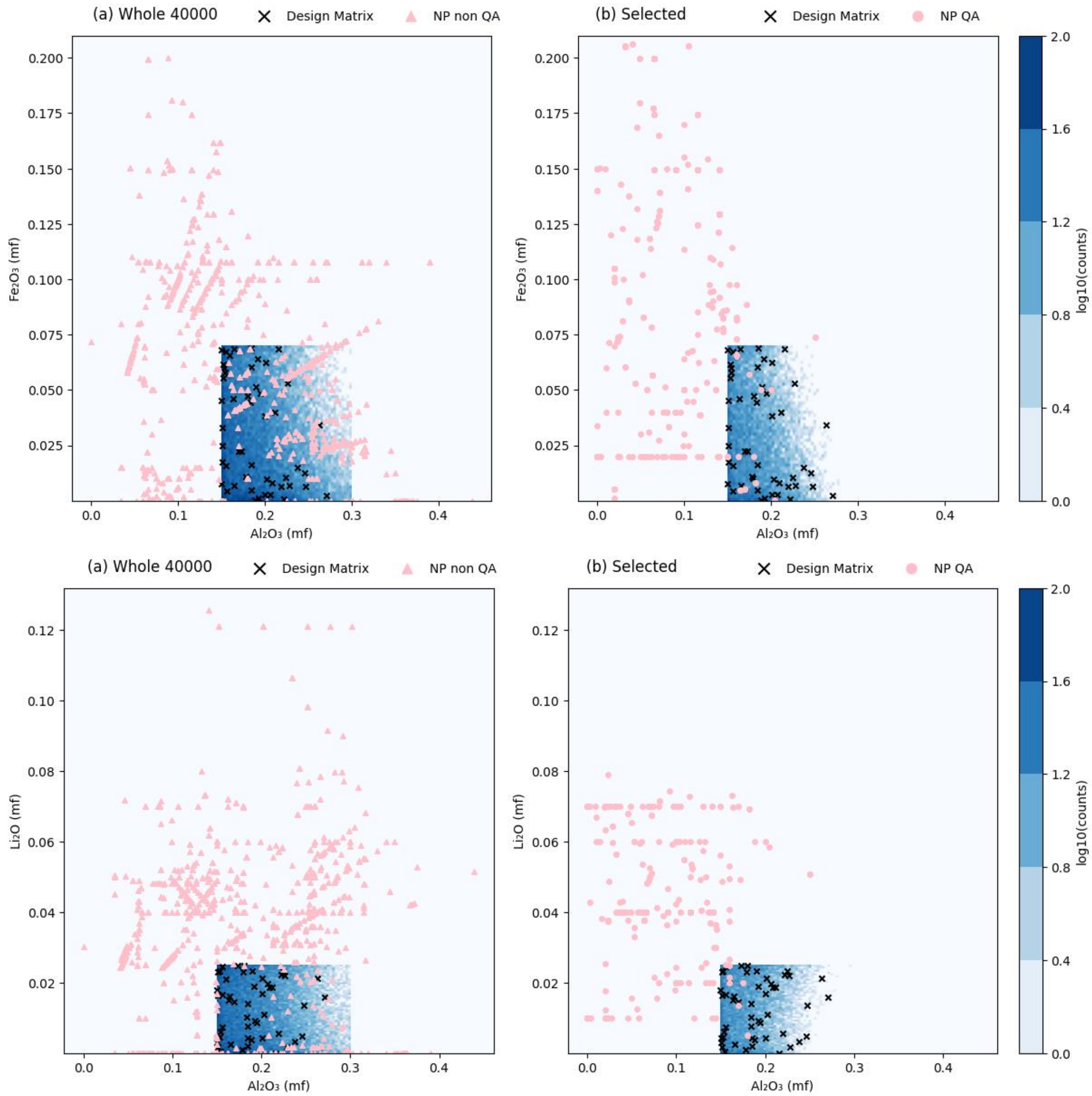

Figure A.3. Heatmaps of Al_2O_3 vs. Fe_2O_3 and Li_2O.

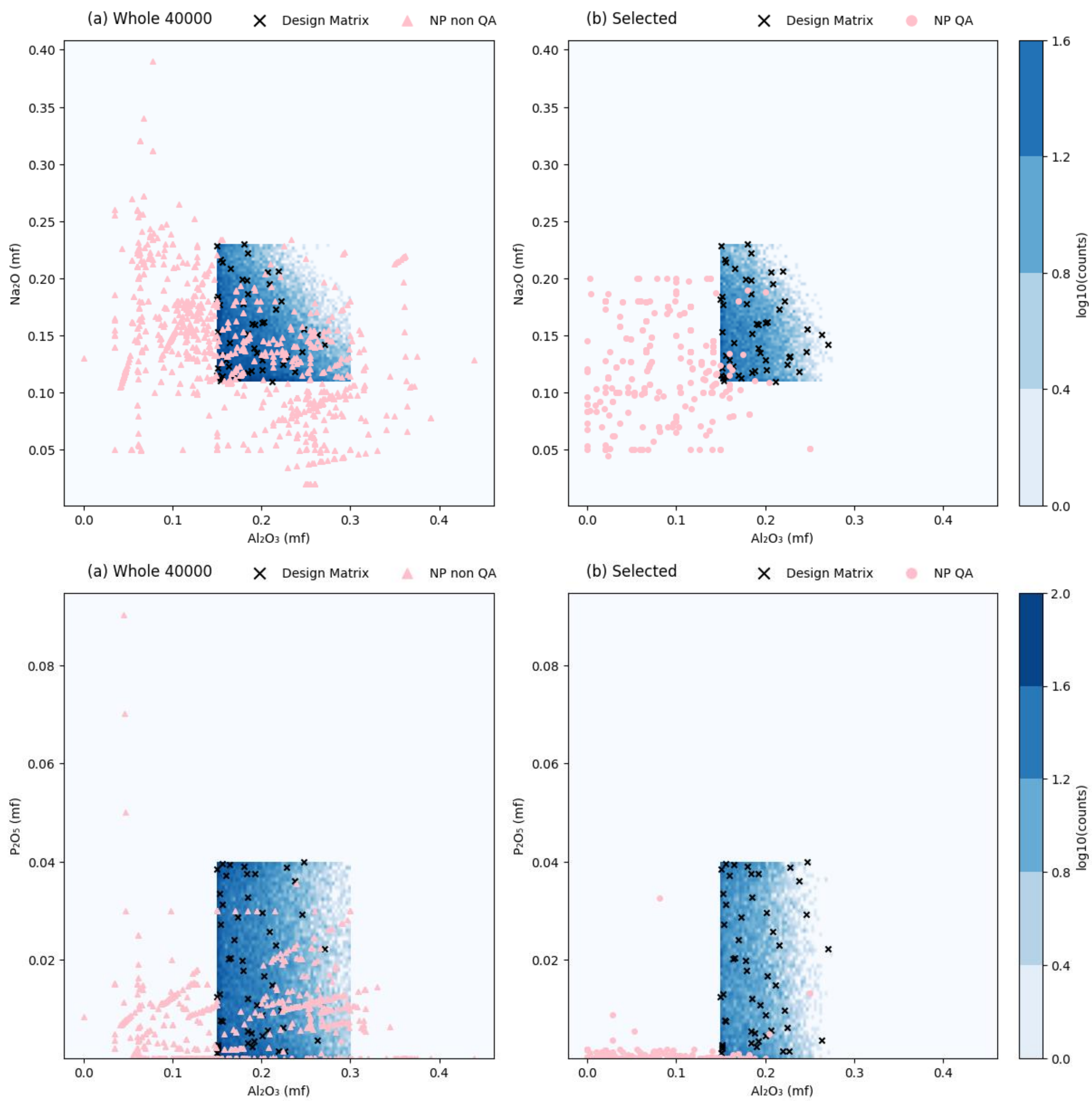

Figure A.4. Heatmaps of Al_2O_3 vs. Na_2O and P_2O_5.

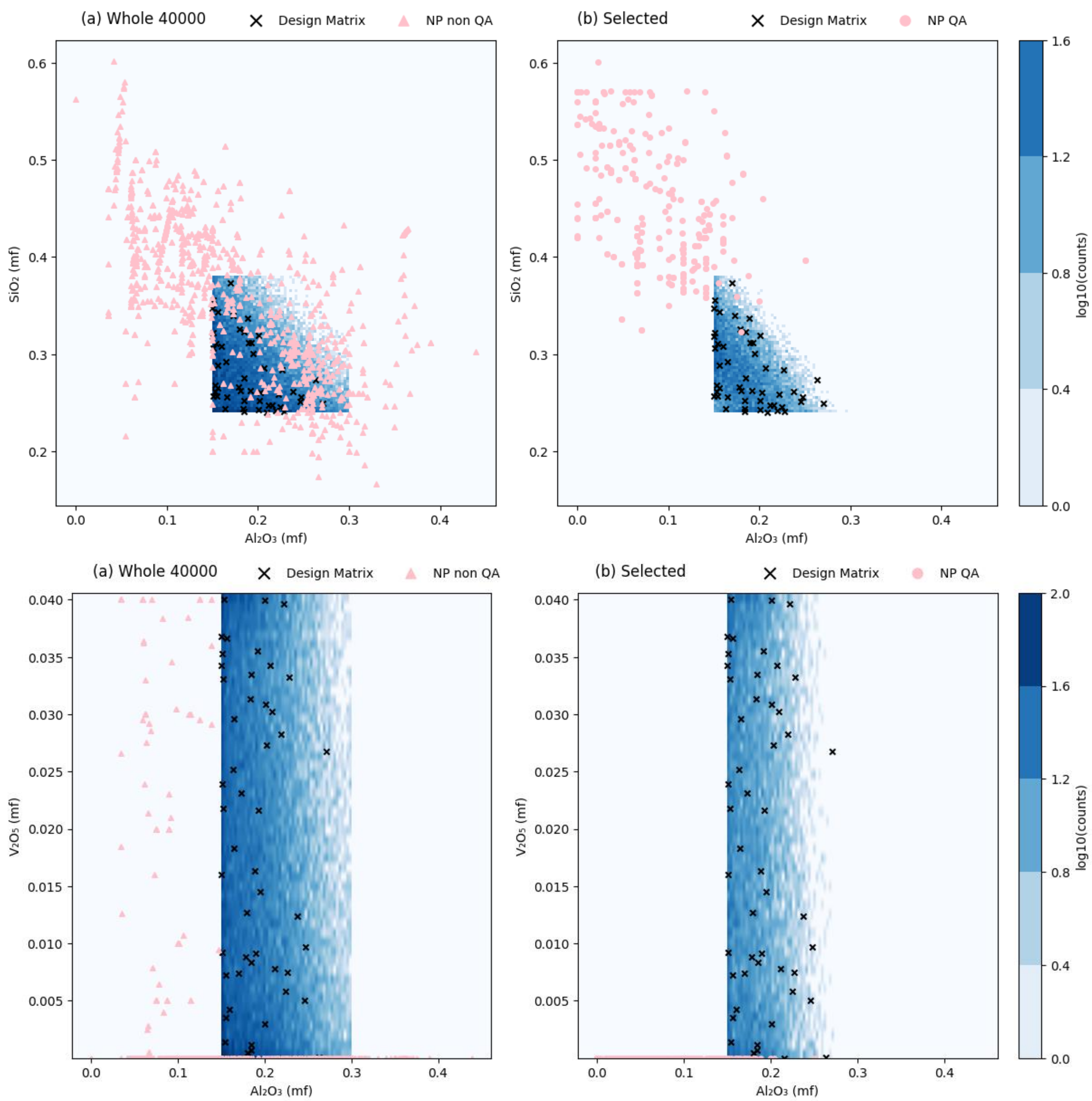

Figure A.5. Heatmaps of Al_2O_3 vs. SiO_2 and V_2O_5.

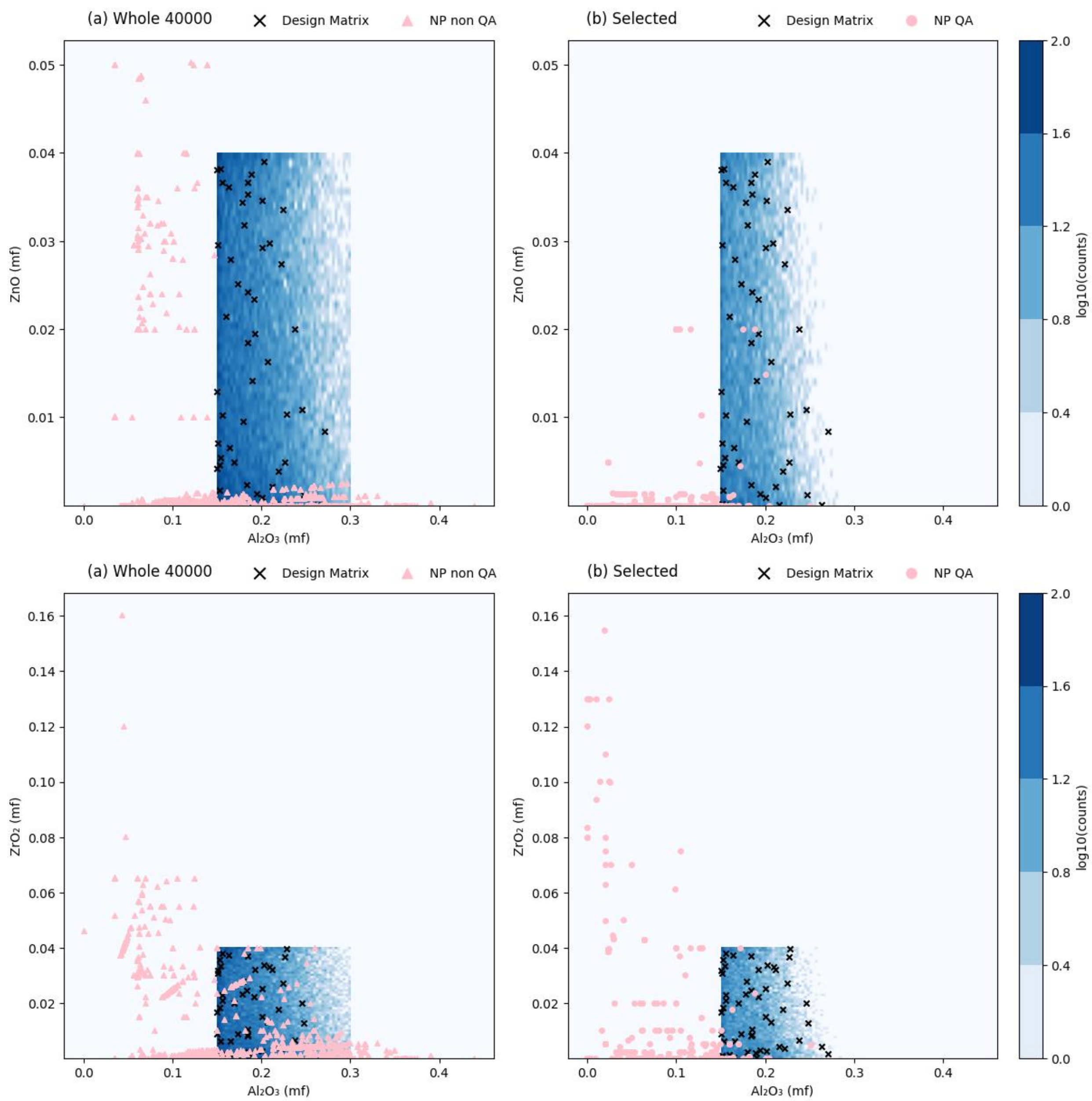

Figure A.6. Heatmaps of Al_2O_3 vs. ZnO and ZrO_2.

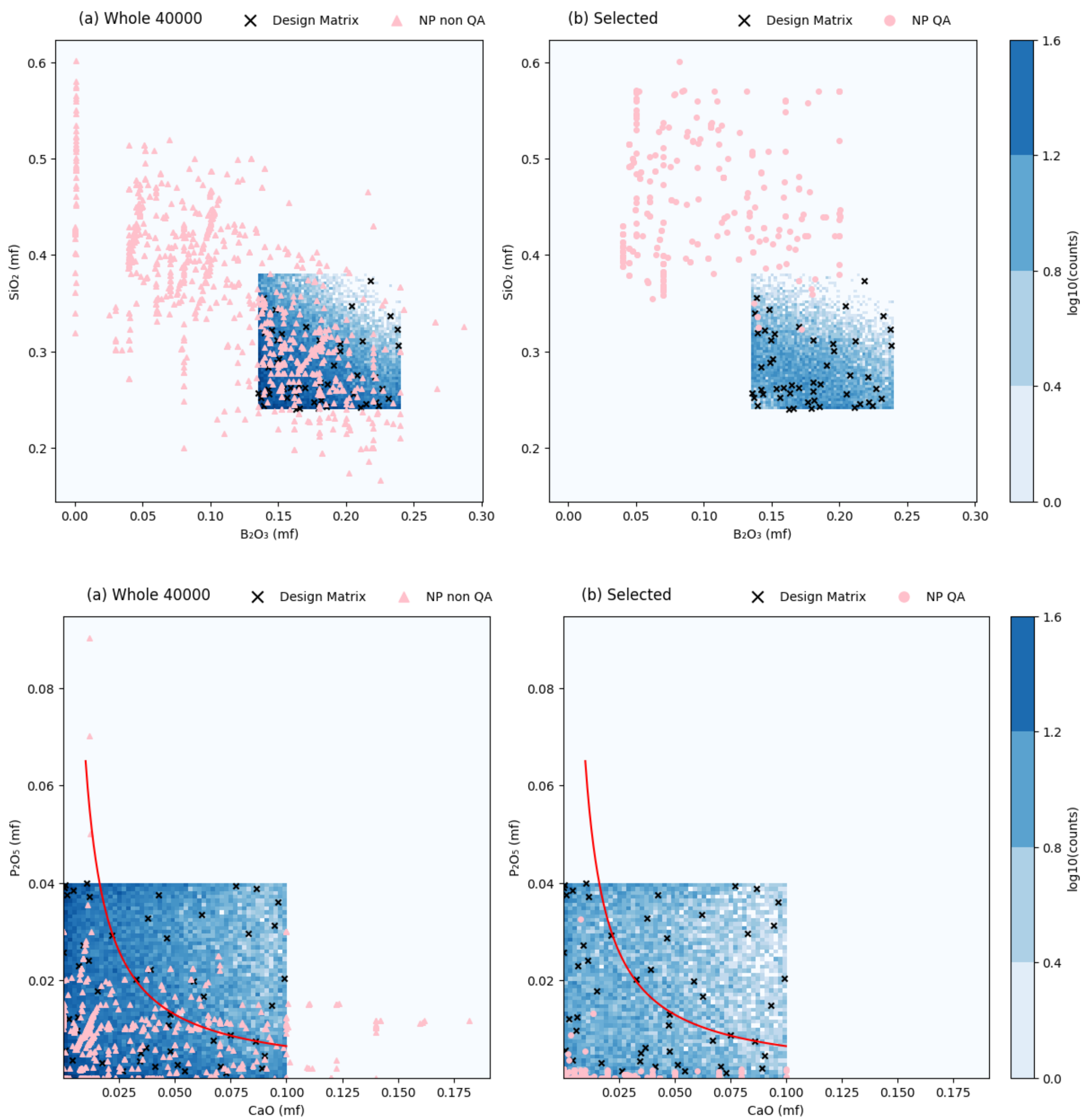

Figure A.7. Heatmaps of CaO vs. SiO_2 and P_2O_5. The red line represents a phosphate phase rule in the WTP baseline algorithm (Vienna and Kim 2014).

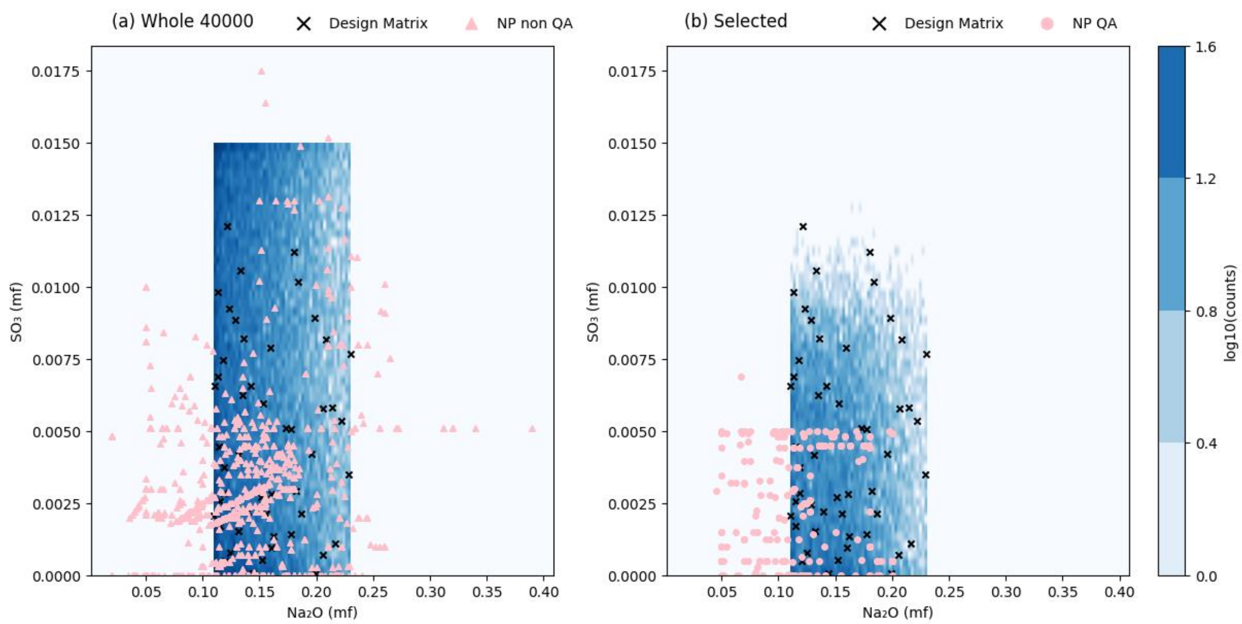

Figure A.8. Heatmaps of Na_2O vs. SiO_2 and SO_3.

Appendix B – Target Masses of Chemical Sources

The target masses of chemical sources from batch sheets of HAL24 glasses are provided.

Table B.1. Target masses of chemical sources.

		HAL24M1-01	HAL24M1-02	HAL24M1-03	HAL24M1-04	HAL24M1-05
Component	Source	Target Mass (g)	Target Mass (g)	Target Mass (g)	Target Mass (g)	Target Mass (g)
Al_2O_3	Al_2O_3	156.04	151.09	152.87	184.73	222.17
B_2O_3	H_3BO_3	264.40	246.92	320.83	422.39	320.44
Bi_2O_3	Bi_2O_3	1.60	0.61	0.70	0.75	0.78
CaO	CaCO3	153.42	91.51	110.76	4.48	10.55
Cl	NaCl	3.15	1.20	1.38	1.48	1.53
Cr_2O_3	Cr_2O_3	1.53	0.80	9.80	9.97	7.09
F	NaF	43.98	40.47	9.92	27.05	42.08
Fe_2O_3	Fe_2O_3	4.44	32.79	61.38	4.61	0.56
K_2O	K_2CO_3	6.02	2.29	2.64	2.82	2.92
Li_2O	Li_2CO_3	60.93	4.53	57.54	4.90	54.80
MgO	MgO	6.89	2.62	3.02	3.23	3.36
MnO	MnO	3.13	1.19	1.37	1.47	1.52
Na_2O	Na_2CO_3	149.34	246.66	141.55	214.63	231.78
Nd_2O_3	Nd_2O_3	0.58	0.22	0.25	0.27	0.28
NiO	NiO	4.30	1.64	1.89	2.02	2.10
P_2O_5	$NaPO_3$	10.88	3.91	48.07	17.37	14.06
PbO	PbO	2.05	0.78	0.90	0.96	1.00
SiO_2	SiO_2	288.38	355.30	267.69	323.06	258.45
SO_3	Na_2SO_4	18.73	18.08	17.44	0.94	19.91
SrO	SrO	0.18	0.07	0.08	0.09	0.09
TiO_2	TiO_2	0.34	0.13	0.15	0.16	0.17
V_2O_5	V_2O_5	36.65	35.32	33.09	1.13	39.62
ZnO	ZnO	36.61	7.08	1.75	35.36	27.36
ZrO_2	ZrO_2	20.85	0.92	35.64	10.28	3.64

Table B.1. Target masses of chemical sources (continued).

		HAL24M1-06	HAL24M1-07	HAL24M1-08	HAL24M1-09	HAL24M1-10
Component	Source	Target Mass (g)	Target Mass (g)	Target Mass (g)	Target Mass (g)	Target Mass (g)
Al_2O_3	Al_2O_3	224.75	153.87	163.37	201.33	159.94
B_2O_3	H_3BO_3	381.65	376.11	397.80	243.60	347.14
Bi_2O_3	Bi_2O_3	1.41	0.56	0.96	0.61	1.17
CaO	CaCO3	65.79	16.12	58.38	147.98	20.51
Cl	NaCl	2.79	1.10	1.90	1.20	2.31
Cr_2O_3	Cr_2O_3	5.60	2.32	8.26	1.66	0.72
F	NaF	39.18	18.26	2.30	29.24	39.72
Fe_2O_3	Fe_2O_3	10.64	59.77	46.01	62.37	65.84
K_2O	K_2CO_3	5.31	2.10	3.61	2.29	4.39
Li_2O	Li_2CO_3	57.76	14.99	37.29	52.20	51.90
MgO	MgO	6.09	2.40	4.15	2.62	5.04
MnO	MnO	2.76	1.09	1.88	1.19	2.29
Na_2O	Na_2CO_3	155.37	136.31	178.26	144.34	127.93
Nd_2O_3	Nd_2O_3	0.51	0.20	0.35	0.22	0.42
NiO	NiO	3.81	1.50	2.59	1.64	3.15
P_2O_5	$NaPO_3$	8.81	39.06	28.93	42.63	53.36
PbO	PbO	1.82	0.72	1.24	0.78	1.50
SiO_2	SiO_2	246.06	311.27	243.54	252.65	307.95
SO_3	Na_2SO_4	1.40	11.66	16.41	0.85	15.74
SrO	SrO	0.16	0.06	0.11	0.07	0.13
TiO_2	TiO_2	0.30	0.12	0.21	0.13	0.25
V_2O_5	V_2O_5	5.79	40.04	25.19	30.90	4.25
ZnO	ZnO	33.62	38.19	36.13	34.65	21.44
ZrO_2	ZrO_2	27.10	6.21	37.33	2.40	1.20

Table B.1. Target masses of chemical sources (continued).

		HAL24M1-11	HAL24M1-12	HAL24M1-13	HAL24M1-14	HAL24M1-15
Component	Source	Target Mass (g)	Target Mass (g)	Target Mass (g)	Target Mass (g)	Target Mass (g)
Al_2O_3	Al_2O_3	237.89	200.80	228.06	164.61	200.68
B_2O_3	H_3BO_3	273.05	248.13	294.40	267.30	329.11
Bi_2O_3	Bi_2O_3	1.63	0.57	0.56	0.72	1.51
CaO	CaCO3	171.97	161.19	154.67	137.77	133.70
Cl	NaCl	3.21	1.14	1.10	1.43	2.98
Cr_2O_3	Cr_2O_3	8.60	7.23	1.37	7.06	4.27
F	NaF	4.15	35.83	10.72	8.42	2.98
Fe_2O_3	Fe_2O_3	14.85	2.94	6.86	68.38	38.10
K_2O	K_2CO_3	6.13	2.16	2.10	2.73	5.69
Li_2O	Li_2CO_3	7.79	41.59	3.96	39.91	10.53
MgO	MgO	7.04	2.47	2.41	3.12	6.52
MnO	MnO	3.19	1.12	1.10	1.42	2.96
Na_2O	Na_2CO_3	163.67	221.70	179.87	204.52	204.05
Nd_2O_3	Nd_2O_3	0.59	0.21	0.20	0.26	0.55
NiO	NiO	4.40	1.55	1.51	1.95	4.08
P_2O_5	$NaPO_3$	51.82	6.59	55.71	56.66	12.71
PbO	PbO	2.10	0.74	0.72	0.93	1.94
SiO_2	SiO_2	261.64	319.62	240.88	292.52	243.15
SO_3	Na_2SO_4	5.04	4.99	2.70	0.12	4.35
SrO	SrO	0.19	0.07	0.06	0.08	0.17
TiO_2	TiO_2	0.35	0.12	0.12	0.16	0.33
V_2O_5	V_2O_5	12.36	2.99	33.24	18.31	39.97
ZnO	ZnO	20.05	0.90	10.37	6.54	29.26
ZrO_2	ZrO_2	6.55	25.21	39.50	0.23	14.85

Table B.1. Target masses of chemical sources (continued).

		HAL24M1-16	HAL24M1-17	HAL24M1-18	HAL24M1-19	HAL24M1-20
Component	Source	Target Mass (g)	Target Mass (g)	Target Mass (g)	Target Mass (g)	Target Mass (g)
Al_2O_3	Al_2O_3	226.79	188.71	173.19	169.68	270.83
B_2O_3	H_3BO_3	252.66	412.53	244.79	387.46	322.43
Bi_2O_3	Bi_2O_3	1.38	1.24	1.53	0.79	0.92
CaO	CaCO3	97.31	61.83	82.65	19.86	69.79
Cl	NaCl	2.72	2.44	3.03	1.57	1.81
Cr_2O_3	Cr_2O_3	8.81	0.36	9.43	0.06	2.22
F	NaF	1.72	0.49	35.56	8.95	34.43
Fe_2O_3	Fe_2O_3	53.02	0.24	22.47	22.41	2.50
K_2O	K_2CO_3	5.18	4.65	5.77	2.98	3.46
Li_2O	Li_2CO_3	54.13	9.05	61.25	36.08	39.07
MgO	MgO	5.94	5.34	6.62	3.41	3.98
MnO	MnO	2.70	2.42	3.00	1.55	1.81
Na_2O	Na_2CO_3	213.08	191.81	115.50	162.38	172.95
Nd_2O_3	Nd_2O_3	0.50	0.45	0.55	0.29	0.33
NiO	NiO	3.71	3.33	4.13	2.13	2.49
P_2O_5	$NaPO_3$	2.11	7.30	41.35	34.67	32.09
PbO	PbO	1.77	1.59	1.97	1.02	1.19
SiO_2	SiO_2	284.40	336.97	339.99	373.72	249.87
SO_3	Na_2SO_4	7.40	6.65	12.21	4.54	11.67
SrO	SrO	0.16	0.14	0.18	0.09	0.11
TiO_2	TiO_2	0.30	0.27	0.33	0.17	0.20
V_2O_5	V_2O_5	7.48	16.34	23.10	7.40	26.77
ZnO	ZnO	4.87	37.57	25.20	4.92	8.36
ZrO_2	ZrO_2	36.73	1.85	8.61	19.88	1.68

Table B.1. Target masses of chemical sources (continued).

		HAL24M1-21	HAL24M1-22	HAL24M1-23	HAL24M1-24	HAL24M1-25
Component	Source	Target Mass (g)	Target Mass (g)	Target Mass (g)	Target Mass (g)	Target Mass (g)
Al_2O_3	Al_2O_3	206.78	247.72	150.53	165.35	184.29
B_2O_3	H_3BO_3	338.63	364.41	240.62	254.45	318.79
Bi_2O_3	Bi_2O_3	0.66	1.66	1.49	0.64	1.28
CaO	CaCO3	1.45	18.56	7.76	177.11	30.57
Cl	NaCl	1.30	3.28	2.93	1.27	2.52
Cr_2O_3	Cr_2O_3	4.91	6.08	6.96	5.83	8.65
F	NaF	6.03	14.85	37.55	21.35	37.15
Fe_2O_3	Fe_2O_3	2.59	6.52	45.04	7.00	60.55
K_2O	K_2CO_3	2.46	6.26	5.60	2.44	4.81
Li_2O	Li_2CO_3	48.69	33.33	10.76	6.31	34.89
MgO	MgO	2.83	7.19	6.42	2.78	5.52
MnO	MnO	1.29	3.26	2.92	1.26	2.51
Na_2O	Na_2CO_3	337.58	211.85	307.64	302.65	320.89
Nd_2O_3	Nd_2O_3	0.24	0.60	0.54	0.23	0.46
NiO	NiO	1.77	4.49	4.01	1.74	3.45
P_2O_5	$NaPO_3$	8.05	57.26	55.20	29.36	4.40
PbO	PbO	0.84	2.14	1.91	0.83	1.65
SiO_2	SiO_2	286.00	256.44	256.61	256.08	241.31
SO_3	Na_2SO_4	1.22	3.78	6.23	14.49	9.53
SrO	SrO	0.08	0.19	0.17	0.07	0.15
TiO_2	TiO_2	0.14	0.36	0.32	0.14	0.28
V_2O_5	V_2O_5	34.29	9.70	16.02	29.58	0.72
ZnO	ZnO	16.36	1.17	38.05	27.92	18.44
ZrO_2	ZrO_2	13.06	12.84	31.67	6.16	8.08

Table B.1. Target masses of chemical sources (continued).

Component	Source	HAL24M1-26 Target Mass (g)	HAL24M1-27 Target Mass (g)	HAL24M1-28 Target Mass (g)	HAL24M1-29 Target Mass (g)	HAL24M1-30 Target Mass (g)
Al_2O_3	Al_2O_3	202.65	183.66	179.40	263.21	215.77
B_2O_3	H_3BO_3	252.73	247.69	301.90	392.63	393.79
Bi_2O_3	Bi_2O_3	1.57	1.26	0.99	0.93	4.56
CaO	CaCO3	111.98	75.80	27.04	7.30	11.94
Cl	NaCl	3.10	2.47	1.96	3.20	3.33
Cr_2O_3	Cr_2O_3	0.11	1.23	4.13	1.31	0.89
F	NaF	13.68	26.85	12.97	4.66	10.06
Fe_2O_3	Fe_2O_3	9.54	44.24	9.95	34.34	68.50
K_2O	K_2CO_3	5.91	4.74	3.74	2.96	0.97
Li_2O	Li_2CO_3	27.18	25.49	56.92	52.70	0.00
MgO	MgO	6.78	5.43	4.29	0.14	0.13
MnO	MnO	3.08	2.46	1.95	3.47	2.84
Na_2O	Na_2CO_3	242.47	263.04	265.96	243.33	256.63
Nd_2O_3	Nd_2O_3	0.57	0.45	0.36	3.25	7.66
NiO	NiO	4.23	3.39	2.68	3.41	5.82
P_2O_5	$NaPO_3$	23.96	53.92	25.57	5.32	33.01
PbO	PbO	2.02	1.62	1.28	1.84	4.86
SiO_2	SiO_2	261.10	243.90	326.28	273.71	247.75
SO_3	Na_2SO_4	2.40	15.84	8.96	4.77	9.05
SrO	SrO	0.18	0.14	0.11	0.00	0.00
TiO_2	TiO_2	0.34	0.27	0.21	0.00	0.00
V_2O_5	V_2O_5	27.31	31.31	12.73	0.03	0.00
ZnO	ZnO	39.00	2.31	9.56	0.07	0.07
ZrO_2	ZrO_2	33.52	24.52	27.67	4.26	4.22

Table B.1. Target masses of chemical sources (continued).

Component	Source	HAL24M2-01 Target Mass (g)	HAL24M2-02 Target Mass (g)	HAL24M2-03 Target Mass (g)	HAL24M2-04 Target Mass (g)	HAL24M2-05 Target Mass (g)
Al_2O_3	Al_2O_3	154.53	180.27	192.61	155.77	189.87
B_2O_3	H_3BO_3	289.61	282.29	320.2	262.95	265.08
Bi_2O_3	Bi_2O_3	1.22	0.65	1.44	0.93	1.66
CaO	$CaCO_3$	119.64	0.57	2.75	1.16	73.32
Cl	NaCl	2.41	1.29	2.84	1.85	3.28
Cr_2O_3	Cr_2O_3	1.12	4.28	2.39	1.68	0.45
F	NaF	31.49	0.62	2.06	15.69	43.12
Fe_2O_3	Fe_2O_3	57.87	47.48	1.06	15.99	51.26
K_2O	K_2CO_3	4.61	2.46	5.41	3.51	6.25
Nd_2O_3	Nd_2O_3	0.44	0.24	0.52	0.34	0.6
Li_2O	Li_2CO_3	0.84	61.2	22.33	18.03	57.22
MgO	MgO	5.28	2.83	6.21	4.03	7.17
MnO	MnO	2.4	1.28	2.82	1.83	3.26
Na_2O	Na_2CO_3	321.38	351.61	228.82	307.49	213.67
NiO	NiO	3.3	1.76	3.88	2.52	4.48
P_2O_5	$NaPO_3$	11.05	56.2	54.08	56.95	3.26
PbO	PbO	1.57	0.84	1.85	1.2	2.14
SiO_2	SiO_2	256.98	262.33	311.56	343.77	312.31
SO_3	Na_2SO_4	1.99	13.61	14	10.29	1.69
SrO	$SrCO_3$	0.199	0.114	0.242	0.157	0.271
TiO_2	TiO_2	0.26	0.14	0.31	0.2	0.36
V_2O_5	V_2O_5	1.44	0.47	21.58	7.28	9.16
ZnO	ZnO	5.42	31.83	19.52	0.12	14.13
ZrO_2	ZrO_2	33.28	2.23	32.01	38.04	0.29

Table B.1. Target masses of chemical sources (continued).

		HAL24M2-06	HAL24M2-07	HAL24M2-08	HAL24M2-09	HAL24M2-10
Component	Source	Target Mass (g)	Target Mass (g)	Target Mass (g)	Target Mass (g)	Target Mass (g)
Al_2O_3	Al_2O_3	150.27	184.28	155.88	152.79	211.86
B_2O_3	H_3BO_3	362.67	277.23	292.72	402.53	313.36
Bi_2O_3	Bi_2O_3	1.1	0.71	1.31	0.57	1.58
CaO	$CaCO_3$	130.24	85.24	168.73	85.28	166.68
Cl	NaCl	2.18	1.42	2.6	1.14	3.13
Cr_2O_3	Cr_2O_3	7.82	3.96	8.3	5.15	2.06
F	NaF	29.02	43.05	42.92	1.66	36.97
Fe_2O_3	Fe_2O_3	7.47	16.3	67.13	55.35	39.75
K_2O	K_2CO_3	4.15	2.7	4.96	2.16	5.97
Nd_2O_3	Nd_2O_3	0.4	0.26	0.48	0.21	0.57
Li_2O	Li_2CO_3	7.54	19.11	40.78	11.55	45.87
MgO	MgO	4.76	3.09	5.68	2.47	6.84
MnO	MnO	2.16	1.4	2.58	1.12	3.11
Na_2O	Na_2CO_3	155.35	256.22	110.31	288.5	124.73
NiO	NiO	2.97	1.93	3.55	1.55	4.28
P_2O_5	$NaPO_3$	1.39	7.8	45.05	18.72	21.45
PbO	PbO	1.42	0.92	1.69	0.74	2.04
SiO_2	SiO_2	347.48	252.16	265.75	261.5	247.52
SO_3	Na_2SO_4	3.05	3.81	7.89	2.52	3.65
SrO	$SrCO_3$	0.185	0.114	0.214	0.1	0.256
TiO_2	TiO_2	0.24	0.15	0.28	0.12	0.34
V_2O_5	V_2O_5	36.75	33.44	3.51	21.74	7.77
ZnO	ZnO	12.9	36.66	10.24	4.64	2.13
ZrO_2	ZrO_2	8.8	36.95	22.76	18.24	31.93

Table B.1. Target masses of chemical sources (continued).

Component	Source	HAL24M2-11 Target Mass (g)	HAL24M2-12 Target Mass (g)	HAL24M2-13 Target Mass (g)	HAL24M2-14 Target Mass (g)	HAL24M2-15 Target Mass (g)
Al_2O_3	Al_2O_3	151.22	209.04	245.9	150.01	178.43
B_2O_3	H_3BO_3	257.39	289.43	410.4	270.55	330.52
Bi_2O_3	Bi_2O_3	0.71	1.09	0.87	1.42	0.7
CaO	$CaCO_3$	125.77	0.107	38.48	11.33	104.48
Cl	NaCl	1.4	2.14	1.71	2.8	1.38
Cr_2O_3	Cr_2O_3	6.51	9.95	9.12	1.33	0.92
F	NaF	0.55	33.92	0.376	23.74	2.78
Fe_2O_3	Fe_2O_3	24.73	8.16	12.67	68.18	10.88
K_2O	K_2CO_3	2.68	4.11	3.29	5.36	2.66
Nd_2O_3	Nd_2O_3	0.26	0.39	0.32	0.52	0.25
Li_2O	Li_2CO_3	56.63	45.99	12.12	44.34	2.45
MgO	MgO	3.08	4.7	3.76	6.15	3.04
MnO	MnO	1.4	2.14	1.71	2.79	1.38
Na_2O	Na_2CO_3	250.26	264.59	198.22	265.82	320.97
NiO	NiO	1.92	2.94	2.35	3.84	1.9
P_2O_5	$NaPO_3$	3.4	36.88	41.95	17.81	28.56
PbO	PbO	0.92	1.4	1.12	1.83	0.91
SiO_2	SiO_2	321.95	240.37	251.53	318.24	266.48
SO_3	Na_2SO_4	10.59	7.45	14.55	5.2	0.106
SrO	$SrCO_3$	0.114	0.185	0.142	0.228	0.114
TiO_2	TiO_2	0.15	0.23	0.19	0.31	0.15
V_2O_5	V_2O_5	23.93	30.24	5	34.24	8.8
ZnO	ZnO	29.61	29.81	10.82	4.18	34.39
ZrO_2	ZrO_2	30.84	33.13	19.99	16.66	23.03

Table B.1. Target masses of chemical sources (continued).

Component	Source	HAL24M2-16 Target Mass (g)	HAL24M2-17 Target Mass (g)	HAL24M2-18 Target Mass (g)	HAL24M2-19 Target Mass (g)	HAL24M2-20 Target Mass (g)
Al_2O_3	Al_2O_3	185.02	151.12	194.66	219.33	191.87
B_2O_3	H_3BO_3	369.38	423.58	347.25	374.5	301.7
Bi_2O_3	Bi_2O_3	0.89	1.51	0.81	0.72	1.02
CaO	$CaCO_3$	67.47	158.86	84.31	47.32	61.4
Cl	NaCl	1.76	2.98	1.62	1.42	2.01
Cr_2O_3	Cr_2O_3	3.49	9.48	8.27	0.09	6.34
F	NaF	10.25	6.83	29.26	31.91	21.81
Fe_2O_3	Fe_2O_3	69.01	17.28	48.33	6.29	64.23
K_2O	K_2CO_3	3.36	5.68	3.07	2.71	3.84
Nd_2O_3	Nd_2O_3	0.32	0.55	0.29	0.26	0.37
Li_2O	Li_2CO_3	10.34	40.68	21.56	13.53	46.61
MgO	MgO	3.85	6.52	3.52	3.11	4.41
MnO	MnO	1.75	2.96	1.6	1.41	2
Na_2O	Na_2CO_3	152.46	178.49	175.83	302.15	203.59
NiO	NiO	2.4	4.07	2.2	1.94	2.75
P_2O_5	$NaPO_3$	46.95	2.96	15.69	2.07	5.03
PbO	PbO	1.15	1.94	1.05	0.93	1.31
SiO_2	SiO_2	275.14	306.01	300.5	242.5	262.33
SO_3	Na_2SO_4	13.27	21.48	11.09	10.25	3.9
SrO	$SrCO_3$	0.142	0.242	0.128	0.114	0.171
TiO_2	TiO_2	0.19	0.33	0.18	0.15	0.22
V_2O_5	V_2O_5	8.34	9.24	14.53	28.29	35.56
ZnO	ZnO	24.19	0.14	1.34	3.89	23.44
ZrO_2	ZrO_2	8.35	0.55	2.82	17.73	22.07

Appendix C – Optical Images of the Quenched Glasses

The optical images of the fabricated HAL24 glasses are shown here. Details of the batching and melting are discussed in Section 2.2.

Figure C.1. Photograph of HAL24M1-01 after the first melt.

Figure C.2. Photograph of HAL24M1-02 after the first melt.

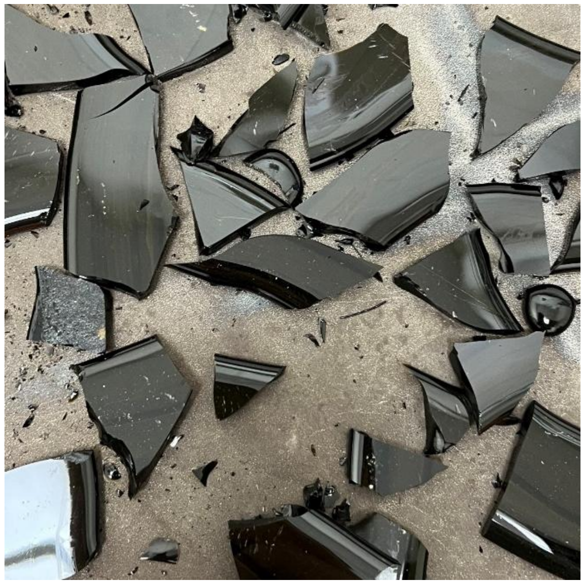

Figure C.3. Photograph of HAL24M1-03 after the first melt.

Figure C.4. Photograph of HAL24M1-04 after the first melt.

Figure C.5. Photograph of HAL24M1-05 after the second melt.

Figure C.6. Photograph of HAL24M1-06 after the first melt.

Figure C.7. Photograph of HAL24M1-07 after the first melt.

Figure C.8. Photograph of HAL24M1-08 after the second melt.

Figure C.9. Photograph of HAL24M1-09 after the first melt.

Figure C.10. Photograph of HAL24M1-10 after the second melt.

Figure C.11. Photograph of HAL24M1-11 after the third melt.

Figure C.12. Photograph of HAL24M1-12 after the third melt.

Figure C.13. Photograph of HAL24M1-13 after the first melt.

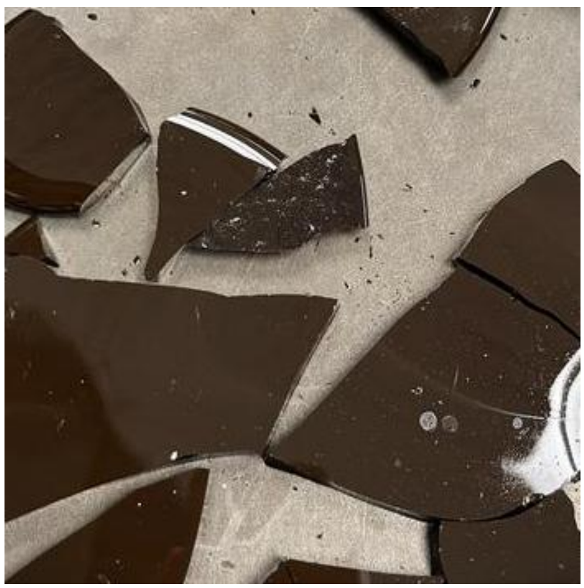

Figure C.14. Photograph of HAL24M1-14 after the second melt.

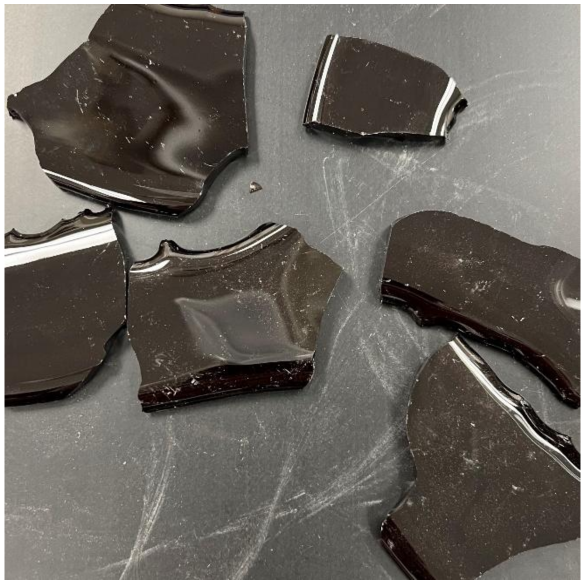

Figure C.15. Photograph of HAL24M1-15 after the first melt.

Figure C.16. Photograph of HAL24M1-16 after the first melt.

Figure C.17. Photograph of HAL24M1-17 after the first melt.

Figure C.18. Photograph of HAL24M1-18 after the second melt.

Figure C.19. Photograph of HAL24M1-19 after the first melt.

Figure C.20. Photograph of HAL24M1-20 after the first melt.

Figure C.21. Photograph of HAL24M1-21 after the first melt.

Figure C.22. Photograph of HAL24M1-22 after the first melt.

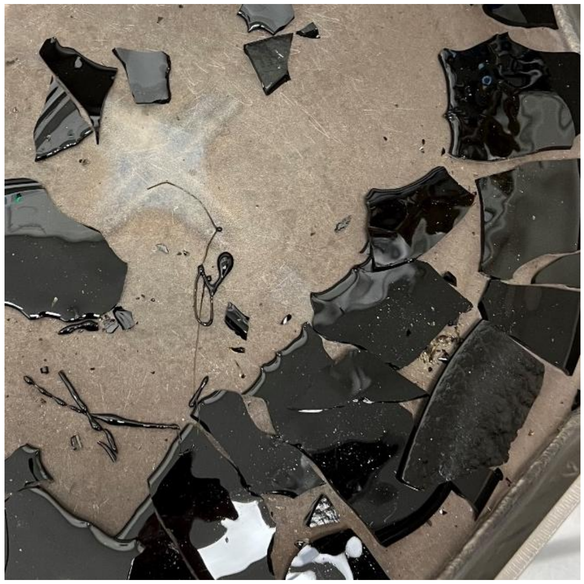

Figure C.23. Photograph of HAL24M1-23 after the first melt.

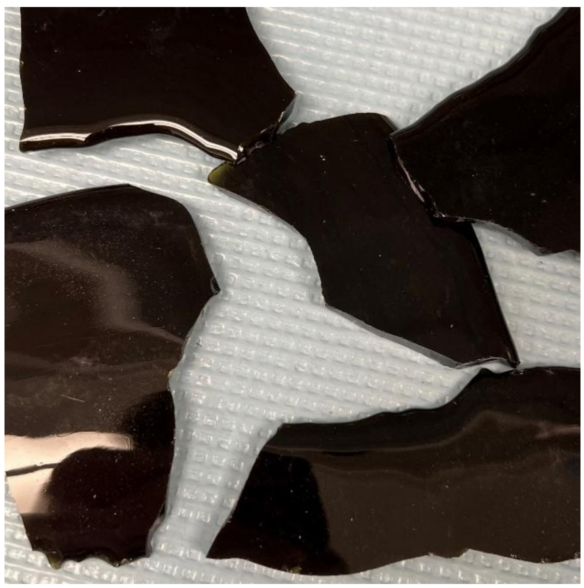

Figure C.24. Photograph of HAL24M1-24 after the second melt.

Figure C.25. Photograph of HAL24M1-25 after the first melt.

Figure C.26. Photograph of HAL24M1-26 after the first melt.

Figure C.27. Photograph of HAL24M1-27 after the second melt.

Figure C.28. Photograph of HAL24M1-28 after the first melt.

Figure C.29. Photograph of HAL24M1-29-1 after the second melt.

Figure C.30. Photograph of HAL24M1-30-1 after the second melt.

Figure C.31. Photograph of HAL24M2-01 glass after the second melt.

Figure C.32. Photograph of HAL24M2-02 glass after the second melt.

Figure C.33. Photograph of HAL24M2-03 glass after the second melt.

Figure C.34. Photograph of HAL24M2-04-1 glass after the third melt.

Figure C.35. Photograph of HAL24M2-05 glass after the second melt.

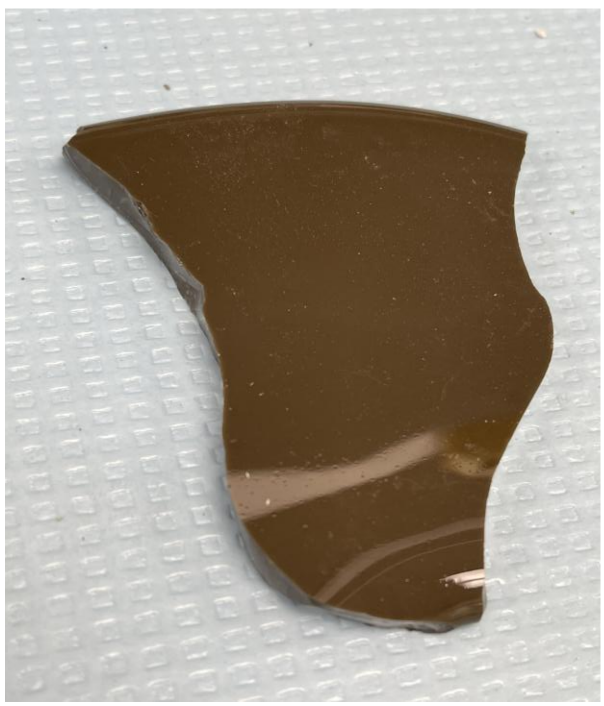

Figure C.36. Photograph of HAL24M2-06 glass after the second melt.

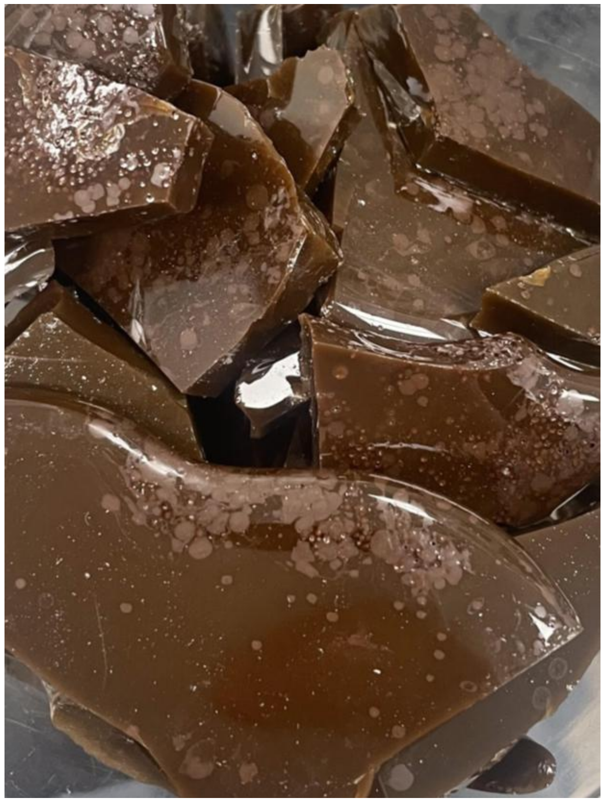

Figure C.37. Photograph of HAL24M2-07 glass after the third melt.

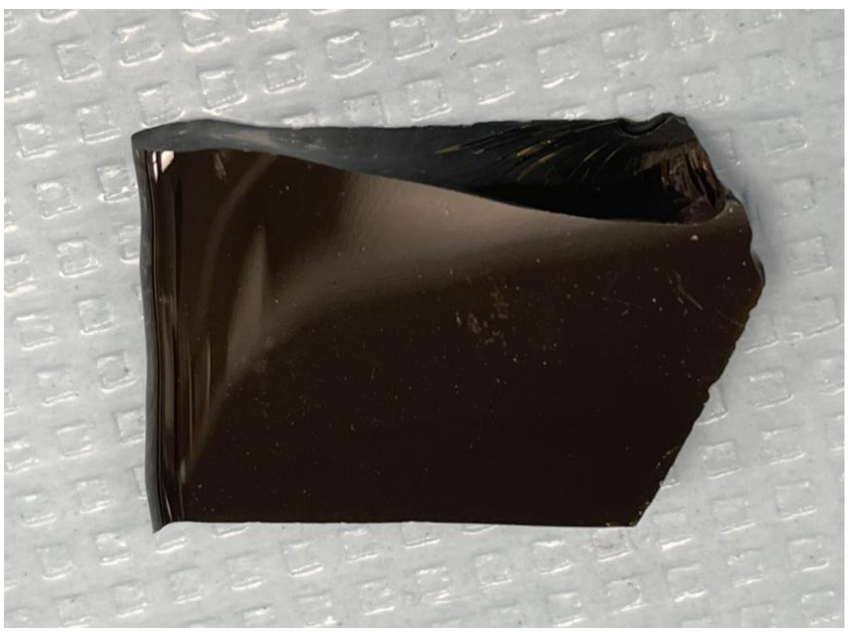

Figure C.38. Photograph of HAL24M2-08 glass after the second melt.

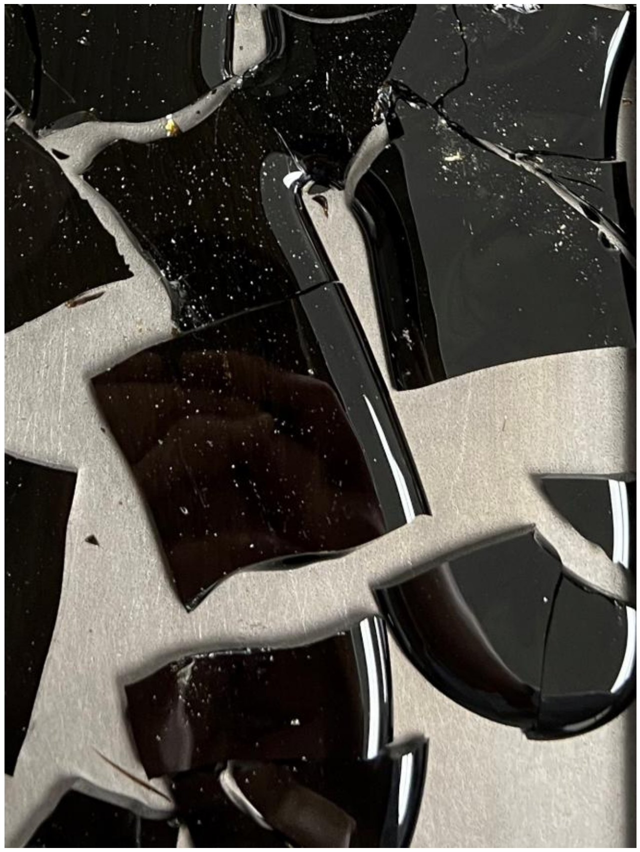

Figure C.39. Photograph of HAL24M2-09 glass after the second melt.

Figure C.40. Photograph of HAL24M2-10 glass after the second melt.

Figure C.41. Photograph of HAL24M2-11 glass after the third melt.

Figure C.42. Photograph of HAL24M2-12 glass after the second melt.

Figure C.43. Photograph of HAL24M2-13 glass after the third melt.

Figure C.44. Photograph of HAL24M2-14 glass after the second melt.

Figure C.45. Photograph of HAL24M2-15 glass after the second melt.

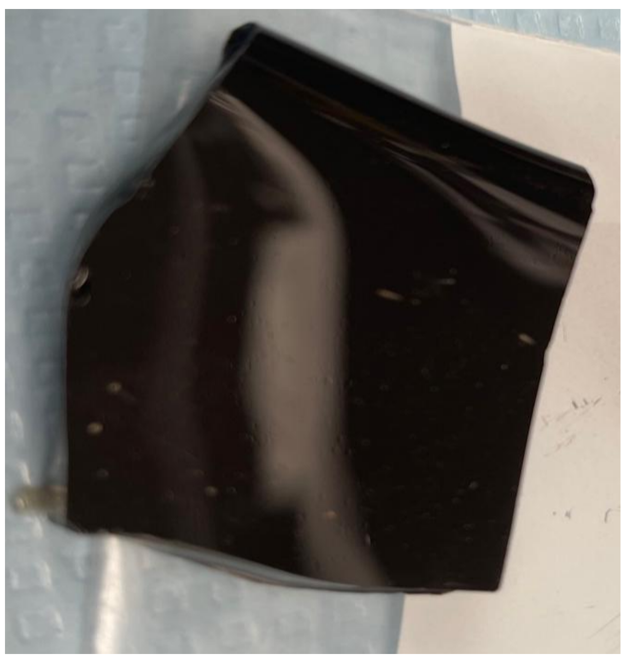

Figure C.46. Photograph of HAL24M2-16 glass after the third melt.

Figure C.47. Photograph of HAL24M2-17 glass after the third melt.

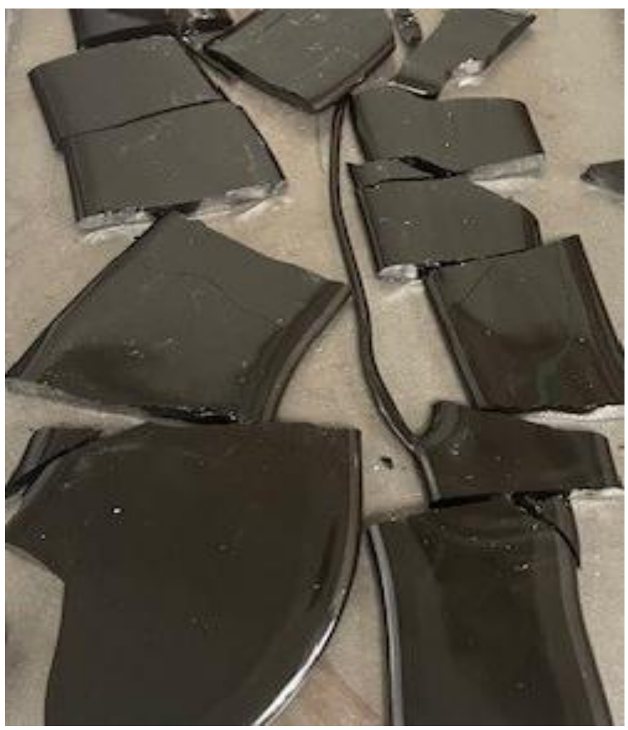

Figure C.48. Photograph of HAL24M2-18 glass after the second melt.

Figure C.49. Photograph of HAL24M2-19 glass after the second melt.

Figure C.50. Photograph of HAL24M2-20 glass after the second melt.

Appendix D – Target and Measured Compositions of HAL24 Glasses

The tables in this appendix compare the target glass compositions with the analyzed glass compositions and the percent difference for the HAL24 glasses.

Table D.1. Target vs. measured compositions of HAL24M1 glasses.

	HAL24M1-01			HAL24M1-02		
Oxide	Target (wt%)	Measured (wt%)	RPD (%)	Target (wt%)	Measured (wt%)	RPD (%)
Al_2O_3	15.60	15.30	-1.94	15.11	15.60	3.23
B_2O_3	14.89	14.38	-3.40	13.90	14.41	3.68
Bi_2O_3	0.16	0.14	-11.75	0.06	0.06	-2.59
CaO	8.60	8.25	-4.01	5.13	4.91	-4.21
Cl	0.19	0.13	-29.42	0.07	0.06	-20.64
Cr_2O_3	0.15	0.12	-19.89	0.08	0.08	-0.26
F	1.99	2.07	4.09	1.83	1.64	-10.46
Fe_2O_3	0.44	0.46	2.69	3.28	3.36	2.59
K_2O	0.41	0.43	3.91	0.16	0.22	42.45
Li_2O	2.46	NM	NM	0.18	NM	NM
MgO	0.69	0.71	2.90	0.26	0.30	16.35
MnO	0.31	0.32	3.69	0.12	0.14	14.86
Na_2O	13.29	13.72	3.23	18.38	18.64	1.43
Nd_2O_3	0.06	0.05	-8.28	0.02	0.03	23.37
NiO	0.43	0.01	-97.68	0.16	0.01	-96.63
P_2O_5	0.76	0.83	10.23	0.27	0.32	16.34
PbO	0.21	0.20	-3.48	0.08	0.06	-17.56
SO_3	1.06	0.47	-55.92	1.02	1.01	-1.05
SiO_2	28.84	29.21	1.30	35.53	35.62	0.25
SrO	0.02	0.00	-100.00	0.01	0.00	-100.00
TiO_2	0.03	0.06	69.26	0.01	0.05	266.92
V_2O_5	3.67	3.56	-2.91	3.53	3.51	-0.60
ZnO	3.66	3.80	3.88	0.71	0.76	8.02
ZrO_2	2.09	2.04	-2.06	0.09	0.13	41.32
SUM	100.00	98.74, 101.20[(a)]		100.00	101.11, 101.29[(a)]	

RPD – relative percentage difference
NM – not measured
(a) Sum including Li_2O

Table D.1. Target vs. measured compositions of HAL24M1 glasses (continued).

	HAL24M1-03			HAL24M1-04		
Oxide	Target (wt%)	Measured (wt%)	RPD (%)	Target (wt%)	Measured (wt%)	RPD (%)
Al_2O_3	15.29	15.23	-0.38	18.47	19.40	5.01
B_2O_3	18.06	16.64	-7.90	23.78	21.59	-9.19
Bi_2O_3	0.07	0.05	-29.44	0.08	0.07	-8.43
CaO	6.21	5.94	-4.27	0.25	0.27	7.58
Cl	0.08	0.05	-37.82	0.09	0.06	-28.75
Cr_2O_3	0.98	0.42	-57.20	1.00	0.22	-77.65
F	0.45	0.41	-8.84	1.22	1.01	-17.85
Fe_2O_3	6.14	5.83	-5.04	0.46	0.47	1.35
K_2O	0.18	0.20	9.12	0.19	0.23	21.99
Li_2O	2.33	NM	NM	0.20	NM	NM
MgO	0.30	0.32	4.70	0.32	0.34	4.79
MnO	0.14	0.14	4.01	0.15	0.16	6.93
Na_2O	11.31	11.49	1.68	15.20	15.32	0.81
Nd_2O_3	0.03	0.03	36.22	0.03	0.03	21.82
NiO	0.19	0.01	-95.50	0.20	0.14	-31.62
P_2O_5	3.35	3.61	8.01	1.21	1.49	23.48
PbO	0.09	0.08	-10.34	0.10	0.08	-15.19
SO_3	0.98	0.63	-36.33	0.05	0.05	-12.98
SiO_2	26.77	27.22	1.69	32.31	32.78	1.48
SrO	0.01	0.00	-100.00	0.01	0.00	-100.00
TiO_2	0.02	0.04	181.38	0.02	0.05	227.36
V_2O_5	3.31	3.19	-3.48	0.11	0.11	-3.40
ZnO	0.18	0.20	14.68	3.54	3.37	-4.57
ZrO_2	3.56	3.49	-2.13	1.03	1.06	2.88
SUM	100.00	97.55, 99.88[a]		100.00	98.51, 98.70[a]	

(a) Sum including Li_2O

Table D.1. Target vs. measured compositions of HAL24M1 glasses (continued).

	HAL24M1-05			HAL24M1-06		
Oxide	Target (wt%)	Measured (wt%)	RPD (%)	Target (wt%)	Measured (wt%)	RPD (%)
Al_2O_3	22.22	22.25	0.13	22.48	22.37	0.13
B_2O_3	18.04	17.21	-4.63	21.49	20.40	-4.63
Bi_2O_3	0.08	0.07	-6.41	0.14	0.12	-6.41
CaO	0.59	0.63	6.94	3.69	3.75	6.94
Cl	0.09	0.06	-35.48	0.17	0.12	-35.48
Cr_2O_3	0.71	0.31	-56.42	0.56	0.13	-56.42
F	1.90	1.78	-6.46	1.77	1.74	-6.46
Fe_2O_3	0.06	0.06	3.57	1.06	0.98	3.57
K_2O	0.20	0.24	18.59	0.36	0.39	18.59
Li_2O	2.22	NM	NM	2.34	NM	NM
MgO	0.34	0.34	2.08	0.61	0.59	2.08
MnO	0.15	0.13	-13.16	0.28	0.27	-13.16
Na_2O	18.04	18.60	3.12	12.45	12.82	3.12
Nd_2O_3	0.03	0.02	-32.14	0.05	0.06	-32.14
NiO	0.21	0.20	-5.71	0.38	0.22	-5.71
P_2O_5	0.98	0.78	-20.43	0.61	0.41	-20.43
PbO	0.10	0.10	-5.00	0.18	0.15	-5.00
SO_3	1.12	0.84	-24.96	0.08	0.07	-24.96
SiO_2	25.85	23.08	-10.70	24.61	22.81	-10.70
SrO	0.01	0.00	-100.00	0.02	0.00	-100.00
TiO_2	0.02	0.06	235.29	0.03	0.08	235.29
V_2O_5	3.96	3.98	0.35	0.58	0.58	0.35
ZnO	2.74	2.47	-9.72	3.36	2.98	-9.72
ZrO_2	0.36	0.33	-10.44	2.71	2.36	-10.44
SUM	100.00	93.52, 95.73[(a)]		100.00	93.36, 95.70[(a)]	

(a) Sum including Li_2O

Table D.1. Target vs. measured compositions of HAL24M1 glasses (continued).

	HAL24M1-07			HAL24M1-08		
Oxide	Target (wt%)	Measured (wt%)	RPD (%)	Target (wt%)	Measured (wt%)	RPD (%)
Al_2O_3	15.39	15.21	-1.16	16.34	15.80	-3.26
B_2O_3	21.17	19.53	-7.76	22.40	20.52	-8.37
Bi_2O_3	0.06	0.05	-3.57	0.10	0.08	-12.50
CaO	0.90	0.94	4.10	3.27	3.27	0.00
Cl	0.07	0.04	-37.31	0.12	0.07	-42.61
Cr_2O_3	0.23	0.24	1.29	0.83	1.37	65.50
F	0.83	0.63	-23.24	0.10	0.10	0.00
Fe_2O_3	5.98	5.61	-6.17	4.60	4.28	-7.00
K_2O	0.14	0.18	25.17	0.25	0.27	9.76
Li_2O	0.61	NM	NM	1.51	NM	NM
MgO	0.24	0.25	4.17	0.42	0.42	0.00
MnO	0.11	0.11	-1.83	0.19	0.36	89.36
Na_2O	11.07	11.58	4.61	12.29	12.54	2.06
Nd_2O_3	0.02	0.02	0.00	0.04	0.03	-14.29
NiO	0.15	0.10	-34.00	0.26	0.23	-10.04
P_2O_5	2.72	1.91	-29.86	2.01	1.41	-30.04
PbO	0.07	0.04	-43.06	0.12	0.10	-17.74
SO_3	0.66	0.10	-84.78	0.93	0.49	-47.03
SiO_2	31.13	29.80	-4.26	24.35	22.46	-7.78
SrO	0.01	0.00	-83.33	0.01	0.00	-72.73
TiO_2	0.01	0.06	375.00	0.02	0.06	171.43
V_2O_5	4.00	3.95	-1.32	2.52	2.43	-3.37
ZnO	3.82	3.60	-5.68	3.61	3.56	-1.49
ZrO_2	0.62	0.56	-9.50	3.73	3.30	-11.65
SUM	100.00	94.51, 95.12[(a)]		100.00	93.15, 94.66[(a)]	

(a) Sum including Li_2O

Table D.1. Target vs. measured compositions of HAL24M1 glasses (continued).

	HAL24M1-09			HAL24M1-10		
Oxide	Target (wt%)	Measured (wt%)	RPD (%)	Target (wt%)	Measured (wt%)	RPD (%)
Al_2O_3	20.13	19.84	-1.48	15.99	15.72	-1.73
B_2O_3	13.71	13.26	-3.35	19.54	17.98	-8.02
Bi_2O_3	0.06	0.05	-13.11	0.12	0.11	-8.55
CaO	8.29	8.32	0.35	1.15	1.20	4.53
Cl	0.07	0.05	-32.88	0.14	0.10	-30.71
Cr_2O_3	0.17	0.12	-28.92	0.07	0.07	-6.94
F	1.32	1.37	3.70	1.80	1.63	-9.57
Fe_2O_3	6.24	5.78	-7.39	6.58	6.19	-6.03
K_2O	0.16	0.19	24.36	0.30	0.32	8.03
Li_2O	2.11	NM	NM	2.10	NM	NM
MgO	0.26	0.26	0.00	0.50	0.49	-2.78
MnO	0.12	0.13	7.56	0.23	0.22	-3.06
Na_2O	12.00	12.41	3.44	12.84	13.07	1.78
Nd_2O_3	0.02	0.02	-27.27	0.04	0.04	4.76
NiO	0.16	0.10	-39.63	0.32	0.24	-22.54
P_2O_5	2.97	2.07	-30.37	3.71	2.54	-31.64
PbO	0.08	0.06	-20.51	0.15	0.14	-10.00
SO_3	0.05	0.06	20.83	0.89	0.71	-19.95
SiO_2	25.27	23.39	-7.44	30.80	29.76	-3.36
SrO	0.01	0.00	-100.00	0.01	0.00	-92.31
TiO_2	0.01	0.05	315.38	0.03	0.06	148.00
V_2O_5	3.09	3.05	-1.23	0.43	0.41	-3.53
ZnO	3.47	3.21	-7.39	2.14	2.06	-3.87
ZrO_2	0.24	0.22	-7.92	0.12	0.12	0.00
SUM	100.00	93.99, 96.11[a]		100.00	93.17, 95.27[a]	

(a) Sum including Li_2O

Table D.1. Target vs. measured compositions of HAL24M1 glasses (continued).

	HAL24M1-11			HAL24M1-12		
Oxide	Target (wt%)	Measured (wt%)	RPD (%)	Target (wt%)	Measured (wt%)	RPD (%)
Al_2O_3	23.79	22.82	-4.08	20.08	19.13	-4.71
B_2O_3	15.37	12.91	-15.99	13.97	12.02	-13.95
Bi_2O_3	0.16	0.14	-11.07	0.06	0.06	5.94
CaO	9.64	9.10	-5.52	9.03	8.83	-2.24
Cl	0.20	0.15	-25.20	0.07	0.05	-24.22
Cr_2O_3	0.86	0.72	-16.61	0.72	0.40	-44.56
F	0.19	0.17	-8.89	1.62	1.62	-0.16
Fe_2O_3	1.49	1.38	-6.81	0.29	0.30	1.91
K_2O	0.42	0.44	5.51	0.15	0.18	20.99
Li_2O	0.32	NM	NM	1.68	NM	NM
MgO	0.70	0.67	-4.12	0.25	0.24	-2.05
MnO	0.32	0.31	-4.03	0.11	0.11	-4.64
Na_2O	11.84	12.12	2.38	16.09	16.32	1.44
Nd_2O_3	0.06	0.06	8.67	0.02	0.03	21.28
NiO	0.44	0.27	-38.26	0.16	0.13	-14.34
P_2O_5	3.61	3.44	-4.64	0.46	0.53	16.08
PbO	0.21	0.16	-25.84	0.07	0.05	-35.17
SO_3	0.28	0.22	-20.78	0.28	0.22	-21.21
SiO_2	26.16	24.92	-4.75	31.96	34.79	8.84
SrO	0.02	0.00	-100.00	0.01	0.00	-100.00
TiO_2	0.04	0.09	153.91	0.01	0.06	361.73
V_2O_5	1.24	1.20	-3.09	0.30	0.27	-8.69
ZnO	2.01	1.95	-2.67	0.09	0.07	-22.20
ZrO_2	0.66	0.57	-12.29	2.52	2.36	-6.56
SUM	100.00	93.84, 94.15[(a)]		100.00	97.76, 99.45[(a)]	

(a) Sum including Li_2O

Table D.1. Target vs. measured compositions of HAL24M1 glasses (continued).

	HAL24M1-13			HAL24M1-14		
Oxide	Target (wt%)	Measured (wt%)	RPD (%)	Target (wt%)	Measured (wt%)	RPD (%)
Al_2O_3	22.81	22.30	-2.22	16.46	15.65	-4.95
B_2O_3	16.57	15.58	-6.02	15.05	13.88	-7.79
Bi_2O_3	0.06	0.04	-23.21	0.07	0.07	-5.48
CaO	8.67	8.66	-0.05	7.72	7.44	-3.66
Cl	0.07	0.05	-19.40	0.09	0.07	-24.08
Cr_2O_3	0.14	0.09	-31.39	0.71	0.57	-18.65
F	0.49	0.48	-0.41	0.38	0.38	-0.86
Fe_2O_3	0.69	0.64	-6.85	6.84	6.64	-2.89
K_2O	0.14	0.16	11.19	0.19	0.21	12.10
Li_2O	0.16	NM	NM	1.61	NM	NM
MgO	0.24	0.25	2.07	0.31	0.30	-4.81
MnO	0.11	0.10	-7.27	0.14	0.15	4.88
Na_2O	13.18	13.31	1.02	14.39	14.59	1.40
Nd_2O_3	0.02	0.02	-5.00	0.03	0.02	-8.65
NiO	0.15	0.00	-97.35	0.20	0.01	-96.47
P_2O_5	3.88	2.78	-28.31	3.94	4.41	11.93
PbO	0.07	0.07	-4.17	0.09	0.06	-36.91
SO_3	0.15	0.08	-47.37	0.01	0.03	274.50
SiO_2	24.09	22.76	-5.52	29.25	31.30	7.00
SrO	0.01	0.00	-66.67	0.01	0.00	-92.86
TiO_2	0.01	0.05	325.00	0.02	0.06	283.83
V_2O_5	3.32	3.24	-2.47	1.83	1.76	-4.04
ZnO	1.04	0.97	-6.36	0.65	0.64	-2.09
ZrO_2	3.95	3.75	-4.99	0.02	0.00	-100.00
SUM	100.00	95.40, 95.56[(a)]		100.00	98.22, 99.83[(a)]	

(a) Sum including Li_2O

Table D.1. Target vs. measured compositions of HAL24M1 glasses (continued).

	HAL24M1-15			HAL24M1-16		
Oxide	Target (wt%)	Measured (wt%)	RPD (%)	Target (wt%)	Measured (wt%)	RPD (%)
Al_2O_3	20.07	19.46	-3.01	22.68	21.28	-6.15
B_2O_3	18.53	17.68	-4.56	14.22	14.39	1.18
Bi_2O_3	0.15	0.11	-24.50	0.14	0.11	-19.47
CaO	7.49	7.49	-0.05	5.45	5.37	-1.59
Cl	0.18	0.13	-30.39	0.17	0.13	-19.78
Cr_2O_3	0.43	0.28	-33.49	0.88	0.66	-25.39
F	0.14	0.10	-25.19	0.08	0.07	-13.64
Fe_2O_3	3.81	3.58	-5.98	5.30	5.08	-4.13
K_2O	0.39	0.40	2.84	0.35	0.38	9.06
Li_2O	0.43	NM	NM	2.19	NM	NM
MgO	0.65	0.63	-3.83	0.59	0.55	-7.42
MnO	0.30	0.28	-6.76	0.27	0.26	-4.97
Na_2O	12.89	13.16	2.10	13.12	13.53	3.16
Nd_2O_3	0.06	0.05	-1.82	0.05	0.04	-28.17
NiO	0.41	0.01	-98.53	0.37	0.00	-99.30
P_2O_5	0.89	0.62	-29.72	0.15	0.15	4.62
PbO	0.19	0.18	-9.79	0.18	0.13	-28.38
SO_3	0.25	0.13	-45.71	0.42	0.32	-23.89
SiO_2	24.32	22.88	-5.90	28.44	27.42	-3.59
SrO	0.02	0.00	-82.35	0.02	0.02	8.89
TiO_2	0.03	0.09	169.70	0.03	0.10	222.41
V_2O_5	4.00	3.92	-2.03	0.75	0.71	-5.50
ZnO	2.93	2.68	-8.54	0.49	0.44	-9.09
ZrO_2	1.49	1.32	-11.45	3.67	3.29	-10.38
SUM	100.00	95.17, 95.60[(a)]		100.00	96.62, 98.81[(a)]	

(a) Sum including Li_2O

Table D.1. Target vs. measured compositions of HAL24M1 glasses (continued.)

	HAL24M1-17			HAL24M1-18		
Oxide	Target (wt%)	Measured (wt%)	RPD (%)	Target (wt%)	Measured (wt%)	RPD (%)
Al_2O_3	18.87	18.67	-1.08	17.32	16.78	-3.13
B_2O_3	23.22	21.71	-6.53	13.78	12.65	-8.20
Bi_2O_3	0.12	0.10	-16.78	0.15	0.13	-14.94
CaO	3.46	3.41	-1.57	4.63	4.30	-7.11
Cl	0.15	0.10	-30.89	0.18	0.12	-33.58
Cr_2O_3	0.04	0.03	-12.74	0.94	0.99	4.72
F	0.02	0.03	26.95	1.61	1.53	-4.69
Fe_2O_3	0.02	0.03	40.95	2.25	2.16	-3.91
K_2O	0.32	0.33	3.06	0.39	0.41	4.33
Li_2O	0.37	NM	NM	2.48	NM	NM
MgO	0.53	0.53	-0.20	0.66	0.67	1.47
MnO	0.24	0.22	-7.85	0.30	0.30	0.48
Na_2O	11.89	12.45	4.70	11.33	11.81	4.25
Nd_2O_3	0.05	0.03	-33.40	0.06	0.04	-24.35
NiO	0.33	0.00	-99.60	0.41	0.01	-98.23
P_2O_5	0.51	0.48	-4.84	2.88	2.78	-3.41
PbO	0.16	0.13	-17.45	0.20	0.21	4.09
SO_3	0.38	0.01	-98.08	0.69	0.23	-67.26
SiO_2	33.70	30.24	-10.25	34.00	34.03	0.09
SrO	0.01	0.01	-40.75	0.02	0.00	-86.83
TiO_2	0.03	0.08	190.18	0.03	0.08	150.08
V_2O_5	1.63	1.62	-0.83	2.31	2.30	-0.60
ZnO	3.76	3.58	-4.68	2.52	2.60	3.25
ZrO_2	0.19	0.14	-22.38	0.86	0.78	-9.29
SUM	100.00	94.31, 94.68[(a)]		100.00	94.91, 97.38[(a)]	

(a) Sum including Li_2O

Table D.1. Target vs. measured compositions of HAL24M1 glasses (continued).

	HAL24M1-19			HAL24M1-20		
Oxide	Target (wt%)	Measured (wt%)	RPD (%)	Target (wt%)	Measured (wt%)	RPD (%)
Al_2O_3	16.97	15.95	-6.02	27.08	25.98	-4.09
B_2O_3	21.81	21.06	-3.46	18.15	17.95	-1.10
Bi_2O_3	0.08	0.06	-18.09	0.09	0.08	-11.98
CaO	1.11	1.13	1.96	3.91	3.89	-0.53
Cl	0.10	0.08	-10.98	0.11	0.09	-20.22
Cr_2O_3	0.01	0.01	44.82	0.22	0.11	-49.88
F	0.41	0.38	-6.82	1.56	1.43	-8.50
Fe_2O_3	2.24	2.14	-4.51	0.25	0.24	-4.10
K_2O	0.20	0.23	13.53	0.24	0.27	13.65
Li_2O	1.46	NM	NM	1.58	NM	NM
MgO	0.34	0.32	-4.93	0.40	0.38	-3.75
MnO	0.16	0.15	-3.83	0.18	0.16	-12.66
Na_2O	11.49	11.60	0.97	14.24	14.77	3.74
Nd_2O_3	0.03	0.02	-14.45	0.03	0.02	-52.06
NiO	0.21	0.01	-96.87	0.25	0.00	-98.22
P_2O_5	2.41	2.44	0.95	2.23	2.38	6.75
PbO	0.10	0.10	-0.94	0.12	0.11	-7.51
SO_3	0.26	0.08	-67.19	0.66	0.20	-69.58
SiO_2	37.37	37.02	-0.95	24.99	24.66	-1.30
SrO	0.01	0.01	-3.06	0.01	0.01	-35.95
TiO_2	0.02	0.06	274.09	0.02	0.09	360.07
V_2O_5	0.74	0.71	-4.41	2.68	2.63	-1.87
ZnO	0.49	0.47	-3.93	0.84	0.76	-8.65
ZrO_2	1.99	1.84	-7.54	0.17	0.13	-24.64
SUM	100.00	97.34, 98.80[a]		100.00	97.91, 99.49[a]	

(a) Sum including Li_2O

Table D.1. Target vs. measured compositions of HAL24M1 glasses (continued).

	HAL24M1-21			HAL24M1-22		
Oxide	Target (wt%)	Measured (wt%)	RPD (%)	Target (wt%)	Measured (wt%)	RPD (%)
Al_2O_3	20.68	20.11	-2.75	24.77	24.16	-2.48
B_2O_3	19.06	18.10	-5.07	20.52	17.68	-13.82
Bi_2O_3	0.07	0.05	-27.26	0.17	0.14	-14.70
CaO	0.08	0.10	28.11	1.04	0.99	-5.23
Cl	0.08	0.07	-9.97	0.20	0.16	-18.94
Cr_2O_3	0.49	0.54	10.59	0.61	0.69	13.45
F	0.27	0.24	-11.83	0.67	0.65	-3.48
Fe_2O_3	0.26	0.26	0.60	0.65	0.64	-1.44
K_2O	0.17	0.22	30.98	0.43	0.46	8.28
Li_2O	1.97	NM	NM	1.35	NM	NM
MgO	0.28	0.28	-1.02	0.72	0.74	2.28
MnO	0.13	0.11	-11.57	0.33	0.33	1.77
Na_2O	20.55	21.49	4.54	15.56	15.60	0.25
Nd_2O_3	0.02	0.01	-48.99	0.06	0.06	-1.55
NiO	0.18	0.01	-95.79	0.45	0.30	-32.21
P_2O_5	0.56	0.60	6.87	3.99	4.00	0.31
PbO	0.08	0.08	-9.95	0.21	0.19	-10.03
SO_3	0.07	0.05	-24.38	0.21	0.19	-11.32
SiO_2	28.60	27.62	-3.43	25.64	24.41	-4.82
SrO	0.01	0.01	61.03	0.02	0.00	-79.46
TiO_2	0.01	0.06	312.33	0.04	0.09	158.42
V_2O_5	3.43	3.33	-2.88	0.97	0.97	-0.26
ZnO	1.64	1.58	-3.21	0.12	0.12	1.76
ZrO_2	1.31	1.24	-5.17	1.28	1.22	-4.81
SUM	100.00	98.13, 100.10[(a)]		100.00	93.80, 95.15[(a)]	

(a) Sum including Li_2O

Table D.1. Target vs. measured compositions of HAL24M1 glasses (continued).

	HAL24M1-23			HAL24M1-24		
Oxide	Target (wt%)	Measured (wt%)	RPD (%)	Target (wt%)	Measured (wt%)	RPD (%)
Al_2O_3	15.05	15.94	5.89	16.54	16.52	-0.10
B_2O_3	13.55	13.58	0.25	14.33	14.09	-1.67
Bi_2O_3	0.15	0.13	-9.44	0.06	0.06	-5.52
CaO	0.44	0.44	1.05	9.92	9.23	-7.03
Cl	0.18	0.14	-21.50	0.08	0.06	-22.42
Cr_2O_3	0.70	0.35	-49.10	0.58	0.37	-37.30
F	1.70	1.68	-0.85	0.97	1.03	6.45
Fe_2O_3	4.50	4.53	0.56	0.70	0.71	1.67
K_2O	0.38	0.44	14.88	0.17	0.20	20.72
Li_2O	0.44	NM	NM	0.26	NM	NM
MgO	0.64	0.73	13.97	0.28	0.31	10.75
MnO	0.29	0.31	7.65	0.13	0.13	3.74
Na_2O	22.87	24.02	5.05	20.87	21.51	3.07
Nd_2O_3	0.05	0.05	-6.35	0.02	0.02	7.10
NiO	0.40	0.27	-32.13	0.17	0.15	-12.32
P_2O_5	3.84	4.42	14.96	2.04	2.41	18.11
PbO	0.19	0.20	2.44	0.08	0.08	-8.46
SO_3	0.35	0.35	0.27	0.82	0.78	-4.88
SiO_2	25.66	25.05	-2.37	25.61	25.27	-1.31
SrO	0.02	0.00	-95.53	0.01	0.00	-100.00
TiO_2	0.03	0.07	114.78	0.01	0.06	303.89
V_2O_5	1.60	1.66	3.38	2.96	3.00	1.38
ZnO	3.81	3.69	-3.01	2.79	2.66	-4.86
ZrO_2	3.17	3.03	-4.29	0.62	0.58	-5.15
SUM	100.00	101.10, 101.53[(a)]		100.00	99.21, 99.47[(a)]	

(a) Sum including Li_2O

Table D.1. Target vs. measured compositions of HAL24M1 glasses (continued).

	HAL24M1-25			HAL24M1-26		
Oxide	Target (wt%)	Measured (wt%)	RPD (%)	Target (wt%)	Measured (wt%)	RPD (%)
Al_2O_3	18.43	18.30	-0.70	20.27	19.02	-6.15
B_2O_3	17.95	16.62	-7.37	14.23	12.60	-11.45
Bi_2O_3	0.13	0.12	-8.07	0.16	0.15	-5.65
CaO	1.71	1.63	-4.61	6.27	6.11	-2.69
Cl	0.15	0.13	-17.30	0.19	0.14	-24.77
Cr_2O_3	0.87	0.82	-5.07	0.01	0.01	28.59
F	1.68	1.67	-0.40	0.62	0.57	-7.99
Fe_2O_3	6.06	6.01	-0.78	0.95	0.94	-1.49
K_2O	0.33	0.36	8.83	0.40	0.41	2.37
Li_2O	1.41	NM	NM	1.10	NM	NM
MgO	0.55	0.59	7.16	0.68	0.68	-0.10
MnO	0.25	0.26	5.21	0.31	0.31	-0.09
Na_2O	22.19	22.80	2.74	16.19	16.75	3.48
Nd_2O_3	0.05	0.06	25.01	0.06	0.06	-0.62
NiO	0.35	0.29	-15.07	0.42	0.42	0.30
P_2O_5	0.31	0.34	11.54	1.67	1.86	11.70
PbO	0.17	0.16	-1.72	0.20	0.19	-5.73
SO_3	0.54	0.52	-2.71	0.14	0.11	-20.29
SiO_2	24.13	23.85	-1.15	26.11	29.43	12.70
SrO	0.02	0.00	-100.00	0.02	0.00	-85.42
TiO_2	0.03	0.07	153.17	0.03	0.08	130.01
V_2O_5	0.07	0.08	8.27	2.73	2.67	-2.19
ZnO	1.84	1.85	0.55	3.90	4.05	3.86
ZrO_2	0.81	0.74	-8.24	3.35	3.09	-7.71
SUM	100.00	97.29, 98.70[a]		100.00	99.65, 100.75[a]	

(a) Sum including Li_2O

Table D.1. Target vs. measured compositions of HAL24M1 glasses (continued).

	HAL24M1-27			HAL24M1-28		
Oxide	Target (wt%)	Measured (wt%)	RPD (%)	Target (wt%)	Measured (wt%)	RPD (%)
Al_2O_3	18.37	17.99	-2.03	17.94	17.36	-3.23
B_2O_3	13.94	12.36	-11.34	17.00	14.31	-15.81
Bi_2O_3	0.13	0.12	-7.70	0.10	0.09	-11.17
CaO	4.25	4.11	-3.28	1.52	1.50	-0.80
Cl	0.15	0.10	-30.94	0.12	0.07	-39.14
Cr_2O_3	0.12	0.14	12.83	0.41	0.40	-4.34
F	1.22	1.16	-4.12	0.59	0.51	-13.04
Fe_2O_3	4.42	4.35	-1.70	1.00	1.00	0.23
K_2O	0.32	0.38	18.76	0.26	0.29	15.32
Li_2O	1.03	NM	NM	2.30	NM	NM
MgO	0.54	0.55	1.06	0.43	0.42	-1.59
MnO	0.25	0.26	4.44	0.20	0.20	0.83
Na_2O	19.83	19.90	0.36	17.78	17.74	-0.23
Nd_2O_3	0.05	0.05	6.95	0.04	0.04	13.38
NiO	0.34	0.35	2.01	0.27	0.26	-1.78
P_2O_5	3.75	4.26	13.46	1.78	2.04	14.67
PbO	0.16	0.14	-13.98	0.13	0.09	-29.64
SO_3	0.89	0.70	-21.70	0.51	0.32	-36.73
SiO_2	24.39	25.65	5.16	32.63	34.32	5.20
SrO	0.01	0.00	-89.11	0.01	0.00	-100.00
TiO_2	0.03	0.07	177.27	0.02	0.06	186.20
V_2O_5	3.13	3.09	-1.29	1.27	1.23	-3.65
ZnO	0.23	0.22	-6.24	0.96	0.97	1.87
ZrO_2	2.45	2.34	-4.43	2.77	2.59	-6.43
SUM	100.00	98.29, 99.32[(a)]		100.00	95.82, 98.12[(a)]	

(a) Sum including Li_2O

Table D.1. Target vs. measured compositions of HAL24M1 glasses (continued).

	HAL24M1-29			HAL24M1-30		
Oxide	Target (wt%)	Measured (wt%)	RPD (%)	Target (wt%)	Measured (wt%)	RPD (%)
Al_2O_3	26.32	24.38	-7.37	21.58	20.85	-3.36
B_2O_3	22.10	22.71	2.73	22.17	23.53	6.12
Bi_2O_3	0.09	0.09	-6.45	0.46	0.41	-9.65
CaO	0.41	0.69	69.68	0.67	0.72	8.22
Cl	0.19	0.15	-24.74	0.20	0.15	-23.76
Cr_2O_3	0.13	0.12	-6.87	0.09	0.11	20.22
F	0.21	0.38	80.57	0.46	0.56	23.30
Fe_2O_3	3.43	3.40	-1.08	6.85	7.09	3.52
K_2O	0.20	0.27	32.67	0.07	0.14	110.61
Li_2O	2.13	NM	NM	0.00	NM	NM
MgO	0.01	0.04	200.00	0.01	0.02	30.77
MnO	0.35	0.35	0.29	0.28	0.30	6.69
Na_2O	15.11	15.02	-0.65	17.32	17.10	-1.28
Nd_2O_3	0.33	0.30	-6.77	0.77	0.44	-43.21
NiO	0.34	0.33	-2.35	0.58	0.60	3.44
P_2O_5	0.37	0.55	48.38	2.30	2.33	1.35
PbO	0.18	0.14	-26.09	0.49	0.47	-3.70
SO_3	0.27	0.23	-13.01	0.51	0.41	-20.59
SiO_2	27.37	26.56	-2.98	24.78	23.57	-4.86
SrO	0.00	0.03	0.00	0.00	0.04	0.00
TiO_2	0.00	0.08	0.00	0.00	0.07	0.00
V_2O_5	0.00	0.18	5800.00	0.00	0.01	0.00
ZnO	0.01	0.05	657.14	0.01	0.02	114.29
ZrO_2	0.43	0.47	9.15	0.42	0.41	-2.61
SUM	100.00	96.50, 98.63[a]		100.00	99.34	

(a) Sum including Li_2O

Table D.2. Target vs. measured compositions of HAL24M2 glasses.

	HAL24M2-01			HAL24M2-02		
Oxide	Target (wt%)	Measured (wt%)	RPD (%)	Target (wt%)	Measured (wt%)	RPD (%)
Al_2O_3	15.45	14.89	-3.63	18.03	17.32	-3.92
B_2O_3	16.30	15.46	-5.17	15.89	14.68	-7.62
Bi_2O_3	0.12	0.12	-4.03	0.07	0.06	-12.31
CaO	6.70	6.97	4.03	0.03	0.07	112.68
Cl	0.15	0.10	-33.24	0.08	0.06	-21.70
Cr_2O_3	0.11	0.10	-8.80	0.43	0.38	-12.17
F	1.43	1.02	-28.67	0.03	0.07	141.10
Fe_2O_3	5.79	5.69	-1.60	4.75	4.67	-1.63
K_2O	0.31	0.32	0.34	0.17	0.19	10.16
Li_2O	0.03	NM	NM	2.48	NM	NM
MgO	0.53	0.47	-10.89	0.28	0.27	-5.47
MnO	0.24	0.24	-0.77	0.13	0.13	1.05
Na_2O	21.67	20.64	-4.75	22.98	22.35	-2.71
Nd_2O_3	0.04	0.04	-14.23	0.02	0.05	94.73
NiO	0.33	0.33	-0.55	0.18	0.18	2.15
P_2O_5	0.77	0.74	-4.22	3.91	3.89	-0.60
PbO	0.16	0.15	-3.53	0.08	0.10	24.81
SO_3	0.11	0.12	7.59	0.77	0.76	-1.50
SiO_2	25.70	25.96	1.01	26.23	26.58	1.32
SrO	0.01	0.03	118.65	0.01	0.02	210.36
TiO_2	0.03	0.08	197.64	0.01	0.05	246.18
V_2O_5	0.14	0.13	-10.90	0.05	0.05	1.25
ZnO	0.54	0.54	-0.30	3.18	3.25	2.24
ZrO_2	3.33	3.28	-1.44	0.22	0.26	17.71
SUM	100.00	97.40, 97.44[(a)]		100.00	95.43, 97.91[(a)]	

(a) Sum including Li_2O

Table D.2. Target vs. measured compositions of HAL24M2 glasses (continued).

	HAL24M2-03			HAL24M2-04-1		
Oxide	Target (wt%)	Measured (wt%)	RPD (%)	Target (wt%)	Measured (wt%)	RPD (%)
Al_2O_3	19.26	18.72	-2.79	15.58	14.97	-3.87
B_2O_3	18.03	16.83	-6.64	14.80	13.77	-7.00
Bi_2O_3	0.14	0.11	-26.82	0.09	0.08	-14.64
CaO	0.15	0.19	20.80	0.07	0.08	29.98
Cl	0.17	0.13	-24.88	0.11	0.08	-24.14
Cr_2O_3	0.24	0.30	24.95	0.17	0.17	2.38
F	0.09	0.01	-87.47	0.71	0.49	-30.87
Fe_2O_3	0.11	0.09	-17.10	1.60	1.60	0.19
K_2O	0.37	0.38	4.14	0.24	0.25	4.23
Li_2O	0.90	NM	NM	0.73	NM	NM
MgO	0.62	0.59	-4.87	0.40	0.38	-6.17
MnO	0.28	0.28	0.76	0.18	0.20	9.98
Na_2O	15.94	15.33	-3.82	21.42	20.66	-3.53
Nd_2O_3	0.05	0.05	-7.75	0.03	0.08	120.97
NiO	0.39	0.40	2.61	0.25	0.24	-4.32
P_2O_5	3.76	3.81	1.35	3.96	3.97	0.25
PbO	0.19	0.17	-10.13	0.12	0.13	9.17
SO_3	0.79	0.59	-25.57	0.58	0.45	-23.14
SiO_2	31.16	31.15	-0.01	34.38	34.80	1.23
SrO	0.02	0.02	36.04	0.01	0.03	140.48
TiO_2	0.03	0.06	106.68	0.02	0.10	395.06
V_2O_5	2.16	2.15	-0.37	0.73	0.68	-7.20
ZnO	1.95	1.98	1.39	0.01	0.02	87.59
ZrO_2	3.20	3.04	-5.07	3.80	3.75	-1.51
SUM	100.00	96.38, 97.28[(a)]		100.00	96.98, 97.71[(a)]	

(a) Sum including Li_2O

Table D.2. Target vs. measured compositions of HAL24M2 glasses (continued).

	HAL24M2-05			HAL24M2-06		
Oxide	Target (wt%)	Measured (wt%)	RPD (%)	Target (wt%)	Measured (wt%)	RPD (%)
Al_2O_3	18.99	18.10	-4.67	15.03	14.37	-4.40
B_2O_3	14.92	14.20	-4.81	20.42	18.76	-8.10
Bi_2O_3	0.17	0.12	-27.86	0.11	0.10	-10.48
CaO	4.11	4.25	3.54	7.30	7.48	2.47
Cl	0.20	0.16	-20.68	0.13	0.09	-29.86
Cr_2O_3	0.05	0.05	12.22	0.78	0.72	-8.56
F	1.95	1.63	-16.32	1.31	1.02	-22.03
Fe_2O_3	5.13	5.01	-2.19	0.75	0.73	-1.62
K_2O	0.43	0.42	-1.51	0.28	0.28	0.53
Li_2O	2.31	NM	NM	0.31	NM	NM
MgO	0.72	0.67	-6.50	0.48	0.43	-9.44
MnO	0.33	0.35	8.10	0.22	0.20	-7.15
Na_2O	16.02	15.43	-3.69	11.52	11.09	-3.71
Nd_2O_3	0.06	0.09	43.73	0.04	0.04	5.75
NiO	0.45	0.45	1.41	0.30	0.28	-5.13
P_2O_5	0.23	0.25	11.23	0.10	0.10	-1.58
PbO	0.21	0.20	-7.39	0.14	0.13	-11.35
SO_3	0.10	0.12	26.84	0.17	0.14	-16.22
SiO_2	31.23	32.04	2.58	34.75	35.22	1.37
SrO	0.02	0.01	-33.01	0.01	0.02	22.23
TiO_2	0.04	0.08	133.23	0.02	0.06	149.30
V_2O_5	0.92	0.89	-3.38	3.68	3.58	-2.70
ZnO	1.41	1.44	1.83	1.29	1.24	-3.51
ZrO_2	0.03	0.03	20.40	0.88	0.83	-5.38
SUM	100.00	96.01, 98.33[(a)]		100.00	96.92, 97.22[(a)]	

(a) Sum including Li_2O

Table D.2. Target vs. measured compositions of HAL24M2 glasses (continued).

	HAL24M2-07			HAL24M2-08		
Oxide	Target (wt%)	Measured (wt%)	RPD (%)	Target (wt%)	Measured (wt%)	RPD (%)
Al_2O_3	18.43	17.74	-3.76	15.59	15.27	-2.06
B_2O_3	15.61	14.77	-5.37	16.48	16.47	-0.05
Bi_2O_3	0.07	0.04	-48.76	0.13	0.12	-6.77
CaO	4.78	4.91	2.88	9.45	9.72	2.78
Cl	0.09	0.07	-21.40	0.16	0.12	-24.65
Cr_2O_3	0.40	0.26	-35.04	0.83	0.75	-9.17
F	1.95	1.82	-6.75	1.94	1.21	-37.77
Fe_2O_3	1.63	1.59	-2.22	6.71	6.41	-4.47
K_2O	0.18	0.20	8.01	0.34	0.33	-2.74
Li_2O	0.77	NM	NM	1.65	NM	NM
MgO	0.31	0.29	-7.52	0.57	0.52	-9.16
MnO	0.14	0.15	9.52	0.26	0.24	-8.17
Na_2O	18.64	18.58	-0.29	11.47	11.22	-2.14
Nd_2O_3	0.03	0.04	60.57	0.05	0.05	-6.04
NiO	0.19	0.20	2.24	0.36	0.36	0.48
P_2O_5	0.54	0.53	-2.99	3.14	3.07	-2.23
PbO	0.09	0.11	14.19	0.17	0.18	6.82
SO_3	0.22	0.19	-12.23	0.45	0.38	-15.43
SiO_2	25.22	25.24	0.08	26.58	26.56	-0.07
SrO	0.01	0.03	311.60	0.02	0.01	-5.09
TiO_2	0.02	0.05	260.68	0.03	0.06	131.29
V_2O_5	3.34	3.24	-3.09	0.35	0.33	-6.17
ZnO	3.67	3.74	1.93	1.02	1.03	0.52
ZrO_2	3.70	3.70	0.17	2.28	2.16	-4.92
SUM	100.00	97.47, 98.25[a]		100.00	96.56, 98.21[a]	

(a) Sum including Li_2O

Table D.2. Target vs. measured compositions of HAL24M2 glasses (continued).

	HAL24M2-09			HAL24M2-10		
Oxide	Target (wt%)	Measured (wt%)	RPD (%)	Target (wt%)	Measured (wt%)	RPD (%)
Al_2O_3	15.28	14.73	-3.61	21.19	20.43	-3.56
B_2O_3	22.66	20.19	-10.89	17.64	16.23	-7.99
Bi_2O_3	0.06	0.06	2.65	0.16	0.12	-22.80
CaO	4.78	4.86	1.79	9.34	9.57	2.47
Cl	0.07	0.06	-19.42	0.19	0.13	-32.35
Cr_2O_3	0.52	0.41	-20.45	0.21	0.20	-4.04
F	0.08	0.00	-100.0	1.67	1.31	-21.58
Fe_2O_3	5.54	5.27	-4.83	3.98	3.79	-4.67
K_2O	0.15	0.15	5.25	0.41	0.39	-3.93
Li_2O	0.47	NM	NM	1.86	NM	NM
MgO	0.25	0.22	-11.96	0.68	0.61	-10.63
MnO	0.11	0.10	-7.54	0.31	0.31	0.93
Na_2O	17.73	16.98	-4.26	11.00	10.52	-4.38
Nd_2O_3	0.02	0.03	26.32	0.06	0.08	37.03
NiO	0.16	0.15	-5.58	0.43	0.43	1.48
P_2O_5	1.30	1.37	5.27	1.49	1.44	-3.64
PbO	0.07	0.09	22.31	0.20	0.19	-4.66
SO_3	0.14	0.15	8.45	0.21	0.19	-6.58
SiO_2	26.15	26.34	0.72	24.75	24.91	0.62
SrO	0.01	0.04	420.89	0.02	0.01	-43.16
TiO_2	0.01	0.08	592.19	0.03	0.12	239.98
V_2O_5	2.17	2.08	-4.16	0.78	0.75	-3.27
ZnO	0.46	0.50	7.00	0.21	0.24	10.94
ZrO_2	1.82	1.83	0.33	3.19	3.05	-4.59
SUM	100.00	95.69, 96.15[(a)]		100.00	95.02, 96.88 [(a)]	

(a) Sum including Li_2O

Table D.2. Target vs. measured compositions of HAL24M2 glasses (continued).

	HAL24M2-11			HAL24M2-12		
Oxide	Target (wt%)	Measured (wt%)	RPD (%)	Target (wt%)	Measured (wt%)	RPD (%)
Al_2O_3	15.12	14.23	-5.89	20.90	19.25	-7.93
B_2O_3	14.49	14.27	-1.52	16.29	15.51	-4.79
Bi_2O_3	0.07	0.06	-15.40	0.11	0.09	-14.12
CaO	7.05	7.19	2.04	0.01	0.03	400.22
Cl	0.09	0.07	-22.21	0.13	0.10	-20.37
Cr_2O_3	0.65	0.40	-38.16	1.00	0.56	-43.46
F	0.03	0.01	-44.95	1.54	1.33	-13.67
Fe_2O_3	2.47	2.36	-4.66	0.82	0.81	-1.19
K_2O	0.18	0.19	4.95	0.28	0.29	4.84
Li_2O	2.29	NM	NM	1.86	NM	NM
MgO	0.31	0.26	-15.04	0.47	0.44	-7.18
MnO	0.14	0.13	-6.95	0.21	0.21	0.04
Na_2O	15.32	14.75	-3.68	19.54	19.32	-1.10
Nd_2O_3	0.03	0.02	-8.58	0.04	0.04	-7.15
NiO	0.19	0.18	-5.61	0.29	0.29	-2.69
P_2O_5	0.24	0.22	-7.56	2.57	2.60	1.45
PbO	0.09	0.07	-26.32	0.14	0.17	19.83
SO_3	0.60	0.56	-5.99	0.42	0.41	-2.12
SiO_2	32.20	32.06	-0.42	24.04	24.63	2.48
SrO	0.01	0.02	170.30	0.01	0.03	161.35
TiO_2	0.02	0.07	396.68	0.02	0.06	182.29
V_2O_5	2.39	2.26	-5.39	3.02	2.96	-2.12
ZnO	2.96	2.90	-2.01	2.98	2.80	-6.19
ZrO_2	3.08	3.00	-2.69	3.31	3.39	2.42
SUM	100.00	95.30, 97.59 [(a)]		100.00	95.33, 97.19 [(a)]	

(a) Sum including Li_2O

Table D.2. Target vs. measured compositions of HAL24M2 glasses (continued).

	HAL24M2-13			HAL24M2-14		
Oxide	Target (wt%)	Measured (wt%)	RPD (%)	Target (wt%)	Measured (wt%)	RPD (%)
Al_2O_3	24.59	22.24	-9.56	15.00	14.32	-4.55
B_2O_3	23.10	21.14	-8.52	15.23	14.74	-3.19
Bi_2O_3	0.09	0.06	-26.20	0.14	0.11	-20.79
CaO	2.16	2.23	3.59	0.64	0.66	4.13
Cl	0.10	0.07	-34.57	0.17	0.12	-31.50
Cr_2O_3	0.91	0.61	-32.67	0.13	0.13	-4.37
F	0.02	0.02	22.95	1.07	0.65	-39.37
Fe_2O_3	1.27	1.24	-2.34	6.82	6.62	-2.91
K_2O	0.22	0.23	4.22	0.37	0.37	1.05
Li_2O	0.49	NM	NM	1.79	NM	NM
MgO	0.38	0.33	-12.01	0.62	0.57	-7.41
MnO	0.17	0.17	-0.30	0.28	0.27	-2.96
Na_2O	13.62	13.08	-3.99	18.21	17.43	-4.29
Nd_2O_3	0.03	0.03	-1.58	0.05	0.08	58.91
NiO	0.24	0.21	-10.09	0.38	0.38	-1.59
P_2O_5	2.92	2.95	0.95	1.24	1.21	-2.10
PbO	0.11	0.06	-49.09	0.18	0.19	2.17
SO_3	0.82	0.56	-31.66	0.29	0.28	-3.18
SiO_2	25.15	25.48	1.31	31.82	31.99	0.53
SrO	0.01	0.02	100.45	0.02	0.02	31.36
TiO_2	0.02	0.09	399.06	0.03	0.08	150.47
V_2O_5	0.50	0.47	-5.50	3.42	3.32	-3.06
ZnO	1.08	0.90	-16.90	0.42	0.43	2.71
ZrO_2	2.00	1.91	-4.44	1.67	1.63	-1.95
SUM	100.00	94.11, 94.60[(a)]		100.00	95.61, 97.40[(a)]	

(a) Sum including Li_2O

Table D.2. Target vs. measured compositions of HAL24M2 glasses (continued).

	HAL24M2-15			HAL24M2-16		
Oxide	Target (wt%)	Measured (wt%)	RPD (%)	Target (wt%)	Measured (wt%)	RPD (%)
Al_2O_3	17.84	17.30	-3.00	18.50	18.17	-1.76
B_2O_3	18.61	17.04	-8.42	20.80	18.63	-10.43
Bi_2O_3	0.07	0.06	-13.46	0.09	0.07	-17.47
CaO	5.85	6.21	6.15	3.78	4.04	6.93
Cl	0.08	0.07	-17.75	0.11	0.06	-45.97
Cr_2O_3	0.09	0.09	0.46	0.35	0.30	-13.88
F	0.13	0.11	-15.89	0.46	0.36	-22.29
Fe_2O_3	1.09	1.06	-3.07	6.90	6.67	-3.35
K_2O	0.18	0.20	12.29	0.23	0.24	3.96
Li_2O	0.10	NM	NM	0.42	NM	NM
MgO	0.30	0.26	-14.63	0.39	0.35	-9.06
MnO	0.14	0.14	-2.02	0.18	0.18	0.43
Na_2O	19.92	19.62	-1.51	11.77	11.63	-1.16
Nd_2O_3	0.03	0.02	-49.07	0.03	0.04	38.86
NiO	0.19	0.19	-0.36	0.24	0.22	-7.35
P_2O_5	1.99	1.92	-3.47	3.27	3.10	-5.10
PbO	0.09	0.06	-35.33	0.12	0.11	-7.86
SO_3	0.01	0.02	121.03	0.75	0.44	-41.11
SiO_2	26.65	27.17	1.96	27.51	28.24	2.67
SrO	0.01	0.03	192.12	0.01	0.04	344.08
TiO_2	0.02	0.06	204.37	0.02	0.06	197.65
V_2O_5	0.88	0.84	-4.49	0.83	0.80	-3.64
ZnO	3.44	3.58	3.94	2.42	2.40	-0.83
ZrO_2	2.30	2.24	-2.47	0.84	0.77	-8.65
SUM	100.01	98.28, 98.38[(a)]		100.02	96.95, 97.37[(a)]	

(a) Sum including Li_2O

Table D.2. Target vs. measured compositions of HAL24M2 glasses (continued).

	HAL24M2-17			HAL24M2-18		
Oxide	Target (wt%)	Measured (wt%)	RPD (%)	Target (wt%)	Measured (wt%)	RPD (%)
Al_2O_3	15.11	14.73	-2.54	19.47	18.96	-2.64
B_2O_3	23.85	22.54	-5.51	19.55	18.03	-7.77
Bi_2O_3	0.15	0.12	-21.82	0.08	0.08	3.48
CaO	8.90	9.46	6.33	4.72	5.05	7.06
Cl	0.18	0.11	-37.74	0.10	0.08	-17.98
Cr_2O_3	0.95	0.80	-16.25	0.83	0.77	-7.34
F	0.31	0.25	-20.83	1.32	1.35	2.43
Fe_2O_3	1.73	1.63	-5.70	4.83	4.69	-2.98
K_2O	0.39	0.39	1.25	0.21	0.23	7.29
Li_2O	1.65	NM	NM	0.87	NM	NM
MgO	0.65	0.60	-7.40	0.35	0.32	-9.67
MnO	0.30	0.28	-5.04	0.16	0.17	3.45
Na_2O	12.13	11.51	-5.15	13.49	12.95	-3.99
Nd_2O_3	0.06	0.07	13.36	0.03	0.06	99.71
NiO	0.41	0.39	-5.39	0.22	0.22	0.06
P_2O_5	0.21	0.22	2.71	1.09	1.08	-1.07
PbO	0.19	0.21	9.33	0.11	0.08	-26.62
SO_3	1.21	1.05	-13.40	0.63	0.53	-16.52
SiO_2	30.60	31.43	2.70	30.05	31.24	3.96
SrO	0.02	0.02	-20.53	0.01	0.04	321.23
TiO_2	0.03	0.08	174.63	0.02	0.07	253.05
V_2O_5	0.92	0.88	-4.29	1.45	1.38	-4.93
ZnO	0.01	0.06	459.02	0.13	0.16	21.57
ZrO_2	0.06	0.05	-23.66	0.28	0.27	-4.03
SUM	100.02	96.85, 98.50[a]		100.00	97.79, 98.66[a]	

(a) Sum including Li_2O

Table D.2. Target vs. measured compositions of HAL24M2 glasses (continued).

	HAL24M2-19			HAL24M2-20		
Oxide	Target (wt%)	Measured (wt%)	RPD (%)	Target (wt%)	Measured (wt%)	RPD (%)
Al_2O_3	21.93	21.77	-0.74	19.19	18.67	-2.73
B_2O_3	21.08	19.54	-7.30	16.99	16.95	-0.22
Bi_2O_3	0.07	0.03	-61.75	0.10	0.07	-29.45
CaO	2.65	2.81	5.94	3.44	3.63	5.47
Cl	0.09	0.07	-27.40	0.12	0.09	-24.35
Cr_2O_3	0.01	0.02	125.34	0.63	0.39	-38.82
F	1.44	1.46	1.13	0.99	1.03	4.18
Fe_2O_3	0.63	0.64	2.28	6.42	6.02	-6.23
K_2O	0.19	0.19	2.14	0.26	0.26	1.86
Li_2O	0.55	NM	NM	1.89	NM	NM
MgO	0.31	0.27	-12.34	0.44	0.40	-9.51
MnO	0.14	0.15	4.15	0.20	0.20	1.75
Na_2O	20.61	19.79	-3.97	13.95	13.63	-2.29
Nd_2O_3	0.03	0.06	91.42	0.04	0.03	-13.81
NiO	0.19	0.21	9.52	0.28	0.22	-22.91
P_2O_5	0.14	0.15	8.83	0.35	0.35	-0.56
PbO	0.09	0.05	-46.82	0.13	0.12	-9.11
SO_3	0.58	0.52	-10.95	0.22	0.24	7.63
SiO_2	24.25	24.83	2.41	26.23	27.40	4.45
SrO	0.01	0.03	213.51	0.01	0.02	127.95
TiO_2	0.02	0.10	408.33	0.02	0.11	446.36
V_2O_5	2.83	2.72	-3.85	3.56	3.43	-3.56
ZnO	0.39	0.42	8.04	2.34	2.26	-3.40
ZrO_2	1.77	1.76	-0.41	2.21	2.19	-1.02
SUM	100.00	97.59, 98.14[a]		100.01	97.71, 99.60[a]	

(a) Sum including Li_2O

Appendix E – XRD Patterns of Samples with Crystalline Phases Present

This appendix presents the refined X-ray diffraction (XRD) data with wt% of crystalline phases. The CeO_2 was added as a standard to quantify the crystalline phases. Red is calculated, and blue is experimental data. The gray line shows the difference between experimental and calculated values. The normalized wt% of crystalline phases are provided in Section 3.1.

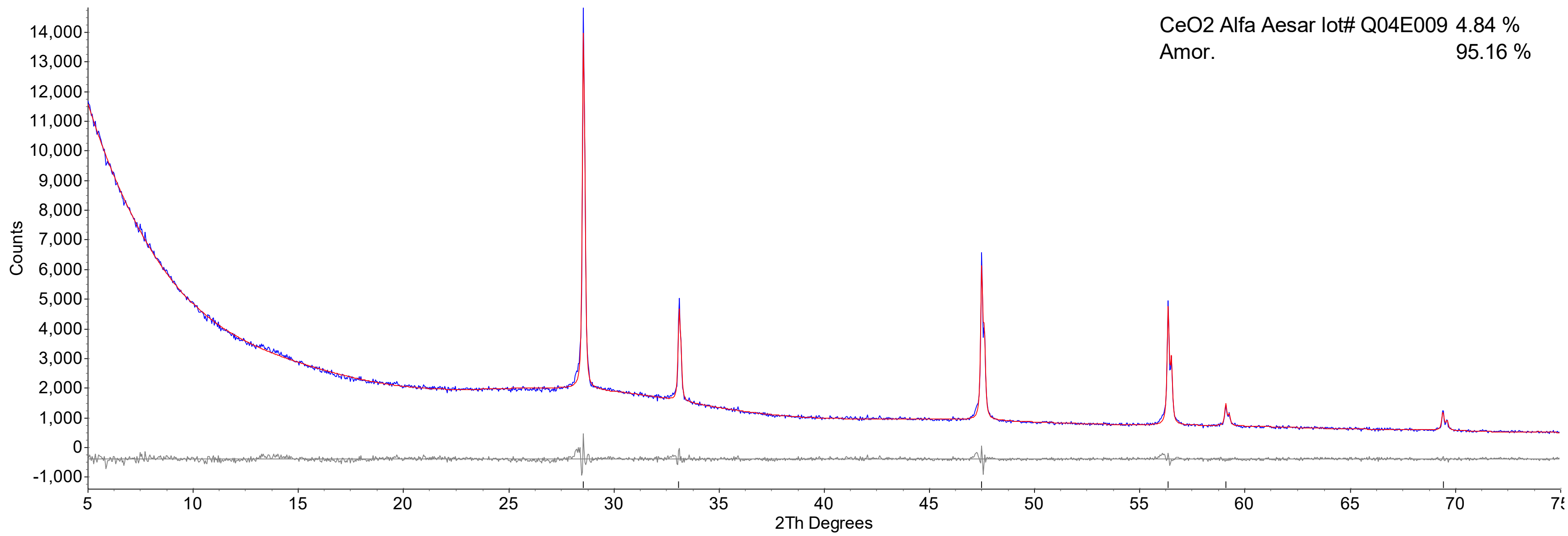

Figure E.1. Refined XRD data of HAL24M1-01.

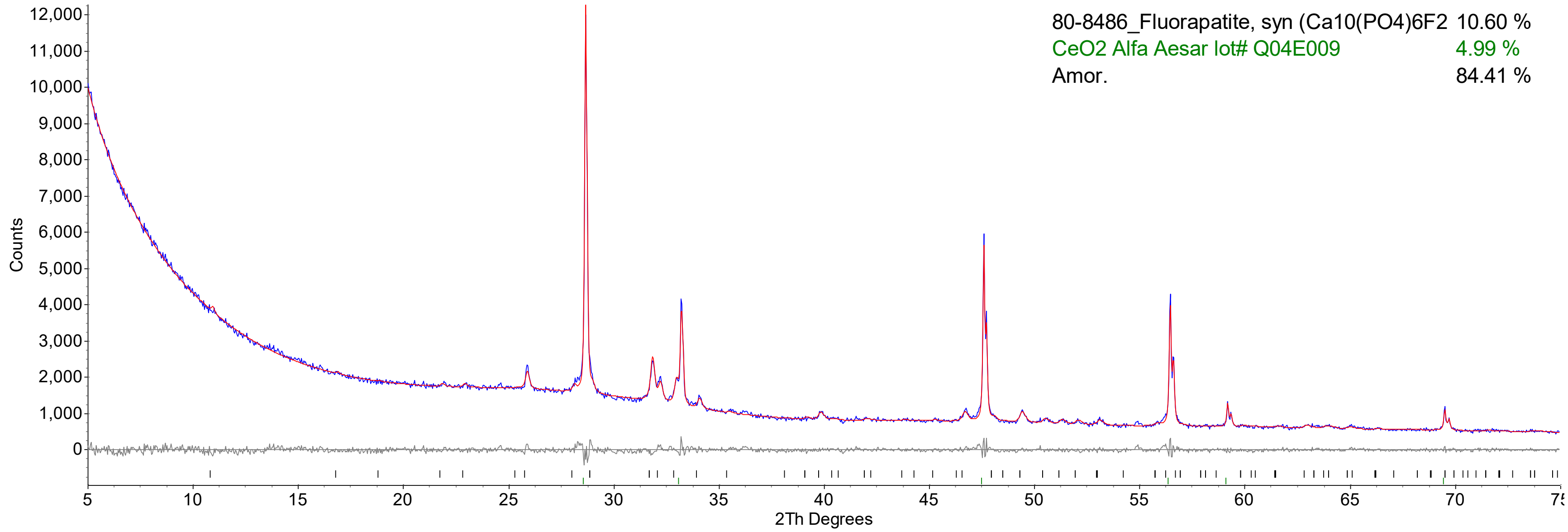

Figure E.2. Refined XRD data of HAL24M1-02.

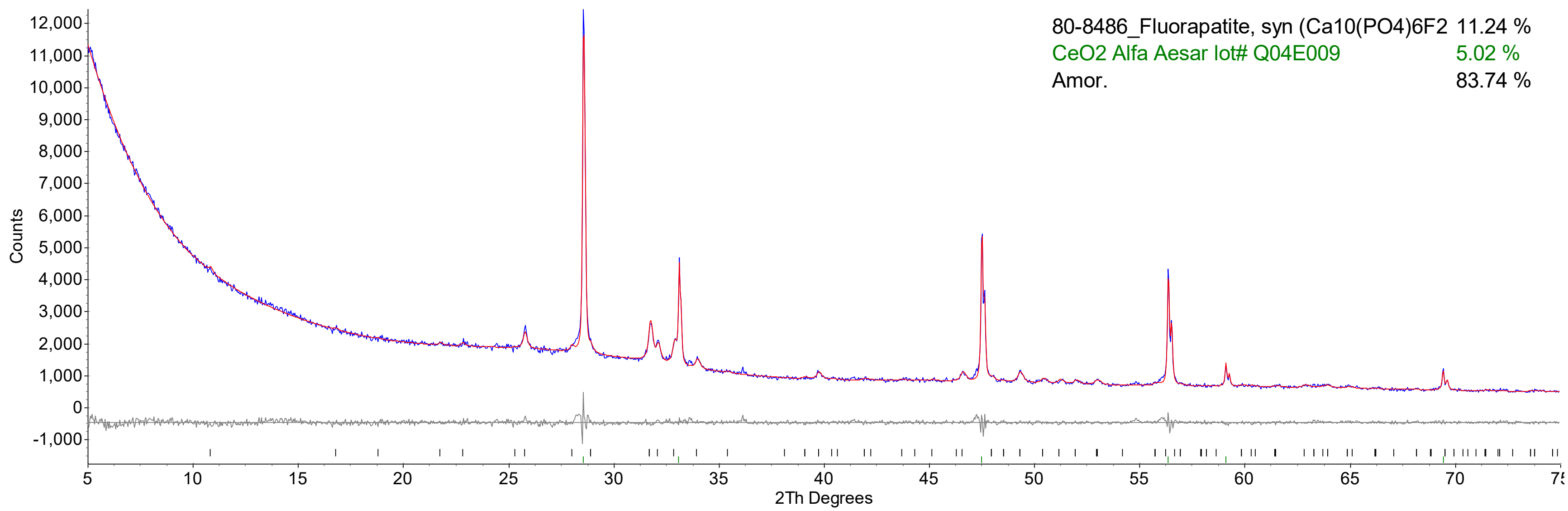

Figure E.3. Refined XRD data of HAL24M1-03.

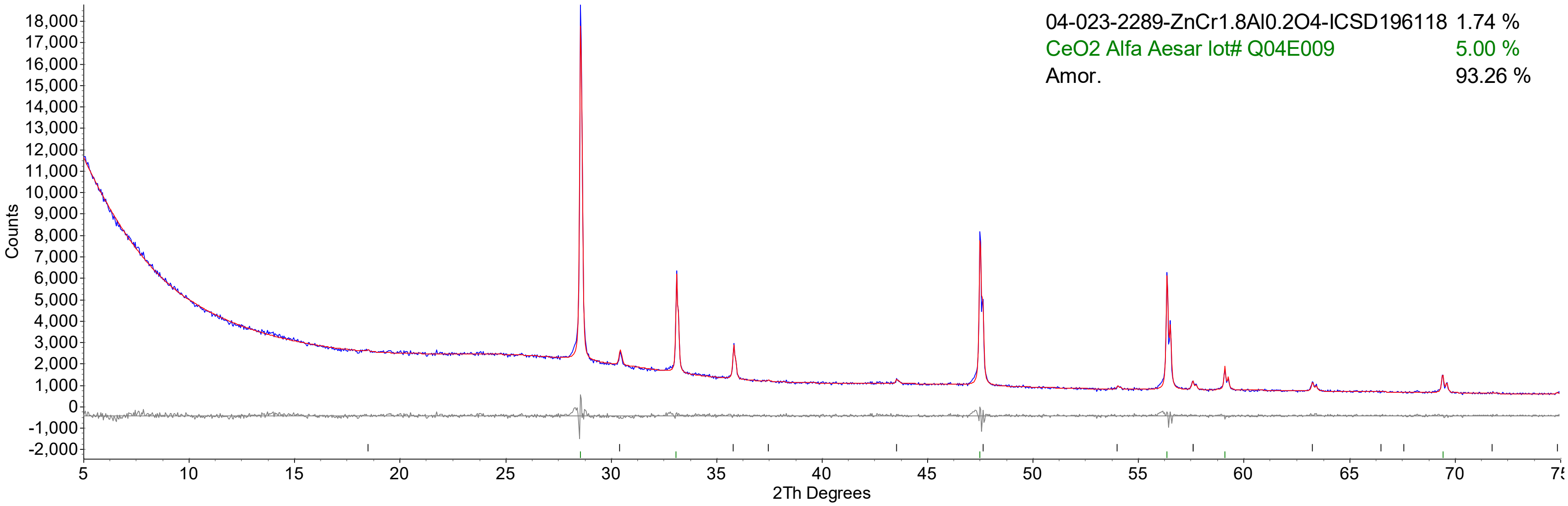

Figure E.4. Refined XRD data of HAL24M1-04.

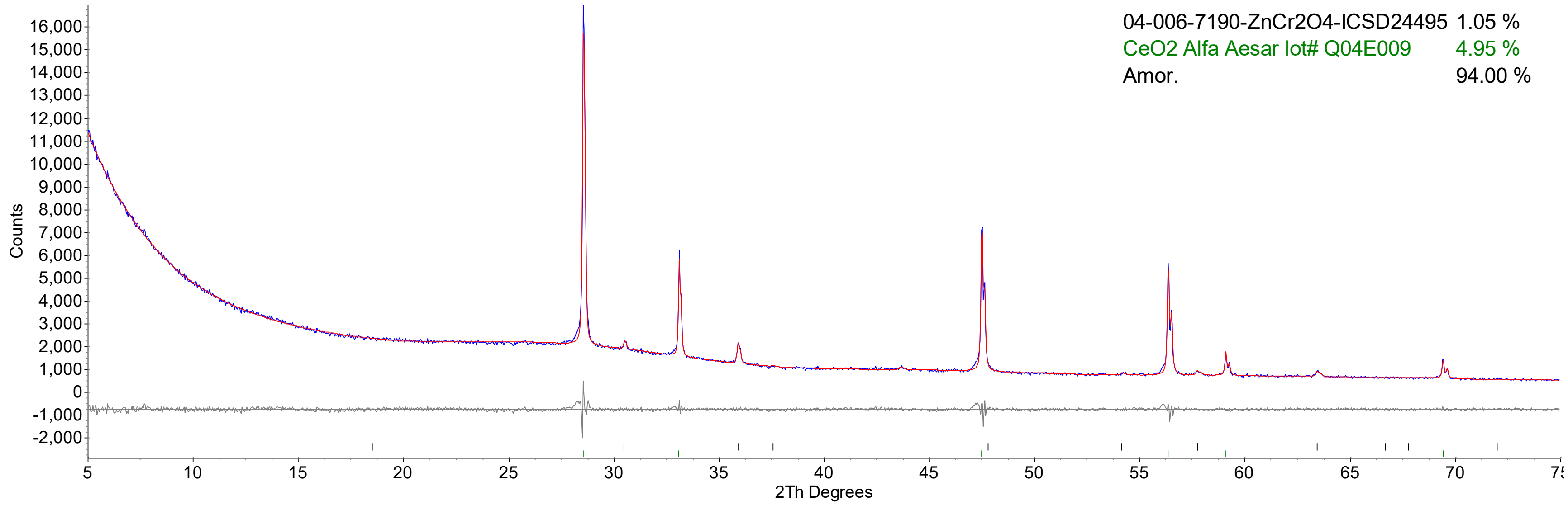

Figure E.5. Refined XRD data of HAL24M1-05.

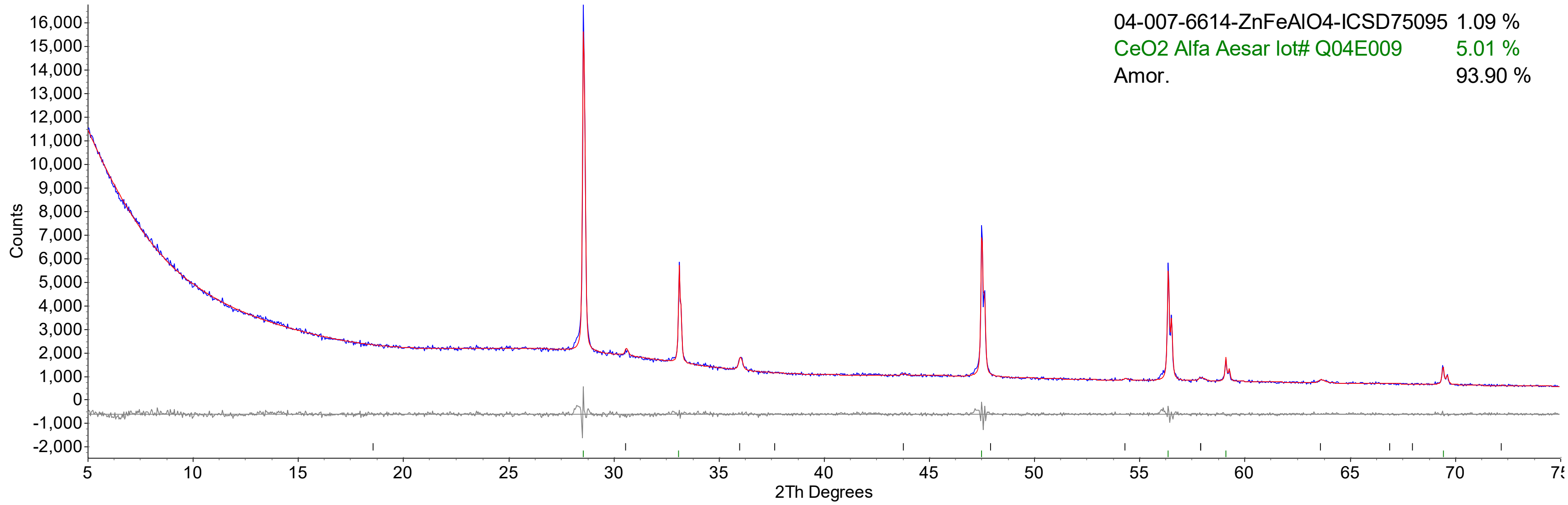

Figure E.6. Refined XRD data of HAL24M1-06.

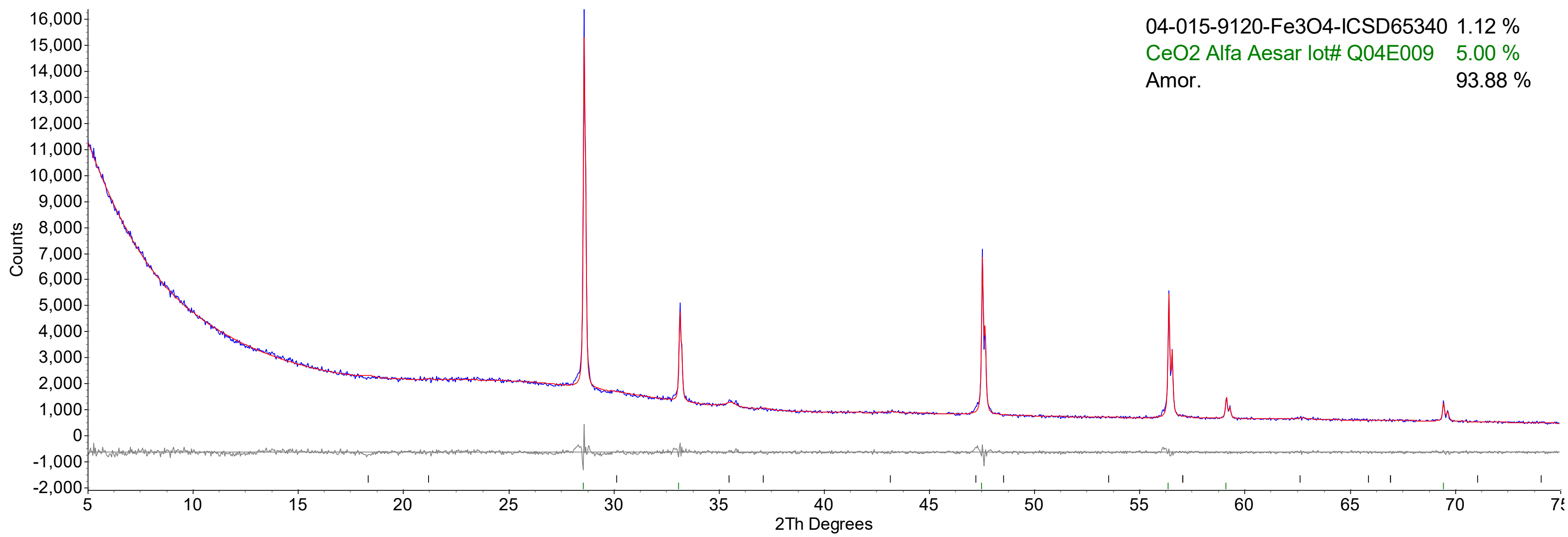

Figure E.7. Refined XRD data of HAL24M1-07.

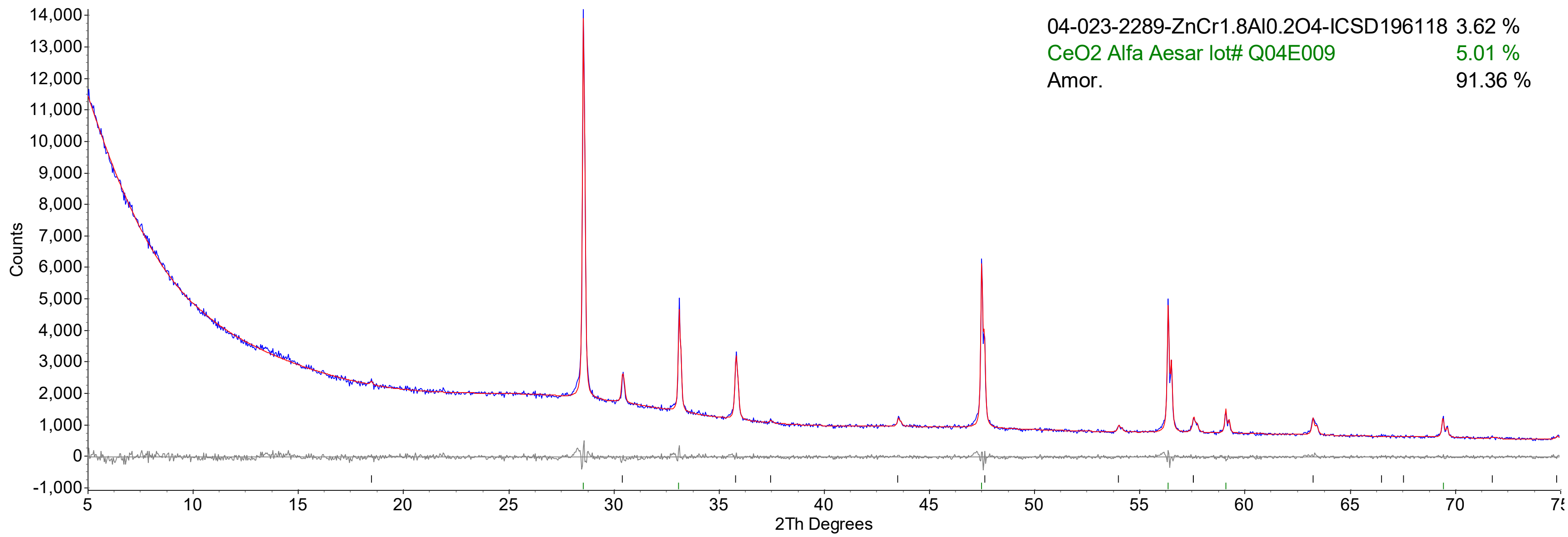

Figure E.8. Refined XRD data of HAL24M1-08.

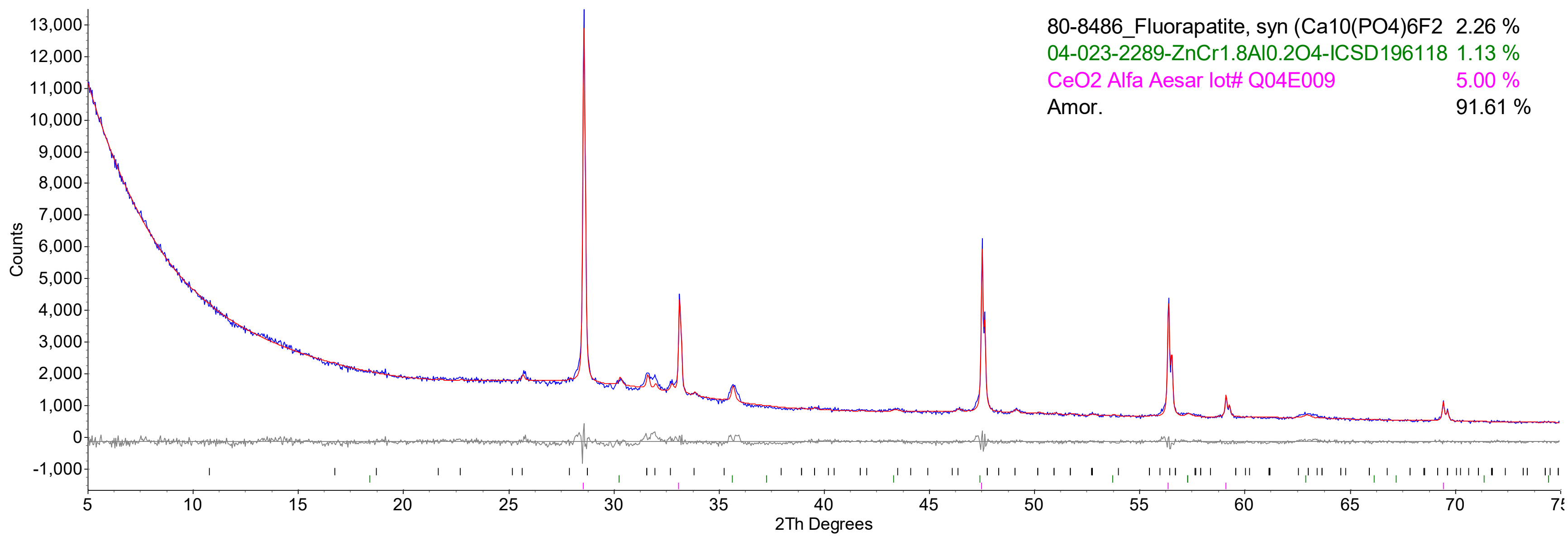

Figure E.9. Refined XRD data of HAL24M1-09.

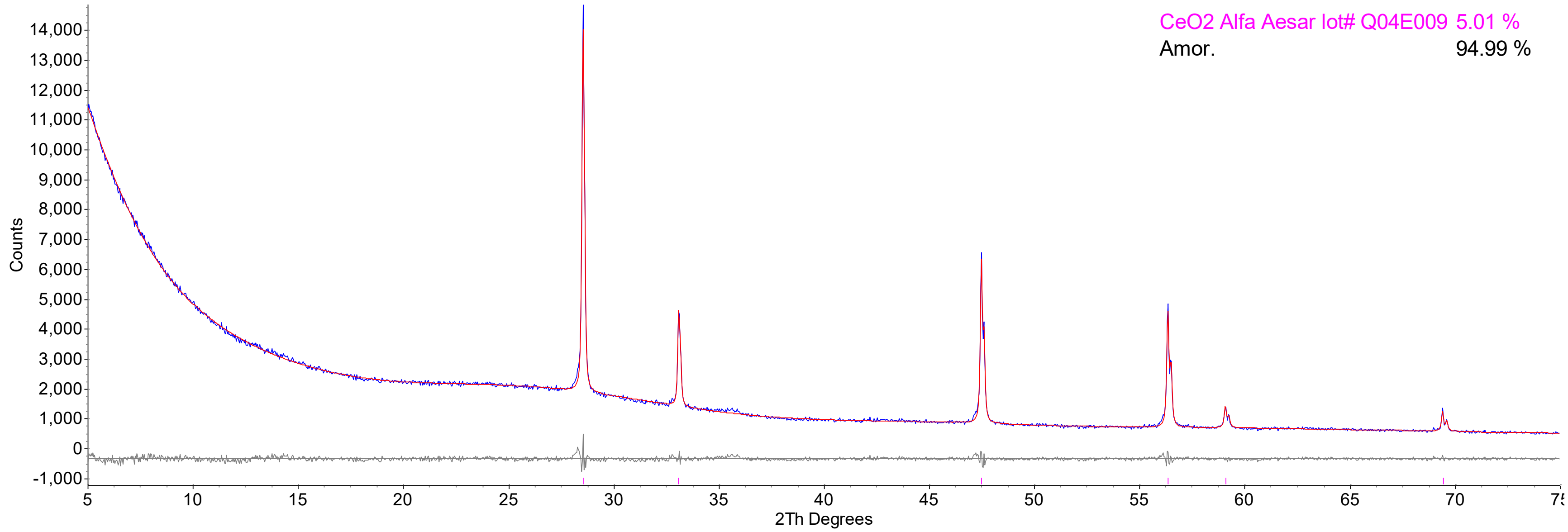

Figure E.10. Refined XRD data of HAL24M1-10.

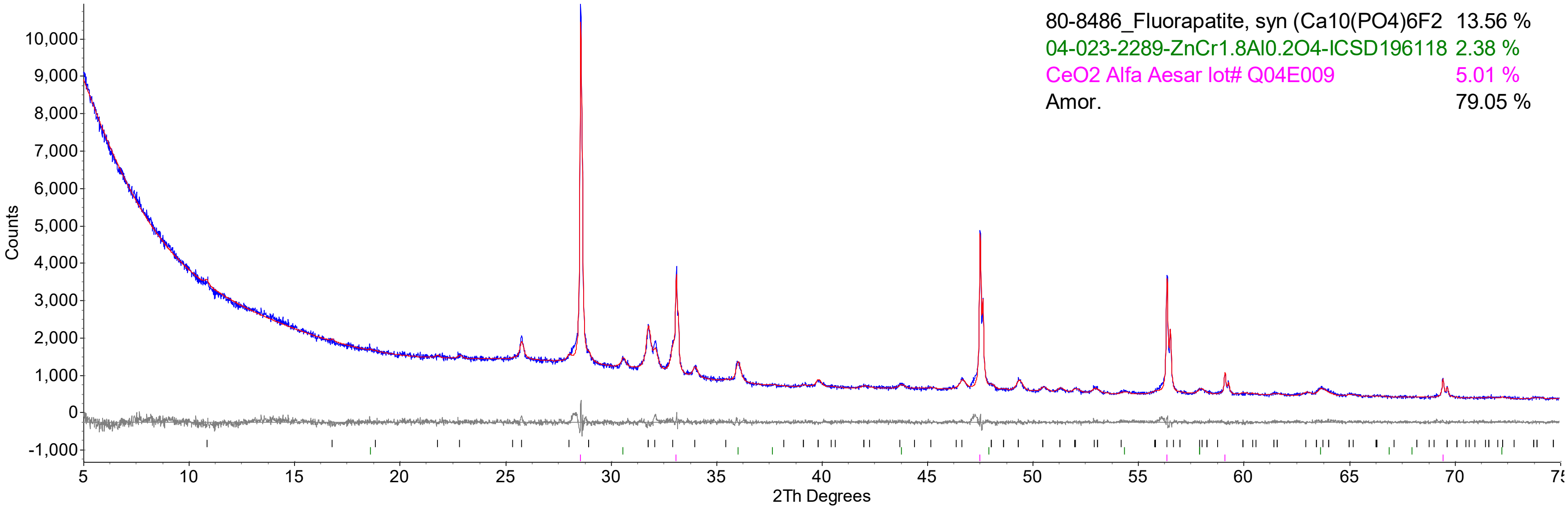

Figure E.11. Refined XRD data of HAL24M1-11.

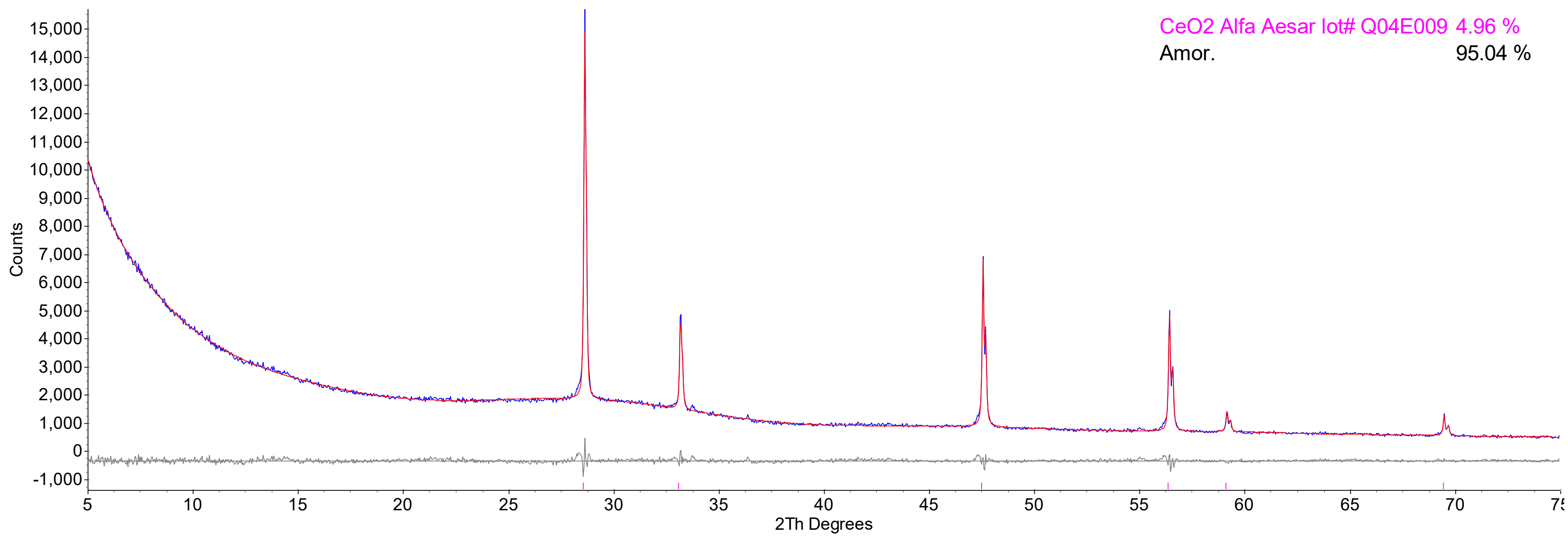

Figure E.12. Refined XRD data of HAL24M1-12.

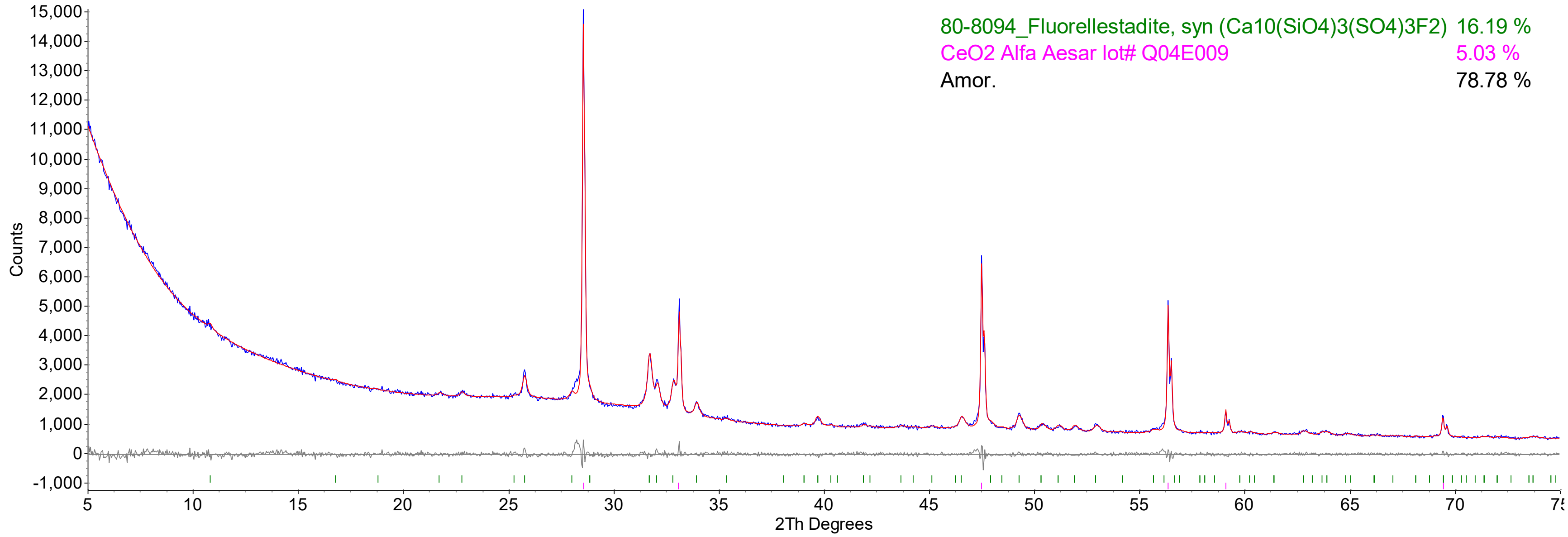

Figure E.13. Refined XRD data of HAL24M1-13-1.

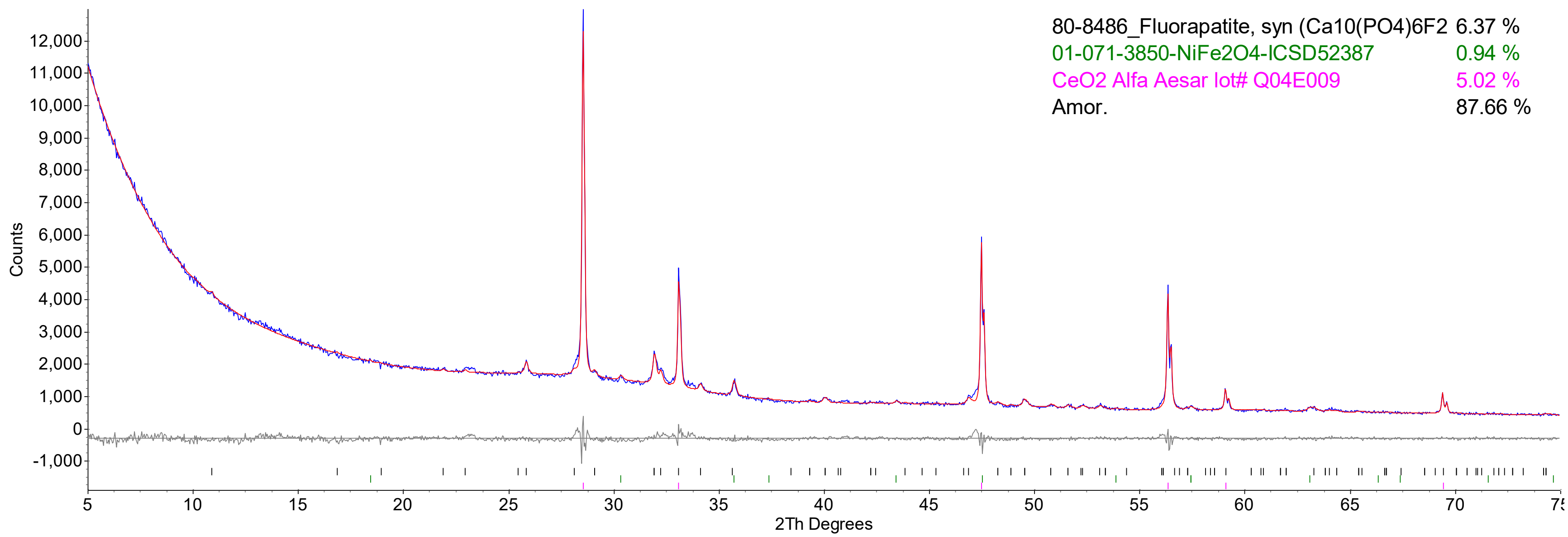

Figure E.14. Refined XRD data of HAL24M1-14.

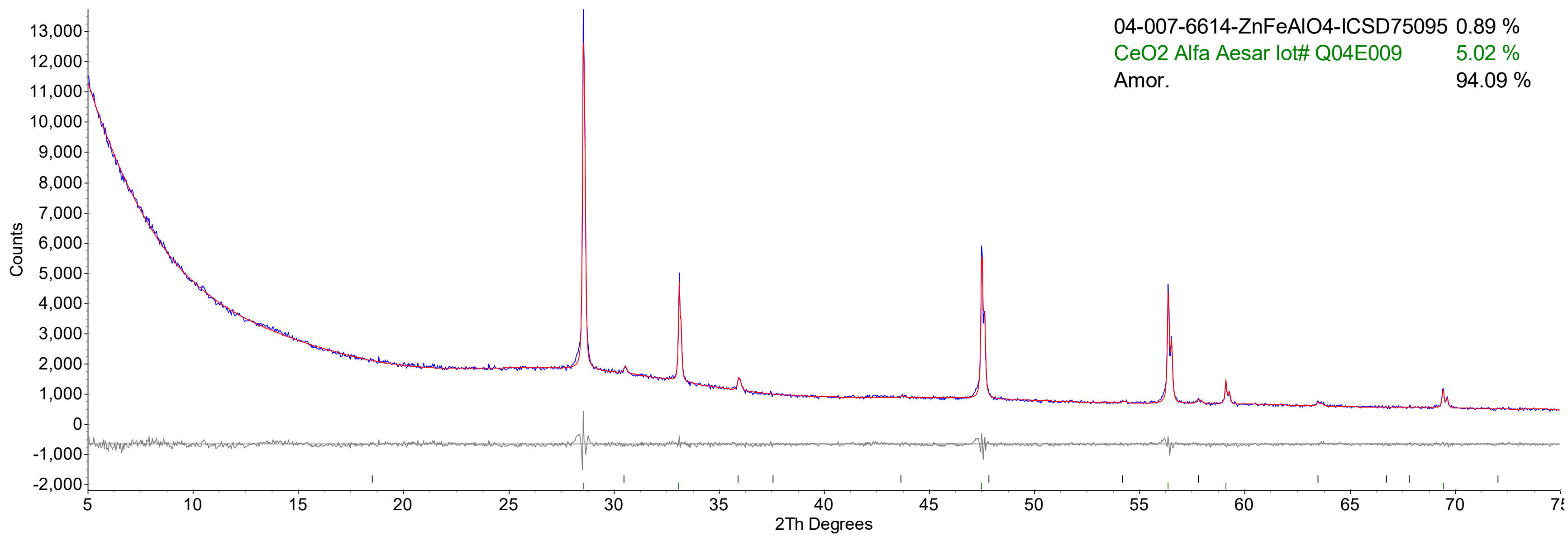

Figure E.15. Refined XRD data of HAL24M1-15.

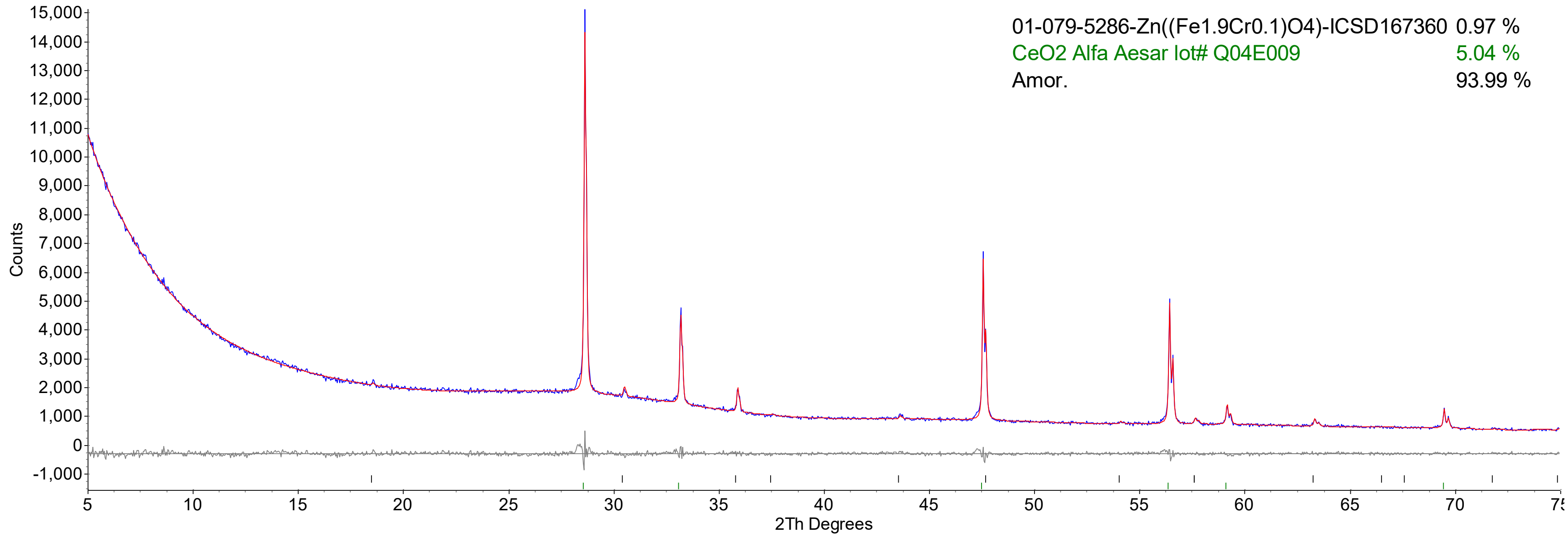

Figure E.16. Refined XRD data of HAL24M1-16.

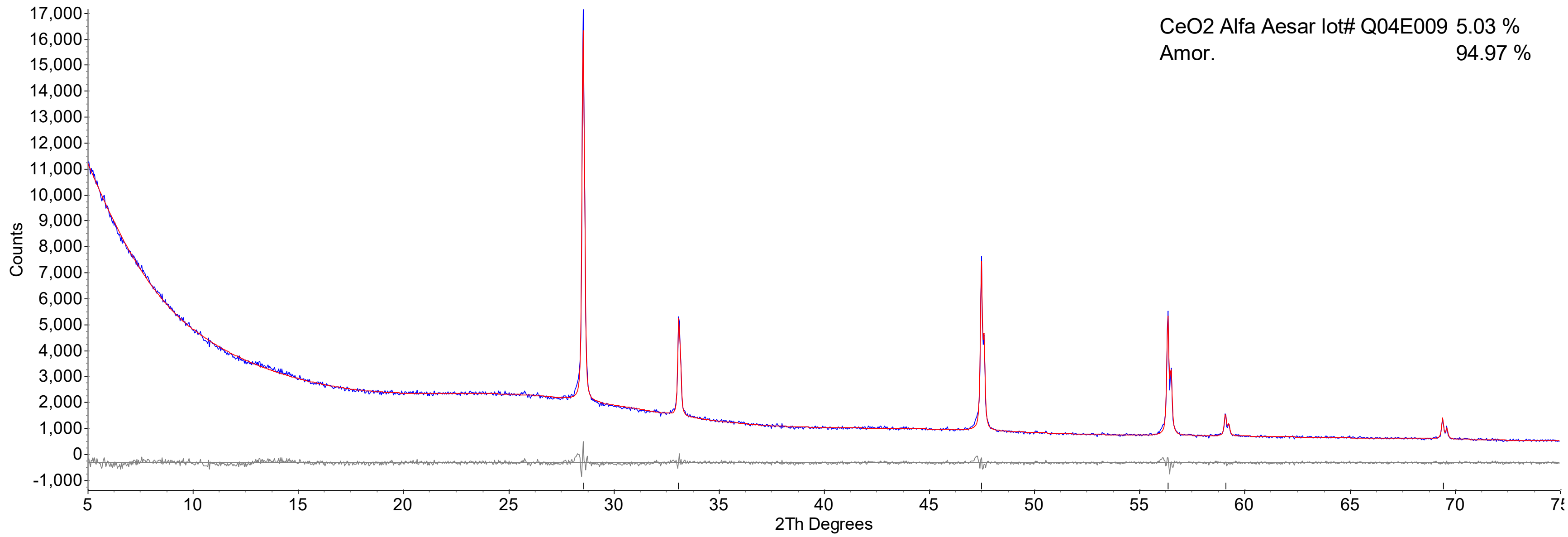

Figure E.17. Refined XRD data of HAL24M1-17.

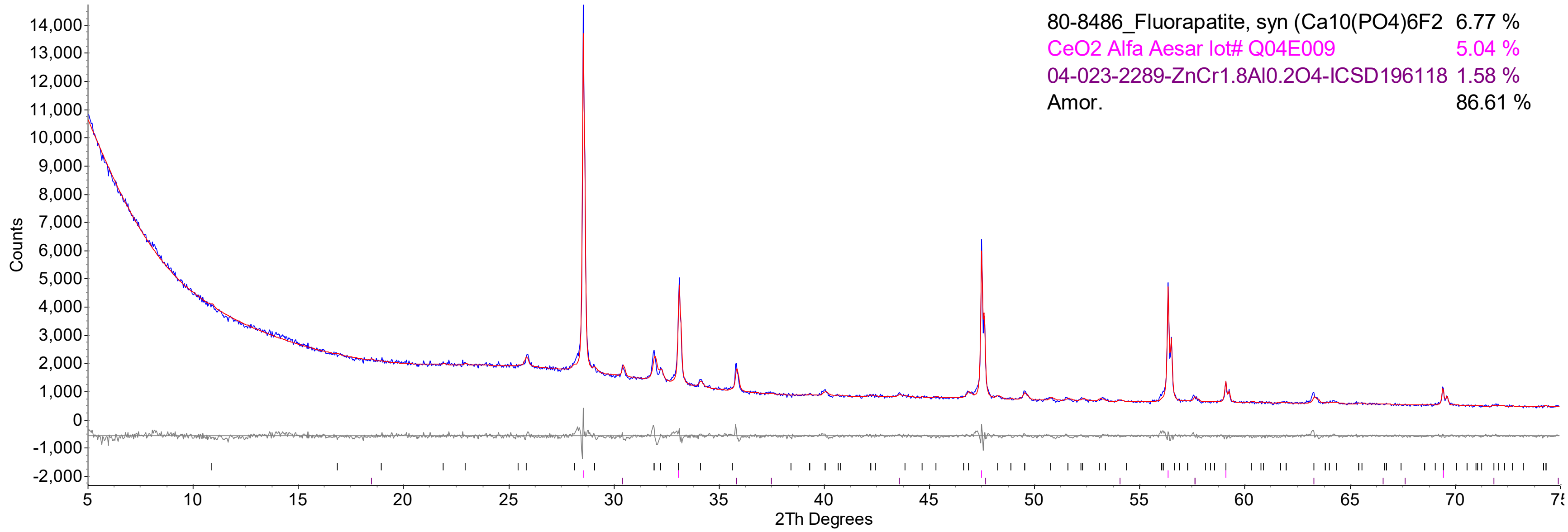

Figure E.18. Refined XRD data of HAL24M1-18.

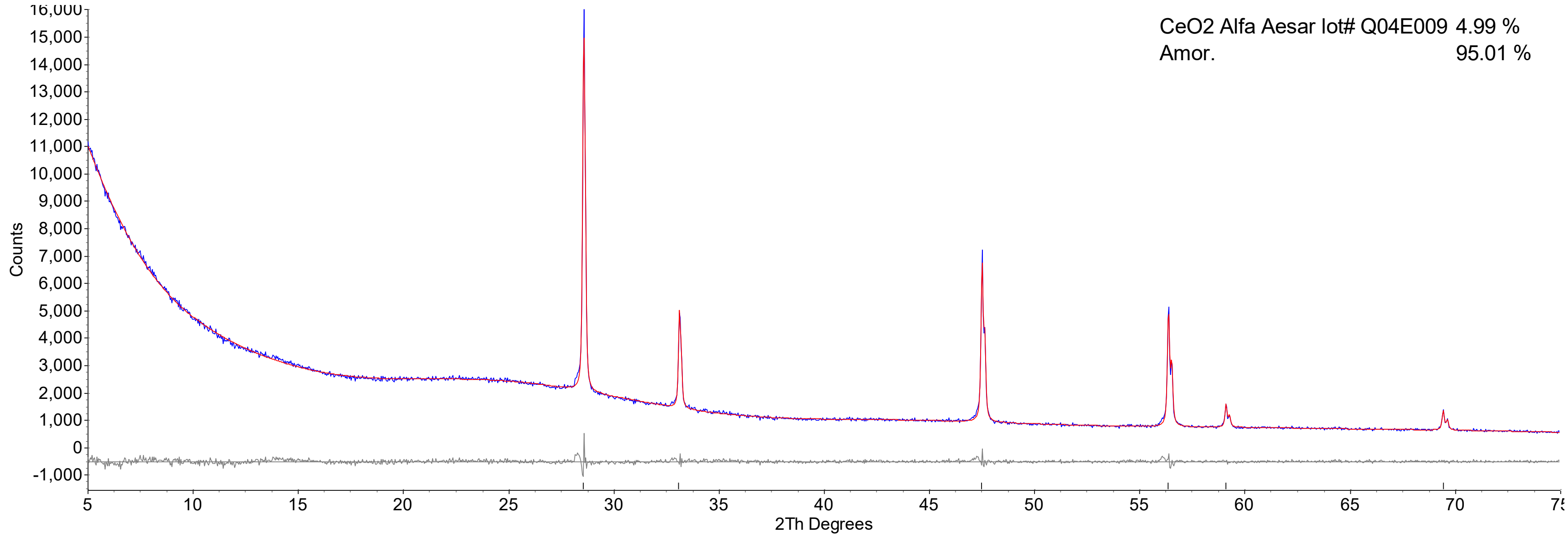

Figure E.19. Refined XRD data of HAL24M1-19.

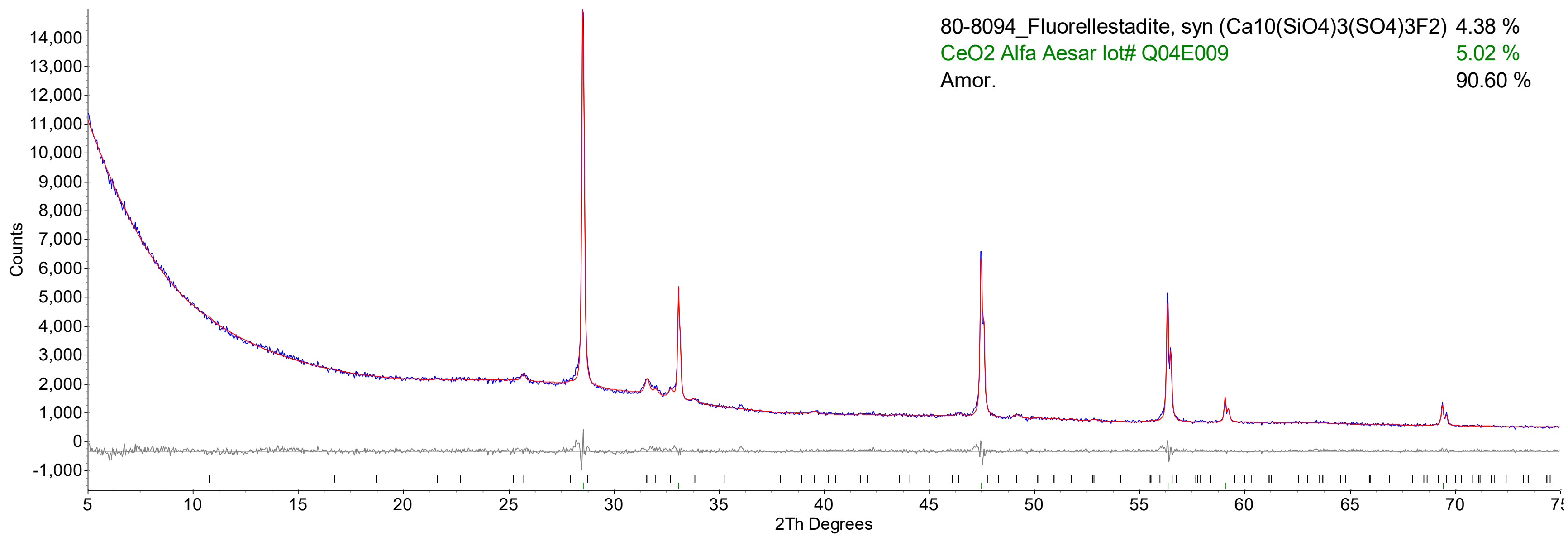

Figure E.20. Refined XRD data of HAL24M1-20.

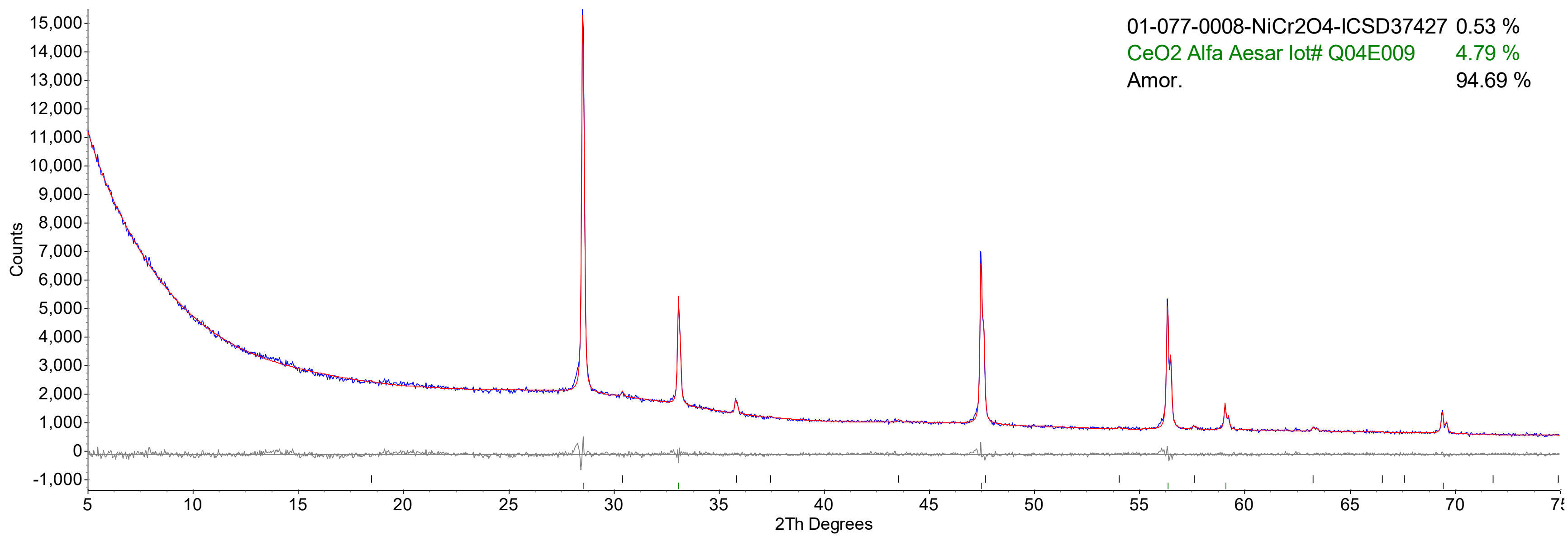

Figure E.21. Refined XRD data of HAL24M1-21.

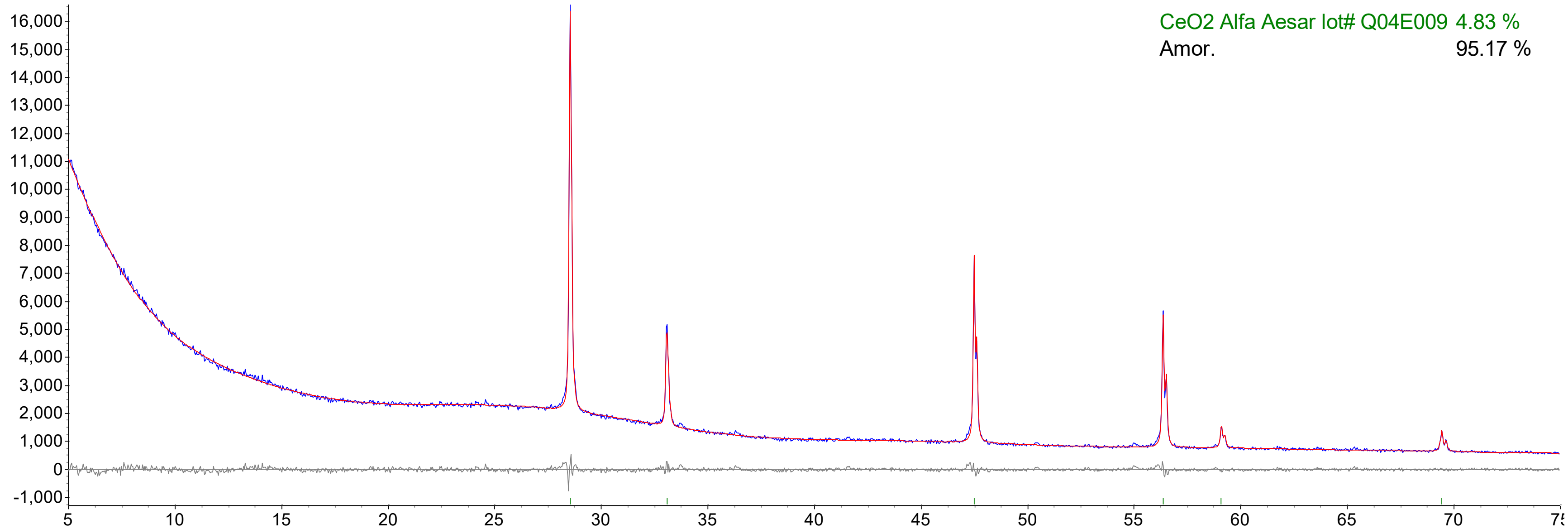

Figure E.22. Refined XRD data of HAL24M1-22.

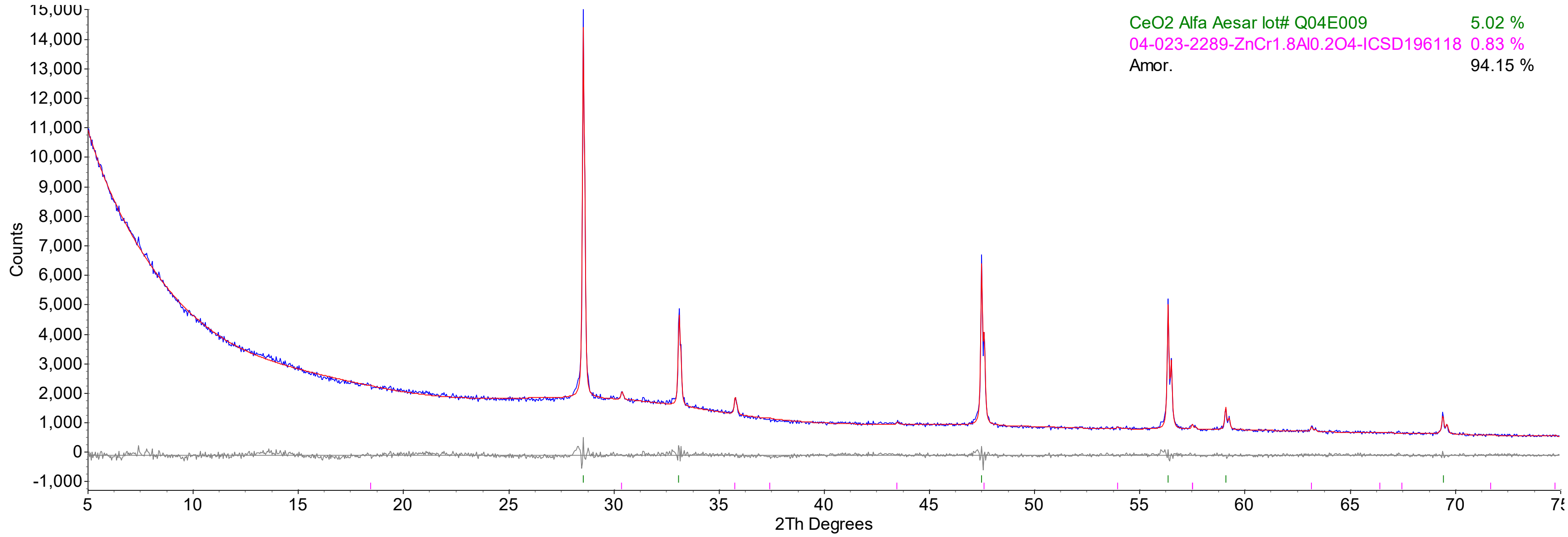

Figure E.23. Refined XRD data of HAL24M1-23.

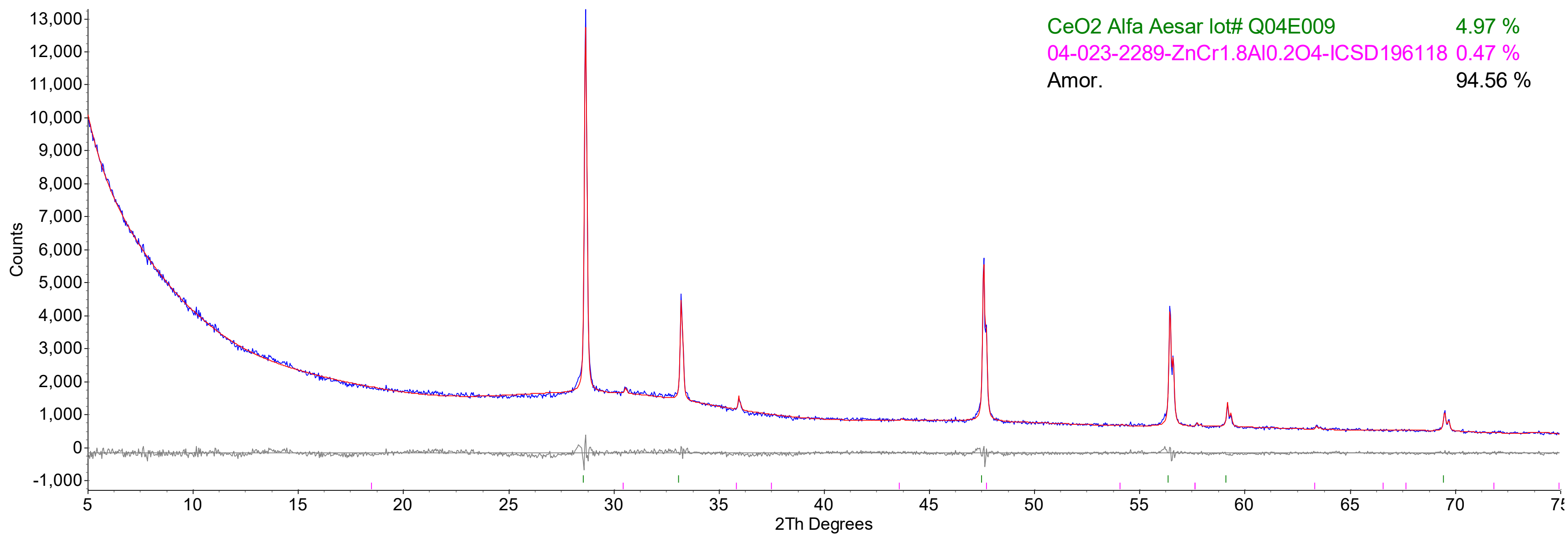

Figure E.24. Refined XRD data of HAL24M1-24.

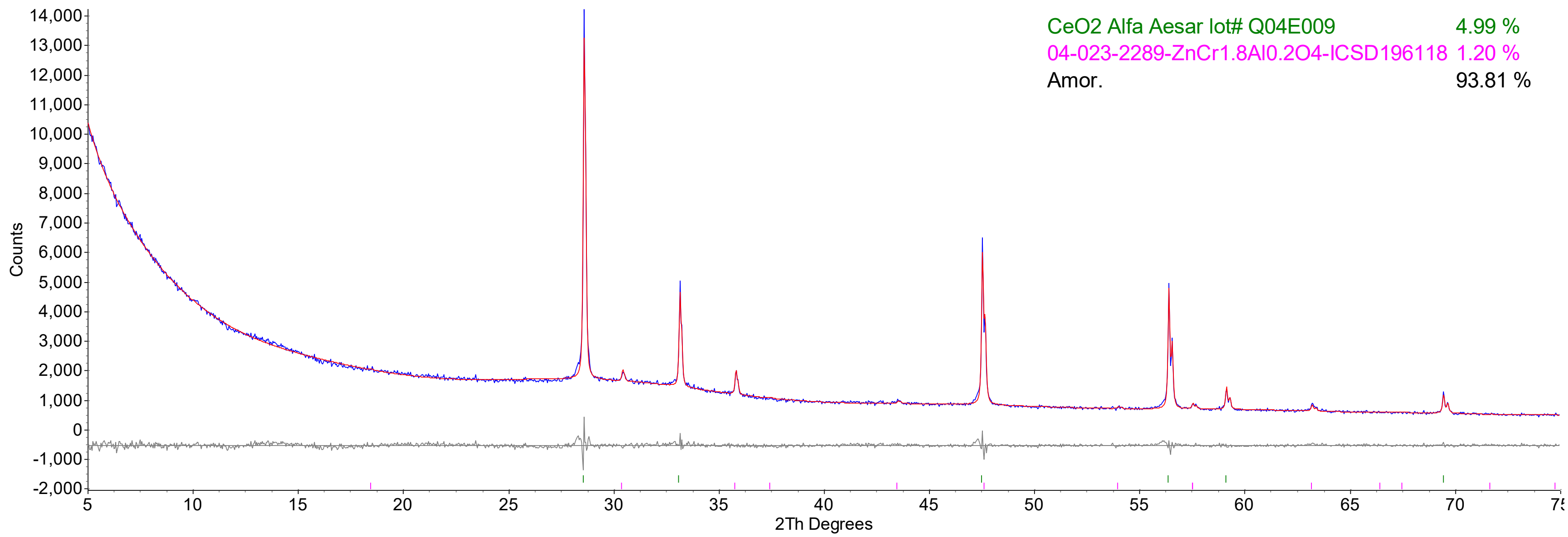

Figure E.25. Refined XRD data of HAL24M1-25.

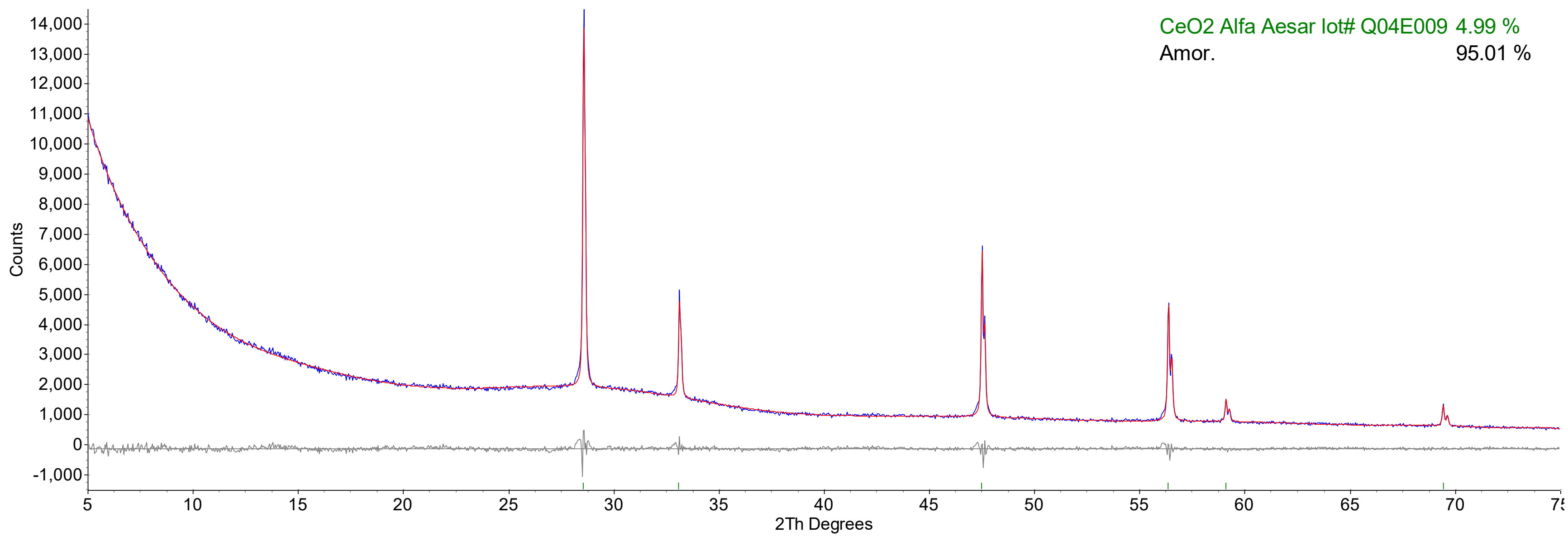

Figure E.26. Refined XRD data of HAL24M1-26.

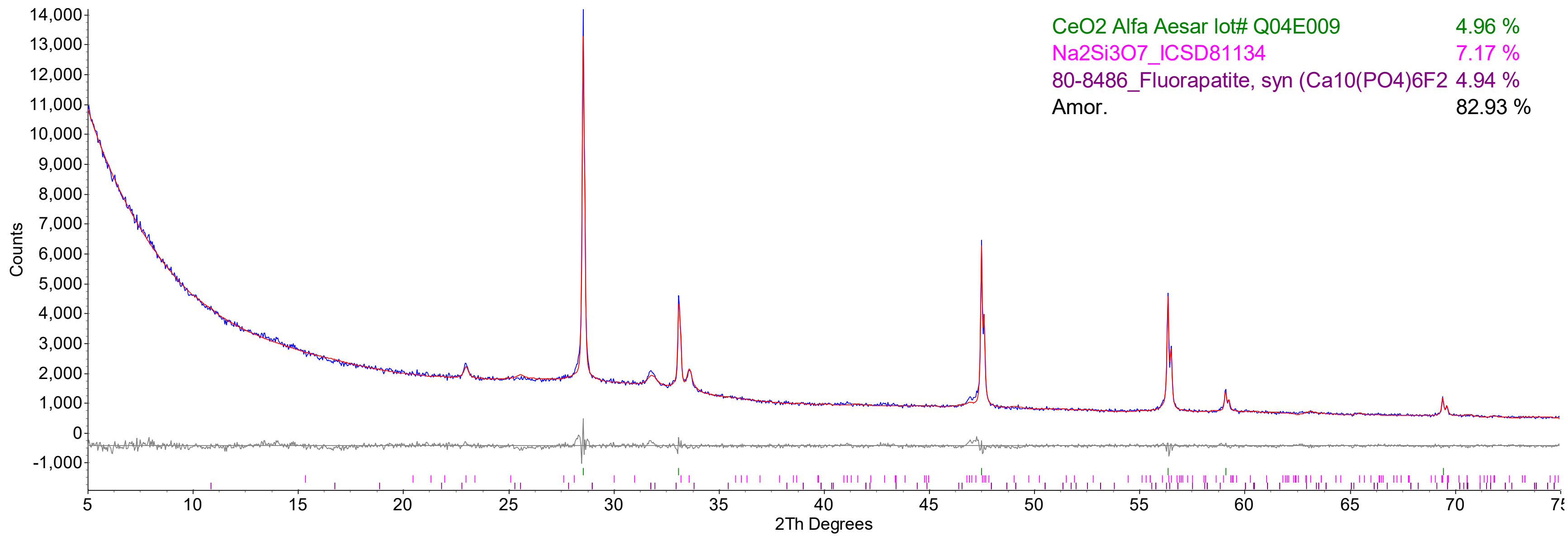

Figure E.27. Refined XRD data of HAL24M1-27.

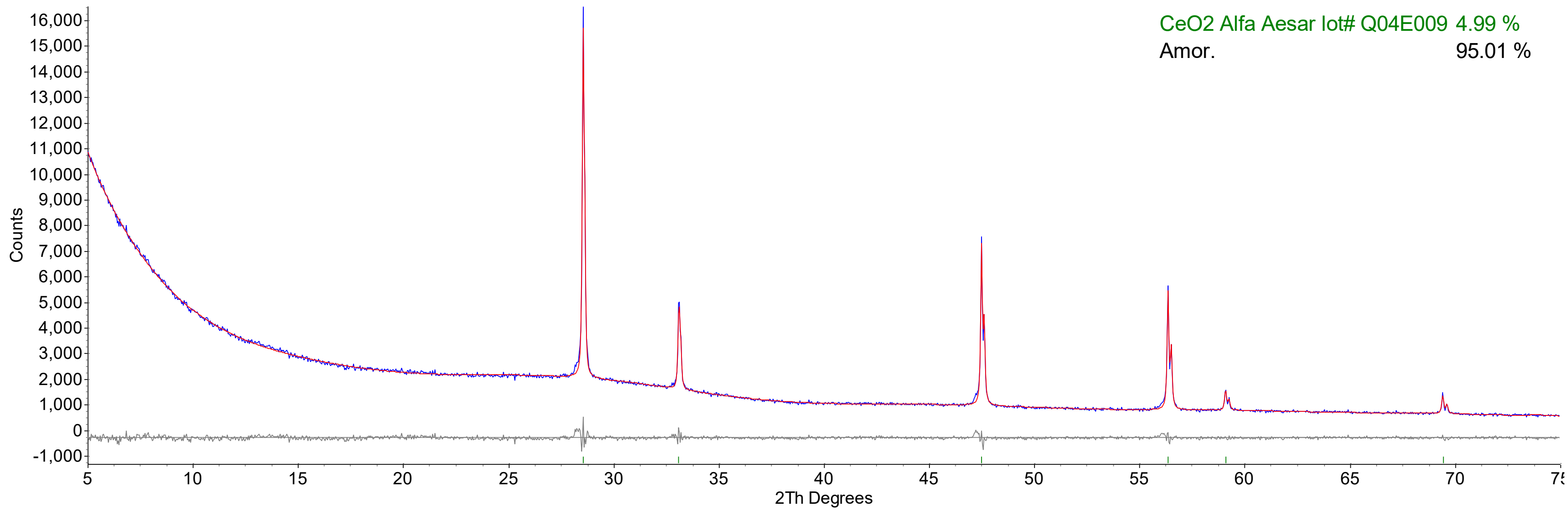

Figure E.28. Refined XRD data of HAL24M1-28.

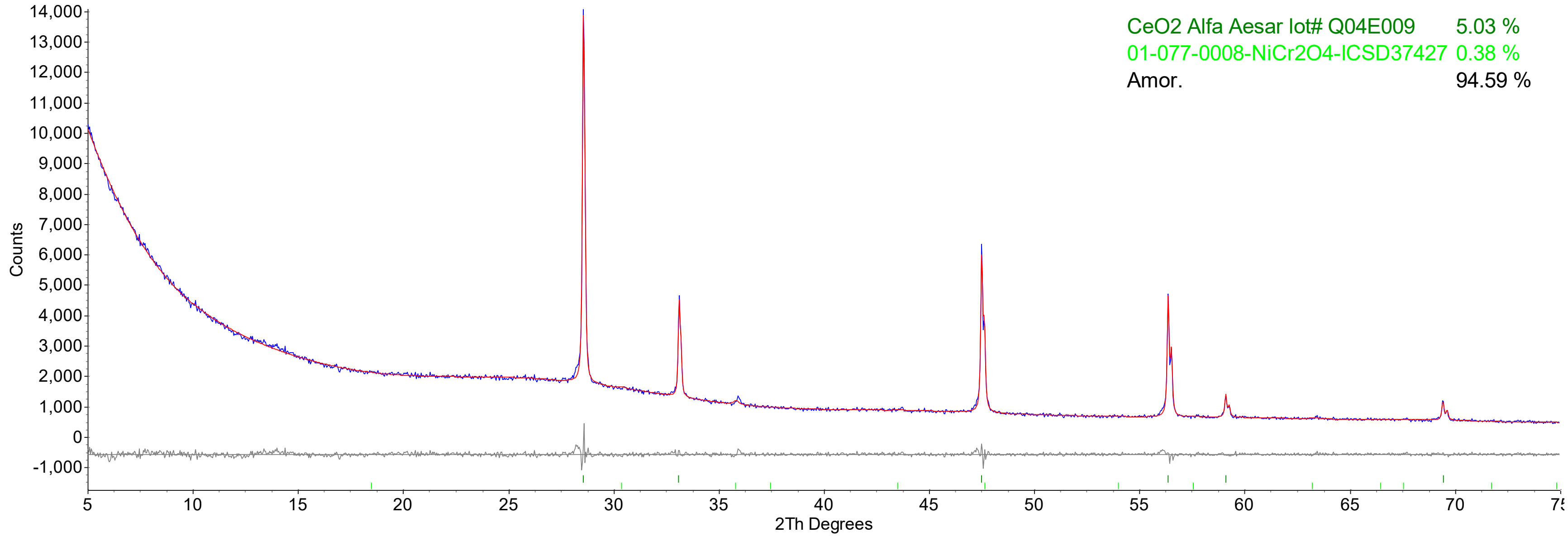

Figure E.29. Refined XRD data of HAL24M1-29-1.

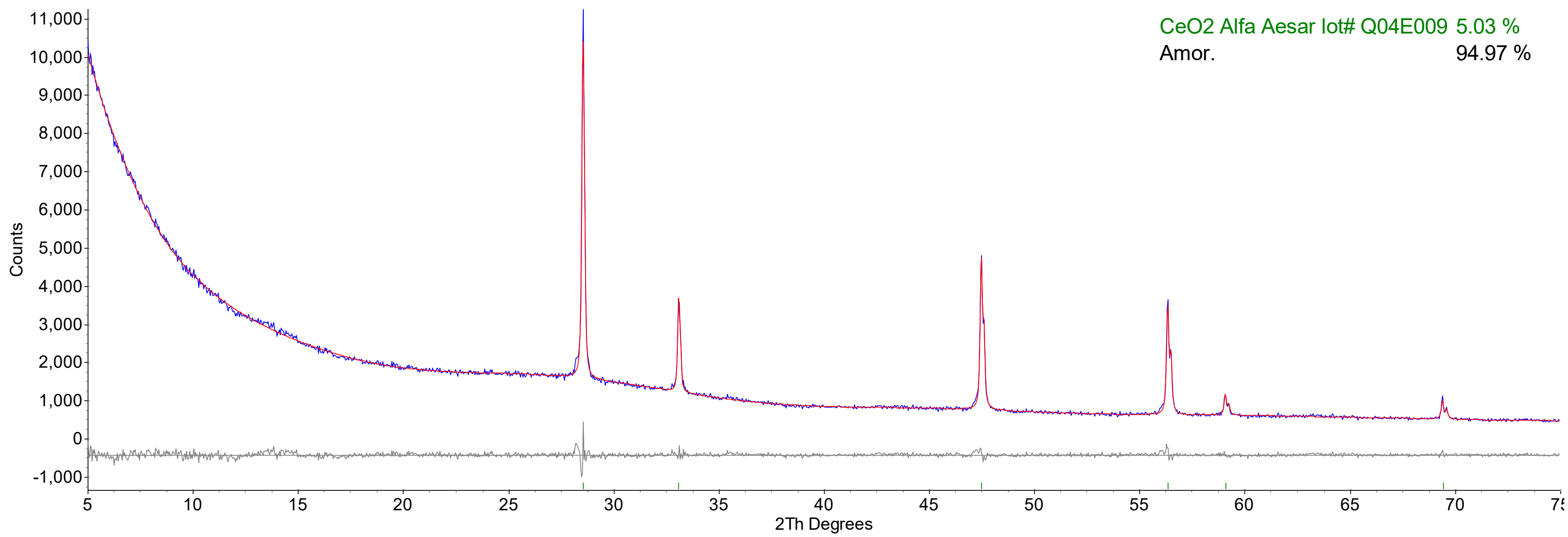

Figure E.30. Refined XRD data of HAL24M1-30-1.

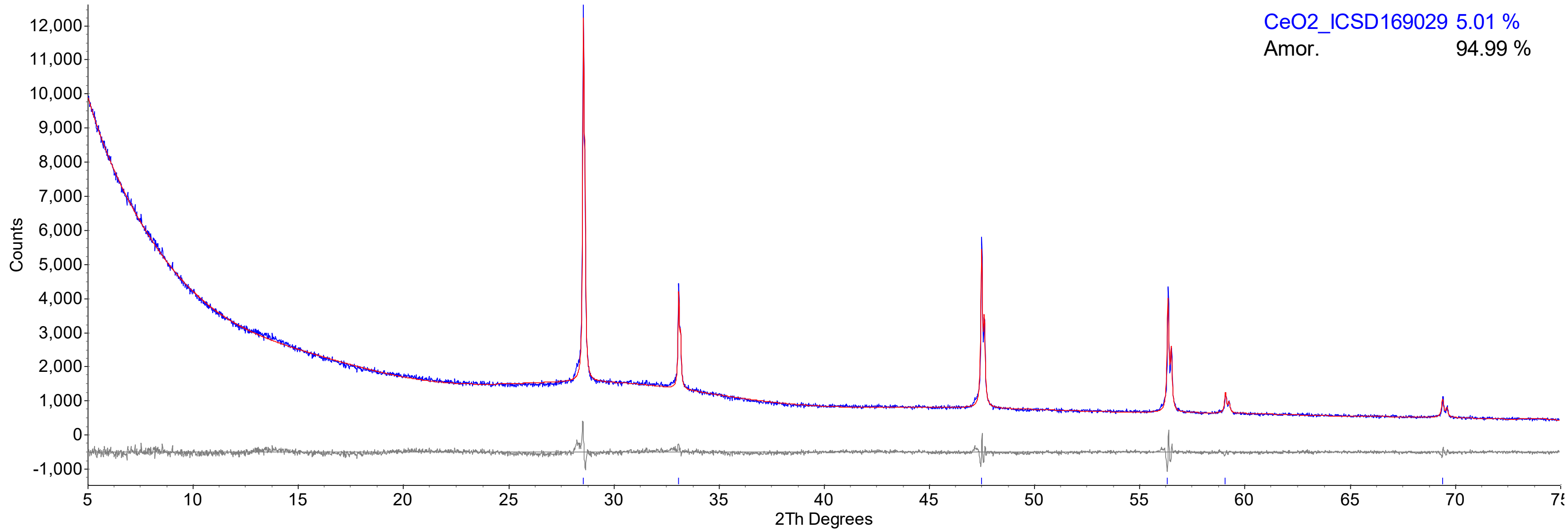

Figure E.31. Refined XRD data of HAL24M2-01.

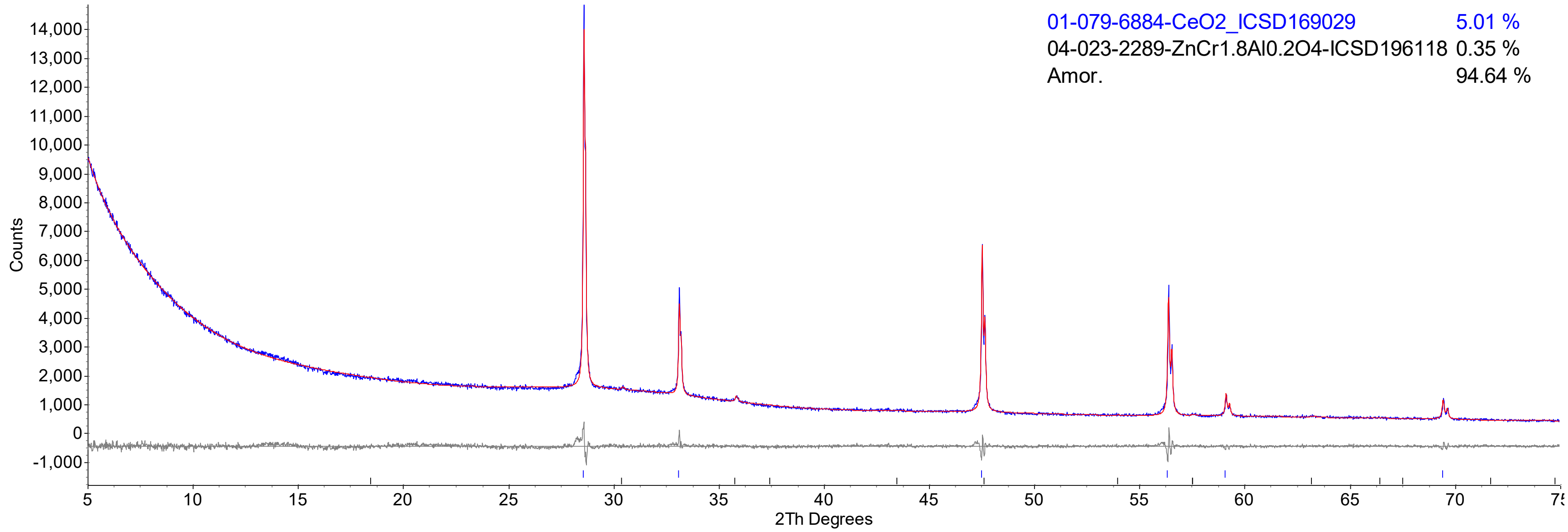

Figure E.32. Refined XRD data of HAL24M2-02.

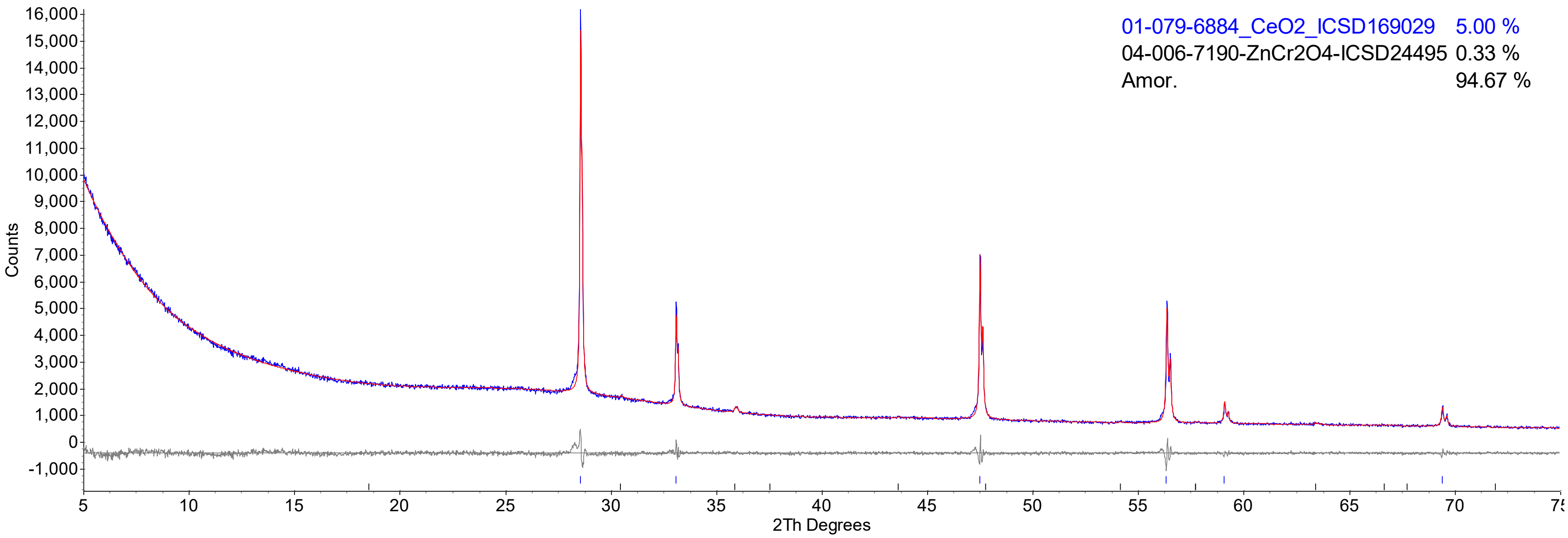

Figure E.33. Refined XRD data of HAL24M2-03.

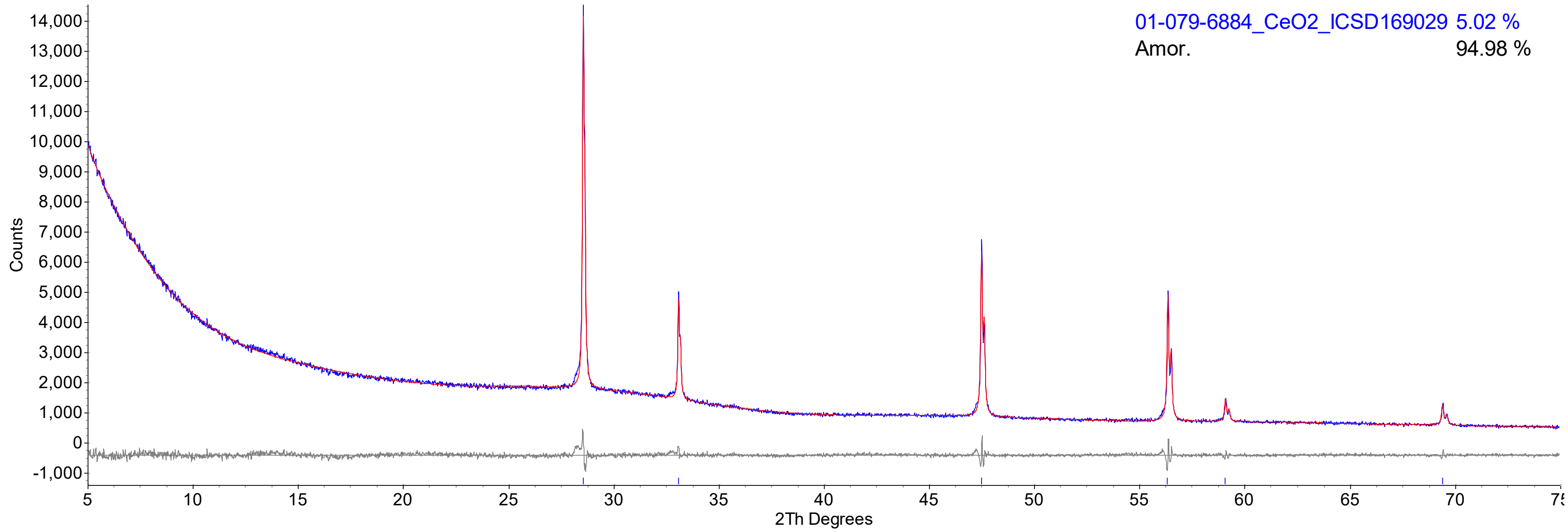

Figure E.34. Refined XRD data of HAL24M2-04-1.

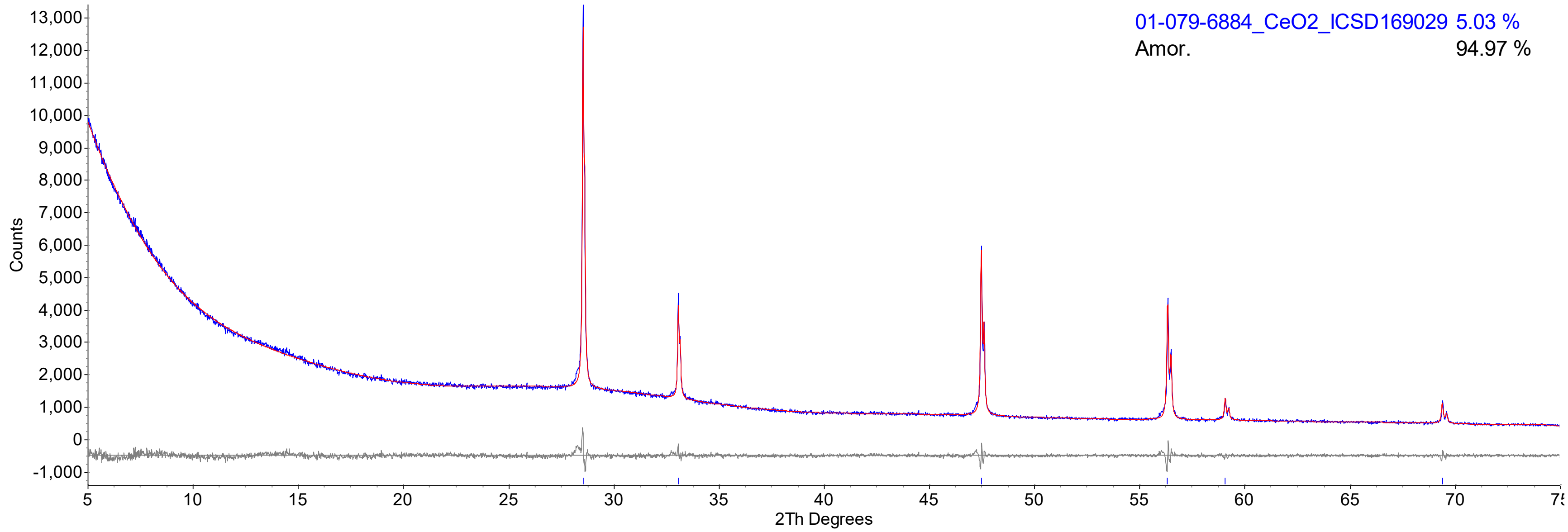

Figure E.35. Refined XRD data of HAL24M2-05.

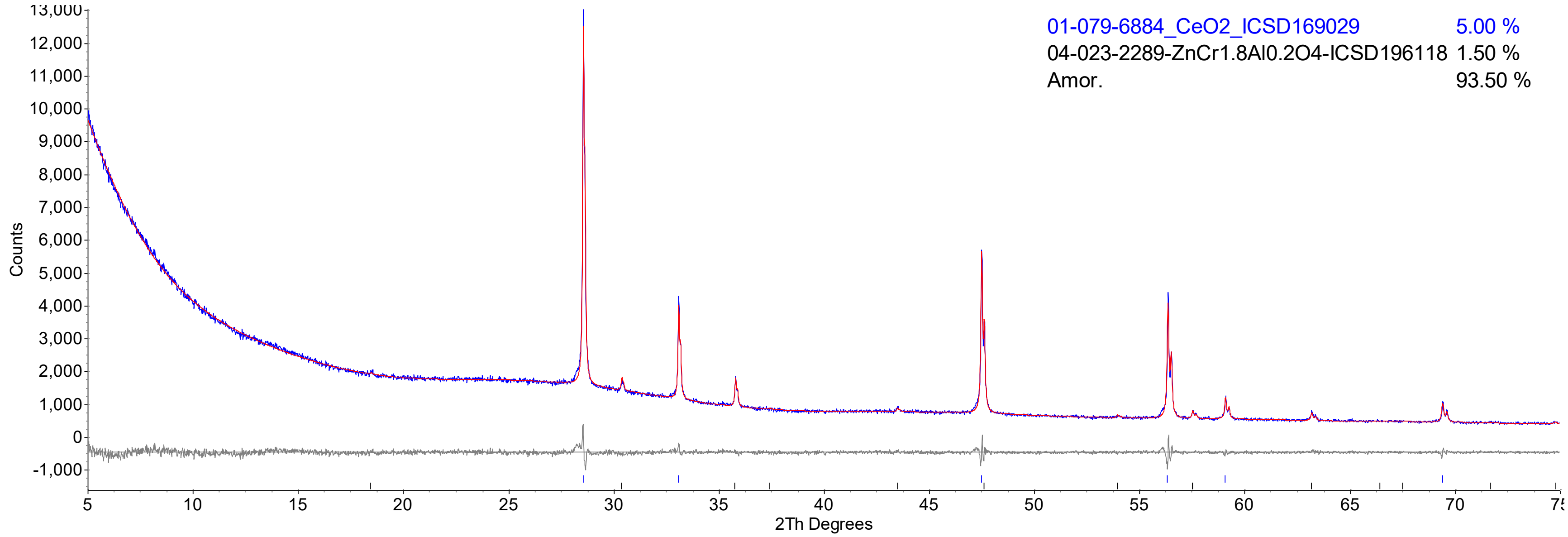

Figure E.36. Refined XRD data of HAL24M2-06.

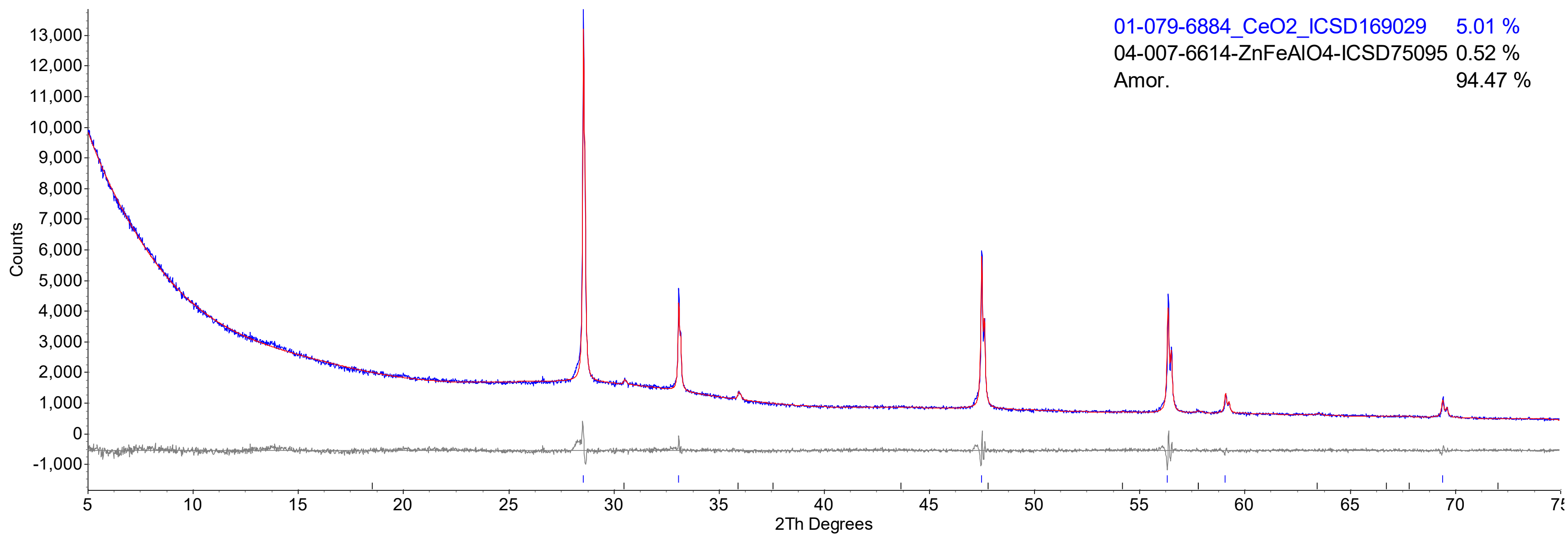

Figure E.37. Refined XRD data of HAL24M2-07.

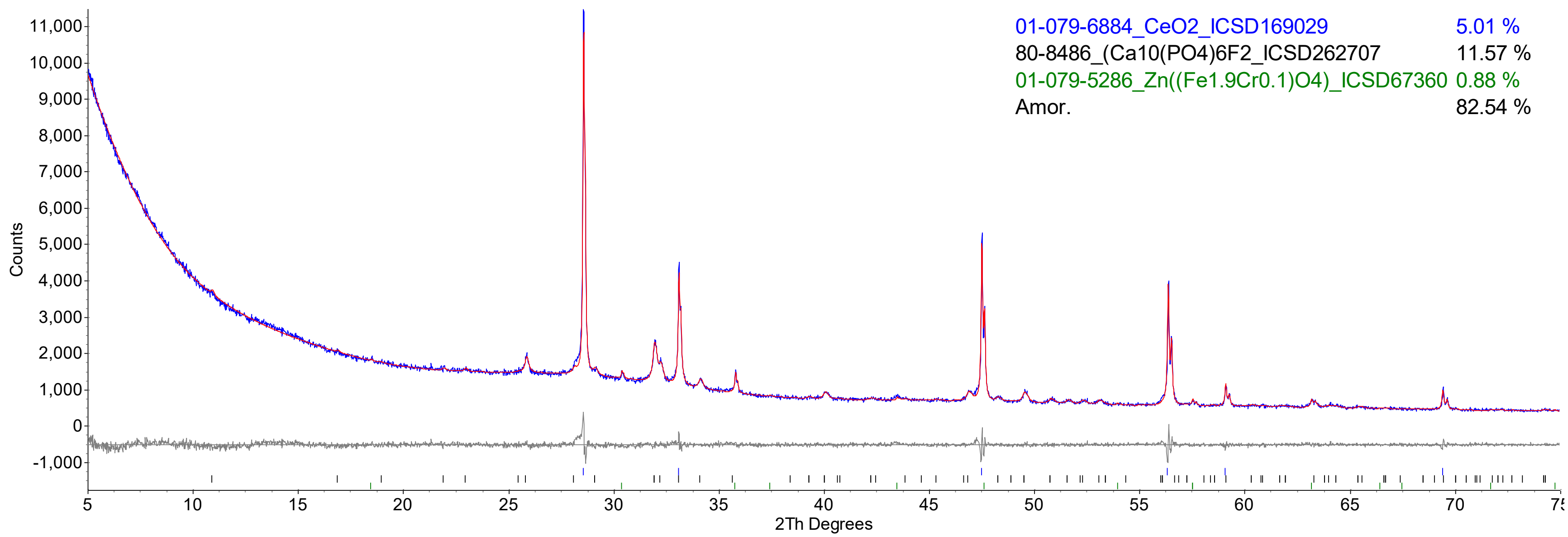

Figure E.38. Refined XRD data of HAL24M2-08.

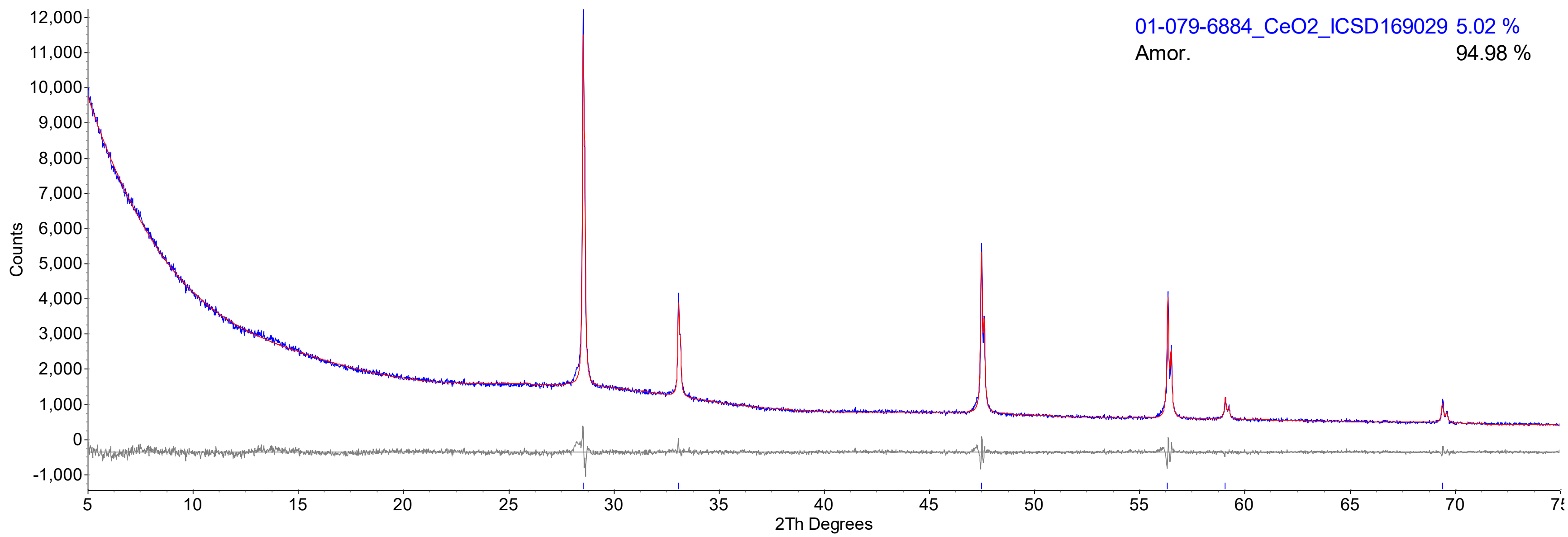

Figure E.39. Refined XRD data of HAL24M2-09.

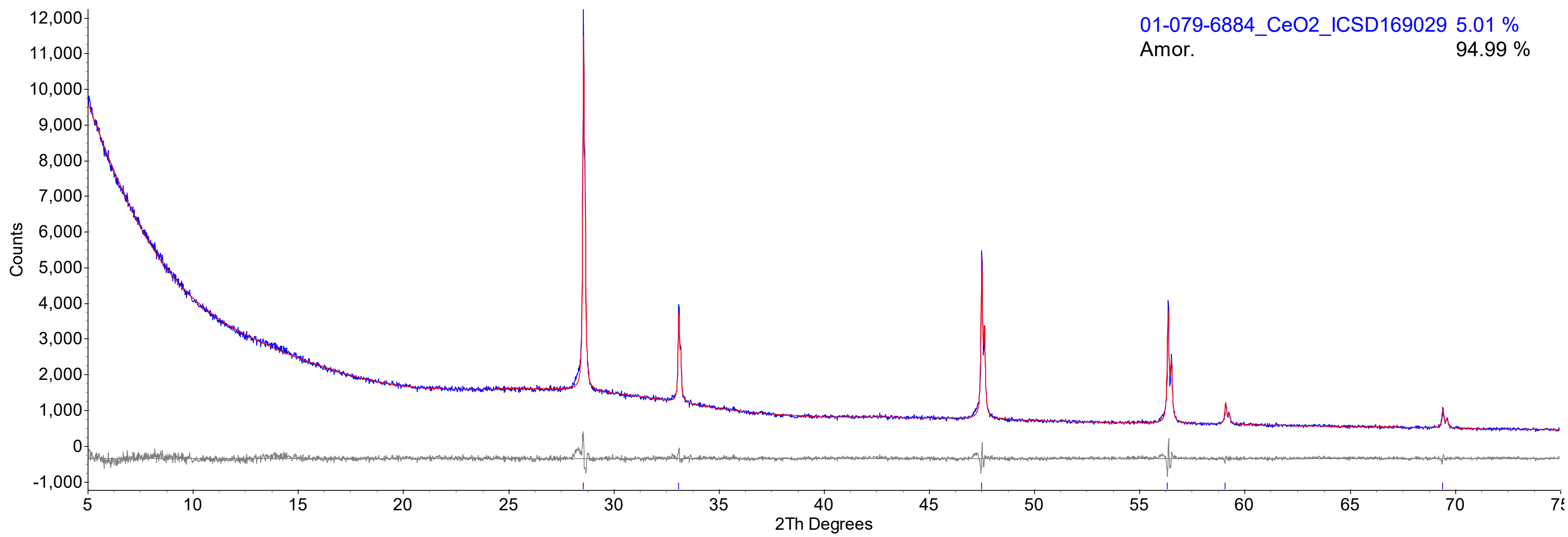

Figure E.40. Refined XRD data of HAL24M2-10.

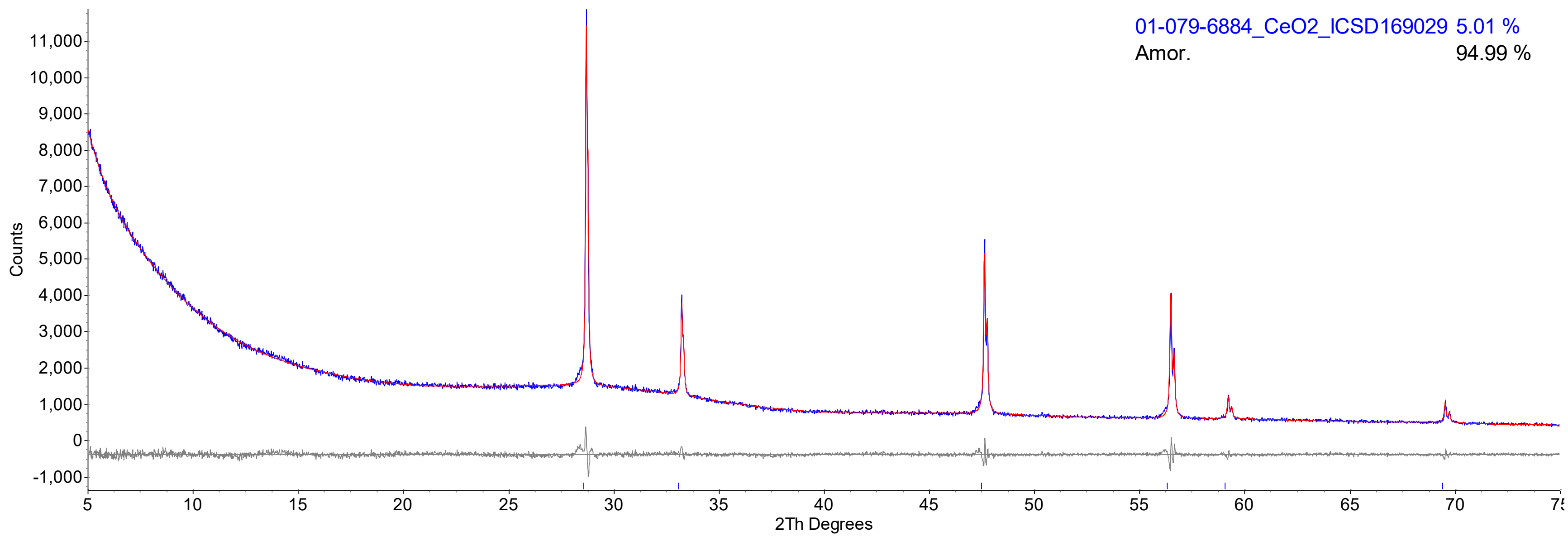

Figure E.41. Refined XRD data of HAL24M2-11.

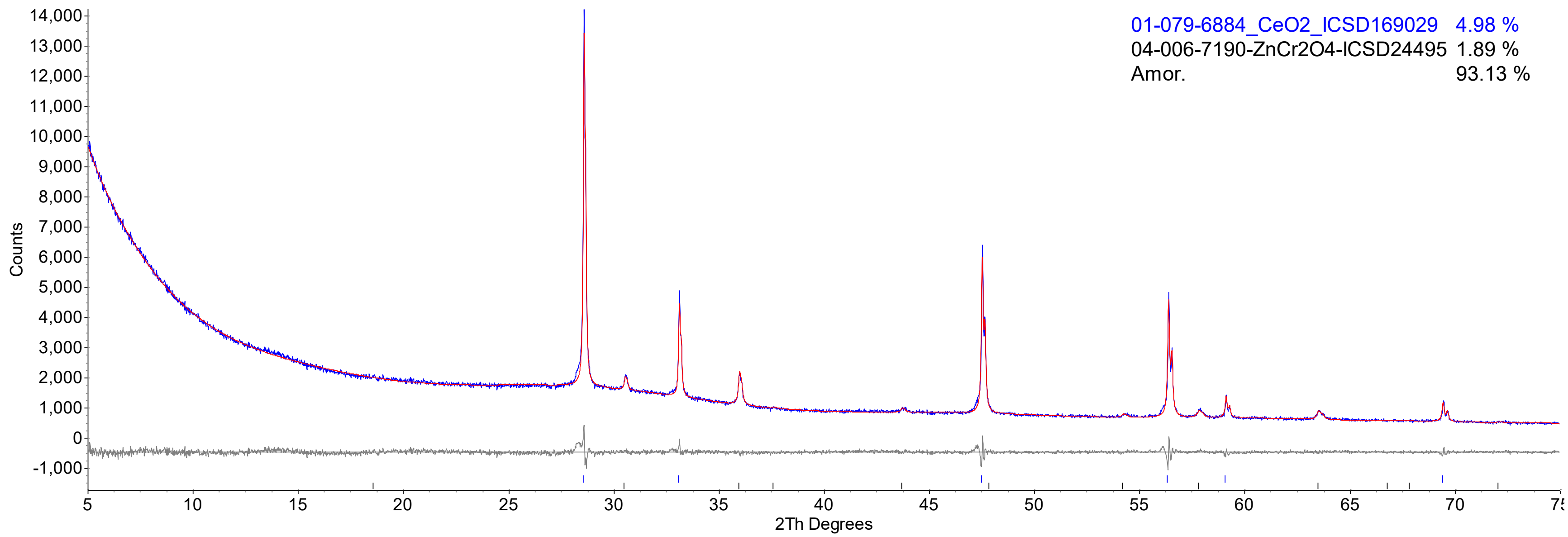

Figure E.42. Refined XRD data of HAL24M2-12.

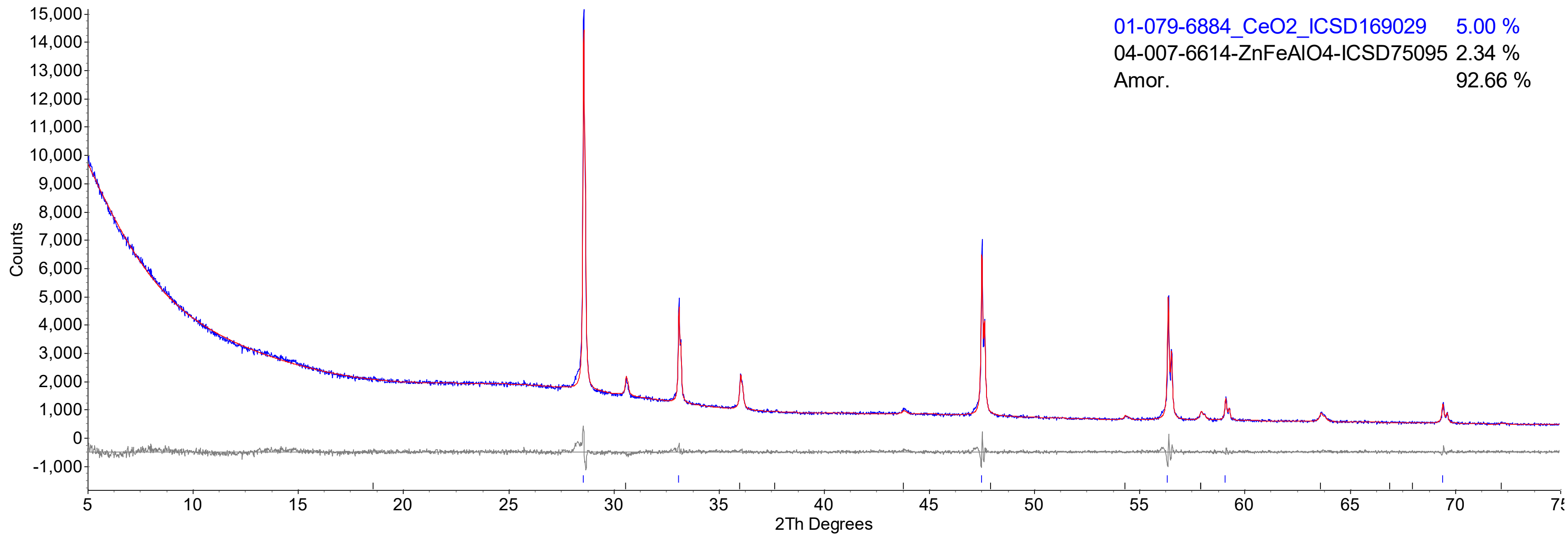

Figure E.43. Refined XRD data of HAL24M2-13.

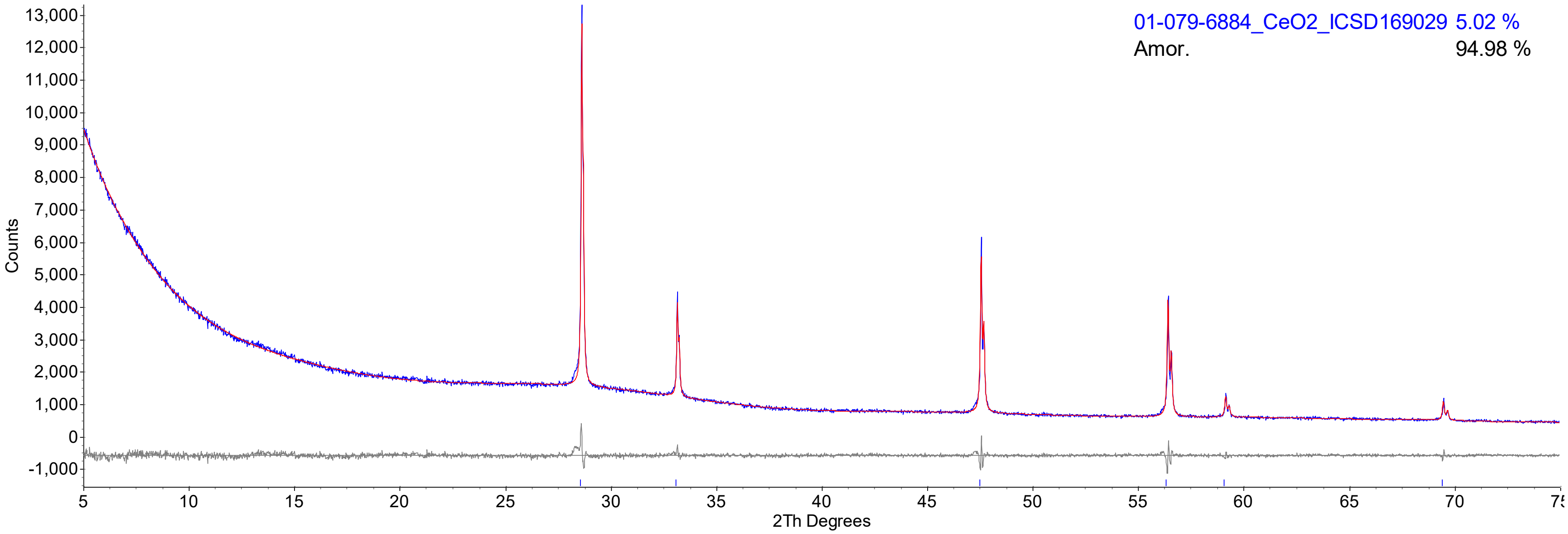

Figure E.44. Refined XRD data of HAL24M2-14.

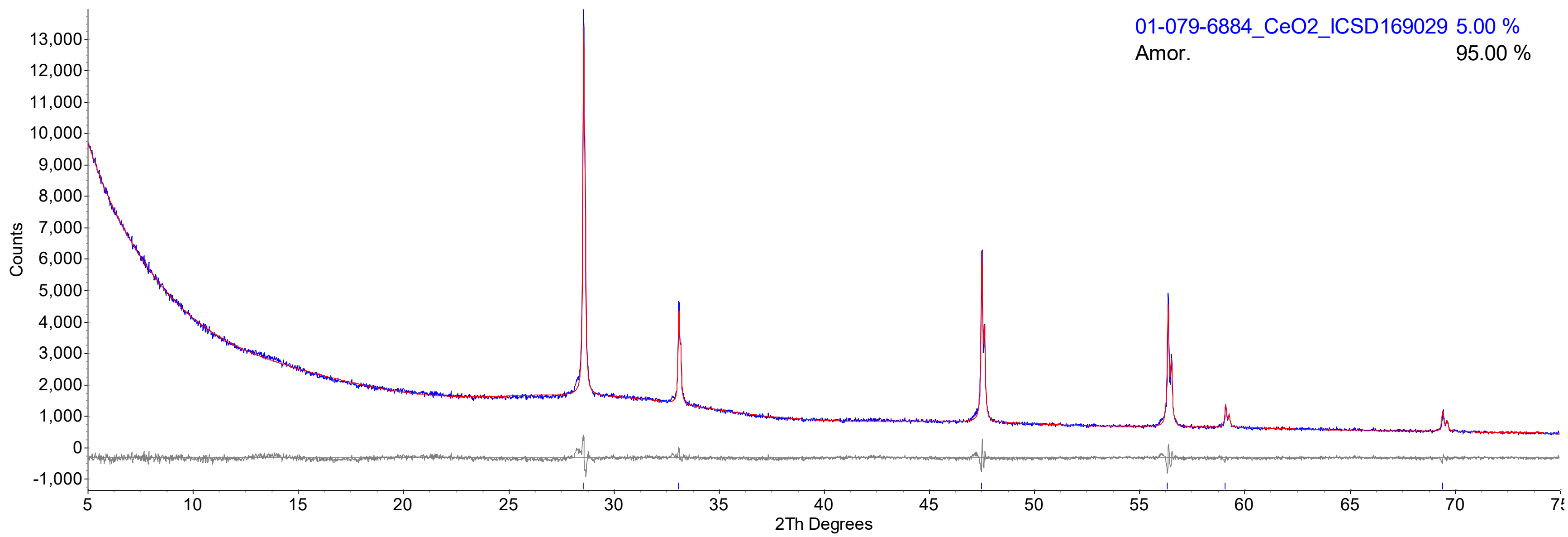

Figure E.45. Refined XRD data of HAL24M2-15.

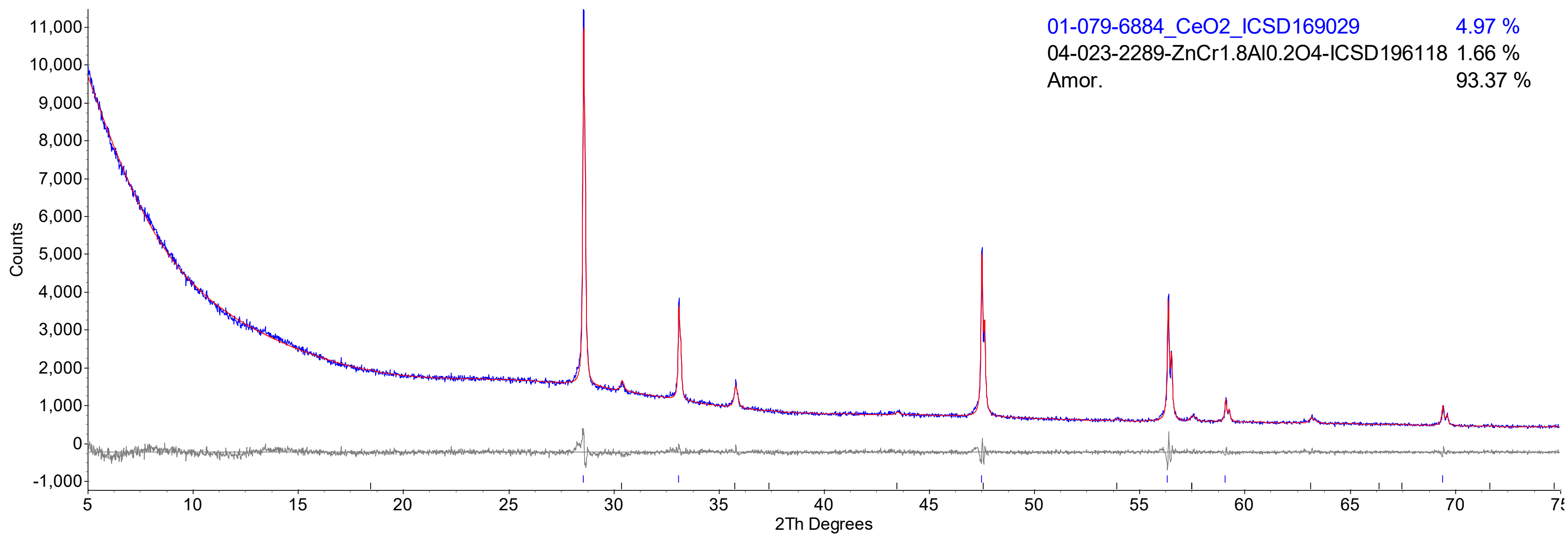

Figure E.46. Refined XRD data of HAL24M2-16.

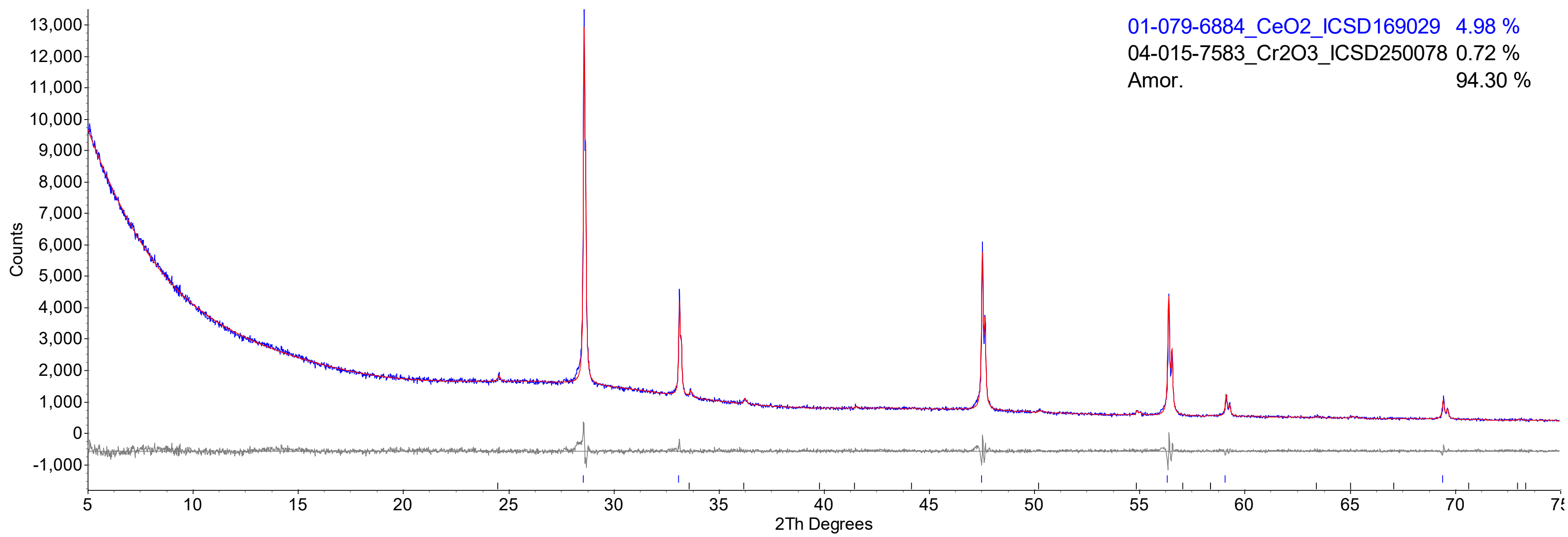

Figure E.47. Refined XRD data of HAL24M2-17.

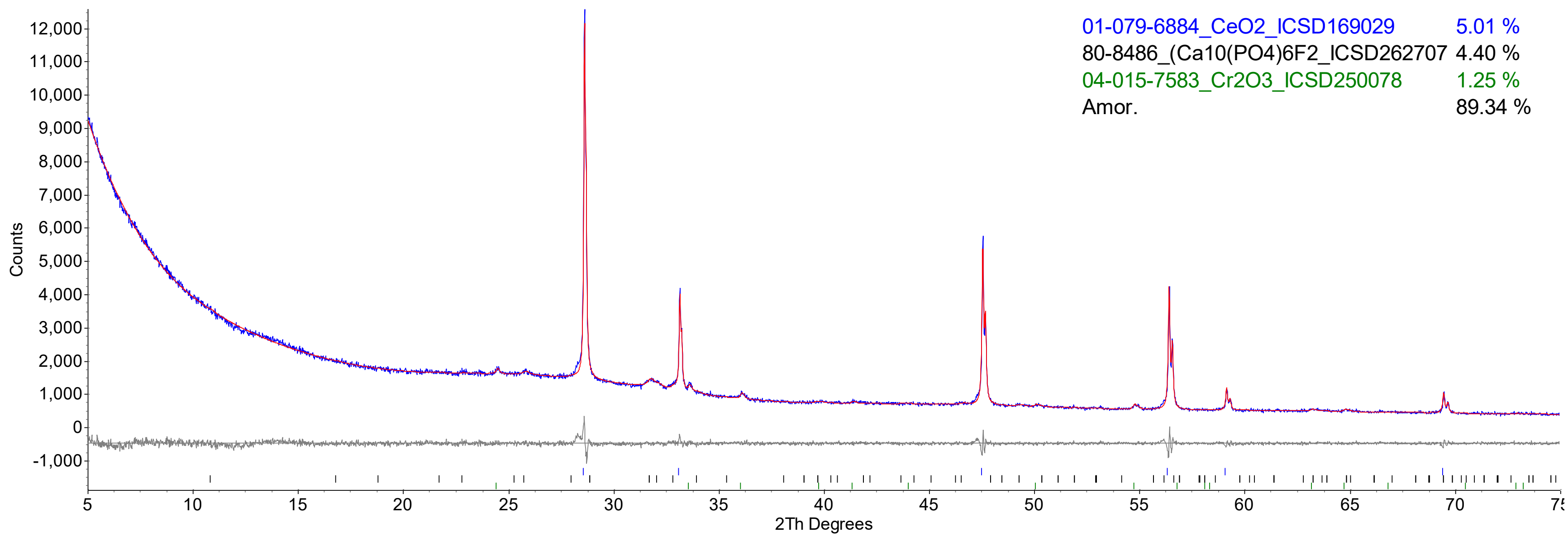

Figure E.48. Refined XRD data of HAL24M2-18.

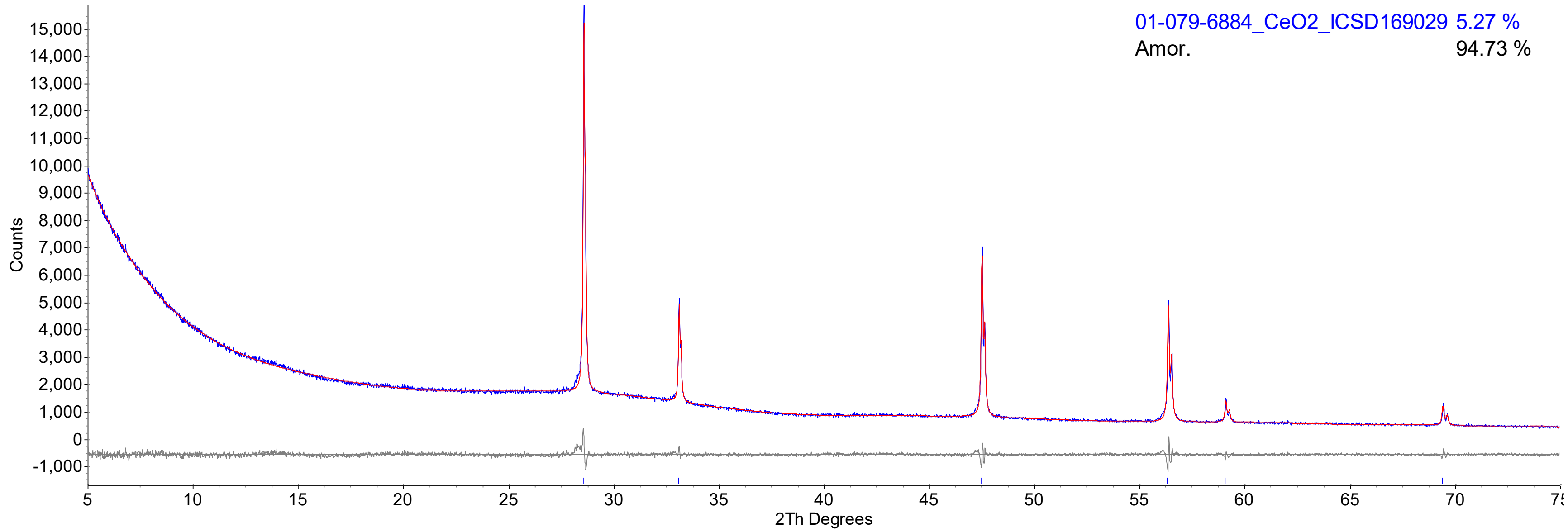

Figure E.49. Refined XRD data of HAL24M2-19.

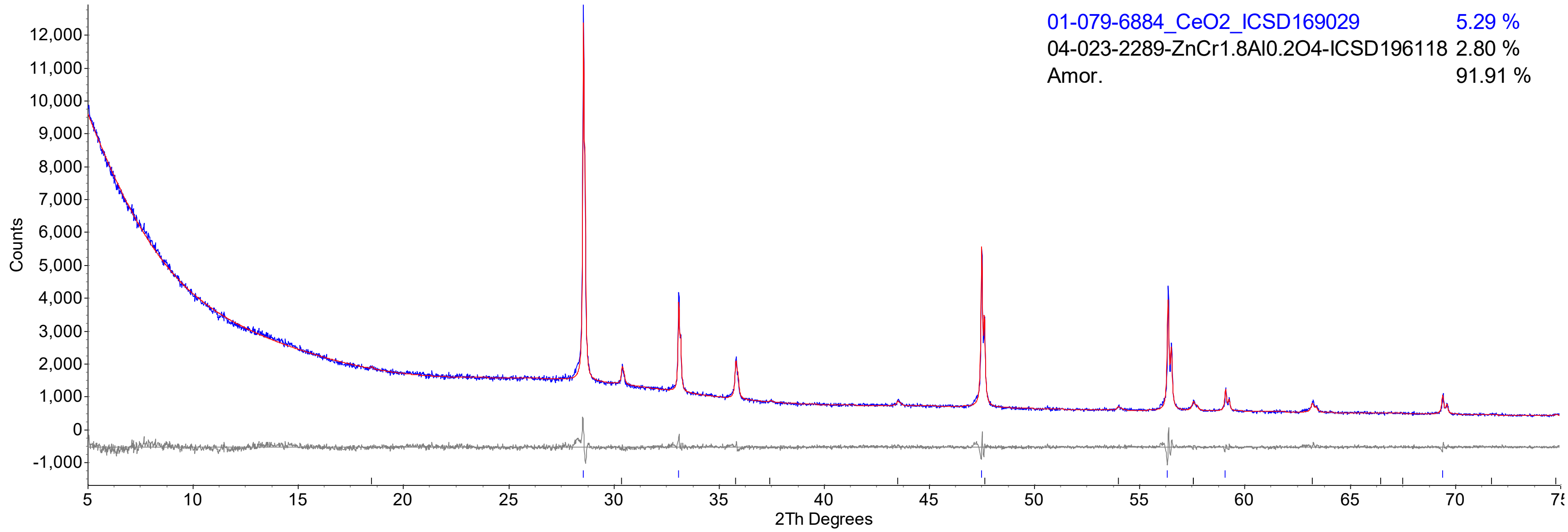

Figure E.50. Refined XRD data of HAL24M2-20.

Appendix F – Morphology/Color of Each Glass after Canister Centerline Cooling

The photographs in this appendix show each glass after canister centerline cooling (CCC) as described in Section 2.3. When applicable, X-ray diffraction scans are reported in Appendix G.

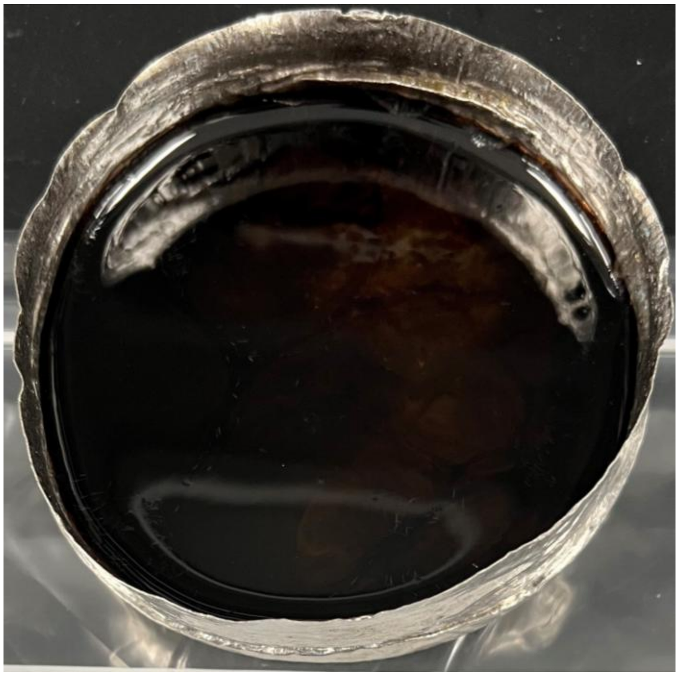

Figure F.1. Glass HAL24M1-01 morphology after CCC.

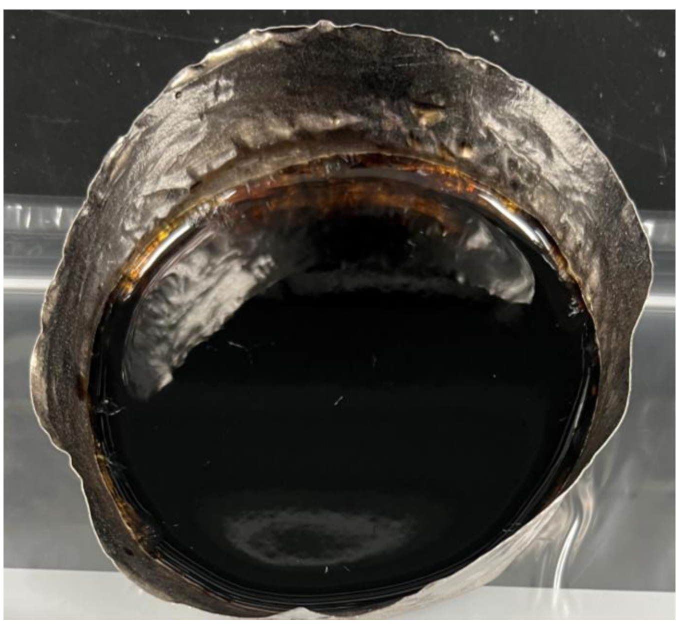

Figure F.2. Glass HAL24M1-02 morphology after CCC.

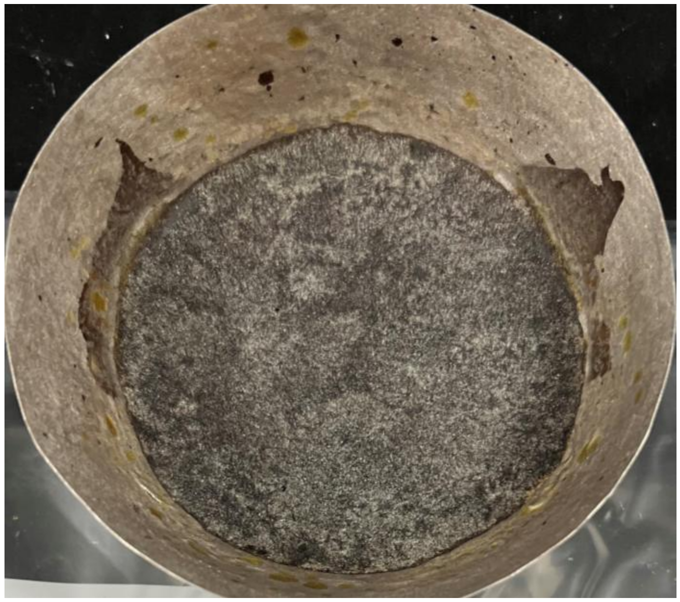

Figure F.3. Glass HAL24M1-03 morphology after CCC.

Figure F.4. Glass HAL24M1-04 morphology after CCC.

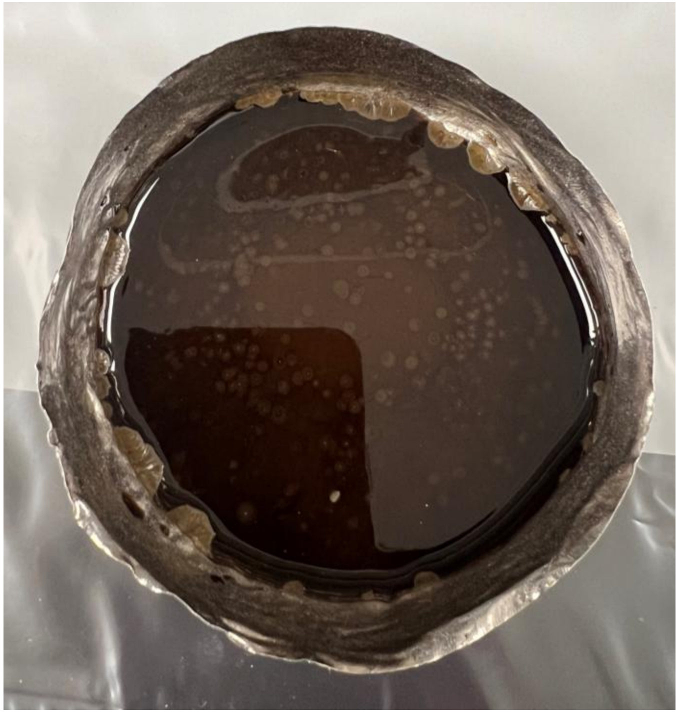

Figure F.5. Glass HAL24M1-05 morphology after CCC.

Figure F.6. Glass HAL24M1-06 morphology after CCC.

Figure F.7. Glass HAL24M1-07 morphology after CCC.

Figure F.8. Glass HAL24M1-08 morphology after CCC.

Figure F.9. Glass HAL24M1-09 morphology after CCC.

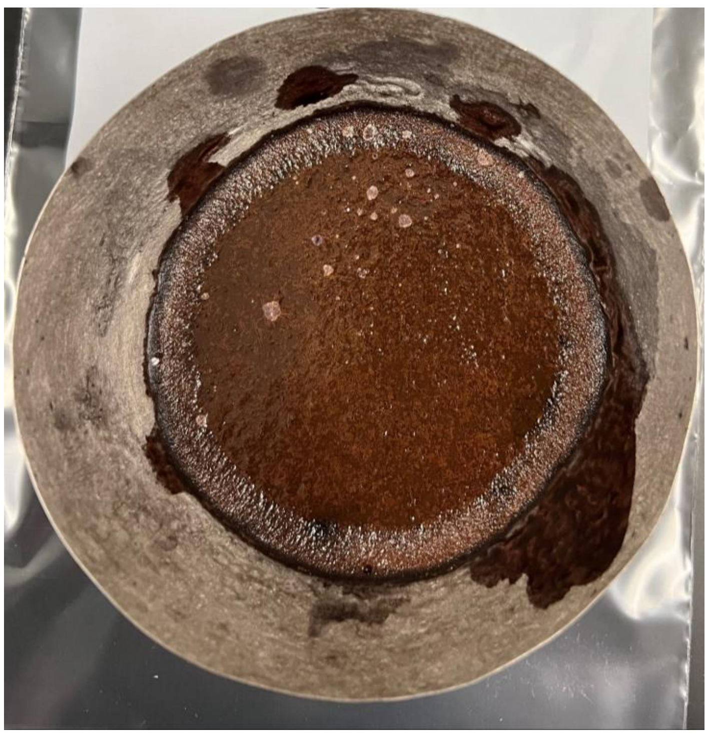

Figure F.10. Glass HAL24M1-10 morphology after CCC.

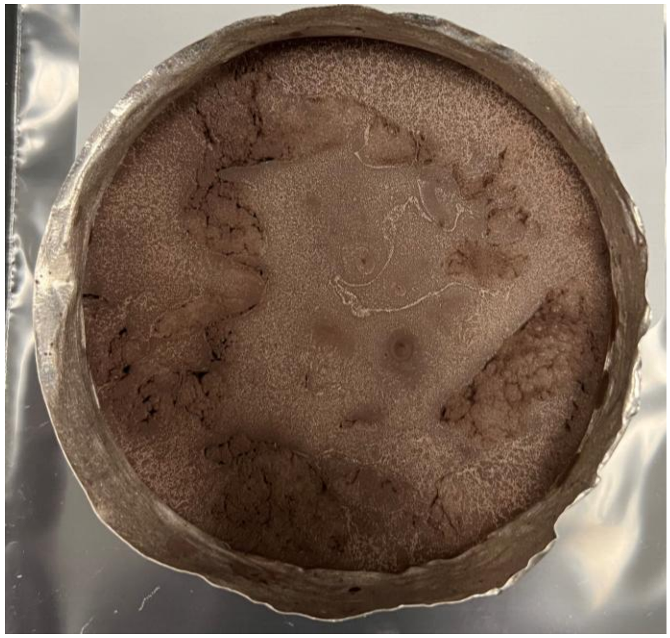

Figure F.11. Glass HAL24M1-11 morphology after CCC.

Figure F.12. Glass HAL24M1-12 morphology after CCC.

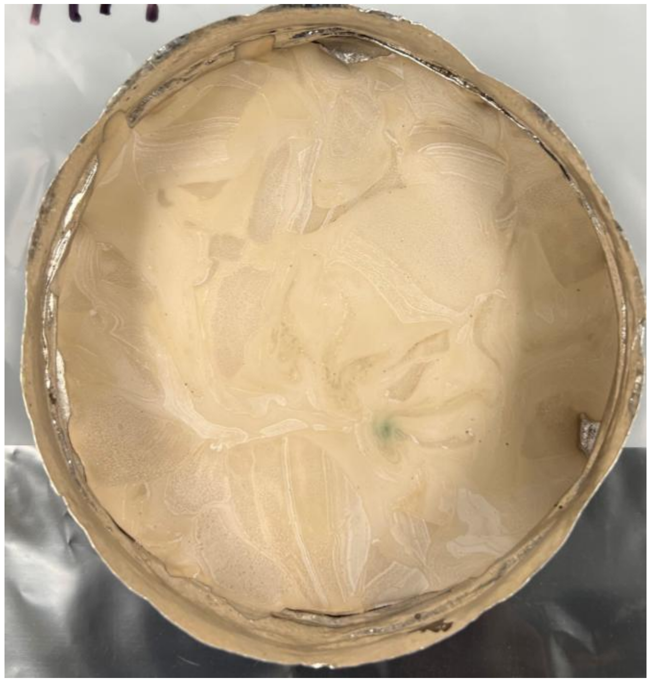

Figure F.13. Glass HAL24M1-13-1 morphology after CCC.

Figure F.14. Glass HAL24M1-14 morphology after CCC.

Figure F.15. Glass HAL24M1-15 morphology after CCC.

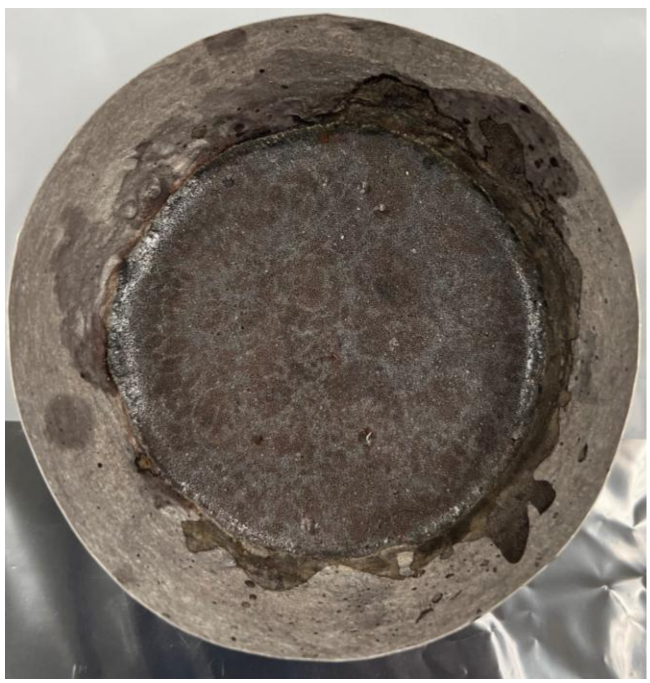

Figure F.16. Glass HAL24M1-16 morphology after CCC.

Figure F.17. Glass HAL24M1-17 morphology after CCC.

Figure F.18. Glass HAL24M1-18 morphology after CCC.

Figure F.19. Glass HAL24M1-19 morphology after CCC.

Figure F.20. Glass HAL24M1-20 morphology after CCC.

Figure F.21. Glass HAL24M1-21 morphology after CCC.

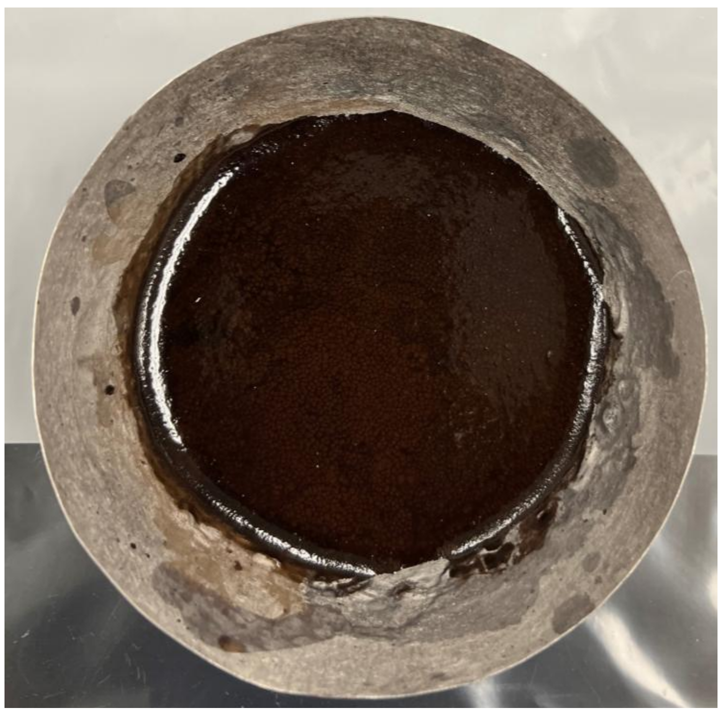

Figure F.22. Glass HAL24M1-22 morphology after CCC.

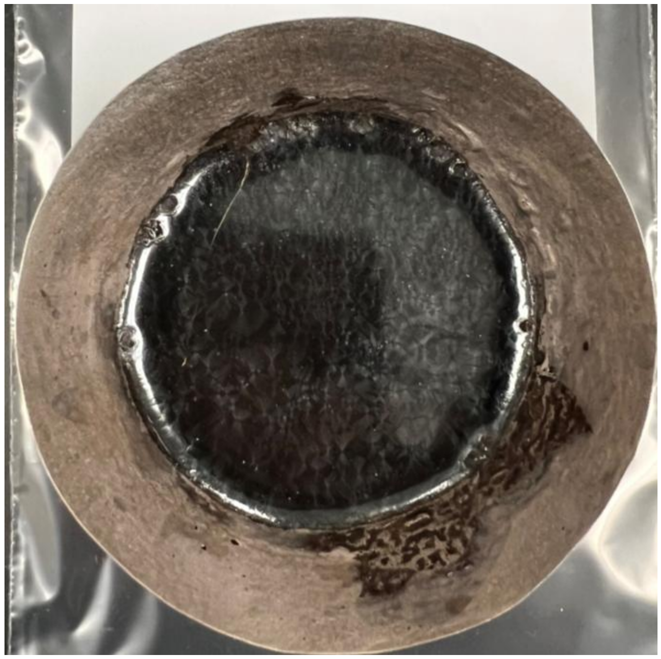

Figure F.23. Glass HAL24M1-23 morphology after CCC.

Figure F.24. Glass HAL24M1-24 morphology after CCC.

Figure F.25. Glass HAL24M1-25 morphology after CCC.

Figure F.26. Glass HAL24M1-26 morphology after CCC.

Figure F.27. Glass HAL24M1-27 morphology after CCC.

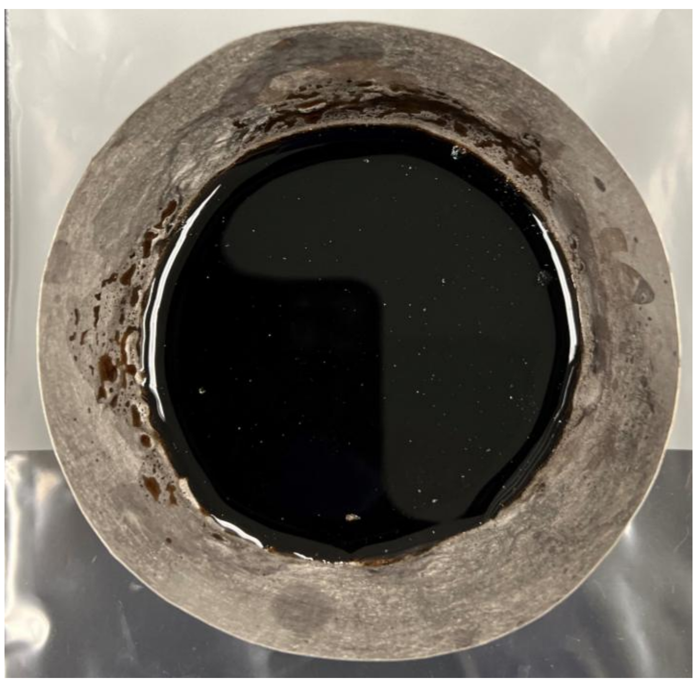

Figure F.28. Glass HAL24M1-28 morphology after CCC.

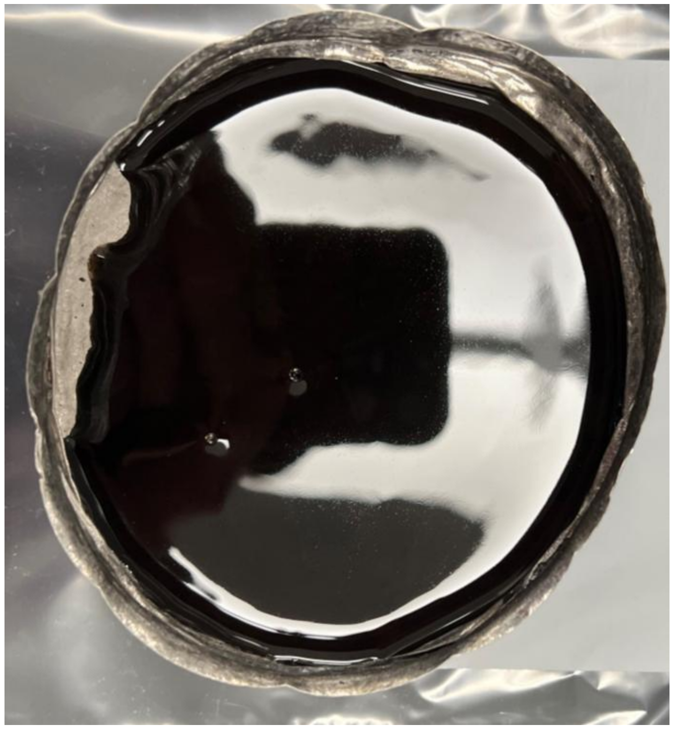

Figure F.29. Glass HAL24M1-29-1 morphology after CCC.

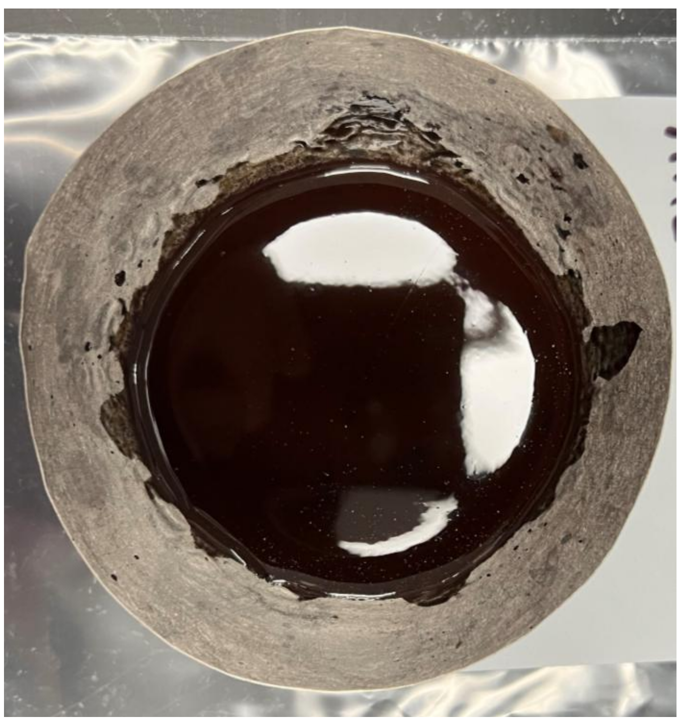

Figure F.30. Glass HAL24M1-30-1 morphology after CCC.

Figure F.31. Glass HAL24M2-01 morphology after CCC.

Figure F.32. Glass HAL24M2-02 morphology after CCC.

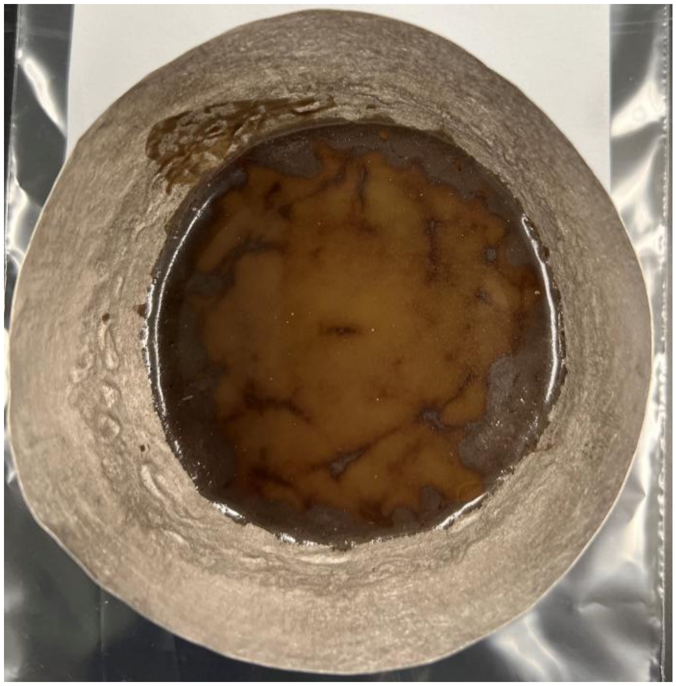

Figure F.33. Glass HAL24M2-03 morphology after CCC.

Figure F.34. Glass HAL24M2-04-1 morphology after CCC.

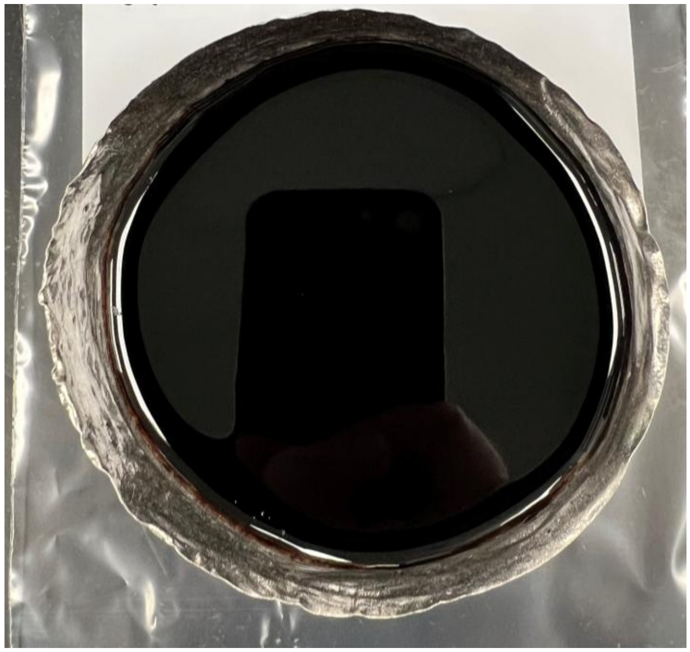

Figure F.35. Glass HAL24M2-05 morphology after CCC.

Figure F.36. Glass HAL24M2-06 morphology after CCC.

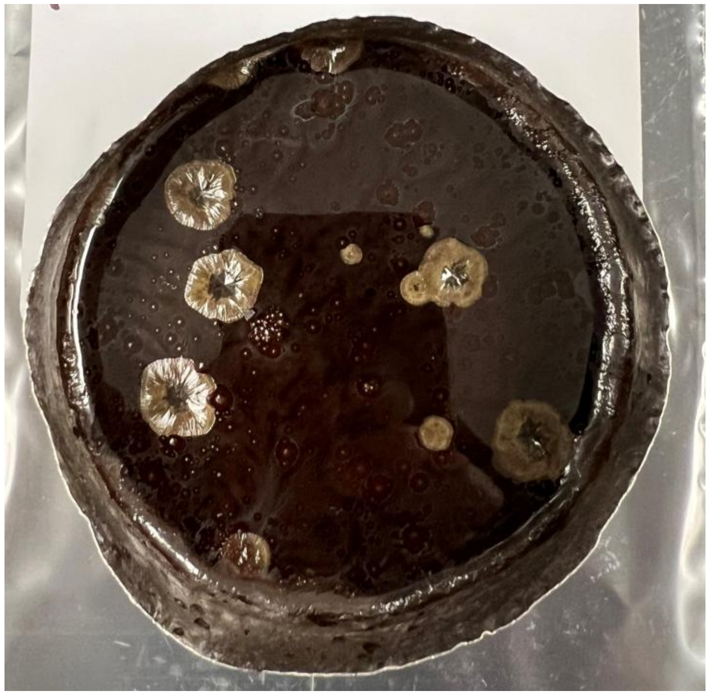

Figure F.37. Glass HAL24M2-07 morphology after CCC.

Figure F.38. Glass HAL24M2-08 morphology after CCC.

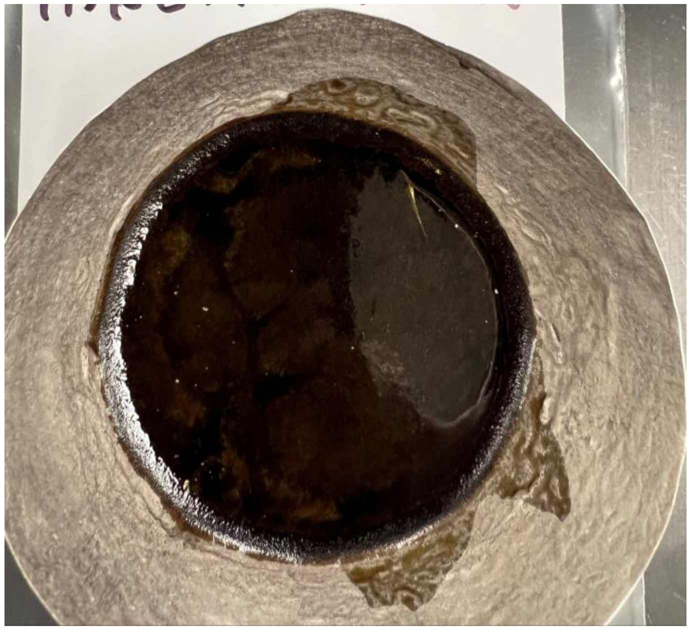

Figure F.39. Glass HAL24M2-09 morphology after CCC.

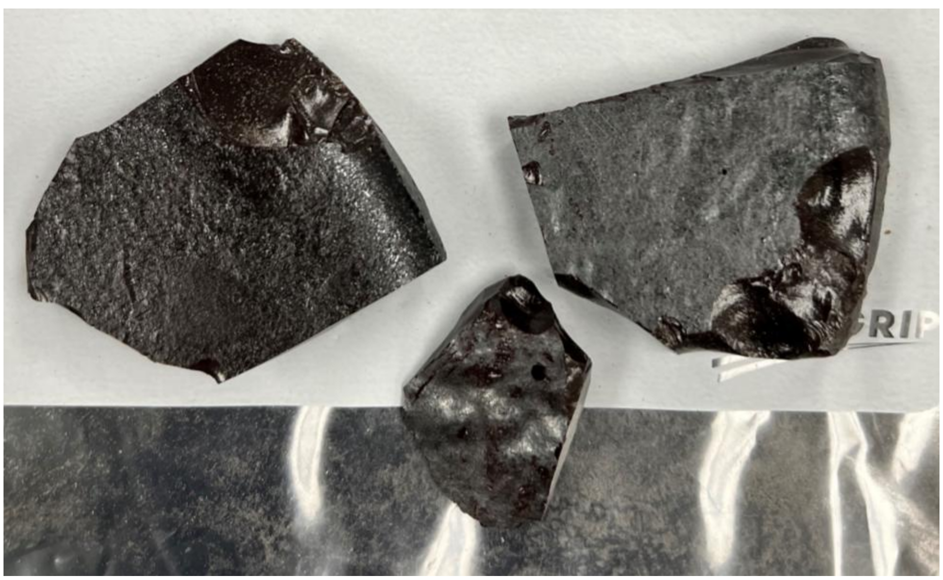

Figure F.40. Glass HAL24M2-10 morphology after CCC.

Figure F.41. Glass HAL24M2-11 morphology after CCC.

Figure F.42. Glass HAL24M2-12 morphology after CCC.

Figure F.43. Glass HAL24M2-13 morphology after CCC.

Figure F.44. Glass HAL24M2-14 morphology after CCC.

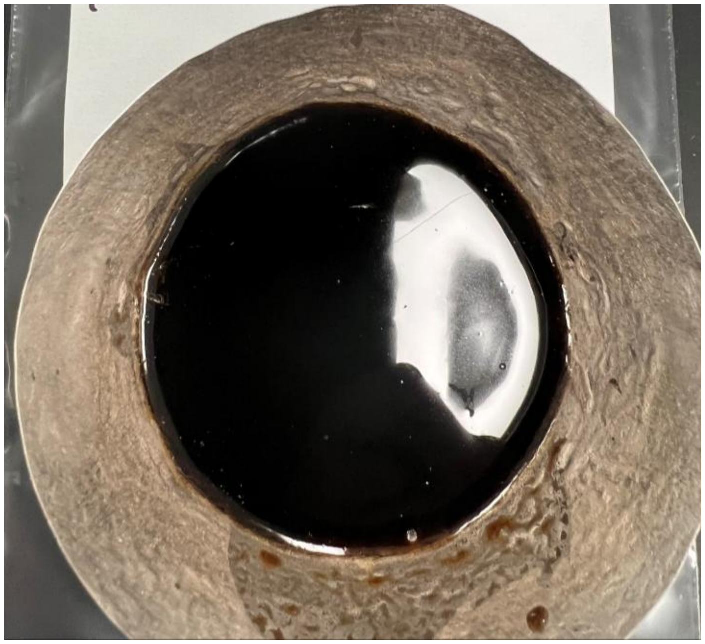

Figure F.45. Glass HAL24M2-15 morphology after CCC.

Figure F.46. Glass HAL24M2-16 morphology after CCC.

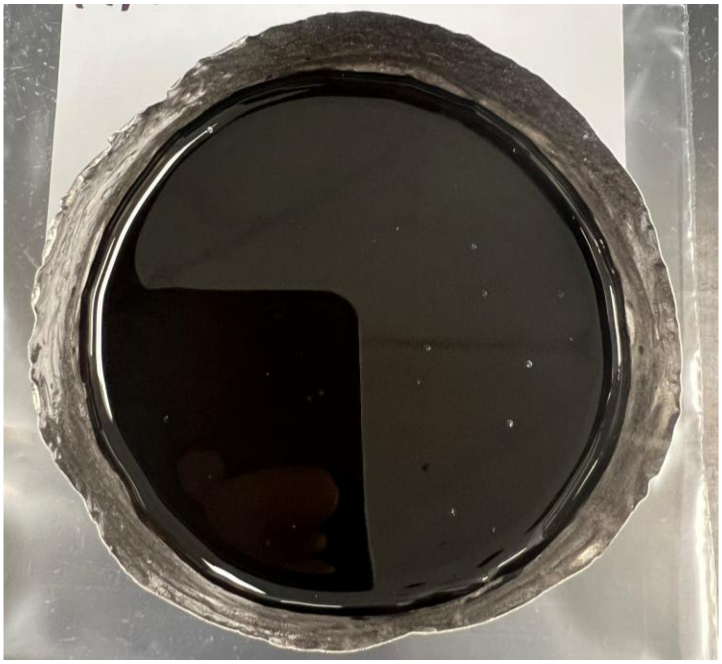

Figure F.47. Glass HAL24M2-17 morphology after CCC.

Figure F.48. Glass HAL24M2-18 morphology after CCC.

Figure F.49. Glass HAL24M2-19 morphology after CCC.

Figure F.50. Glass HAL24M2-20 morphology after CCC.

Appendix G – XRD Scans after Canister Centerline Cooling

This appendix presents the X-ray diffraction (XRD) scans showing the main crystal phases present after canister centerline cooling (CCC) of the glasses shown in Appendix F. The percentage of crystal content reported in the XRD scans is presented before any adjustments were made from spiking with 5 wt% of high-purity cerium oxide. The data is corrected not only for the amount of cerium oxide introduced into the samples, but also for the fact that the cerium oxide used was only 51% crystalline. XRD scans are not included when the glass maintains an amorphous structure.

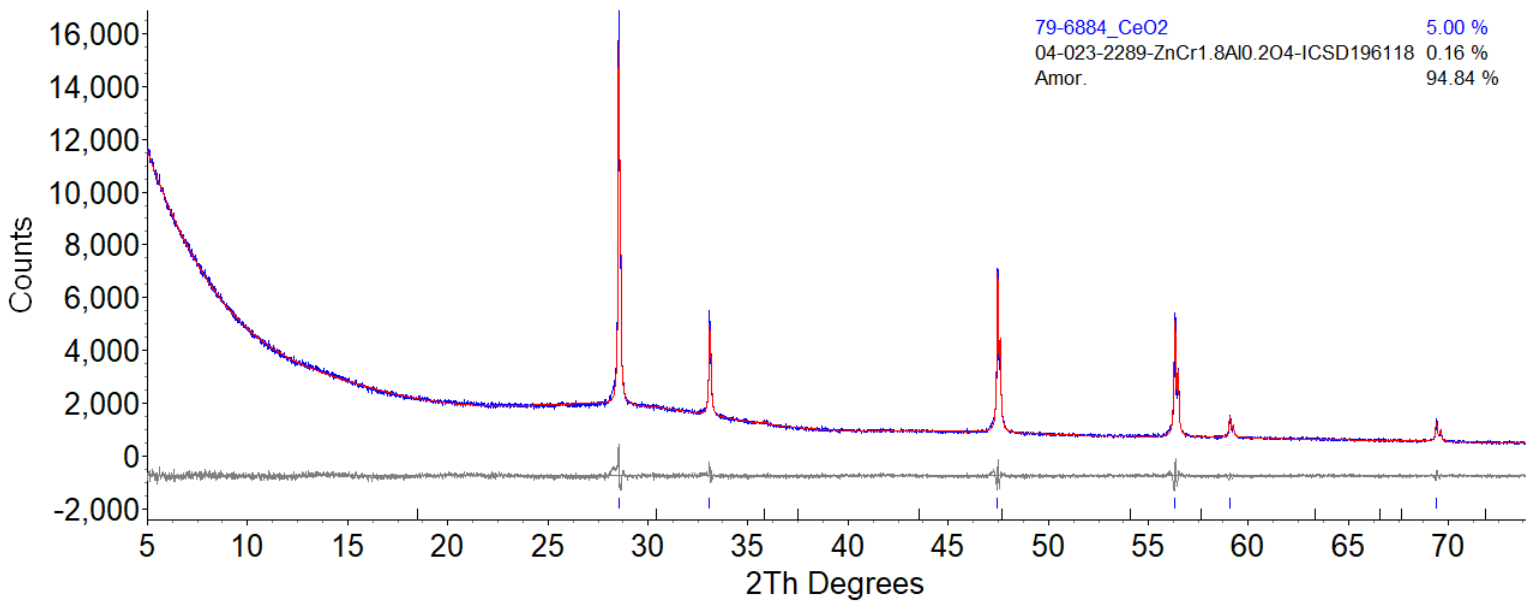

Phase Name	wt% Measured	wt% Corrected	wt% Normalized
CeO_2	5.00	2.57	-
$ZnCr_{1.8}$ $Al_{0.2}O_4$	0.16	0.082	0.086

Figure G.1. XRD scan of glass HAL24M1-01 after CCC.

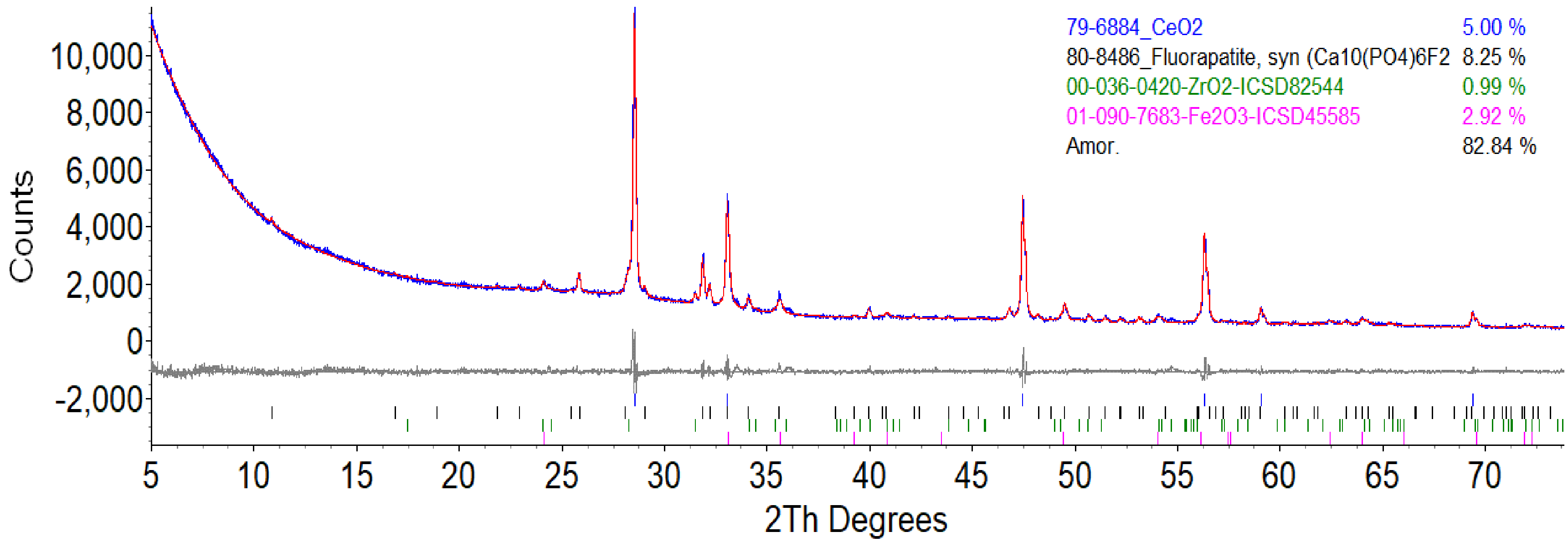

Phase Name	wt% Measured	wt% Corrected	wt% Normalized
CeO_2	5.00	2.57	-
$Ca_{10}(PO_4)_6F_2$	8.25	4.23	4.45
ZrO_2	0.99	0.51	0.54
Fe_2O_3	2.92	1.50	1.58

Figure G.2. XRD scan of glass HAL24M1-03 after CCC.

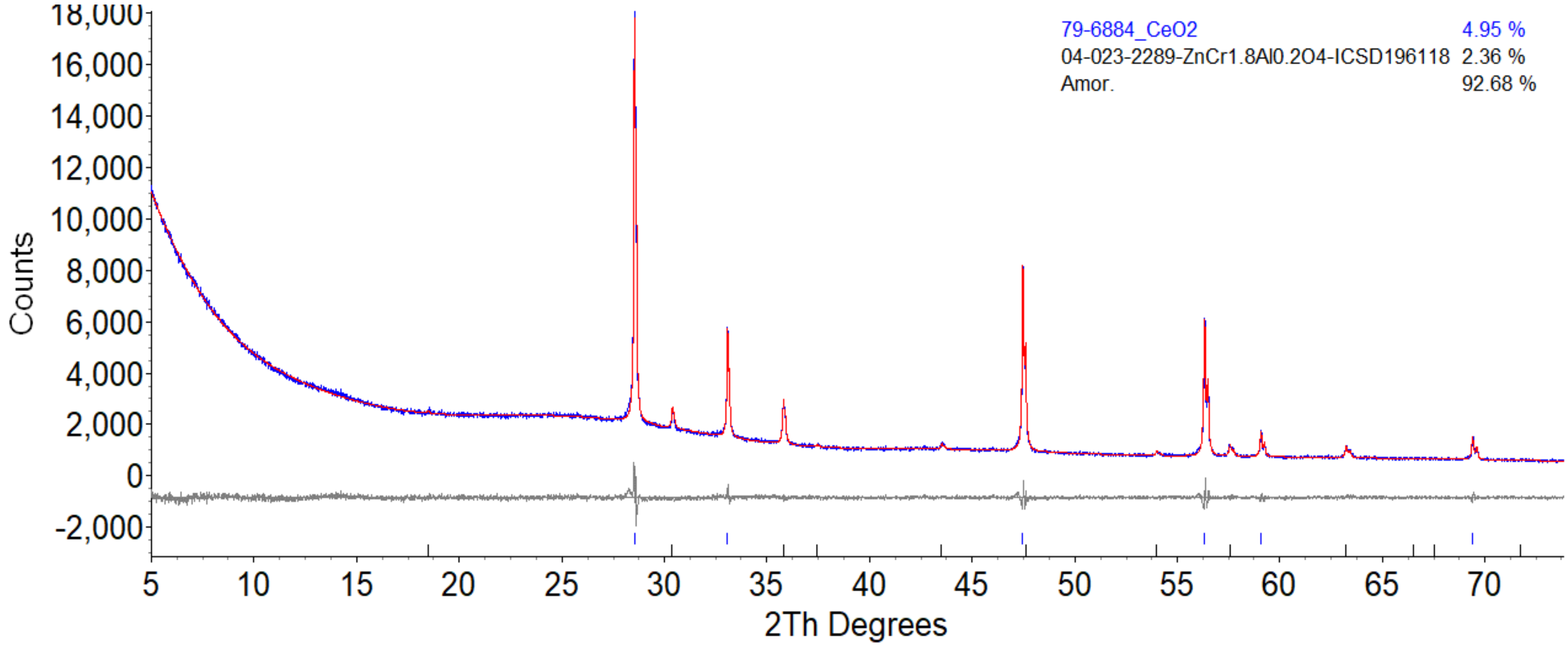

Phase Name	wt% Measured	wt% Corrected	wt% Normalized
CeO_2	4.95	2.54	-
$ZnCr_{1.8}Al_{0.2}O_4$	2.36	1.21	1.27

Figure G.3. XRD scan of glass HAL24M1-04 after CCC.

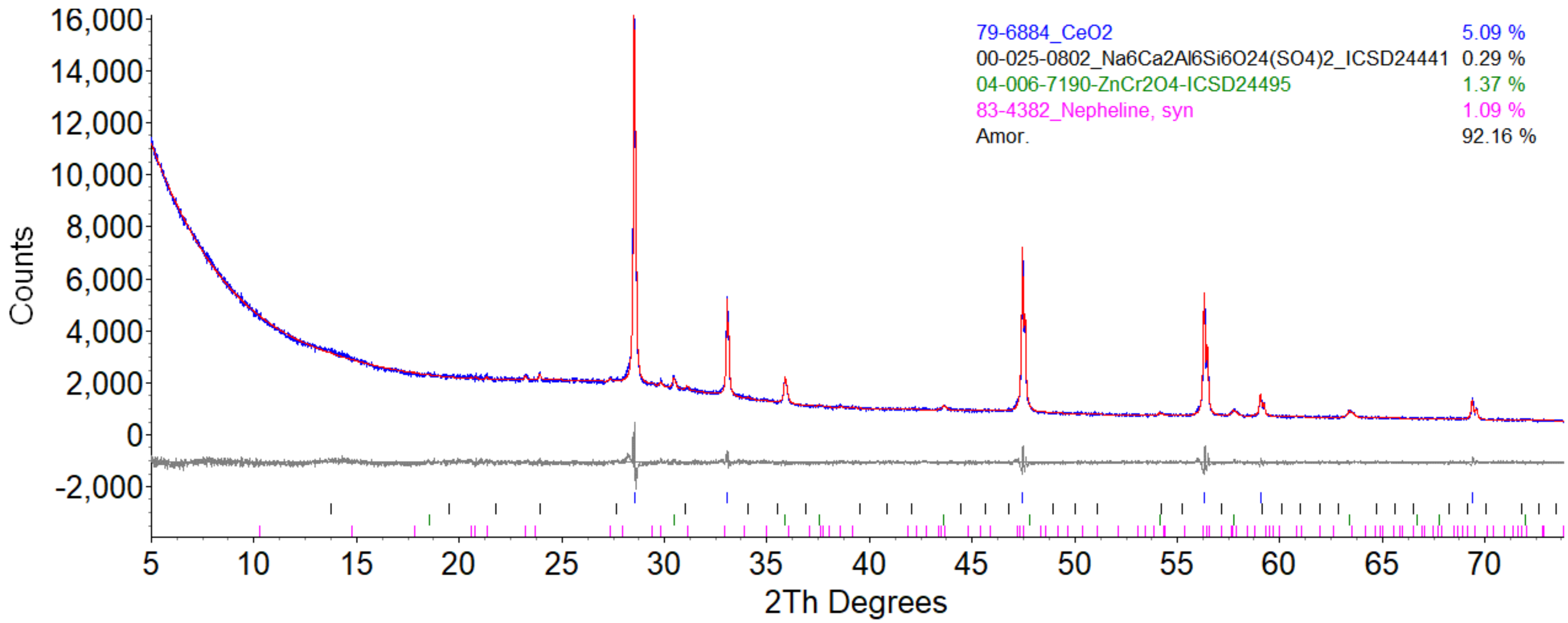

Phase Name	wt% Measured	wt% Corrected	wt% Normalized
CeO_2	5.09	2.61	-
$Na_6Ca_2Al_6Si_6O_{24}(SO_4)_2$	0.29	0.15	0.16
$ZnCr_2O_4$	1.37	0.70	0.74
Nepheline	1.09	0.56	0.59

Figure G.4. XRD scan of glass HAL24M1-05 after CCC.

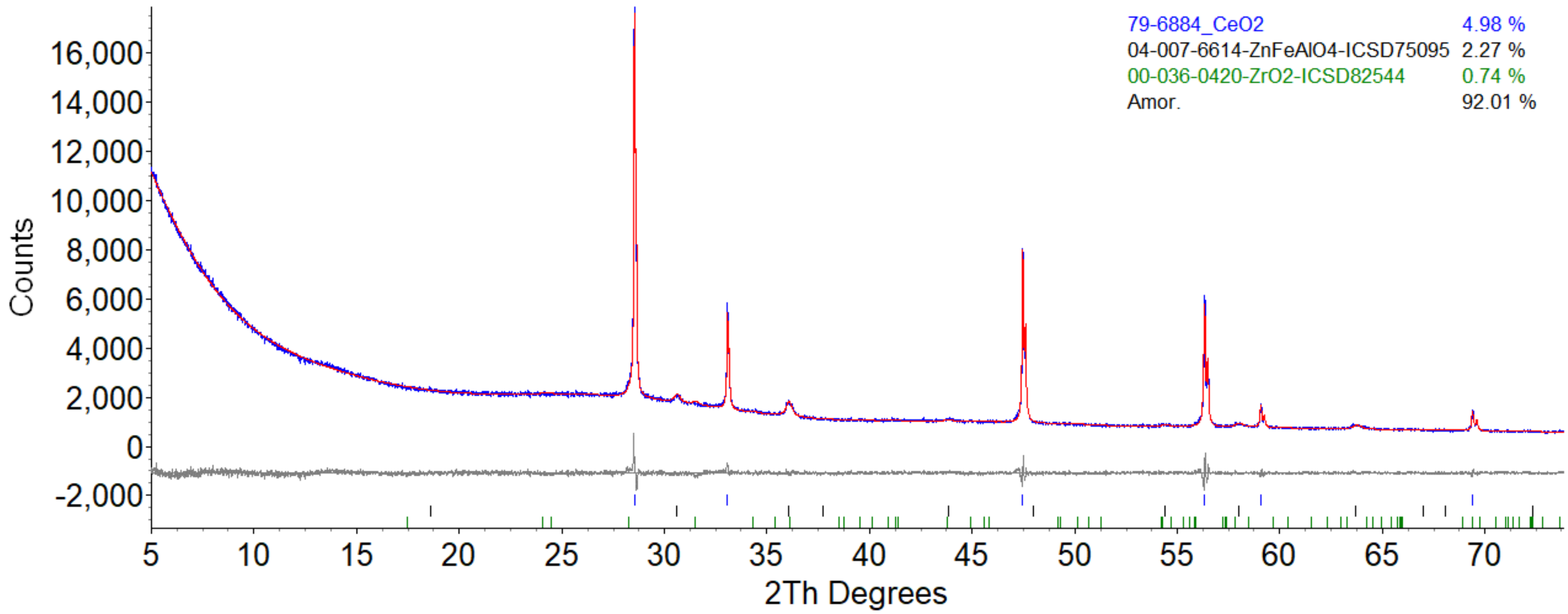

Phase Name	wt% Measured	wt% Corrected	wt% Normalized
CeO_2	4.98	2.55	-
$ZnFeAlO_4$	2.27	1.17	1.23
ZrO_2	0.74	0.38	0.40

Figure G.5. XRD scan of glass HAL24M1-06 after CCC.

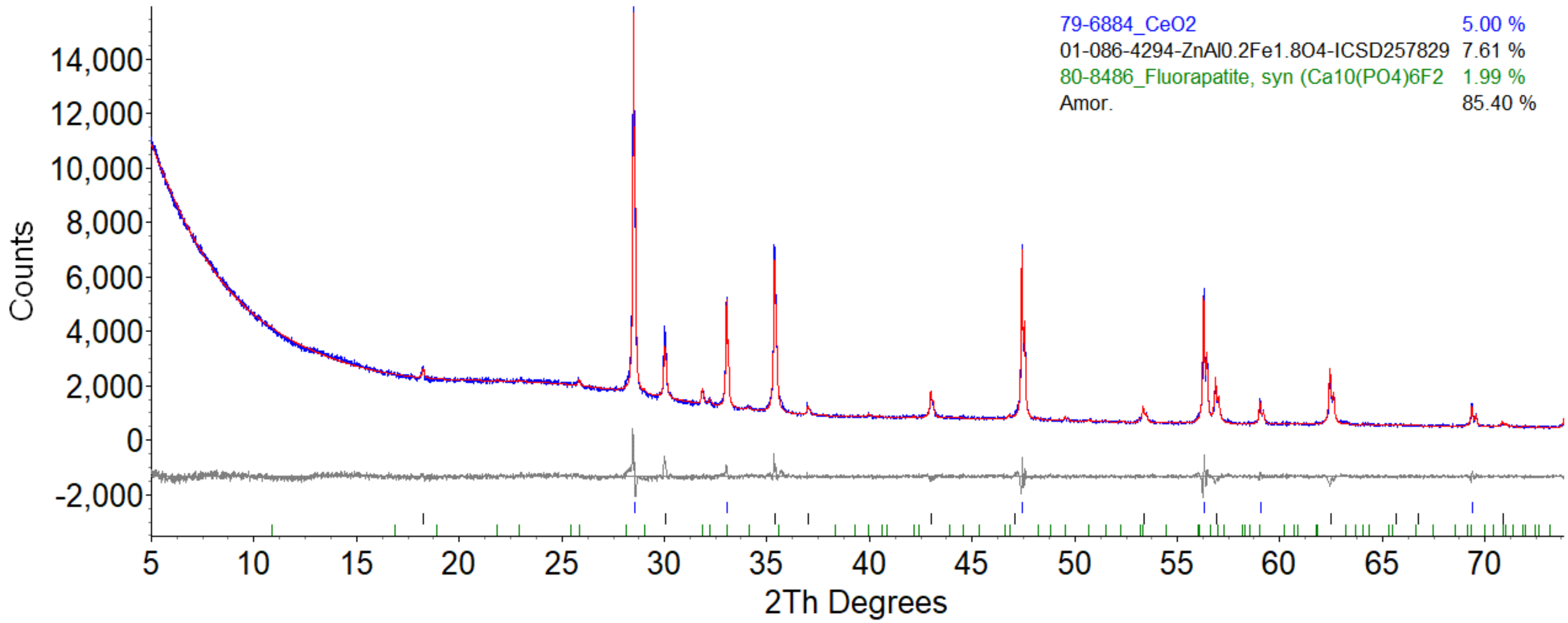

Phase Name	wt% Measured	wt% Corrected	wt% Normalized
CeO_2	5.00	2.57	-
$ZnAl_{0.2}Fe_{1.8}O_4$	7.61	3.90	4.11
$Ca_{10}(PO_4)_6F_2$	1.99	1.02	1.08

Figure G.6. XRD scan of glass HAL24M1-07 after CCC.

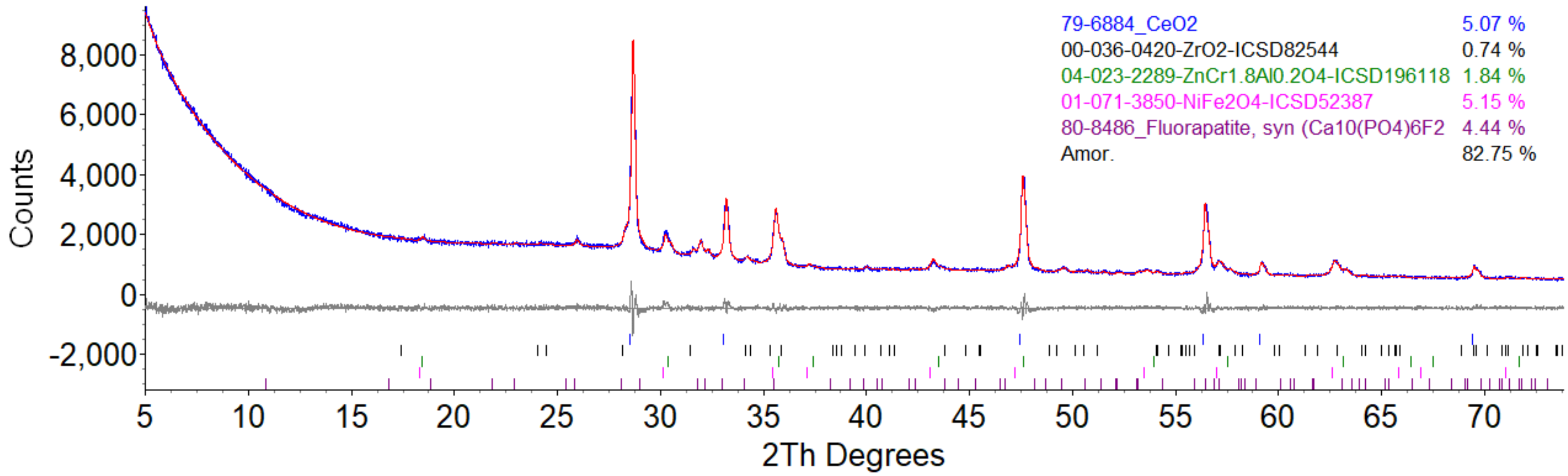

Phase Name	wt% Measured	wt% Corrected	wt% Normalized
CeO_2	5.07	2.60	-
ZrO_2	0.74	0.38	0.40
$ZnCr_{1.8}Al_{0.2}O_4$	1.84	0.94	1.00
$NiFe_2O_4$	5.15	2.64	2.78
$Ca_{10}(PO_4)_6F_2$	4.44	2.28	2.40

Figure G.7. XRD scan of glass HAL24M1-08 after CCC.

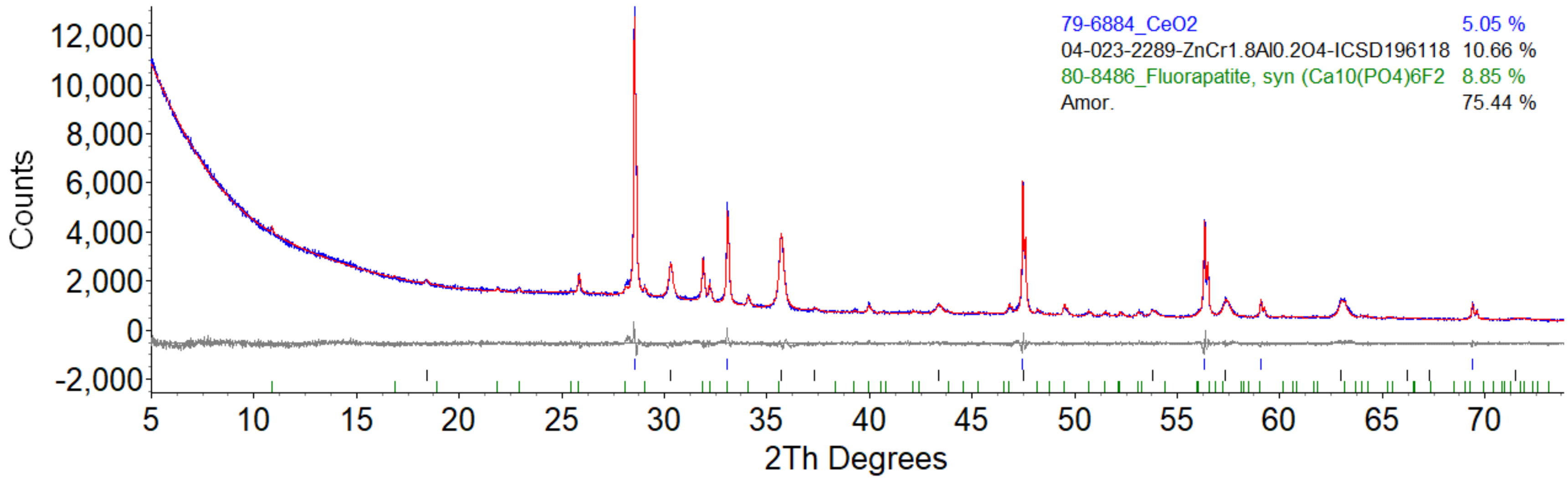

Phase Name	wt% Measured	wt% Corrected	wt% Normalized
CeO_2	5.05	2.59	-
$ZnCr_{1.8}Al_{0.2}O_4$	10.66	5.47	5.76
$Ca_{10}(PO_4)_6F_2$	8.85	4.54	4.78

Figure G.8. XRD scan of glass HAL24M1-09 after CCC.

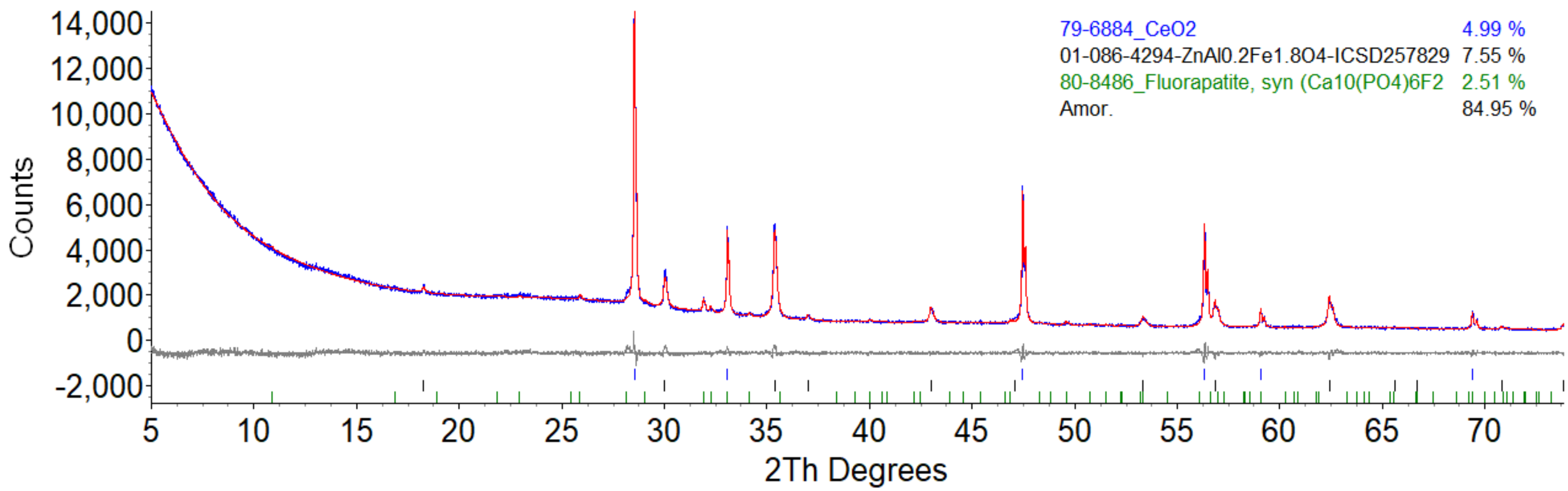

Phase Name	wt% Measured	wt% Corrected	wt% Normalized
CeO_2	4.99	2.56	-
$ZnAl_{0.2}Fe_{1.8}O_4$	7.55	3.87	4.08
$Ca_{10}(PO_4)_6F_2$	2.51	1.29	1.35

Figure G.9. XRD scan of glass HAL24M1-10 after CCC.

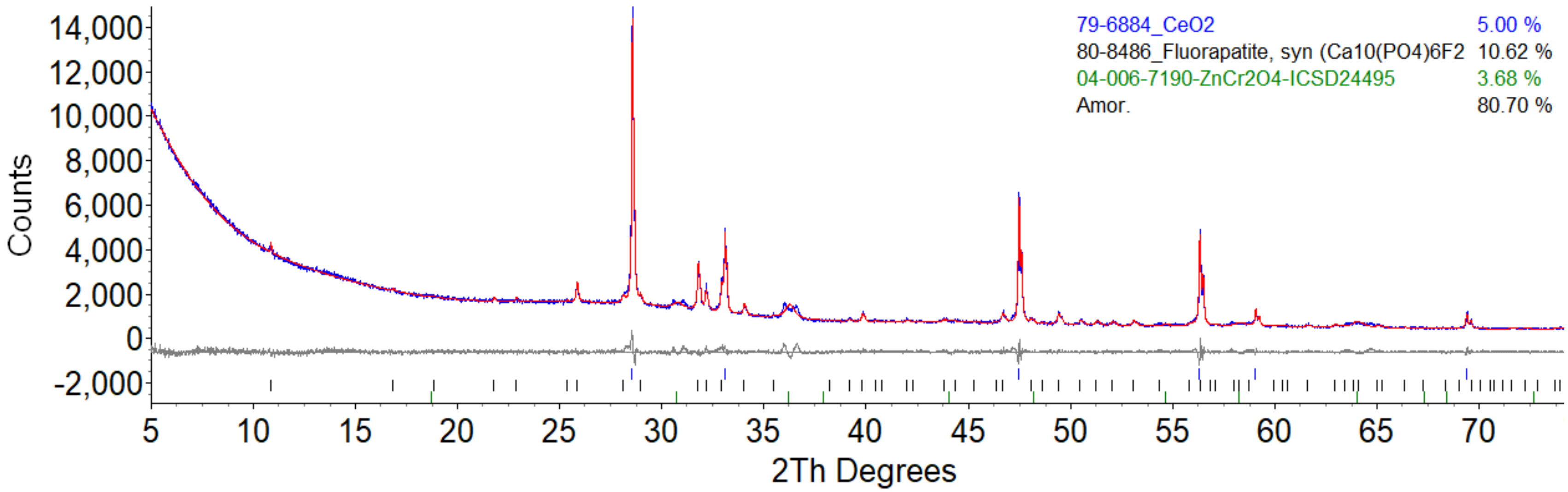

Phase Name	wt% Measured	wt% Corrected	wt% Normalized
CeO_2	5.00	2.57	-
$Ca_{10}(PO_4)_6F_2$	10.62	5.45	5.73
$ZnCr_2O_4$	3.68	1.89	1.99

Figure G.10. XRD scan of glass HAL24M1-11 after CCC.

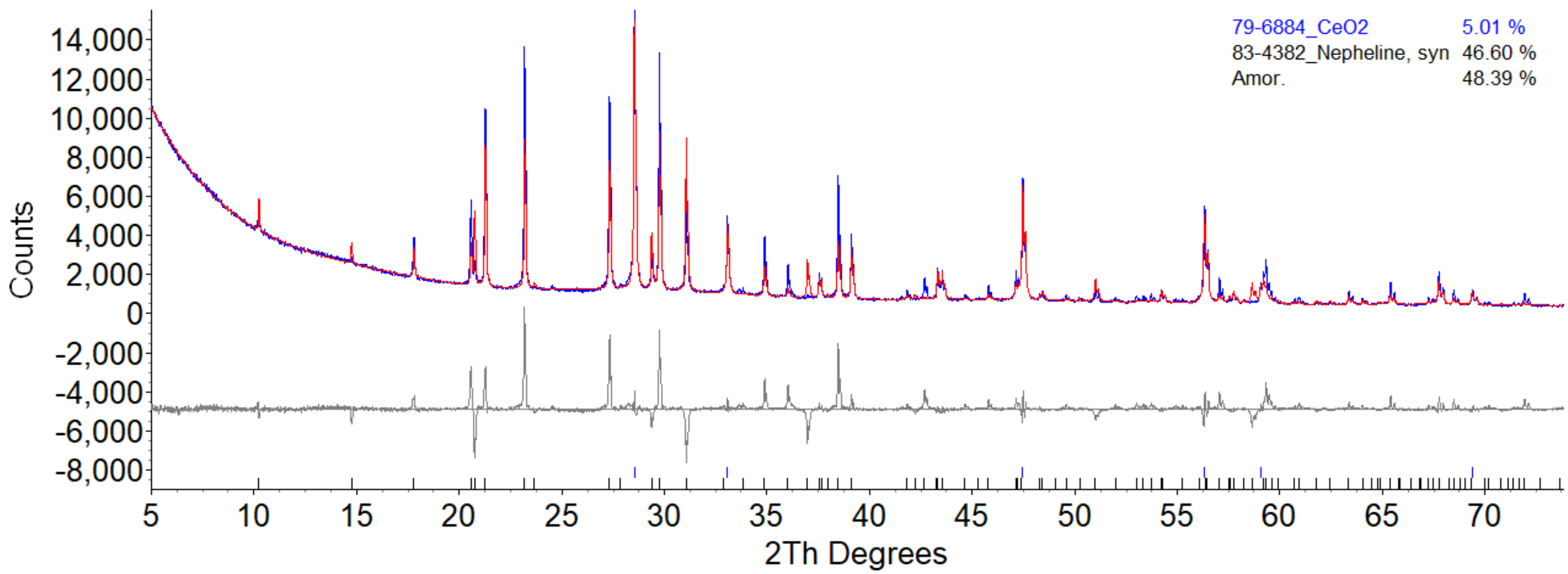

Phase Name	wt% Measured	wt% Corrected	wt% Normalized
CeO_2	5.01	2.57	-
Nepheline	46.60	23.89	25.15

Figure G.11. XRD scan of glass HAL24M1-12 after CCC.

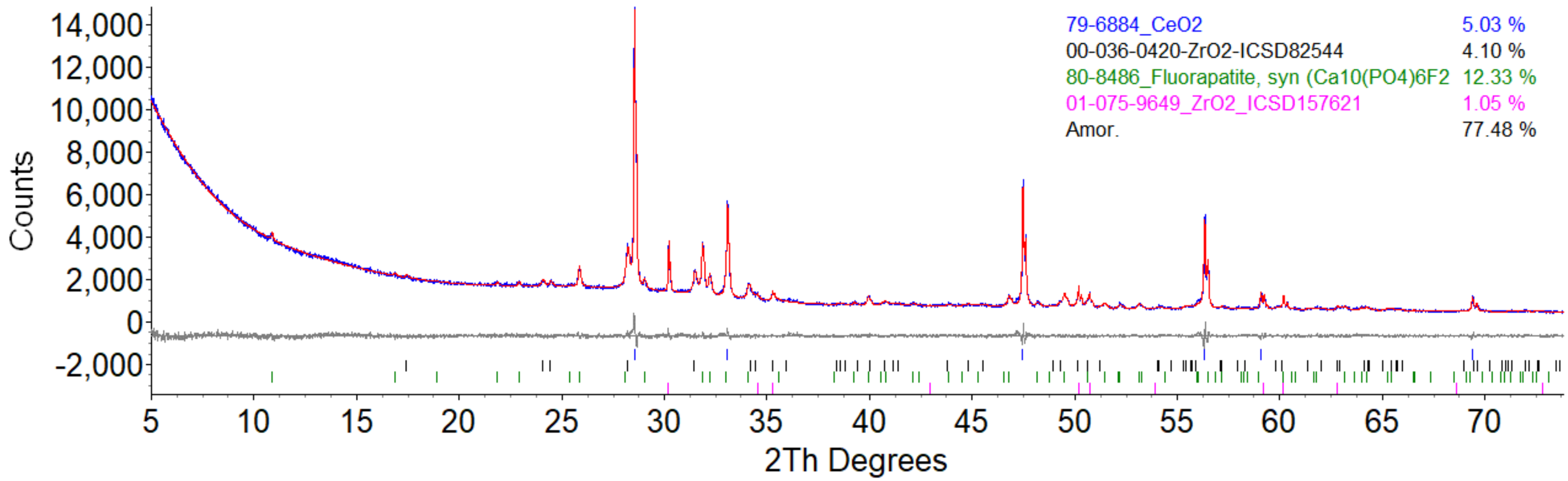

Phase Name	wt% Measured	wt% Corrected	wt% Normalized
CeO_2	5.03	2.58	-
ZrO_2	5.15	2.64	2.78
$Ca_{10}(PO_4)_6F_2$	12.33	6.32	6.66

Figure G.12. XRD scan of glass HAL24M1-13-1 after CCC.

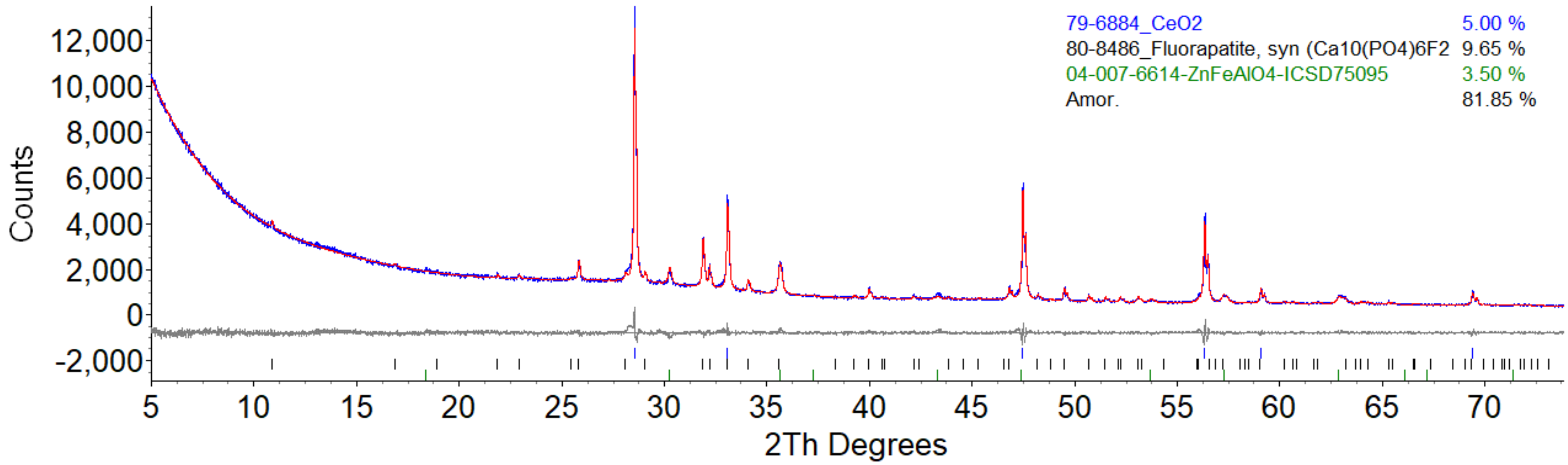

Phase Name	wt% Measured	wt% Corrected	wt% Normalized
CeO_2	5.00	2.56	-
$Ca_{10}(PO_4)_6F_2$	9.65	4.95	5.21
$ZnFeAlO_4$	3.50	1.80	1.89

Figure G.13. XRD scan of glass HAL24M1-14 after CCC.

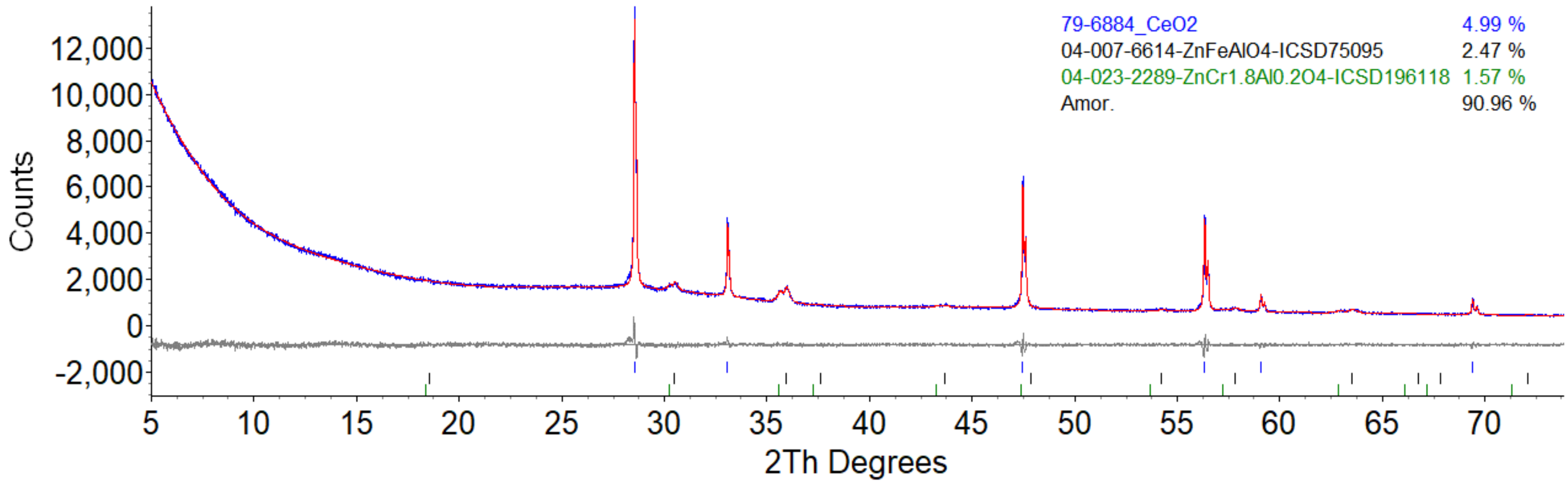

Phase Name	wt% Measured	wt% Corrected	wt% Normalized
CeO_2	4.99	2.56	-
$ZnFeAlO_4$	2.47	1.27	1.33
$ZnCr_{1.8}Al_{0.2}O_4$	1.57	0.81	0.85

Figure G.14. XRD scan of glass HAL24M1-15 after CCC.

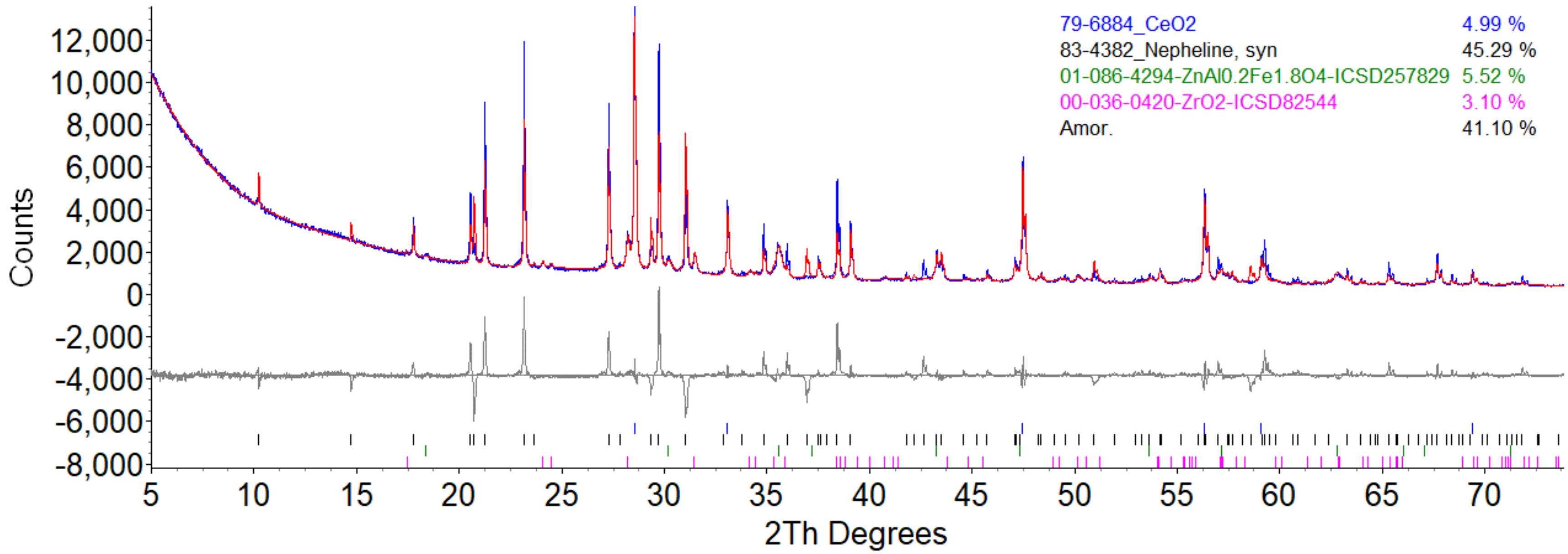

Phase Name	wt% Measured	wt% Corrected	wt% Normalized
CeO_2	4.99	2.56	-
Nepheline	45.29	23.22	24.44
$ZnAl_{0.2}Fe_{1.8}O_4$	5.52	2.83	2.98
ZrO_2	3.10	1.59	1.67

Figure G.15. XRD scan of glass HAL24M1-16 after CCC.

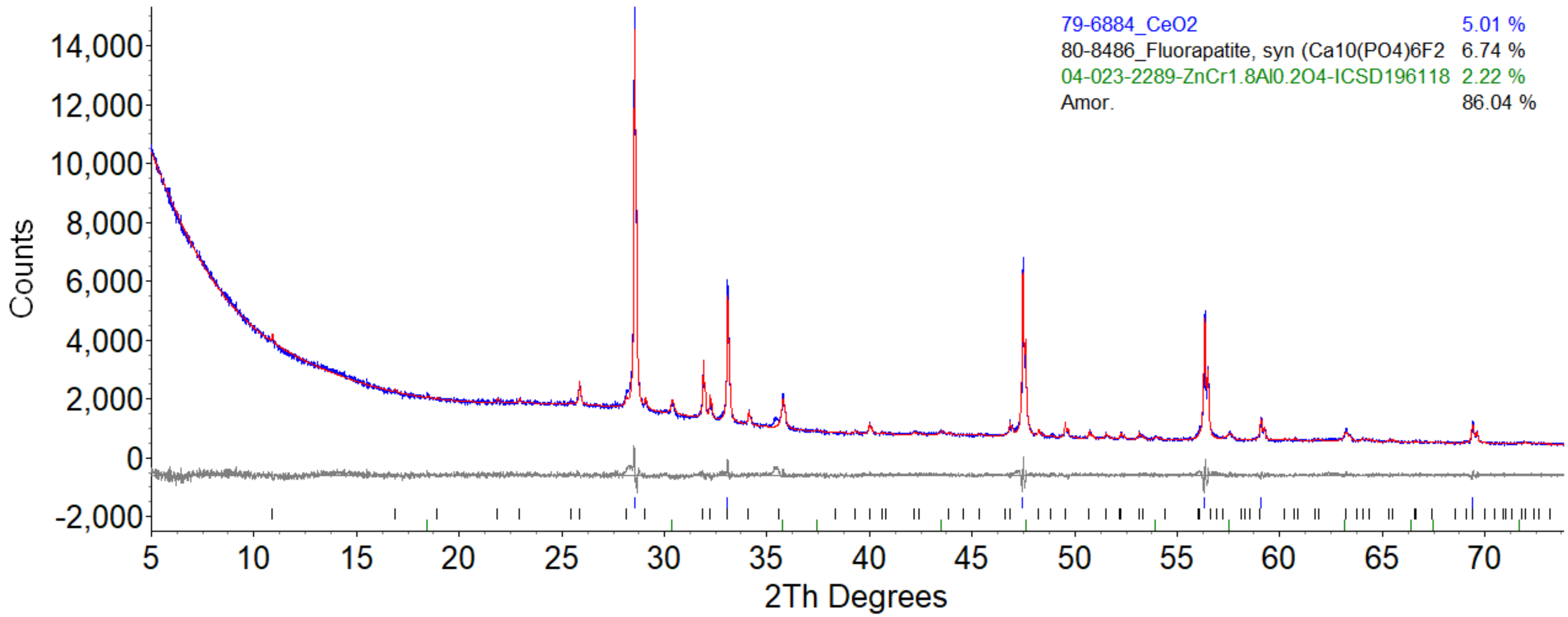

Phase Name	wt% Measured	wt% Corrected	wt% Normalized
CeO_2	5.01	2.57	-
$Ca_{10}(PO_4)_6F_2$	6.74	3.45	3.64
$ZnCr_{1.8}Al_{0.2}O_4$	2.22	1.14	1.20

Figure G.16. XRD scan of glass HAL24M1-18 after CCC.

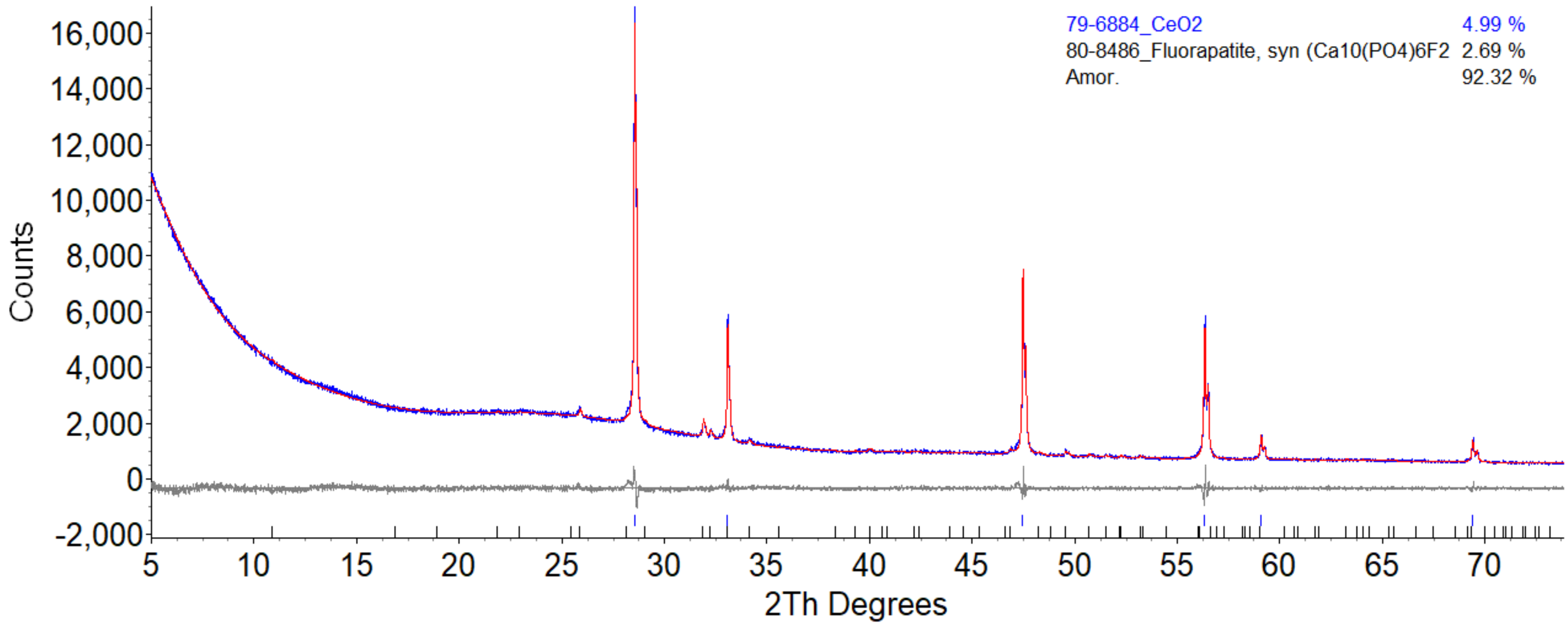

Phase Name	wt% Measured	wt% Corrected	wt% Normalized
CeO_2	4.99	2.56	-
$Ca_{10}(PO_4)_6F_2$	2.69	1.38	1.45

Figure G.17. XRD scan of glass HAL24M1-19 after CCC.

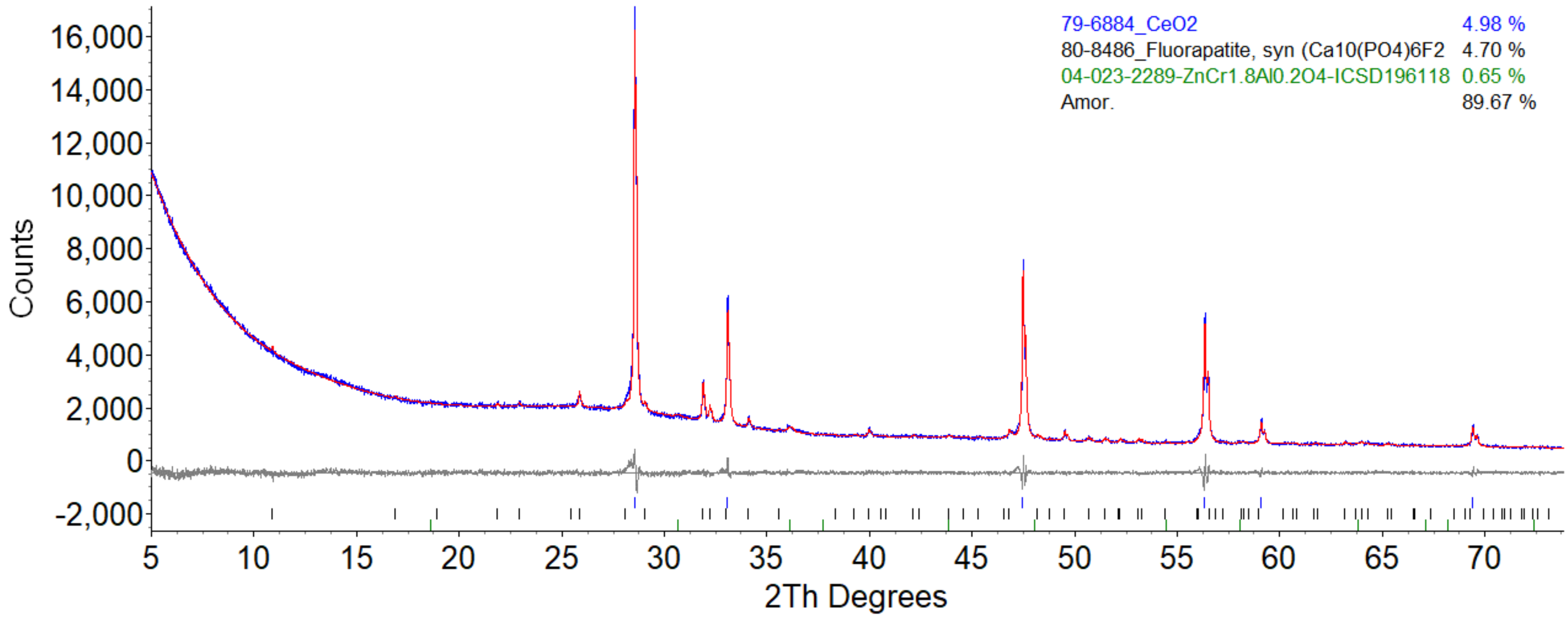

Phase Name	wt% Measured	wt% Corrected	wt% Normalized
CeO_2	4.98	2.55	-
$Ca_{10}(PO_4)_6F_2$	4.70	2.41	2.54
$ZnCr_{1.8}Al_{0.2}O_4$	0.65	0.33	0.35

Figure G.18. XRD scan of glass HAL24M1-20 after CCC.

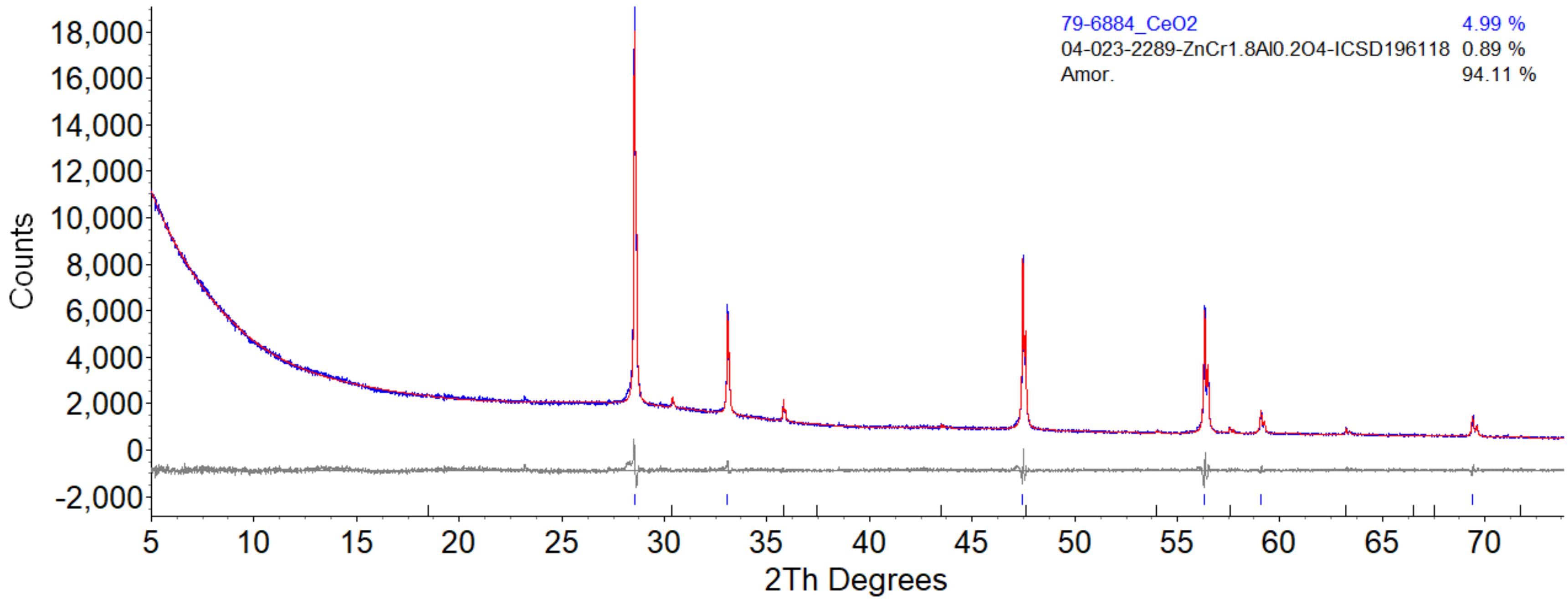

Phase Name	wt% Measured	wt% Corrected	wt% Normalized
CeO_2	4.99	2.56	-
$ZnCr_{1.8}Al_{0.2}O_4$	0.89	0.46	0.48

Figure G.19. XRD scan of glass HAL24M1-21 after CCC.

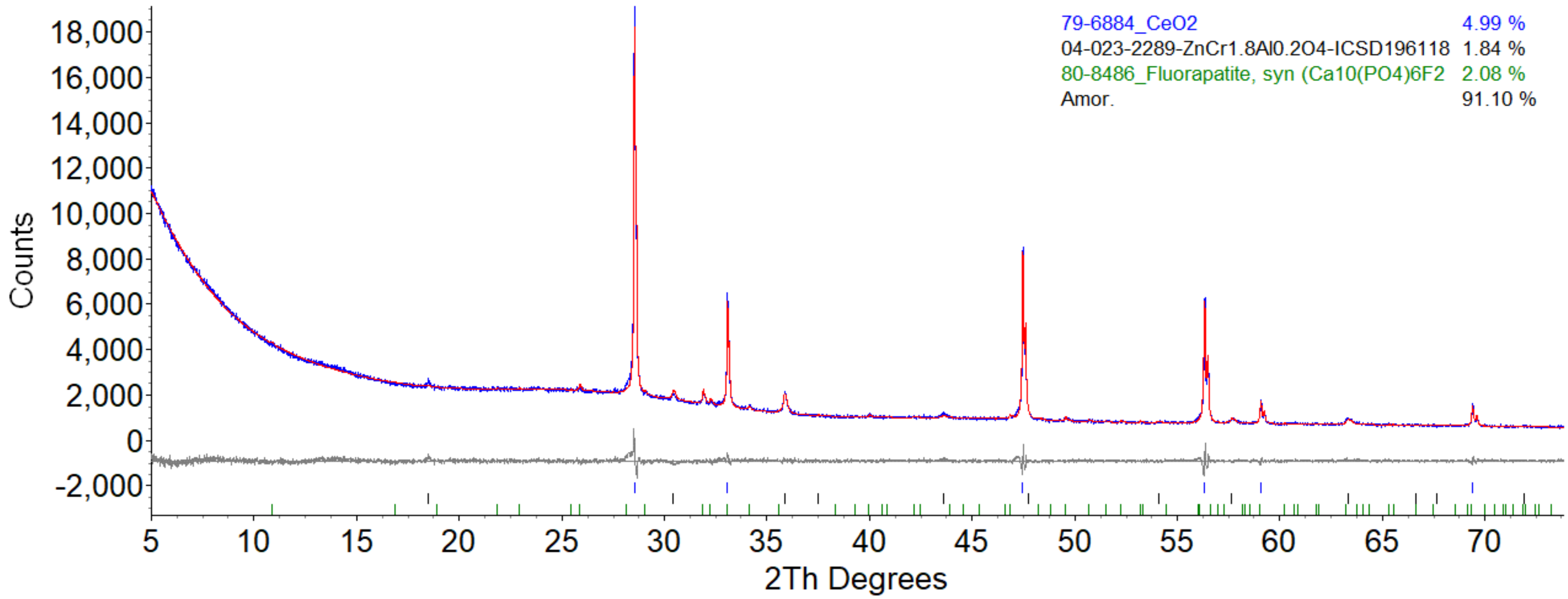

Phase Name	wt% Measured	wt% Corrected	wt% Normalized
CeO_2	4.99	2.56	-
$ZnCr_{1.8}Al_{0.2}O_4$	1.84	0.94	0.99
$Ca_{10}(PO_4)_6F_2$	2.08	1.07	1.12

Figure G.20. XRD scan of glass HAL24M1-22 after CCC.

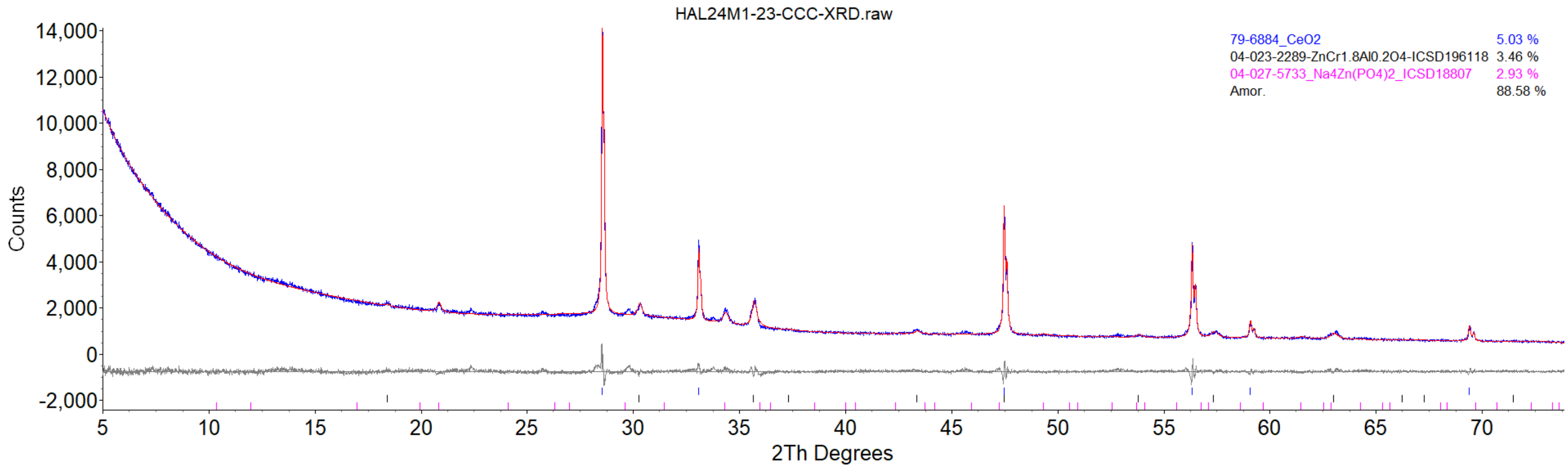

Phase Name	wt% Measured	wt% Corrected	wt% Normalized
CeO_2	5.03	2.58	-
$ZnCr_{1.8}Al_{0.2}O_4$	3.46	1.78	1.87
$Na_4Zn(PO_4)_2$	2.93	1.50	1.60

Figure G.21. XRD scan of glass HAL24M1-23 after CCC.

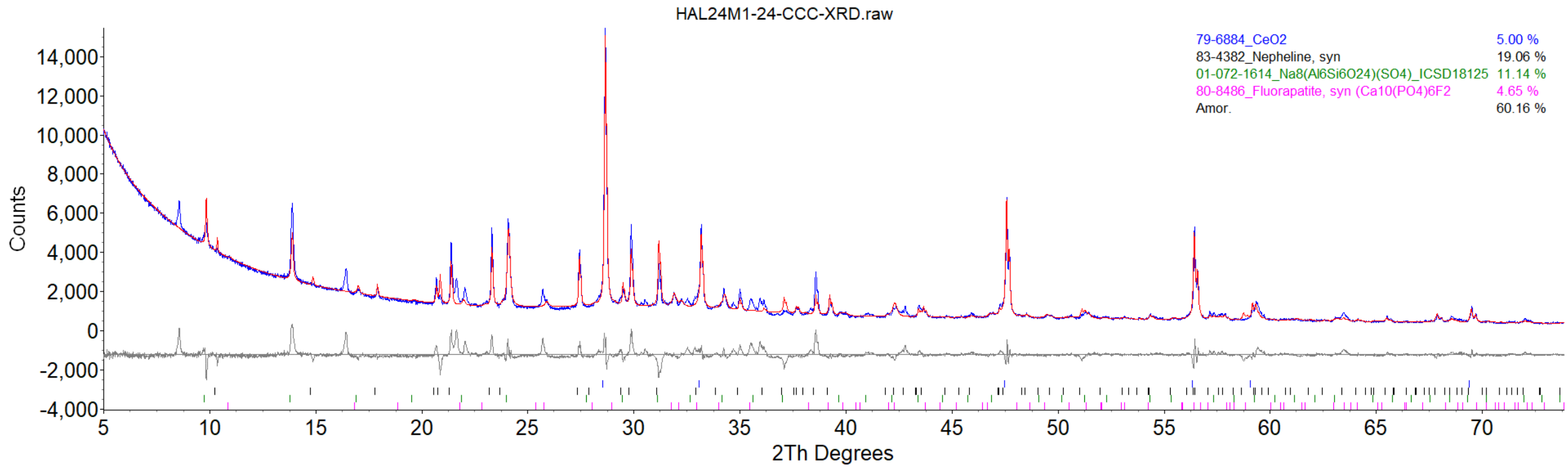

Phase Name	wt% Measured	wt% Corrected	wt% Normalized
CeO_2	5.00	2.56	-
Nepheline	19.06	9.77	10.29
$Na_8(Al_6Si_6O_{24})(SO_4)$	11.14	5.71	6.01
$Ca_{10}(PO_4)_6F_2$	4.65	2.38	2.51

Figure G.22. XRD scan of glass HAL24M1-24 after CCC.

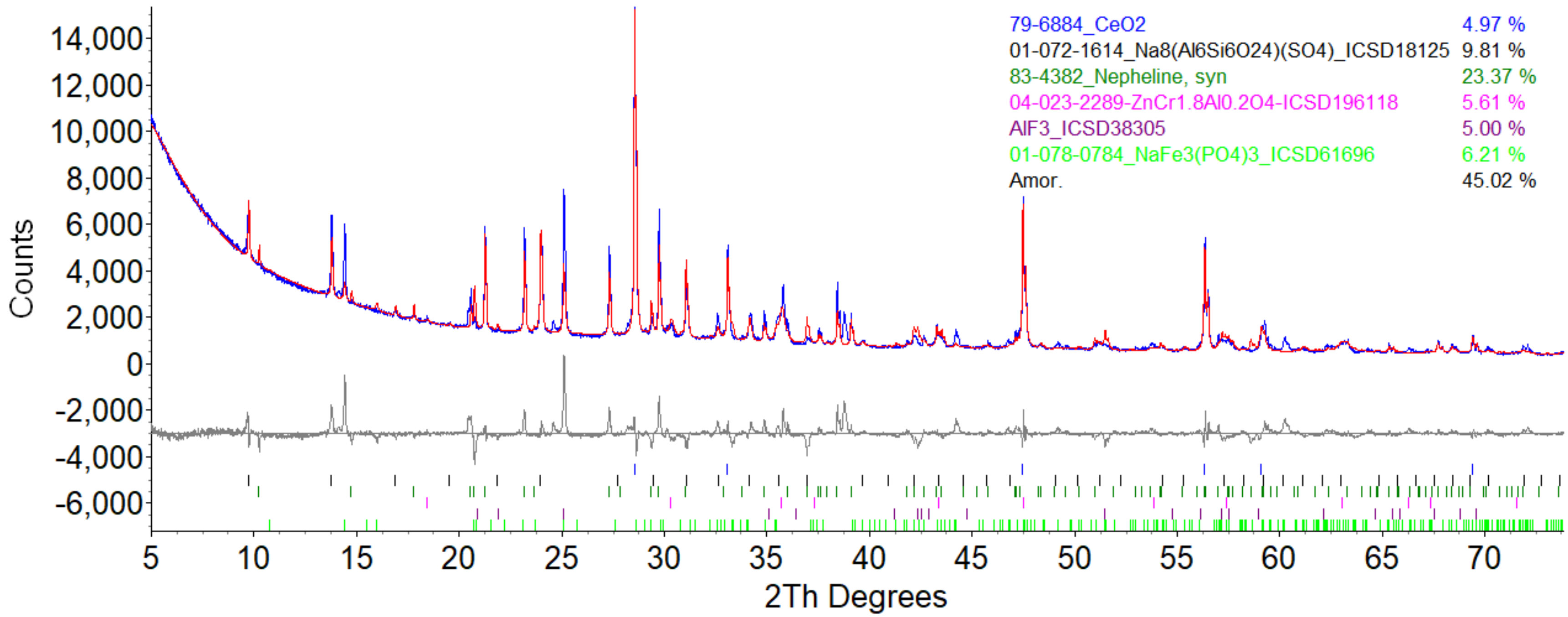

Phase Name	wt% Measured	wt% Corrected	wt% Normalized
CeO_2	4.97	2.55	-
$Na_8(Al_6Si_6O_{24})(SO_4)$	9.81	5.03	5.29
Nepheline	23.37	11.98	12.61
$ZnCr_{1.8}Al_{0.2}O_4$	5.61	2.88	3.03
AlF_3	5.00	2.56	2.70
$NaFe_3(PO_4)_3$	6.21	3.19	3.35

Figure G.23. XRD scan of glass HAL24M1-25 after CCC.

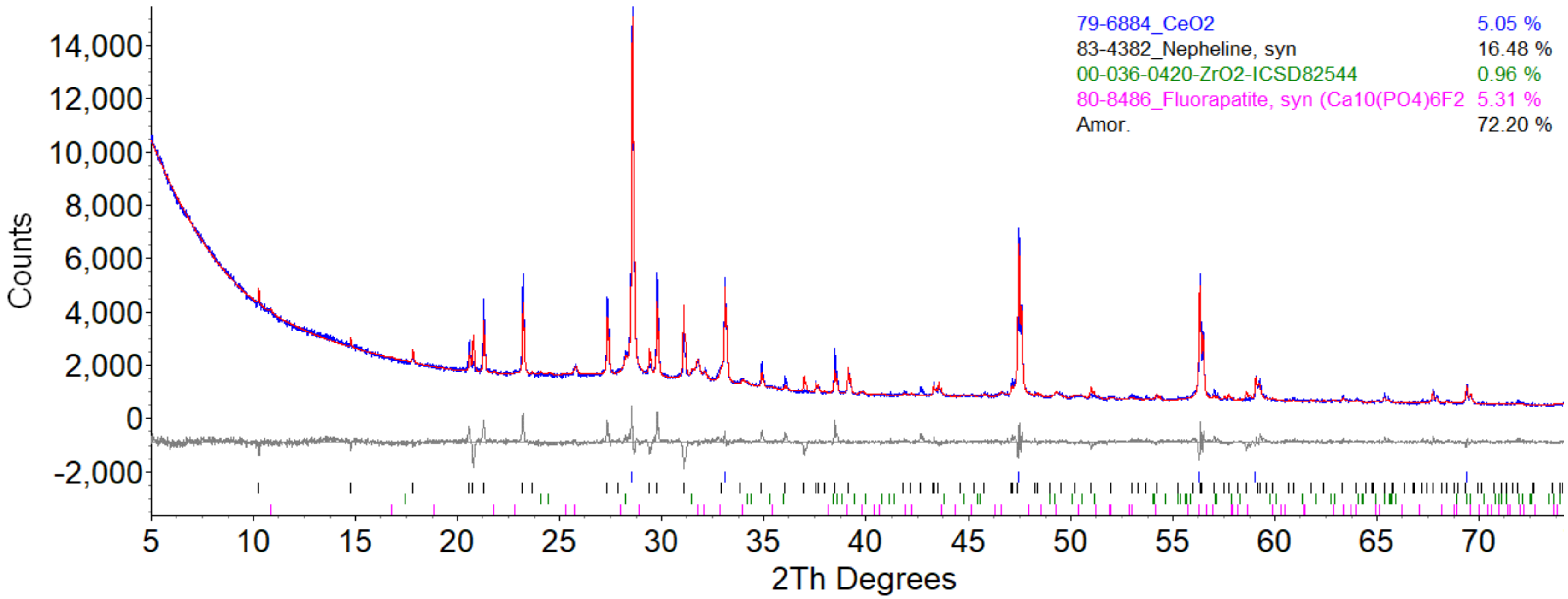

Phase Name	wt% Measured	wt% Corrected	wt% Normalized
CeO_2	5.05	2.59	-
Nepheline	16.48	8.45	8.90
ZrO_2	0.96	0.49	0.52
$Ca_{10}(PO_4)_6F_2$	5.31	2.72	2.86

Figure G.24. XRD scan of glass HAL24M1-26 after CCC.

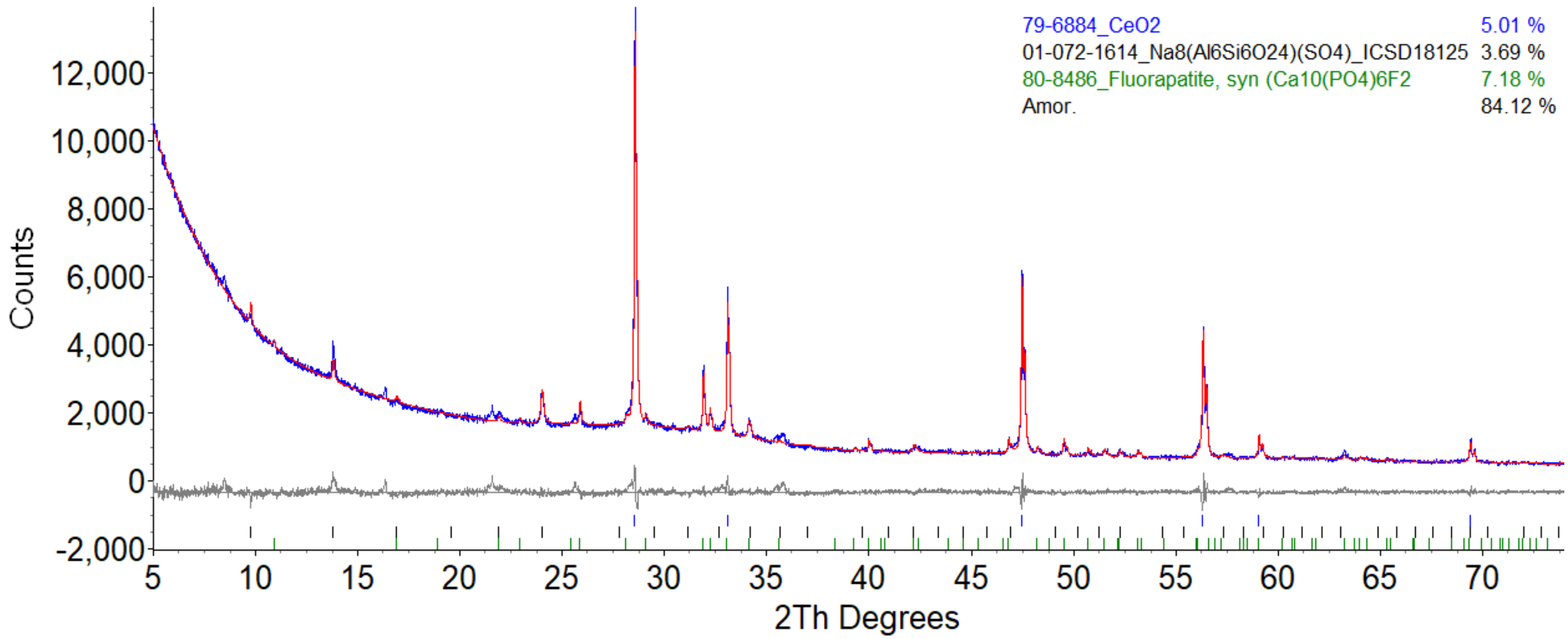

Phase Name	wt% Measured	wt% Corrected	wt% Normalized
CeO_2	5.01	2.57	-
$Na_8(Al_6Si_6O_{24})(SO_4)$	3.69	1.89	1.99
$Ca_{10}(PO_4)_6F_2$	7.18	3.68	3.87

Figure G.25. XRD scan of glass HAL24M1-27 after CCC.

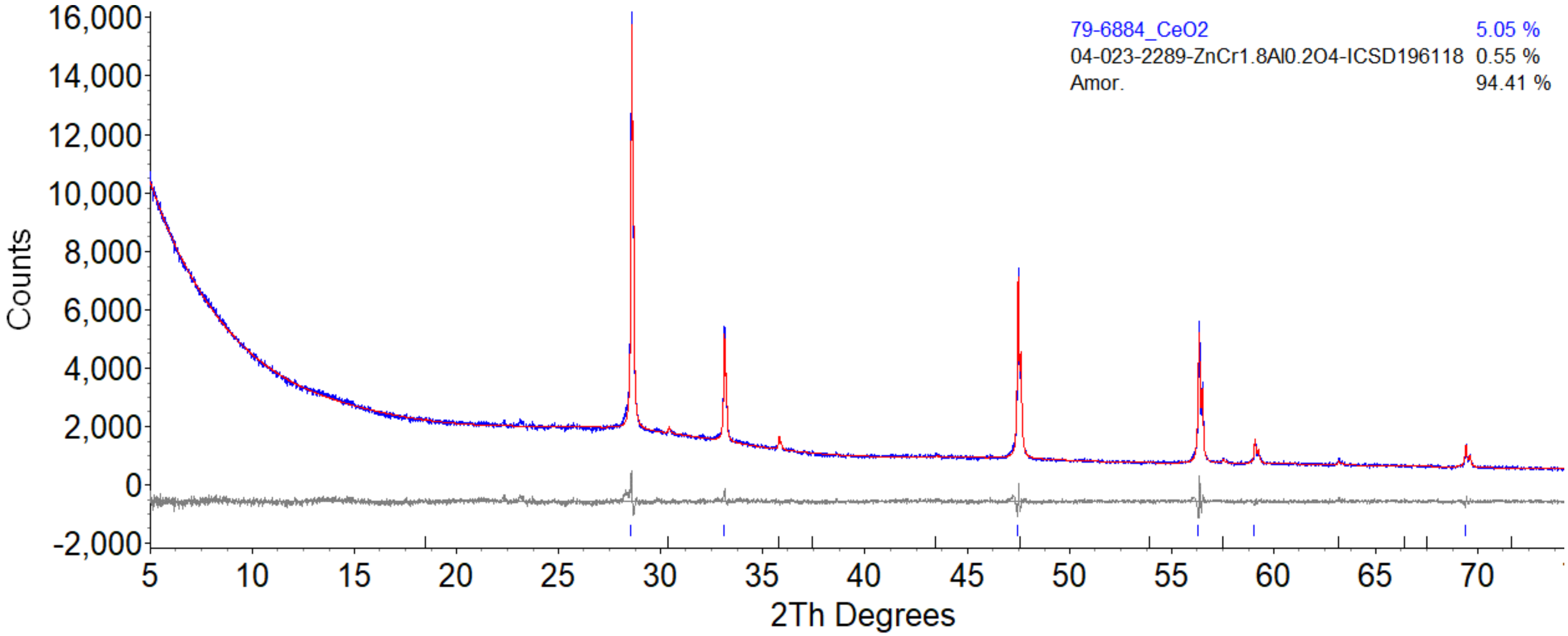

Phase Name	wt% Measured	wt% Corrected	wt% Normalized
CeO_2	5.05	2.59	-
$ZnCr_{1.8}Al_{0.2}O_4$	0.55	0.28	0.29

Figure G.26. XRD scan of glass HAL24M1-28 after CCC.

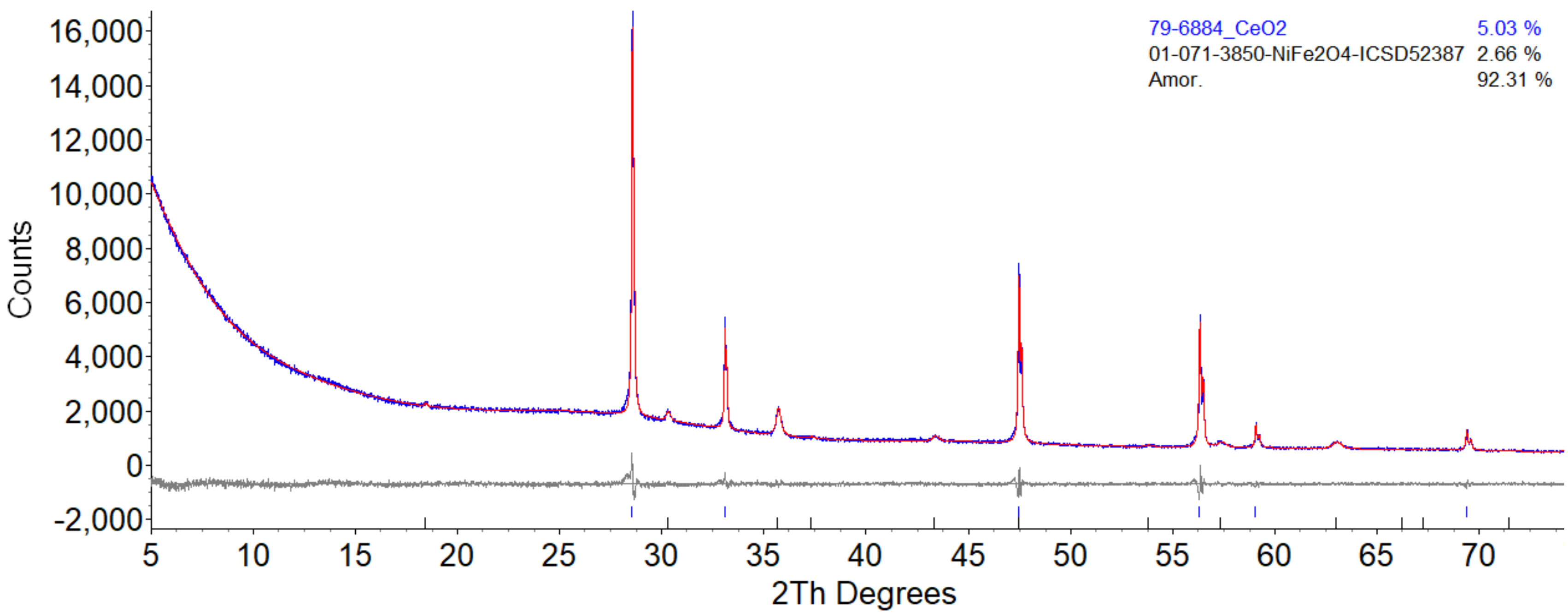

Phase Name	wt% Measured	wt% Corrected	wt% Normalized
CeO_2	5.03	2.58	-
$NiFe_2O_4$	2.66	1.37	1.44

Figure G.27. XRD scan of glass HAL24M1-29-1 after CCC.

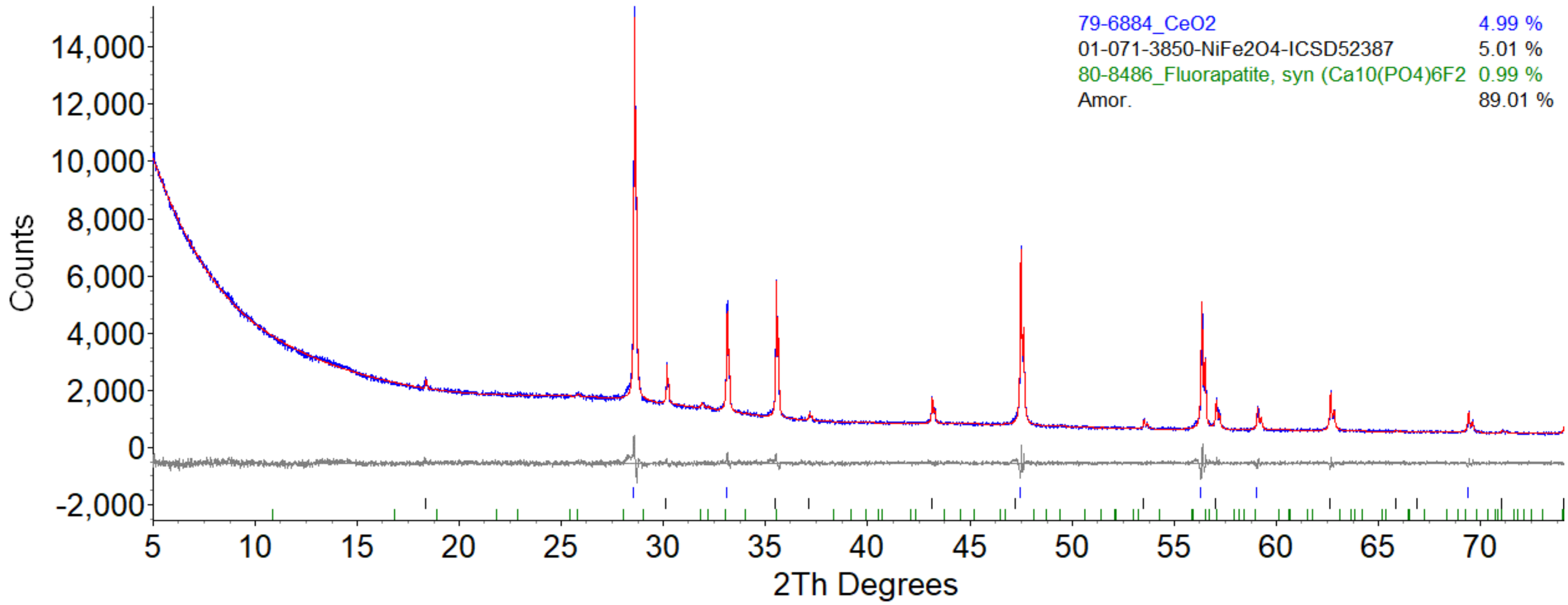

Phase Name	wt% Measured	wt% Corrected	wt% Normalized
CeO_2	4.99	2.56	-
$NiFe_2O_4$	5.01	2.57	2.70
$Ca_{10}(PO_4)_6F_2$	0.99	0.51	0.54

Figure G.28. XRD scan of glass HAL24M1-30-1 after CCC.

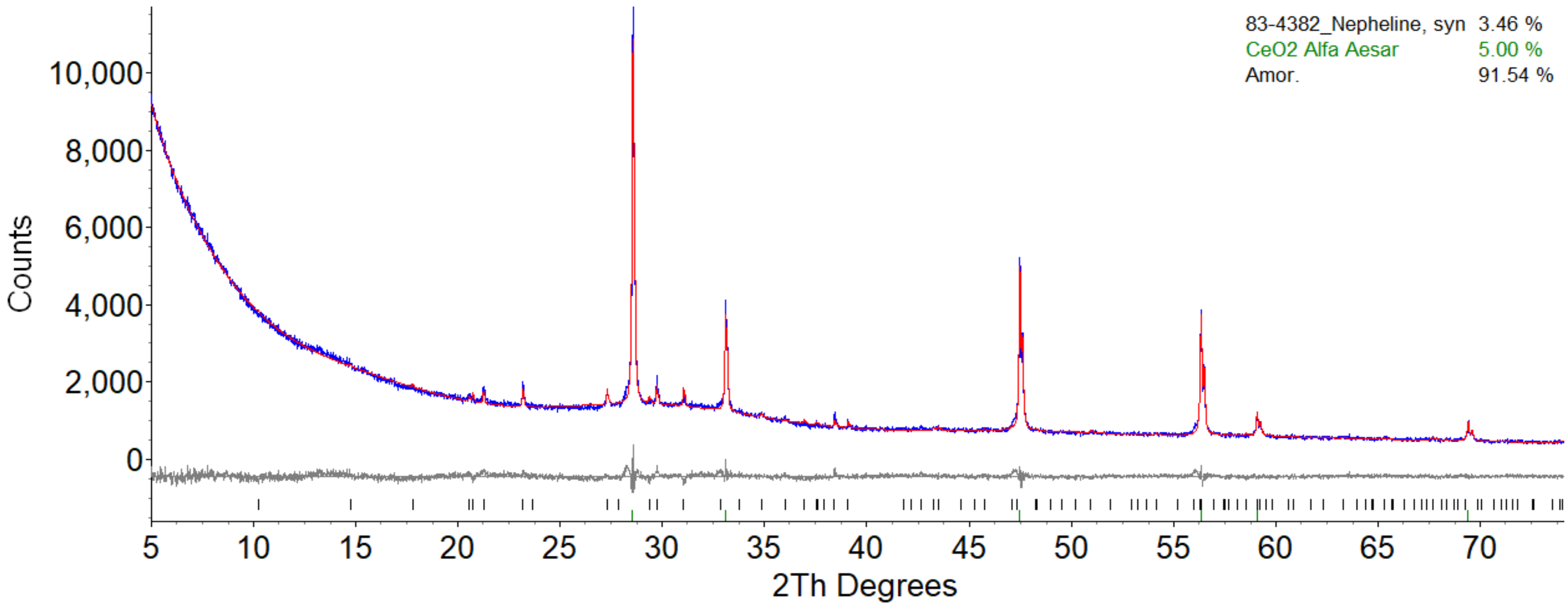

Phase Name	wt% Measured	wt% Corrected	wt% Normalized
CeO_2	5.00	2.58	-
Nepheline	3.46	1.78	1.88

Figure G.29. XRD scan of glass HAL24M2-01 after CCC.

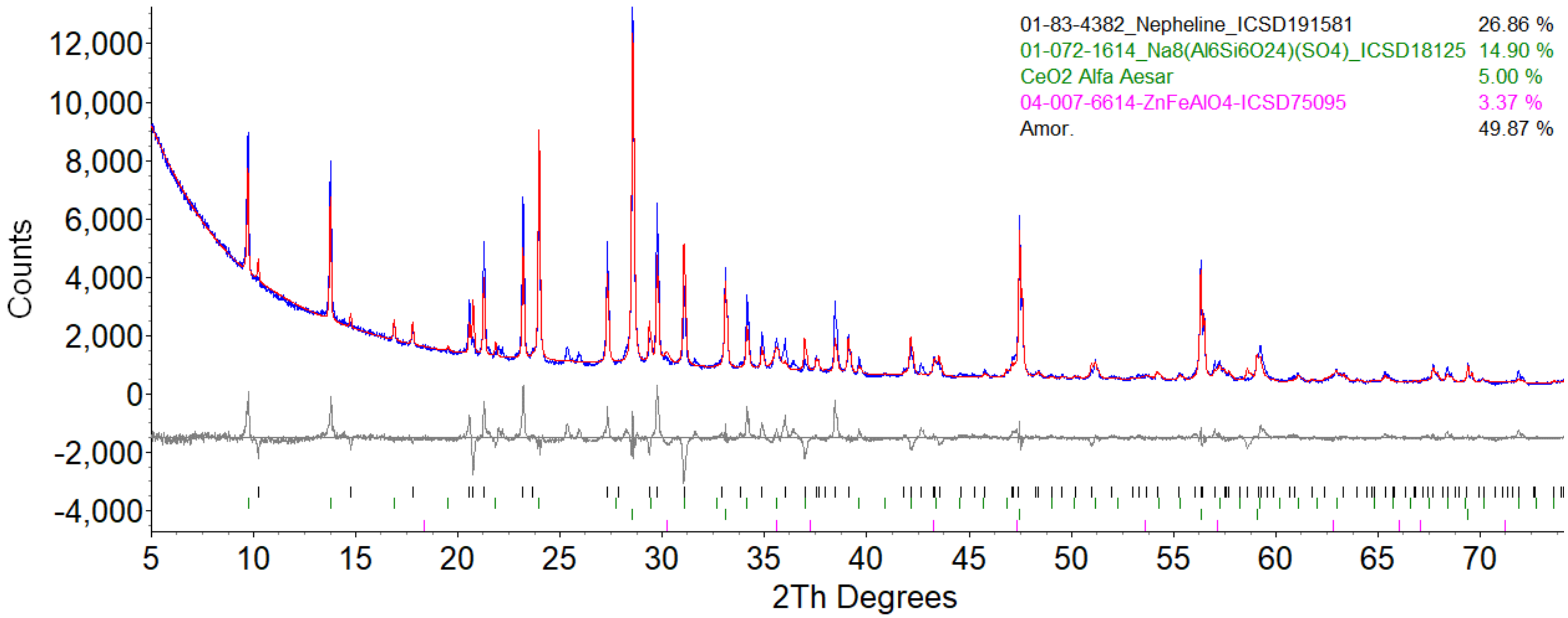

Phase Name	wt% Measured	wt% Corrected	wt% Normalized
CeO_2	5.00	2.58	-
Nepheline	26.86	13.84	14.57
$Na_8(Al_6Si_6O_{24})(SO_4)$	14.90	7.68	8.08
$ZnFeAlO_4$	3.37	1.74	1.83

Figure G.30. XRD scan of glass HAL24M2-02 after CCC.

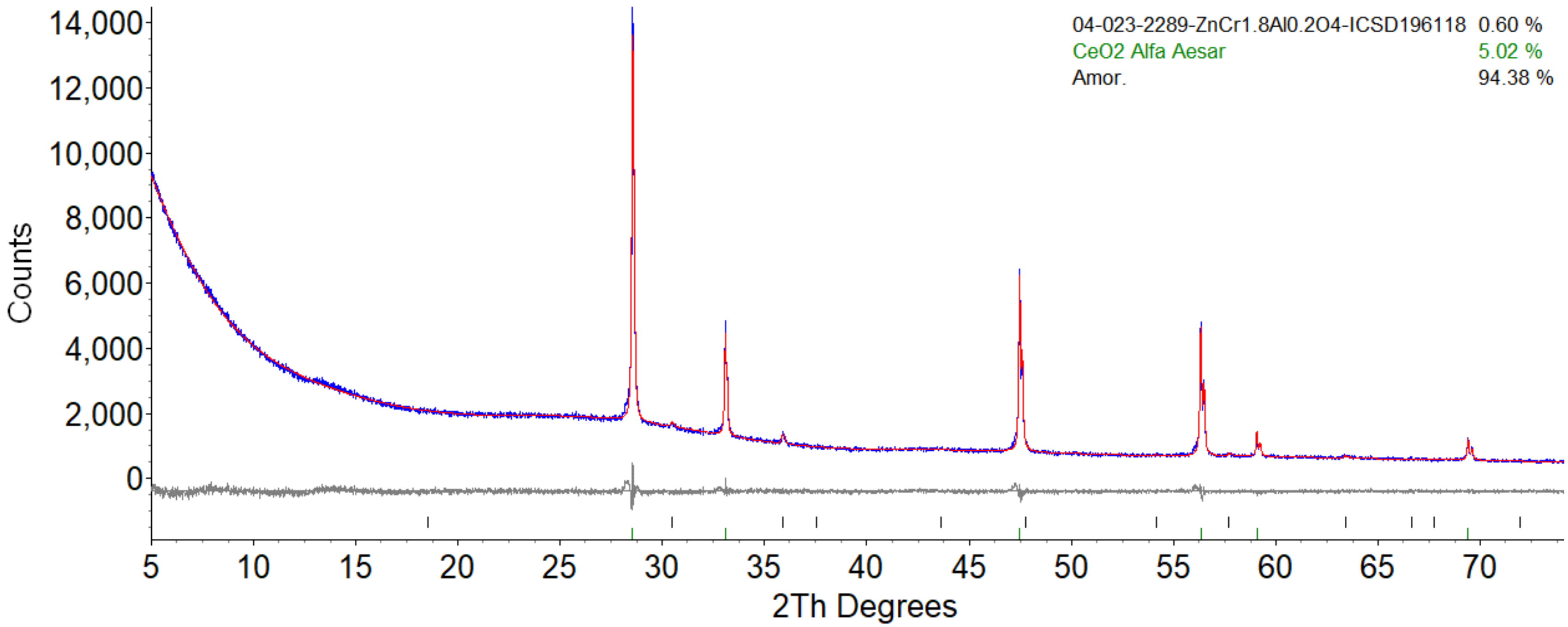

Phase Name	wt% Measured	wt% Corrected	wt% Normalized
CeO_2	5.02	2.59	-
$ZnCr_{1.8}Al_{0.2}O_4$	0.60	0.31	0.33

Figure G.31. XRD scan of glass HAL24M2-03 after CCC.

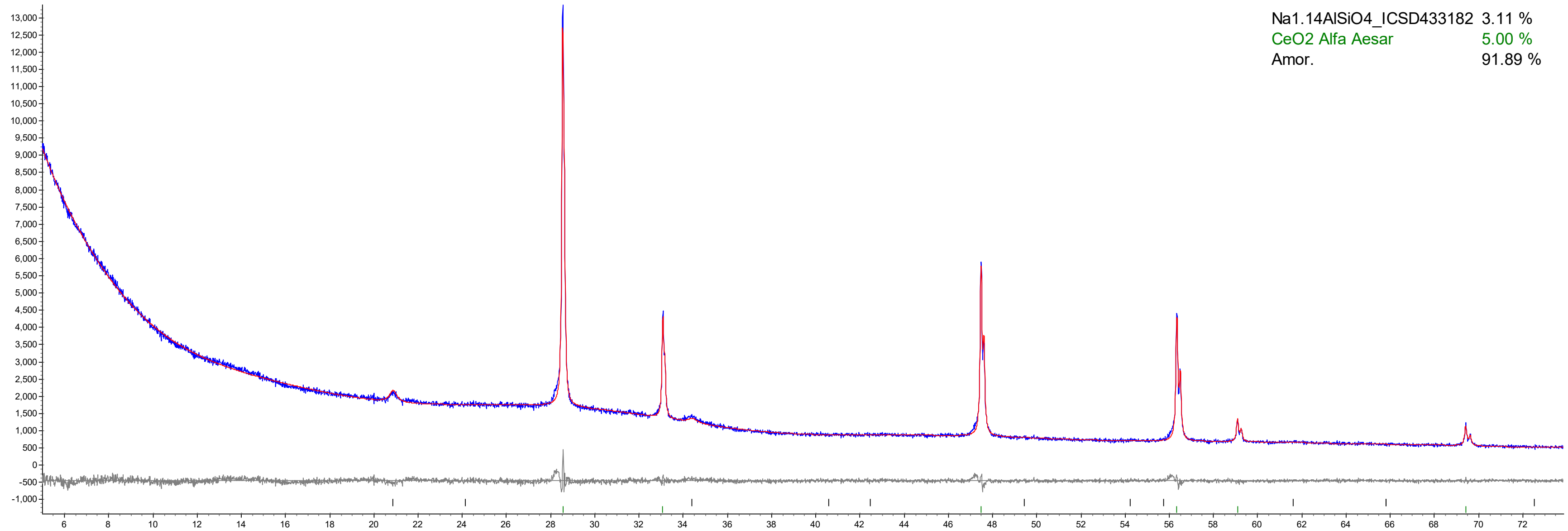

Phase Name	wt% Measured	wt% Corrected	wt% Normalized
CeO_2	5.00	2.58	-
$Na_{1.14}AlSiO_4$	3.11	1.60	1.69

Figure G.32. XRD scan of glass HAL24M2-04-1 after CCC.

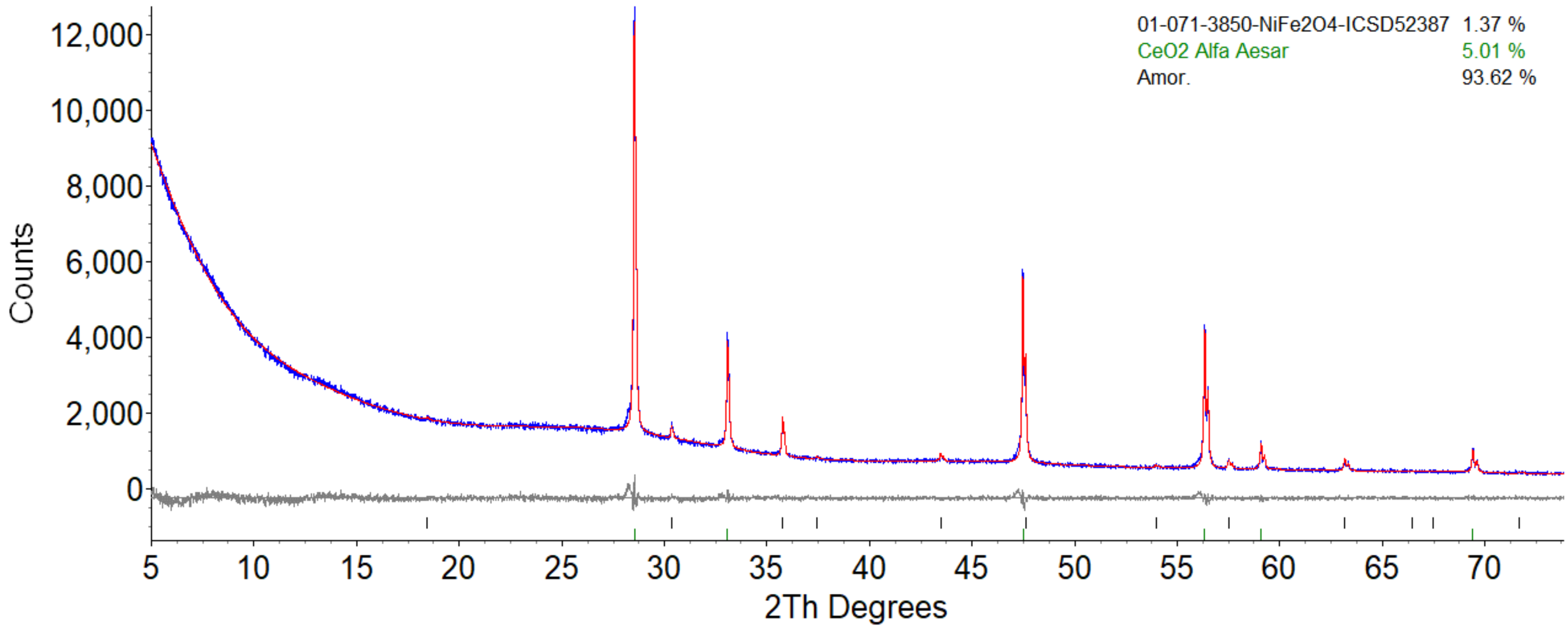

Phase Name	wt% Measured	wt% Corrected	wt% Normalized
CeO_2	5.01	2.58	-
$NiFe_2O_4$	1.37	0.70	0.74

Figure G.33. XRD scan of glass HAL24M2-06 after CCC.

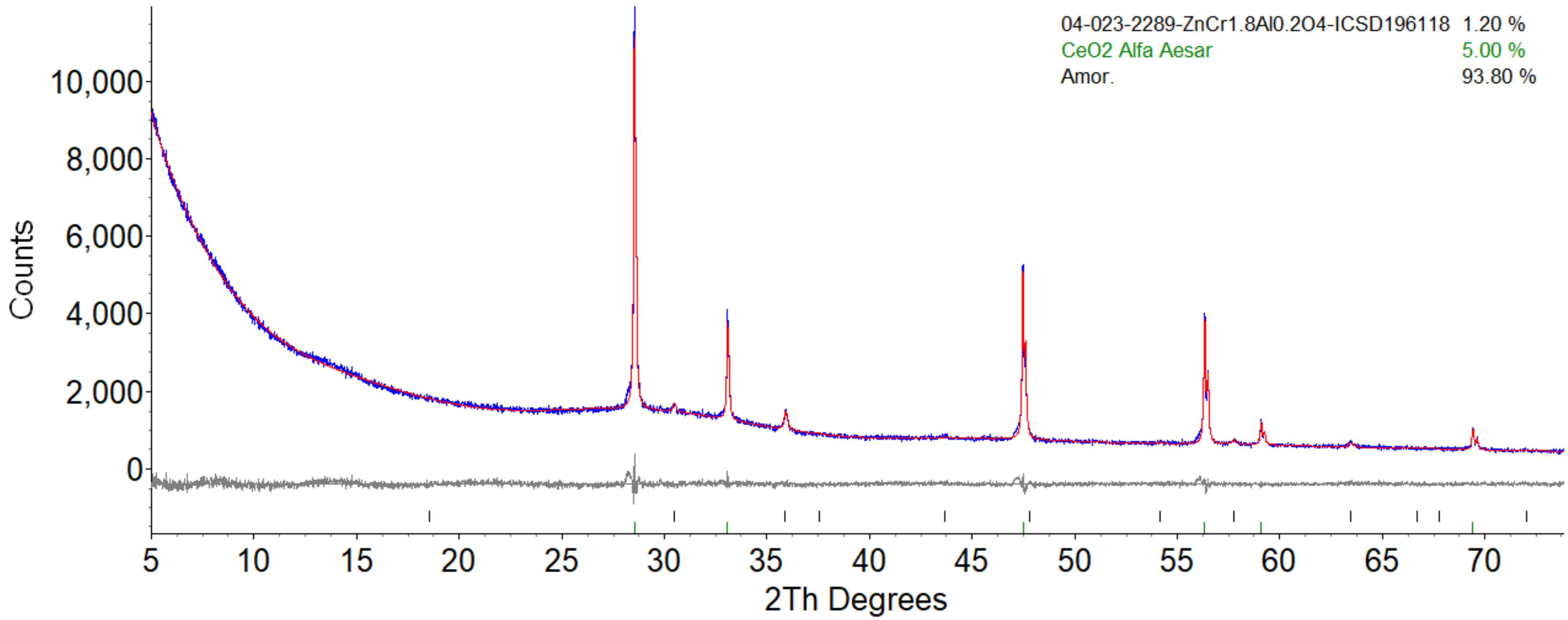

Phase Name	wt% Measured	wt% Corrected	wt% Normalized
CeO_2	5.00	2.58	-
$ZnCr_{1.8}\,Al_{0.2}\,O_4$	1.20	0.62	0.65

Figure G.34. XRD scan of glass HAL24M2-07 after CCC.

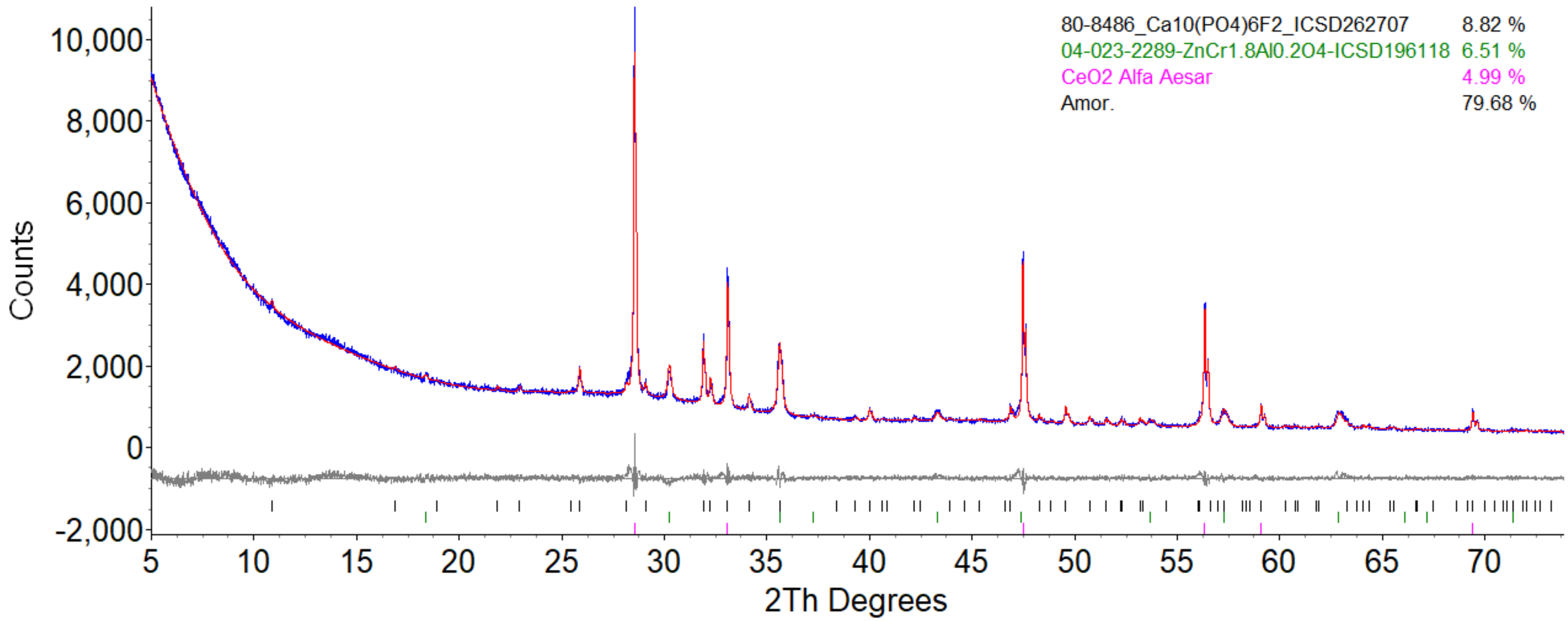

Phase Name	wt% Measured	wt% Corrected	wt% Normalized
CeO_2	4.99	2.57	-
$Ca_{10}(PO_4)_6F_2$	8.82	4.54	4.78
$ZnCr_{1.8}Al_{0.2}O_4$	6.51	3.36	3.53

Figure G.35. XRD scan of glass HAL24M2-08 after CCC.

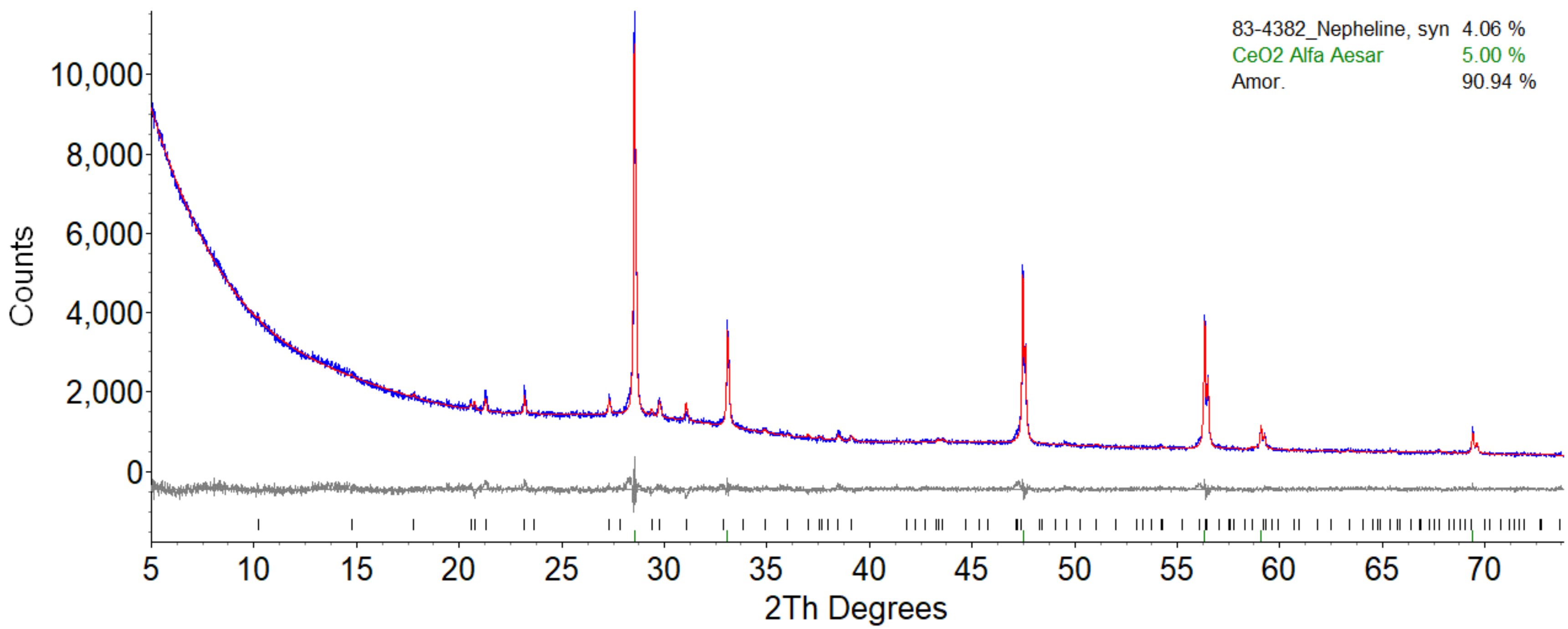

Phase Name	wt% Measured	wt% Corrected	wt% Normalized
CeO_2	5.00	2.58	-
Nepheline	4.06	2.09	2.20

Figure G.36. XRD scan of glass HAL24M2-09 after CCC.

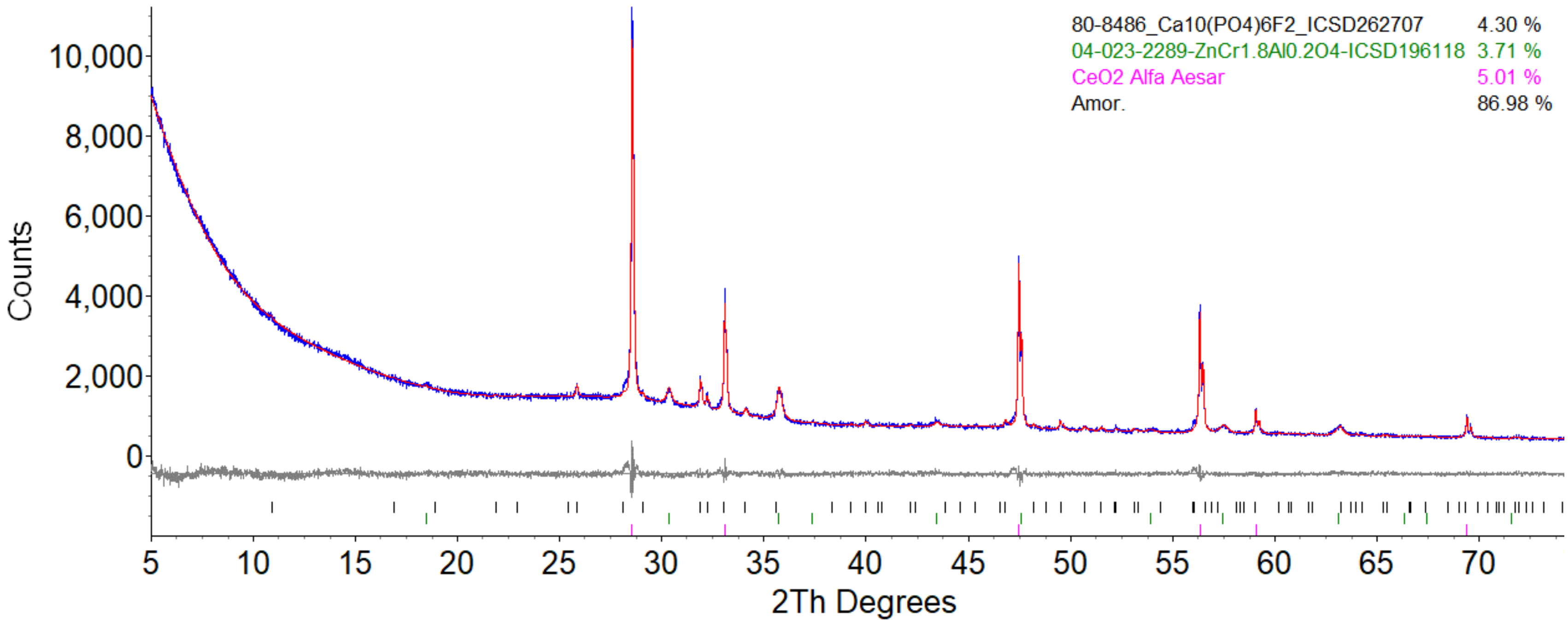

Phase Name	wt% Measured	wt% Corrected	wt% Normalized
CeO_2	5.01	2.58	-
$Ca_{10}(PO_4)_6F_2$	4.30	2.22	2.33
$ZnCr_{1.8}\ Al_{0.2}\ O_4$	3.71	1.91	2.01

Figure G.37. XRD scan of glass HAL24M2-10 after CCC.

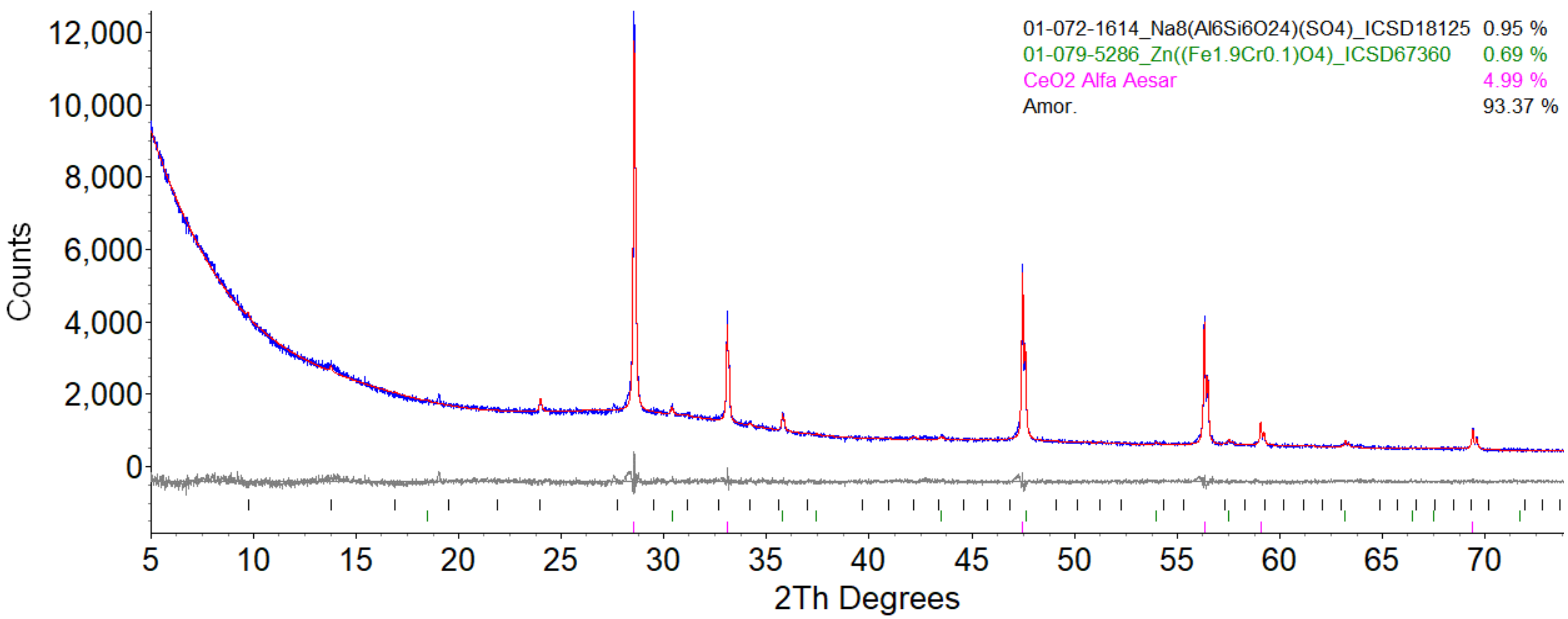

Phase Name	wt% Measured	wt% Corrected	wt% Normalized
CeO_2	4.99	2.57	-
Nosean ($Na_8(Al_6Si_6O_{24})(SO_4)$)	0.95	0.49	0.52
$Zn((Fe_{1.9}Cr_{0.1})O_4)$	0.69	0.36	0.38

Figure G.38. XRD scan of glass HAL24M2-11 after CCC.

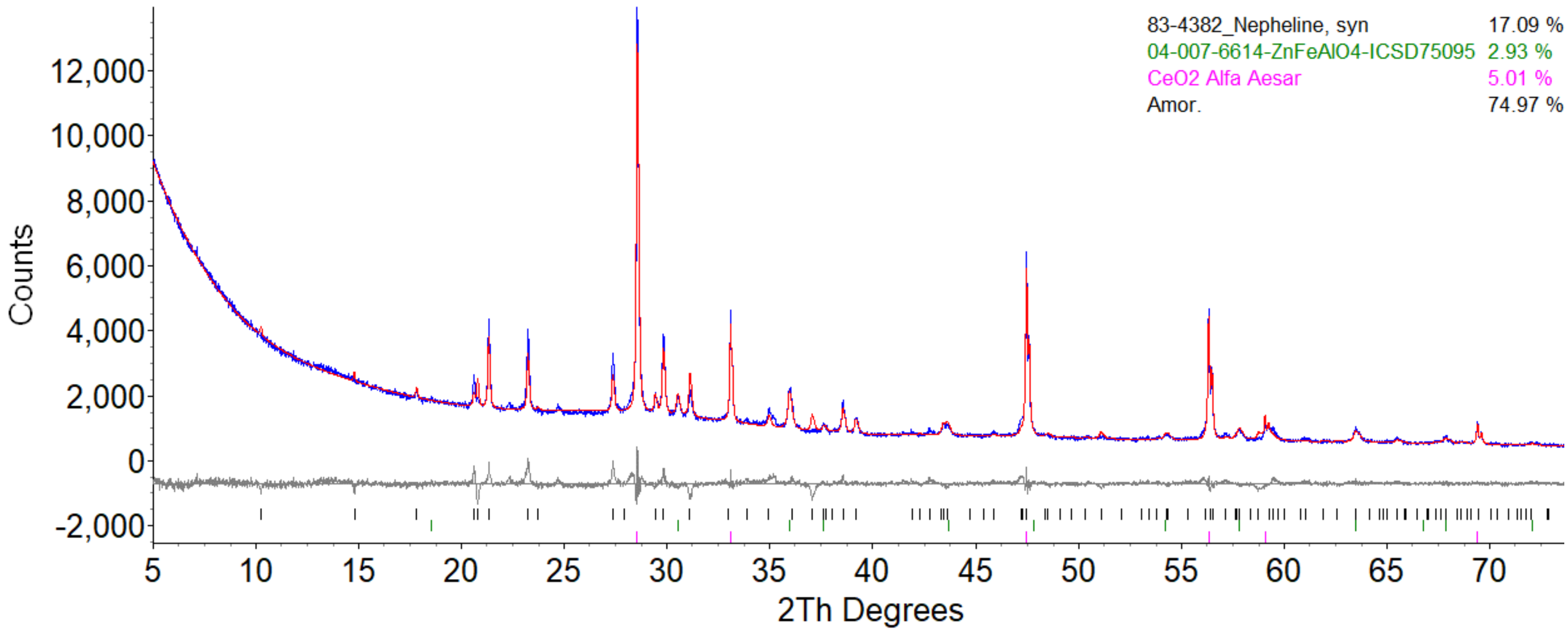

Phase Name	wt% Measured	wt% Corrected	wt% Normalized
CeO_2	5.01	2.58	-
Nepheline	17.09	8.81	9.27
$ZnFeAlO_4$	2.93	1.51	1.59

Figure G.39. XRD scan of glass HAL24M2-12 after CCC.

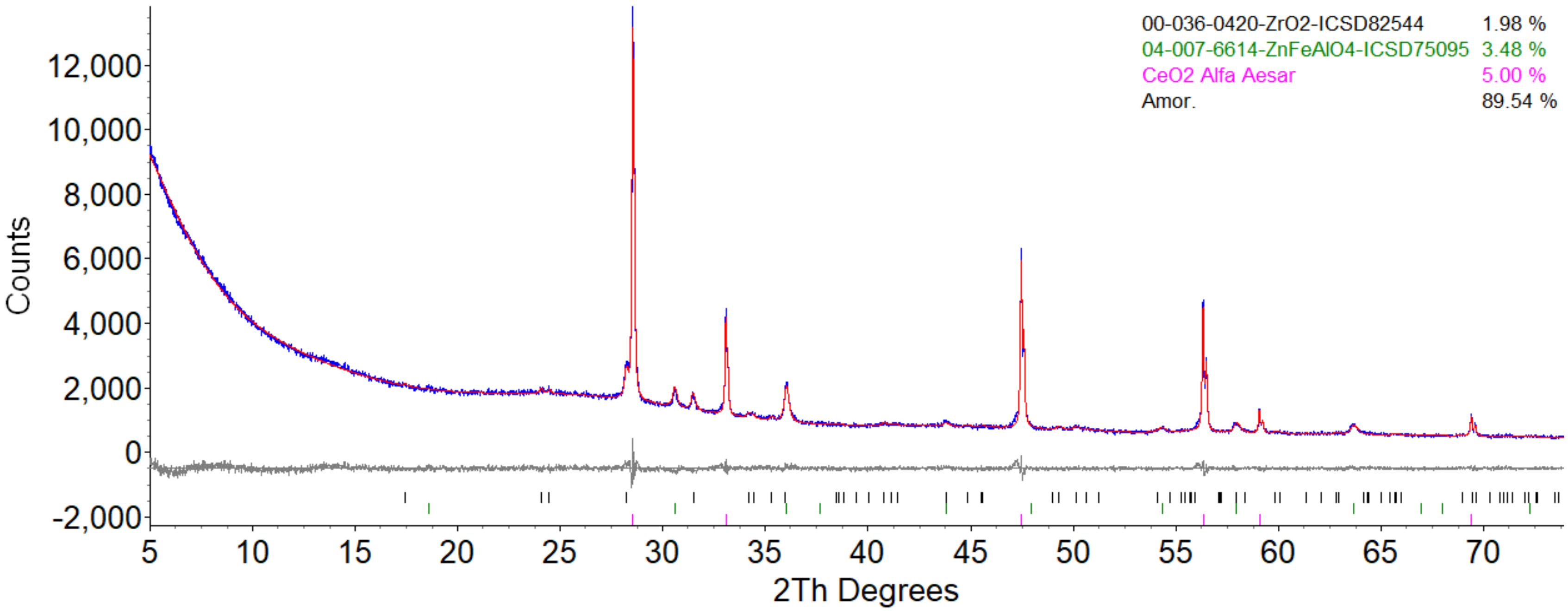

Phase Name	wt% Measured	wt% Corrected	wt% Normalized
CeO_2	5.00	2.58	-
ZrO_2	1.98	1.02	1.07
$ZnFeAlO_4$	3.48	1.79	1.89

Figure G.40. XRD scan of glass HAL24M2-13 after CCC.

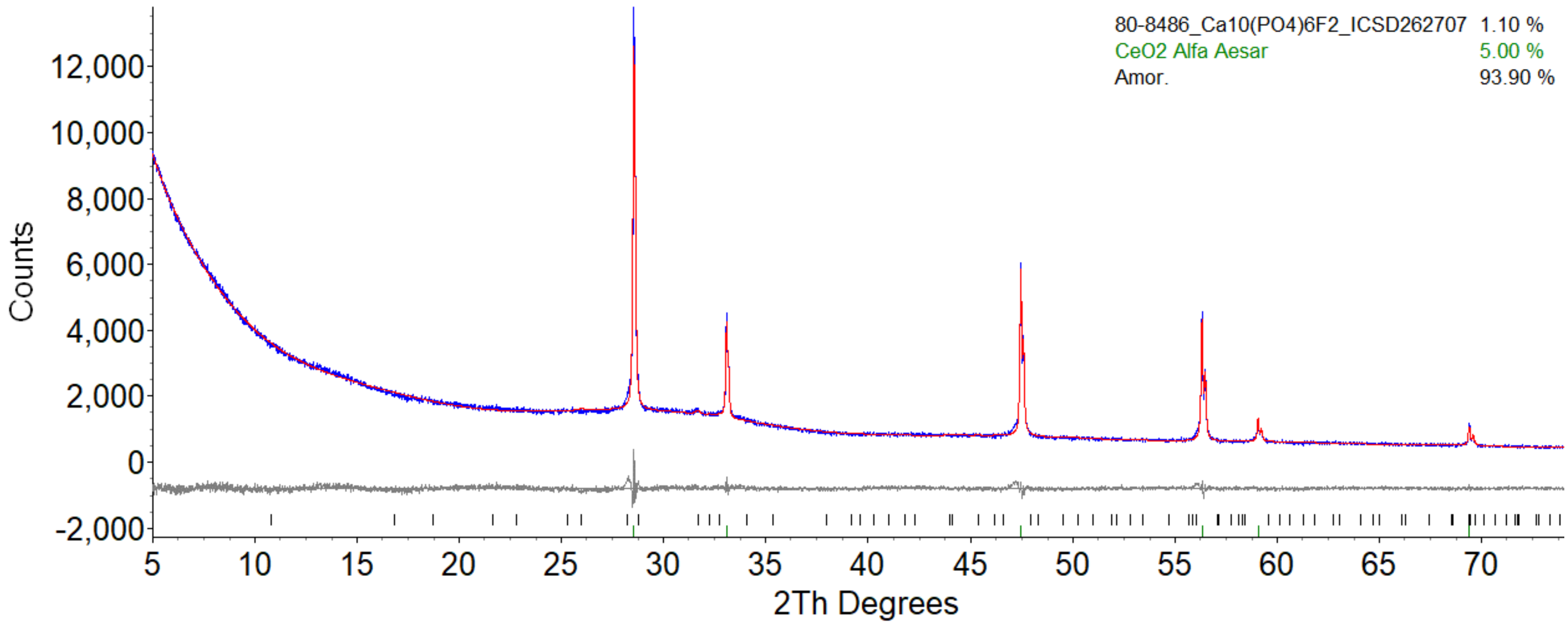

Phase Name	wt% Measured	wt% Corrected	wt% Normalized
CeO_2	5.00	2.58	-
$Ca_{10}(PO_4)_6F_2$	1.10	0.57	0.60

Figure G.41. XRD scan of glass HAL24M2-15 after CCC.

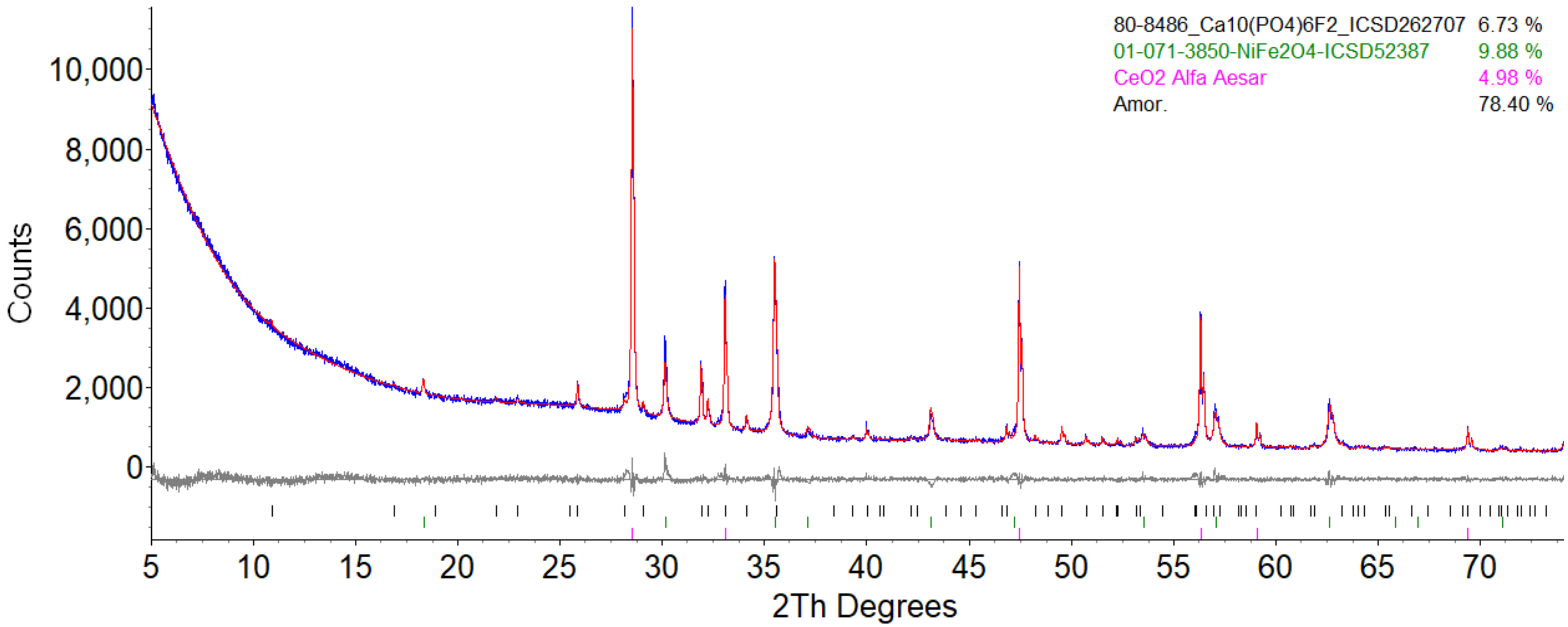

Phase Name	wt% Measured	wt% Corrected	wt% Normalized
CeO_2	4.98	2.57	-
$Ca_{10}(PO_4)_6F_2$	6.73	3.47	3.65
$NiFe_2O_4$	9.88	5.09	5.36

Figure G.42. XRD scan of glass HAL24M2-16 after CCC.

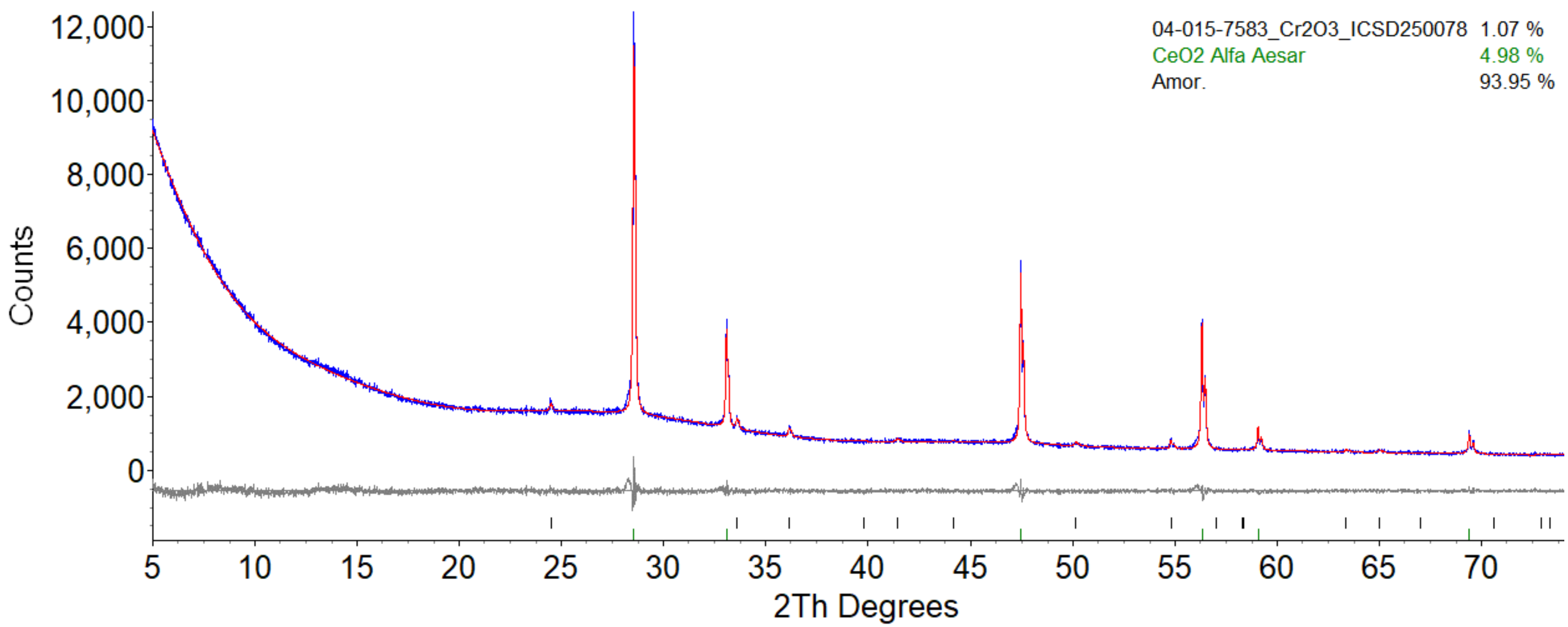

Phase Name	wt% Measured	wt% Corrected	wt% Normalized
CeO_2	4.98	2.57	-
Cr_2O_3	1.07	0.55	0.58

Figure G.43. XRD scan of glass HAL24M2-17 after CCC.

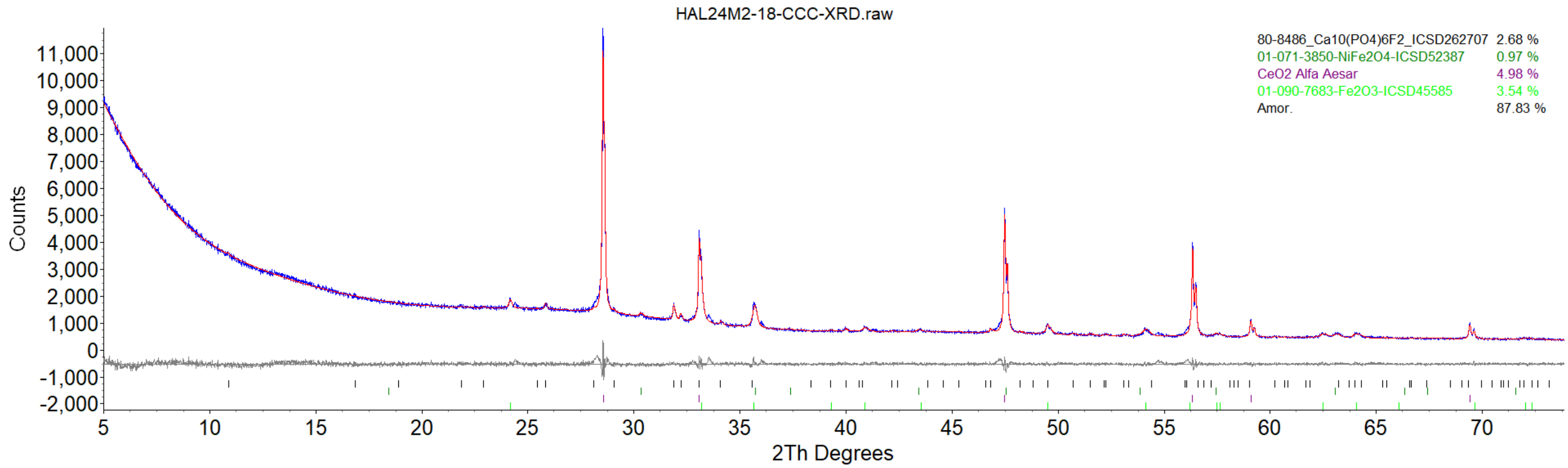

Phase Name	wt% Measured	wt% Corrected	wt% Normalized
CeO_2	4.98	2.57	-
$Ca_{10}(PO_4)_6F_2$	2.68	1.38	1.45
$NiFe_2O_4$	0.97	0.50	0.53
Fe_2O_3	3.54	1.83	1.92

Figure G.44. XRD scan of glass HAL24M2-18 after CCC.

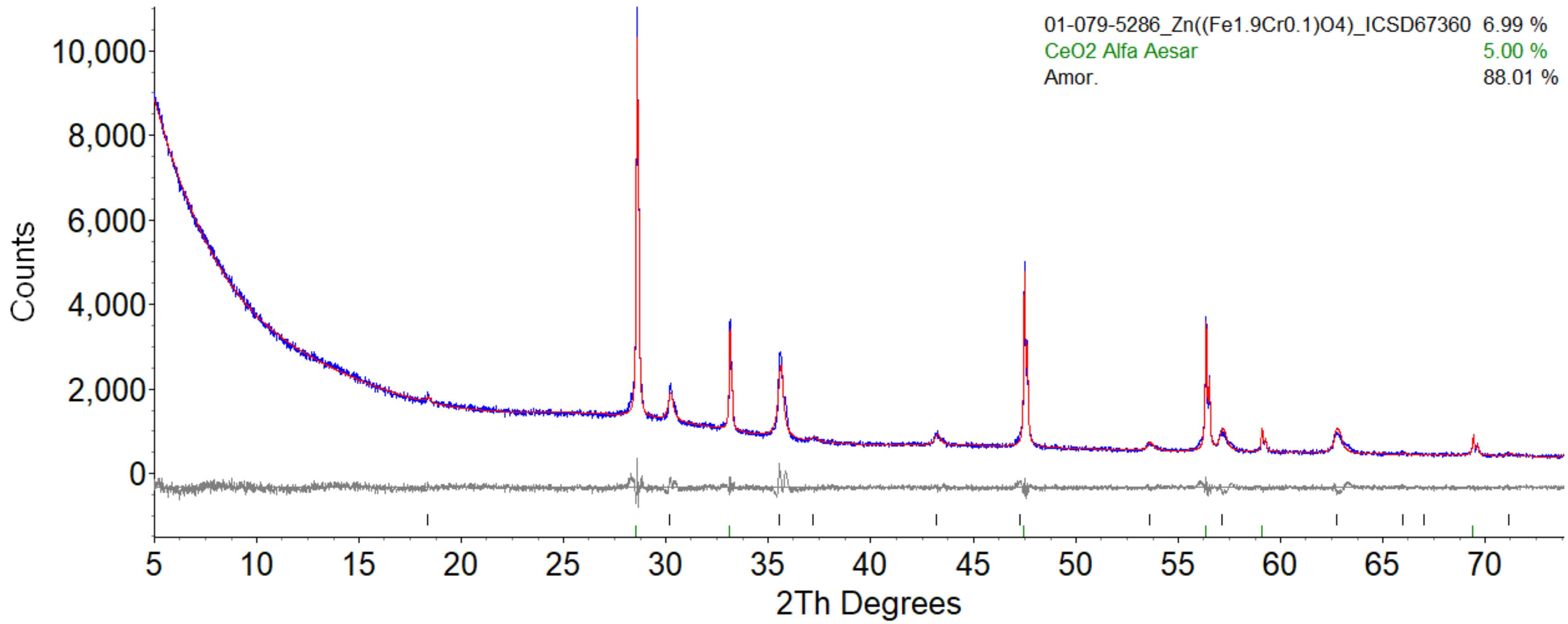

Phase Name	wt% Measured	wt% Corrected	wt% Normalized
CeO_2	5.00	2.58	-
$Zn((Fe_{1.9}Cr_{0.1})O_4)$	6.99	3.61	3.79

Figure G.45. XRD scan of glass HAL24M2-20 after CCC.

Appendix H – Morphology of Isothermally Heat-Treated Glasses at or near 950 °C

The morphology of the glasses after being heat-treated at 950 °C for 24 h is expected to conservatively represent the potential presence of crystal fractions at this idling temperature. The X-ray diffraction scans of the glasses with crystal fractions are shown in Appendix G. If crystal fractions were not observed at lower temperatures or photographs were not taken, the morphology at 900 °C or 1050 °C is shown instead.

HAL24M1-01-CF-900 °C


HAL24M1-02-CF-900 °C


HAL24M1-03-CF-950 °C


HAL24M1-04-CF-950 °C


HAL24M1-05-CF-950 °C


HAL24M1-06-CF-950 °C


HAL24M1-07-CF-950 °C


HAL24M1-08-CF-950 °C


HAL24M1-09-CF-950 °C

Figure H.1. Glass morphology after isothermal heat treatment.


HAL24M1-10-CF-950 °C


HAL24M1-11-CF-950 °C


HAL24M1-12-CF-950 °C


HAL24M1-13-1-CF-950 °C

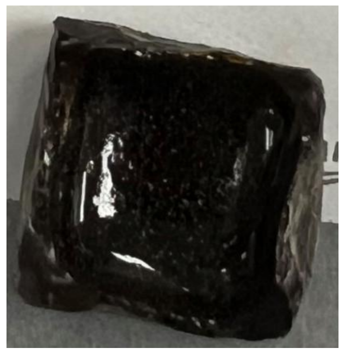
HAL24M1-14-CF-950 °C


HAL24M1-15-CF-950 °C

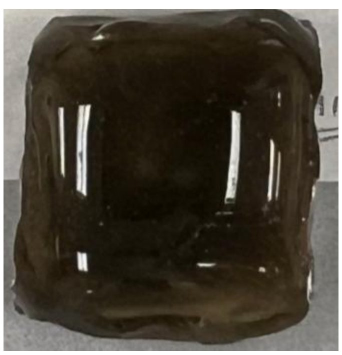
HAL24M1-16-CF-950 °C

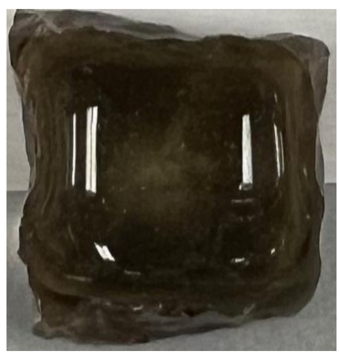
HAL24M1-17-CF-950 °C


HAL24M1-18-CF-950 °C

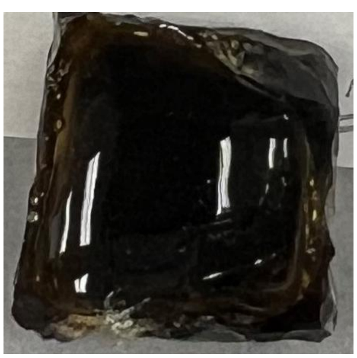
HAL24M1-19-CF-950 °C


HAL24M1-20-CF-950 °C


HAL24M1-21-CF-950 °C

Figure H.2. Glass morphology after isothermal heat treatment.


HAL24M1-22-CF-950 °C

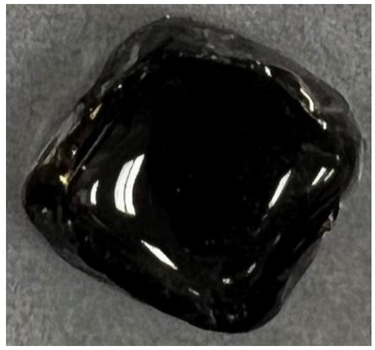
HAL24M1-23-CF-950 °C


HAL24M1-24-CF-950 °C


HAL24M1-25-CF-950 °C


HAL24M1-26-CF-950 °C


HAL24M1-27-CF-950 °C


HAL24M1-28-CF-950 °C

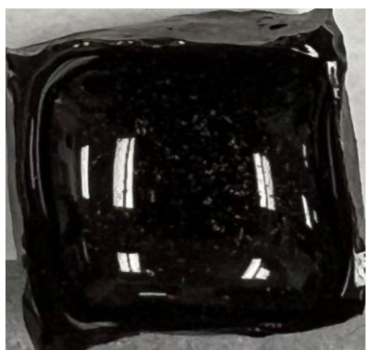
HAL24M1-29-1-CF-950 °C


HAL24M1-30-1-CF-950 °C


HAL24M2-01-CF-950 °C


HAL24M2-02-CF-950 °C


HAL24M2-03-CF-950 °C

Figure H.3. Glass morphology after isothermal heat treatment.

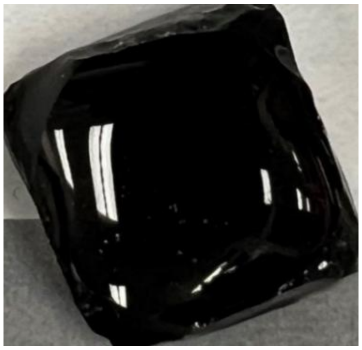
HAL24M2-04-1-CF-950 °C

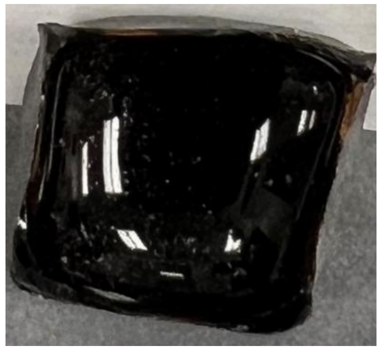
HAL24M2-05-CF-950 °C

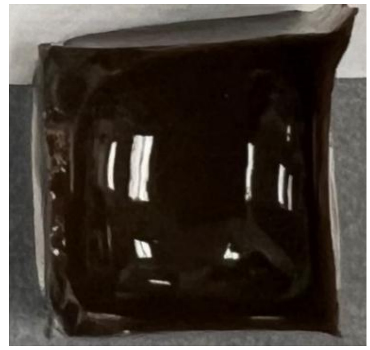
HAL24M2-06-CF-950 °C


HAL24M2-07-CF-950 °C


HAL24M2-08-CF-950 °C


HAL24M2-09-CF-1050 °C


HAL24M2-10-CF-950 °C

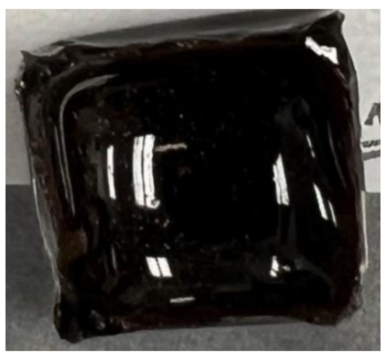
HAL24M2-11-CF-950 °C

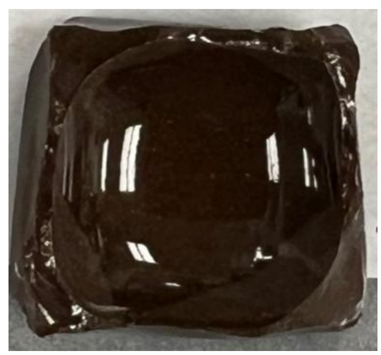
HAL24M2-12-CF-950 °C

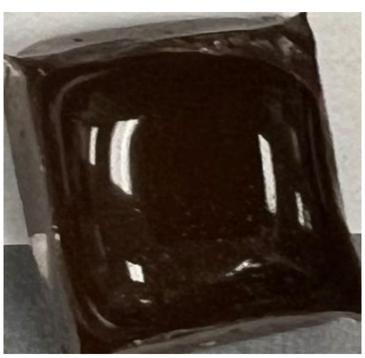
HAL24M2-13-CF-950 °C


HAL24M2-14-CF-950 °C


HAL24M2-15-CF-950 °C

Figure H.4. Glass morphology after isothermal heat treatment.


HAL24M2-16-CF-950 °C

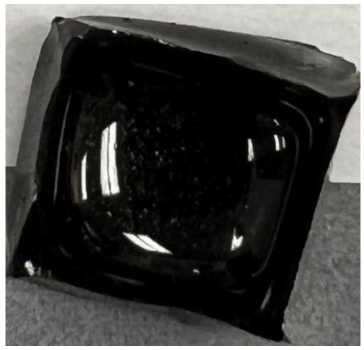
HAL24M2-17-CF-950 °C

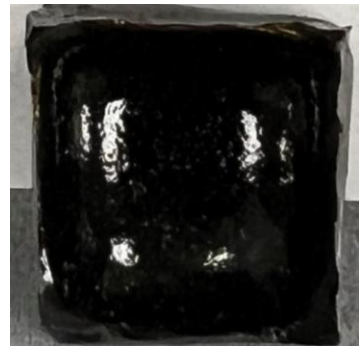
HAL24M2-18-CF-950 °C


HAL24M2-19-CF-950 °C


HAL24M2-20-CF-950 °C

Figure H.5. Glass morphology after isothermal heat treatment.

Appendix I – XRD and Liquidus Temperature Plots for CF Glasses

The X-ray diffraction (XRD) and liquidus temperature (T_L) plots help predict the temperatures at which crystal phases will form, which is vital for its mechanical strength and durability - especially for waste immobilization purposes. When T_L was estimated to be greater than 850 °C, the glass included measured temperatures (°C), crystal content (mass percentage), and a plot of the main crystalline phase. The XRD analysis is also included in these cases. The percentage of crystal content reported in the XRD images is presented before any adjustment was made from spiking with 5 wt% of a high purity cerium oxide. XRD scans are not included when the glass maintains an amorphous structure.

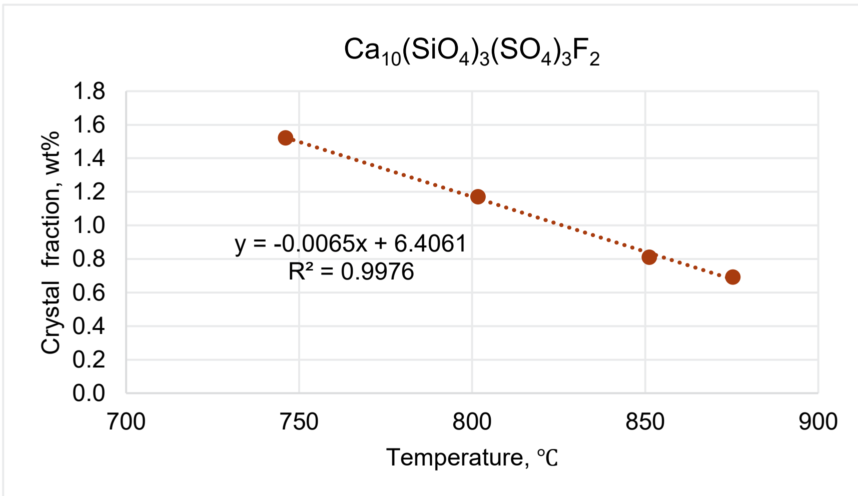

Figure I.1. The liquidus temperature plot for $Ca_{10}(SiO_4)_3(SO_4)_3F_2$ in glass HAL24M1-01 shows a linear T_L at 979 °C (R^2 = 0.9976), but HAL24M1-01 at 900 °C was fully amorphous and showed no presence of $Ca_{10}(SiO_4)_3(SO_4)_3F_2$. The T_L is between 875 °C and 900 °C.

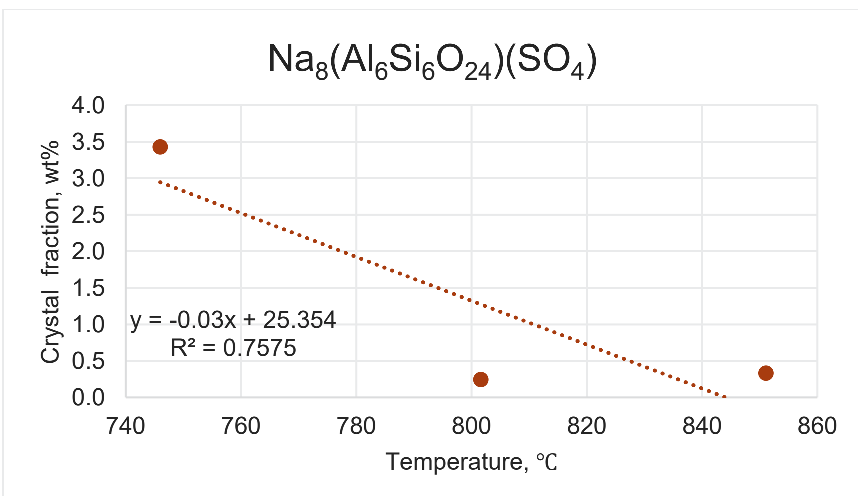

Figure I.2. The liquidus temperature plot for $Na_8(Al_6Si_6O_{24})(SO_4)$ in glass HAL24M1-02 shows the linear T_L was 844 °C (R^2 = 0.7575). The XRD of HAL24M1-02 at 950 °C revealed an amorphous structure (XRD scan not included.)

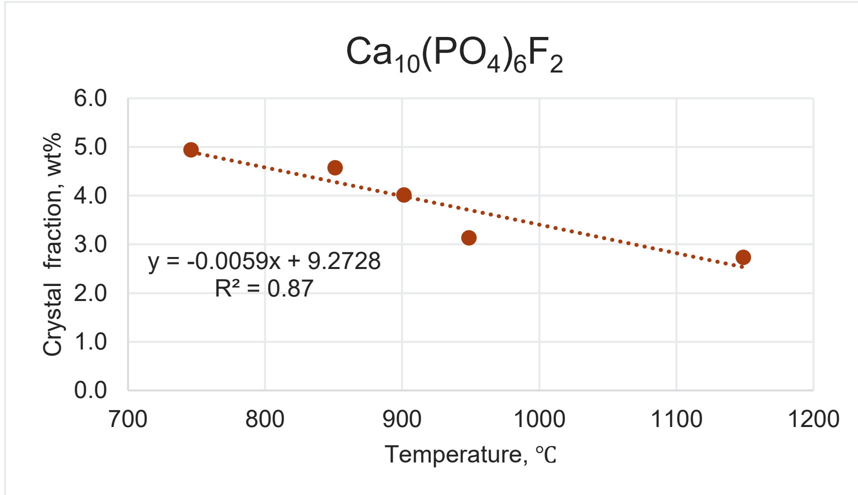

Figure I.3. The liquidus temperature (T_L) plot for fluorapatite ($Ca_{10}(PO_4)_6F_2$) in glass HAL24M1-03 shows linear T_L at 1580 °C (R^2=0.87).

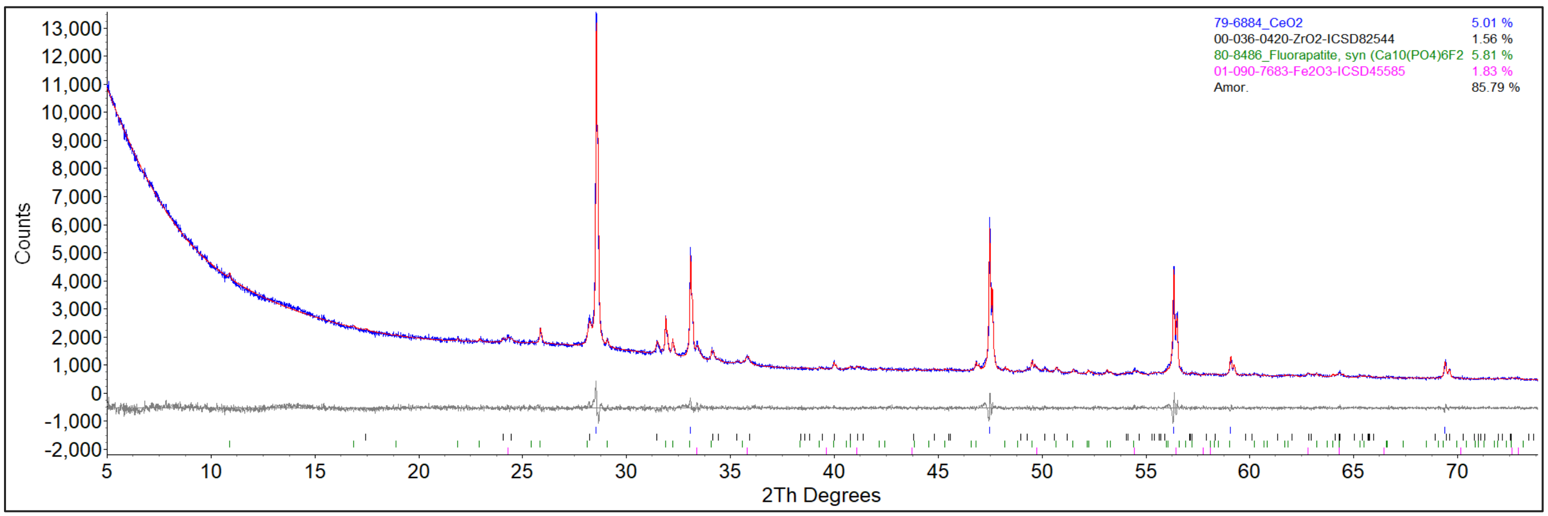

Figure I.4. XRD scan of glass HAL24M1-03 at 950 °C showing three crystalline phases: ZrO_2, Fluorapatite ($Ca_{10}(PO_4)_6F_2$), and Fe_2O_3.

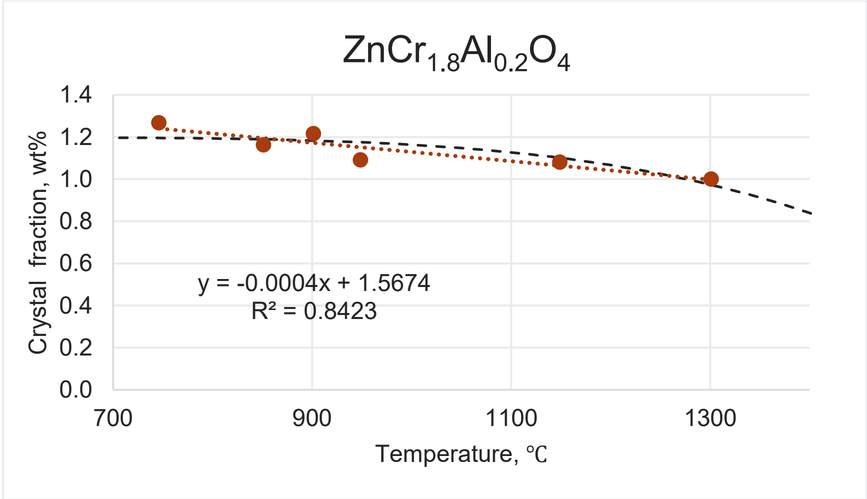

Figure I.5. The liquidus temperature plot for $ZnCr_{1.8}Al_{0.2}O_4$ in glass HAL24M1-04 shows a linear T_L at 3922 °C (R^2 = 0.8423) and the non-linear (black dash line) T_L at 1727 °C. Although the highest measured temperature was 1300 °C, both methods indicate a T_L above 1700 °C.

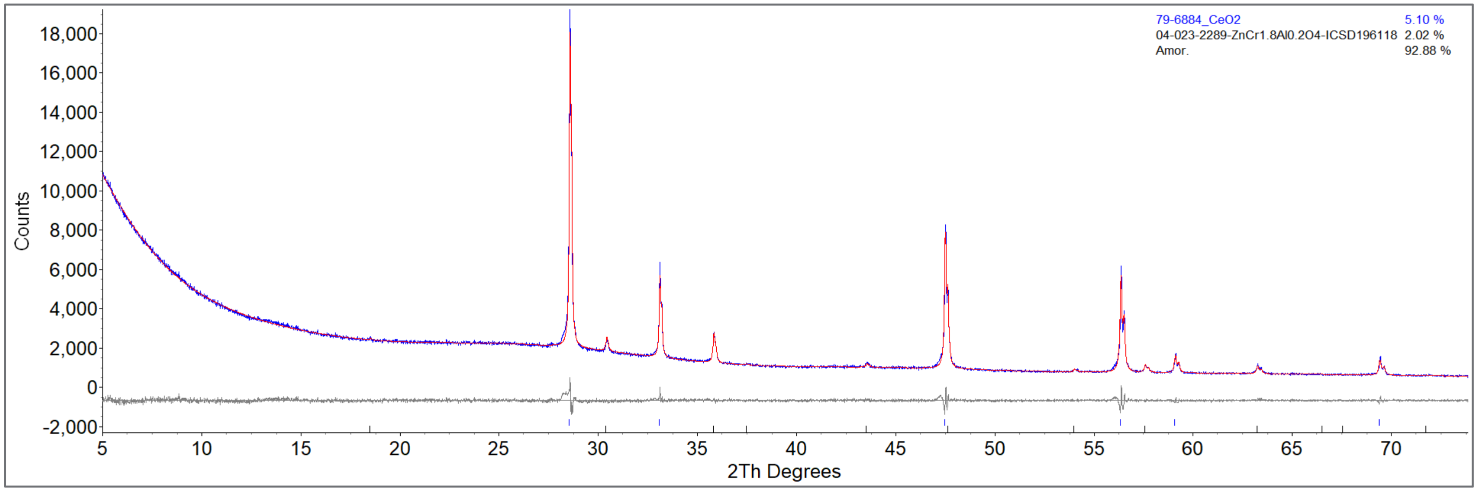

Figure I.6. XRD of glass HAL24M1-04 at 950 °C showing crystalline phase, $ZnCr_{1.8}Al_{0.2}O_4$.

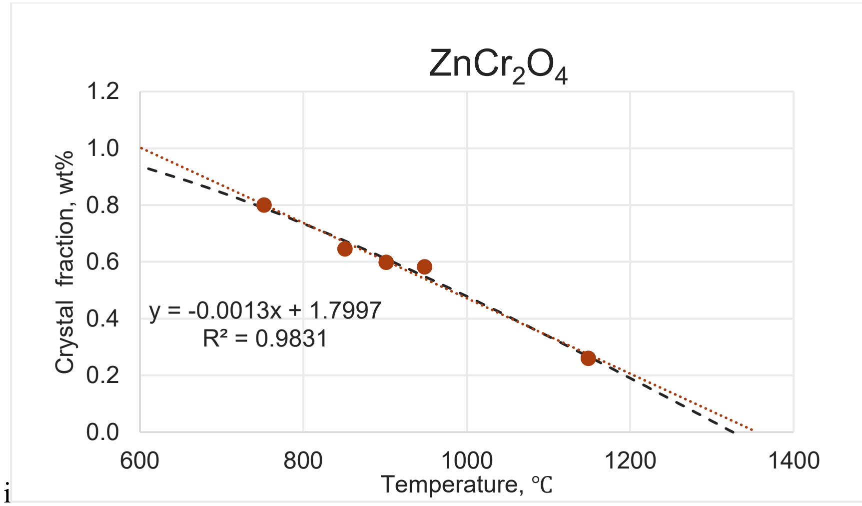

i

Figure I.7. The liquidus temperature plot for $ZnCr_2O_4$ in glass HAL24M1-05 shows a T_L at 1355 °C (R^2 = 0.9831) from linear fitting and a T_L at 1326 °C by non-linear fitting (black dash line). At 1150 °C, a new spinel phase of $ZrCr_{0.4}Al_{1.6}O_4$ was observed along with a small amount of $ZnCr_2O_4$, indicating a phase transformation. At 1301 °C, only $ZrCr_{0.4}Al_{1.6}O_4$ was present. This plot shows the T_L of $ZnCr_2O_4$.

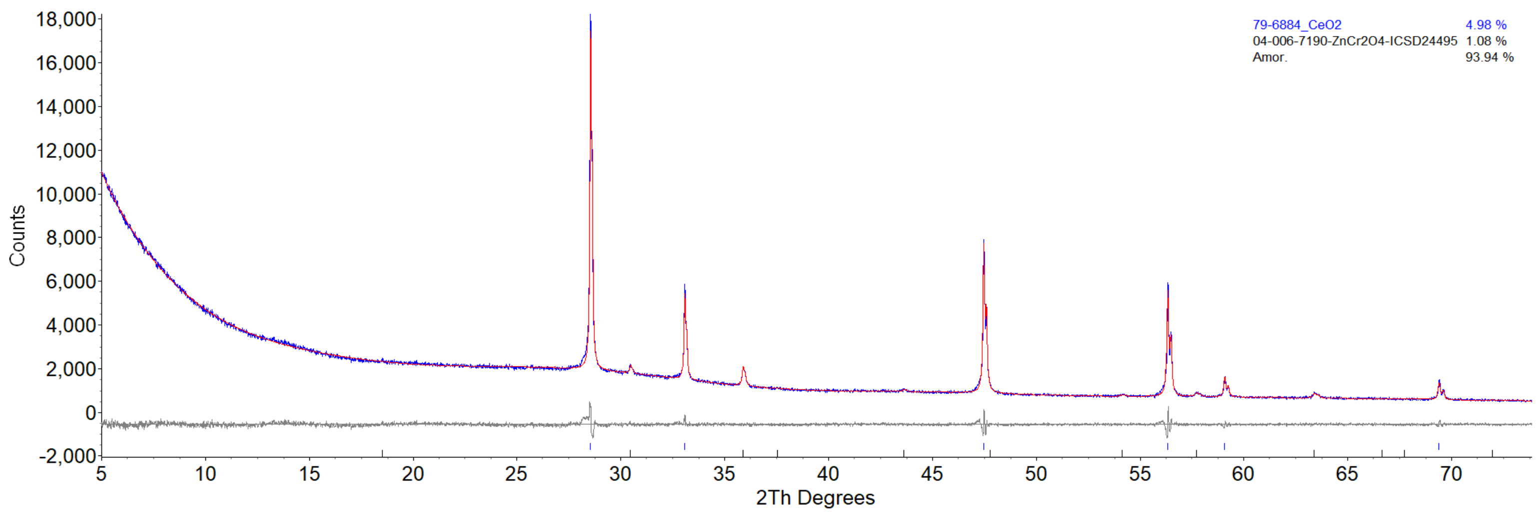

Figure I.8. XRD of glass HAL24M1-05 at 950 °C showing crystalline phase, $ZnCr_2O_4$.

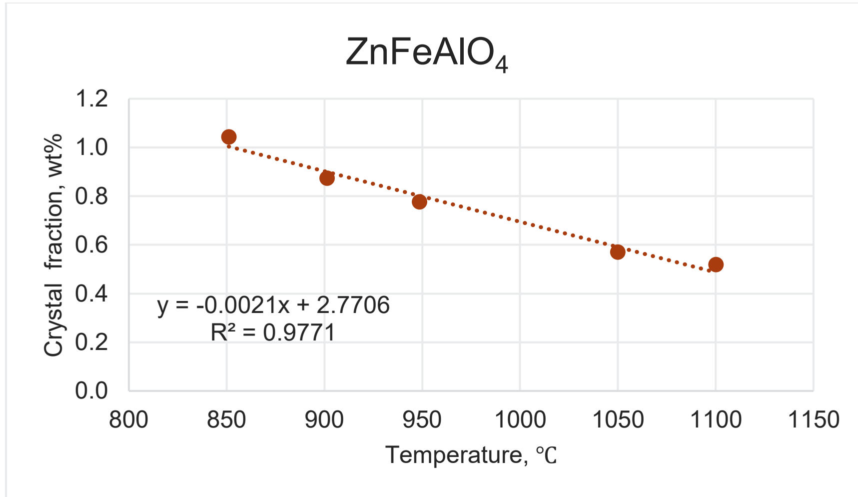

Figure I.9. The liquidus temperature plot for $ZnFeAlO_4$ in glass HAL24M1-06 shows the linear T_L at 1335 °C ($R^2 = 0.9771$).

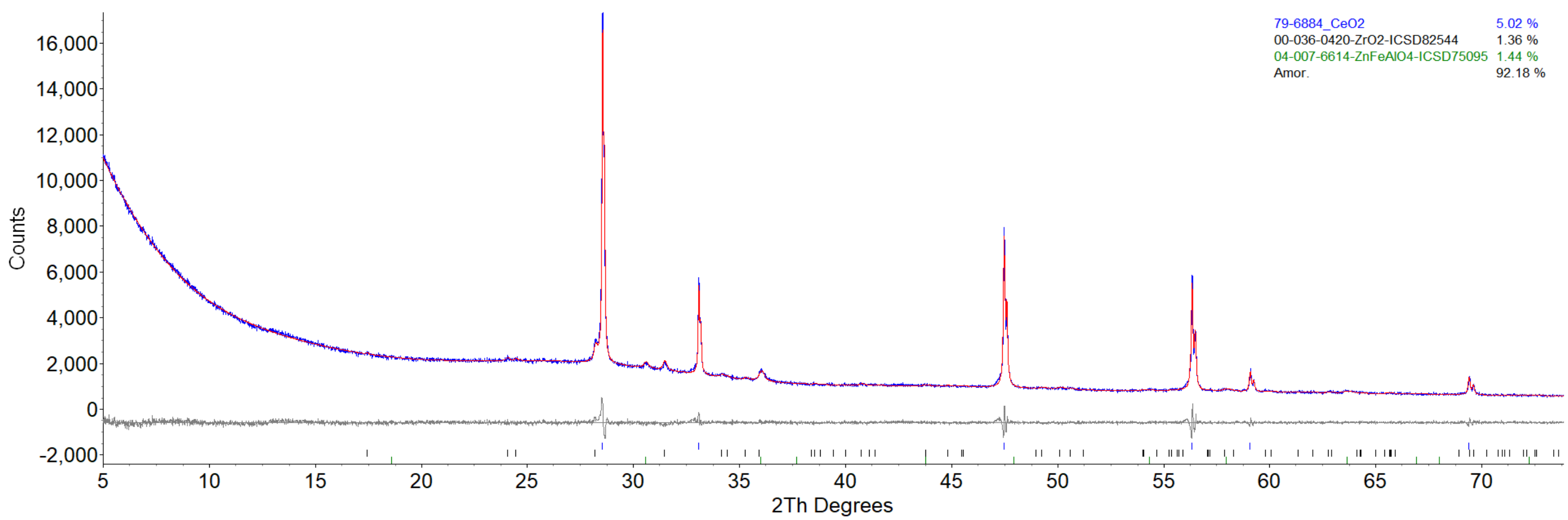

Figure I.10. XRD of glass HAL24M1-06 at 950 °C showing two crystalline phases: $ZnFeAlO_4$ and ZrO_2.

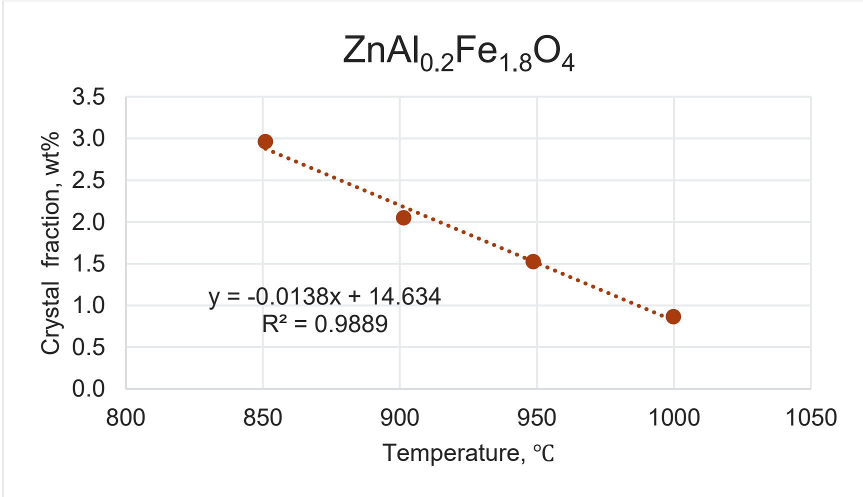

Figure I.11. The liquidus temperature plot for $ZnAl_{0.2}Fe_{1.8}O_4$ in glass HAL24M1-07 showing the linear T_L at 1059 °C ($R^2 = 0.9889$).

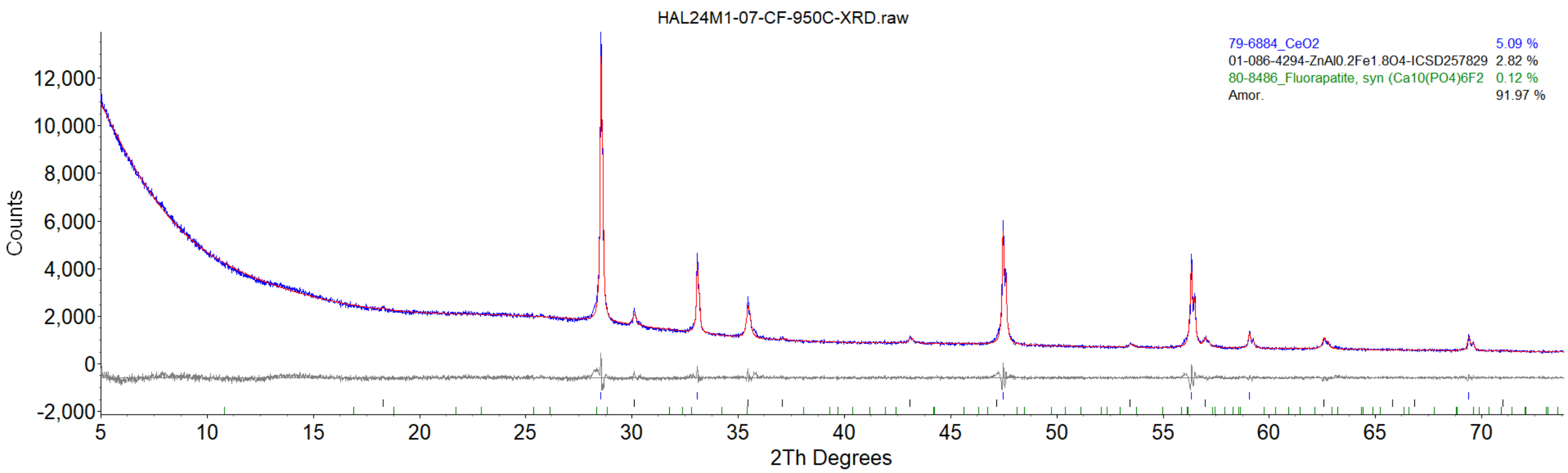

Figure I.12. XRD of glass HAL24M1-07 at 950 °C showing two crystalline phases: $ZnAl_{0.2}Fe_{1.8}O_4$ and $Ca_{10}(PO_4)_6F_2$.

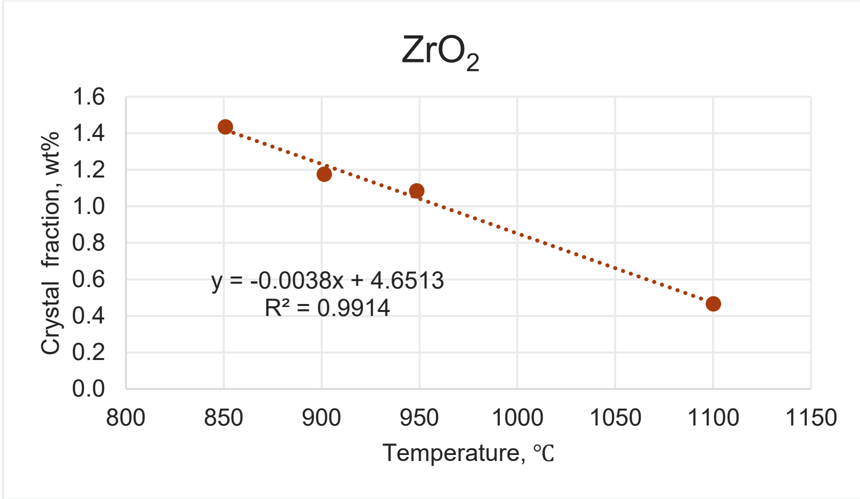

Figure I.13. The liquidus temperature plot for ZrO_2 in glass HAL24M1-08 showing the linear T_L at 1224 °C (R^2 = 0.9914).

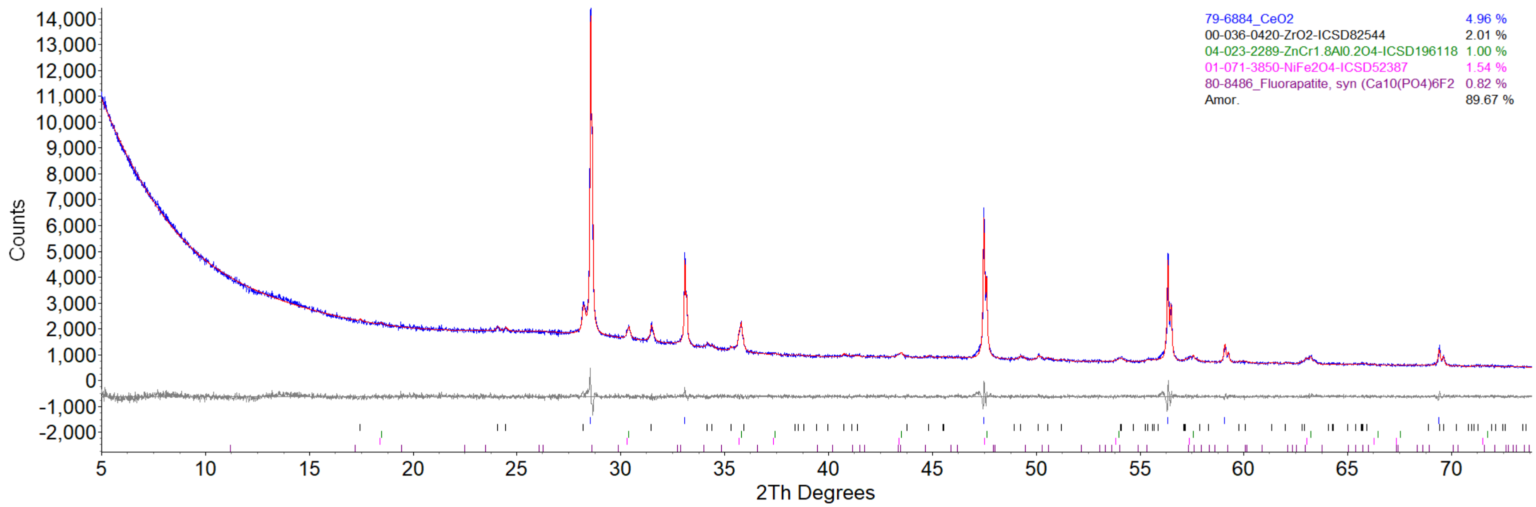

Figure I.14. XRD of glass HAL24M1-08 at 950 °C showing four crystalline phases: ZrO_2, $ZnCr_{1.8}Al_{0.2}O_4$, $NiFe_2O_4$, and $Ca_{10}(PO_4)_6F_2$.

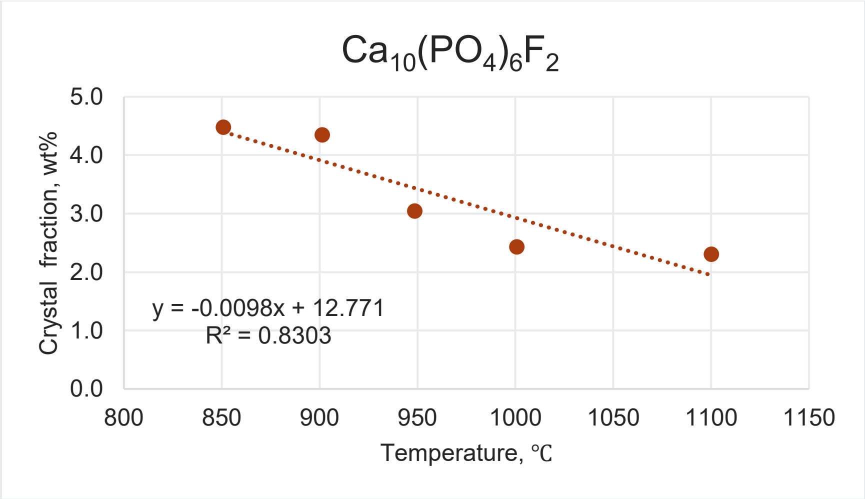

Figure I.15. The liquidus temperature plot for $Ca_{10}(PO_4)_6F_2$ in glass HAL24M1-09 showing the linear T_L at 1298 °C ($R^2 = 0.8303$).

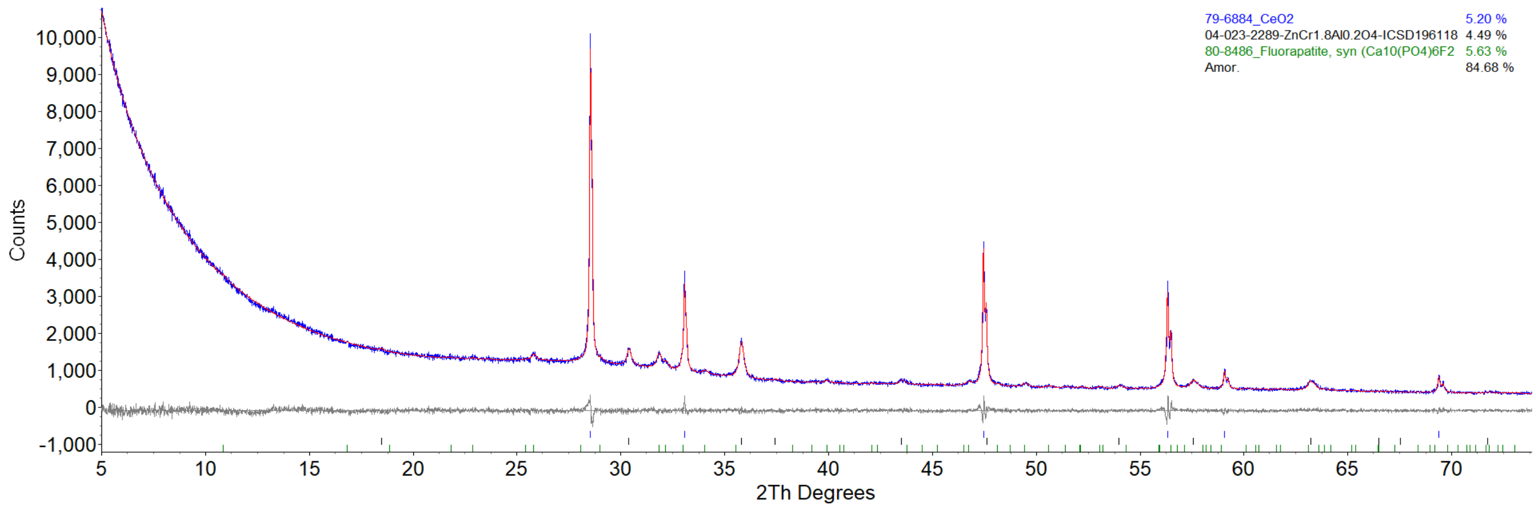

Figure I.16. XRD of glass HAL24M1-09 at 950 °C showing two crystalline phases, $ZnCr_{1.8}Al_{0.2}O_4$, and $Ca_{10}(PO_4)_6F_2$.

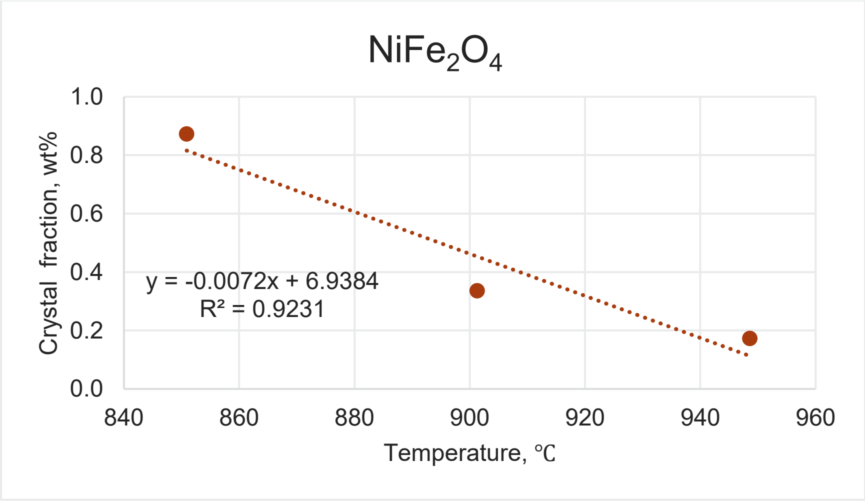

Figure I.17. The liquidus temperature plot for $NiFe_2O_4$ in glass HAL24M1-10 showing the linear T_L at 964 °C (R^2 = 0.9231).

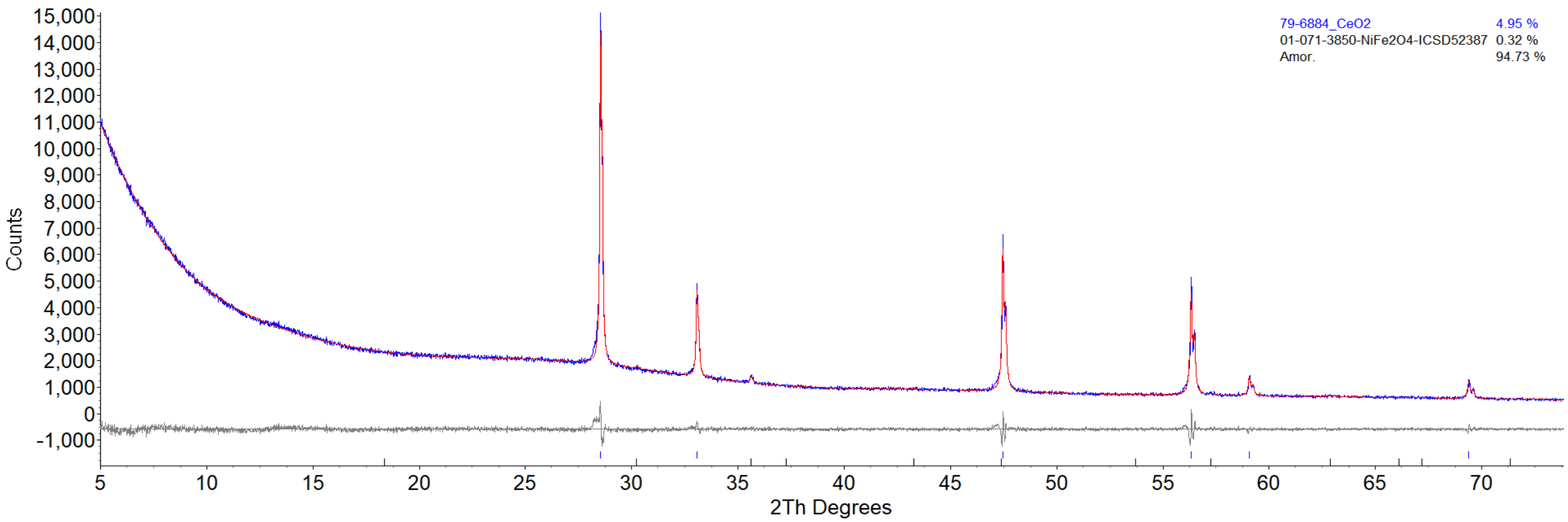

Figure I.18. XRD of glass HAL24M1-10 at 950 °C showing crystalline phase, $NiFe_2O_4$.

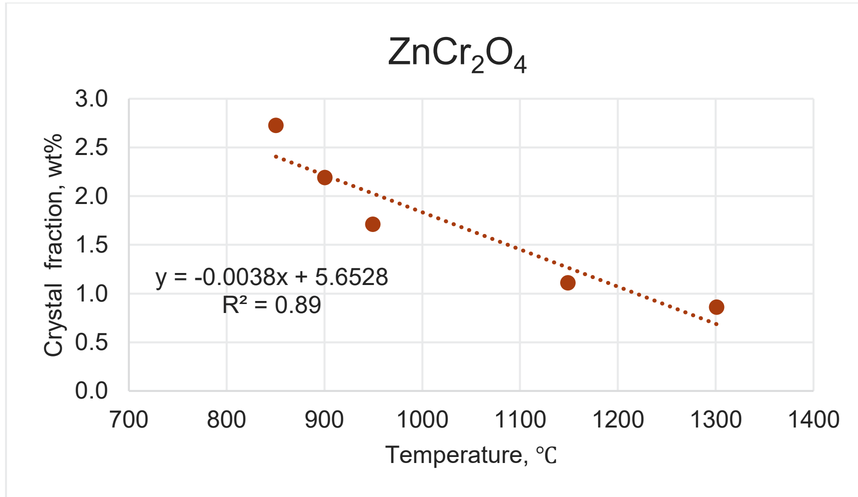

Figure I.19. The liquidus temperature plot for $ZnCr_2O_4$ in glass HAL24M1-11 showing the linear at 1480 °C (R^2 = 0.89).

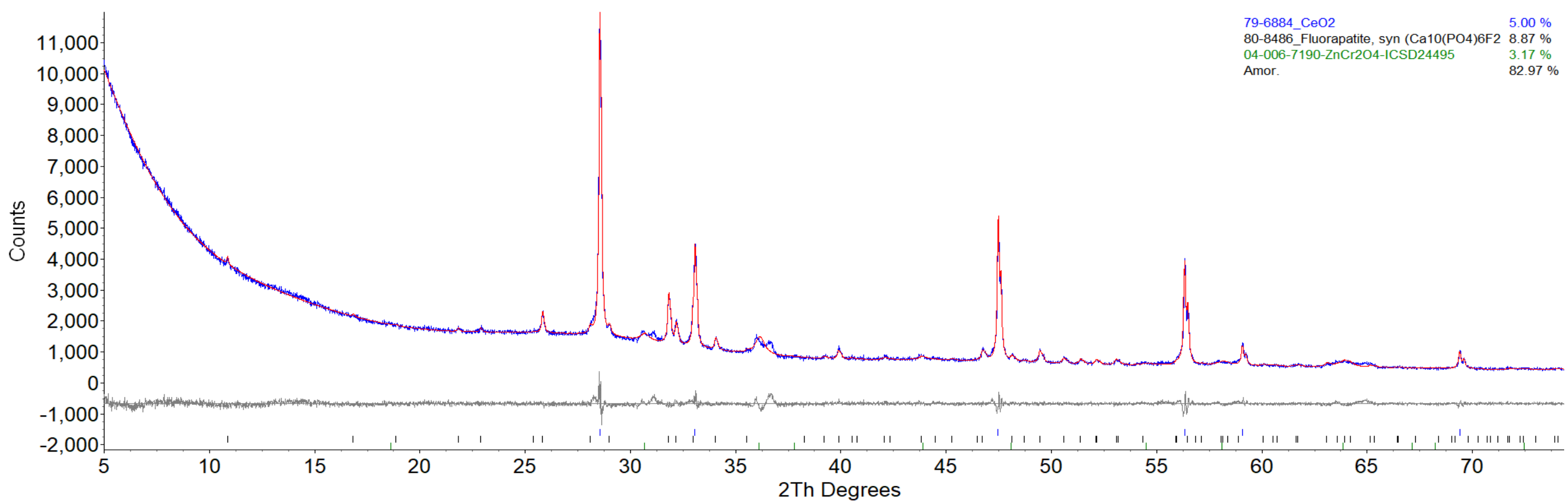

Figure I.20. XRD of glass HAL24M1-11 at 950 °C showing two crystalline phases, $ZnCr_2O_4$ and $Ca_{10}(PO_4)_6F_2$.

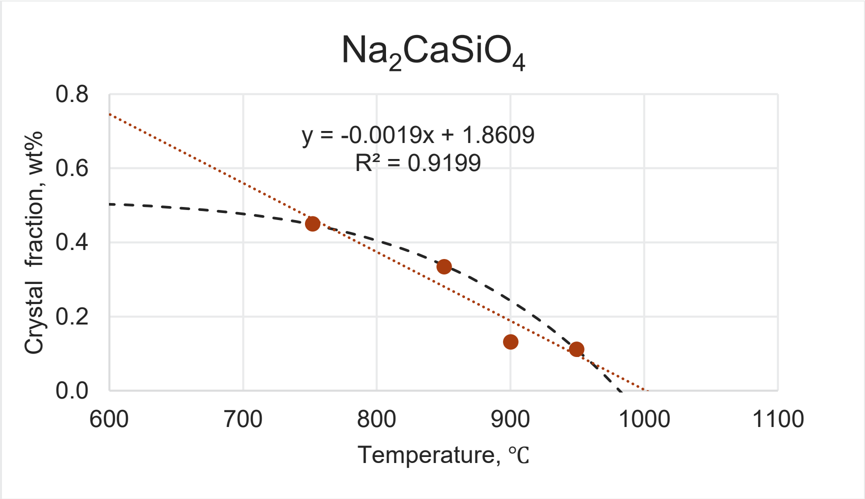

Figure I.21. The liquidus temperature plot for Na_2CaSiO_4 in glass HAL24M1-12 showing the linear T_L at 1001 °C (R^2 = 0.9199) and the non-linear (black dash line) T_L at 982 °C. The linear fitting includes all four temperature datapoints while the non-linear fitting excludes 900 °C as an outlier.

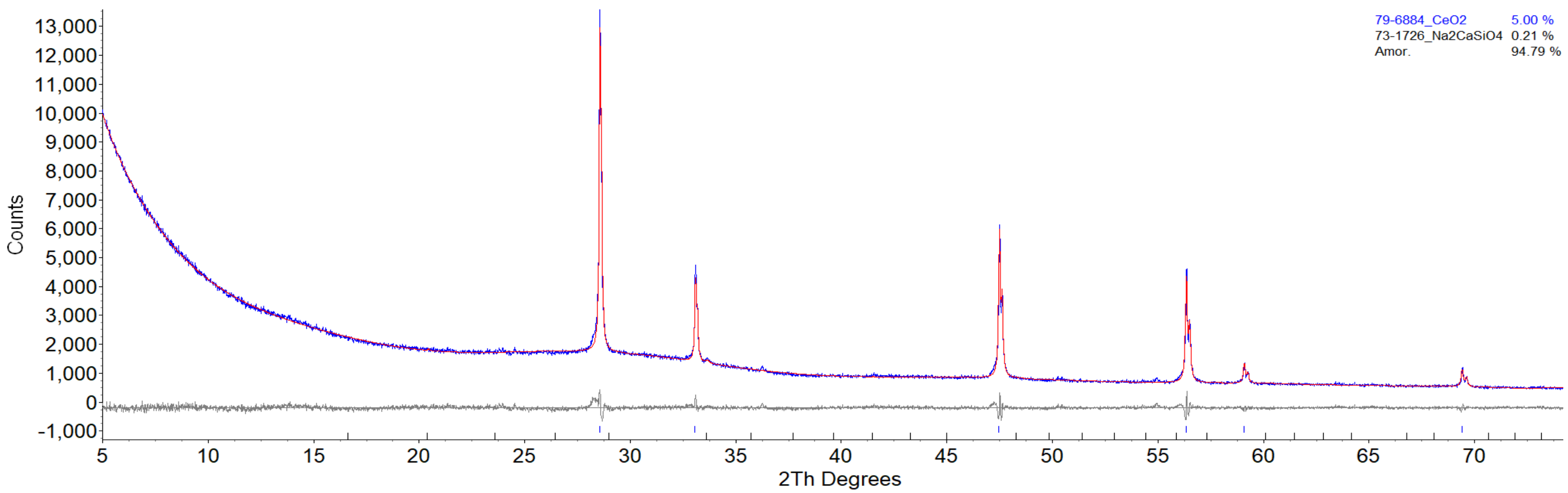

Figure I.22. XRD of glass HAL24M1-12 at 950 °C showing single crystalline phase, Na_2CaSiO_4.

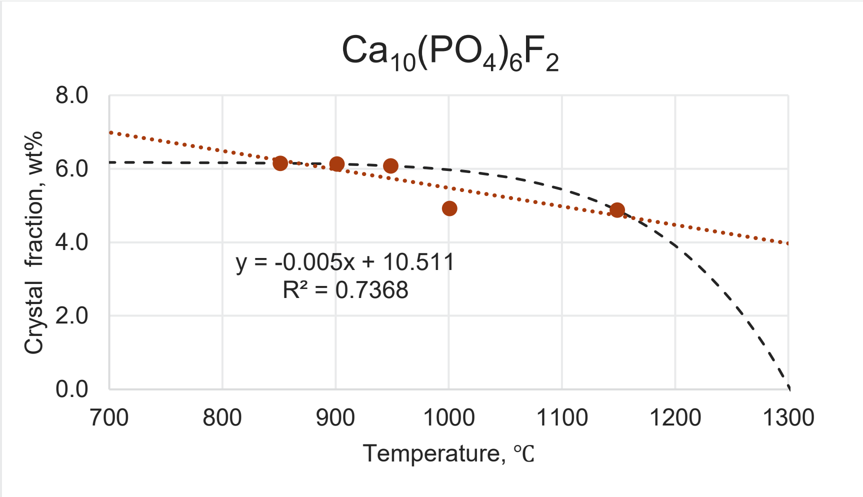

Figure I.23. The liquidus temperature plot for $Ca_{10}(PO_4)_6F_2$ in glass HAL24M1-13-1 showing the linear T_L at 2089 °C ($R^2 = 0.7368$) and the non-linear (black dash line) T_L at 1302 °C. The linear fitting includes all five temperature datapoints while the non-linear fitting excludes 1000 °C as an outlier.

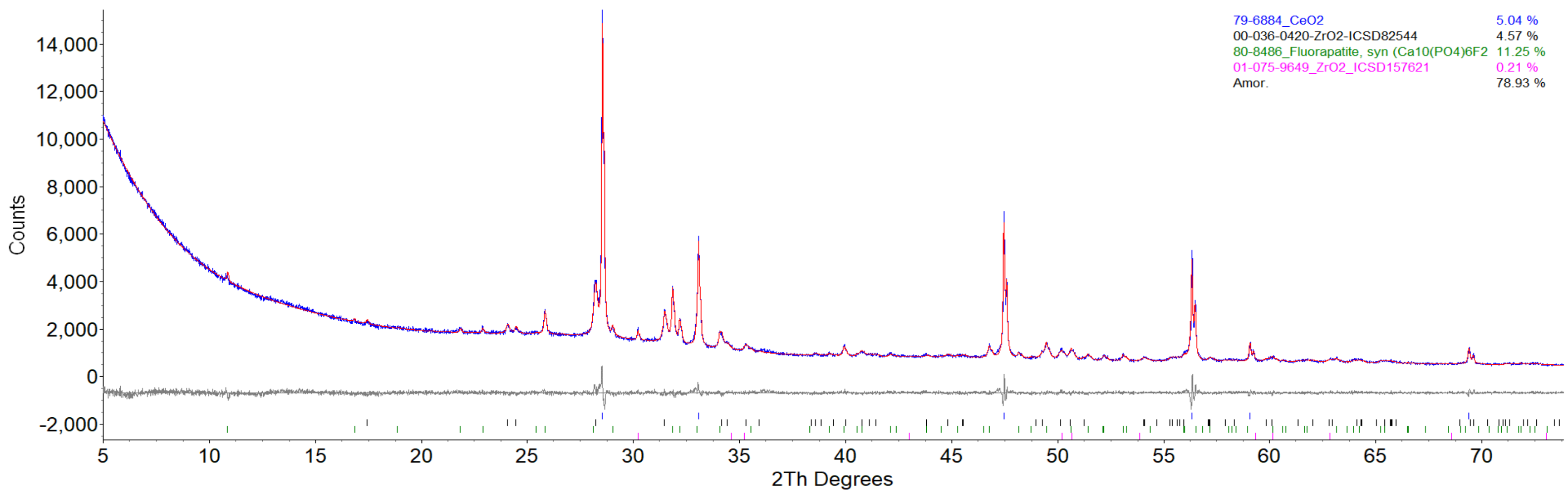

Figure I.24. XRD of glass HAL24M1-13-1 at 950 °C showing crystalline phases, ZrO_2 and $Ca_{10}(PO_4)_6F_2$.

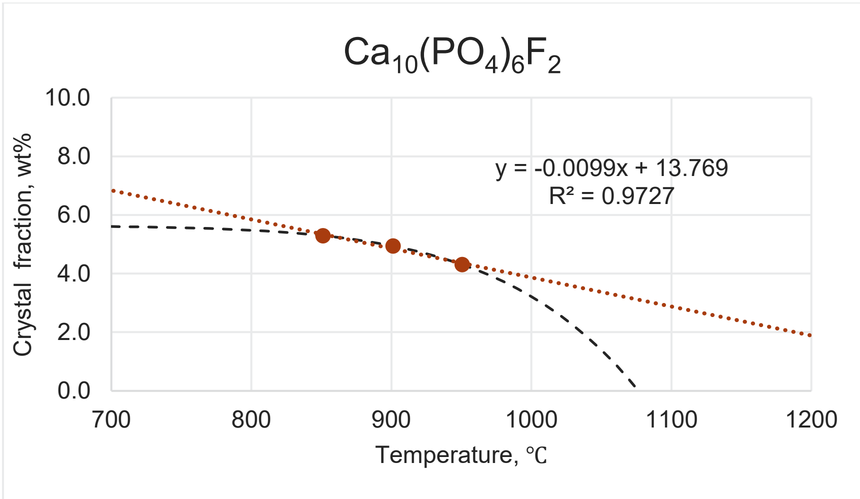

Figure I.25. The liquidus temperature plot for $Ca_{10}(PO_4)_6F_2$ in glass HAL24M1-14 showing the linear T_L at 1391 °C ($R^2 = 0.9727$) and the non-linear (black dash line) T_L at 1077 °C.

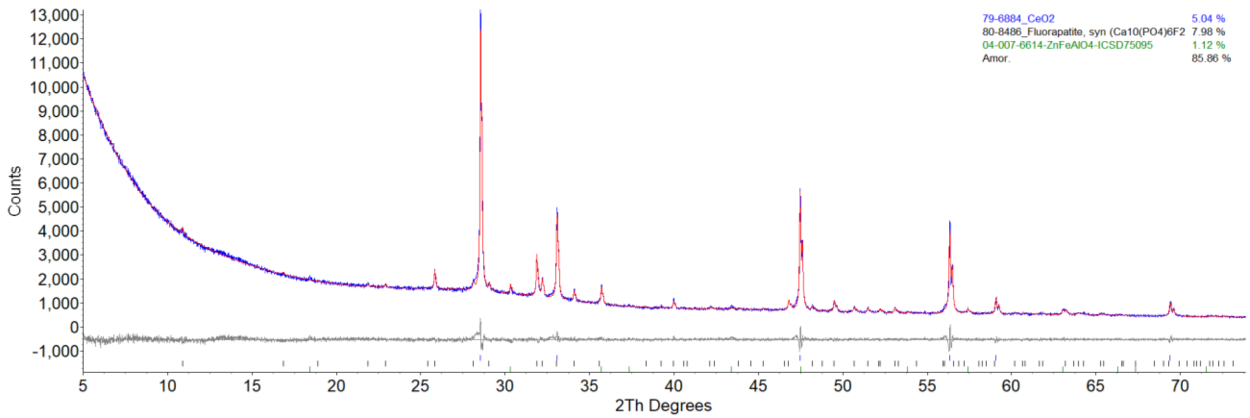

Figure I.26. XRD of glass HAL24M1-14 at 950 °C showing crystalline phases, $Ca_{10}(PO_4)_6F_2$ and $ZnFeAlO_4$.

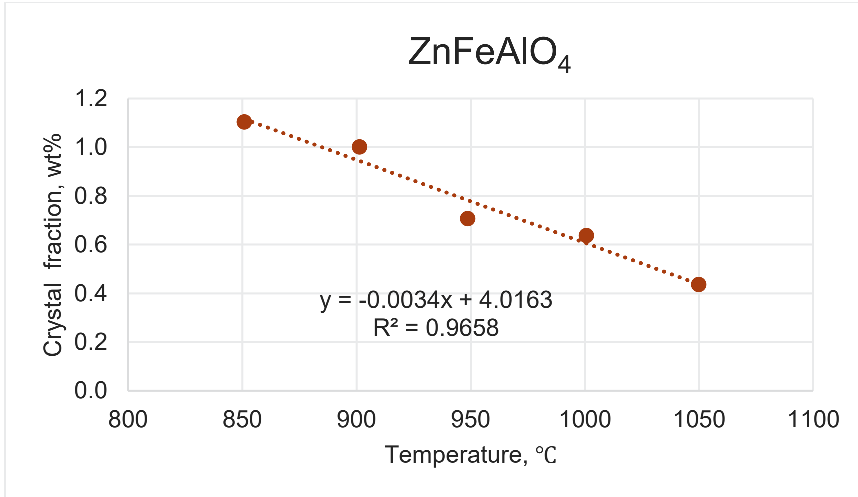

Figure I.27. The liquidus temperature plot for $ZnFeAlO_4$ in glass HAL24M1-15 showing the linear T_L at 1178 °C (R^2 = 0.9658).

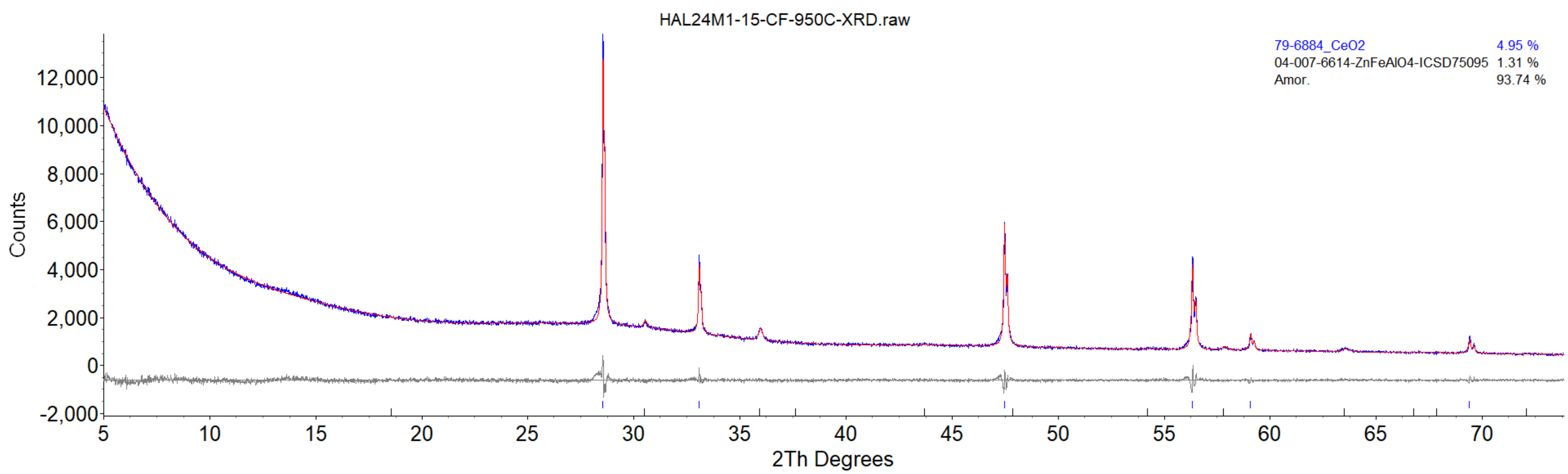

Figure I.28. XRD of glass HAL24M1-15 at 950 °C showing crystalline phase of $ZnFeAlO_4$.

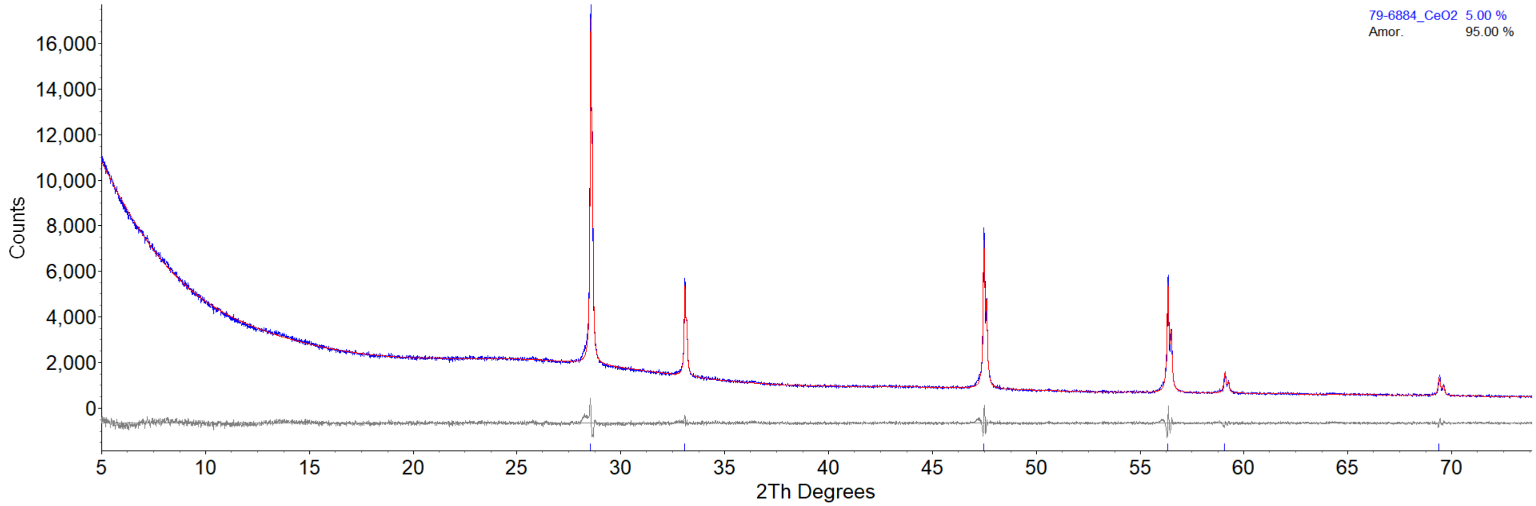

Figure I.29. The XRD of HAL24M1-16 at 950 °C revealed an amorphous structure.

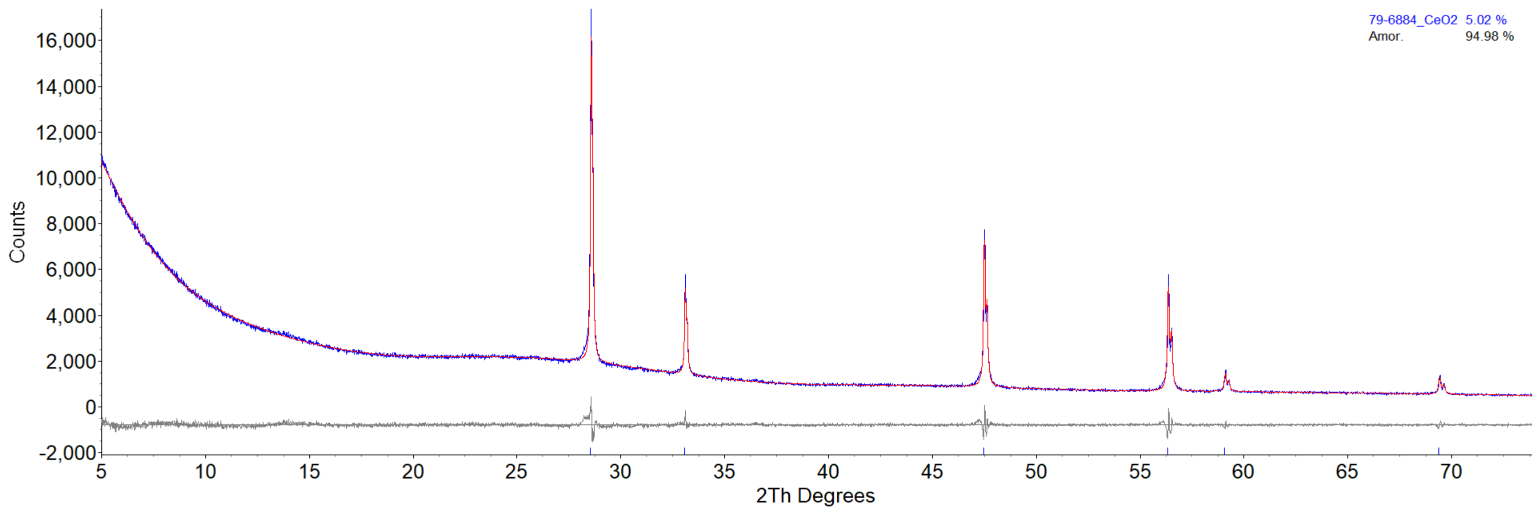

Figure I.30. The XRD of HAL24M1-17 at 950 °C revealed an amorphous structure.

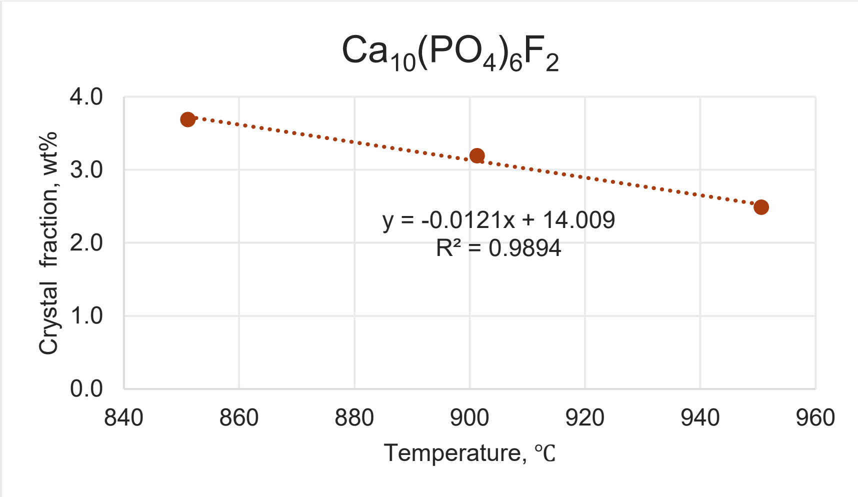

Figure I.31. The liquidus temperature plot for $Ca_{10}(PO_4)_6F_2$ in glass HAL24M1-18 showing the linear T_L at 1159 °C ($R^2 = 0.9894$).

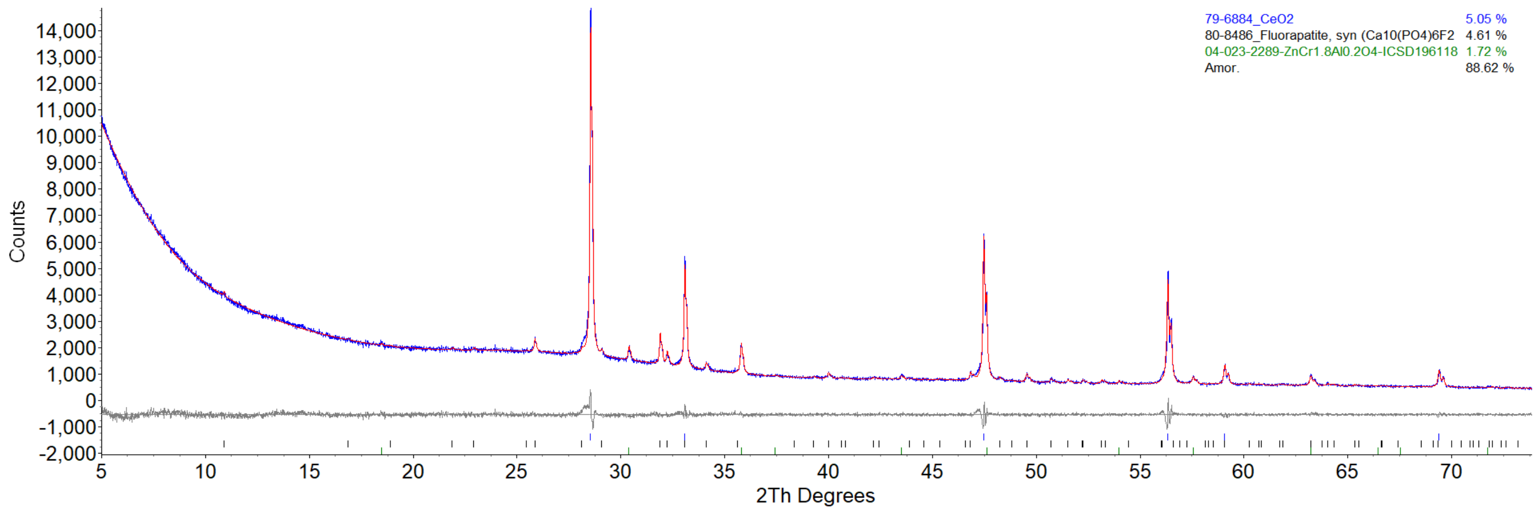

Figure I.32. XRD of glass HAL24M1-18 at 950 °C showing crystalline phase, $Ca_{10}(PO_4)_6F_2$ and $ZnCr_{1.8}Al_{0.2}O_4$.

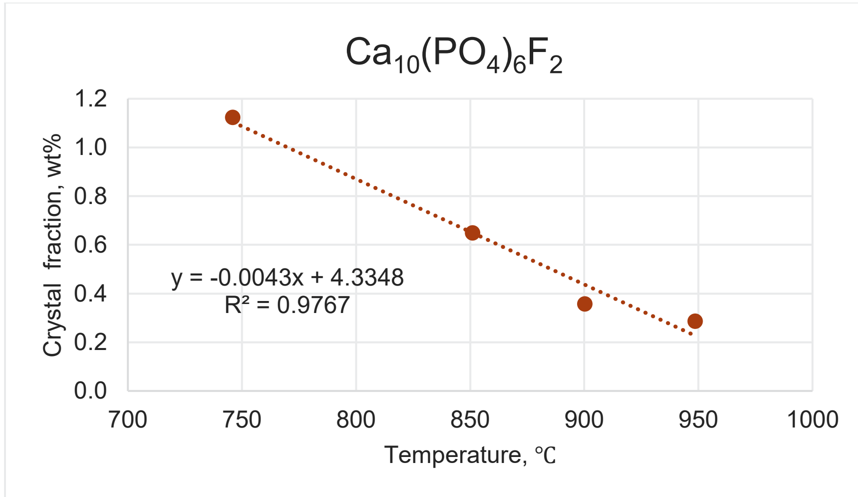

Figure I.33. The liquidus temperature plot for $Ca_{10}(PO_4)_6F_2$ in glass HAL24M1-19 showing the linear T_L at 1001 °C ($R^2 = 0.9767$).

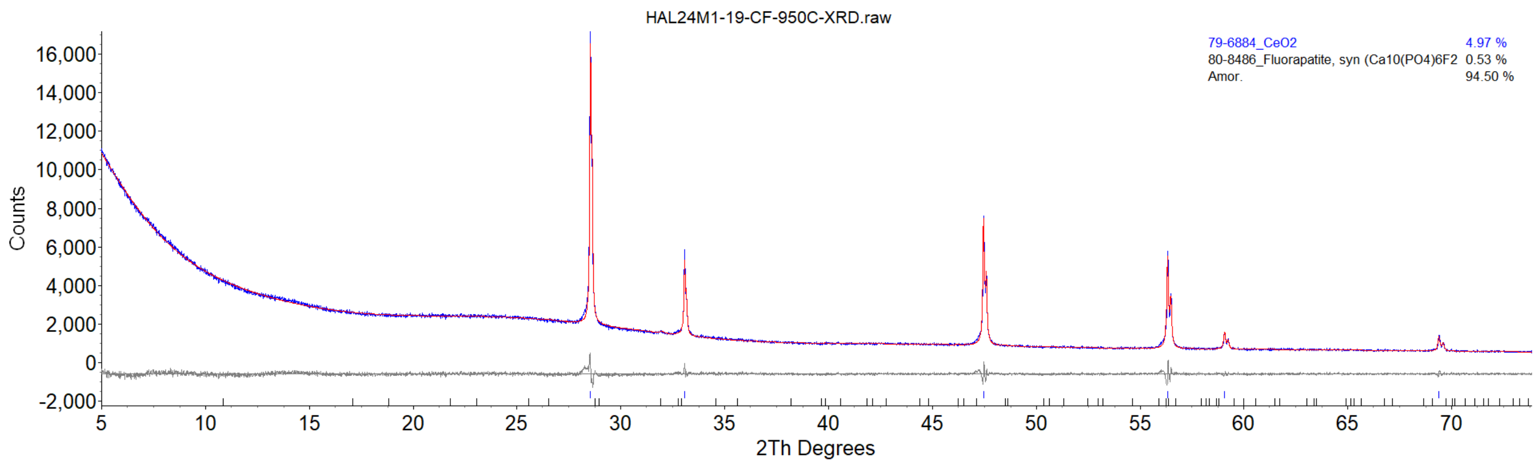

Figure I.34. XRD of glass HAL24M1-19 at 950 °C showing crystalline phase, $Ca_{10}(PO_4)_6F_2$.

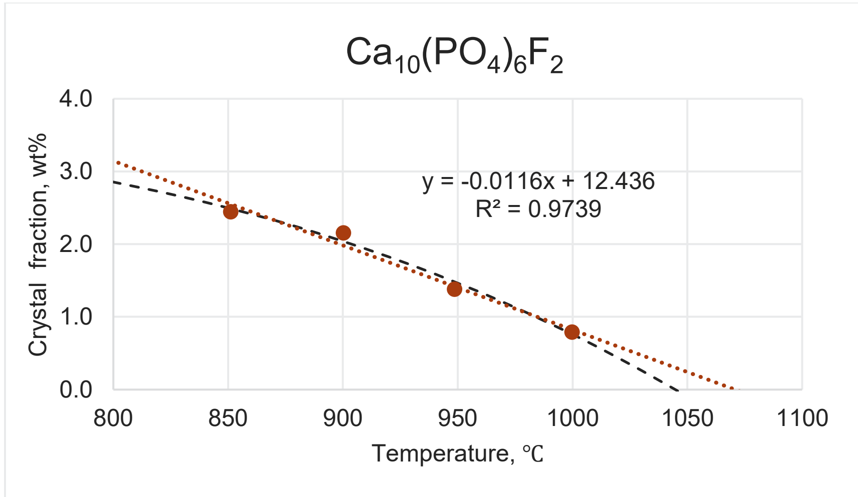

Figure I.35. The liquidus temperature plot for $Ca_{10}(PO_4)_6F_2$ in glass HAL24M1-20 showing the linear T_L at 1071 °C ($R^2 = 0.9739$) and the non-linear (black dash line) T_L at 1045 °C.

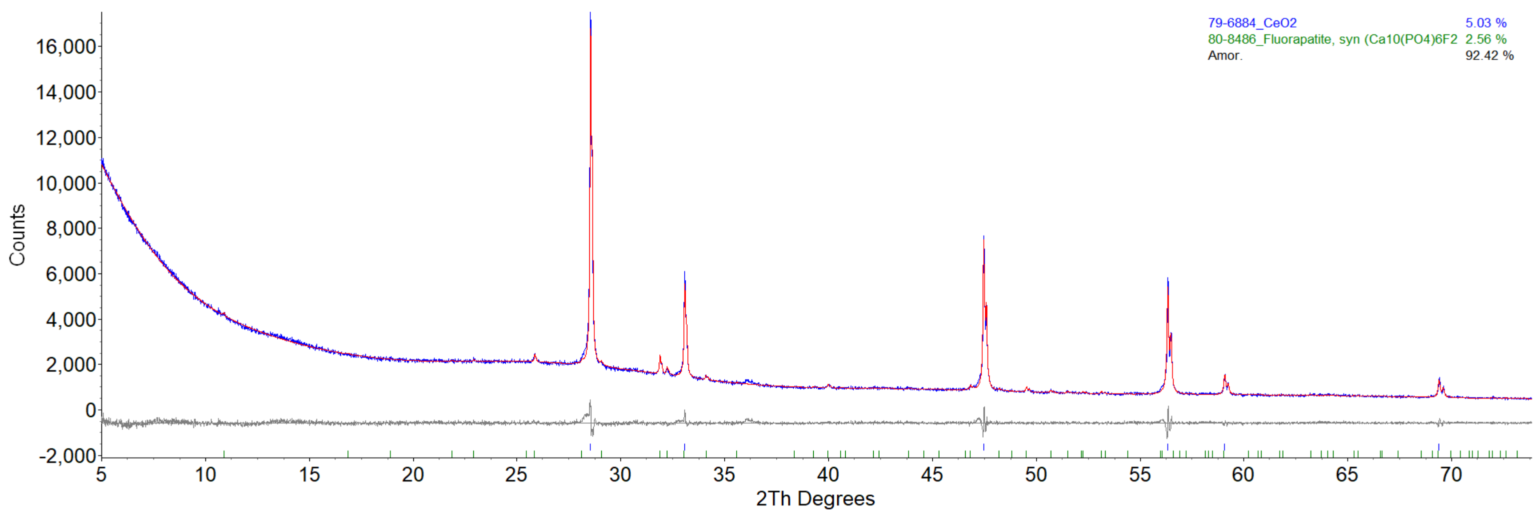

Figure I.36. XRD of glass HAL24M1-20 at 950 °C showing crystalline phase, $Ca_{10}(PO_4)_6F_2$.

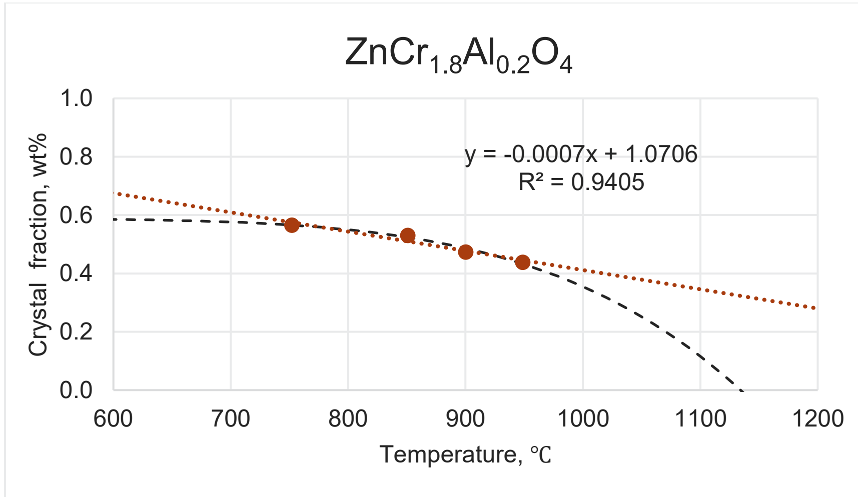

Figure I.37. The liquidus temperature plot for $ZnCr_{1.8}Al_{0.2}O_4$ in glass HAL24M1-21 showing the linear T_L at 1624 °C ($R^2 = 0.9405$) and the non-linear (black dash line) T_L at 1134 °C.

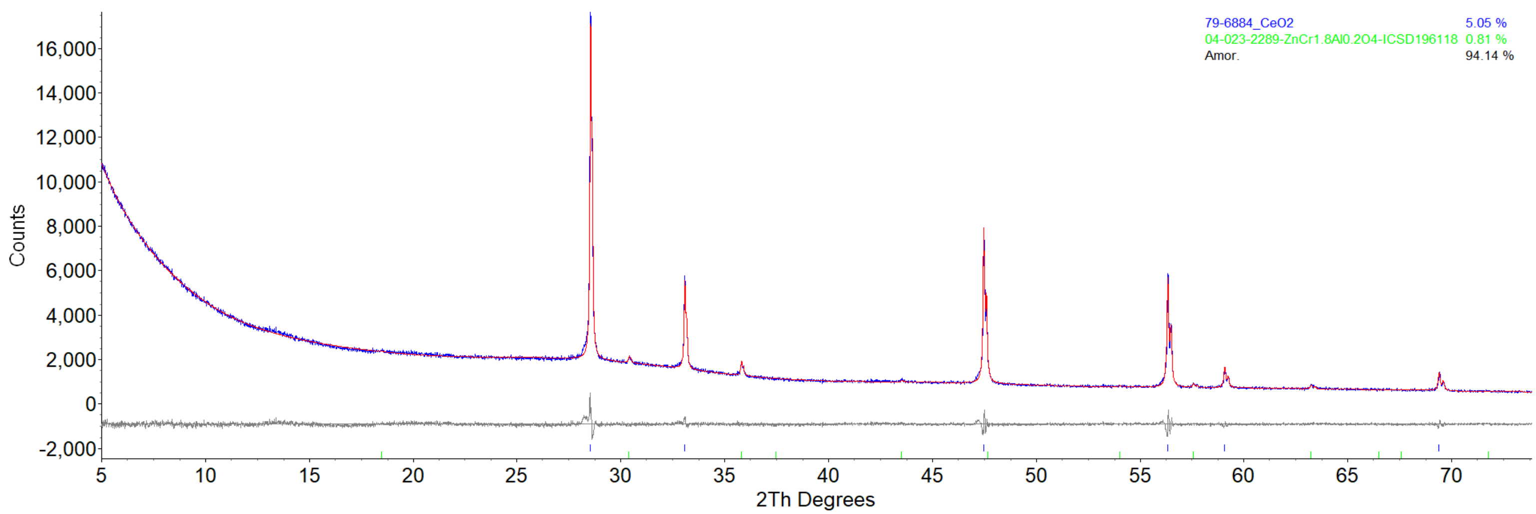

Figure I.38. XRD of glass HAL24M1-21 at 950 °C showing crystalline phase, $ZnCr_{1.8}Al_{0.2}O_4$.

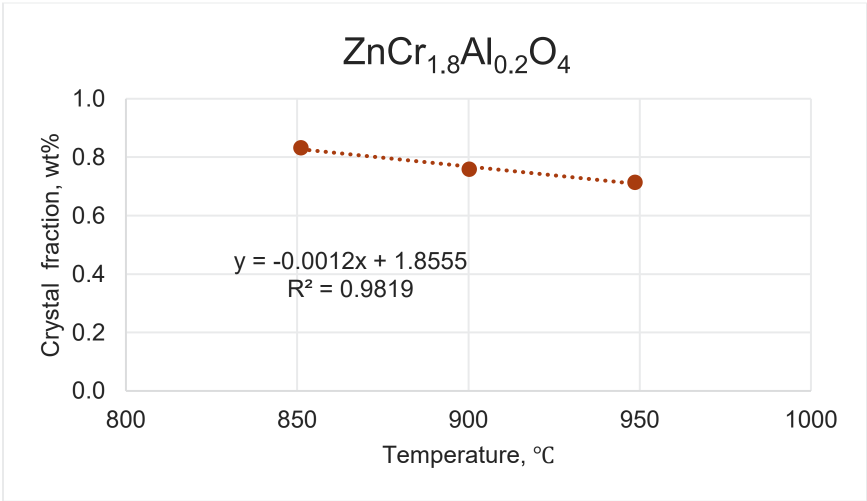

Figure I.39. The liquidus temperature plot for $ZnCr_{1.8}Al_{0.2}O_4$ in glass HAL24M1-22 showing the linear T_L at 1536 °C (R^2 = 0.9819).

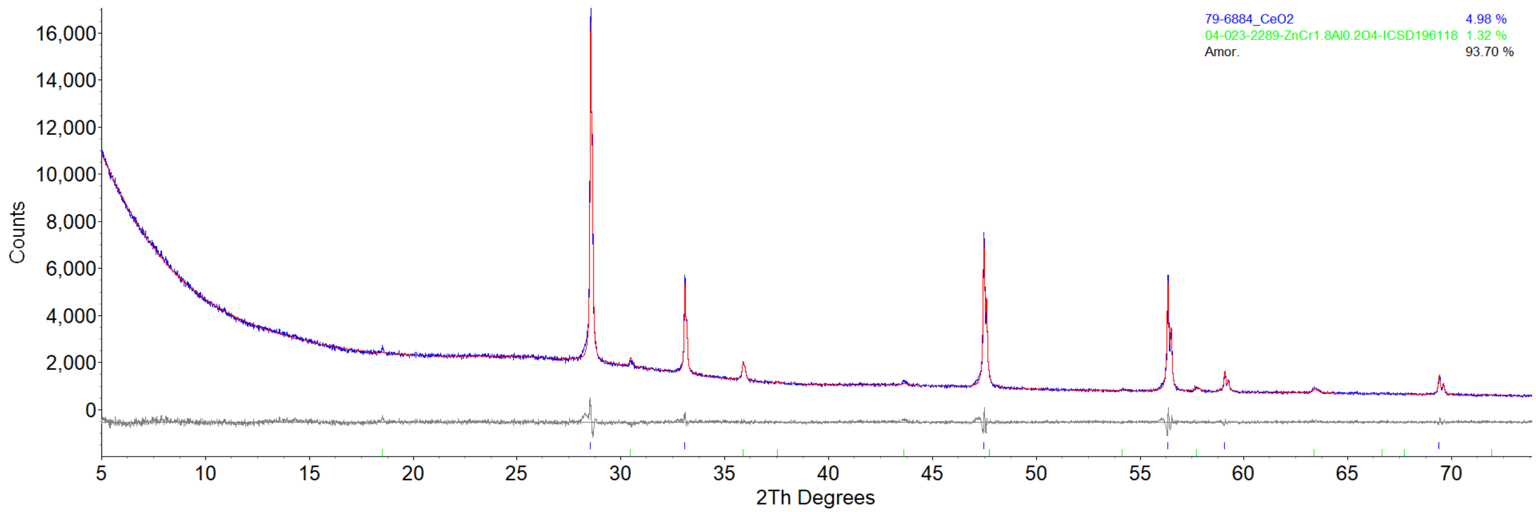

Figure I.40. XRD of glass HAL24M1-22 at 950 °C showing crystalline phase, $ZnCr_{1.8}Al_{0.2}O_4$.

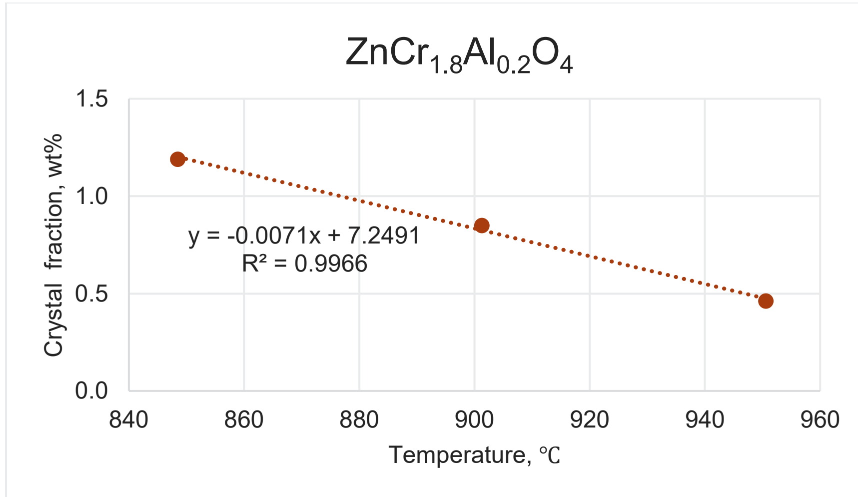

Figure I.41. The liquidus temperature plot for $ZnCr_{1.8}Al_{0.2}O_4$ in glass HAL24M1-23 showing the linear T_L at 1017 °C ($R^2 = 0.9966$).

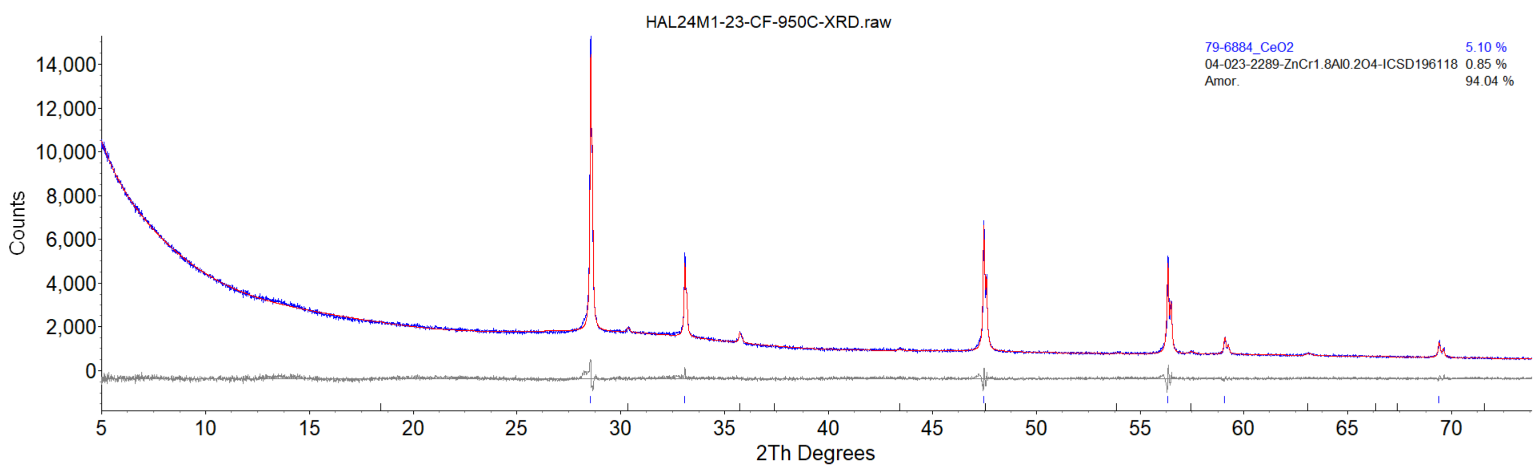

Figure I.42. XRD of glass HAL24M1-23 at 950 °C showing crystalline phase, $ZnCr_{1.8}Al_{0.2}O_4$.

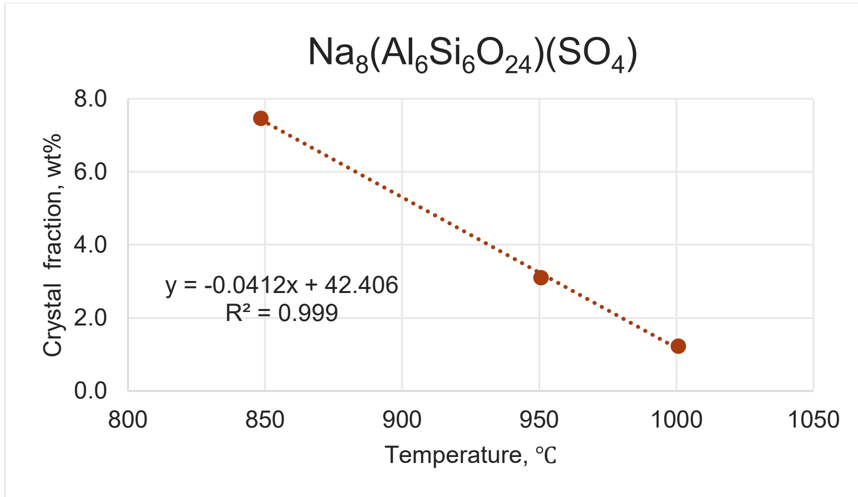

Figure I.43. The liquidus temperature plot for $Na_8(Al_6Si_6O_{24})(SO_4)$ in glass HAL24M1-24 showing the linear T_L at 1029 °C ($R^2 = 0.999$).

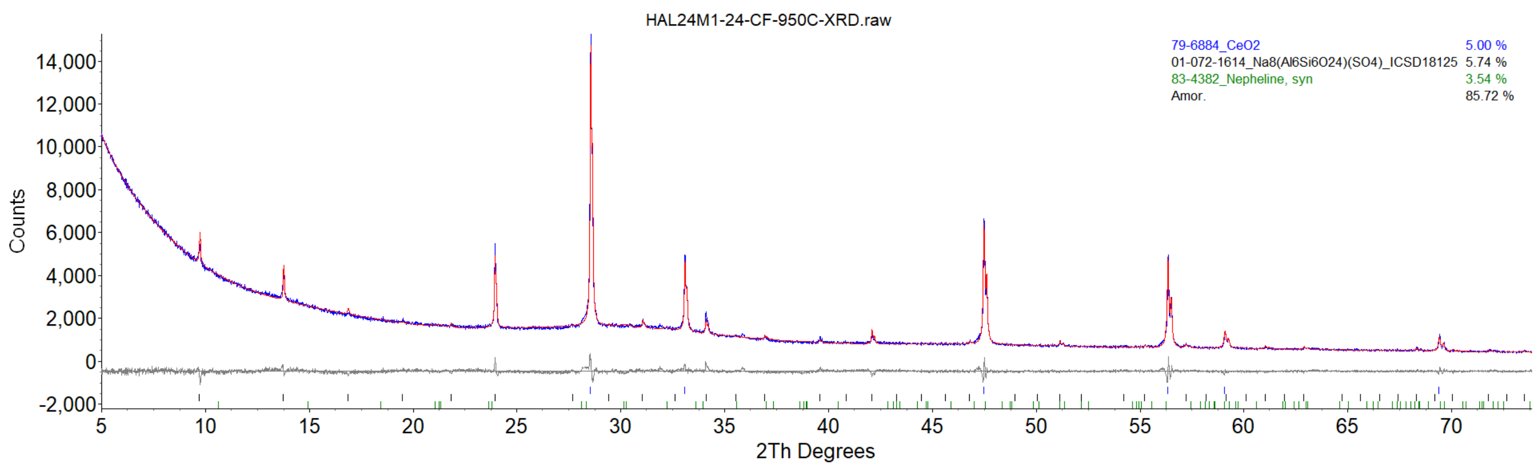

Figure I.44. XRD of glass HAL24M1-24 at 950 °C showing crystalline phase, $Na_8(Al_6Si_6O_{24})(SO_4)$ and nepheline.

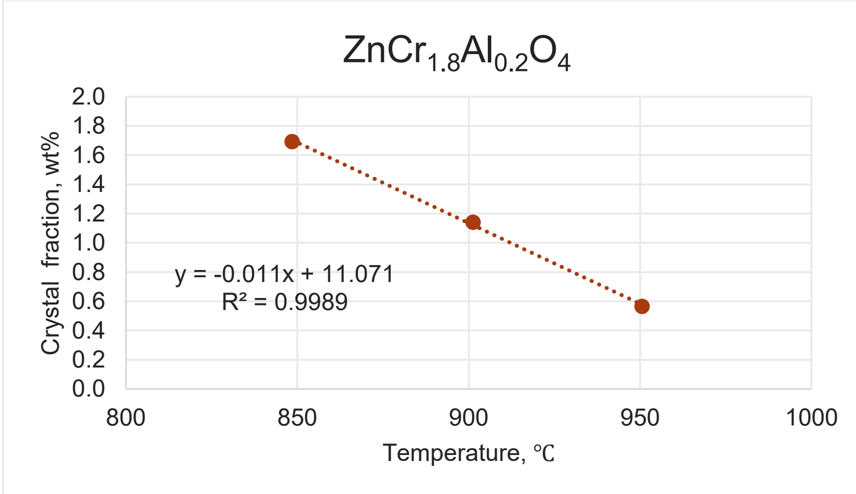

Figure I.45. The liquidus temperature plot for $ZnCr_{1.8}Al_{0.2}O_4$ in glass HAL24M1-25 showing the linear T_L at 1003 °C ($R^2 = 0.9989$).

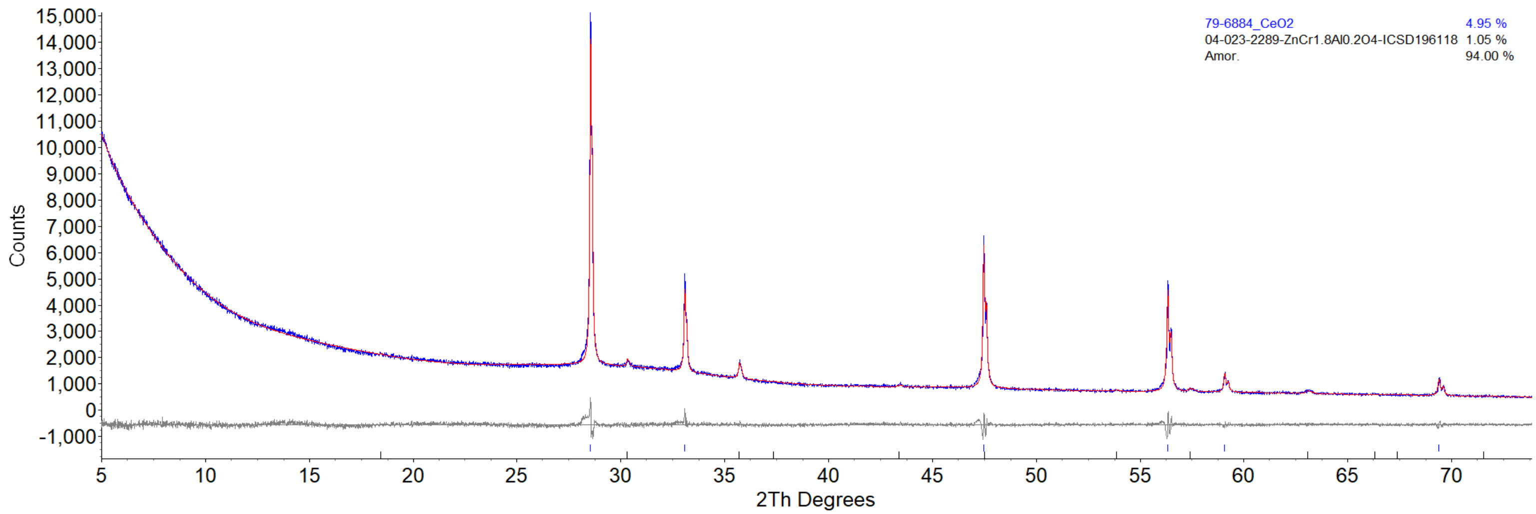

Figure I.46. XRD of glass HAL24M1-25 at 950 °C showing crystalline phase, $ZnCr_{1.8}Al_{0.2}O_4$.

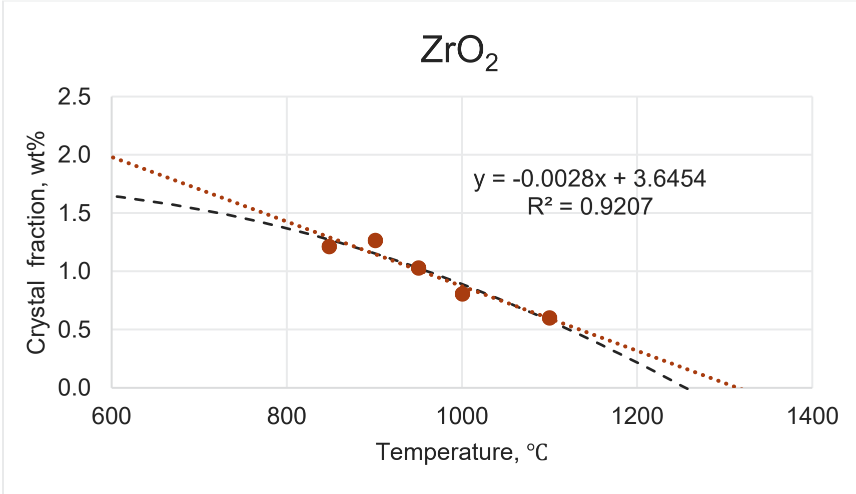

Figure I.47. The liquidus temperature plot for ZrO_2 in glass HAL24M1-26 showing the linear T_L at 1315 °C (R^2 = 0.9207) and the non-linear (black dash line) T_L at 1255 °C.

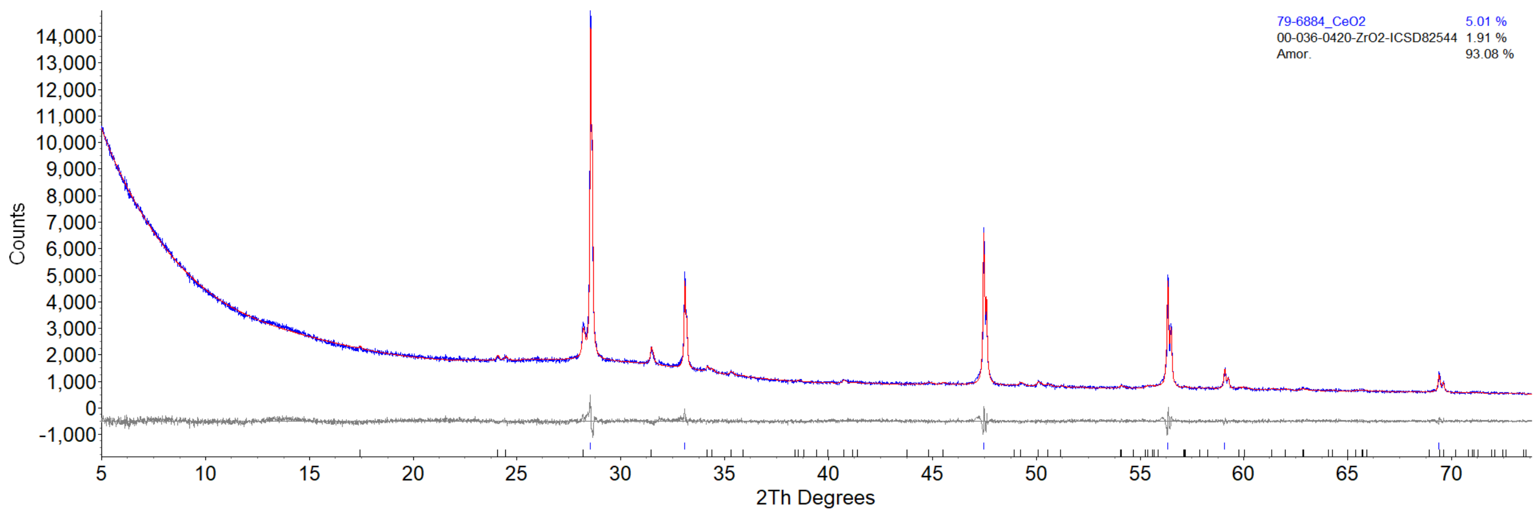

Figure I.48. XRD of glass HAL24M1-26 at 950 °C showing crystalline phase, ZrO_2.

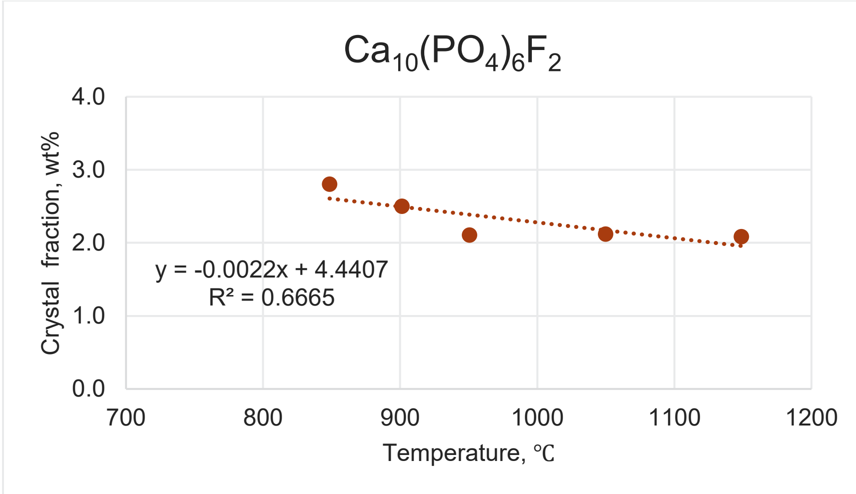

Figure I.49. The liquidus temperature plot for $Ca_{10}(PO_4)_6F_2$ in glass HAL24M1-27 showing the linear T_L at 2055 °C (R^2 = 0.6665).

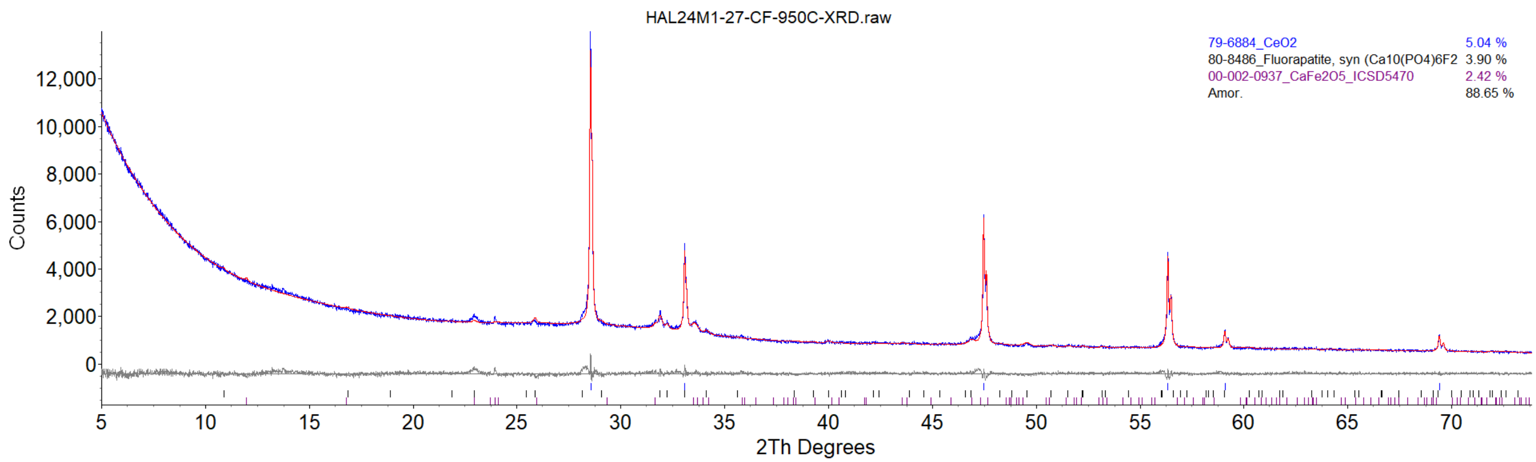

Figure I.50. XRD of glass HAL24M1-27 at 950 °C showing crystalline phase, $Ca_{10}(PO_4)_6F_2$ and $CaFe_2O_5$.

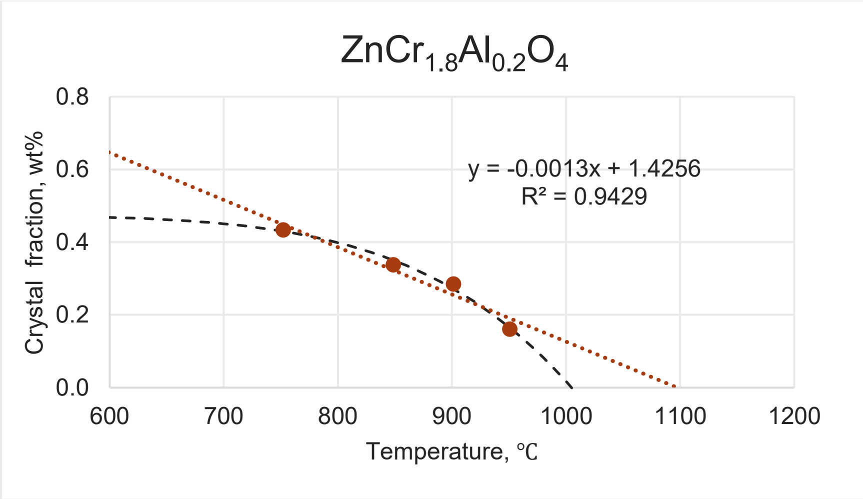

Figure I.51. The liquidus temperature plot for $ZnCr_{1.8}Al_{0.2}O_4$ in glass HAL24M1-28 showing the linear T_L at 1097 °C (R^2 = 0.9429) and the non-linear (black dash line) T_L at 1005 °C.

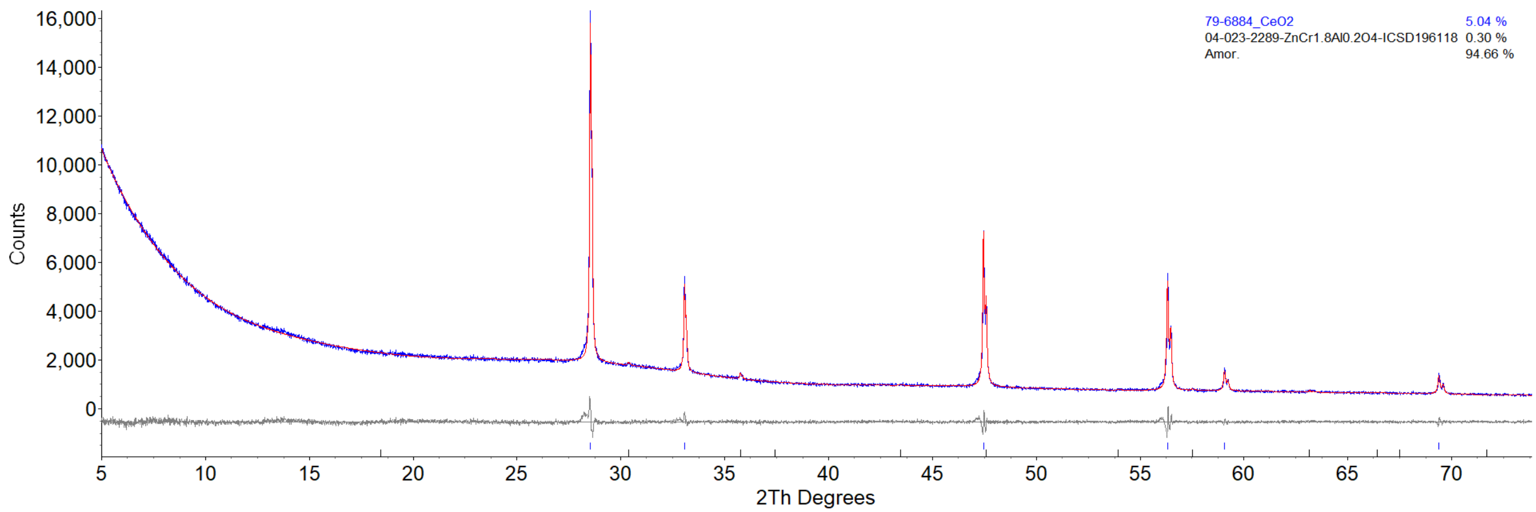

Figure I.52. XRD of glass HAL24M1-28 at 950 °C showing crystalline phase, $ZnCr_{1.8}Al_{0.2}O_4$.

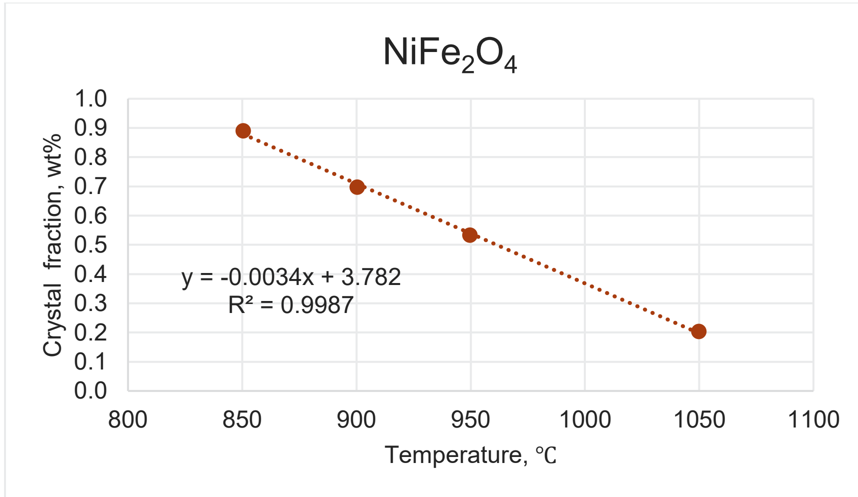

Figure I.53. The liquidus temperature plot for $FeNi_2O_4$ in glass HAL24M1-29-1 showing the linear T_L at 1108 °C (R^2 = 0.9987).

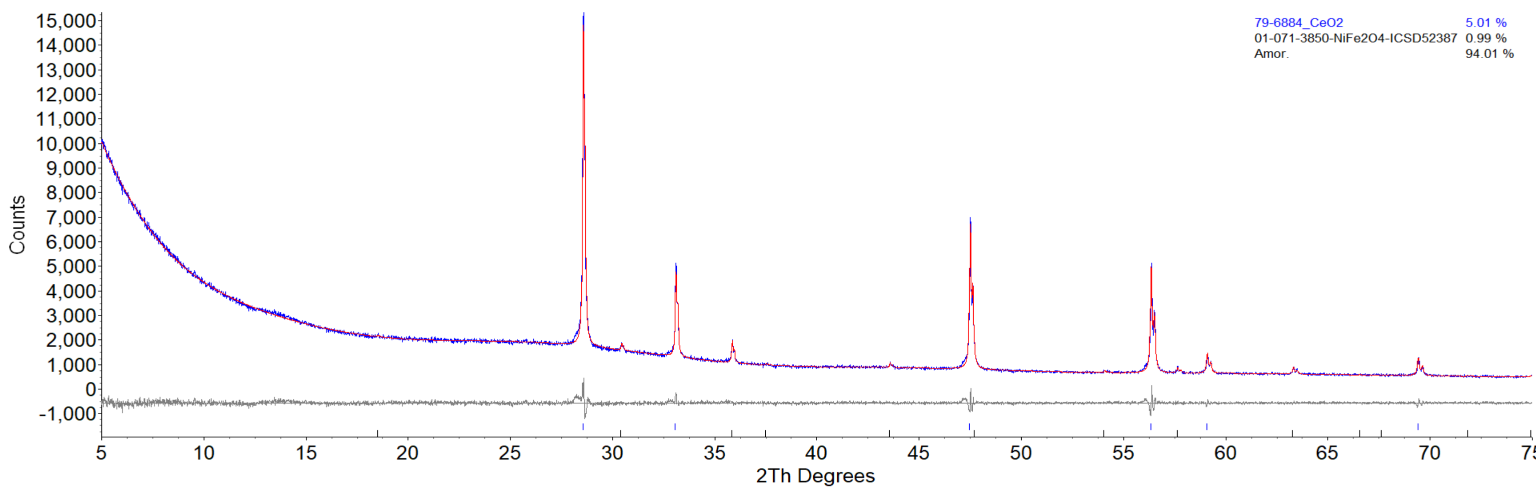

Figure I.54. XRD of glass HAL24M1-29-1 at 950 °C showing crystalline phase, $FeNi_2O_4$.

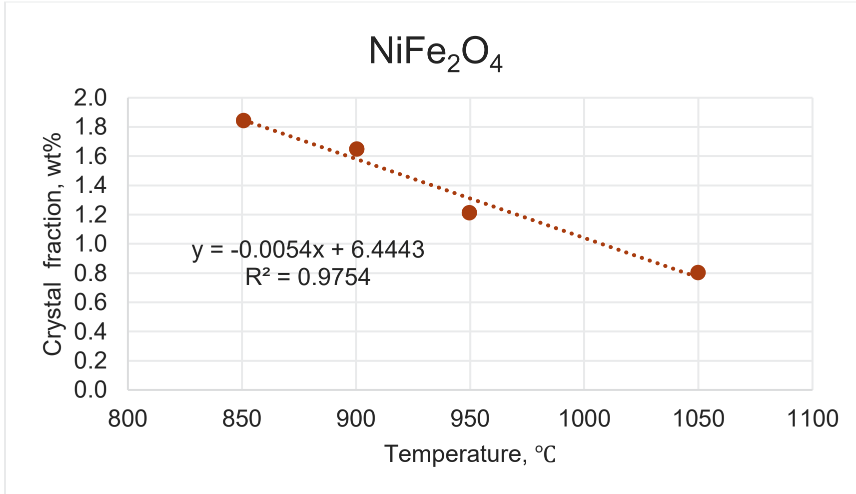

Figure I.55. The liquidus temperature plot for $NiFe_2O_4$ in glass HAL24M1-30-1 showing the linear T_L at 1193 °C (R^2 = 0.9754).

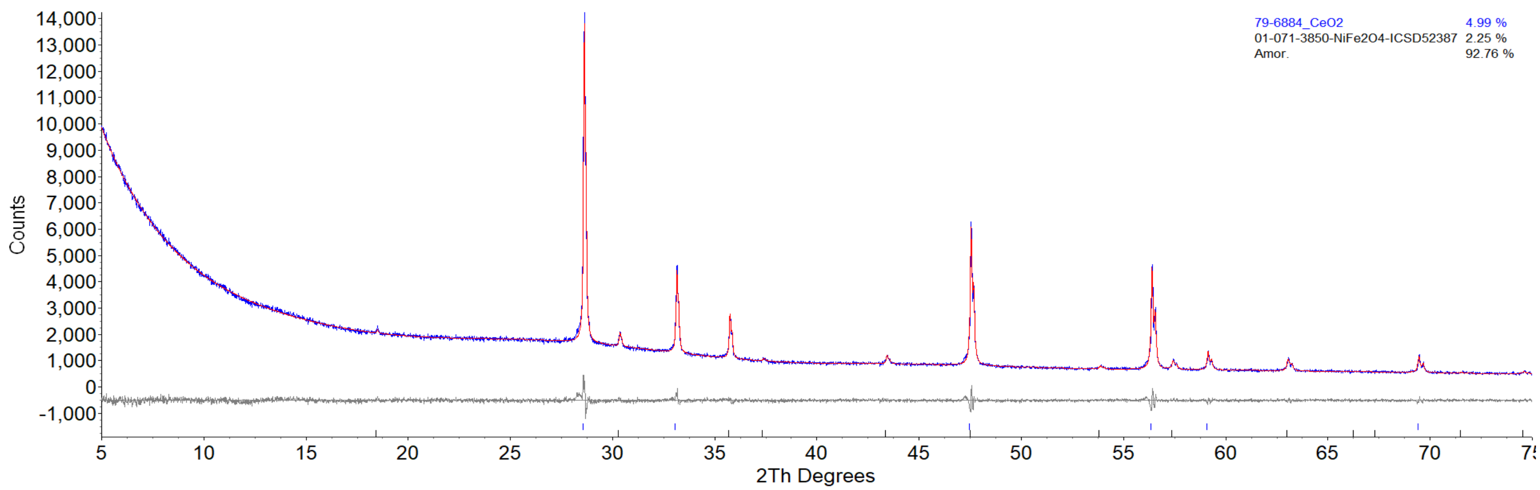

Figure I.56. XRD of glass HAL24M1-30-1 at 950 °C showing crystalline phase, $NiFe_2O_4$.

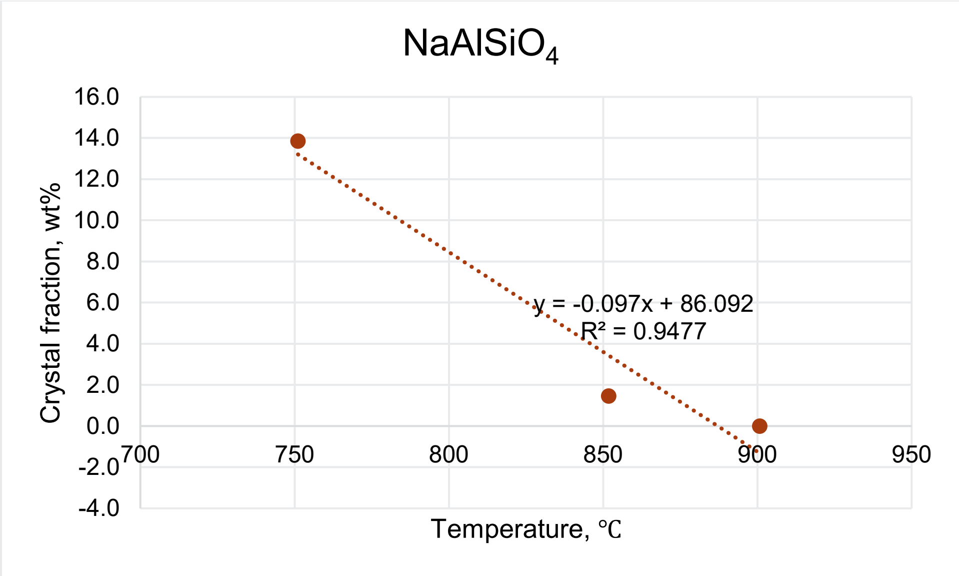

Figure I.57. The liquidus temperature plot for nepheline in glass HAL24M2-01 showing the linear T_L at 888 °C (R^2 = 0.9477).

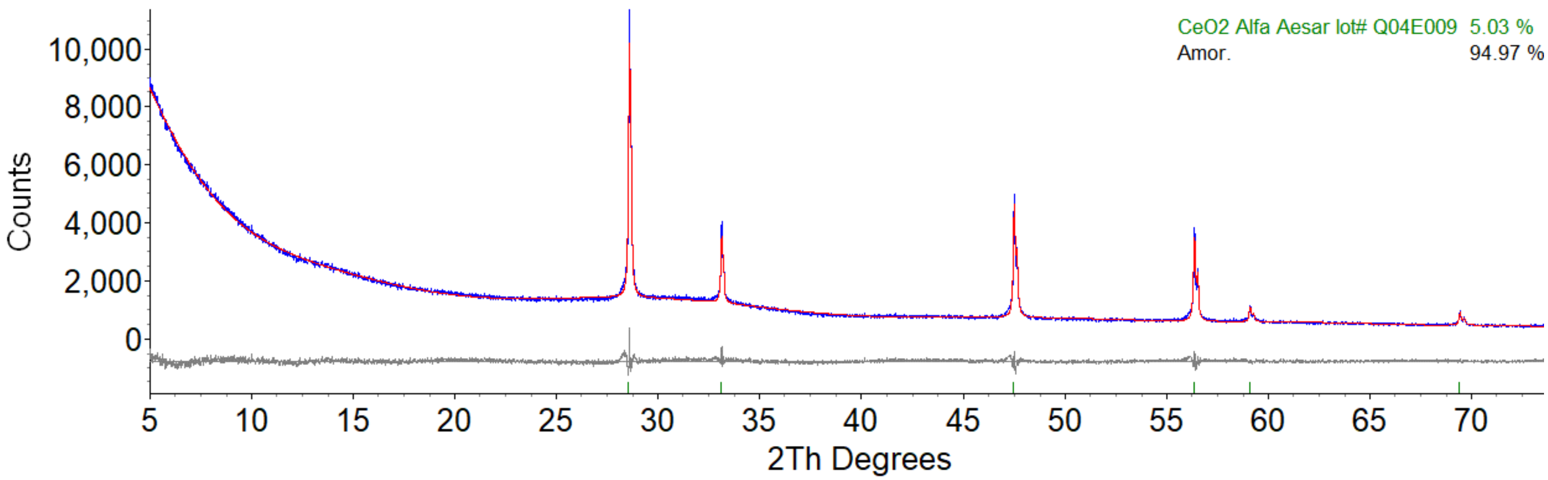

Figure I.58. XRD pattern of HAL24M2-01 at 950 °C.

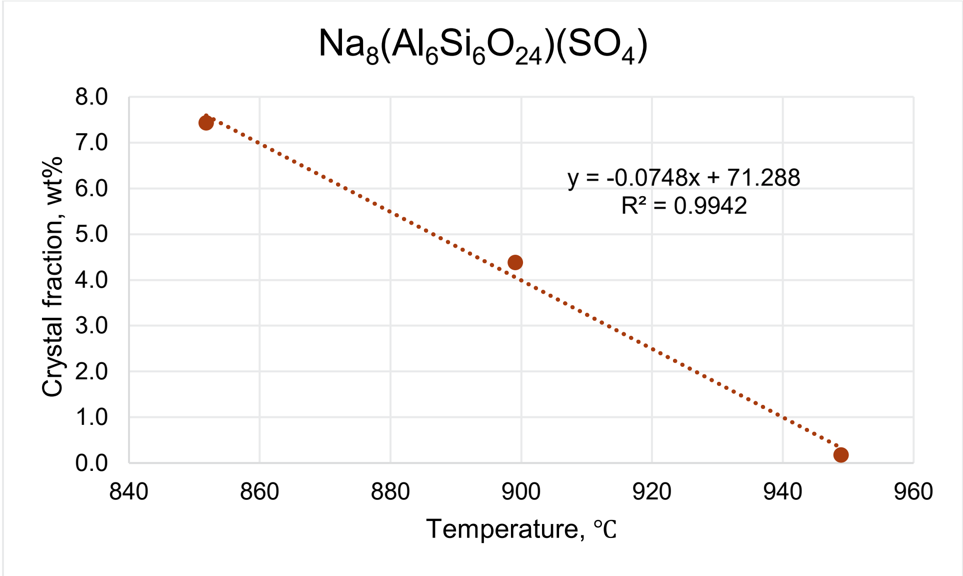

Figure I.59. The liquidus temperature plot for Nosean ($Na_8(Al_6Si_6O_{24})(SO_4)$) in glass HAL24M2-02 showing the linear T_L at 953 °C (R^2 = 0.9942).

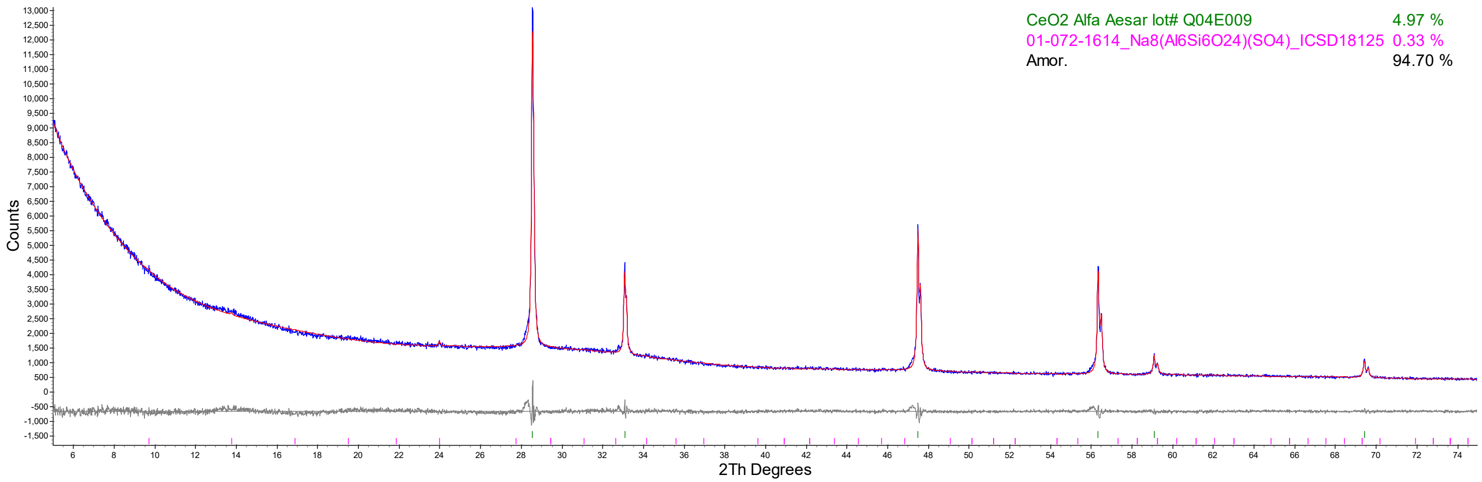

Figure I.60. XRD of glass HAL24M2-02 at 950 °C showing crystalline phase, Nosean ($Na_8(Al_6Si_6O_{24})(SO_4)$).

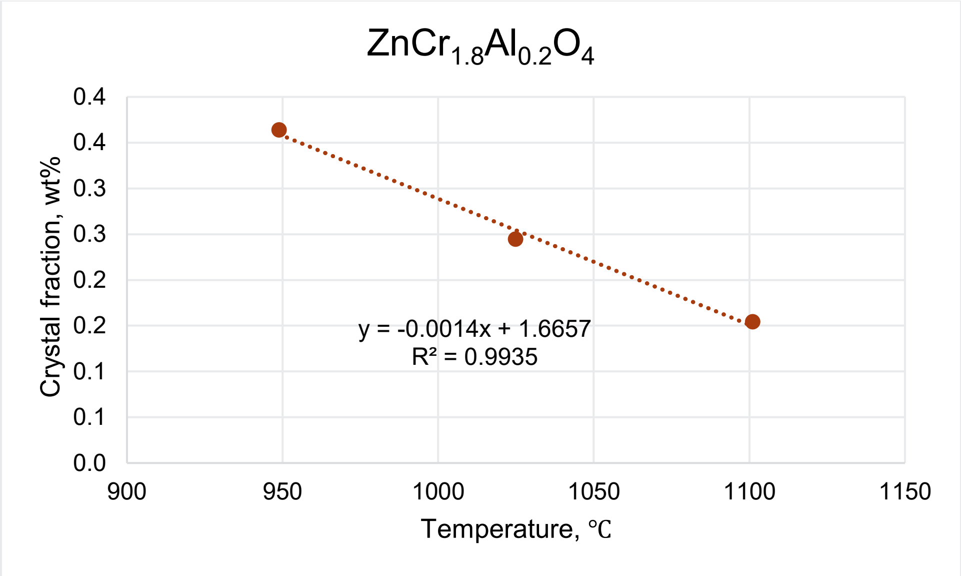

Figure I.61. The liquidus temperature plot for $ZnCr_{1.8}Al_{0.2}O_4$ in glass HAL24M2-03 showing the linear T_L at 1208 °C ($R^2 = 0.9935$).

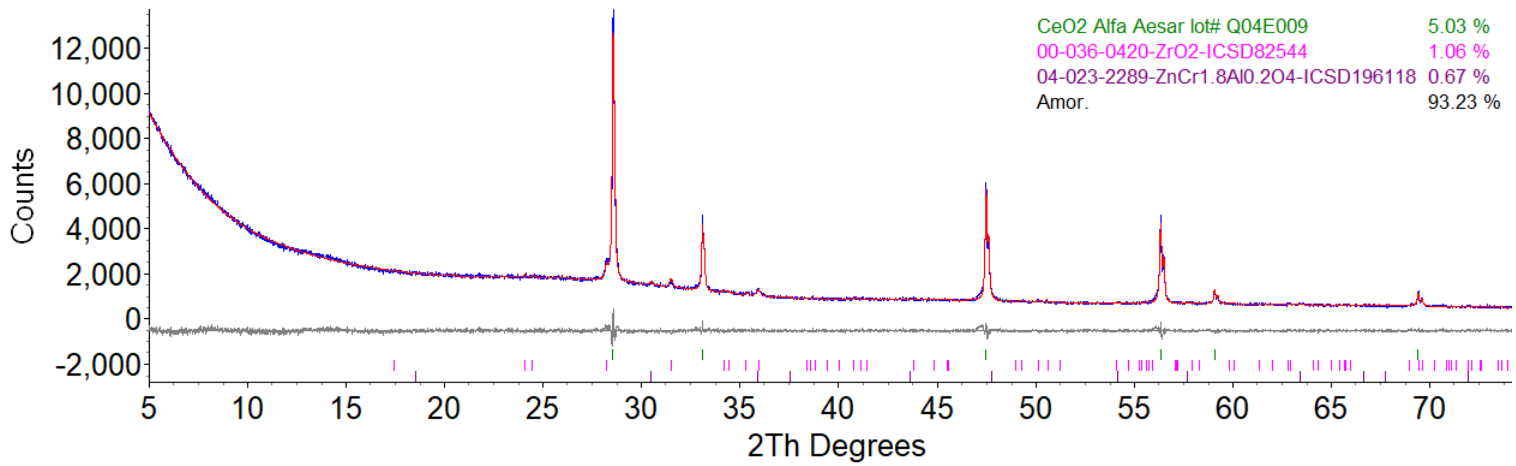

Figure I.62. XRD of glass HAL24M2-03 at 950 °C showing crystalline phases: ZrO_2 and $ZnCr_{1.8}Al_{0.2}O_4$.

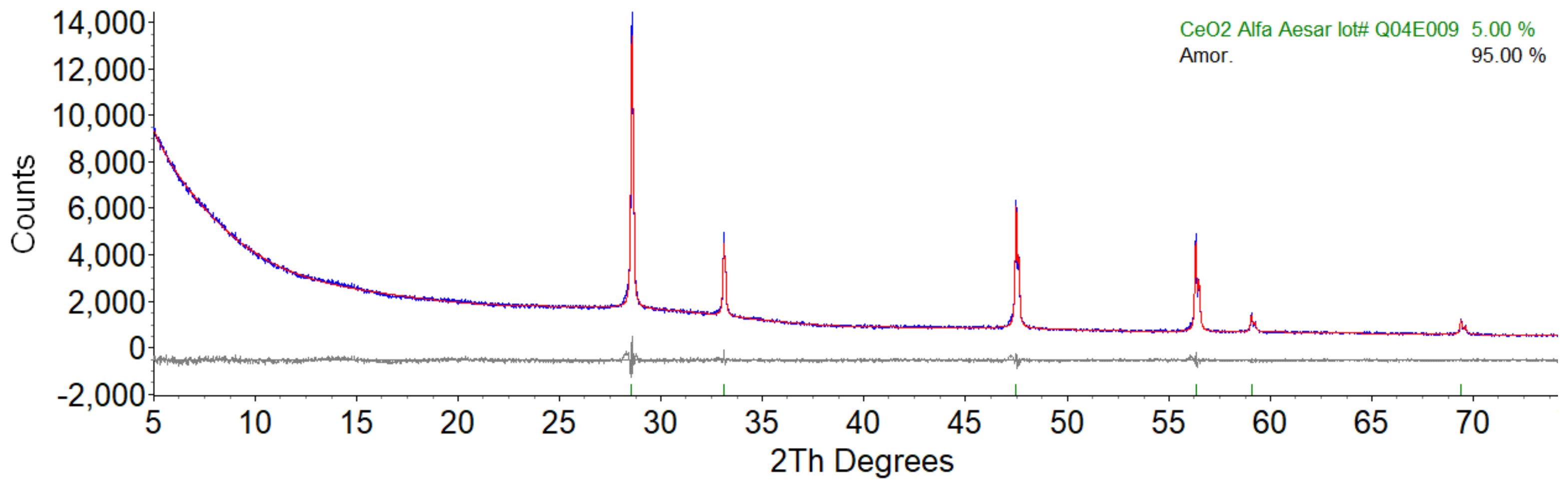

Figure I.63. XRD of glass HAL24M2-04 at 950 °C revealed an amorphous structure. The glass was fully amorphous at 850, 950, and 1100 °C, and the liquidus temperature is < 850 °C.

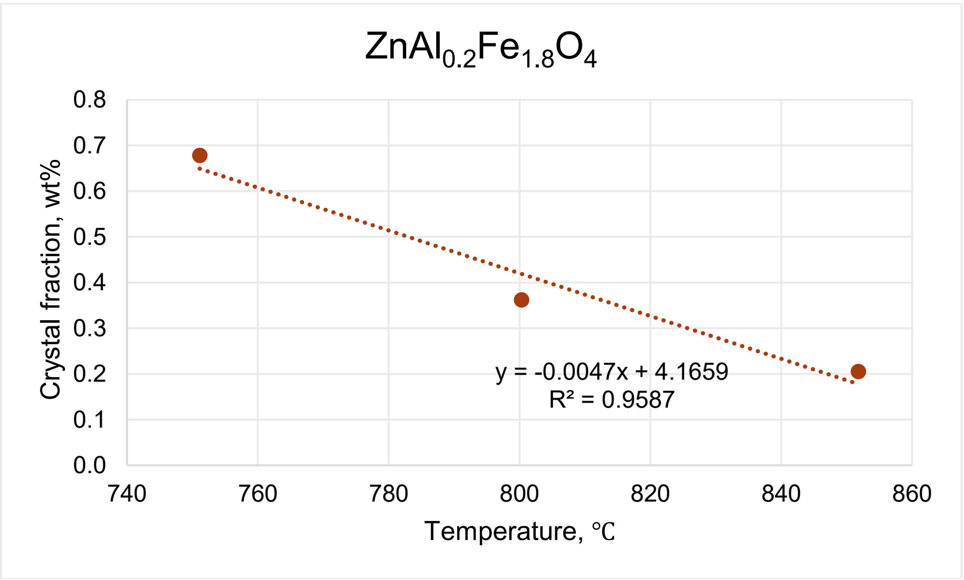

Figure I.64. The liquidus temperature plot for $ZnAl_{0.2}Fe_{1.8}O_4$ in glass HAL24M2-05 showing the linear T_L at 890 °C ($R^2 = 0.9587$).

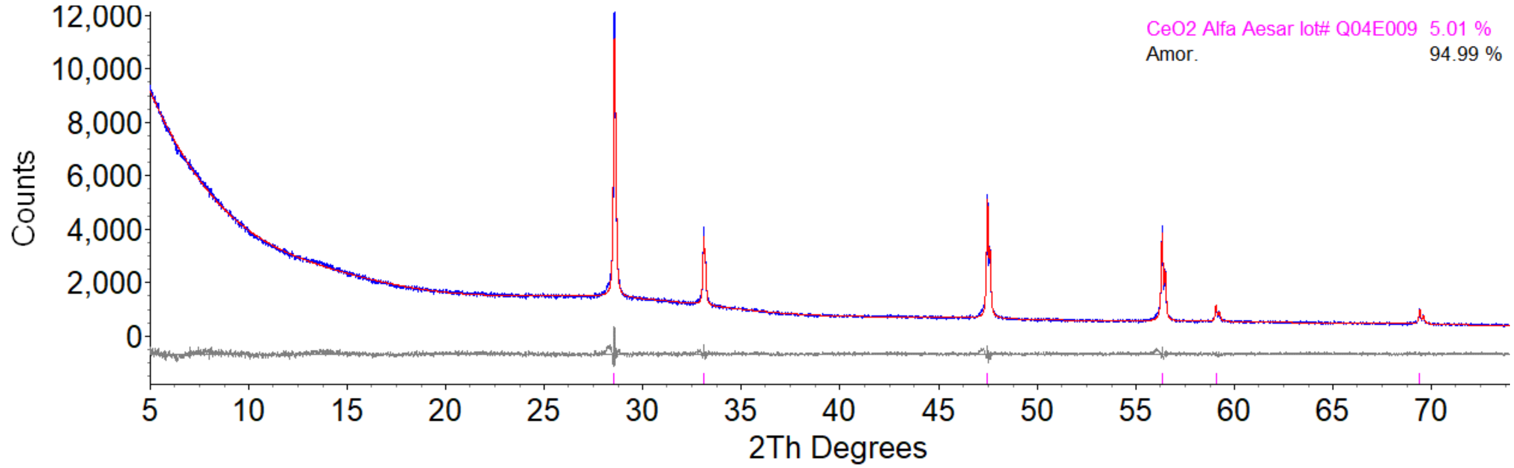

Figure I.65. XRD of glass HAL24M2-05 at 950 °C revealed an amorphous structure.

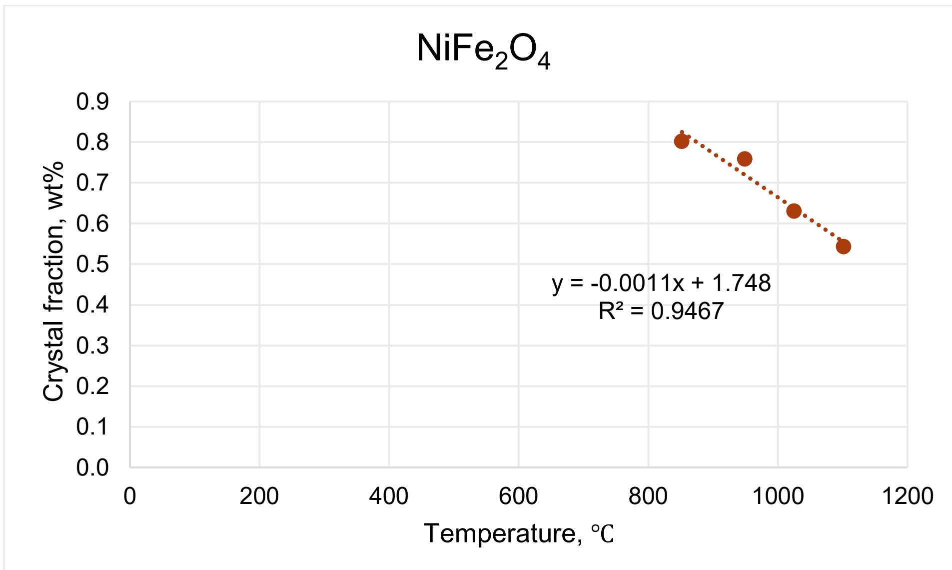

Figure I.66. The liquidus temperature plot for $NiFe_2O_4$ in glass HAL24M2-06 showing the linear T_L at 1613 °C (R^2 = 0.9467).

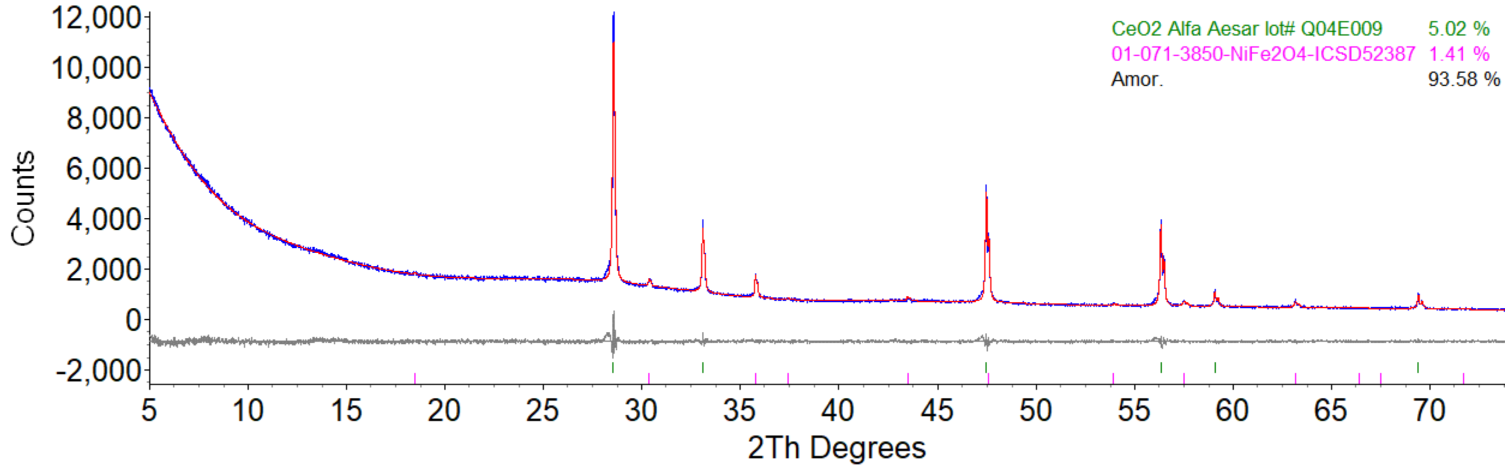

Figure I.67. XRD of glass HAL24M2-06 at 950 °C showing crystalline phase, $NiFe_2O_4$.

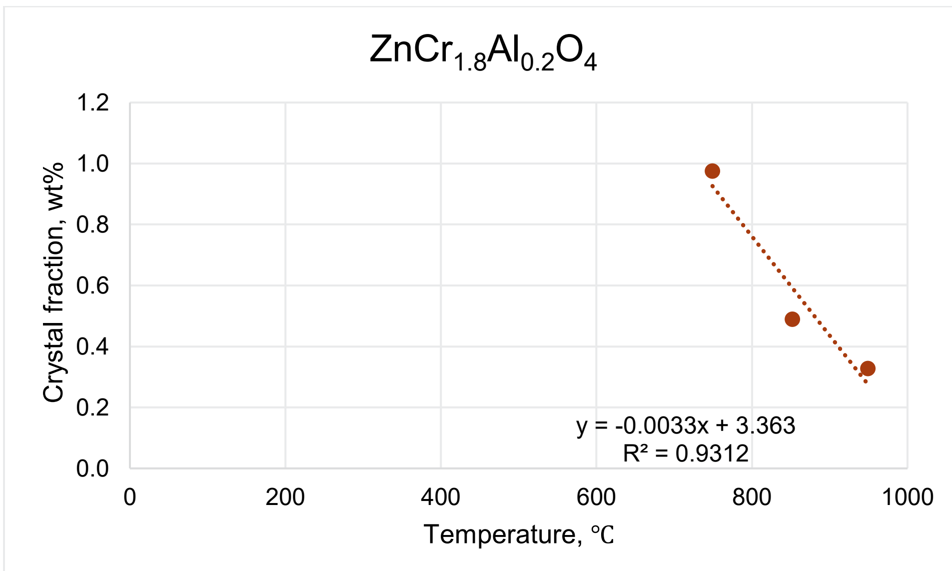

Figure I.68. The liquidus temperature plot for $ZnCr_{1.8}Al_{0.2}O_4$ in glass HAL24M2-07 showing the linear T_L at 1034 °C ($R^2 = 0.9312$).

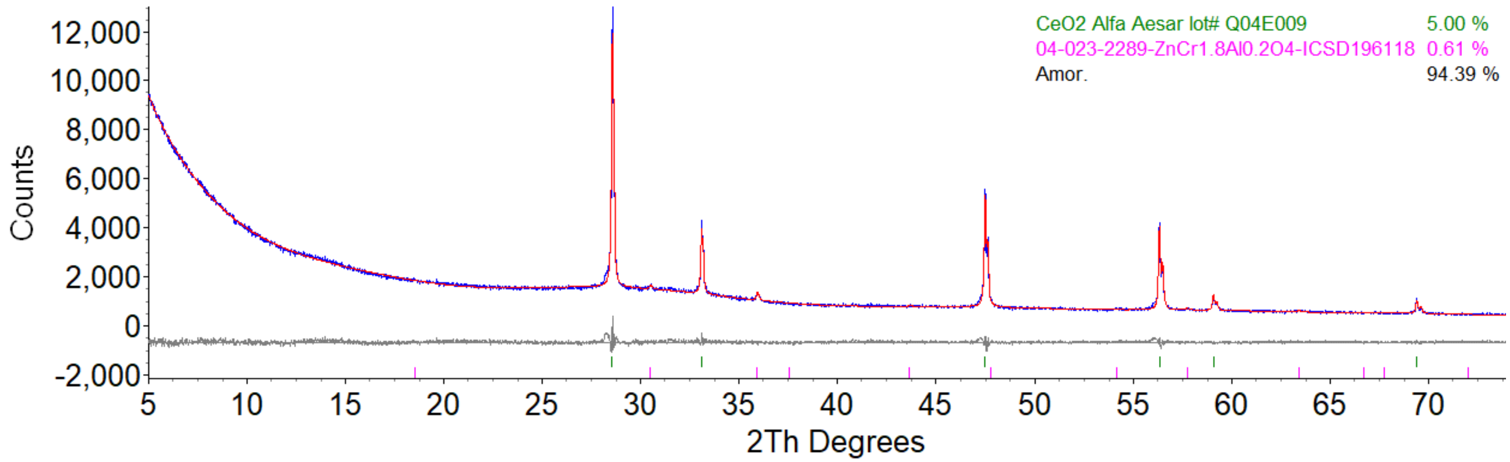

Figure I.69. XRD of glass HAL24M2-07 at 950 °C showing crystalline phase, $ZnCr_{1.8}Al_{0.2}O_4$.

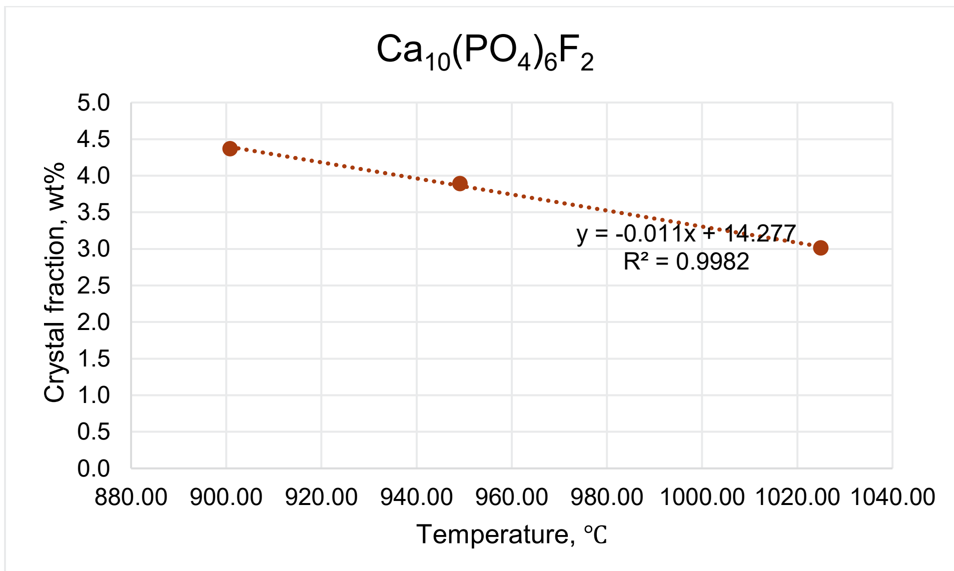

Figure I.70. The liquidus temperature plot for $Ca_{10}(PO_4)_6F_2$ in glass HAL24M2-08 showing the linear T_L at 1301 °C (R^2 = 0.9982).

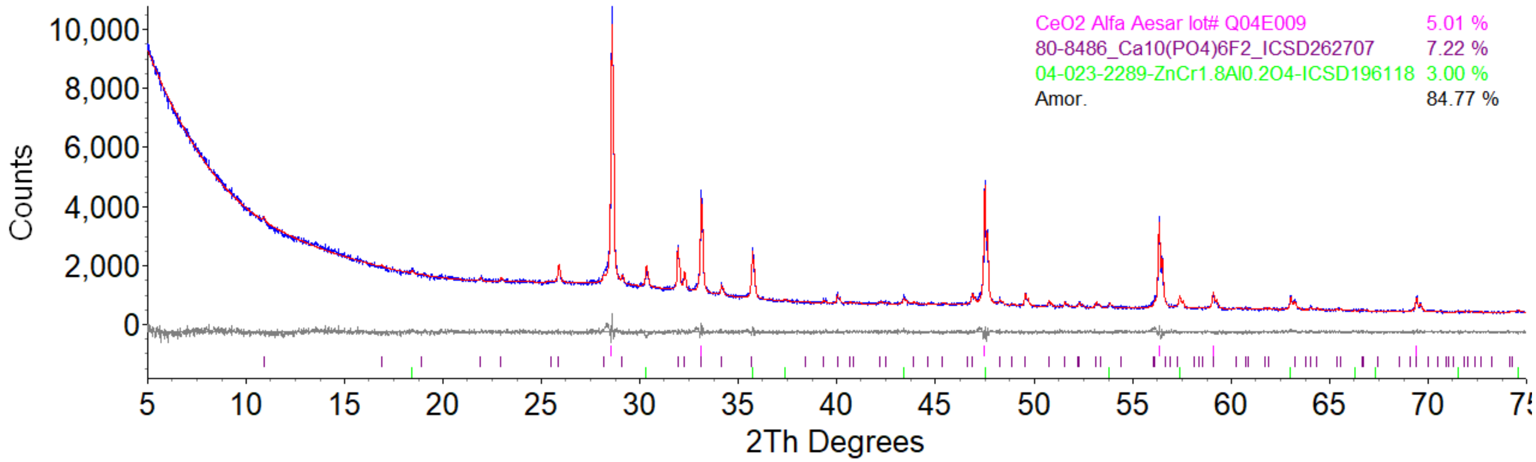

Figure I.71. XRD of glass HAL24M2-08 at 950 °C showing crystalline phase, $Ca_{10}(PO_4)_6F_2$ and $ZnCr_{1.8}Al_{0.2}O_4$.

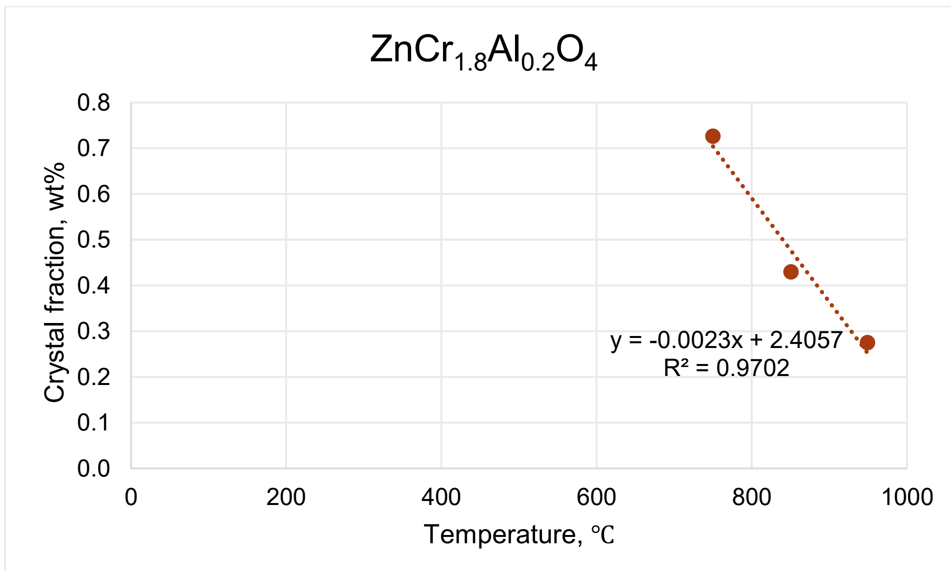

Figure I.72. The liquidus temperature plot for $ZnCr_{1.8}Al_{0.2}O_4$ in glass HAL24M2-09 showing the linear T_L at 1060 °C ($R^2 = 0.9702$).

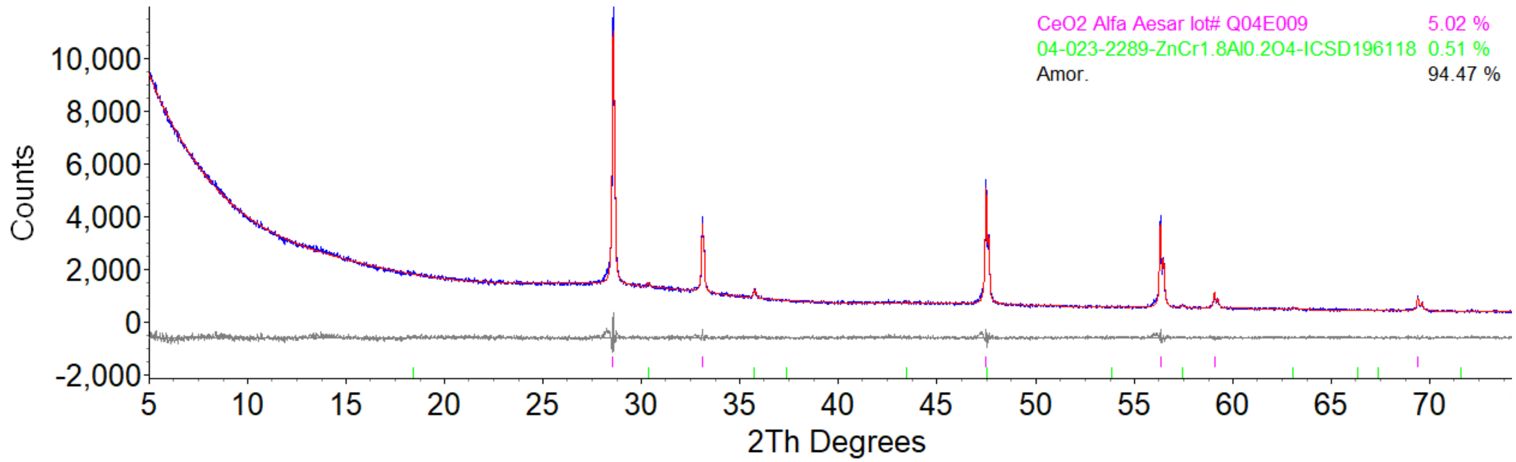

Figure I.73. XRD of glass HAL24M2-09 at 950 °C showing crystalline phase, $ZnCr_{1.8}Al_{0.2}O_4$.

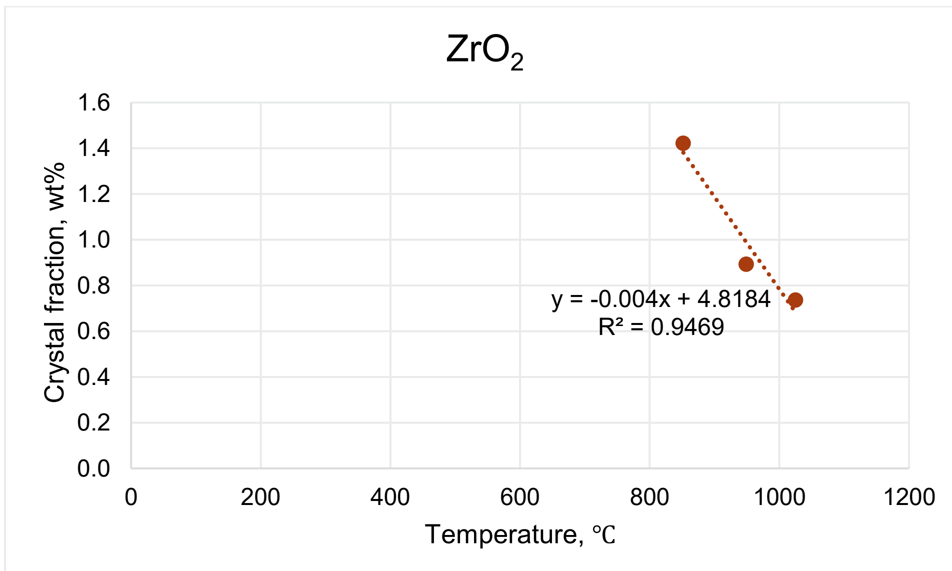

Figure I.74. The liquidus temperature plot for ZrO_2 in glass HAL24M2-10 showing the linear T_L at 1194 °C ($R^2 = 0.9469$).

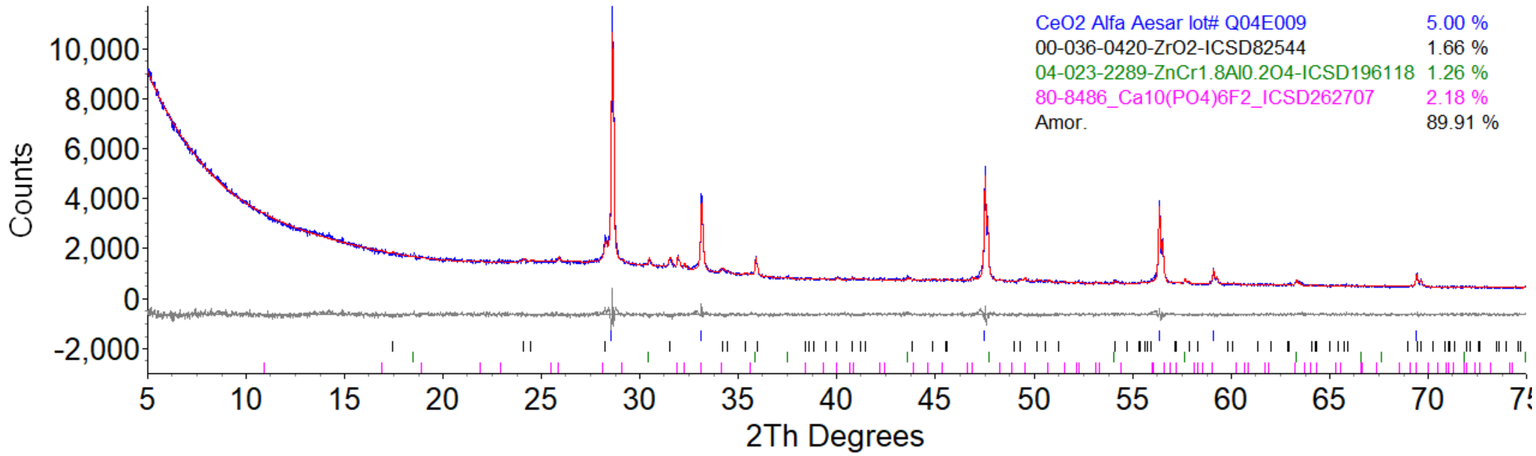

Figure I.75. XRD of glass HAL24M2-10 at 950 °C showing crystalline phases, ZrO_2, $ZnCr_{1.8}Al_{0.2}O_4$, and $Ca_{10}(PO_4)_6F_2$.

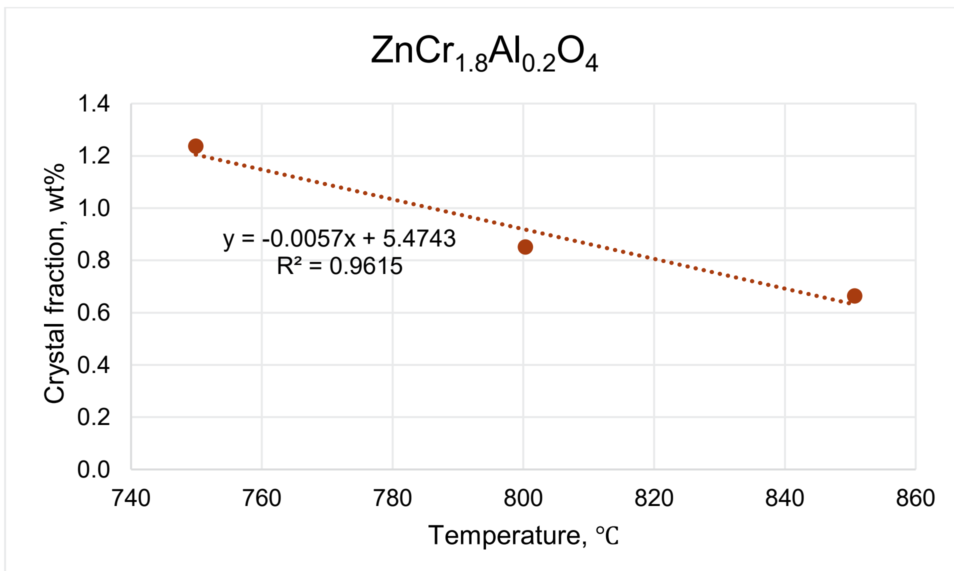

Figure I.76. The liquidus temperature plot for $ZnCr_{1.8}Al_{0.2}O_4$ in glass HAL24M2-11 showing the linear T_L at 962 °C ($R^2 = 0.9672$).

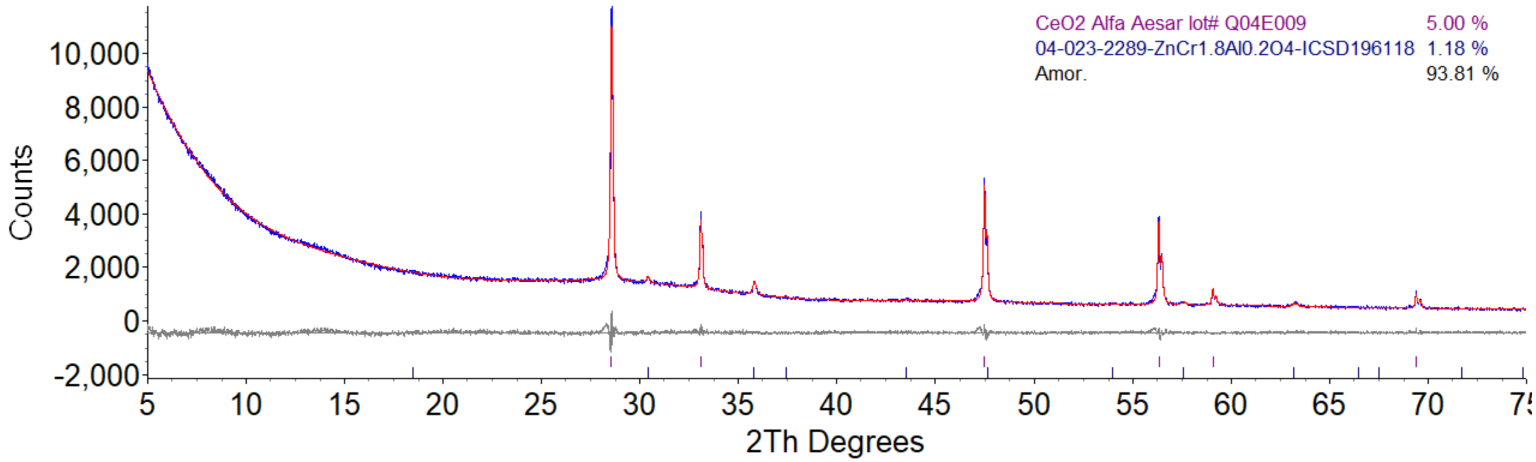

Figure I.77. XRD of glass HAL24M2-11 at 950 °C showing crystalline phase, $ZnCr_{1.8}Al_{0.2}O_4$.

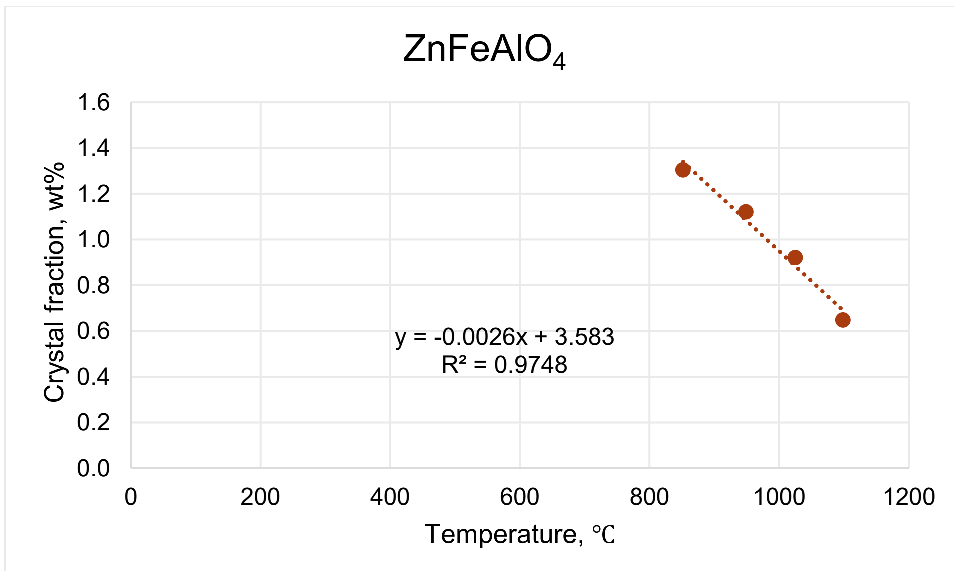

Figure I.78. The liquidus temperature plot for $ZnFeAlO_4$ in glass HAL24M2-12 showing the linear T_L at 1360 °C ($R^2 = 0.9748$).

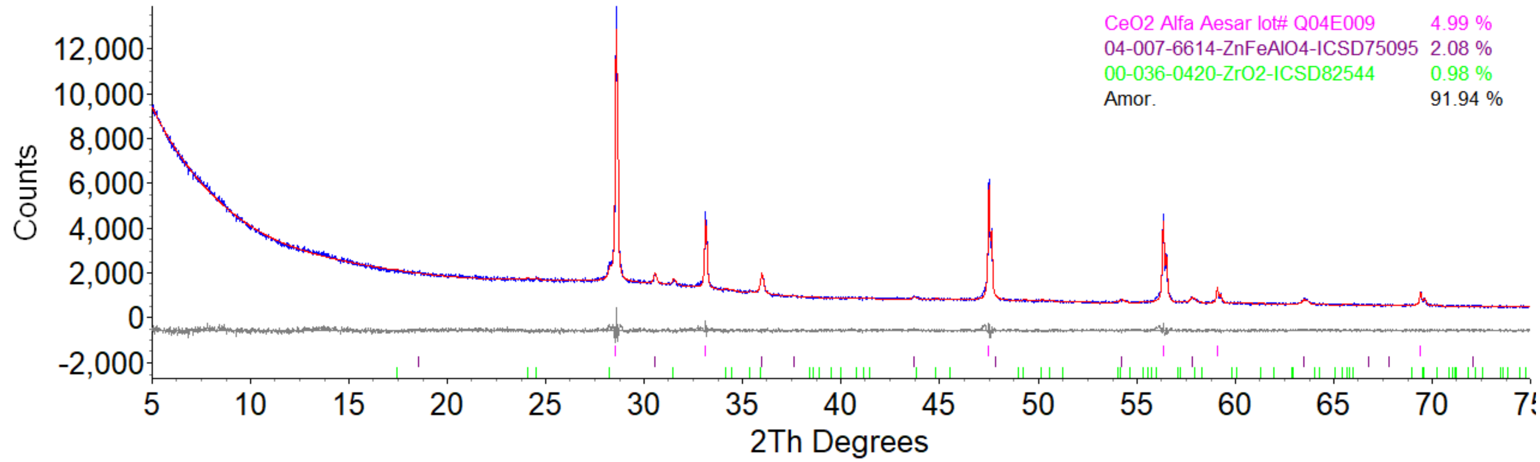

Figure I.79. XRD of glass HAL24M2-12 at 950 °C showing crystalline phases, $ZnFeAlO_4$ and ZrO_2.

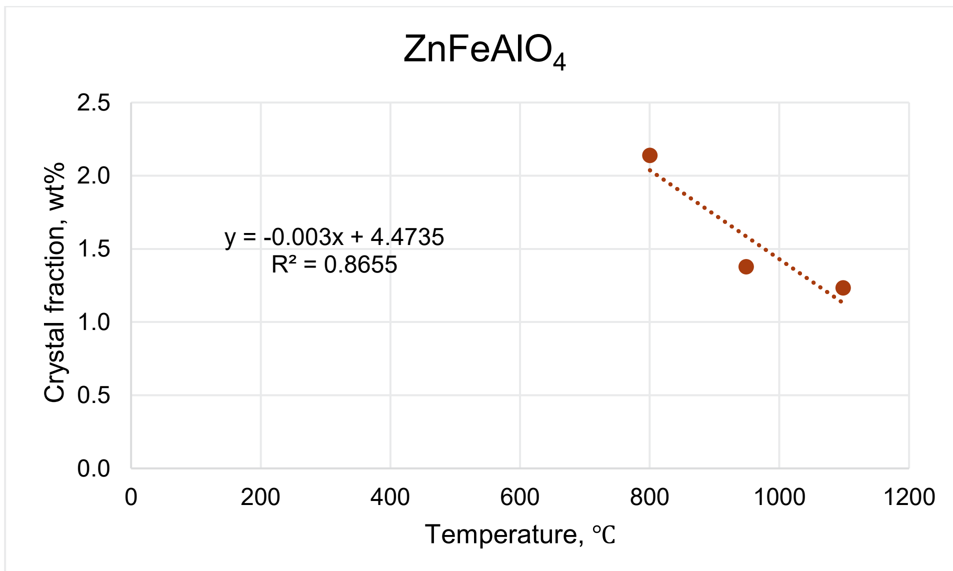

Figure I.80. The liquidus temperature plot for $ZnFeAlO_4$ in glass HAL24M2-13 showing the linear T_L at 1470 °C (R^2 = 0.8655).

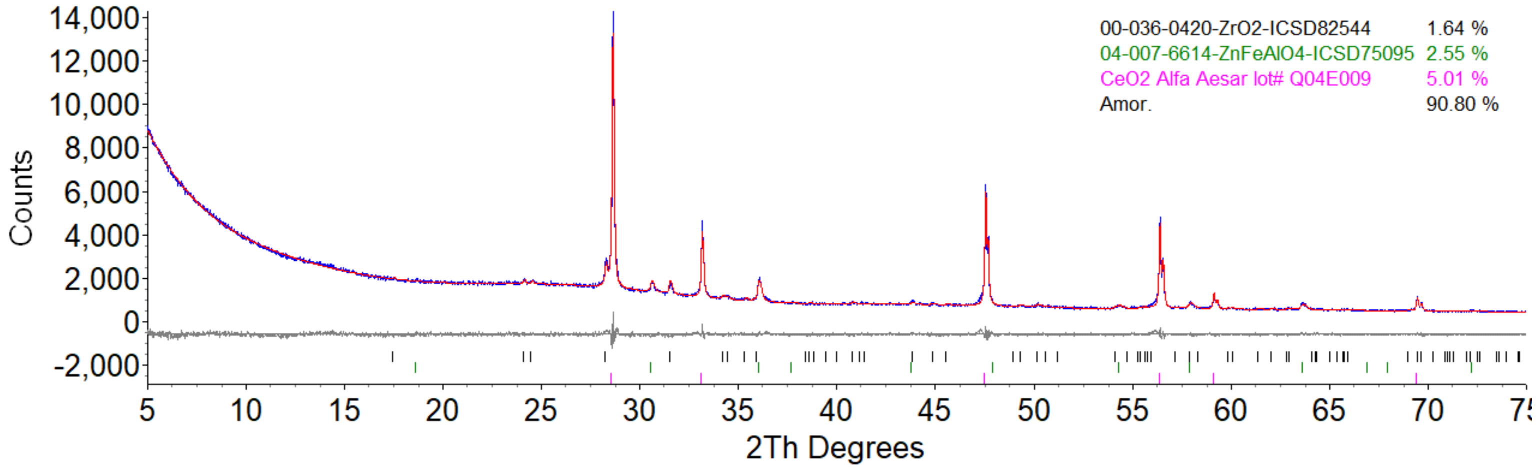

Figure I.81. XRD of glass HAL24M2-13 at 950 °C showing crystalline phase, ZrO_2 and $FeNi_2O_4$.

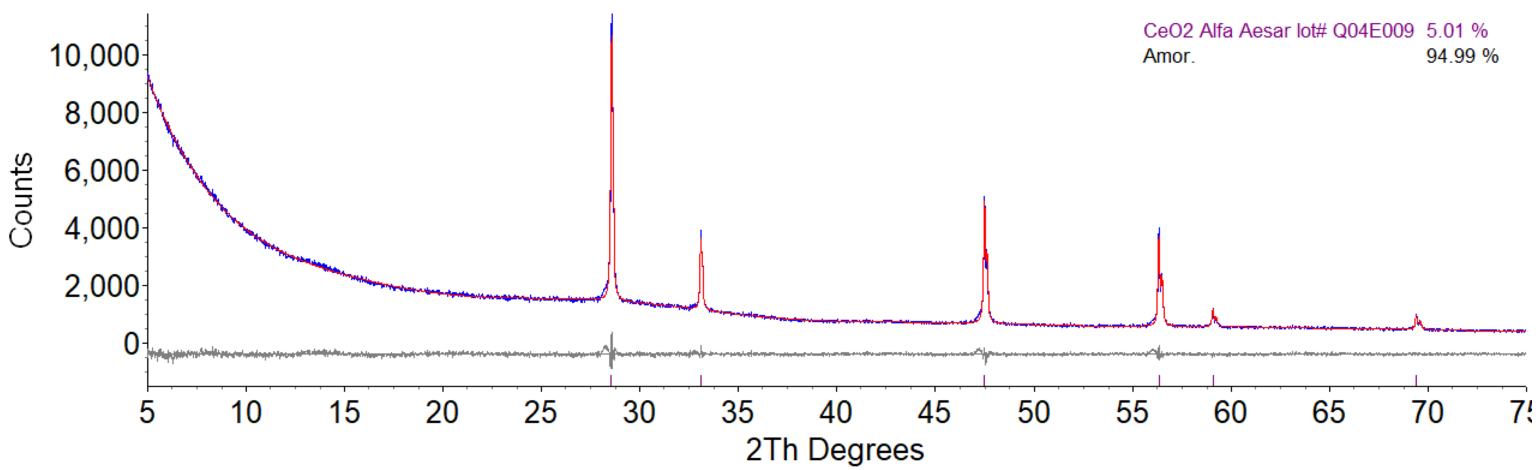

Figure I.82. XRD of glass HAL24M2-14 at 950 °C revealed an amorphous structure. The glass was fully amorphous at 900 °C, and the liquidus temperature is between 850 °C and 900 °C.

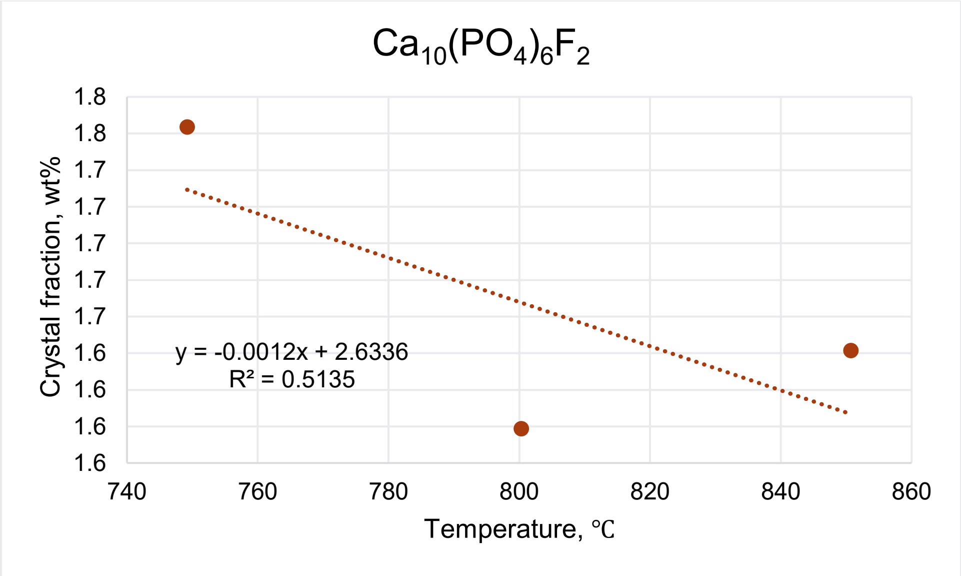

Figure I.83. The glass HAL24M2-15 was fully amorphous at 900 °C, and the liquidus temperature is between 850 °C and 900 °C. Fitting was bad to project the linear T_L.

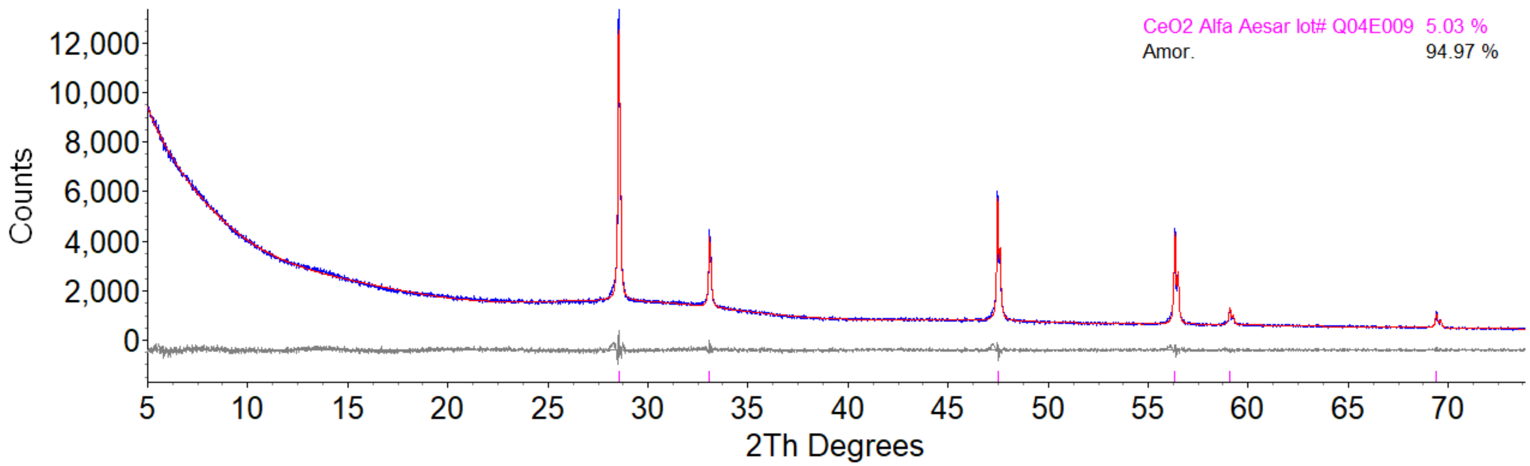

Figure I.84. XRD of glass HAL24M2-15 at 950 °C revealed an amorphous structure.

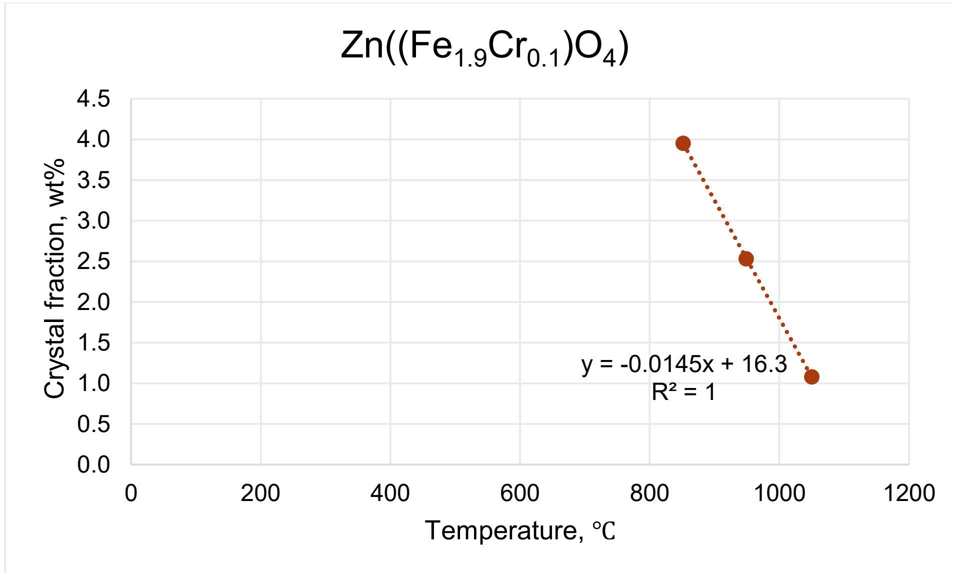

Figure I.85. The liquidus temperature plot for $Zn((Fe_{1.9}Cr_{0.1})O_4)$ in glass HAL24M2-16 showing the linear T_L at 1124 °C ($R^2 = 1$).

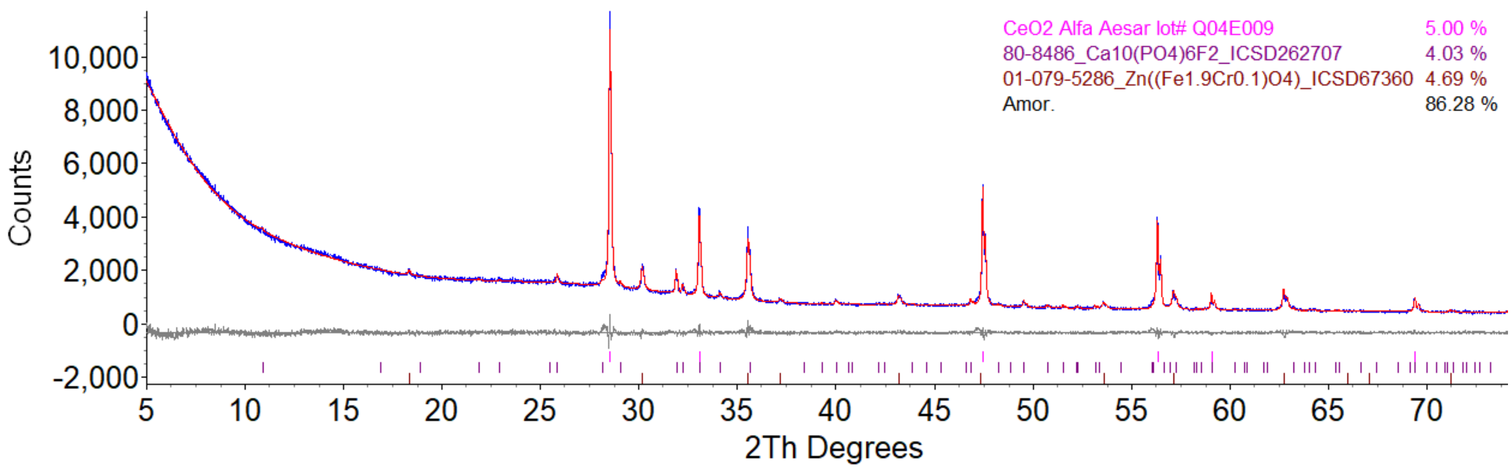

Figure I.86. XRD of glass HAL24M2-16 at 950 °C showing crystalline phase, $Ca_{10}(PO_4)_6F_2$ and $Zn((Fe_{1.9}Cr_{0.1})O_4)$.

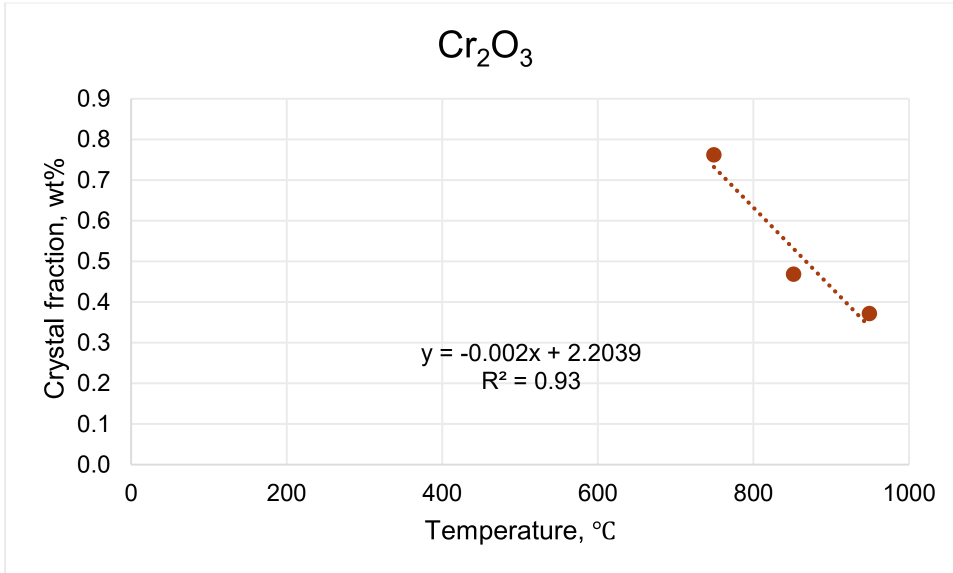

Figure I.87. The liquidus temperature plot for Cr_2O_3 in glass HAL24M2-17 showing the linear T_L at 1122 °C (R^2 = 0.93).

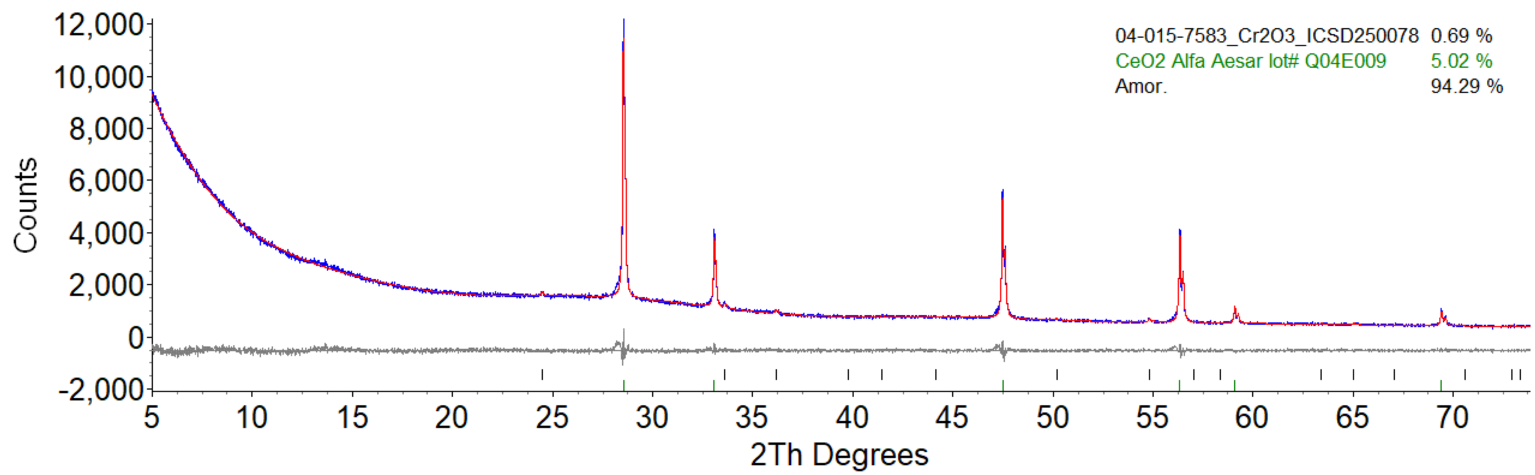

Figure I.88. XRD of glass HAL24M2-17 at 950 °C showing crystalline phase, Cr_2O_3.

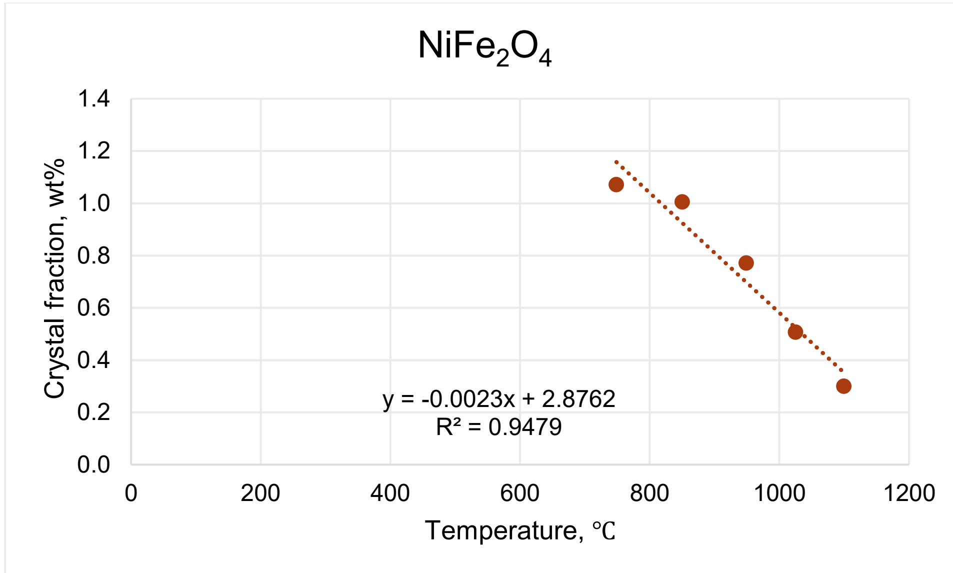

Figure I.89. The liquidus temperature plot for $NiFe_2O_4$ in glass HAL24M2-18 showing the linear T_L at 1253 °C (R^2 = 0.9479).

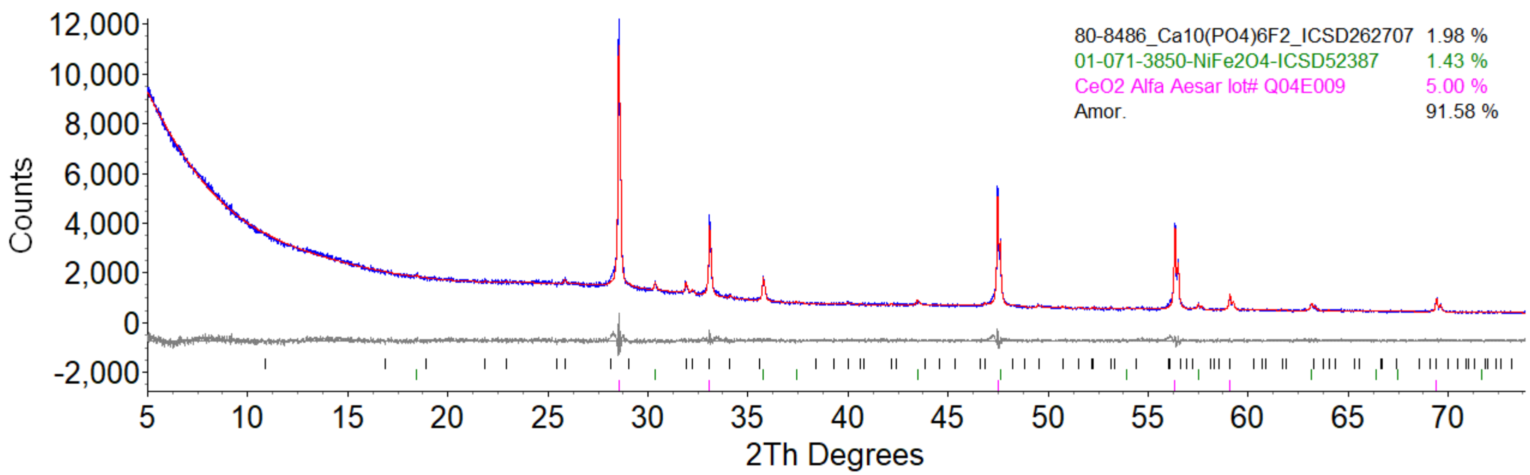

Figure I.90. XRD of glass HAL24M2-18 at 950 °C showing crystalline phase, $Ca_{10}(PO_4)_6F_2$ and $NiFe_2O_4$.

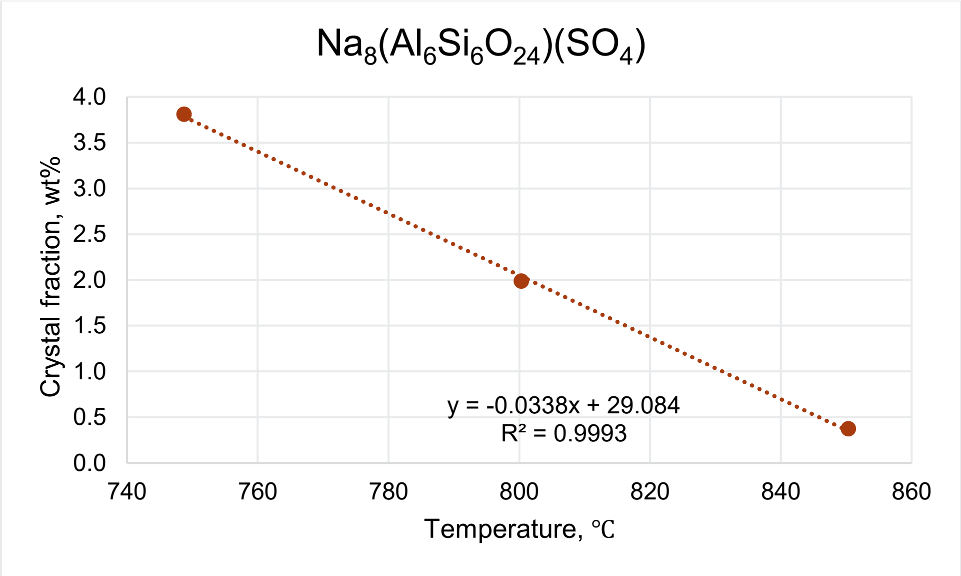

Figure I.91. The liquidus temperature plot for Nosean ($Na_8(Al_6Si_6O_{24})(SO_4)$) in glass HAL24M2-19 showing the linear T_L at 861 °C ($R^2 = 0.9993$).

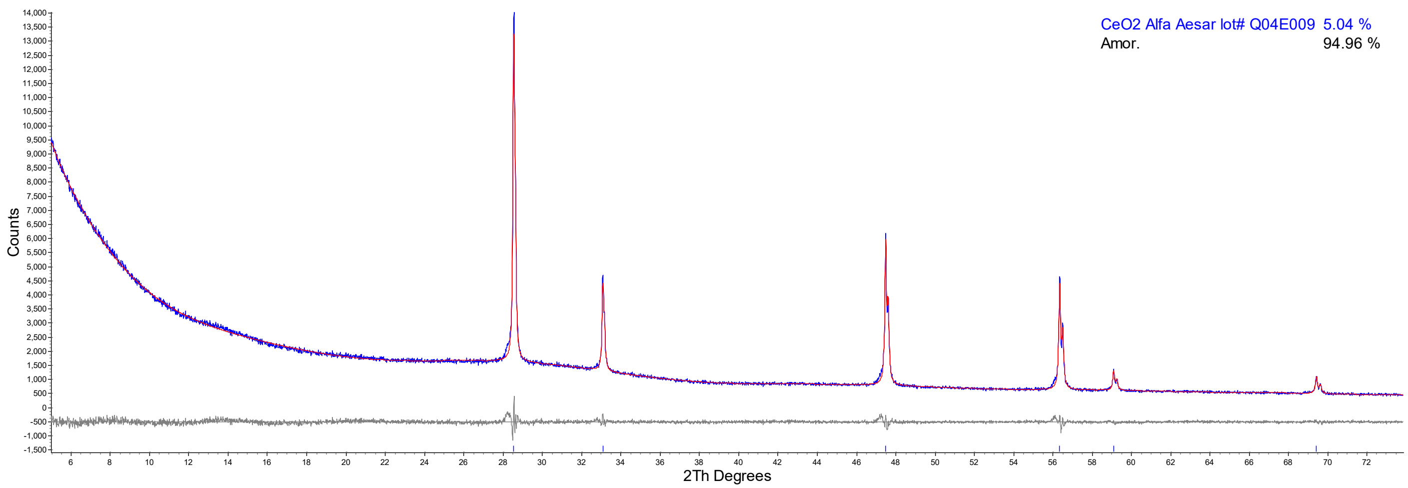

Figure I.92. XRD of glass HAL24M2-19 at 950 °C showing crystalline phase, Nosean ($Na_8(Al_6Si_6O_{24})(SO_4)$).

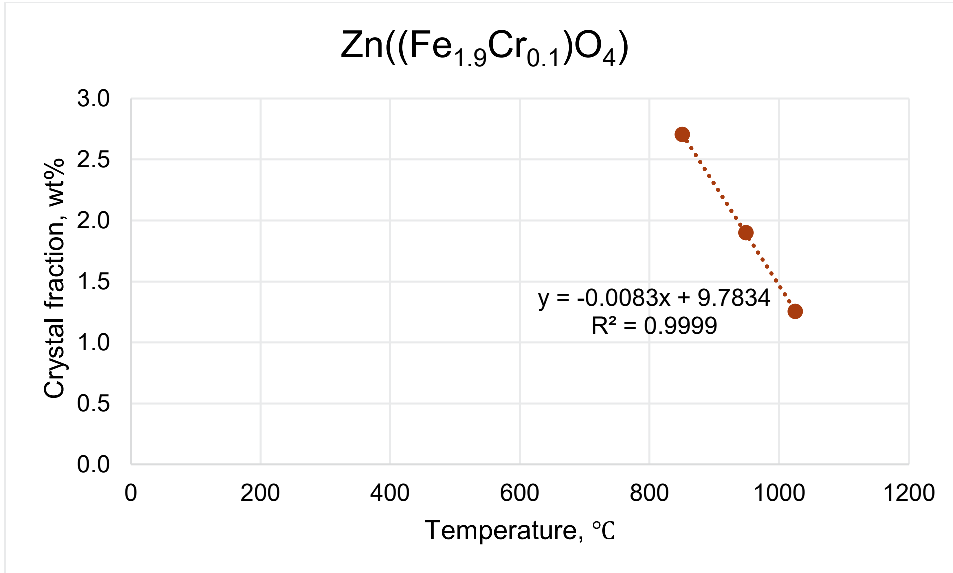

Figure I.93. The liquidus temperature plot for $Zn((Fe_{1.9}Cr_{0.1})O_4)$ in glass HAL24M2-20 showing the linear T_L at 1176 °C ($R^2 = 0.9999$).

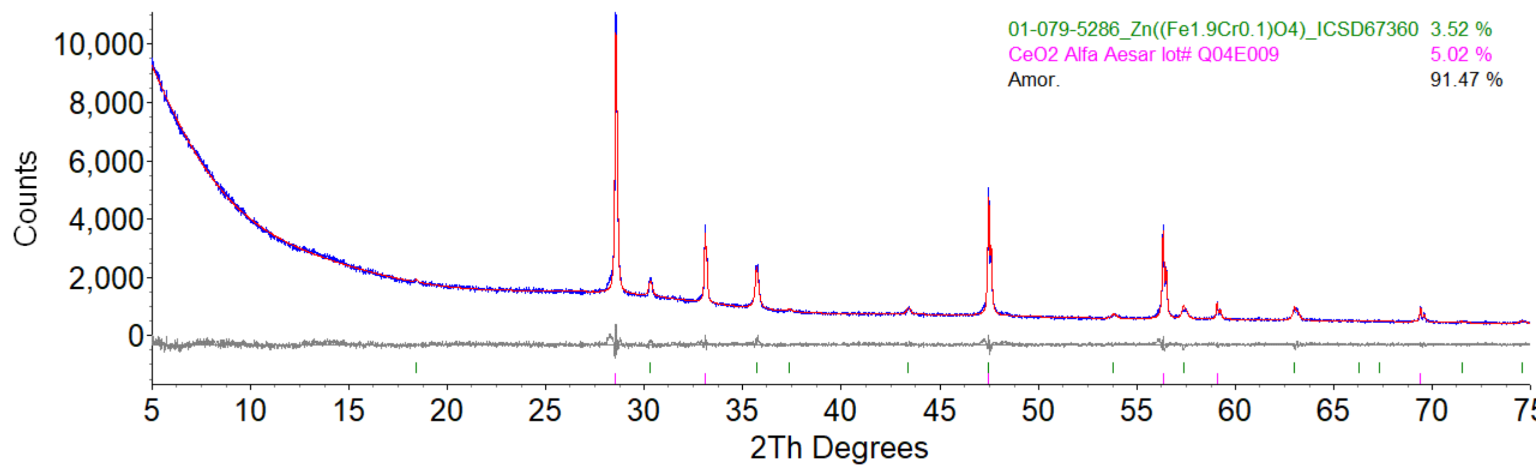

Figure I.94. XRD of glass HAL24M2-20 at 950 °C showing crystalline phase, $Zn((Fe_{1.9}Cr_{0.1})O_4)$.

Appendix J – Viscosity Data

This appendix contains the temperatures at which viscosity was measured (Table J.1), and the measured viscosity data, also found in Table 3.6, for each of the glasses in this matrix. The actual temperatures at which the viscosity was measured were not recorded for the HAL24M1 glasses.

The plots shown in this appendix are fitted to the Arrhenius equation:

$$\ln(\eta) = A + \frac{B}{T_K} \quad \text{(J.1)}$$

where A and B are independent of temperature and temperature (T_K) is in K (T(°C) + 273.15).

Table J.1. Temperatures (°C) at which the viscosities have been measured in order of measurement.

Glass ID	Temperature (°C)					
HAL24M2-01	1155	1067	975	1158	1249	1159
HAL24M2-02	1156	1067	975	1158	1247	1157
HAL24M2-03	1158	1067	975	1158	1248	1158
HAL24M2-04-1	1155	1067	975	1158	1248	1157
HAL24M2-05	1157	1068	975	1157	1247	1158
HAL24M2-06	1158	1068	976	1158	1248	1159
HAL24M2-07	1156	1067	925	1158	1248	1157
HAL24M2-08	1157	1068	NM	1158	1247	1158
HAL24M2-09	1155	1066	975	1157	1247	1157
HAL24M2-10	1158	1068	NM	1158	1247	1157
HAL24M2-11	1156	1066	974	1157	1246	1156
HAL24M2-12	1157	1067	949	1155	1248	1158
HAL24M2-13	1157	1066	976	1157	1248	1157
HAL24M2-14	1158	1067	975	1157	1248	1158
HAL24M2-15	1157	1067	976	1158	1248	1158
HAL24M2-16	1155	1065	NM	1157	1247	1157
HAL24M2-17	1158	1066	978	1158	1248	1158
HAL24M2-18	1158	1058	974	1158	1247	1156
HAL24M2-19	1158	1068	976	1158	1248	1159
HAL24M2-20	1158	1068	975	1159	1249	1159

NM = not measured

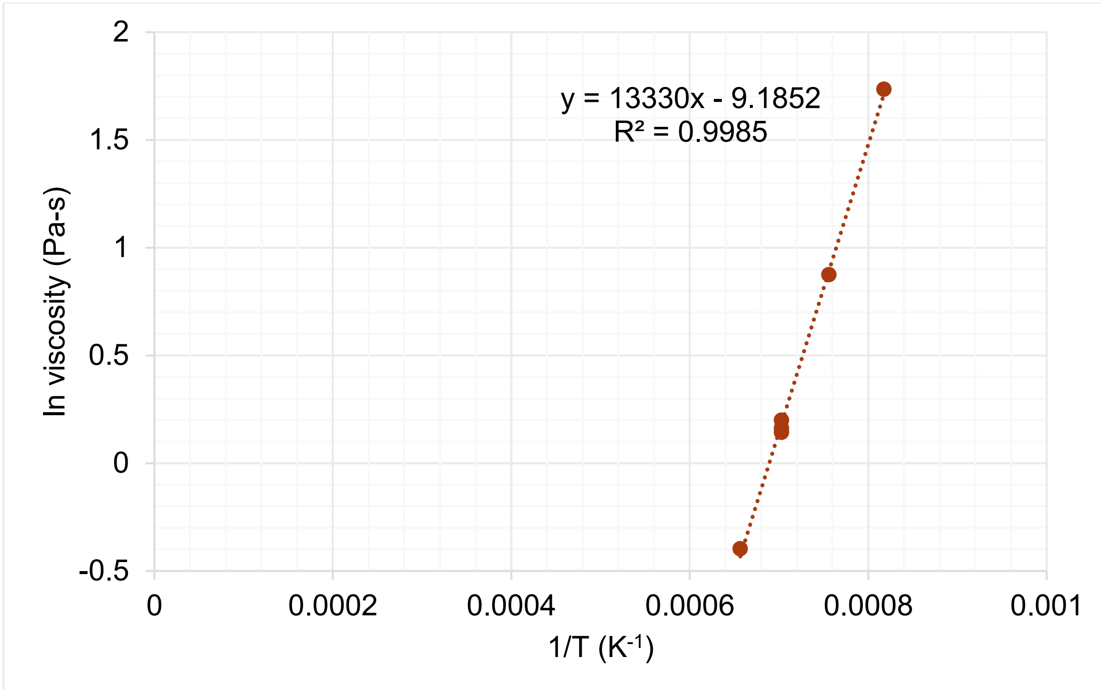

Figure J.1. Viscosity-temperature data and Arrhenius equation fit for HAL24M1-01.

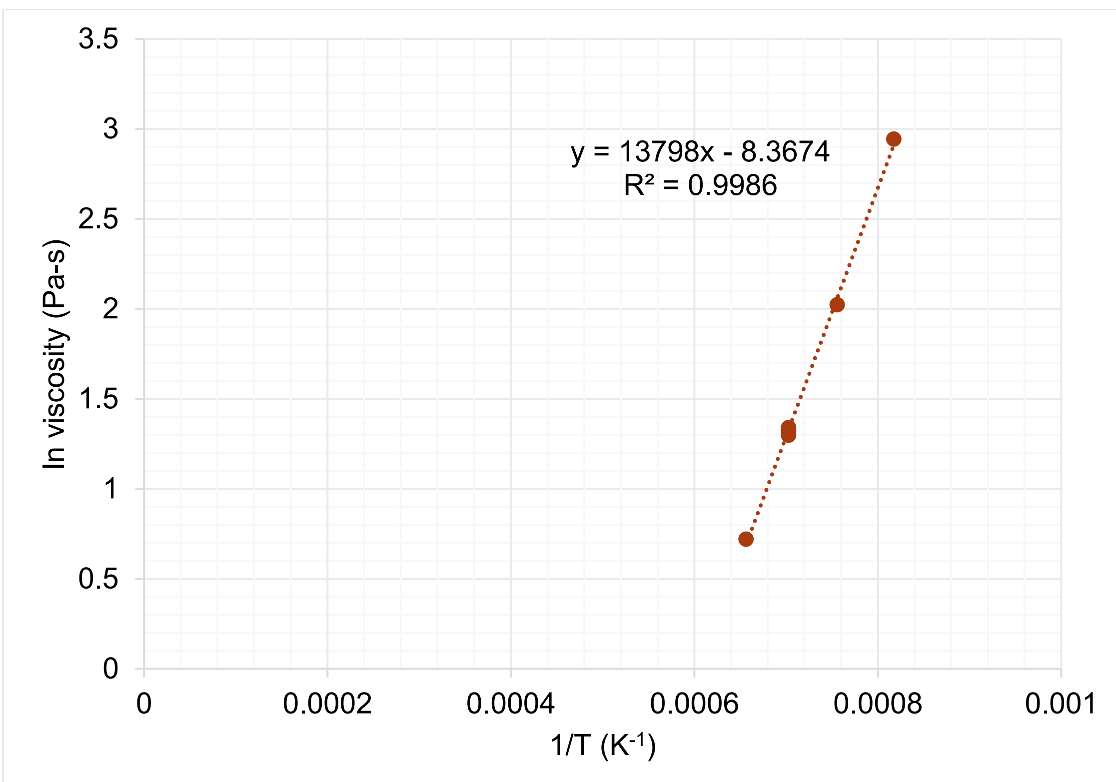

Figure J.2. Viscosity-temperature data and Arrhenius equation fit for HAL24M1-02.

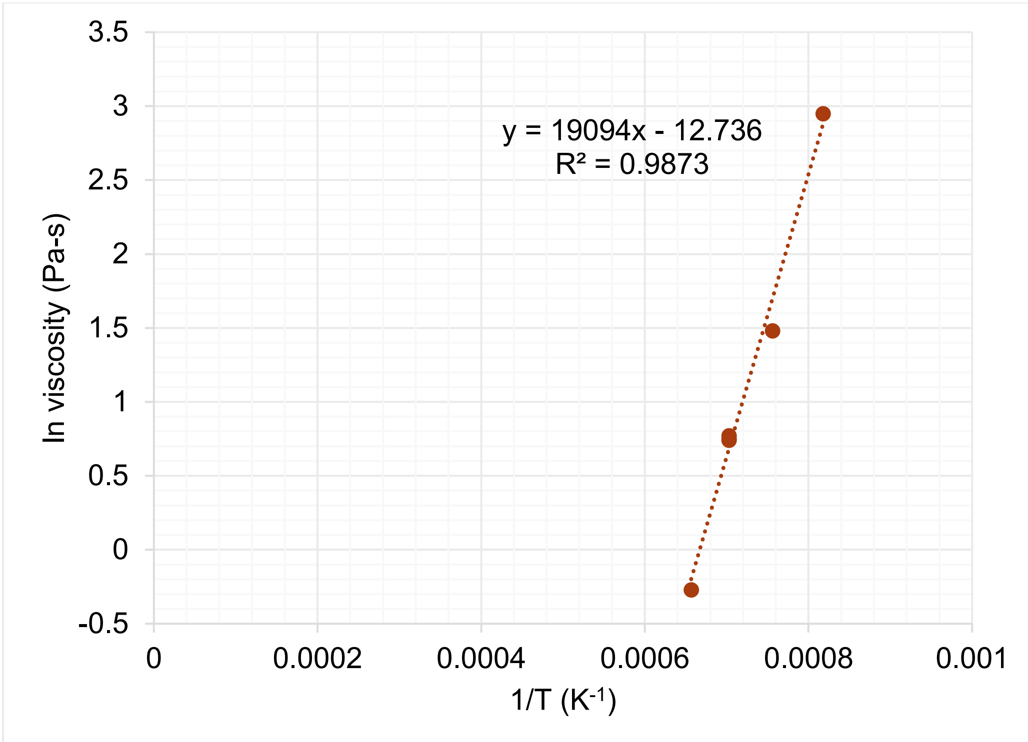

Figure J.3. Viscosity-temperature data and Arrhenius equation fit for HAL24M1-03.

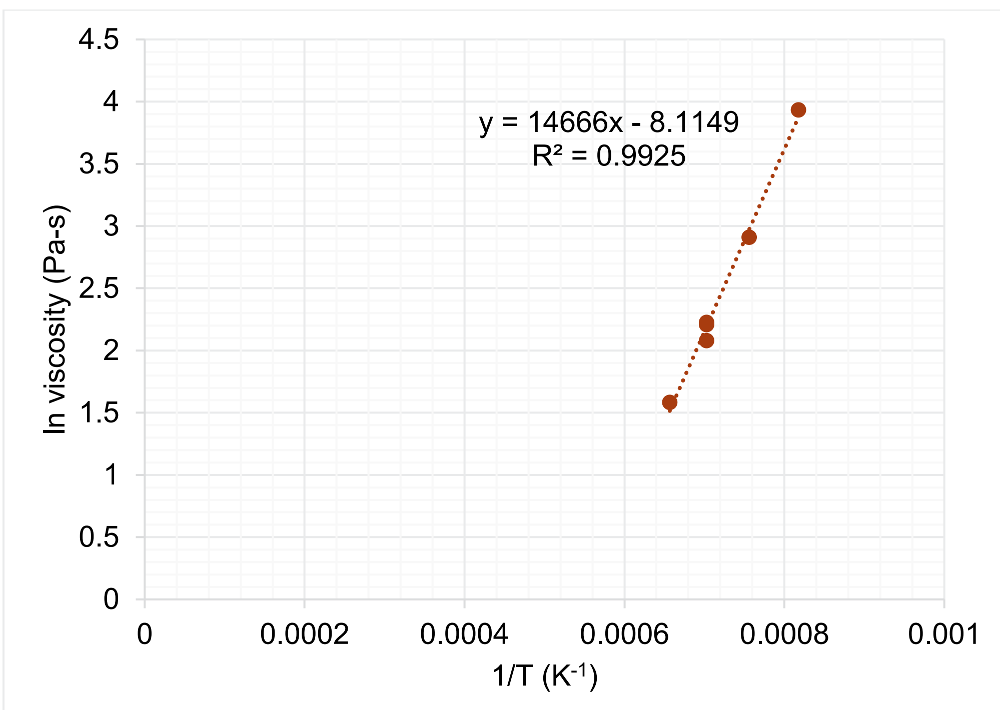

Figure J.4. Viscosity-temperature data and Arrhenius equation fit for HAL24M1-04.

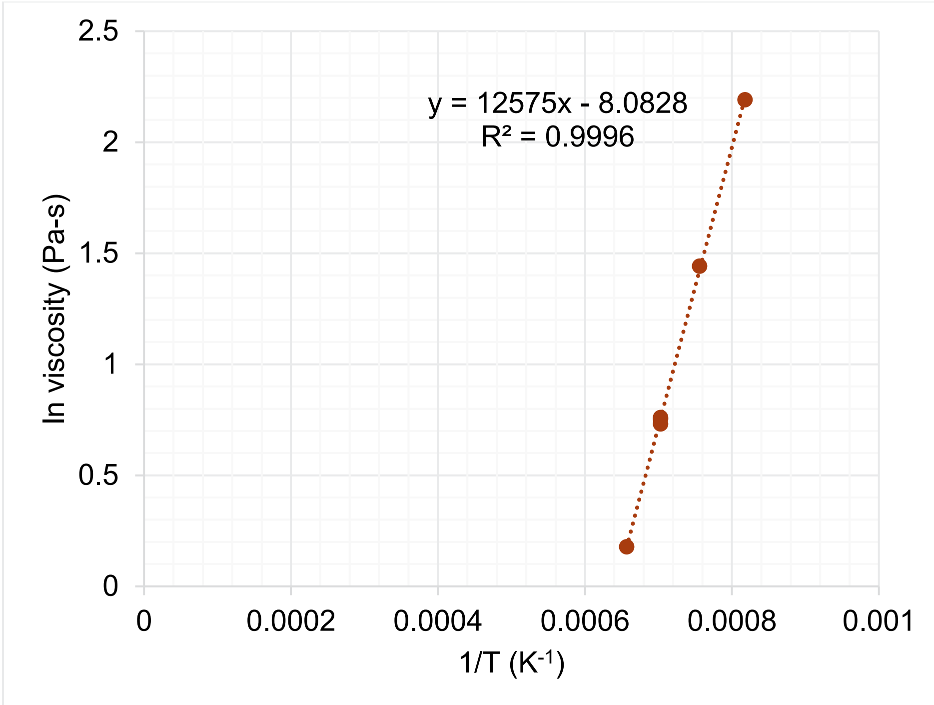

Figure J.5. Viscosity-temperature data and Arrhenius equation fit for HAL24M1-05.

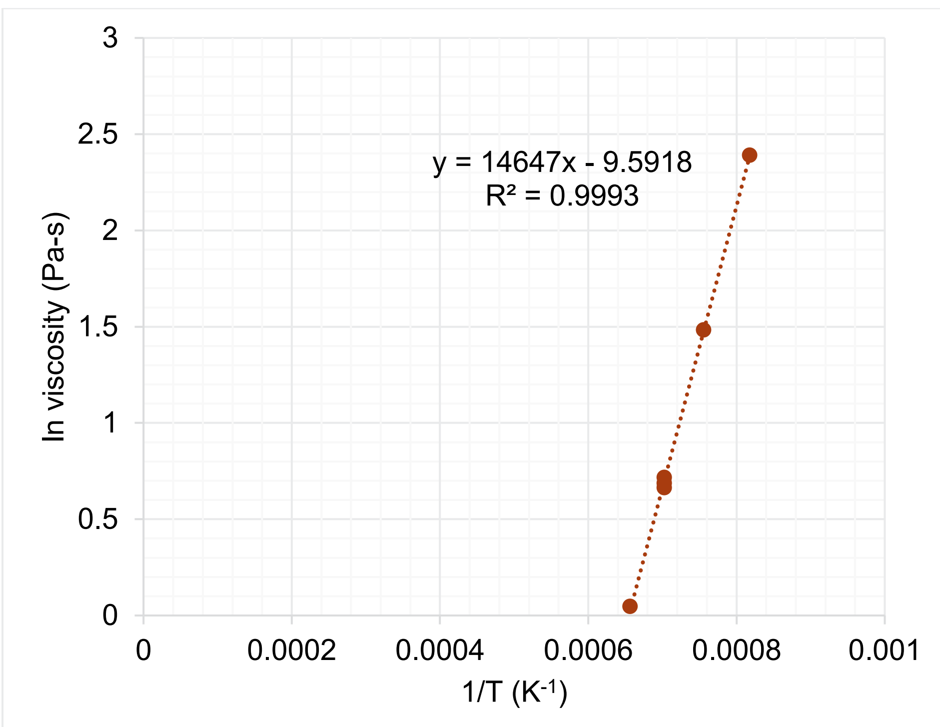

Figure J.6. Viscosity-temperature data and Arrhenius equation fit for HAL24M1-06.

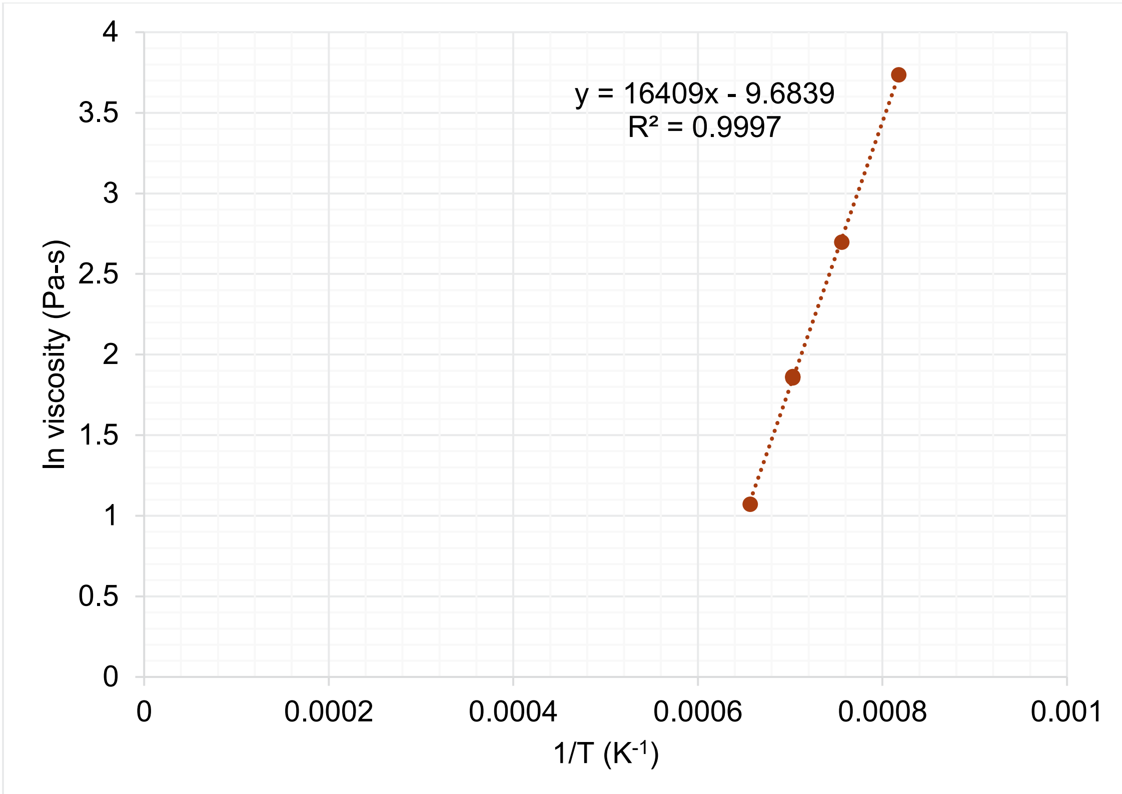

Figure J.7. Viscosity-temperature data and Arrhenius equation fit for HAL24M1-07.

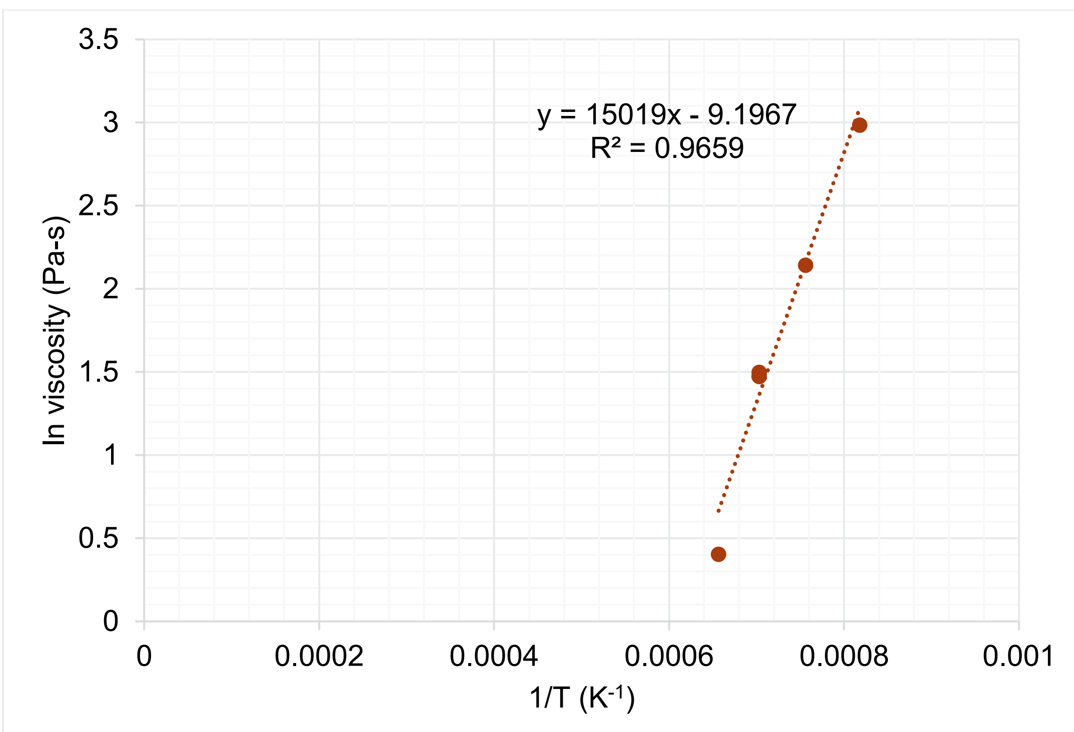

Figure J.8. Viscosity-temperature data and Arrhenius equation fit for HAL24M1-08.

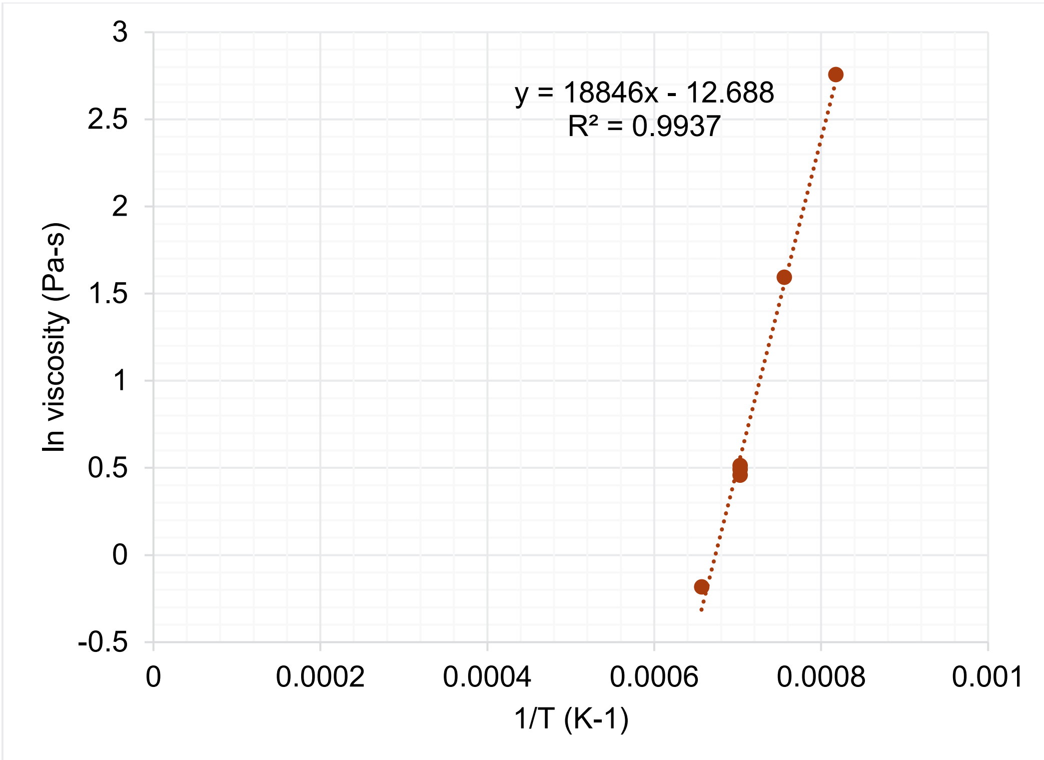

Figure J.9. Viscosity-temperature data and Arrhenius equation fit for HAL24M1-09.

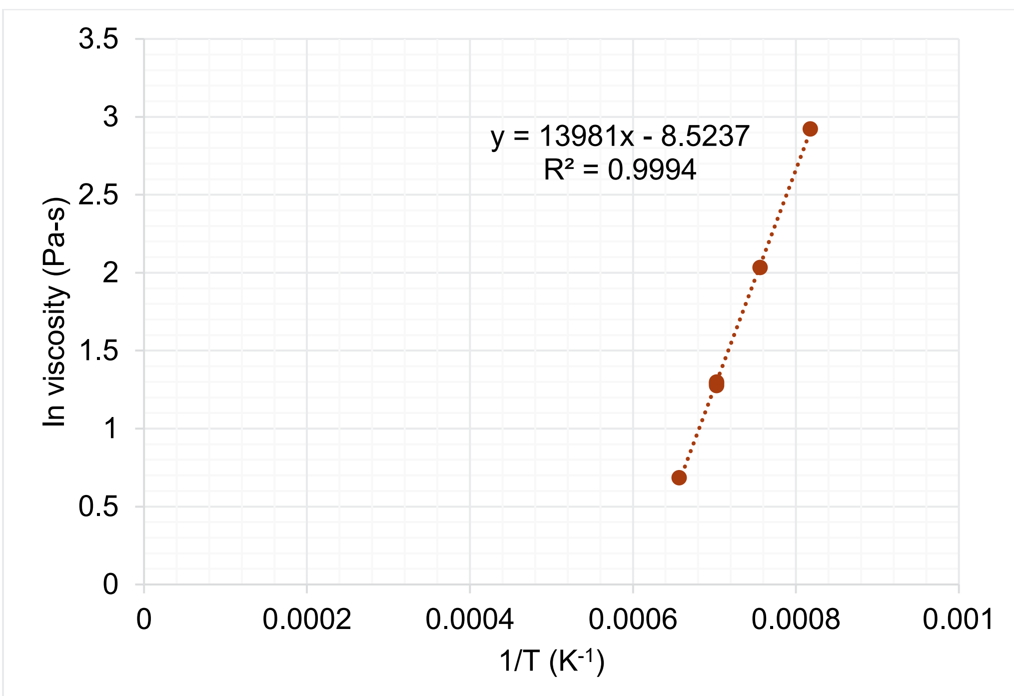

Figure J.10. Viscosity-temperature data and Arrhenius equation fit for HAL24M1-10.

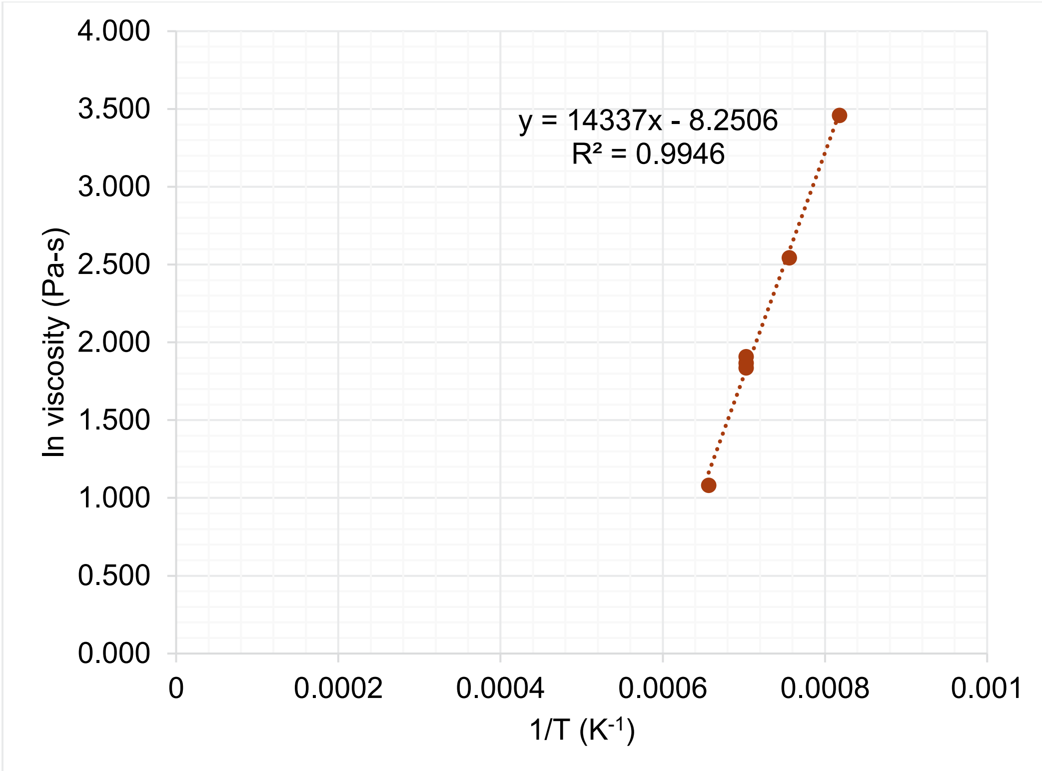

Figure J.11. Viscosity-temperature data and Arrhenius equation fit for HAL24M1-11.

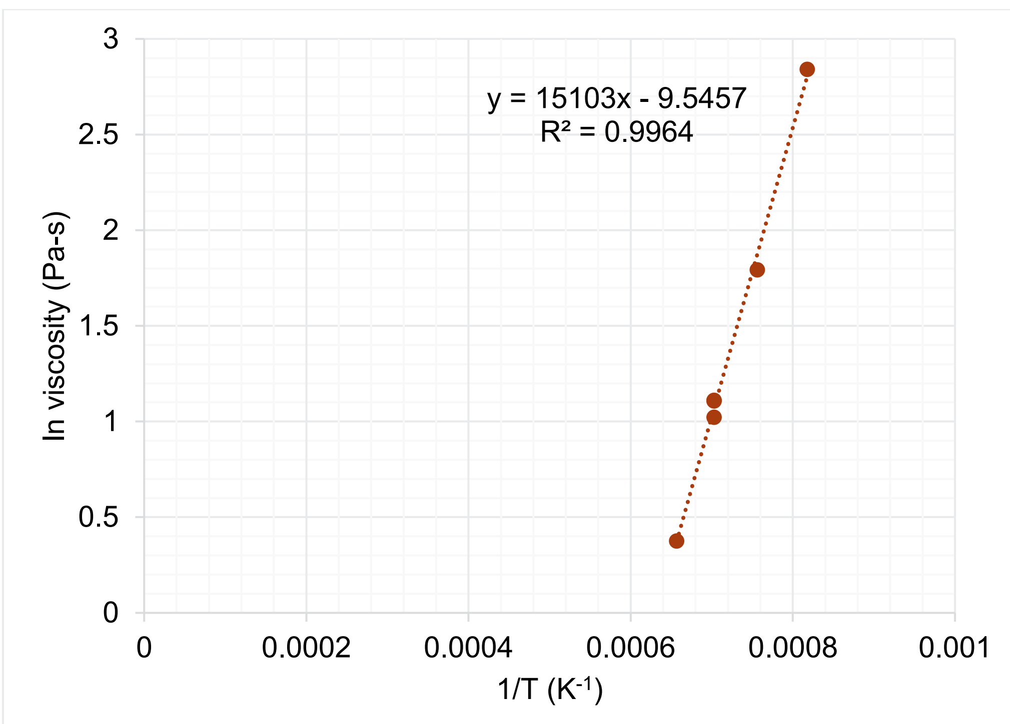

Figure J.12. Viscosity-temperature data and Arrhenius equation fit for HAL24M1-12.

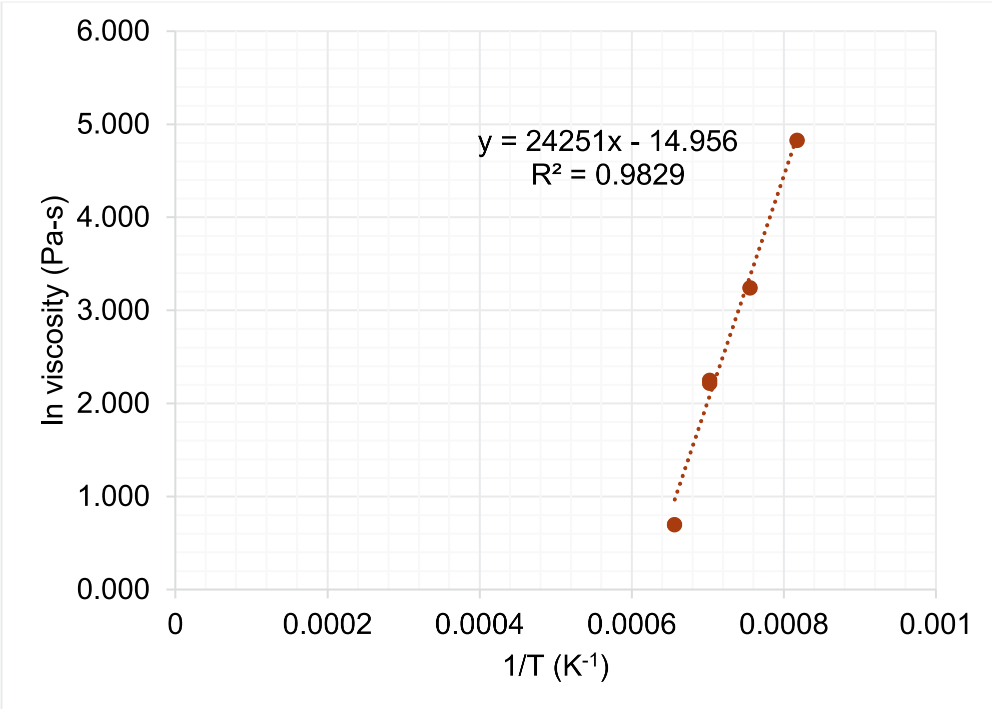

Figure J.13. Viscosity-temperature data and Arrhenius equation fit for HAL24M1-13-1.

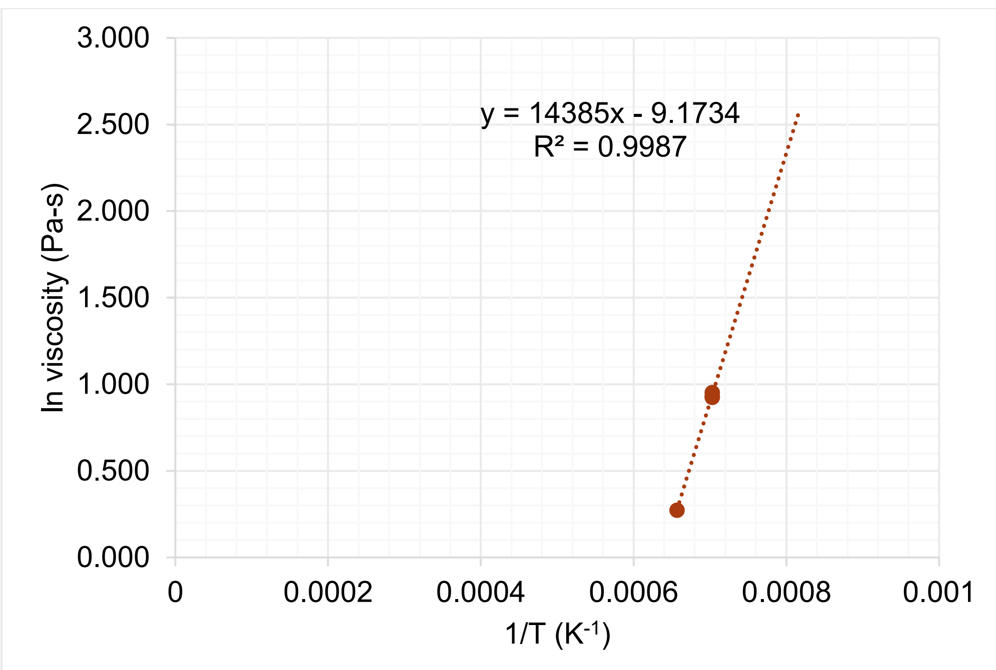

Figure J.14. Viscosity-temperature data and Arrhenius equation fit for HAL24M1-14.

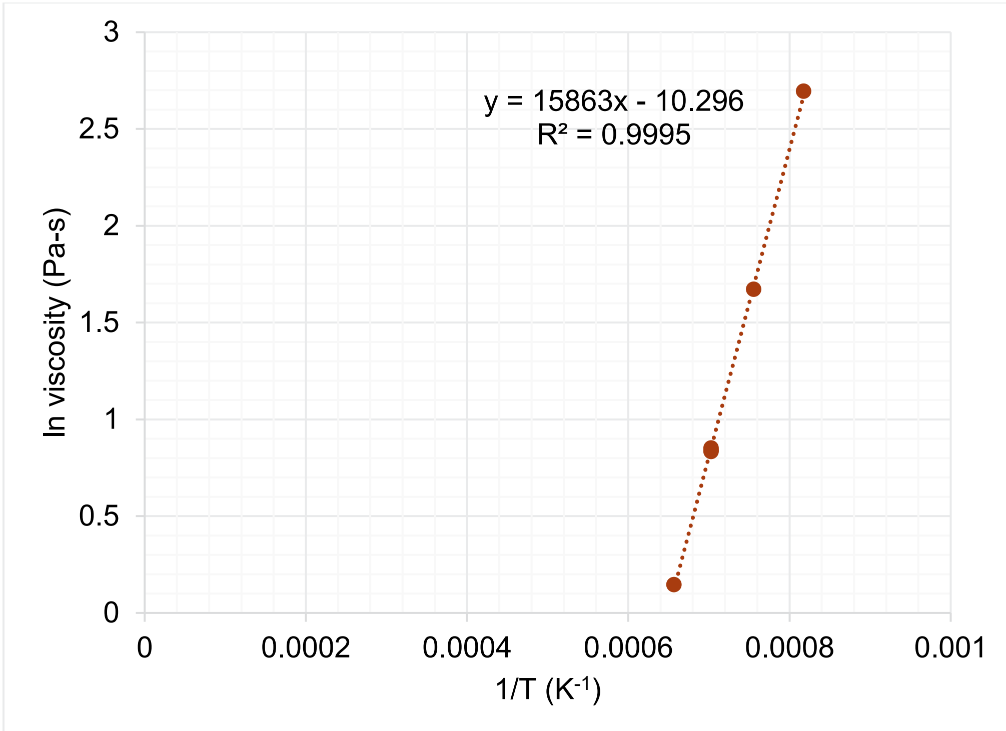

Figure J.15. Viscosity-temperature data and Arrhenius equation fit for HAL24M1-15.

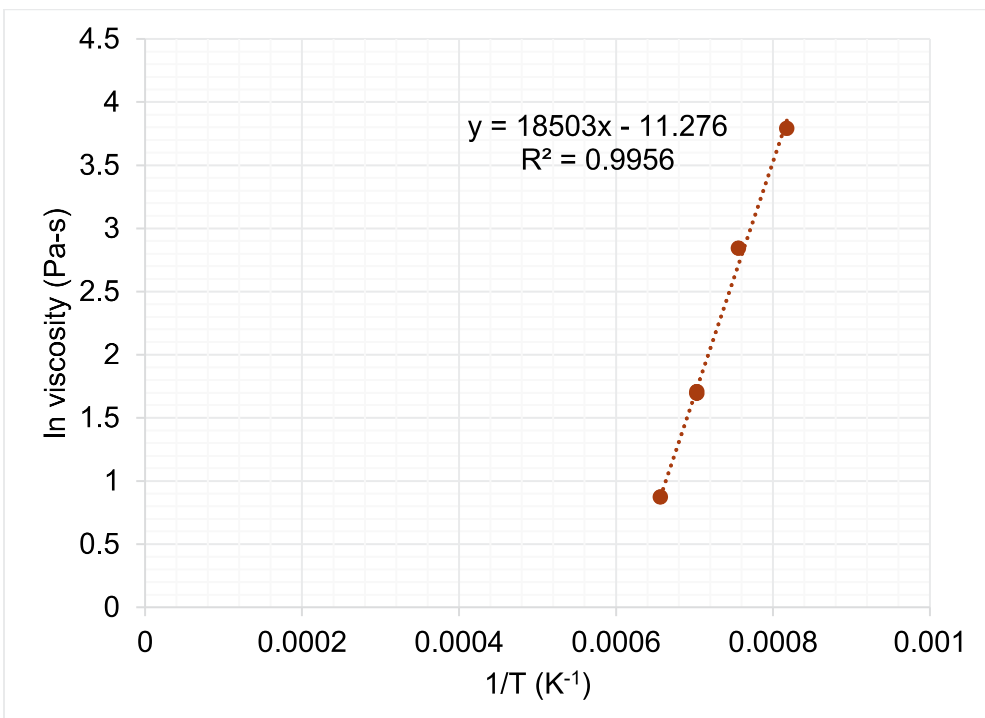

Figure J.16. Viscosity-temperature data and Arrhenius equation fit for HAL24M1-16.

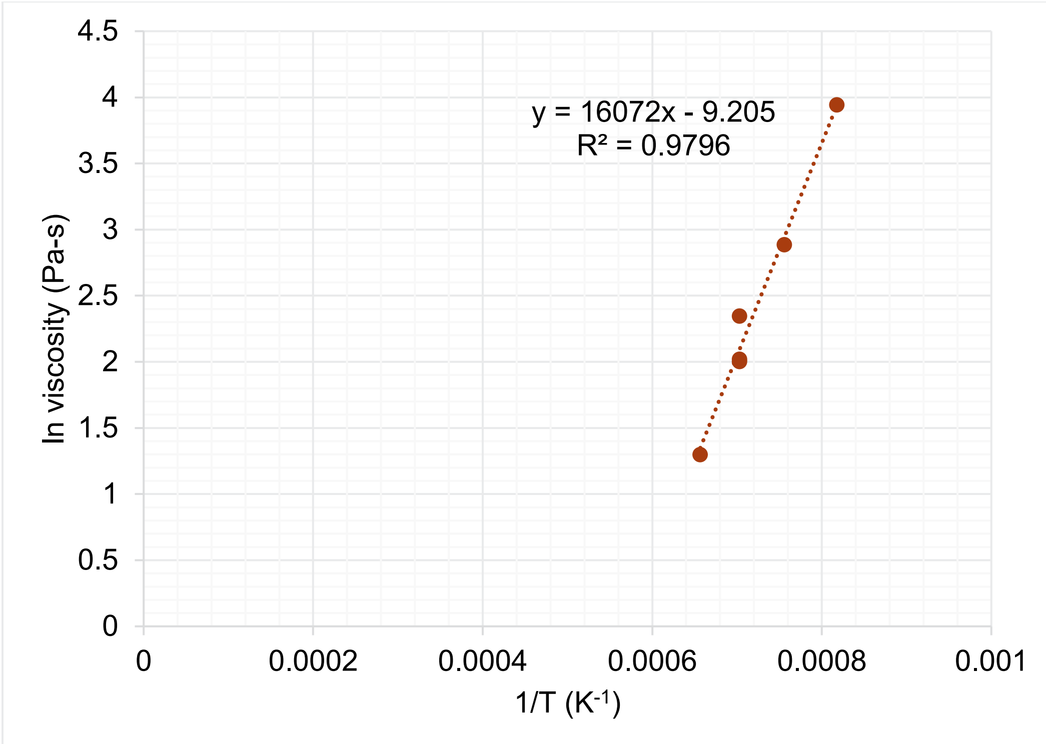

Figure J.17. Viscosity-temperature data and Arrhenius equation fit for HAL24M1-17.

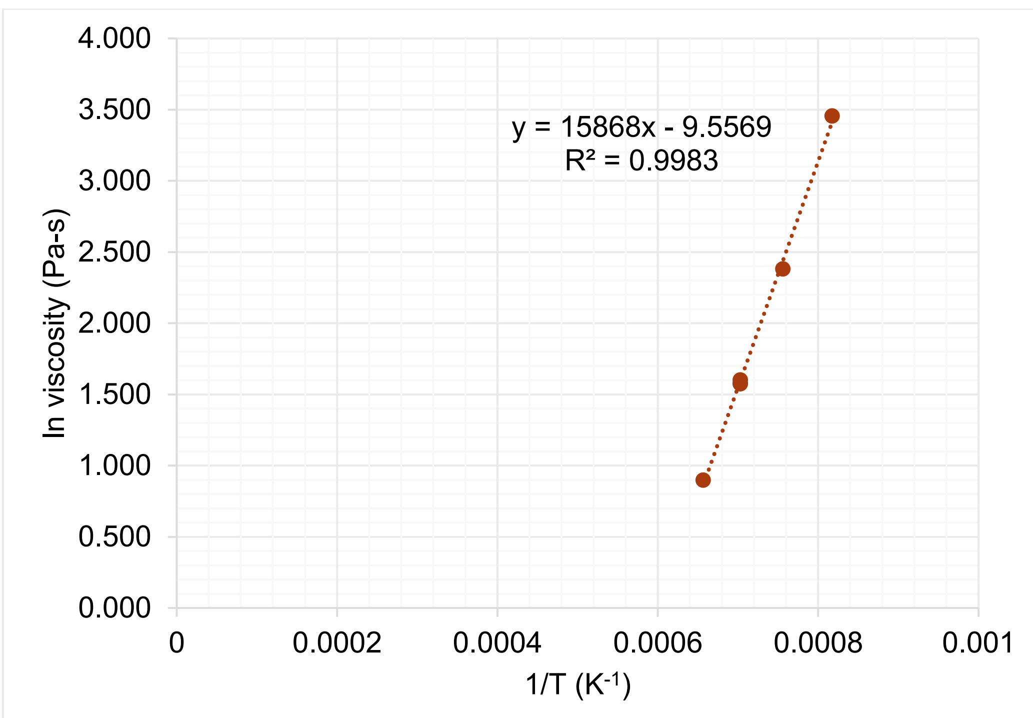

Figure J.18. Viscosity-temperature data and Arrhenius equation fit for HAL24M1-18.

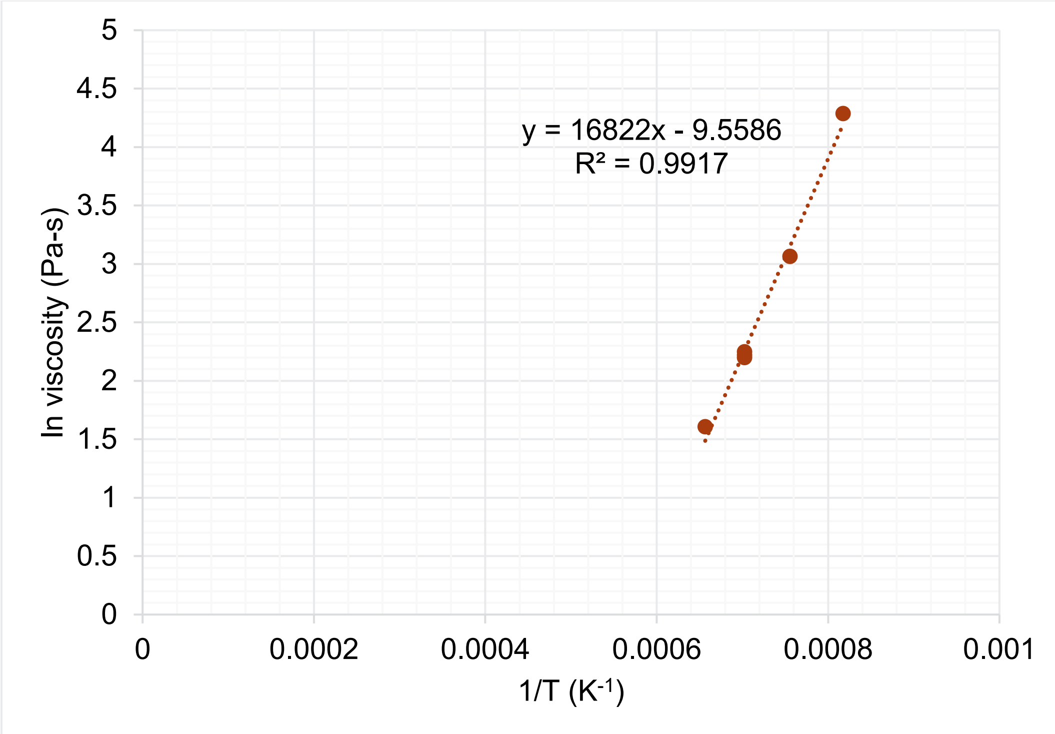

Figure J.19. Viscosity-temperature data and Arrhenius equation fit for HAL24M1-19.

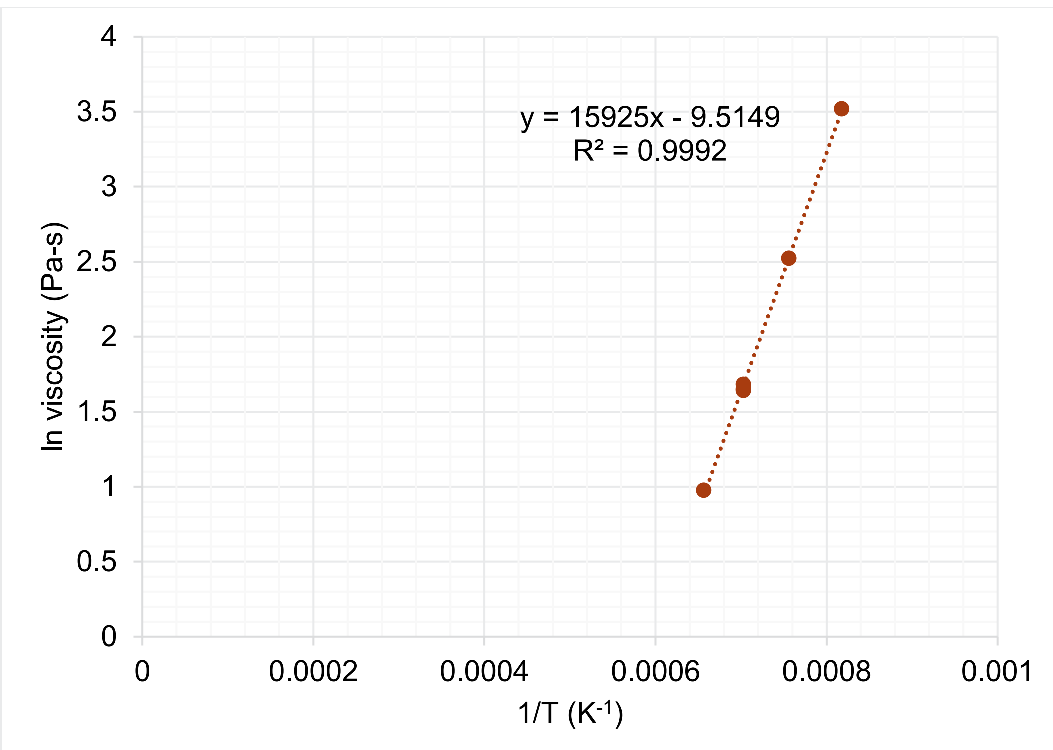

Figure J.20. Viscosity-temperature data and Arrhenius equation fit for HAL24M1-20.

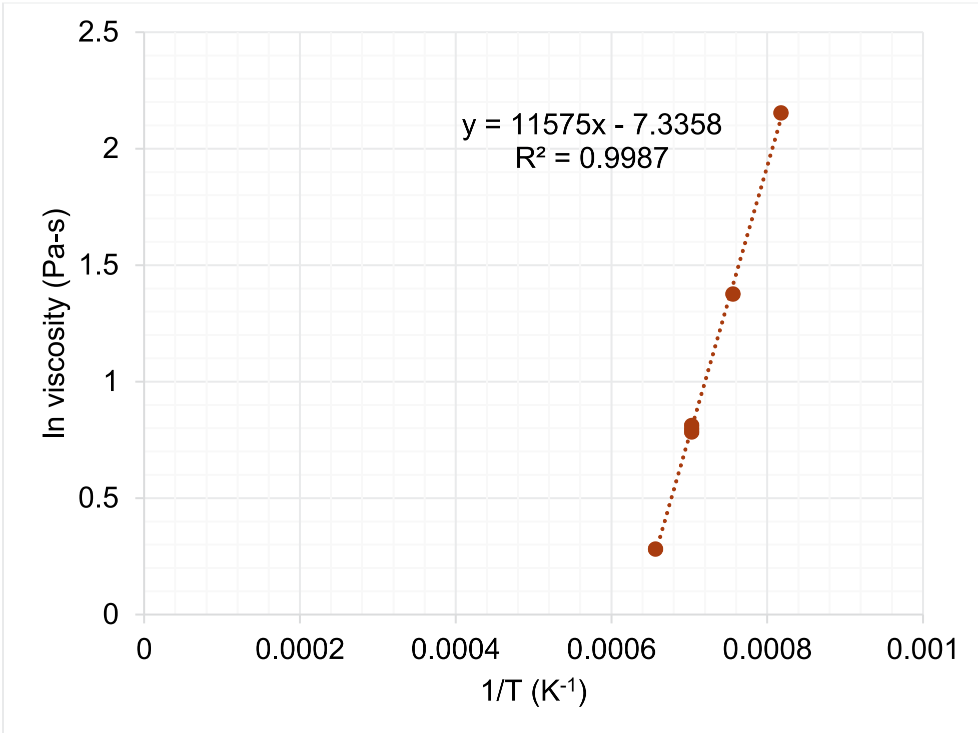

Figure J.21. Viscosity-temperature data and Arrhenius equation fit for HAL24M1-21.

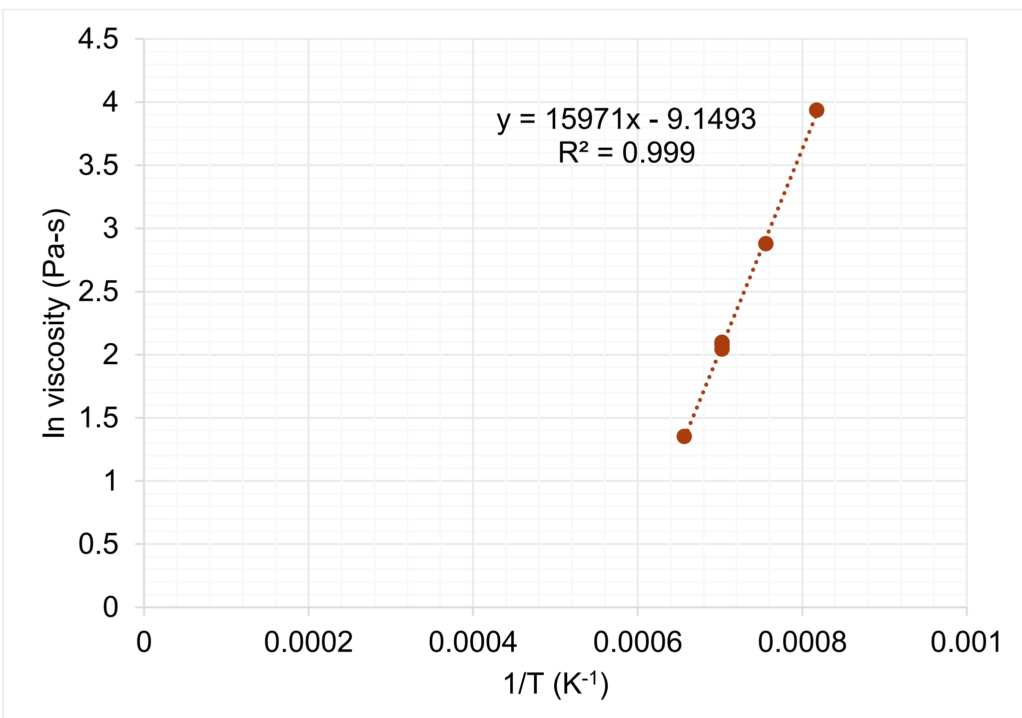

Figure J.22. Viscosity-temperature data and Arrhenius equation fit for HAL24M1-22.

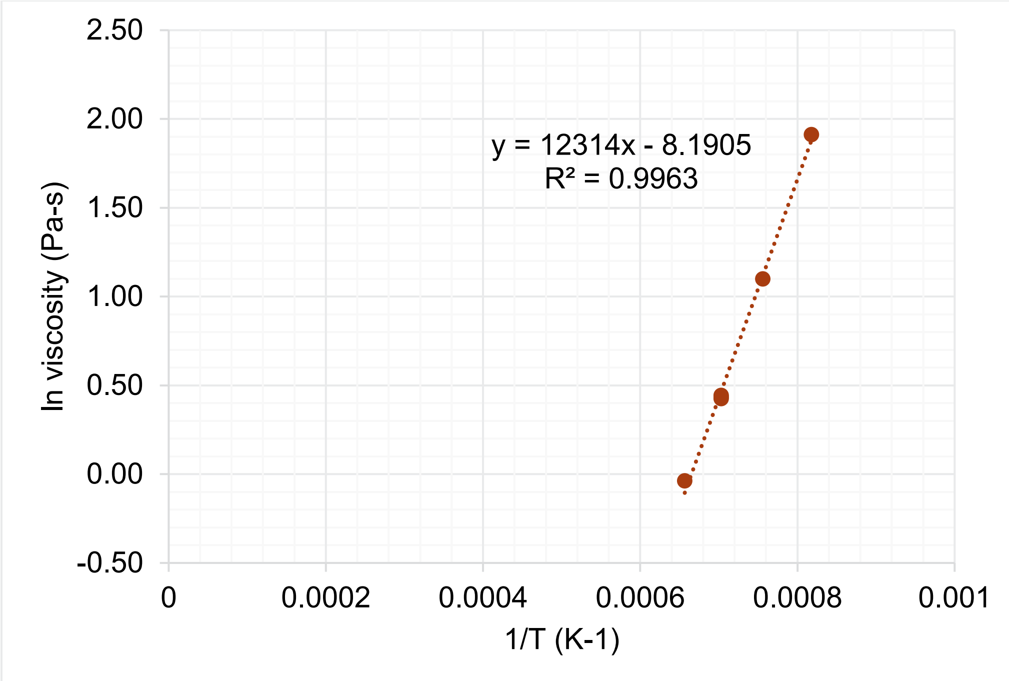

Figure J.23. Viscosity-temperature data and Arrhenius equation fit for HAL24M1-23.

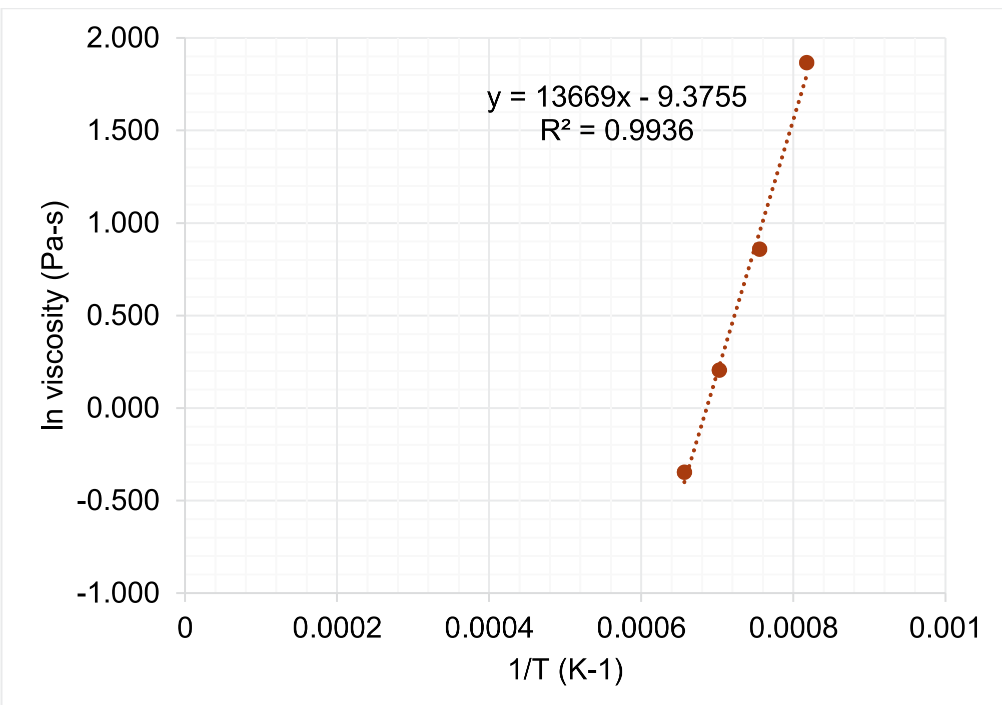

Figure J.24. Viscosity-temperature data and Arrhenius equation fit for HAL24M1-24.

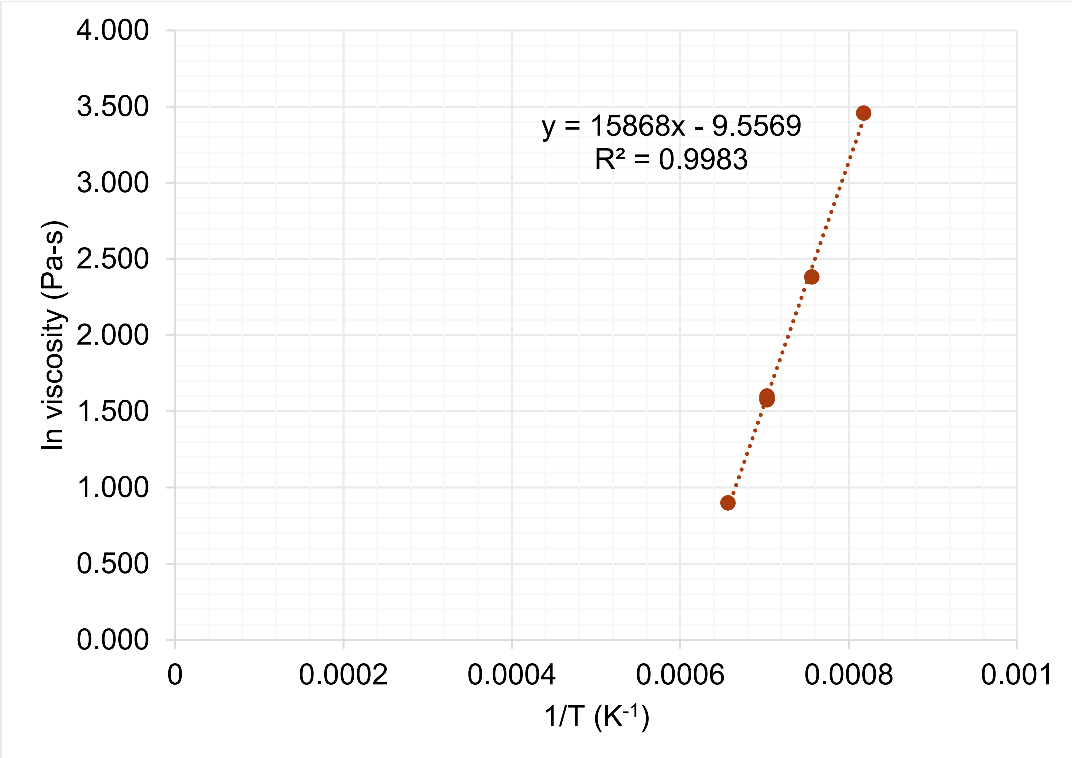

Figure J.25. Viscosity-temperature data and Arrhenius equation fit for HAL24M1-25.

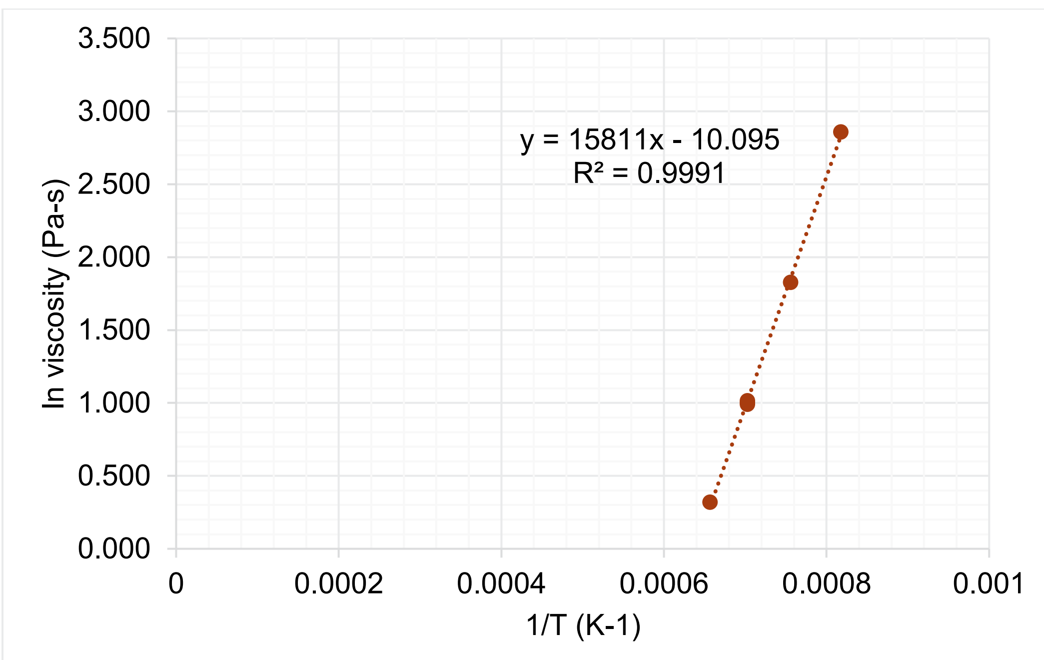

Figure J.26. Viscosity-temperature data and Arrhenius equation fit for HAL24M1-26.

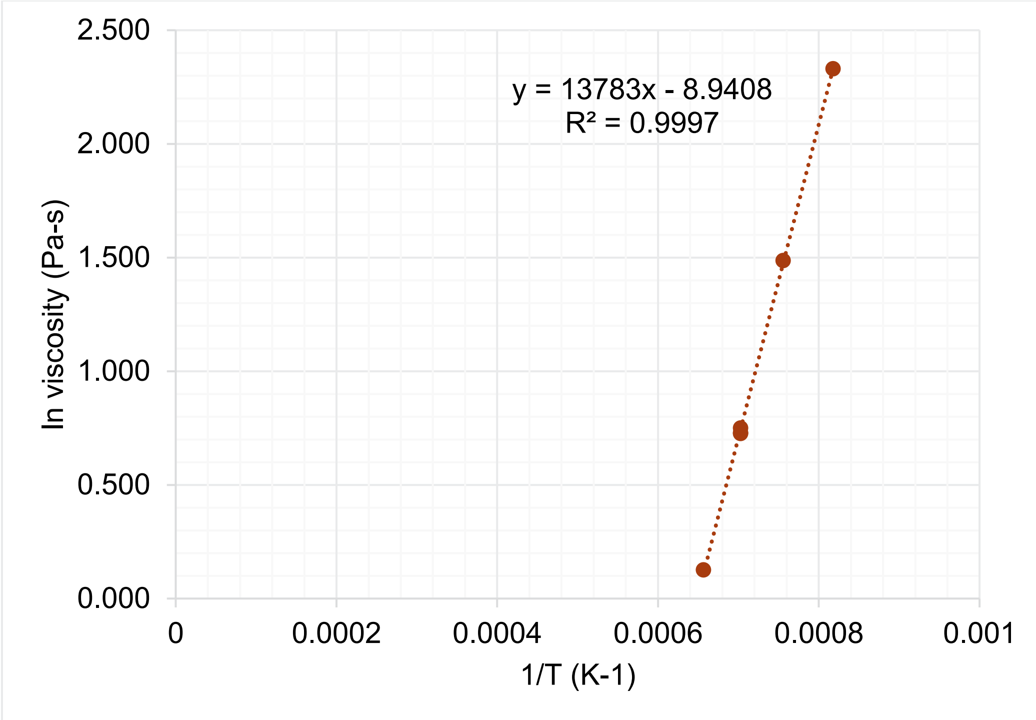

Figure J.27. Viscosity-temperature data and Arrhenius equation fit for HAL24M1-27.

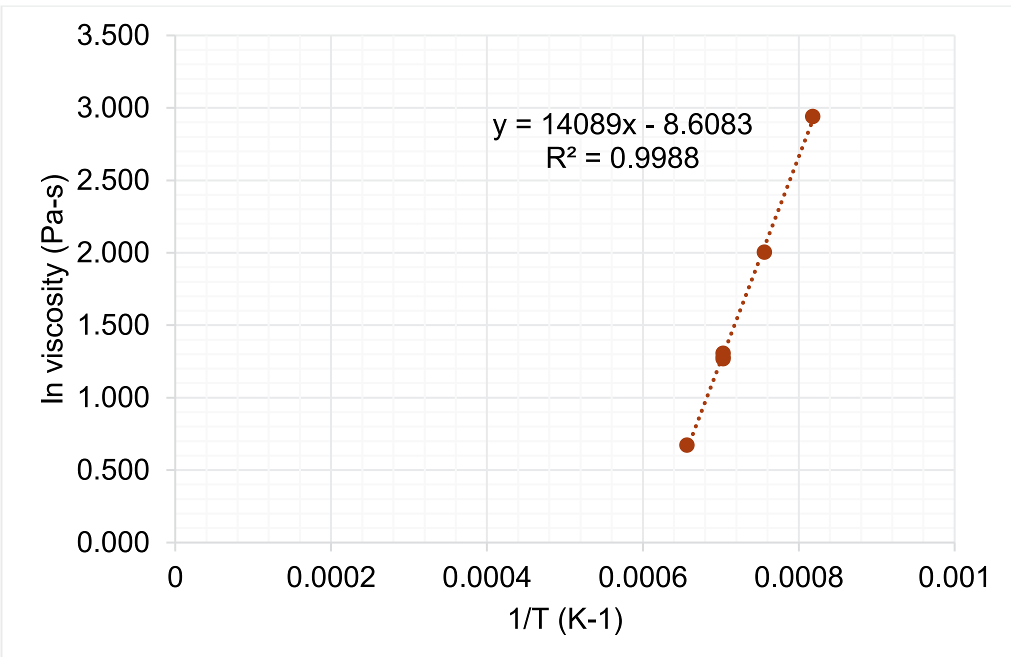

Figure J.28. Viscosity-temperature data and Arrhenius equation fit for HAL24M1-28.

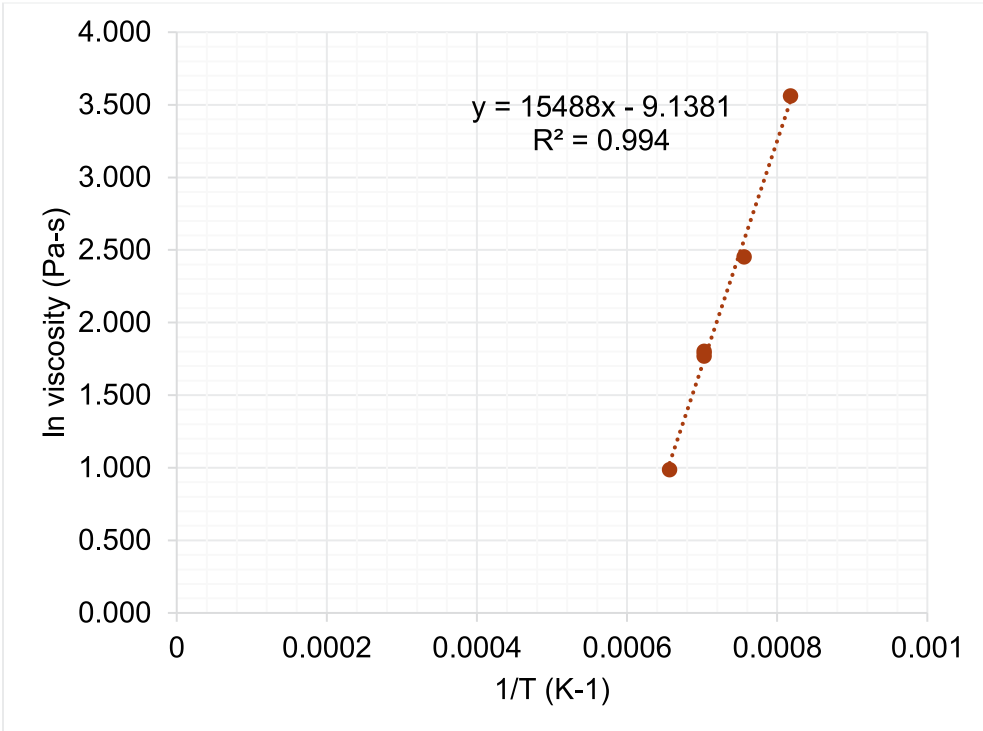

Figure J.29. Viscosity-temperature data and Arrhenius equation fit for HAL24M1-29-1.

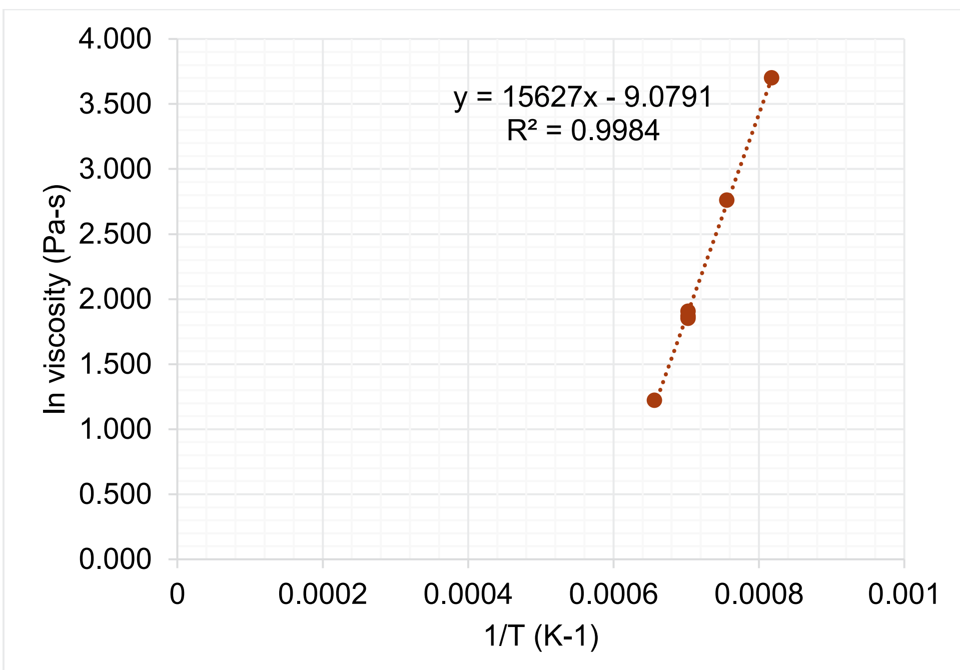

Figure J.30. Viscosity-temperature data and Arrhenius equation fit for HAL24M1-30-1.

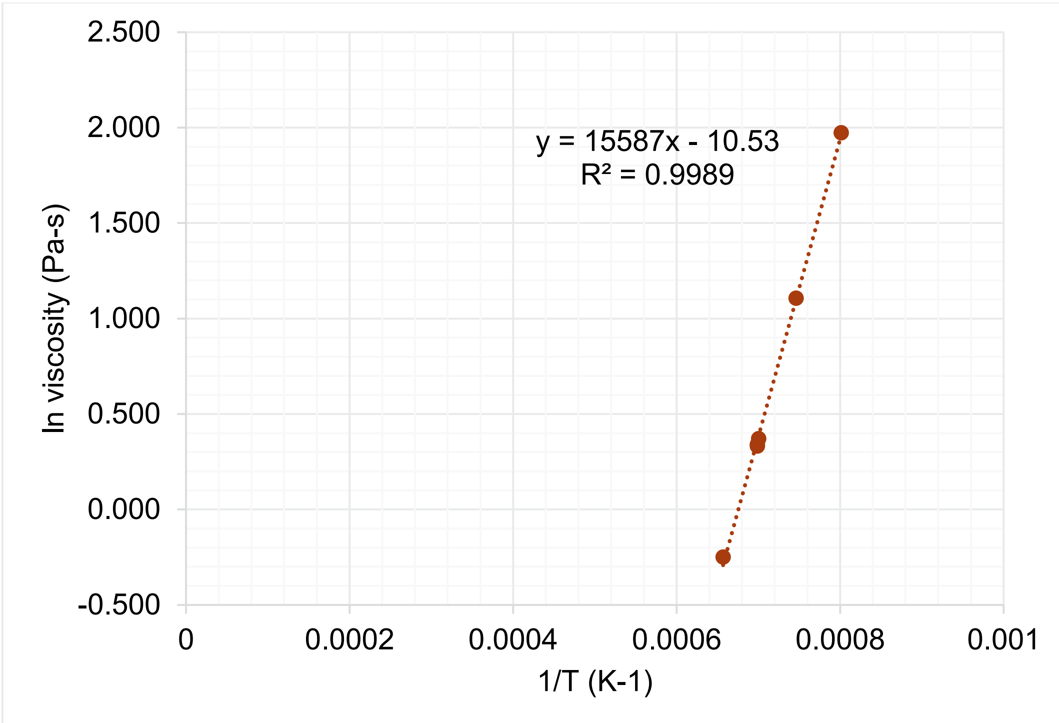

Figure J.31. Viscosity-temperature data and Arrhenius equation fit for HAL24M2-01.

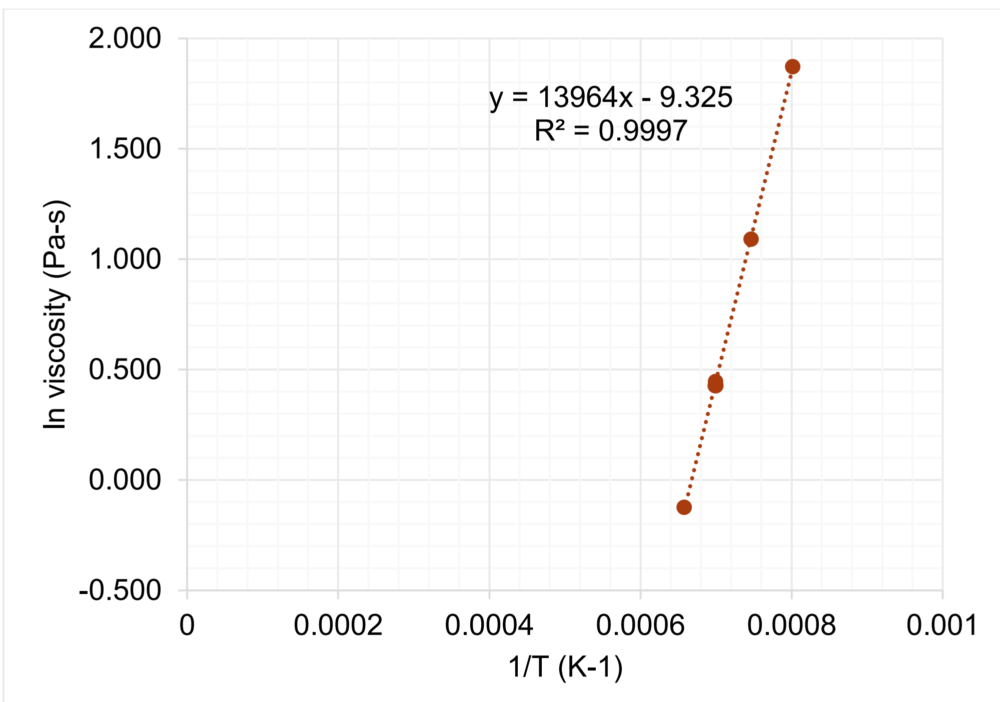

Figure J.32. Viscosity-temperature data and Arrhenius equation fit for HAL24M2-02.

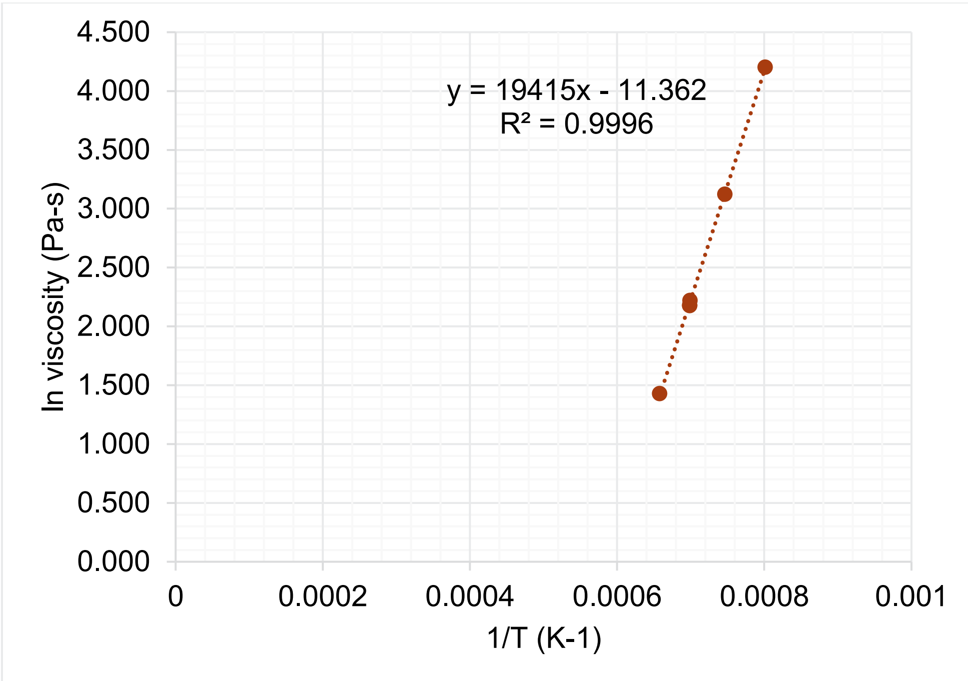

Figure J.33. Viscosity-temperature data and Arrhenius equation fit for HAL24M2-03.

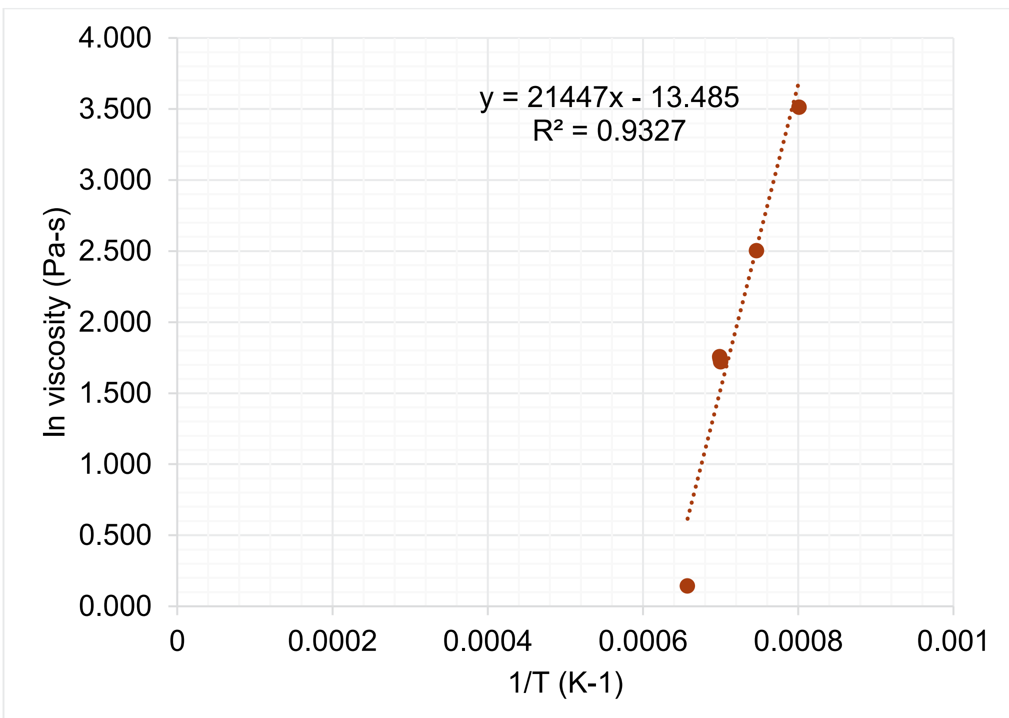

Figure J.34. Viscosity-temperature data and Arrhenius equation fit for HAL24M2-04-1.

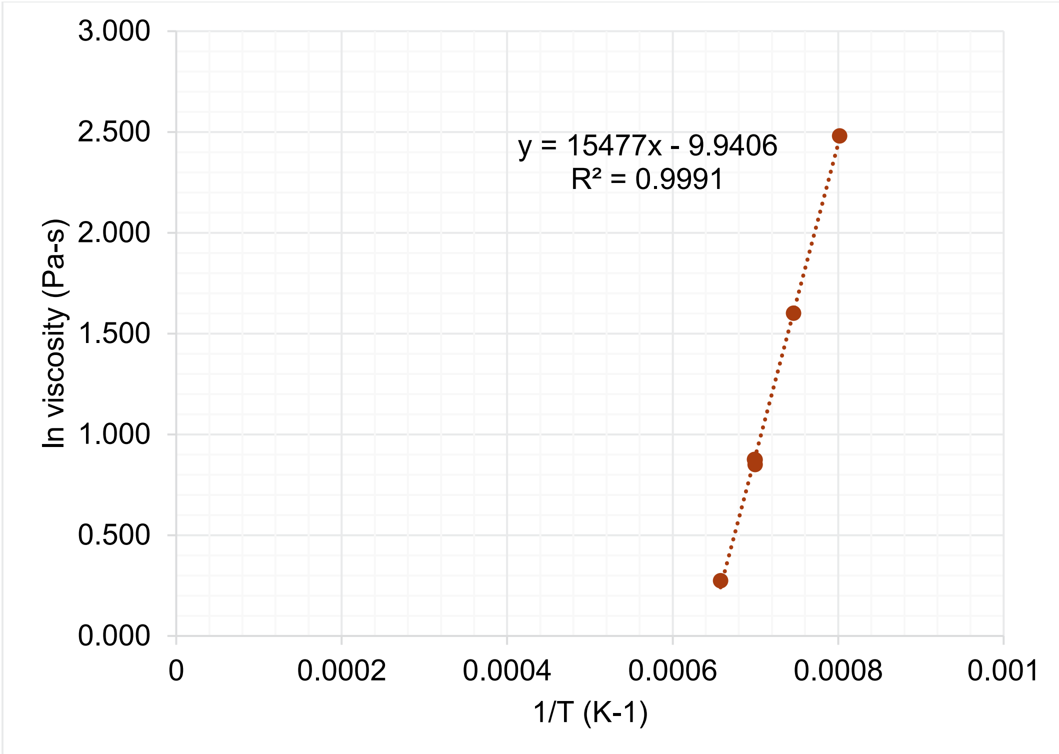

Figure J.35. Viscosity-temperature data and Arrhenius equation fit for HAL24M2-05.

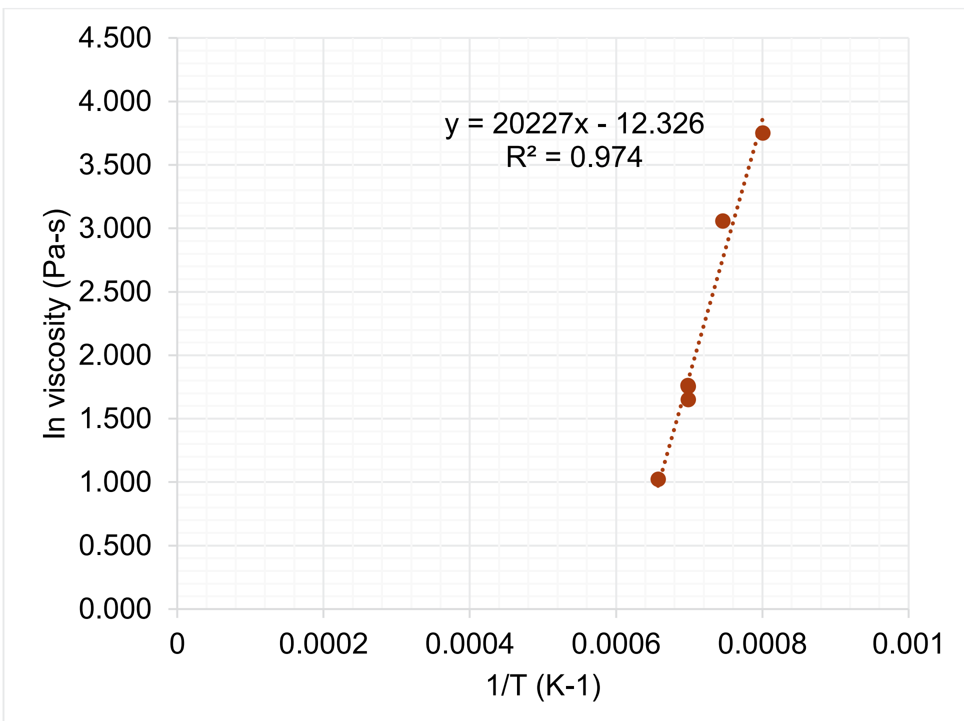

Figure J.36. Viscosity-temperature data and Arrhenius equation fit for HAL24M2-06.

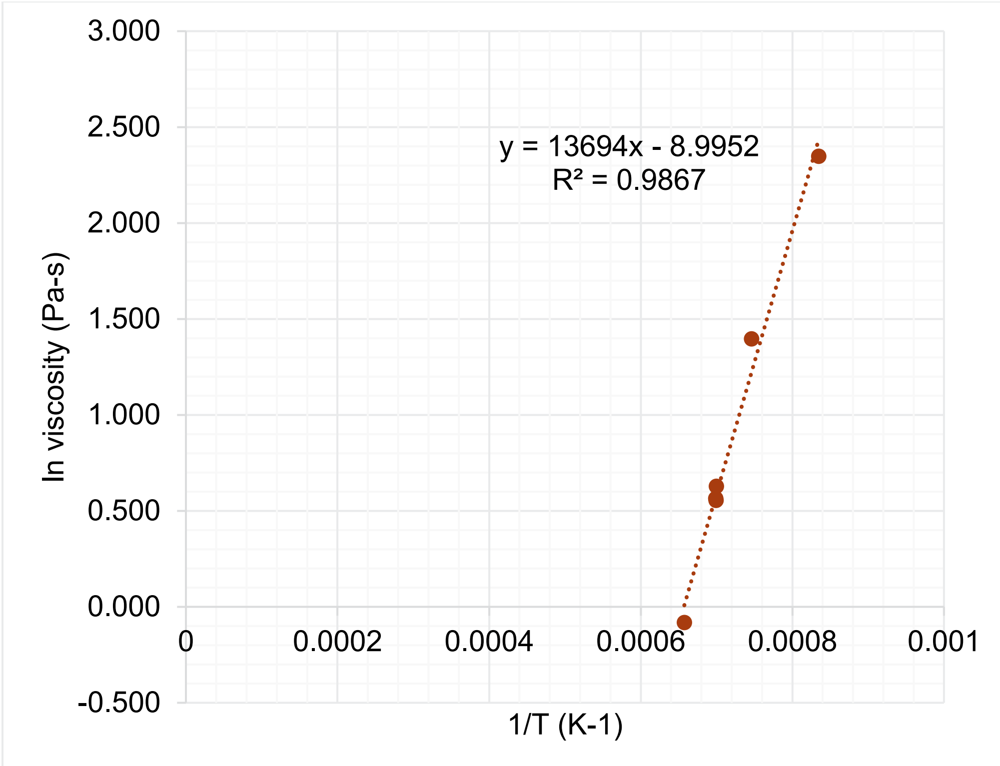

Figure J.37. Viscosity-temperature data and Arrhenius equation fit for HAL24M2-07.

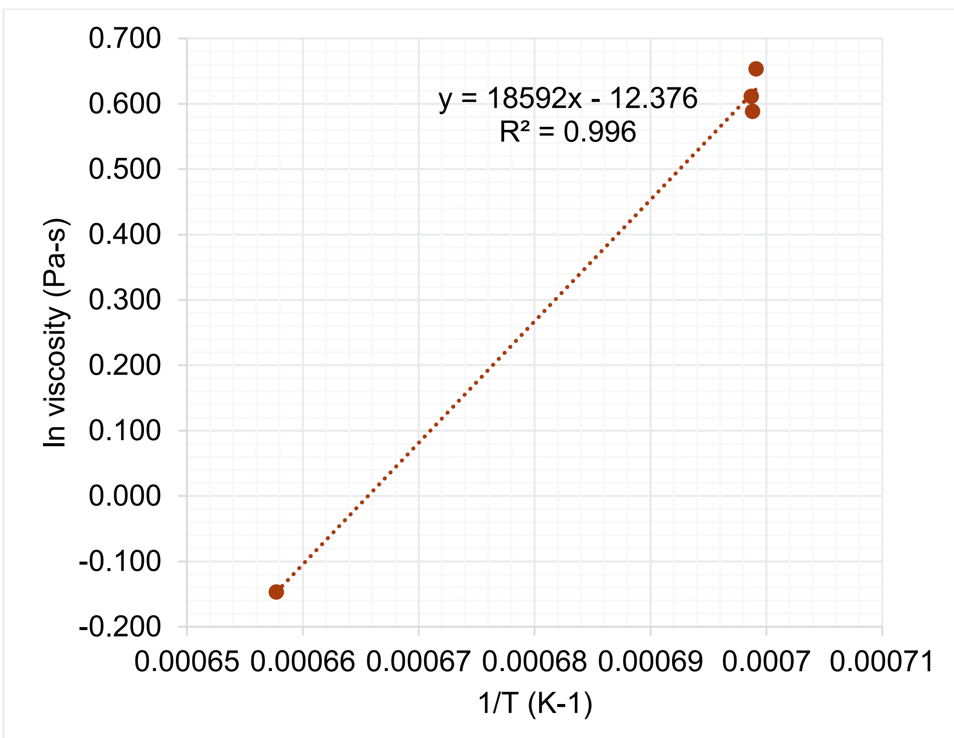

Figure J.38. Viscosity-temperature data and Arrhenius equation fit for HAL24M2-08.

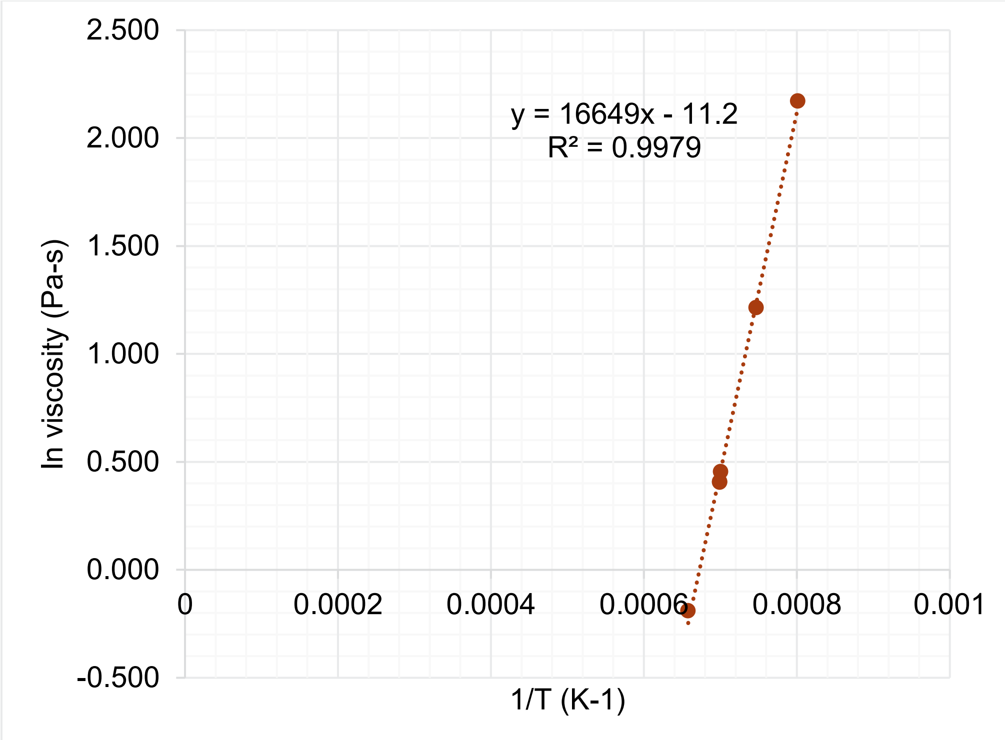

Figure J.39. Viscosity-temperature data and Arrhenius equation fit for HAL24M2-09.

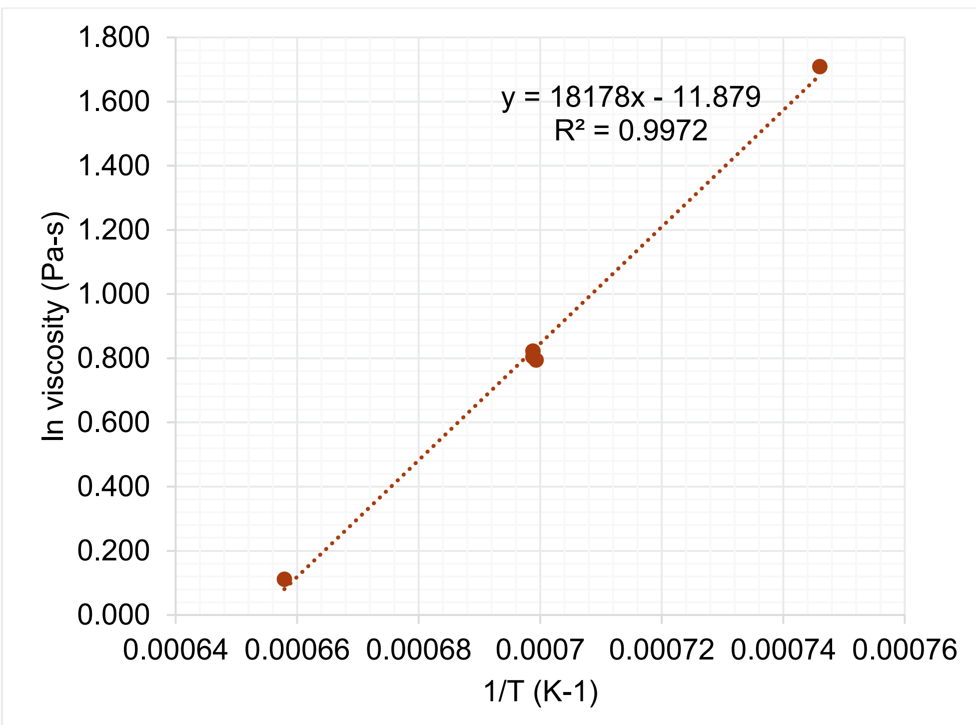

Figure J.40. Viscosity-temperature data and Arrhenius equation fit for HAL24M2-10.

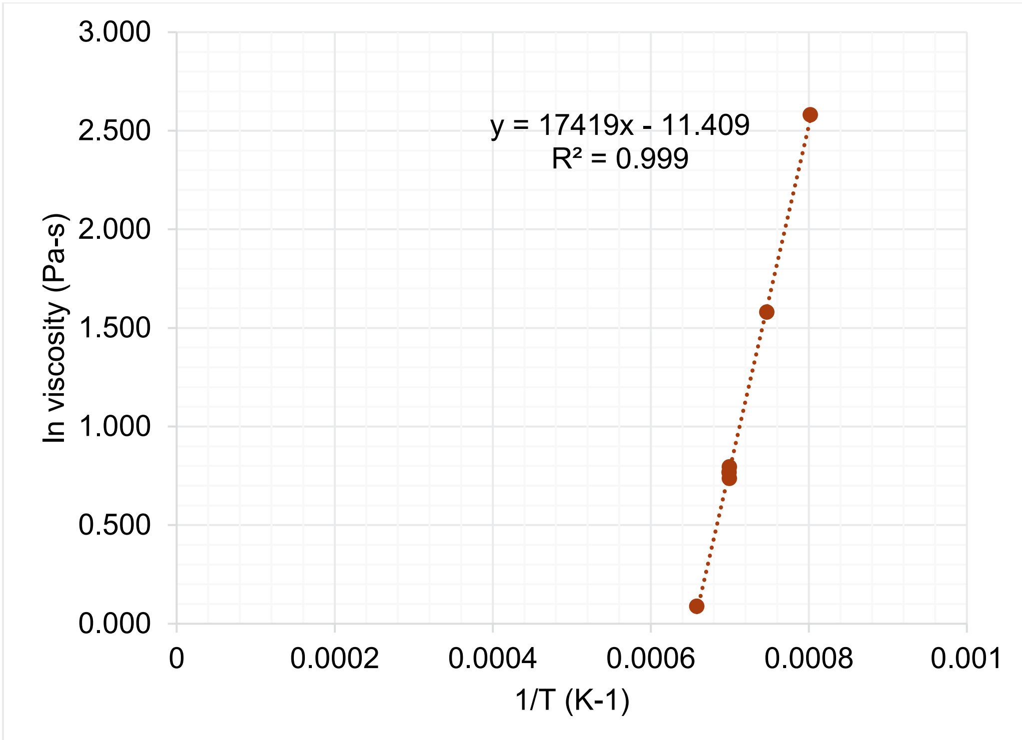

Figure J.41. Viscosity-temperature data and Arrhenius equation fit for HAL24M2-11.

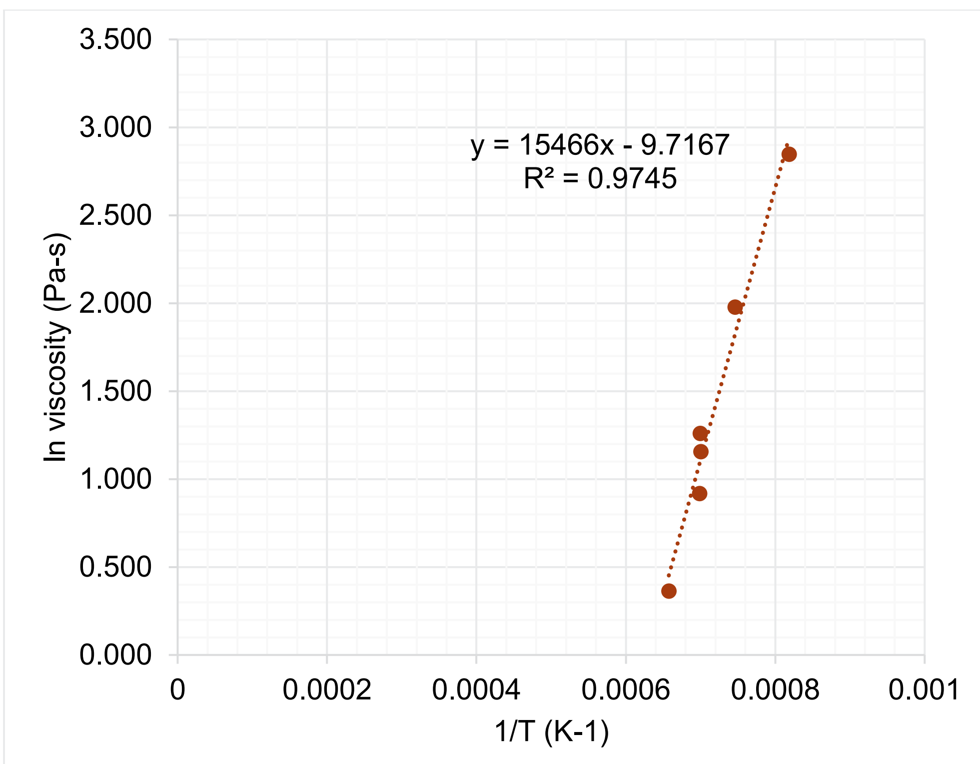

Figure J.42. Viscosity-temperature data and Arrhenius equation fit for HAL24M2-12.

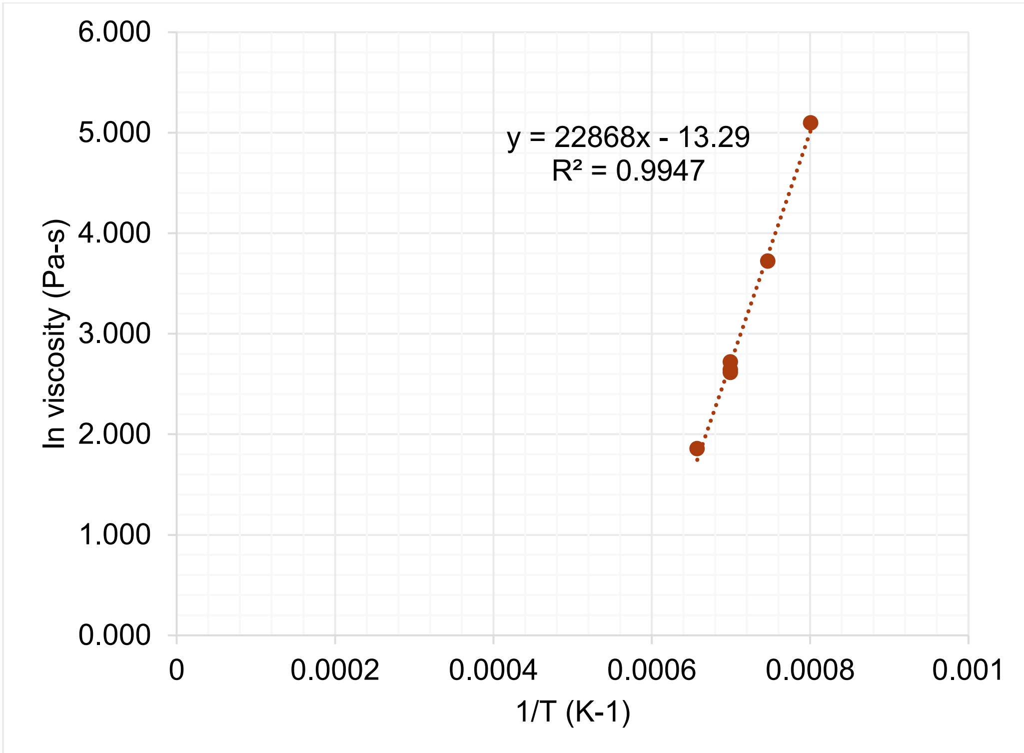

Figure J.43. Viscosity-temperature data and Arrhenius equation fit for HAL24M2-13.

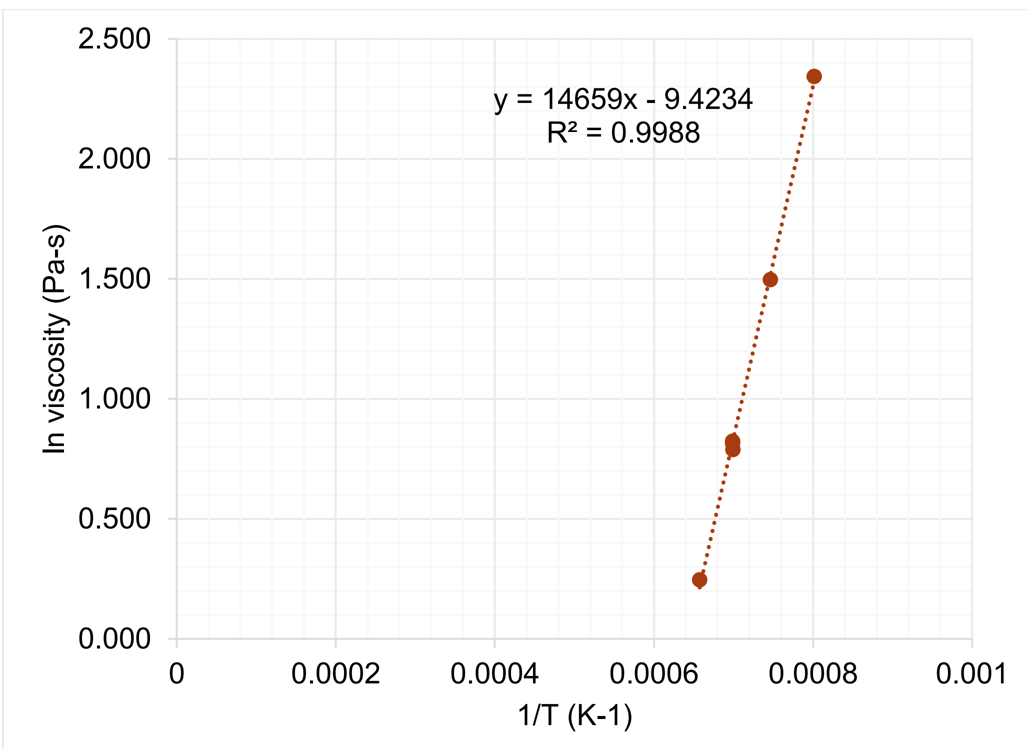

Figure J.44. Viscosity-temperature data and Arrhenius equation fit for HAL24M2-14.

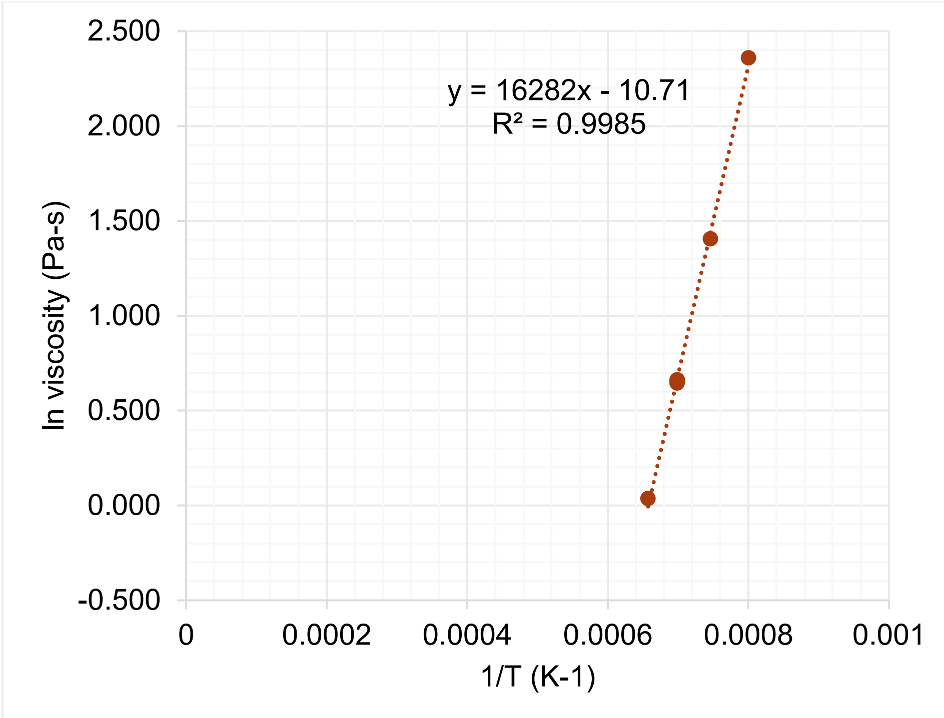

Figure J.45. Viscosity-temperature data and Arrhenius equation fit for HAL24M2-15.

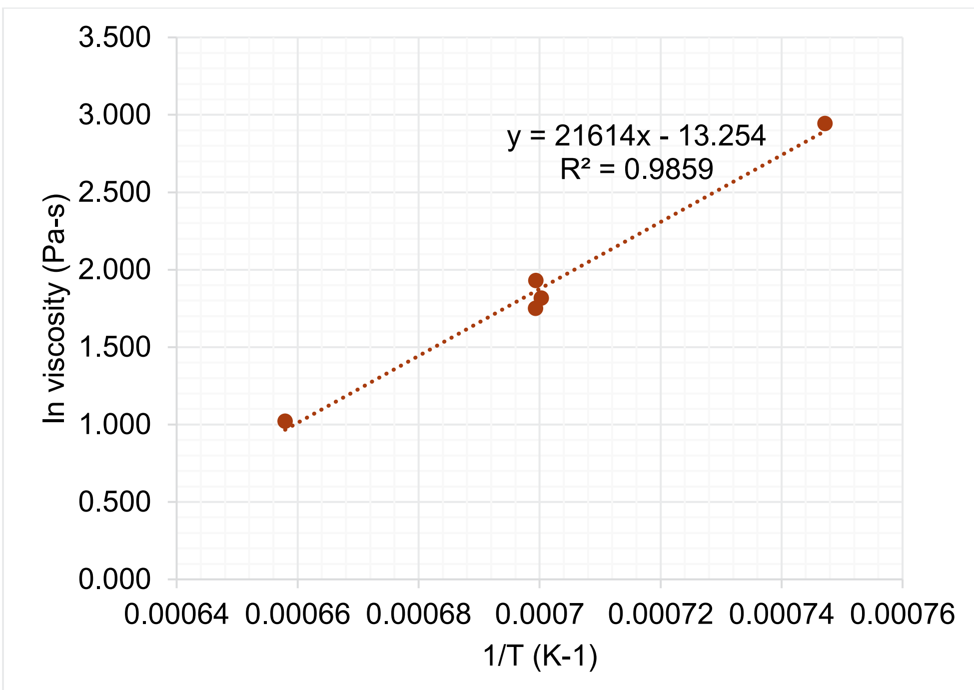

Figure J.46. Viscosity-temperature data and Arrhenius equation fit for HAL24M2-16.

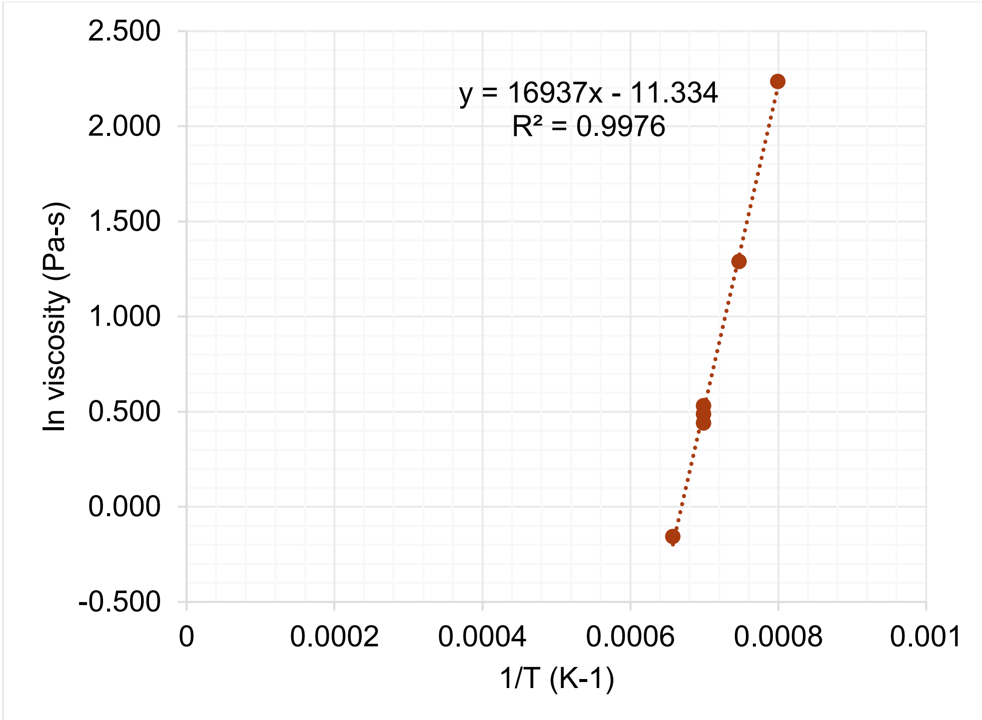

Figure J.47. Viscosity-temperature data and Arrhenius equation fit for HAL24M2-17.

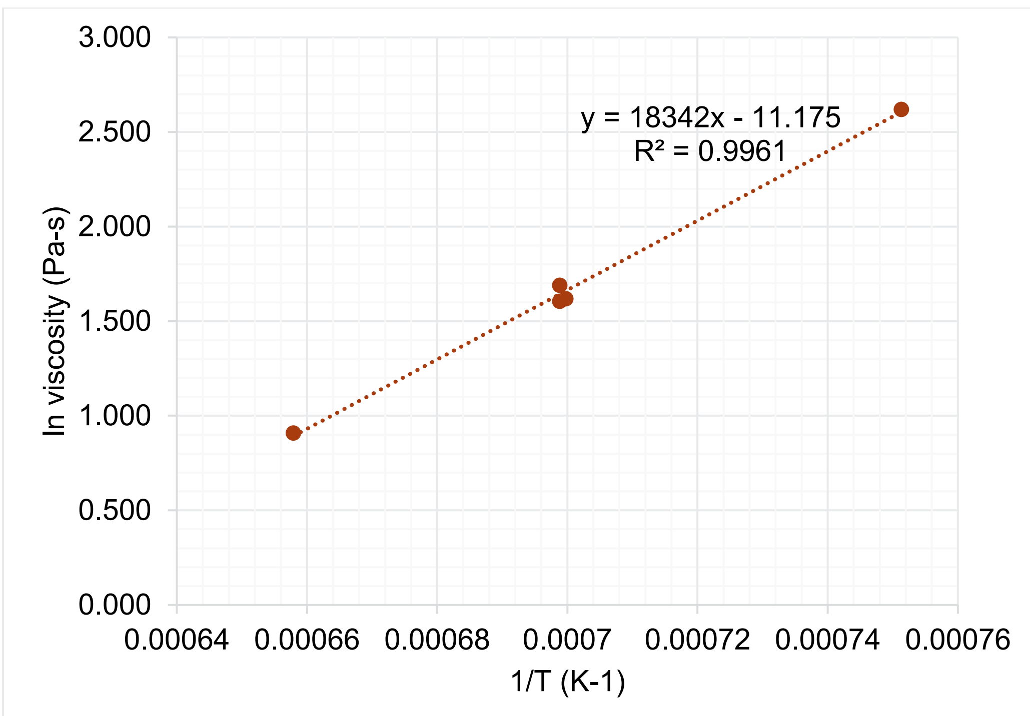

Figure J.48. Viscosity-temperature data and Arrhenius equation fit for HAL24M2-18.

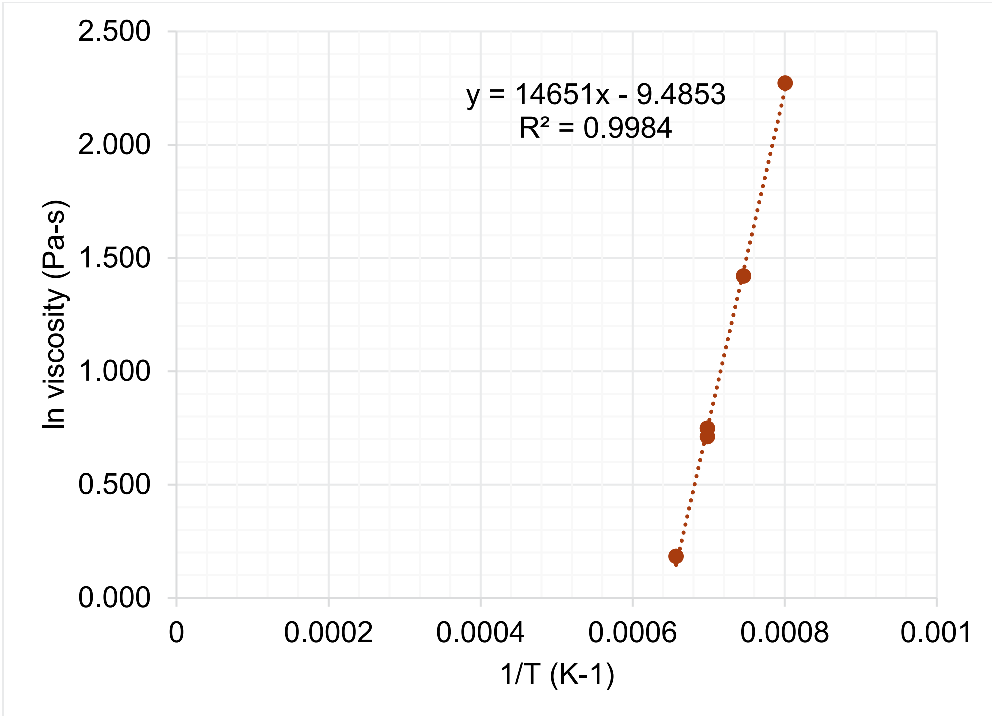

Figure J.49. Viscosity-temperature data and Arrhenius equation fit for HAL24M2-19.

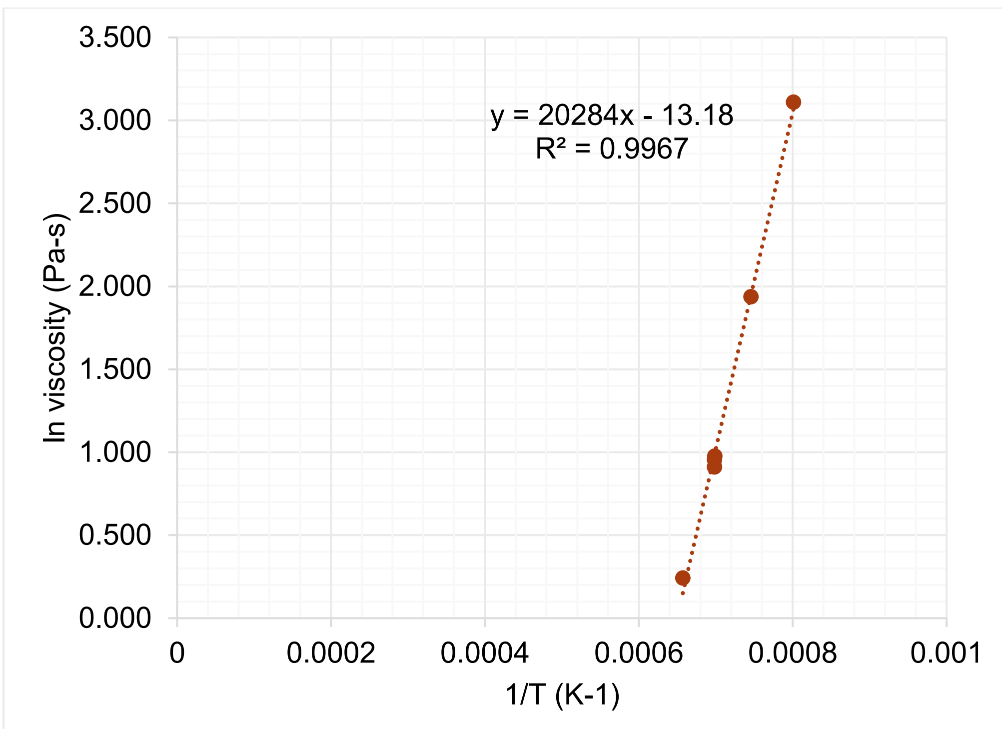

Figure J.50. Viscosity-temperature data and Arrhenius equation fit for HAL24M2-20.

Appendix K – Electrical Conductivity Data

This appendix contains the measured electrical conductivity data for each of the glasses in this matrix following Section 2.10.

The plots shown in this appendix are fitted to the Arrhenius equation, which is shown below:

$$\ln(\varepsilon) = A + B/T_K \quad \text{(K.1)}$$

where A and B are independent of temperature and temperature (T_K) is in K (T(°C) + 273.15).

The main intent of the figures and Arrhenius equation fits shown in this appendix is to assess trends in the data and provide observations about whether there may be sufficient curvature in the data to consider Vogel–Fulcher–Tammann (VFT) fits in the subsequent work that will decide between fitting the data to the Arrhenius or VFT equations for the electrical conductivity-temperature data for each glass that is being made.

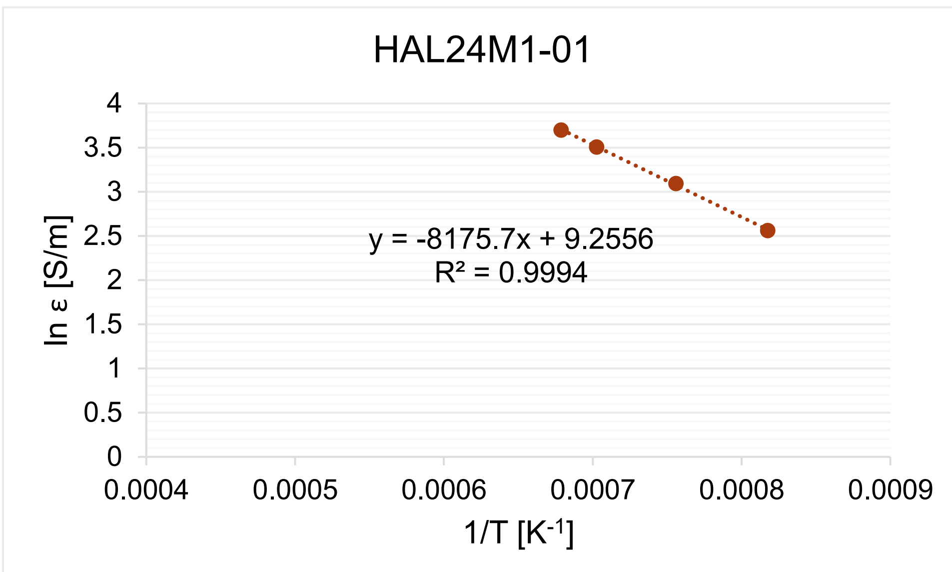

Figure K.1. Electrical conductivity-temperature data and Arrhenius equation fit for glass HAL24M1-01.

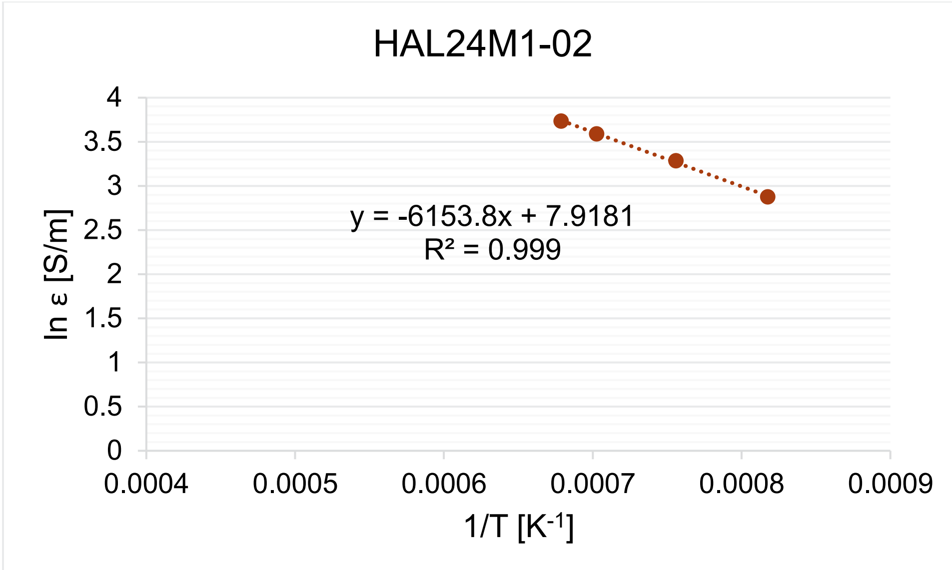

Figure K.2. Electrical conductivity-temperature data and Arrhenius equation fit for glass HAL24M1-02.

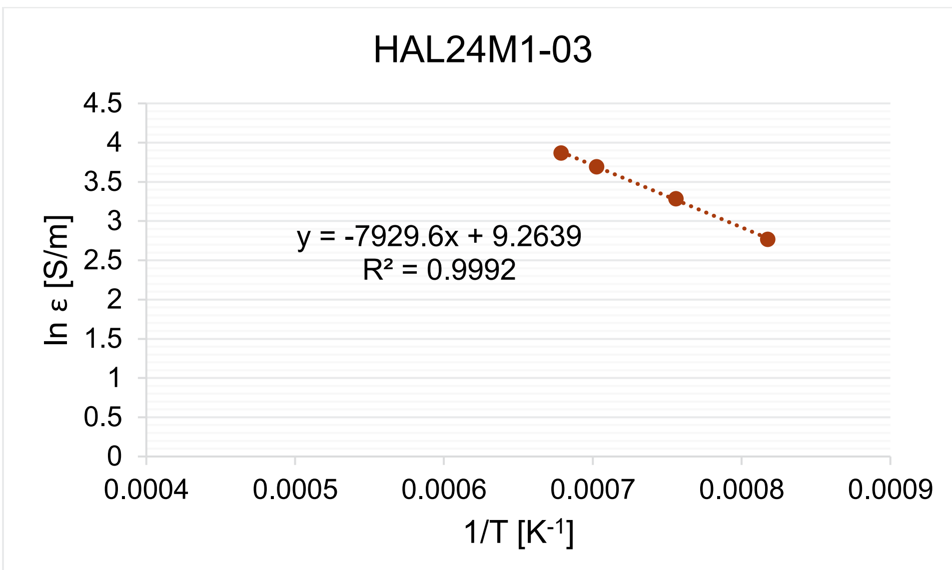

Figure K.3. Electrical conductivity-temperature data and Arrhenius equation fit for glass HAL24M1-03.

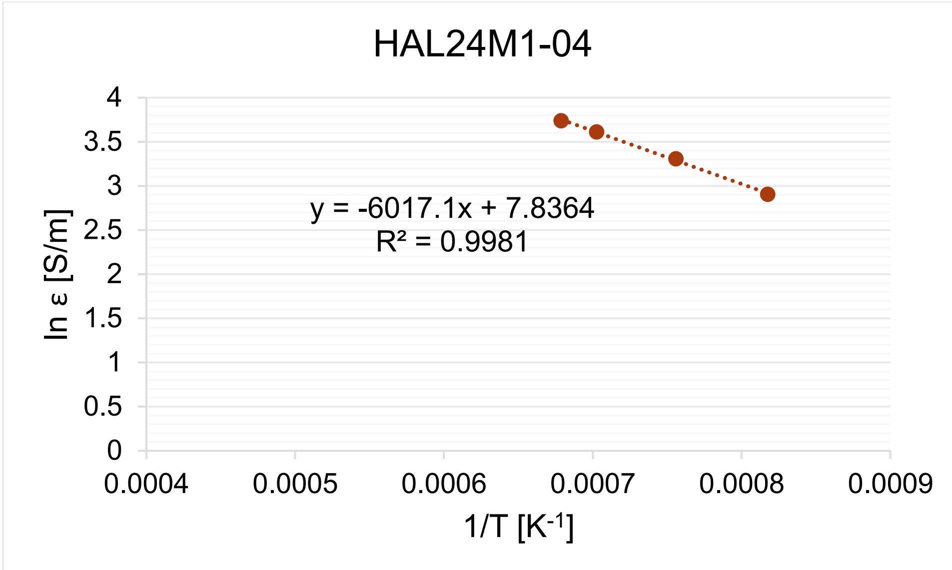

Figure K.4. Electrical conductivity-temperature data and Arrhenius equation fit for glass HAL24M1-04.

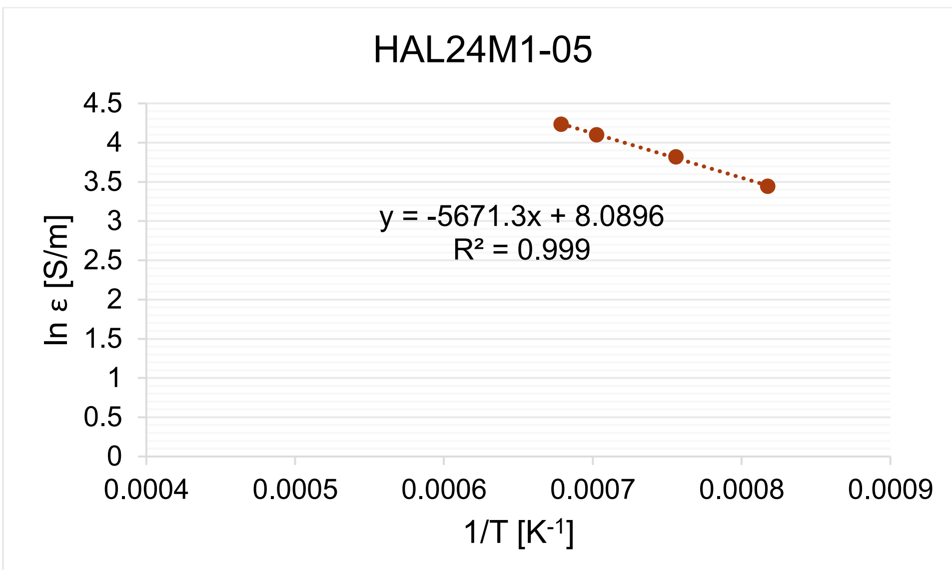

Figure K.5. Electrical conductivity-temperature data and Arrhenius equation fit for glass HAL24M1-05.

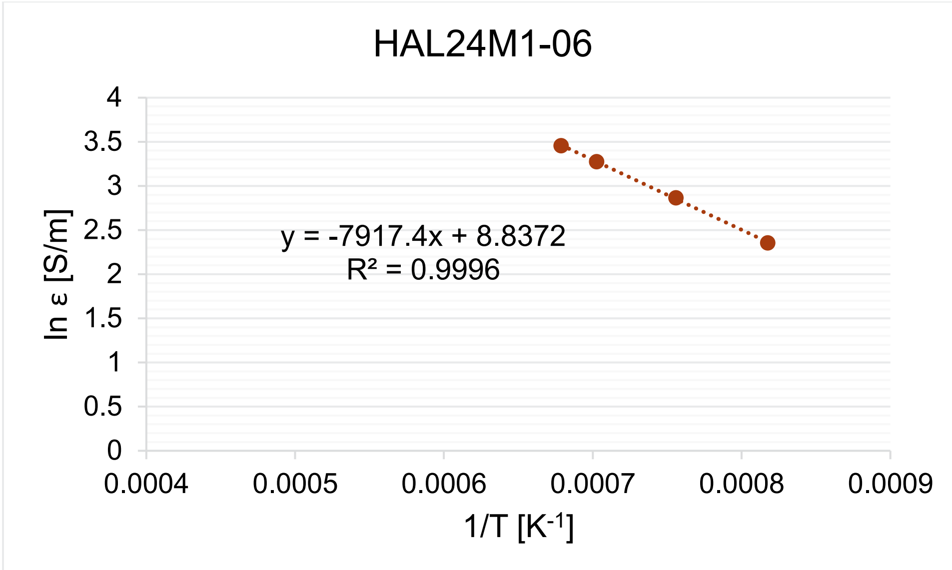

Figure K.6. Electrical conductivity-temperature data and Arrhenius equation fit for glass HAL24M1-06.

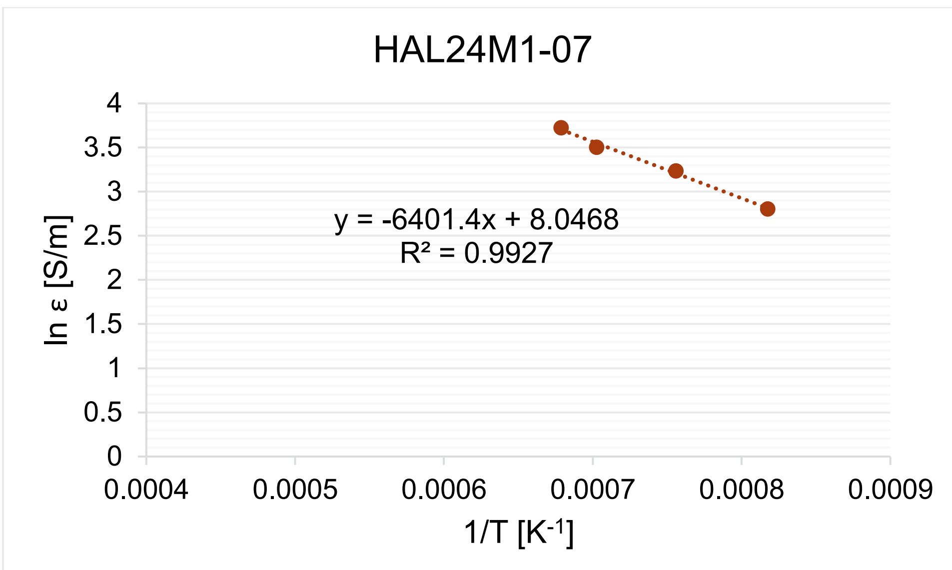

Figure K.7. Electrical conductivity-temperature data and Arrhenius equation fit for glass HAL24M1-07.

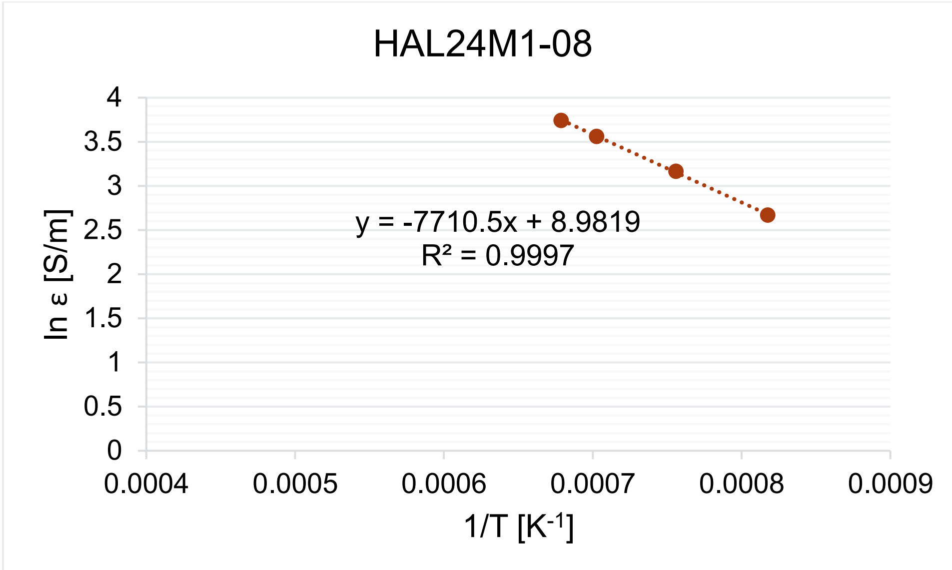

Figure K.8. Electrical conductivity-temperature data and Arrhenius equation fit for glass HAL24M1-08.

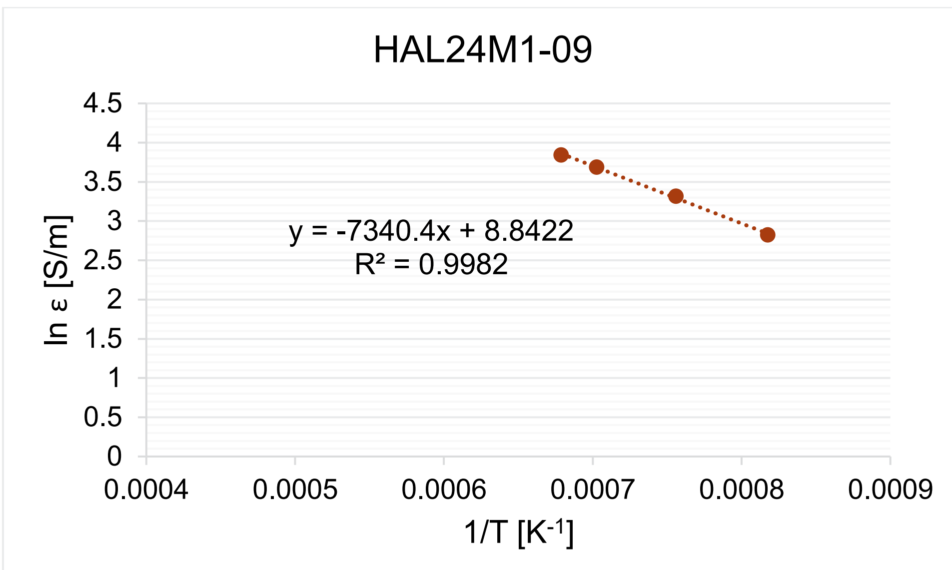

Figure K.9. Electrical conductivity-temperature data and Arrhenius equation fit for glass HAL24M1-09.

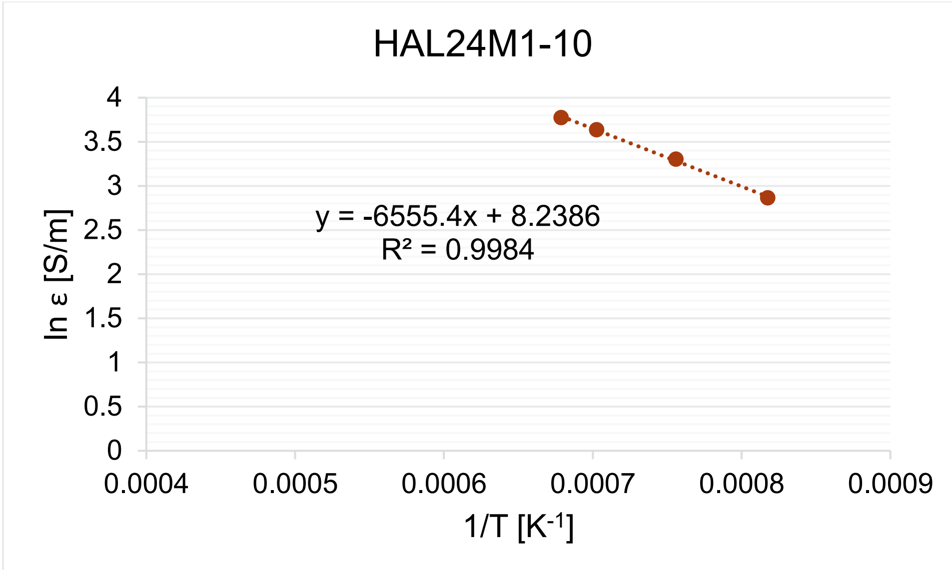

Figure K.10. Electrical conductivity-temperature data and Arrhenius equation fit for glass HAL24M1-10.

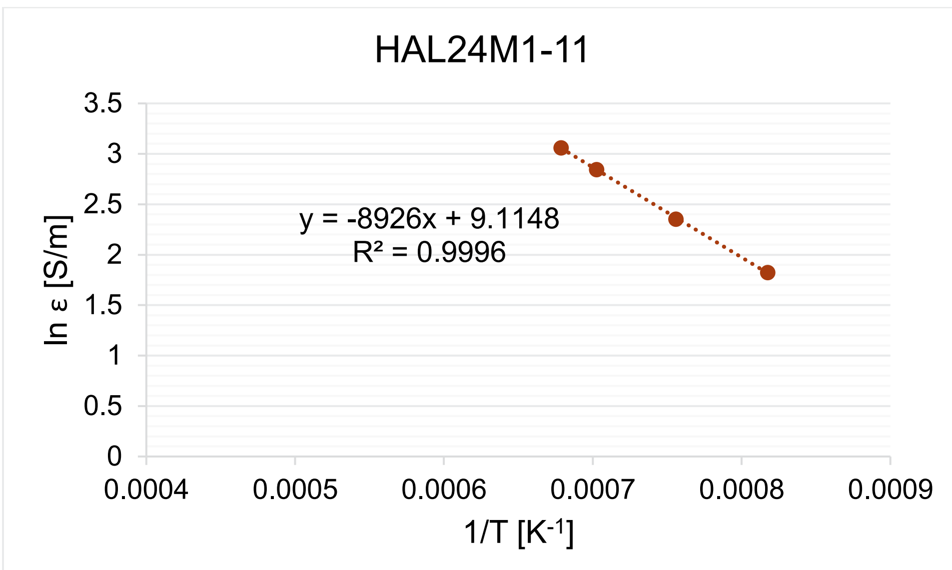

Figure K.11. Electrical conductivity-temperature data and Arrhenius equation fit for glass HAL24M1-11.

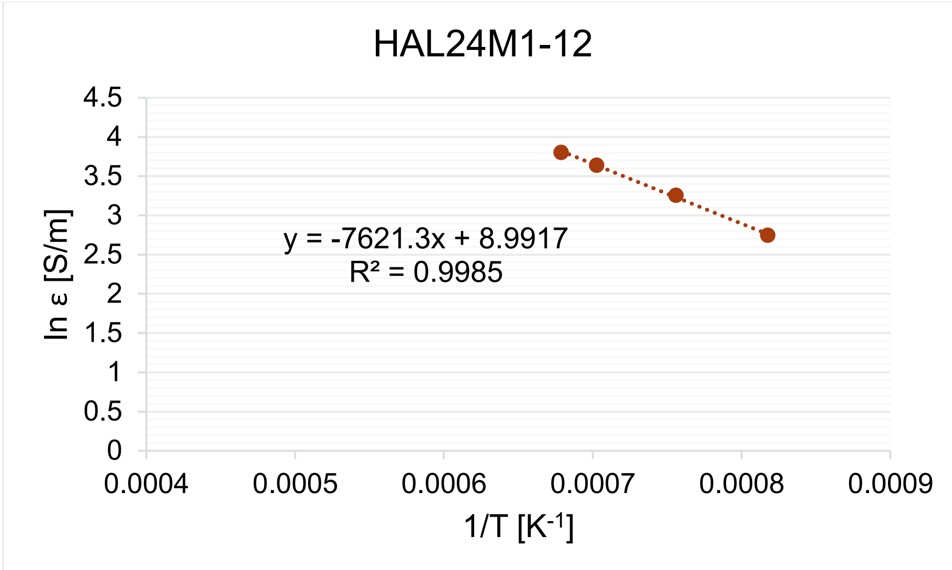

Figure K.12. Electrical conductivity-temperature data and Arrhenius equation fit for glass HAL24M1-12.

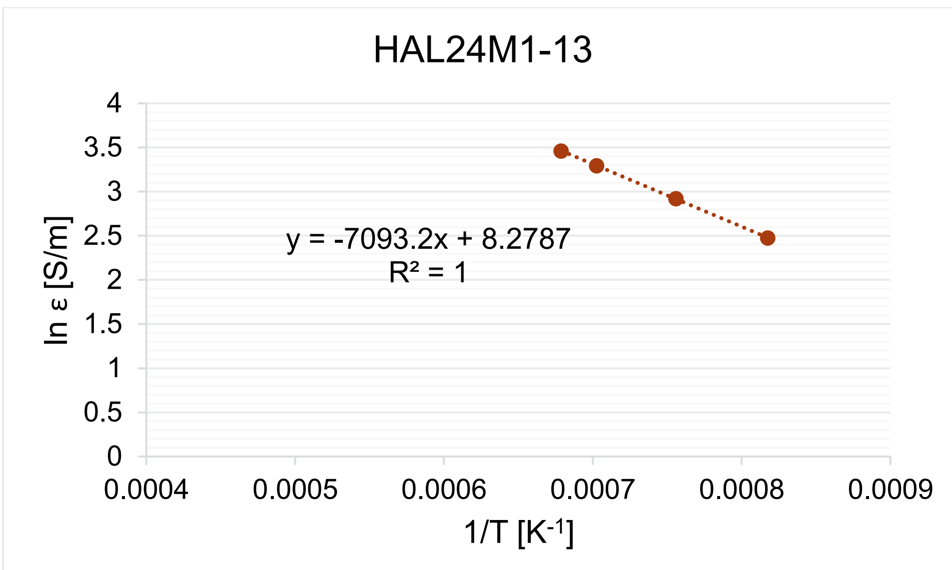

Figure K.13. Electrical conductivity-temperature data and Arrhenius equation fit for glass HAL24M1-13-1.

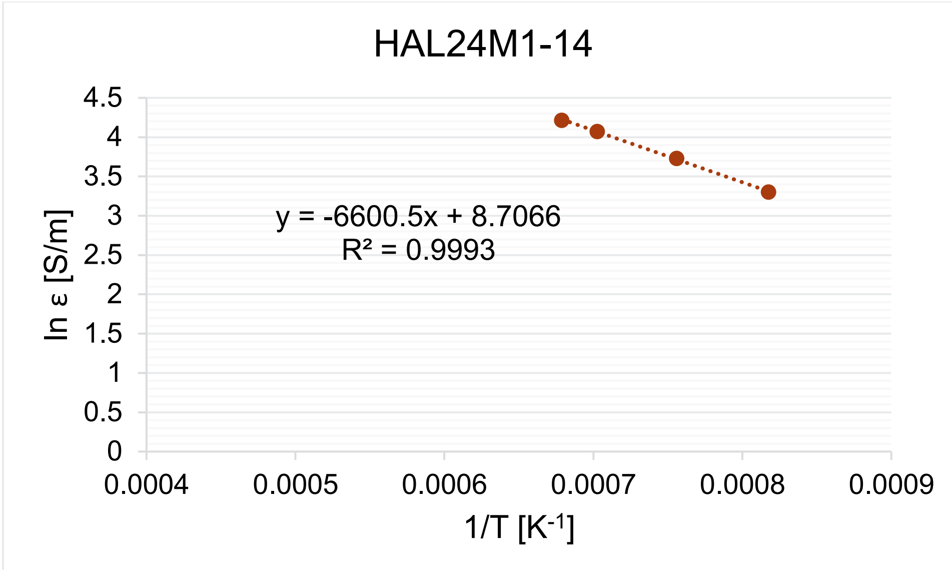

Figure K.14. Electrical conductivity-temperature data and Arrhenius equation fit for glass HAL24M1-14.

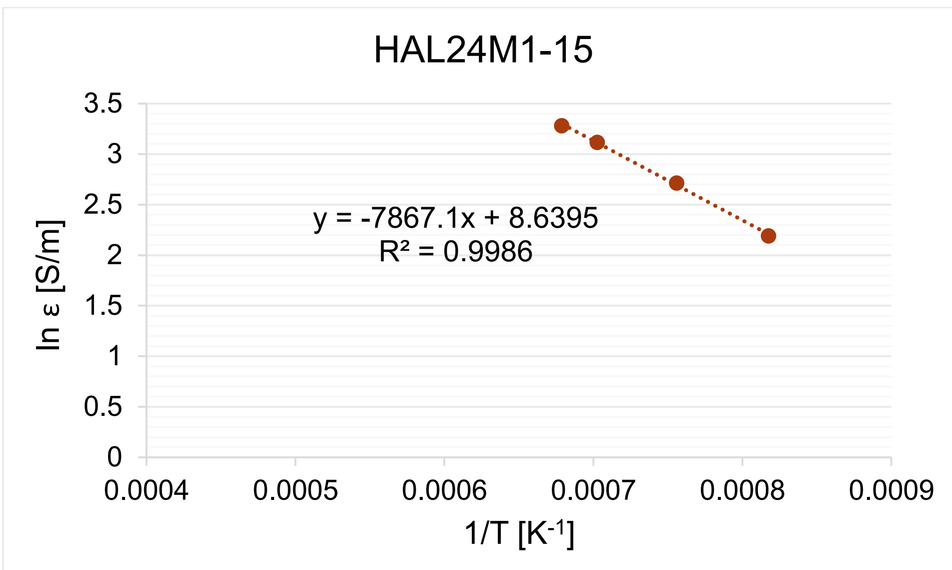

Figure K.15. Electrical conductivity-temperature data and Arrhenius equation fit for glass HAL24M1-15.

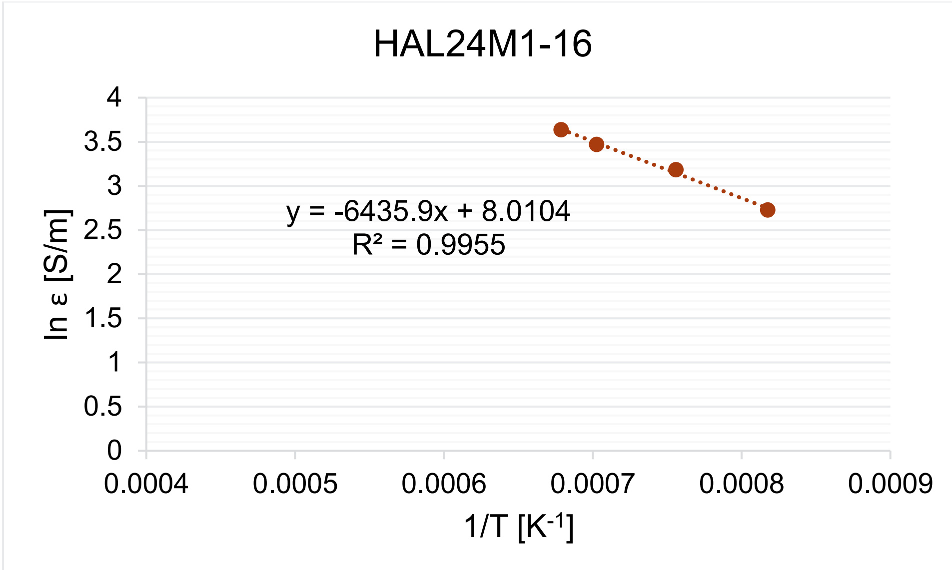

Figure K.16. Electrical conductivity-temperature data and Arrhenius equation fit for glass HAL24M1-16.

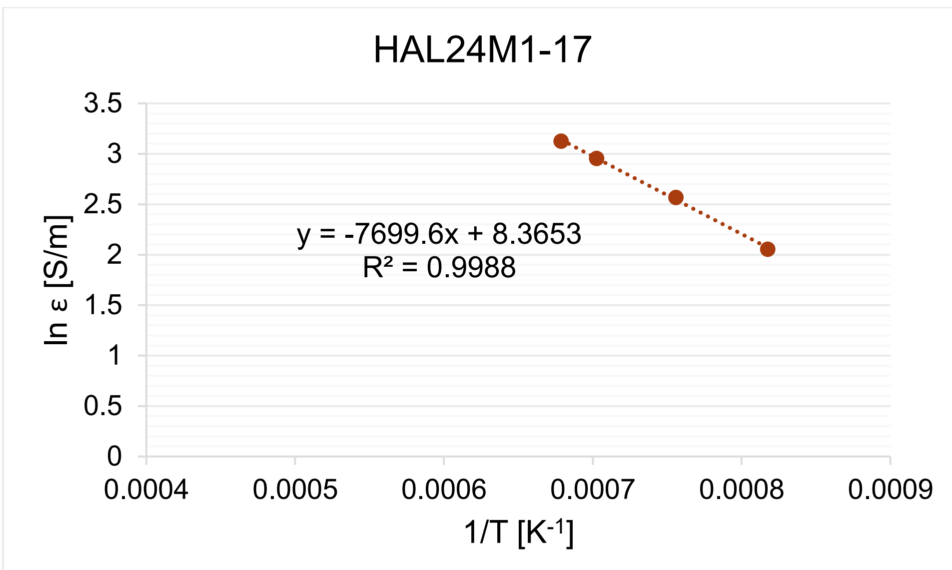

Figure K.17. Electrical conductivity-temperature data and Arrhenius equation fit for glass HAL24M1-17.

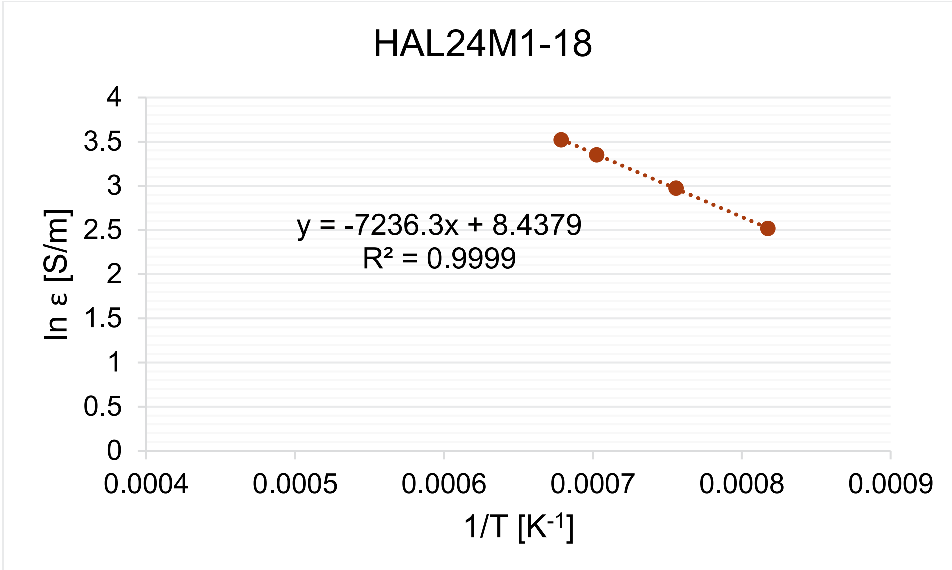

Figure K.18. Electrical conductivity-temperature data and Arrhenius equation fit for glass HAL24M1-18.

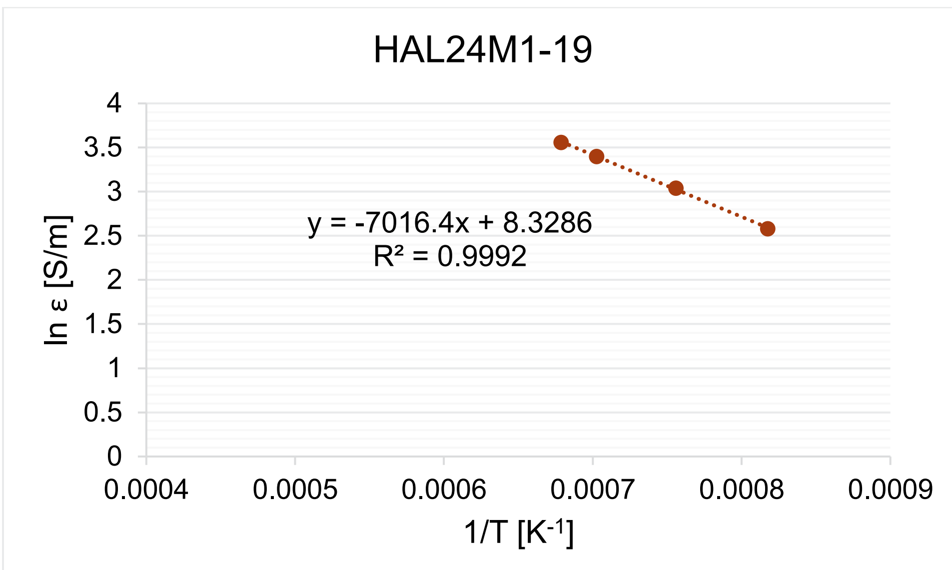

Figure K.19. Electrical conductivity-temperature data and Arrhenius equation fit for glass HAL24M1-19.

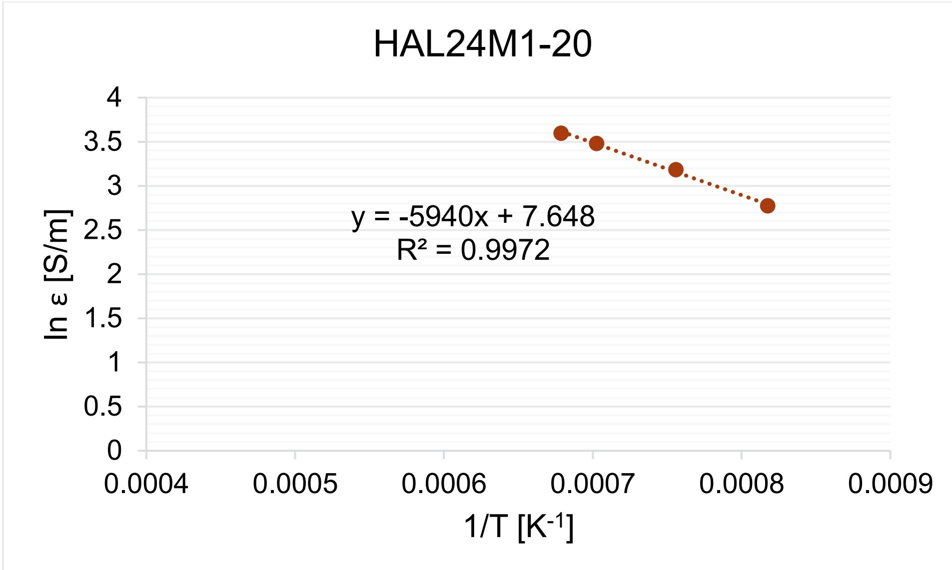

Figure K.20. Electrical conductivity-temperature data and Arrhenius equation fit for glass HAL24M1-20.

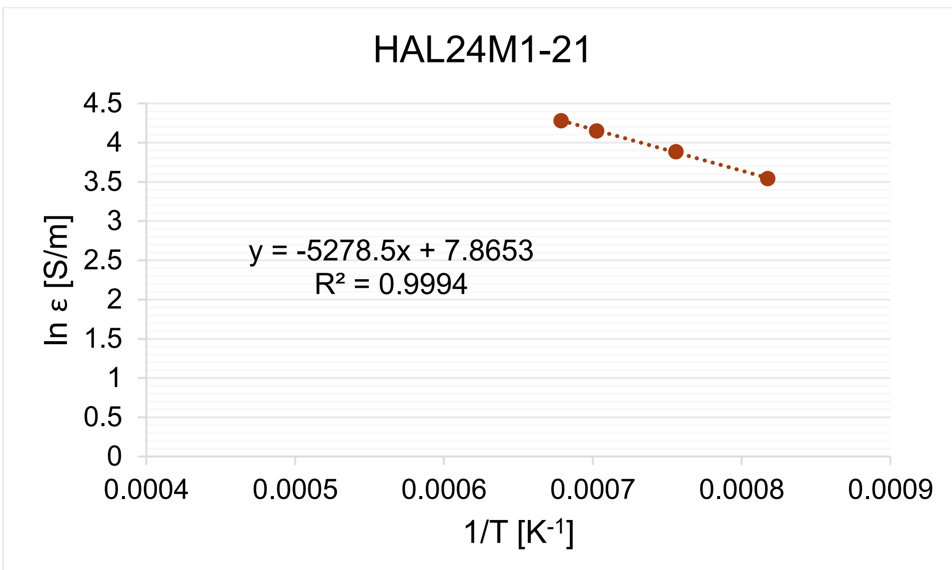

Figure K.21. Electrical conductivity-temperature data and Arrhenius equation fit for glass HAL24M1-21.

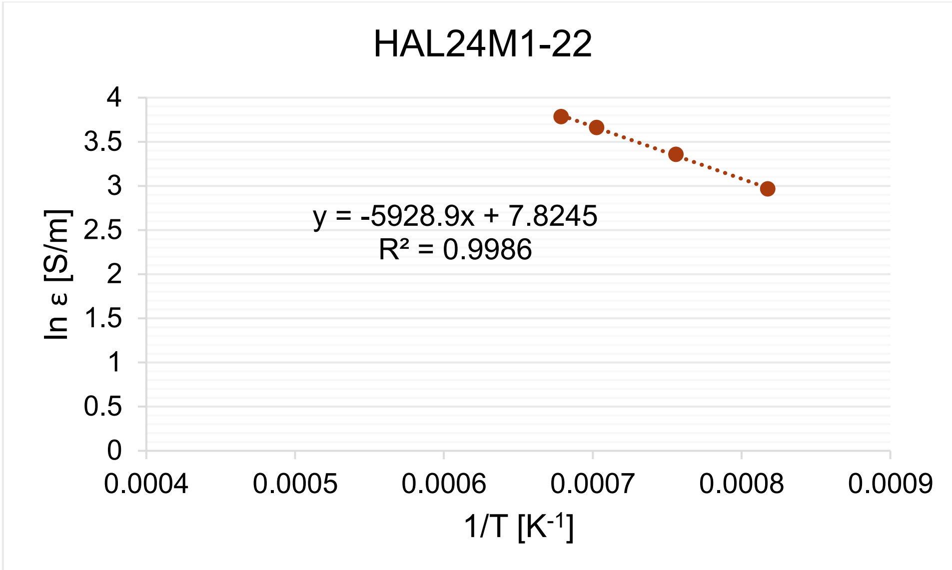

Figure K.22. Electrical conductivity-temperature data and Arrhenius equation fit for glass HAL24M1-22.

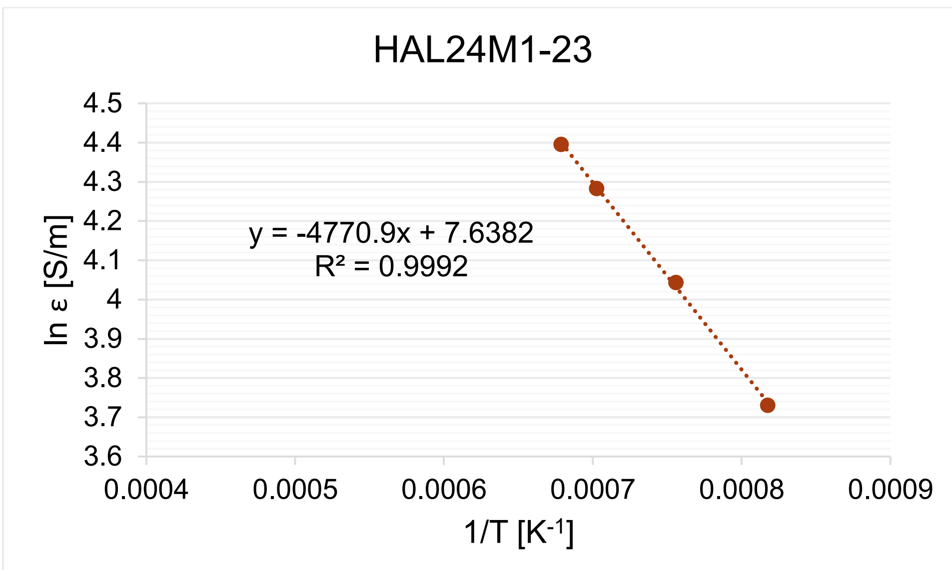

Figure K.23. Electrical conductivity-temperature data and Arrhenius equation fit for glass HAL24M1-23.

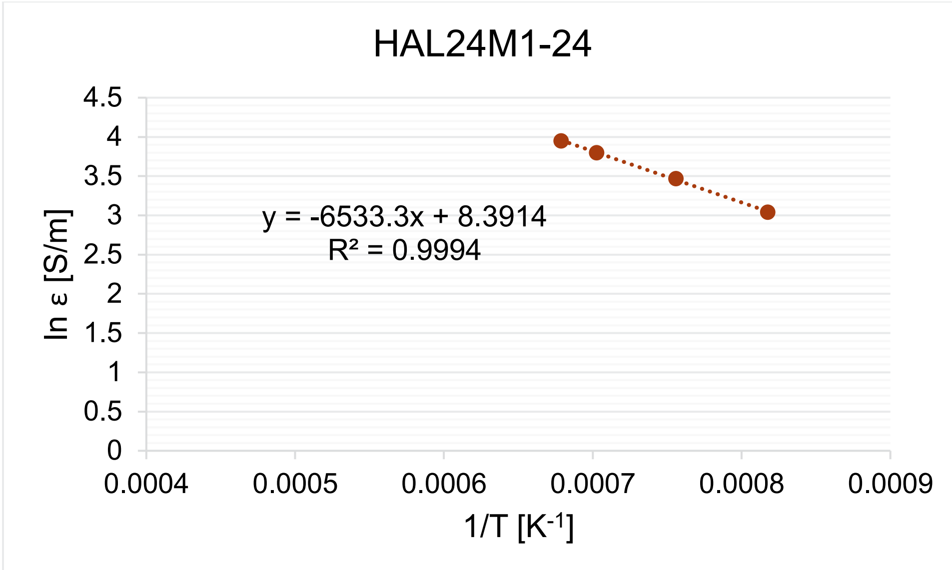

Figure K.24. Electrical conductivity-temperature data and Arrhenius equation fit for glass HAL24M1-24.

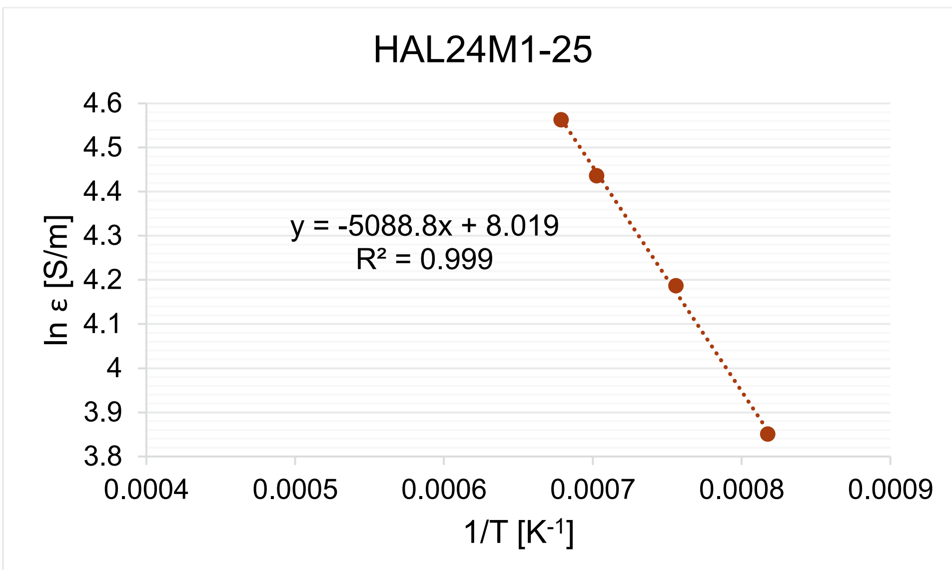

Figure K.25. Electrical conductivity-temperature data and Arrhenius equation fit for glass HAL24M1-25.

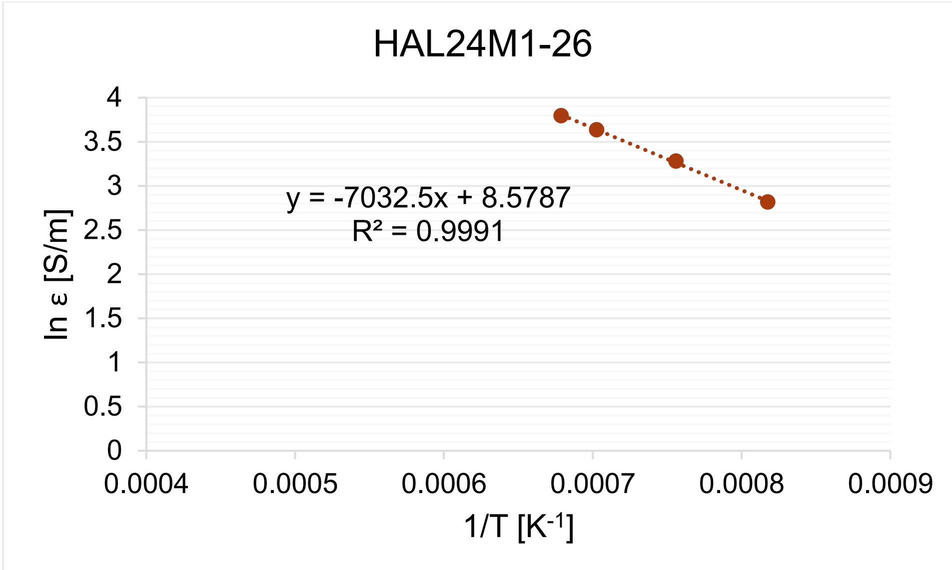

Figure K.26. Electrical conductivity-temperature data and Arrhenius equation fit for glass HAL24M1-26.

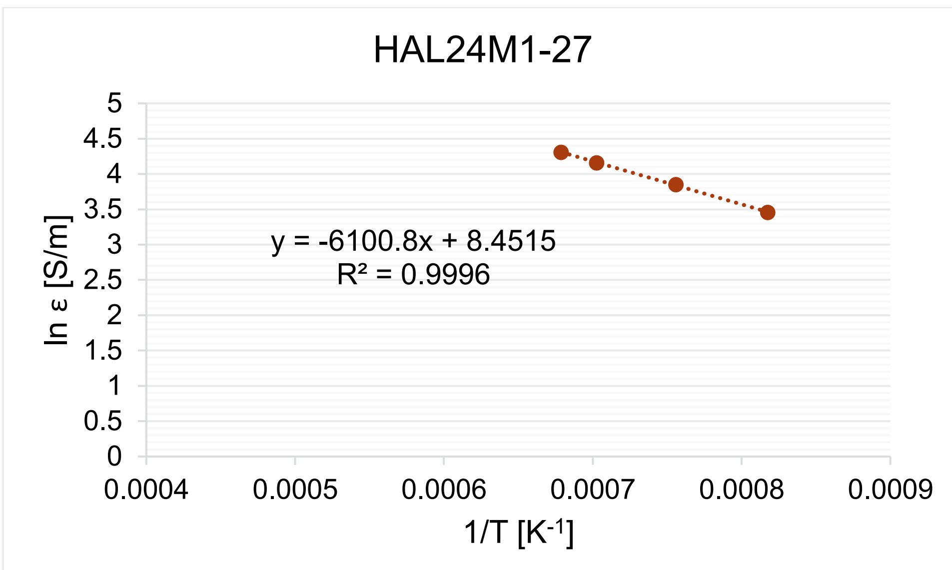

Figure K.27. Electrical conductivity-temperature data and Arrhenius equation fit for glass HAL24M1-27.

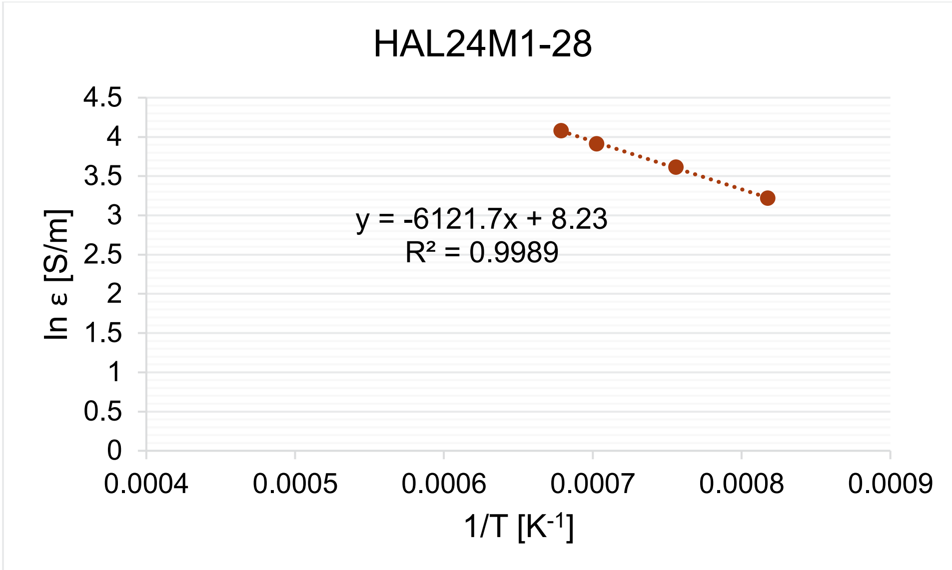

Figure K.28. Electrical conductivity-temperature data and Arrhenius equation fit for glass HAL24M1-28.

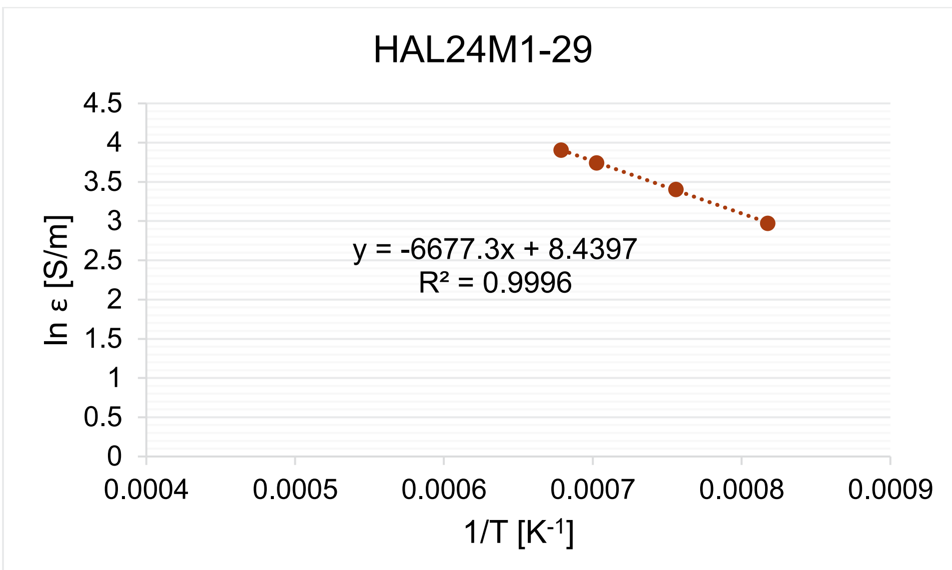

Figure K.29. Electrical conductivity-temperature data and Arrhenius equation fit for glass HAL24M1-29-1.

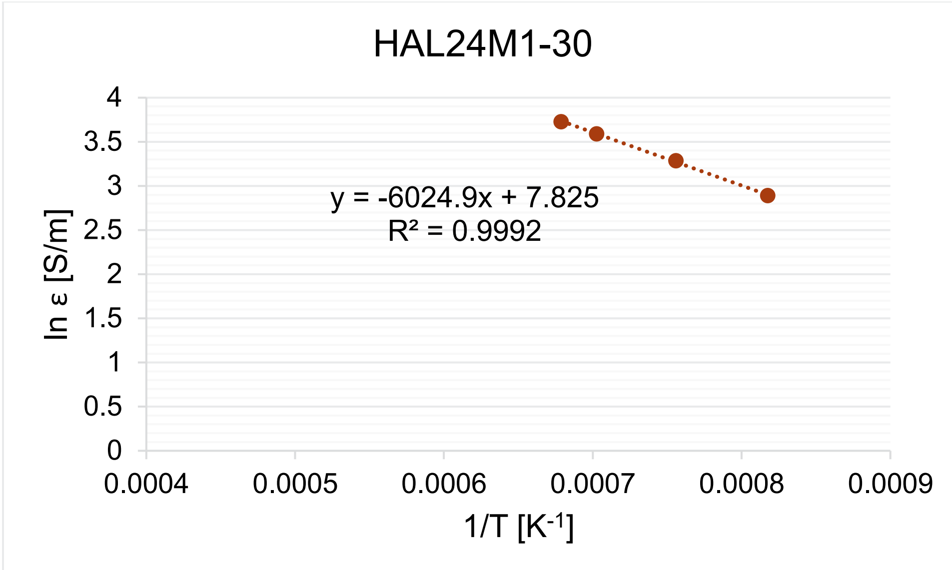

Figure K.30. Electrical conductivity-temperature data and Arrhenius equation fit for glass HAL24M1-30-1.

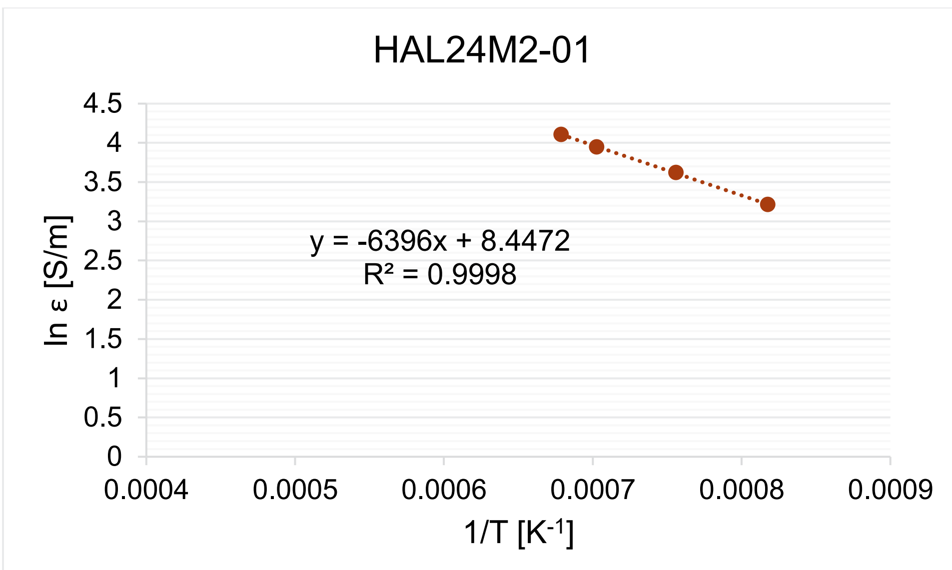

Figure K.31. Electrical conductivity-temperature data and Arrhenius equation fit for glass HAL24M2-01.

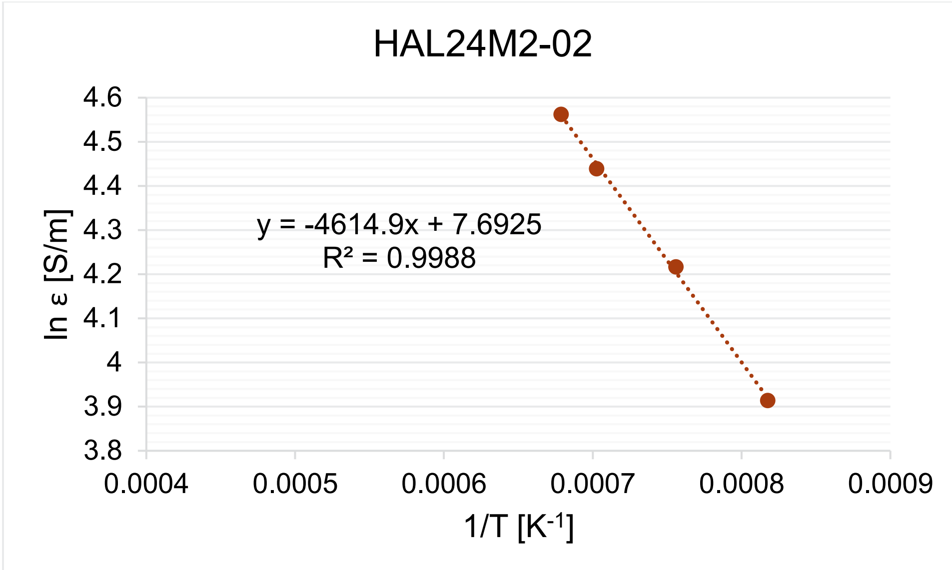

Figure K.32. Electrical conductivity-temperature data and Arrhenius equation fit for glass HAL24M2-02.

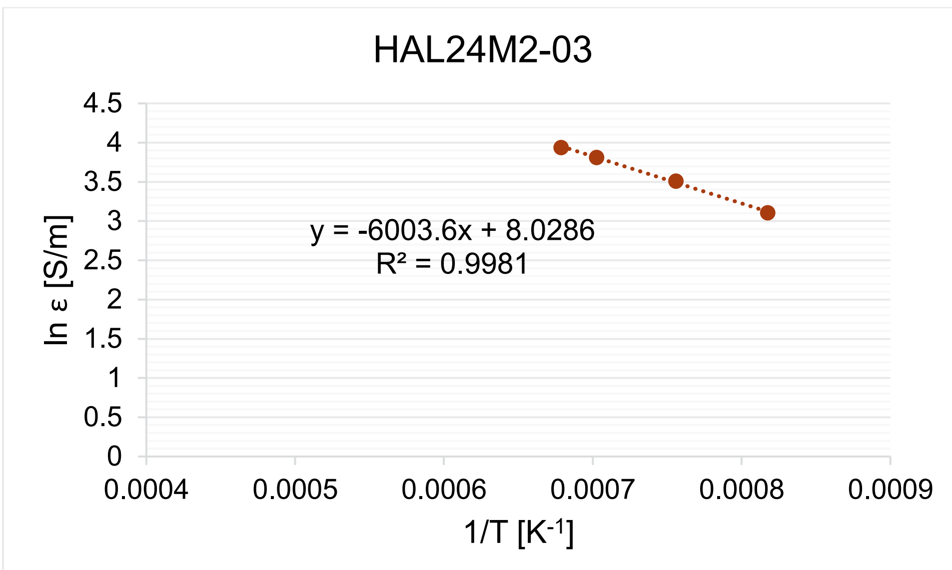

Figure K.33. Electrical conductivity-temperature data and Arrhenius equation fit for glass HAL24M2-03.

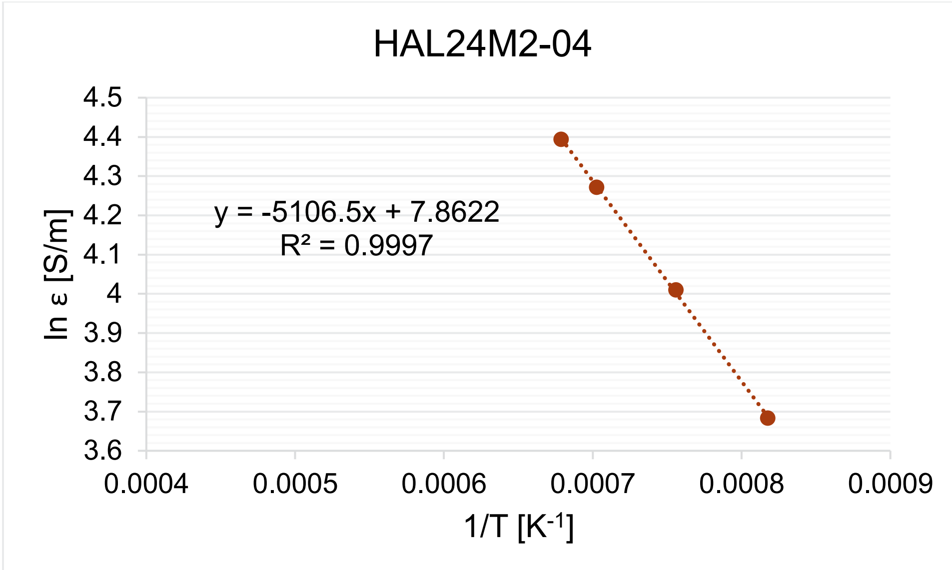

Figure K.34. Electrical conductivity-temperature data and Arrhenius equation fit for glass HAL24M2-04-1.

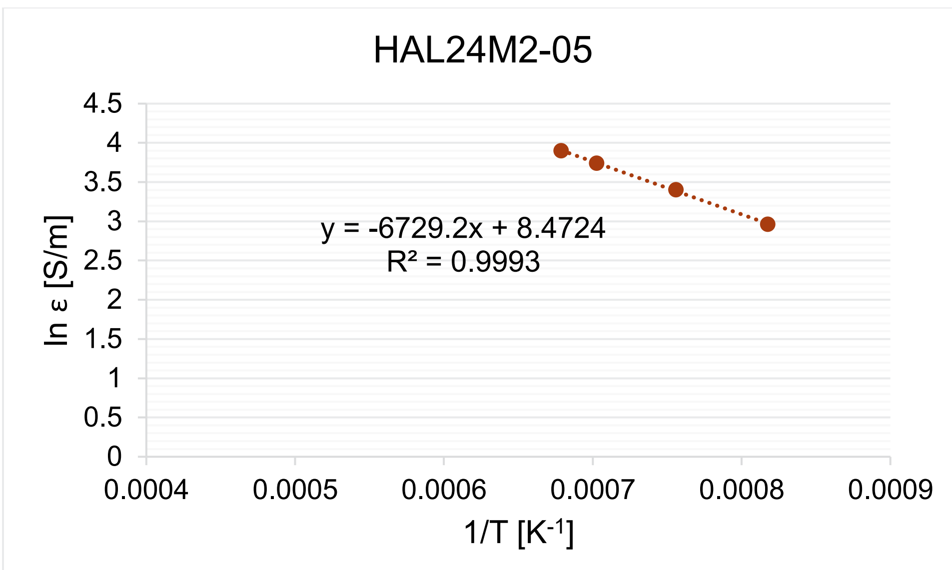

Figure K.35. Electrical conductivity-temperature data and Arrhenius equation fit for glass HAL24M2-05.

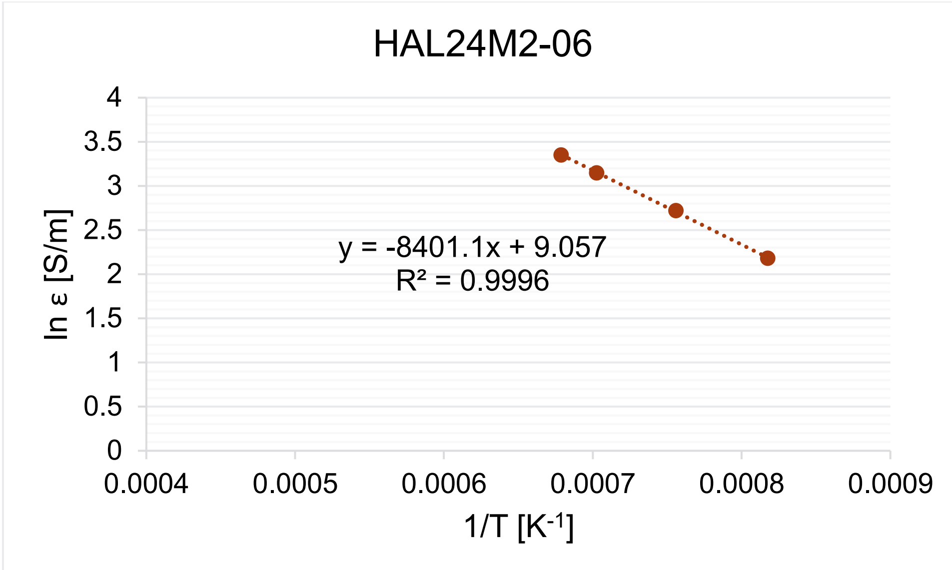

Figure K.36. Electrical conductivity-temperature data and Arrhenius equation fit for glass HAL24M2-06.

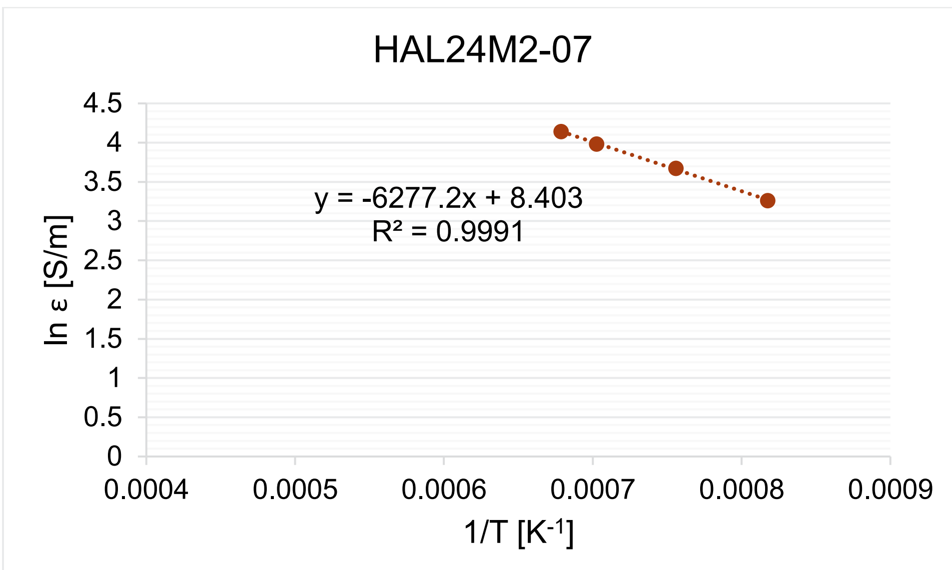

Figure K.37. Electrical conductivity-temperature data and Arrhenius equation fit for glass HAL24M2-07.

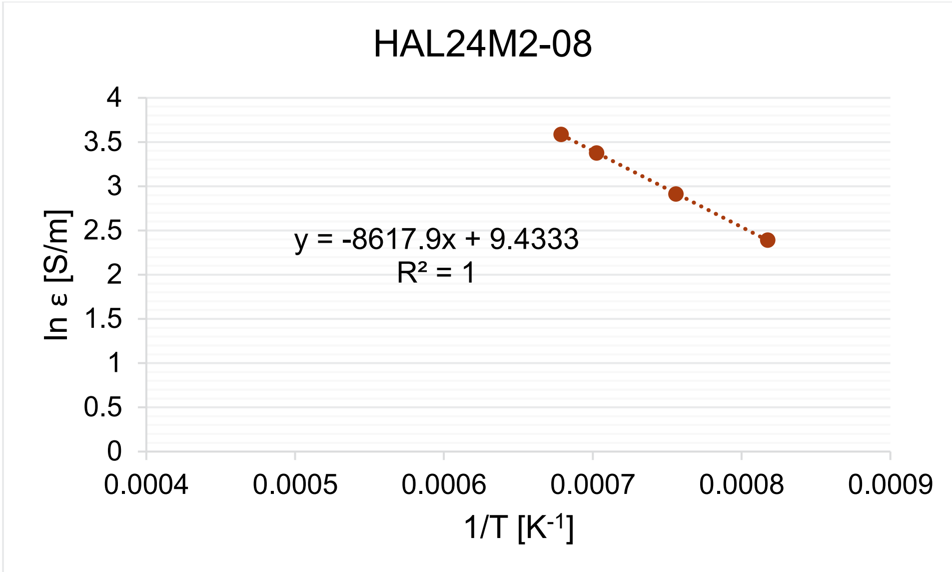

Figure K.38. Electrical conductivity-temperature data and Arrhenius equation fit for glass HAL24M2-08.

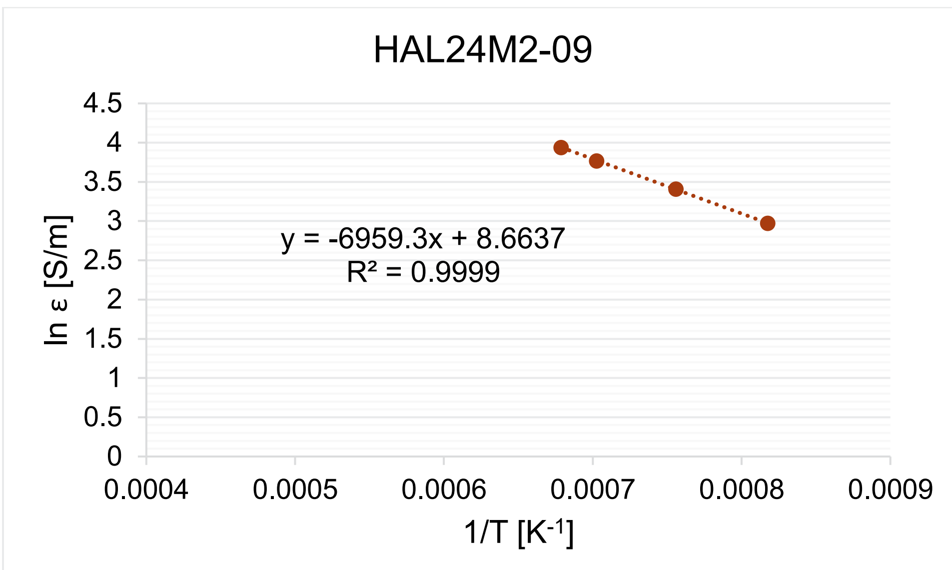

Figure K.39. Electrical conductivity-temperature data and Arrhenius equation fit for glass HAL24M2-09.

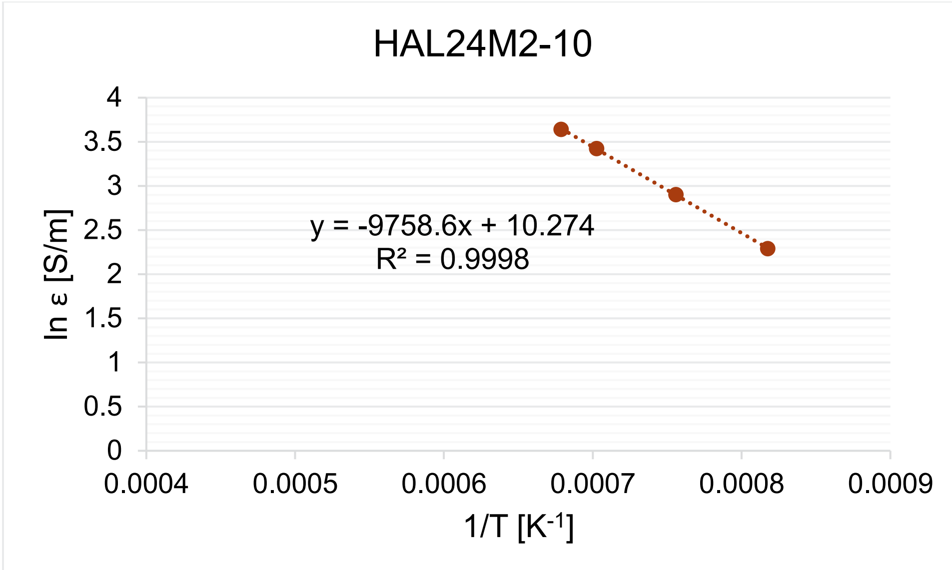

Figure K.40. Electrical conductivity-temperature data and Arrhenius equation fit for glass HAL24M2-10.

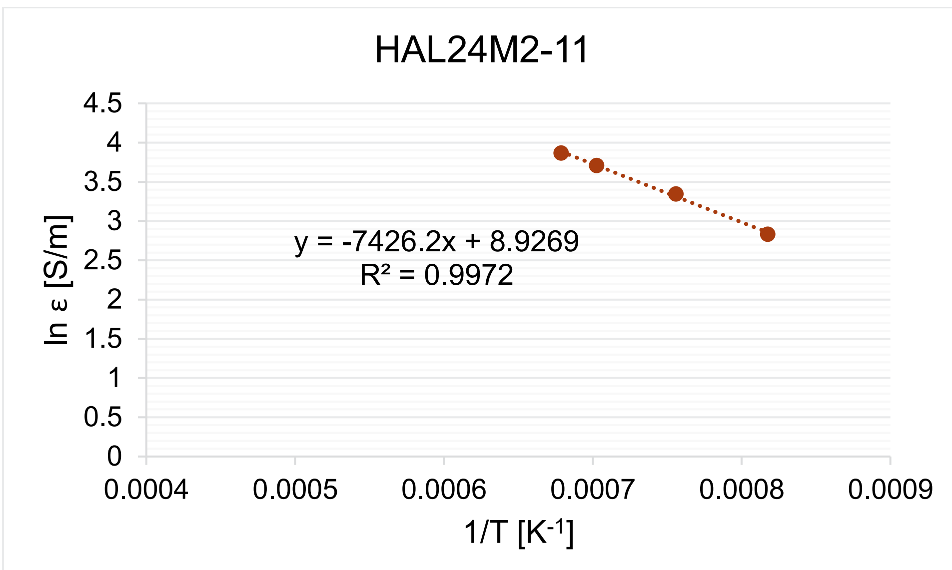

Figure K.41. Electrical conductivity-temperature data and Arrhenius equation fit for glass HAL24M2-11.

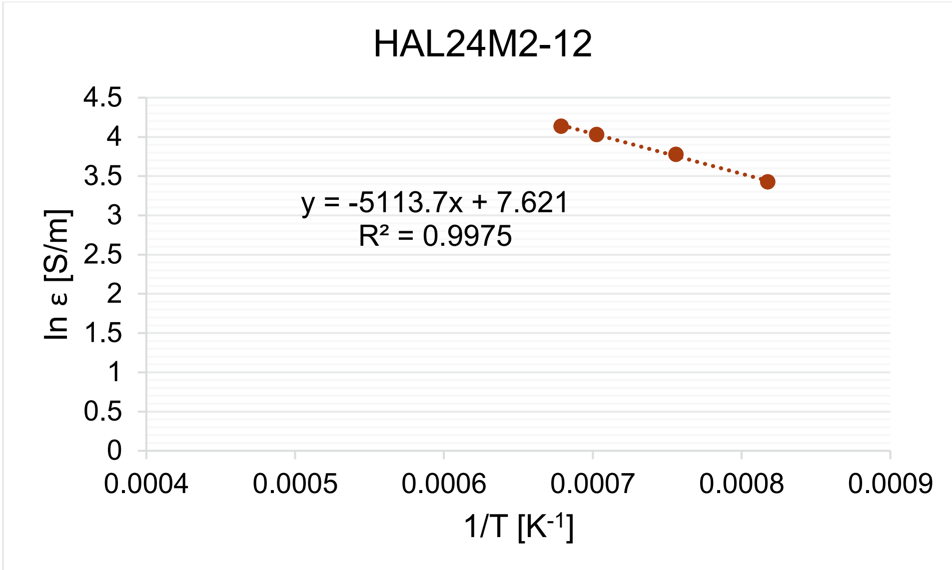

Figure K.42. Electrical conductivity-temperature data and Arrhenius equation fit for glass HAL24M2-12.

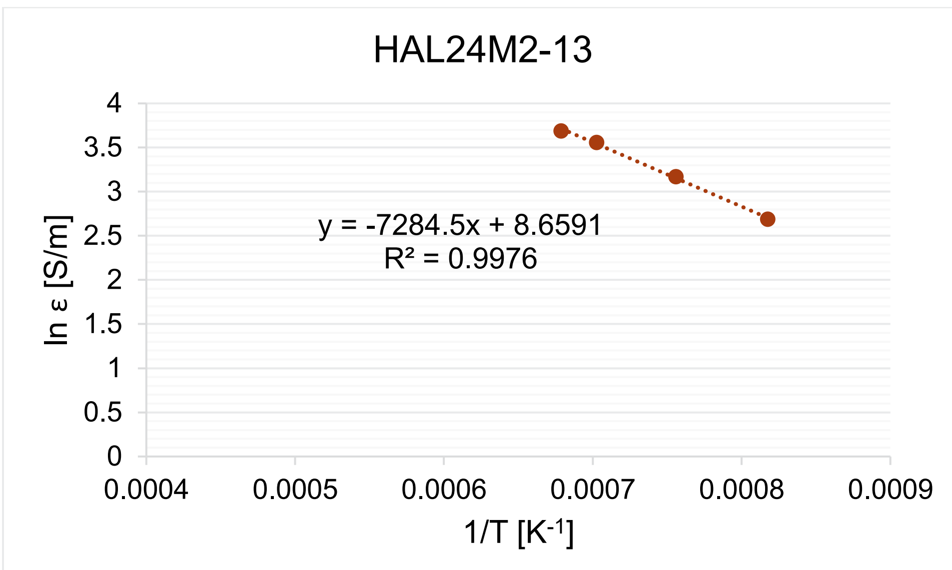

Figure K.43. Electrical conductivity-temperature data and Arrhenius equation fit for glass HAL24M2-13.

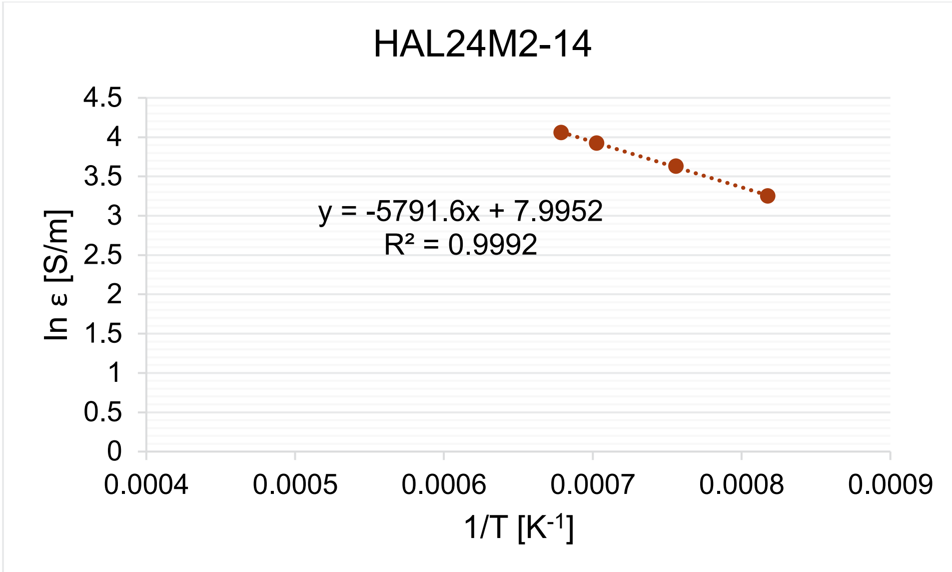

Figure K.44. Electrical conductivity-temperature data and Arrhenius equation fit for glass HAL24M2-14.

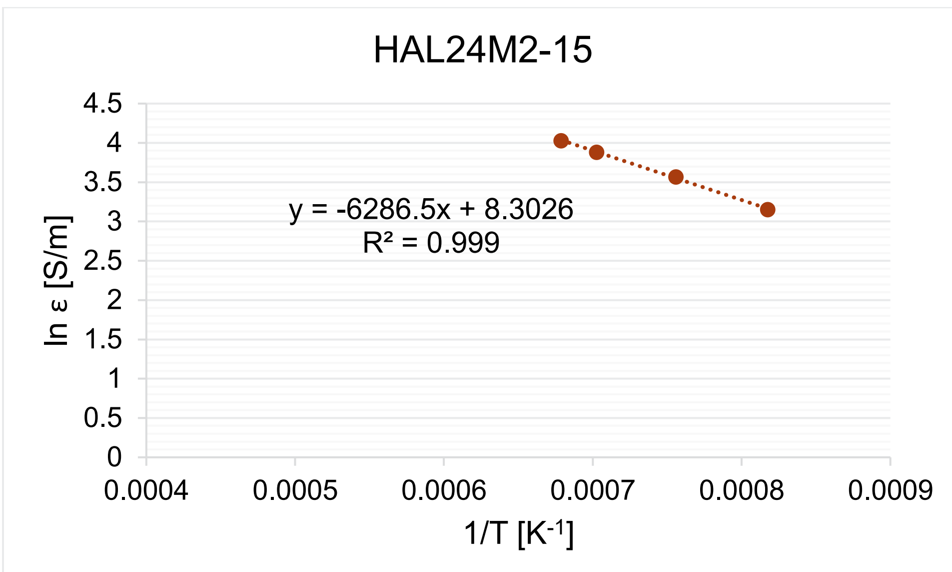

Figure K.45. Electrical conductivity-temperature data and Arrhenius equation fit for glass HAL24M2-15.

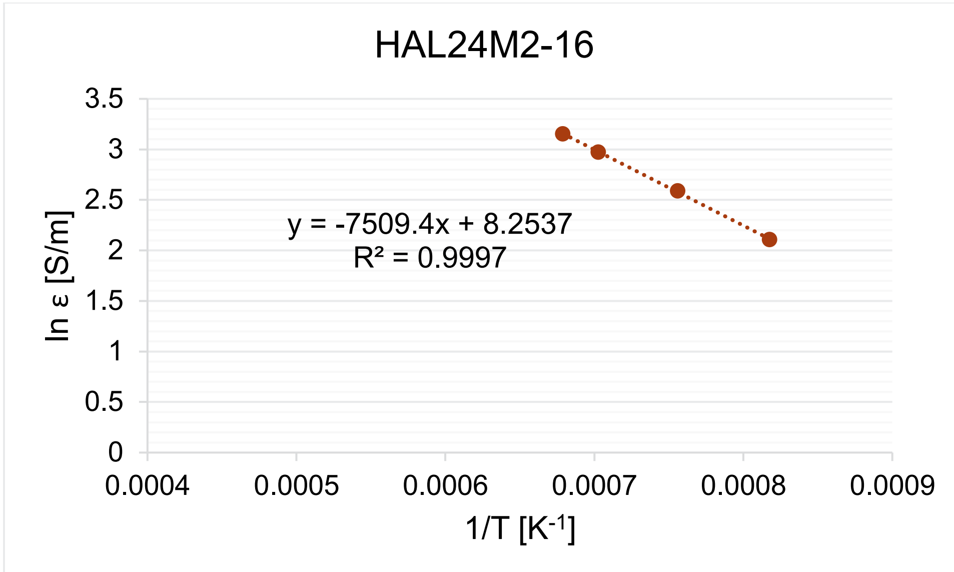

Figure K.46. Electrical conductivity-temperature data and Arrhenius equation fit for glass HAL24M2-16.

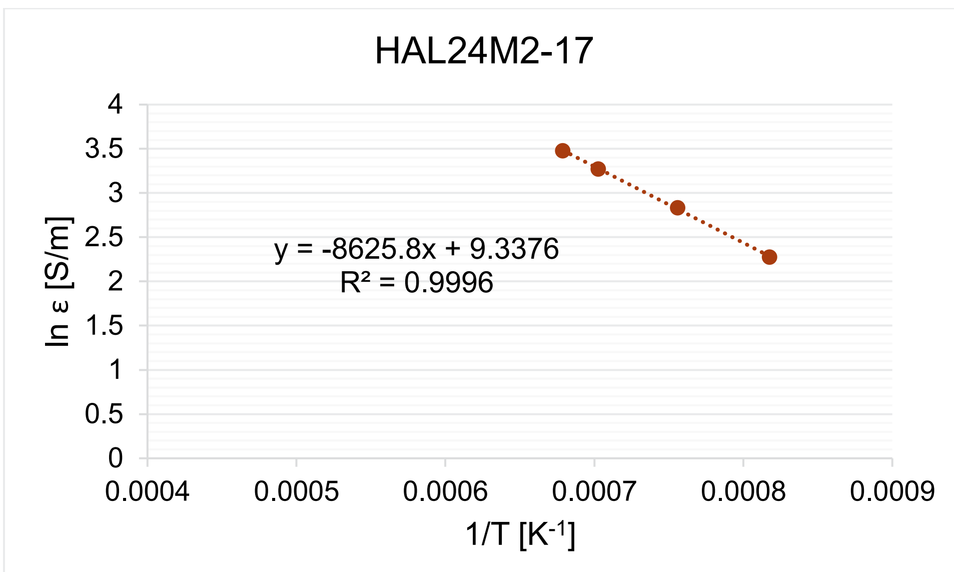

Figure K.47. Electrical conductivity-temperature data and Arrhenius equation fit for glass HAL24M2-17.

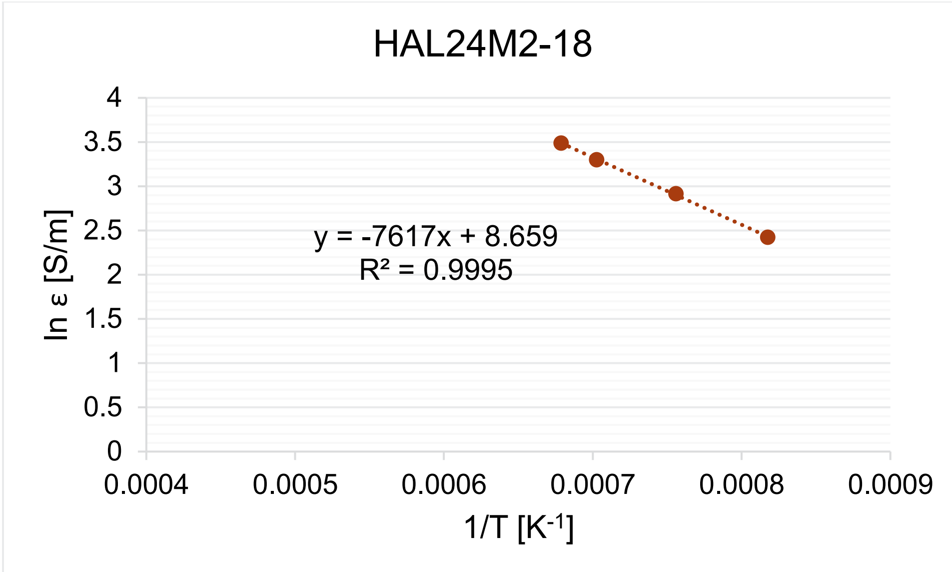

Figure K.48. Electrical conductivity-temperature data and Arrhenius equation fit for glass HAL24M2-18.

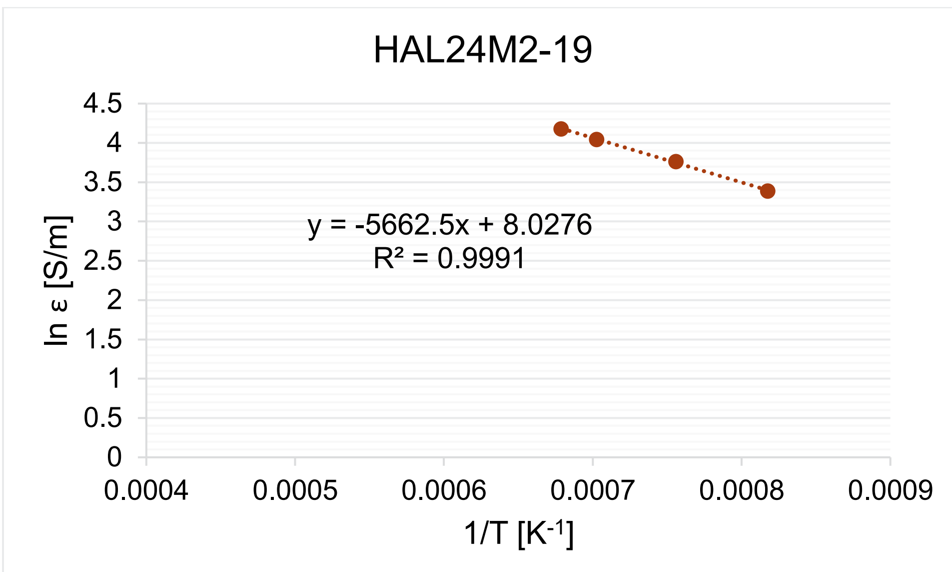

Figure K.49. Electrical conductivity-temperature data and Arrhenius equation fit for glass HAL24M2-19.

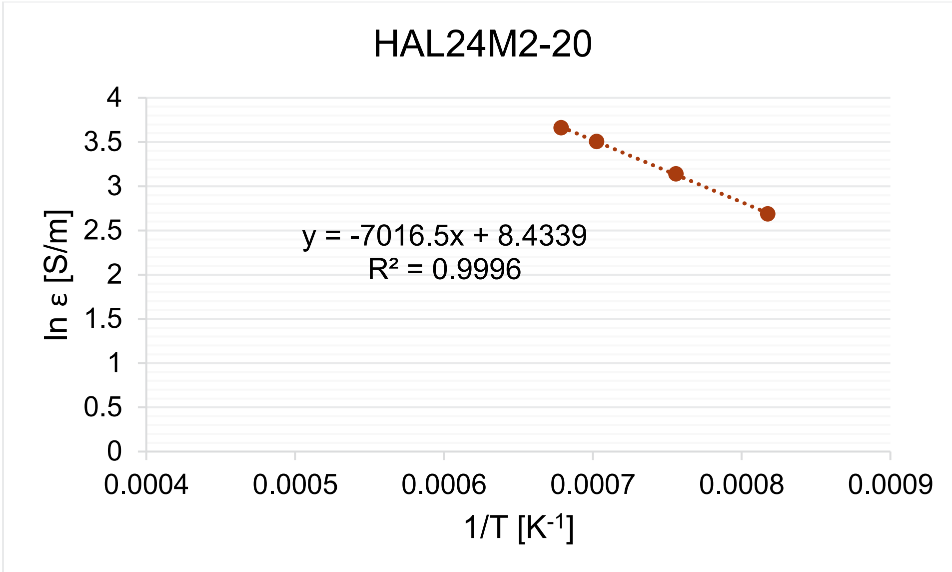

Figure K.50. Electrical conductivity-temperature data and Arrhenius equation fit for glass HAL24M2-50.

Appendix L – PCT Full Results

The complete list of product consistency test (PCT) results is shown in this appendix in a manner that the quenched (Q) and canister centerline cooled (CCC) glasses can be compared easily.

Table L.1. PCT normalized concentrations (g/L) of B, Si, Na, and Li for Q and CCC HAL24 glasses. N/A = not applicable as the glass does not contain Li.

	Normalized Concentrations (NC_i) in g/L			
Sample ID	Boron	Silicon	Sodium	Lithium
HAL24M1-01-Q	0.94 ± 0.01	0.17 ± 0.00	1.02 ± 0.02	0.90 ± 0.01
HAL24M1-02-Q	2.38 ± 0.06	0.26 ± 0.01	1.84 ± 0.04	1.82 ± 0.04
HAL24M1-03-Q	2.79 ± 0.08	0.25 ± 0.00	1.72 ± 0.04	2.44 ± 0.05
HAL24M1-04-Q	11.56 ± 0.08	0.17 ± 0.00	6.11 ± 0.05	9.46 ± 0.09
HAL24M1-05-Q	9.31 ± 0.16	0.22 ± 0.00	5.73 ± 0.08	7.48 ± 0.09
HAL24M1-06-Q	2.32 ± 0.03	0.23 ± 0.01	2.03 ± 0.03	2.26 ± 0.04
HAL24M1-07-Q	9.33 ± 0.04	0.20 ± 0.00	3.95 ± 0.02	6.64 ± 0.04
HAL24M1-08-Q	4.94 ± 0.04	0.19 ± 0.00	3.46 ± 0.01	4.30 ± 0.03
HAL24M1-09-Q	0.74 ± 0.01	0.31 ± 0.00	0.77 ± 0.00	0.76 ± 0.01
HAL24M1-10-Q	7.52 ± 0.11	0.22 ± 0.01	3.73 ± 0.06	5.50 ± 0.10
HAL24M1-11-Q	0.29 ± 0.00	0.13 ± 0.00	0.40 ± 0.00	0.52 ± 0.00
HAL24M1-12-Q	0.43 ± 0.01	0.11 ± 0.00	0.53 ± 0.01	0.37 ± 0.01
HAL24M1-13-1-Q	0.68 ± 0.03	0.25 ± 0.00	0.74 ± 0.02	1.03 ± 0.00
HAL24M1-14-Q	0.52 ± 0.01	0.23 ± 0.00	0.61 ± 0.01	0.52 ± 0.01
HAL24M1-15-Q	0.67 ± 0.01	0.14 ± 0.00	0.76 ± 0.01	0.64 ± 0.01
HAL24M1-16-Q	0.60 ± 0.00	0.17 ± 0.00	0.68 ± 0.00	0.64 ± 0.00
HAL24M1-17-Q	3.45 ± 0.02	0.21 ± 0.00	2.36 ± 0.02	3.18 ± 0.01
HAL24M1-18-Q	0.46 ± 0.01	0.25 ± 0.00	0.42 ± 0.01	0.65 ± 0.01
HAL24M1-19-Q	8.16 ± 0.11	0.20 ± 0.00	3.12 ± 0.04	5.87 ± 0.06
HAL24M1-20-Q	2.85 ± 0.02	0.32 ± 0.01	2.13 ± 0.02	2.62 ± 0.02
HAL24M1-21-Q	10.26 ± 0.05	0.25 ± 0.00	6.02 ± 0.06	7.96 ± 0.11
HAL24M1-22-Q	5.33 ± 0.01	0.23 ± 0.00	3.36 ± 0.00	4.22 ± 0.00
HAL24M1-23-Q	6.97 ± 0.09	0.29 ± 0.00	4.63 ± 0.04	4.16 ± 0.03
HAL24M1-24-Q	1.42 ± 0.03	0.32 ± 0.00	1.62 ± 0.04	0.81 ± 0.02
HAL24M1-25-Q	6.43 ± 0.02	0.37 ± 0.01	5.30 ± 0.03	5.26 ± 0.03
HAL24M1-26-Q	1.13 ± 0.01	0.20 ± 0.00	1.19 ± 0.00	0.99 ± 0.00
HAL24M1-27-Q	2.33 ± 0.04	0.28 ± 0.00	1.90 ± 0.02	1.41 ± 0.01
HAL24M1-28-Q	3.78 ± 0.05	0.25 ± 0.00	2.31 ± 0.04	2.93 ± 0.05
HAL24M1-29-1-Q	5.62 ± 0.05	0.24 ± 0.00	3.72 ± 0.02	4.57 ± 0.03
HAL24M1-30-1-Q	9.23 ± 0.06	0.20 ± 0.00	5.84 ± 0.04	NA
HAL24M2-01-Q	2.18 ± 0.02	0.26 ± 0.00	2.12 ± 0.01	4.79 ± 0.00
HAL24M2-02-Q	7.70 ± 0.11	0.62 ± 0.02	5.34 ± 0.05	4.39 ± 0.01
HAL24M2-03-Q	5.00 ± 0.07	0.20 ± 0.00	2.38 ± 0.04	3.62 ± 0.06
HAL24M2-04-1-Q	6.56 ± 0.06	0.22 ±0.00	3.63 ± 0.02	3.58 ± 0.03
HAL24M2-05-Q	1.21 ± 0.04	0.30 ± 0.00	1.10 ± 0.02	0.97 ± 0.02

Sample ID	Normalized Concentrations (NC_i) in g/L			
	Boron	Silicon	Sodium	Lithium
HAL24M2-06-Q	2.74 ± 0.02	0.14 ± 0.00	2.29 ± 0.04	2.66 ± 0.04
HAL24M2-07-Q	2.38 ± 0.02	0.23 ± 0.00	2.09 ± 0.02	1.84 ± 0.01
HAL24M2-08-Q	0.65 ± 0.00	0.16 ± 0.00	0.72 ± 0.00	0.68 ± 0.00
HAL24M2-09-Q	5.16 ± 0.04	0.20 ± 0.00	4.00 ± 0.03	4.61 ± 0.06
HAL24M2-10-Q	0.55 ± 0.00	0.09 ± 0.00	0.63 ± 0.01	0.61 ± 0.00
HAL24M2-11-Q	0.77 ± 0.02	0.20 ± 0.00	0.92 ± 0.03	0.71 ± 0.02
HAL24M2-12-Q	8.08 ± 0.19	0.20 ± 0.00	5.31 ± 0.12	6.23 ± 0.16
HAL24M2-13-Q	5.33 ± 0.04	0.22 ± 0.00	3.55 ± 0.02	4.48 ± 0.03
HAL24M2-14-Q	6.32 ± 0.09	0.25 ± 0.00	3.69 ± 0.05	4.69 ± 0.07
HAL24M2-15-Q	2.53 ± 0.04	0.27 ± 0.00	2.31 ± 0.03	1.75 ± 0.06
HAL24M2-16-Q	2.06 ± 0.03	0.24 ± 0.00	1.60 ± 0.02	1.97 ± 0.03
HAL24M2-17-Q	2.01 ± 0.01	0.17 ± 0.00	2.02 ± 0.01	2.10 ± 0.01
HAL24M2-18-Q	2.26 ± 0.06	0.24 ± 0.00	1.70 ± 0.05	2.13 ± 0.05
HAL24M2-19-Q	7.40 ± 0.03	0.22 ± 0.00	5.69 ± 0.03	6.39 ± 0.05
HAL24M2-20-Q	1.56 ± 0.03	0.27 ± 0.00	1.32 ± 0.02	1.47 ± 0.03
HAL24M1-01-CCC	1.03 ± 0.01	0.18 ± 0.00	1.17 ± 0.01	1.13 ± 0.02
HAL24M1-02-CCC	1.45 ± 0.05	0.27 ± 0.00	1.23 ± 0.03	1.18 ± 0.05
HAL24M1-03-CCC	4.43 ± 0.01	0.27 ± 0.00	2.51 ± 0.01	3.69 ± 0.02
HAL24M1-04-CCC	10.04 ± 0.11	0.18 ± 0.00	5.36 ± 0.04	8.28 ± 0.09
HAL24M1-05-CCC	12.07 ± 0.13	0.21 ± 0.00	6.69 ± 0.06	9.23 ± 0.06
HAL24M1-06-CCC	2.02 ± 0.03	0.27 ± 0.00	1.78 ± 0.02	1.98 ± 0.03
HAL24M1-07-CCC	20.36 ± 0.24	0.22 ± 0.00	6.80 ± 0.09	13.83 ± 0.25
HAL24M1-08-CCC	8.11 ± 0.10	0.23 ± 0.00	4.92 ± 0.04	6.89 ± 0.05
HAL24M1-09-CCC	0.54 ± 0.01	0.18 ± 0.00	0.51 ± 0.01	0.57 ± 0.00
HAL24M1-10-CCC	11.90 ± 0.05	0.22 ± 0.00	4.99 ± 0.02	7.39 ± 0.03
HAL24M1-11-CCC	0.29 ± 0.01	0.13 ± 0.00	0.36 ± 0.01	0.52 ± 0.00
HAL24M1-12-CCC	6.42 ± 0.14	0.06 ± 0.00	2.95 ± 0.06	7.56 ± 0.16
HAL24M1-13-1-CCC	0.74 ± 0.02	0.29 ± 0.00	0.78 ± 0.03	1.03 ± 0.00
HAL24M1-14-CCC	1.36 ± 0.01	0.25 ± 0.00	0.99 ± 0.01	1.15 ± 0.01
HAL24M1-15-CCC	0.51 ± 0.01	0.14 ± 0.00	0.60 ± 0.01	0.54 ± 0.01
HAL24M1-16-CCC	41.87 ± 0.23	0.05 ± 0.00	13.83 ± 0.10	51.53 ± 0.39
HAL24M1-17-CCC	2.87 ± 0.05	0.21 ± 0.00	2.01 ± 0.02	2.65 ± 0.04
HAL24M1-18-CCC	0.50 ± 0.00	0.32 ± 0.00	0.43 ± 0.00	0.66 ± 0.01
HAL24M1-19-CCC	7.52 ± 0.07	0.20 ± 0.00	2.71 ± 0.03	5.22 ± 0.03
HAL24M1-20-CCC	2.59 ± 0.00	0.32 ± 0.00	1.96 ± 0.02	2.43 ± 0.04
HAL24M1-21-CCC	10.34 ± 0.11	0.24 ± 0.00	5.83 ± 0.05	8.01 ± 0.08
HAL24M1-22-CCC	6.20 ± 0.07	0.24 ± 0.00	3.70 ± 0.04	4.76 ± 0.06
HAL24M1-23-CCC	5.04 ± 0.03	0.25 ± 0.00	4.42 ± 0.01	3.97 ± 0.01
HAL24M1-24-CCC	24.52 ± 0.49	0.31 ± 0.00	18.71 ± 0.32	28.27 ± 0.45
HAL24M1-25-CCC	89.25 ± 0.81	0.12 ± 0.00	43.26 ± 0.35	78.77 ± 0.69
HAL24M1-26-CCC	21.54 ± 0.15	0.07 ± 0.00	10.89 ± 0.04	20.38 ± 0.10
HAL24M1-27-CCC	44.44 ± 0.14	0.13 ± 0.00	18.67 ± 0.04	34.46 ± 0.24

Sample ID	Normalized Concentrations (NC_i) in g/L			
	Boron	Silicon	Sodium	Lithium
HAL24M1-28-CCC	3.71 ± 0.01	0.21 ± 0.00	2.18 ± 0.01	2.78 ± 0.02
HAL24M1-29-1-CCC	5.12 ± 0.03	0.25 ± 0.00	3.32 ± 0.02	4.04 ± 0.03
HAL24M1-30-1-CCC	10.93 ± 0.13	0.21 ± 0.00	6.49 ± 0.06	NA
HAL24M2-01-CCC	8.99 ± 0.19	0.15 ± 0.00	6.83 ± 0.15	6.15 ± 0.08
HAL24M2-02-CCC	83.45 ± 0.44	0.17 ± 0.00	34.21 ± 0.12	22.30 ± 0.16
HAL24M2-03-CCC	3.89 ± 0.03	0.24 ± 0.01	1.92 ± 0.02	2.76 ± 0.01
HAL24M2-04-1-CCC	4.38 ± 0.03	0.23 ± 0.00	2.43 ± 0.01	1.40 ± 0.01
HAL24M2-05-CCC	0.78 ± 0.02	0.21 ± 0.00	0.70 ± 0.01	0.68 ± 0.01
HAL24M2-06-CCC	0.39 ± 0.01	0.11 ± 0.00	0.43 ± 0.01	0.53 ± 0.00
HAL24M2-07-CCC	2.43 ± 0.04	0.17 ± 0.00	1.88 ± 0.03	1.94 ± 0.02
HAL24M2-08-CCC	0.80 ± 0.02	0.19 ± 0.00	0.81 ± 0.02	0.80 ± 0.02
HAL24M2-09-CCC	20.58 ± 0.15	0.11 ± 0.00	13.76 ± 0.05	20.45 ± 0.12
HAL24M2-10-CCC	0.38 ± 0.00	0.10 ± 0.00	0.40 ± 0.01	0.42 ± 0.01
HAL24M2-11-CCC	0.72 ± 0.03	0.19 ± 0.00	0.82 ± 0.03	0.74 ± 0.03
HAL24M2-12-CCC	46.46 ± 0.34	0.14 ± 0.00	23.07 ± 0.18	23.14 ± 0.25
HAL24M2-13-CCC	5.76 ± 0.06	0.24 ± 0.00	3.68 ± 0.03	4.64 ± 0.05
HAL24M2-14-CCC	3.68 ± 0.02	0.27 ± 0.00	2.26 ± 0.01	2.86 ± 0.02
HAL24M2-15-CCC	3.15 ± 0.02	0.22 ± 0.00	2.62 ± 0.01	2.41 ± 0.03
HAL24M2-16-CCC	10.26 ± 0.07	0.22 ± 0.00	4.75 ± 0.01	7.33 ± 0.04
HAL24M2-17-CCC	1.81 ± 0.04	0.17 ± 0.00	1.82 ± 0.04	1.87 ± 0.05
HAL24M2-18-CCC	3.25 ± 0.02	0.24 ± 0.01	2.19 ± 0.02	2.88 ± 0.02
HAL24M2-19-CCC	6.66 ± 0.04	0.19 ± 0.00	4.96 ± 0.02	5.69 ± 0.02
HAL24M2-20-CCC	2.01 ± 0.10	0.28 ± 0.00	1.55 ± 0.06	1.81 ± 0.08

Appendix M – TCLP Full Results

This appendix presents the complete list of toxicity characteristic leaching procedure (TCLP) results for this study.

Table M.1. TCLP leachate concentrations of B, Cr, Ni, Pb, V, and Zn for quenched (Q) and canister centerline cooled (CCC) HAL24 glasses in mg·L^{-1}. The delisting limits (Blumenkranz 2006) for the constituents of concern are provided as a reference. Values represented by detection limits are presented in red font.

	Element					
Sample ID	B	Cr	Ni	Pb	V	Zn
Delisting Limits:	N/A	4.95	22.6	5.00	16.9	225
HAL24M1-01-Q	15.4 ± 3.43	≤0.25	≤0.38	≤0.5	4.3 ± 0.56	9.99 ± 1.92
HAL24M1-02-Q	7.04 ± 0.21	≤0.25	≤0.38	≤0.51	2.28 ± 0	1.04 ± 0.01
HAL24M1-03-Q	≤5.05	≤0.25	≤0.38	≤0.5	0.52 ± 0.02	≤0.76
HAL24M1-04-Q	10.16 ± 0.12	≤0.25	≤0.38	≤0.5	≤0.25	3.54 ± 0.09
HAL24M1-05-Q	20.08 ± 0.57	≤0.25	0.48 ± 0.05	≤0.51	6.49 ± 0.6	6.45 ± 0.54
HAL24M1-06-Q	22.8 ± 2.43	≤0.25	0.56 ± 0.07	0.51 ± 0.01	0.49 ± 0.03	8.76 ± 0.88
HAL24M1-07-Q	5.65 ± 0.83	≤0.25	≤0.38	≤0.51	0.75 ± 0.04	1.55 ± 0.05
HAL24M1-08-Q	6.51 ± 2.06	≤0.25	≤0.38	≤0.5	0.51 ± 0.08	2.54 ± 0.77
HAL24M1-09-Q	11.8 ± 3.52	≤0.25	≤0.38	≤0.5	1.53 ± 0.47	7.21 ± 2
HAL24M1-10-Q	≤5.05	≤0.25	≤0.38	≤0.51	≤0.25	1.68 ± 0.06
HAL24M1-11-Q	8.42 ± 0.82	≤0.25	≤0.38	≤0.5	0.57 ± 0.03	3.49 ± 0.92
HAL24M1-12-Q	9.49 ± 1.62	≤0.25	≤0.38	≤0.5	0.26 ± 0.01	≤0.76
HAL24M1-13-1-Q	≤5.06	≤0.25	≤0.38	≤0.51	0.81 ± 0.05	1 ± 0.08
HAL24M1-14-Q	≤5.06	≤0.25	≤0.38	≤0.51	0.52 ± 0	≤0.76
HAL24M1-15-Q	13.08 ± 0.43	≤0.25	≤0.38	≤0.51	2.37 ± 0.09	5.35 ± 0.21
HAL24M1-16-Q	6.7 ± 0.46	≤0.25	≤0.38	≤0.51	≤0.25	≤0.76
HAL24M1-17-Q	6.38 ± 0.17	≤0.25	≤0.38	≤0.51	0.59 ± 0.02	2.92 ± 0.11
HAL24M1-18-Q	≤5.13	≤0.26	≤0.38	≤0.51	0.65 ± 0	1.1 ± 0.03
HAL24M1-19-Q	≤5.12	≤0.26	≤0.38	≤0.51	≤0.26	≤0.77
HAL24M1-20-Q	11.7 ± 1.94	≤0.26	≤0.39	≤0.51	2.11 ± 0.3	1.88 ± 0.22
HAL24M1-21-Q	18.69 ± 0.35	≤0.25	≤0.38	≤0.5	4.59 ± 0.08	5.8 ± 2.61
HAL24M1-22-Q	≤5.06	≤0.25	≤0.38	≤0.51	0.26 ± 0.02	0.87 ± 0.17
HAL24M1-23-Q	≤5.08	≤0.25	≤0.38	≤0.51	0.43 ± 0.02	2.84 ± 0.14
HAL24M1-24-Q	25.61 ± 3.02	0.47 ± 0.05	0.66 ± 0.08	≤0.51	4.61 ± 0.41	12.05 ± 1.44
HAL24M1-25-Q	18.33 ± 0	0.58 ± 0.01	1.03 ± 0.18	0.51 ± 0.01	≤0.25	4.5 ± 0.04
HAL24M1-26-Q	6.89 ± 0.97	≤0.25	0.5 ± 0.06	≤0.51	1.72 ± 0.2	5.24 ± 0.69
HAL24M1-27-Q	9.44 ± 2.12	≤0.25	0.57 ± 0.11	≤0.5	1.99 ± 0.34	≤0.76
HAL24M1-28-Q	5.49 ± 0.27	≤0.25	≤0.38	≤0.5	0.6 ± 0.02	0.88 ± 0.07
HAL24M1-29-1-Q	13.06 ± 0.15	≤0.25	0.38 ± 0	≤0.51	≤0.25	1.2 ± 0.62
HAL24M1-30-1-Q	6.68 ± 0.7	≤0.25	≤0.38	≤0.5	≤0.25	2.27 ± 2.14
HAL24M1-01-CCC	25.98 ± 3.79	≤0.25	≤0.38	≤0.5	6.42 ± 0.64	16.61 ± 1.86
HAL24M1-02-CCC	7.97 ± 1.42	≤0.25	≤0.38	≤0.5	2.61 ± 0.31	1.12 ± 0.22
HAL24M1-03-CCC	8.81 ± 0.48	≤0.25	≤0.38	≤0.51	1.43 ± 0.06	0.78 ± 0.03
HAL24M1-04-CCC	7.62 ± 0.92	≤0.25	≤0.38	≤0.51	≤0.25	2.78 ± 0.02
HAL24M1-05-CCC	39.54 ± 7.07	≤0.25	0.82 ± 0.15	≤0.51	10.36 ± 1.34	13.75 ± 2.12

Sample ID	Element					
	B	Cr	Ni	Pb	V	Zn
Delisting Limits:	N/A	4.95	22.6	5.00	16.9	225
HAL24M1-06-CCC	23.15 ± 6.24	≤0.25	≤0.38	0.52 ± 0.02	0.54 ± 0.11	9.67 ± 1.23
HAL24M1-07-CCC	≤5.08	≤0.25	≤0.38	≤0.51	1.33 ± 0.05	0.98 ± 0.06
HAL24M1-08-CCC	10.17 ± 0.07	≤0.25	≤0.38	≤0.51	1.09 ± 0.01	2.35 ± 0.01
HAL24M1-09-CCC	43.37 ± 4.04	≤0.25	≤0.38	≤0.51	21.81 ± 1.91	8.51 ± 0.74
HAL24M1-10-CCC	≤5.08	≤0.25	≤0.38	≤0.51	≤0.25	0.84 ± 0.11
HAL24M1-11-CCC	15.18 ± 0.69	≤0.25	≤0.38	≤0.51	1.26 ± 0.13	9.11 ± 8.04
HAL24M1-12-CCC	9.7 ± 0.6	≤0.25	≤0.38	≤0.51	≤0.25	1.04 ± 0.4
HAL24M1-13-1-CCC	43.43 ± 3.94	≤0.26	≤0.38	≤0.51	10.45 ± 0.84	6.19 ± 0.59
HAL24M1-14-CCC	≤5.1	≤0.25	≤0.38	≤0.51	0.46 ± 0	1.01 ± 0.35
HAL24M1-15-CCC	17.18 ± 3.51	≤0.25	≤0.38	≤0.51	2.67 ± 0.29	6.8 ± 1.25
HAL24M1-16-CCC	6.43 ± 0.79	≤0.25	≤0.38	≤0.51	≤0.25	≤0.76
HAL24M1-17-CCC	6.69 ± 0.21	≤0.25	≤0.38	≤0.51	0.75 ± 0.03	3.14 ± 0.15
HAL24M1-18-CCC	≤5.11	≤0.26	≤0.38	≤0.51	0.58 ± 0.06	1.68 ± 0.43
HAL24M1-19-CCC	≤5.11	≤0.26	≤0.38	≤0.51	≤0.26	1.43 ± 0.94
HAL24M1-20-CCC	24.58 ± 7.81	≤0.25	≤0.38	≤0.51	4.87 ± 1.29	3.08 ± 1.93
HAL24M1-21-CCC	23.62 ± 2.58	≤0.25	≤0.38	≤0.51	5.04 ± 0.43	5.64 ± 1.51
HAL24M1-22-CCC	≤5.09	≤0.25	≤0.38	≤0.51	0.46 ± 0.04	1.36 ± 0.67
HAL24M1-23-CCC	16.2 ± 2.27	≤0.25	≤0.38	≤0.51	1.81 ± 0.21	15.69 ± 4.42
HAL24M1-24-CCC	242.44 ± 4.56	0.91 ± 0.05	5.23 ± 0.08	≤0.51	39.32 ± 0.02	45.3 ± 7.75
HAL24M1-25-CCC	849.28 ± 18.61	2.3 ± 0.29	0.39 ± 0.01	≤0.51	≤0.25	104.89 ± 3.59
HAL24M1-26-CCC	223.15 ± 18.91	≤0.25	10.45 ± 0.8	≤0.51	5.41 ± 0.92	146.75 ± 8.32
HAL24M1-27-CCC	151.03 ± 12.91	0.27 ± 0.01	2.5 ± 0.18	≤0.51	3.38 ± 0.32	5.35 ± 0.47
HAL24M1-28-CCC	9.09 ± 2.92	≤0.25	0.44 ± 0.08	≤0.51	0.74 ± 0.09	1.37 ± 0.44
HAL24M1-29-1-CCC	15.51 ± 3.87	≤0.25	≤0.38	≤0.51	0.26 ± 0.01	≤0.76
HAL24M1-30-1-CCC	≤5.1	≤0.25	≤0.38	≤0.51	≤0.25	≤0.77
HAL24M2-01-Q	7.94 ± 0.42	≤0.13	0.4 ± 0.02	≤0.25	≤0.13	0.76 ± 0.04
HAL24M2-02-Q	4.05 ± 0.08	≤0.13	≤0.19	≤0.25	≤0.13	2.05 ± 0.11
HAL24M2-03-Q	≤2.52	≤0.13	≤0.19	≤0.25	0.44 ± 0.02	0.66 ± 0.03
HAL24M2-04-1-Q	≤2.51	≤0.13	≤0.19	≤0.25	≤0.13	≤0.38
HAL24M2-05-Q	19.12 ± 0.94	≤0.13	1.43 ± 0.06	0.63 ± 0	1.01 ± 0.03	4.94 ± 0.22
HAL24M2-06-Q	10.07 ± 0.39	≤0.13	0.32 ± 0.02	≤0.25	2.84 ± 0.1	1.46 ± 0.08
HAL24M2-07-Q	9.63 ± 0.38	≤0.13	0.28 ± 0	≤0.25	1.87 ± 0.08	5.88 ± 0.11
HAL24M2-08-Q	6.1 ± 0.01	0.16 ± 0	0.23 ± 0.01	≤0.25	≤0.13	0.96 ± 0
HAL24M2-09-Q	7.81 ± 0.09	0.14 ± 0	≤0.19	≤0.25	0.58 ± 0.01	0.5 ± 0.01
HAL24M2-10-Q	7.46 ± 0.28	≤0.13	0.47 ± 0.02	≤0.26	0.24 ± 0	≤0.38
HAL24M2-11-Q	4.19 ± 0.36	≤0.13	≤0.19	≤0.26	0.81 ± 0.02	2.34 ± 0.16
HAL24M2-12-Q	4.24 ± 0.01	≤0.13	≤0.19	≤0.25	1.04 ± 0	1.81 ± 0.03
HAL24M2-13-Q	2.65 ± 0.03	≤0.13	≤0.19	≤0.26	≤0.13	≤0.38
HAL24M2-14-Q	3.49 ± 0.01	≤0.13	0.23 ± 0.01	≤0.25	0.85 ± 0.02	≤0.38
HAL24M2-15-Q	6.78 ± 0.43	≤0.13	≤0.19	≤0.25	0.35 ± 0.01	3.43 ± 0.21
HAL24M2-16-Q	2.84 ± 0.07	≤0.13	≤0.19	≤0.25	0.14 ± 0	0.9 ± 0.01
HAL24M2-17-Q	31.63 ± 1.86	0.38 ± 0.01	1.26 ± 0.08	0.53 ± 0.05	0.98 ± 0.03	≤0.38
HAL24M2-18-Q	8.55 ± 0.3	≤0.13	0.23 ± 0.01	≤0.25	0.61 ± 0	≤0.38
HAL24M2-19-Q	18.91 ± 2.8	≤0.13	0.44 ± 0.07	≤0.25	3.37 ± 0.37	1.05 ± 0.18
HAL24M2-20-Q	9.83 ± 0.86	≤0.13	≤0.19	≤0.25	1.49 ± 0.06	3.01 ± 0.27

Sample ID	Element					
	B	Cr	Ni	Pb	V	Zn
Delisting Limits:	N/A	4.95	22.6	5.00	16.9	225
HAL24M2-01-CCC	163.68 ± 6.41	1.37 ± 0.06	7.32 ± 0.21	≤0.25	≤0.13	11.91 ± 0.07
HAL24M2-02-CCC	838.5 ± 37.23	12.42 ± 0.79	0.39 ± 0.06	≤0.25	1.2 ± 0.18	77.41 ± 29.18
HAL24M2-03-CCC	≤2.54	≤0.13	≤0.19	≤0.25	0.4 ± 0	0.63 ± 0.01
HAL24M2-04-1-CCC	≤2.53	≤0.13	≤0.19	≤0.25	≤0.13	≤0.38
HAL24M2-05-CCC	21.64 ± 1.79	≤0.13	1.22 ± 0.09	0.52 ± 0.01	0.96 ± 0.04	5.45 ± 0.42
HAL24M2-06-CCC	4.33 ± 0.17	≤0.13	≤0.19	≤0.25	1.29 ± 0.04	0.67 ± 0.01
HAL24M2-07-CCC	32.44 ± 7.02	0.24 ± 0.06	0.67 ± 0.14	≤0.25	3.23 ± 0.42	18.8 ± 4.08
HAL24M2-08-CCC	14.65 ± 0.21	≤0.13	≤0.19	0.27 ± 0.02	0.16 ± 0	1.11 ± 0.01
HAL24M2-09-CCC	95 ± 8.46	0.18 ± 0	1.33 ± 0.13	≤0.25	0.92 ± 0.04	4.35 ± 0.32
HAL24M2-10-CCC	14.55 ± 0.22	≤0.13	≤0.19	0.39 ± 0.02	0.49 ± 0.02	0.56 ± 0.23
HAL24M2-11-CCC	6.77 ± 0.16	0.36 ± 0.02	≤0.19	≤0.25	1.28 ± 0.03	3.45 ± 0.12
HAL24M2-12-CCC	161.03 ± 1.63	≤0.13	2.8 ± 0.02	≤0.26	9.33 ± 0.03	45.52 ± 0.56
HAL24M2-13-CCC	3.71 ± 0.07	≤0.13	≤0.19	≤0.26	≤0.13	≤0.39
HAL24M2-14-CCC	4.39 ± 0.02	≤0.13	0.25 ± 0.01	≤0.26	0.95 ± 0.02	0.67 ± 0.36
HAL24M2-15-CCC	6.73 ± 0.29	≤0.13	≤0.19	≤0.26	0.37 ± 0.01	3.52 ± 0.22
HAL24M2-16-CCC	5.08 ± 0.03	≤0.13	≤0.19	≤0.25	0.3 ± 0	≤0.38
HAL24M2-17-CCC	43.9 ± 0.71	0.35 ± 0.01	1.74 ± 0.02	0.54 ± 0	1.3 ± 0	≤0.38
HAL24M2-18-CCC	16.37 ± 0.22	≤0.13	≤0.19	≤0.26	1.57 ± 0.01	≤0.38
HAL24M2-19-CCC	25.14 ± 1.3	≤0.13	0.55 ± 0.04	≤0.25	4.11 ± 0.28	1.34 ± 0.12
HAL24M2-20-CCC	15.56 ± 0.37	≤0.13	≤0.19	≤0.25	2.94 ± 0.1	2.12 ± 0.15

Pacific Northwest National Laboratory

902 Battelle Boulevard
P.O. Box 999
Richland, WA 99354

1-888-375-PNNL (7665)

www.pnnl.gov